Imperial College London

USING BIOMECHANICS TO DEFINE THE ROLE OF THE UPPER EXTREMITY IN ROWING PERFORMANCE

Caryn Alexa Urbanczyk

A thesis submitted in fulfillment of requirements for the degree of Doctor of Philosophy

Department of Bioengineering & Department of Surgery and Cancer

Imperial College London

September 2021

DECLARATION OF ORIGINALITY

I declare that to the best of my knowledge, all material in this dissertation is the result of my own work and all else is appropriately referenced. This work has not been previously submitted, in part or whole, to any university or institution for any degree, diploma, or other qualification.

DECLARATION OF COPYRIGHT

ACKNOWLEDGEMENTS

"In rowing I found a sport that demanded

some skill, granted, but placed a much higher

premium on plain hard work and persistence."

- Harry Parker

This has been a fascinating four-year journey. I wish to thank my advisors Prof. Anthony Bull and Prof. Alison McGregor for the opportunity to carry out this research and for years of support, guidance, encouragement.

I have many people to thank at Imperial College London including all the colleagues and collaborators of the MSK Lab and the Musculoskeletal mechanics group: Peter Reilly, Shruti Turner, Yewande Adesida, Biranavan Sivapuratharasu, Matthew Hopkins, Christian Klemt, Samuel Smith, Michael Berthaume, and Paul Thompson, who were supportive throughout my doctoral research in many ways – technically, socially, professionally, and personally; contributing time, expertise, and enthusiasm. Many thanks to the athletes, coaches, and staff that helped make this work possible, including my masters' students, Alessandro Bonfiglio and Emma Miller, that helped run a bunch of crazy long experimental days. To the Avalanche UK community and all the friends I've made there.

I am grateful to the Imperial College President's PhD Scholarship committee, who enabled me, financially to pursue this PhD degree and who have offered over the years a great deal of professional development support.

To the best person I have met on this journey and the least expected: Nick, I love you. Last and certainly not least, to my family, who have always been there for me, through all the highs and lows, with unwavering support.

LIST OF PUBLICATIONS

- **Urbanczyk CA,** McGregor AH, Bull AMJ. "Modelling scapular biomechanics to enhance interpretation of kinematics and performance data in rowing." *Proceedings of the 37th International Conference of Biomechanics in Sports.* 2019; 37(1), Article 31.
- **Urbanczyk CA,** Miller E, McGregor AH, Bull, AMJ. "Fatigue Leads to Altered Spinal Kinematics During High Performance Ergometer Rowing." *Proceedings of the 38th International Conference of Biomechanics in Sports.* 2020; 38(1), Article 29.
- **Urbanczyk, CA,** Bonfiglio A, McGregor AH, Bull AMJ. "Comparing Optical and Electromagnetic Tracking Systems to Facilitate Compatibility in Sports Kinematics" *International Biomechanics.* (Accepted).

ABSTRACT

Performance and injury risk are strongly affected by an athlete's ability to consistently execute effective rowing technique. Previous rowing biomechanics studies focused on kinematic descriptions of the lower extremity and lumbar spine. Detailed biomechanical analyses of the upper extremity during rowing are limited, despite repetitive, high intensity loading across the shoulder complex and the prevalence of long-lasting upper extremity overuse injuries.

This thesis aims to examine upper body biomechanics in ergometer rowing (for performance enhancement and injury mitigation), by developing kinematic and kinetic descriptions of technique. Computational modelling examined internal biomechanics, external kinematics, and performance metrics, across athletes of various ages and skill levels. Optical motion capture and bespoke instrumentation were used in whole-body tracking during ergometer rowing. Kinetic and kinematic data drove a multibody inverse dynamics model. Joint and muscle force patterns were analyzed to quantify upper extremity influence and create a biofeedback structure for rowers and coaches.

As stroke rate increases, significant changes to the shape and timing of seat force profiles, shoulder joint angle profiles, and lumbar and thoracic spinal flexion, arose. Muscle force patterns highlight the importance of rotator cuff support for load transfer across the glenohumeral joint, with subscapularis and infraspinatus stabilizing the upper extremity before the finish and catch, respectively. Sex and age-related comparisons indicated differential prioritization of scapula stabilizers and prime movers in muscle force distribution. Masters rowers recruit arm accessory muscles but decrease rotator cuff force. Muscle forces impact external movement, joint forces, contact patterns, and shoulder stability, which over many cycles, have implications on performance and injury risk.

Musculoskeletal modelling enhances spatio-temporal analyses, offering population-wide insight into how muscle and joint forces relate to traditional power metrics. Parameters provided deeper context on technique optimization for individual's performance by identifying important muscles and the timing of their loading.

TABLE OF CONTENTS

LIST OF FIGURES

LIST OF TABLES

NOMENCLATURE AND ABBREVIATIONS

α	Alpha angle i.e., flexion-extension inter-segmental angle
β	Beta angle i.e., abduction-adduction, side flexion inter-segmental angle
γ	Gamma angle i.e., internal external rotation, twist inter-segmental angle
A/P	Anterior-posterior
AA	Acromial angle
AC	Acromioclavicular
AI	Inferior angle
AJC	Ankle joint center
ASI	Asymmetry Index
ANOVA	Analysis of variance
CMC	Coefficients of multiple correlation
CoP	Center of pressure
CorEM	Capture latency corrected electromagnetic data
ELB	Elbow
EM	Electromagnetic
EMG	Electromyography
FoB1 – FoB4	Electromagnetic system (Flock of Birds) sensors
GH	Glenohumeral
HF-RoC	Rate of handle force development
HI1	First inflection point in handle velocity
HI2	Second inflection point in handle velocity
HJC	Hip joint center
IDA	Inverse dynamics analysis
IMU	Inertial measurement unit

IQR	Interquartile range
KJC	Knee joint center
L1-L5	Lumbar spinal segments
LASIS	Left anterior superior iliac spine – anatomical landmark
LPSIS	Left posterior superior iliac spine – anatomical landmark
M/L	Medio-lateral
MA	Jugular notch
MFF	Maximum footplate force
MHF	Maximum handle force
MSF	Maximum seat force
MSK	Musculoskeletal
OMC	Optical motion capture
port	Port sweep rowers - athlete group
PR1	Arms-shoulders – para-rowing classification
PR2	Trunk-arms – para-rowing classification
PR3	Leg-trunk-arms – para-rowing classification
RASIS	Right anterior superior iliac spine – anatomical landmark
RMS	Root mean square
RoC	Rate of change
RoM	Range of motion
RPSIS	Right posterior superior iliac spine – anatomical landmark
S/I	Superior-inferior
S1	Sacrum spinal segment
SC	Sternoclavicular
SI1	First inflection of seat trajectory

SI2	Second inflection of seat trajectory
spm	Strokes per minute
SS	Seat suspension
SS-RoC	Seat suspension rate of change
SSR	Shoulder stability ratio
starboard	Starboard sweep rowers - athlete group
ST	Scapulothoracic
std	Standard deviation
ste	Standard error of the mean
T1 - T12	Thoracic spinal segments
TS	Trigonum spinae
UKNSM	United Kingdom National Shoulder Model
X	Laboratory medial-lateral axis
xBW	Times body weight
XI	Xiphoid process – anatomical landmark
Y	Laboratory anterior-posterior axis
Z	Laboratory superior-inferior axis

1. CHAPTER 1: INTRODUCTION

1.1 BACKGROUND AND MOTIVATION

Rowing demands flexibility, coordination, physical power, mental toughness, and cardiovascular endurance. Athletes train for years to reach the highest echelons of the sport and coaches are constantly seeking new ways to achieve higher performances, because in elite competition the margin between winning and losing can be exceedingly small. Outside of elite, competitive circles, growing participation in rowing and ergometer rowing has spurred institutional efforts to further diversify the community by welcoming new members of all ages and ability, and by investing in rowing as an activity for rehabilitation or recreation (British Rowing, 2016; US Rowing, 2018).

To help rowing athletes at any level, training often focuses on improving physiological capacity, primarily in terms of the cardiovascular and musculoskeletal (MSK) systems. The biomechanics involved in entraining good rowing habits plays a major role in performance. Understanding how biomechanical factors affect rowing performance, helps athletes and coaches optimize training (McGregor *et al.*, 2016). Biomechanical assessments have been used to help predict boat velocity and analyze rowing technique, by profiling body kinematics using optical motion capture (OMC), or electromagnetic (EM) systems, and matching them to force and power measured on instrumented ergometers or boats (Hume, 2017). Biomechanics offers a framework within which to describe execution of the rowing movement and accuracy in motion tracking for biomechanical assessments is important in providing accurate feedback to athletes and coaches. Parameters derived from kinematics and force-time profiles offer sports scientists more precise information about rowing dynamics with which may be utilized to guide training, technique optimization, and longitudinal athlete development.

Previously published studies have focused on lower extremity contributions to performance (Buckeridge *et al.*, 2012; Soper, Reid & Hume, 2004) and pathomechanics of injury at the lumbosacral spine (Holt *et al.*, 2003; Bull & McGregor, 2000). Few studies have assessed upper extremity or shoulder contributions to rowing, despite its key role in the rowing kinetic chain. The shoulder provides the largest range of motion (RoM) of any joint in the human body, offering mobility by low congruency of the articulating structures and coupled movement of the scapula, through the scapulohumeral rhythm. Shoulder joint stability is achieved through activation of surrounding musculature and passive ligamentous tissue (Itoi, Morrey & An, 2009). Effective load transfer across the shoulder complex is essential to consistent, high quality rowing performance.

However, anatomically a lack of articular constraint predisposes the shoulder to instability. Age and pathology can decrease the shoulder's stabilization ability. Reviews of injury prevalence among rowers at the junior, senior, and masters levels have shown that shoulder and upper limb injuries account for approximately 7-15% of all reported injuries but represent one of the largest risks of long-lasting overuse injuries (Smoljanović *et al.*, 2018; Smoljanovic *et al.*, 2009, 2015). While the shoulder and upper limb comprise the third most reported musculoskeletal injury sight in rowing, gaps in the literature exist as to the pathomechanics of such injuries. Clinically, these injuries include rotator cuff tendinopathy, anterior instability, stretching of the posterior capsule, and impingement (Thornton *et al.*, 2017a). Quantitative information on the biomechanics of the upper extremity in rowing can have implications for strength and conditioning, yield insights into causes of pain or injury and guide teaching technique to maximize proficiency for athletes at all skill levels.

1.2 THESIS AIMS AND SCOPE

The overarching hypothesis for this work is that the upper extremity has a significant role in rowing performance, rowing technique and propensity for injury. This led to the creation of the following sub-hypotheses, each with specific aims and objectives.

The role of the upper extremity can be quantified during ergometer rowing

- Develop a motion tracking methodology with OMC and ergometer instrumentation to build a biomechanical model of the upper extremity during rowing.
- Adapt the computational multibody dynamics United Kingdom National Shoulder Model (UKNSM) to quantify muscle and joint forces in the upper extremity during ergometer rowing.

The upper extremity contributes to quality of rowing performance and is influenced by posture and lower limb kinematic patterns.

- Demonstrate the use of the selected upper limb motion tracking technology to measure established and accepted performance metrics used by athletes and coaches with respect to the spine and lower extremity, to provide a single motion tracking technology for all rowing biomechanics analyses.
- Identify biomechanical parameters of the upper extremity and spine that impact whole body movement patterns. Interpret these parameters to produce hypotheses on the relationship of shoulder complex mechanics to predicting performance or highlighting potential injury risk during in rowing.

Variation in rowing speed and intensity influence shoulder kinematics and performance.

- Attain external kinetic and kinematic data on different levels of rowing athletes at various rowing intensities using a progressive fatiguing exercise protocol and assess the effects of changing rowing speed and intensity on upper extremity movement patterns.

Shoulder and body kinematics and kinetics differ amongst different groups of rowing athletes.

- Compare and discriminate movement patterns and muscle mechanics across rowing athlete cohorts, grouped by sex, age, experience, and rowing modality. Link variations in internal muscle and joint mechanics to external kinematic changes.

Information about upper extremity biomechanics has the potential to inform performance benefits and predict injury risk.

- Develop and deliver a quantitative feedback structure to athletes and coaches addressing influential parameters identified from computational modelling to enhance interpretation of performance metrics in biomechanical context.

1.3 THESIS STRUCTURE

This thesis is organized into 9 chapters, divided into three core areas – analysis of the literature, primary experimental results, and computational modelling:

Chapter 2: Functional anatomy of the shoulder complex – is described in terms of its relevance within the context of the biomechanics of rowing. Details of foundational concepts in musculoskeletal mechanics used throughout this thesis including anatomical coordinate frames, Euler rotations, and matrix transformations are described.

Chapter 3: Rowing fundamentals and research paradigms – introduces rowing terminology for training, racing, and physiology. A literature review of current research methods in the biomechanics of rowing performance and injury, with a focus on motion analysis technologies, is undertaken. Key publications related to the aims of this thesis are outlined and critically assessed.

Chapter 4: Optical and EM systems in static and dynamic tracking – simultaneously recorded ergometer apparatus and athlete movements during a series of indoor rowing trials using the selected OMC system and an EM tracking system. Data were compared statistically across systems for accuracy and precision.

Chapter 5: Dynamic tracking and spatio-temporal analysis in ergometer rowing – describes the materials and methods utilized for OMC during indoor rowing on an instrumented ergometer. Results from ergometer derived kinetics are discussed in relation to performance metrics; their sequence and timing assessed relative to critical stroke events.

Chapter 6: Fatigue leads to altered kinematics during high performance ergometer rowing – assesses form differences across athletes using relative motion between body segments throughout the stroke cycle and relative to critical stroke events. The influence of sagittal, transverse, and frontal plane rotations on force output and declining postural control with time, intensity and speed are discussed. Links between the movement patterns in the spine and the shoulder girdle are proposed.

Chapter 7: Modelling scapular biomechanics to enhance interpretation of performance data in rowing – introduces the computational modelling tools used for biomechanical analysis in this thesis and evaluates comprehensive musculoskeletal analysis of the shoulder complex during ergometer rowing in an adult population of competitive rowers. Joint and muscle forces are compared across a range of stroke rates and athlete sub-populations.

Chapter 8: Enhancing athlete feedback with biomechanics – utilized a case study athlete to illustrate the utility of quantifying subject specific biomechanical parameters during performance evaluation by creating a feedback structure for coaches and athletes, which may form a foundation from which to recommend means to improve an individual's performance.

Chapter 9: Conclusions and future directions – summarizes the important findings and implications of the research in this thesis. Limitations are discussed and potential directions for future rowing research are highlighted.

2. CHAPTER 2: FUNCTIONAL ANATOMY OF THE SHOULDER COMPLEX

Rowing is a cyclical, closed kinetic chain movement involving motion at every joint in the body. The drive phase of the rowing stroke, in which boat propulsion is created, requires the transfer of torque and force from the foot through the ankle, knee, and hip to the spine, and from the hands and wrist through to the elbow. The shoulder, as the most mobile joint in the body, sits at the intersection of these. This chapter reviews the functional anatomy of the shoulder in the context of rowing.

2.1 THE SHOULDER IN ROWING

Large, superficial back and shoulder muscles contribute to force production in the drive phase of the rowing stroke (Soper & Hume, 2004). Latissimus dorsi and trapezius extend and adduct the shoulder. Pectoralis major, latissimus, and subscapularis also internally rotate the upper arm (see Itoi, Morrey & An, 2009). During the drive phase serratus anterior and trapezius move the scapula from a protracted and anterior tilted position at the catch to a retracted position into the finish. Through the finish, the scapula is rotated downward by pectoralis minor (Mazzone, 1988) and on the recovery, triceps brachii extend the elbows until full extension. Moving into the catch, deltoid, coracobrachialis, and biceps contract, raising the arms (Mazzone, 1988).

The scapula is pivotal in proximal to distal sequencing of the kinetic chain - transferring large forces from the legs and trunk, through the kinematic chain, to accelerate the hands and oar handle. This is accomplished most efficiently when the shoulder acts as a stable platform (Ben Kibler, 1998). But common technical faults, such as “taking the catch with the shoulders” instead of first engaging the leg drive, and hyperextension of the upper limb in an effort to increase effective stroke length, can negatively affect horizontal force generation or pulling of the oar to the body (Bull & McGregor, 2000; Paine & Voight, 1993). Exaggerated GH RoM can produce insufficient scapular stabilization, create muscle force imbalances at the GH joint (Bey *et al.*, 2010), and alter contact patterns between the humeral head and glenoid socket, resulting in high shear forces (Ben Kibler, 1998).

2.2 FUNCTIONAL ANATOMY OF THE SHOULDER

To understand which biomechanical factors play significant roles during rowing requires an understanding of how rowing kinematics are predicted by shoulder anatomy. The shoulder joint has one of the highest degrees of complexity in the human body, accommodating a large RoM but leaving it

susceptible to instability and injury. Shoulder mobility is derived from the combination of three bones (humerus, scapula, and clavicle) articulating at four joints (see Jobe, Phipatanakul & Coen, 2009).

Motion of the human body or body segments is described in relation to three anatomical planes: sagittal, frontal, and transverse (Figure 2.1). Clinical terminology describes movement of the upper limbs in rotational and translation directions. Proximal / distal refer to the relative position of body segments in relation to distance away from the torso, with distal referring to the farther segment. Motions of the upper limb relative to any proximal segment can be defined in clinical terms (Figure 2.2). Abduction/adduction used to describe the relative rotation between proximal and distal segments in the frontal plane. Flexion/extension is the relative rotation between proximal and distal segments in the sagittal plane; and internal/external rotation refers to rotations about the proximal segment longitudinal axis (Figure 2.2). Descriptions of clavicle, humerus, forearm, and scapula rotations relative to the thorax can be similarly described (Figure 2.2). When considering complex movements of the upper limbs, large abduction angles are made possible by humeral elevation combined with upward rotation of the scapula. This rotational assistance is referred to as a scapula-humeral rhythm and thus is it useful to describe humeral joint angles relative to the scapula anatomical frame.

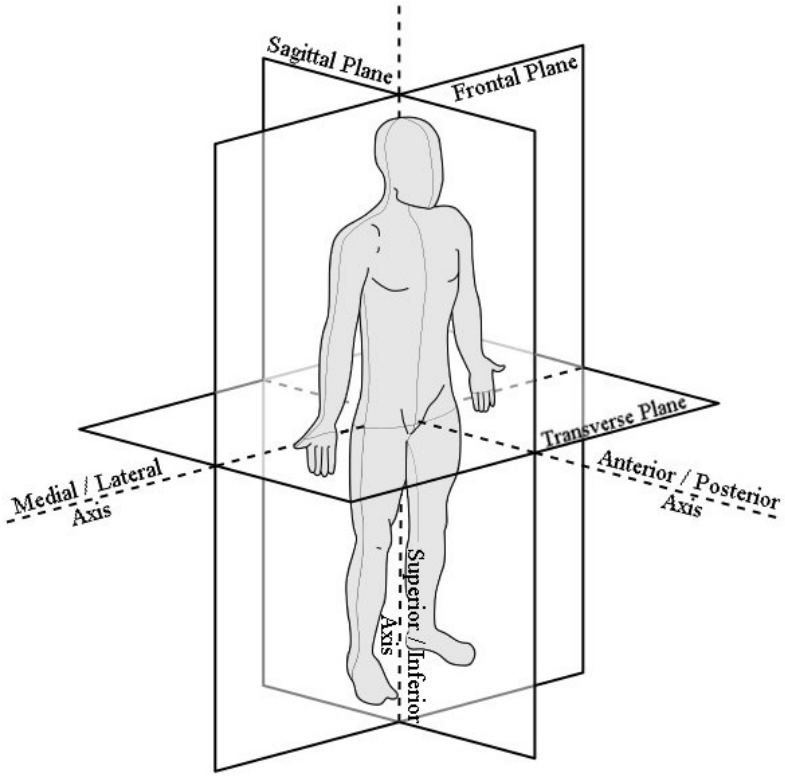

Figure 2.1: Anatomical planes and axes used to describe the human body (Adapted from CFCF, 2014).

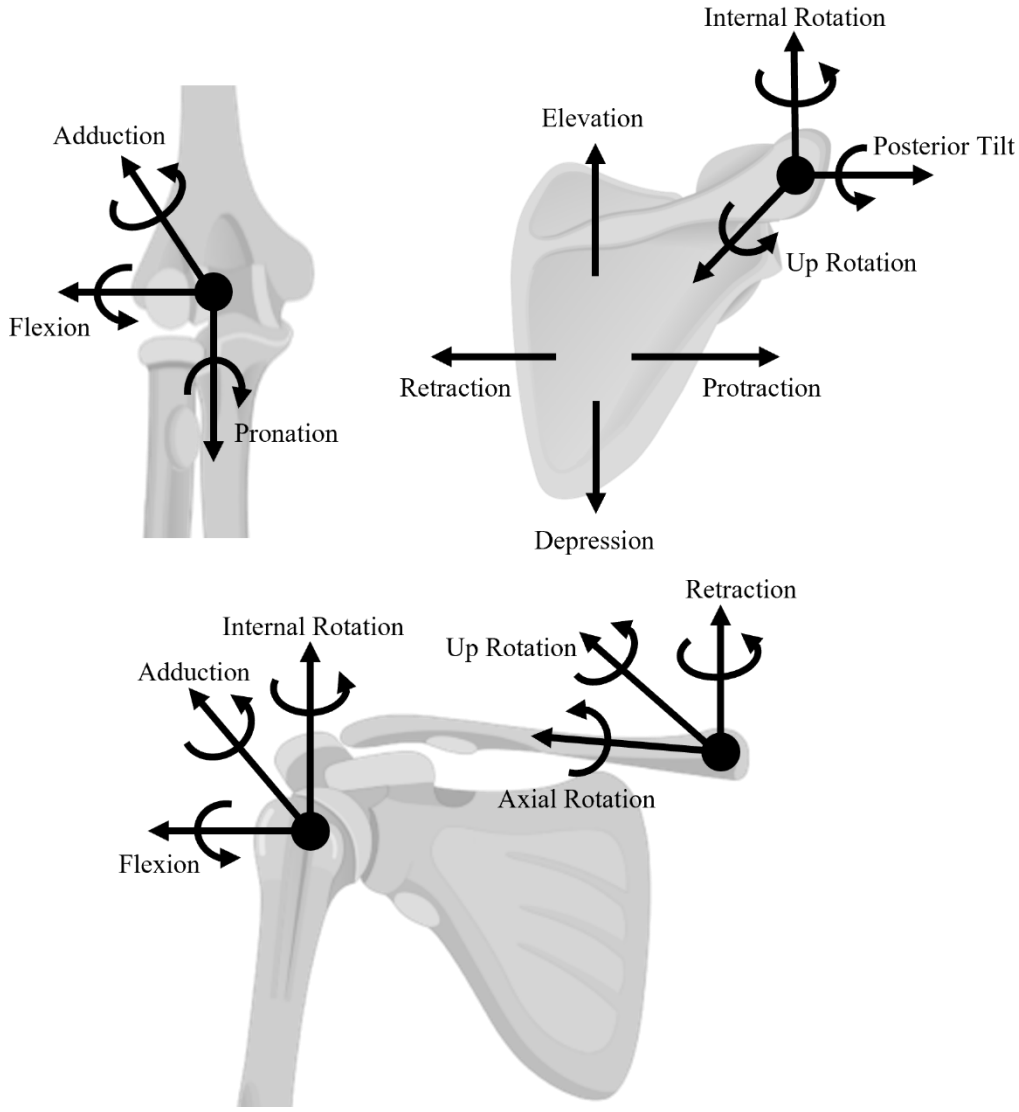

Figure 2.2: Schematic axes and anatomical descriptions of positive joint rotations used for a right arm, at the elbow (*top-left, anterior view*), scapula (*top-right, posterior view*), clavicle (*bottom-right, anterior view*), and humerus (*bottom-left, anterior view*). Adapted from (Charlton, 2003; Prinold, 2012; Get Body Smart, 2021)

2.2.1 Anatomical Structures of the Shoulder Complex

The shoulder complex comprises the clavicle, scapula, and humerus (Figure 2.3). Due to the synergistic movements of these bones, the shoulder can generate the largest RoM of any joint in the human body. In rowing, the range of shoulder motion occurs mostly at low humeral elevation (< 90º) but may involve an extreme range of scapula protraction/retraction and scapular internal/external rotation (Figure 2.2). The mobility in the shoulder complex is provided by four articulating structures (Jobe, Phipatanakul & Coen, 2009): the sternoclavicular (SC) joint, acromioclavicular (AC) joint, GH joint and the scapulothoracic (ST) joint. The first three are diarthrodial articulations, constructed with little bony

congruence and relying mainly on passive and active stabilizing mechanisms including surrounding ligaments and muscles. Motion of the ST articulation is determined mainly by the opposing surfaces of the ribcage and scapula. About one third of the total elevation takes place in this part of the shoulder; the remainder occurs in the GH joint. The ratio of GH-to-ST motion in scapular plane abduction is about 2:1 (see Itoi, Morrey & An, 2009). All anatomical and functional structures of the shoulder complex are briefly discussed below.

2.2.1.1 Osseous Anatomy

The **clavicle** links the axial skeleton to the appendicular skeleton (Figure 2.3). It extends between the SC joint at the medial end and the AC joint at the lateral end, and it acts as a strut around which the shoulder complex rotates in the frontal plane (Kibler & Sciascia, 2010). Three ligaments that help constrain movement of the clavicle are the costoclavicular ligament at the proximal end, the conoid ligament and trapezoid ligament at the distal end. The clavicle is important in supporting axial loads, particularly when humerothoracic (HT) muscles such as pectoralis major and latissimus dorsi are active (van der Helm & Pronk, 1994). In rowing, the clavicle provides torsional stability to the shoulder complex during glenohumeral forward flexion and adduction at the catch.

The **humerus** is the largest long bone in the upper limb. The proximal end comprises a hemispherical articular surface called the humeral head, which articulates with the glenoid fossa of the scapula (Terry & Chopp, 2000), while the distal end articulates at the elbow joint with the ulna and radius (Figure 2.3). There are twelve muscles that attach along the length of the humerus, including the latissimus dorsi, teres major, deltoid, pectoralis major, and the rotator cuff muscles. Important bony features include the greater and lesser tuberosities, medial and lateral epicondyles, and the bicipital groove, through which the long head of the biceps passes (Jobe, Phipatanakul & Coen, 2009).

The **scapula** is a large, flat, bony structure located on the posterolateral, superior region of the torso (Figure 2.3). The scapula plays a vital role in shoulder movement and stability, contributing to generating long stroke lengths in rowing through large RoM in protraction & retraction (Figure 2.2). The scapula comprises no bony attachments to the torso, instead, being wrapped within many layers of connective tissue, it moves relative to the torso along the scapulothoracic gliding plane. Several prominent bony features of the scapula, including the acromion, scapular spine, and coracoid process, host attachment sites for eighteen different ST muscles. These muscles can leverage the triangular shape of the scapula to gain large moment arms around the SC and AC joints (Veeger & van der Helm, 2007). This is important for distributed load transfer across the shoulder complex during the *drive phase.*

The scapular spine, running horizontally along the posterior side of the scapula, divides the surface into the upper supraspinatus fossa and the lower infraspinatus fossa. The acromion is located at the antero-lateral, superior corner of the scapula. It forms one half of the AC joint and is positioned over the top of the GH joint, under which the rotator cuff muscles pass (Jobe, Phipatanakul & Coen, 2009). This subacromial space between the acromion and the rotator cuff muscles is small and this area is a common site of injury and inflammation (Ben Kibler, 1998; Ludewig & Cook, 2000). Lastly, the glenoid fossa is the lateral articulating surface of the scapula at the GH joint. This shallow cavity, and its relatively low conformity to the opposing humeral head articulating surface, contributes to producing the large RoM in the shoulder complex.

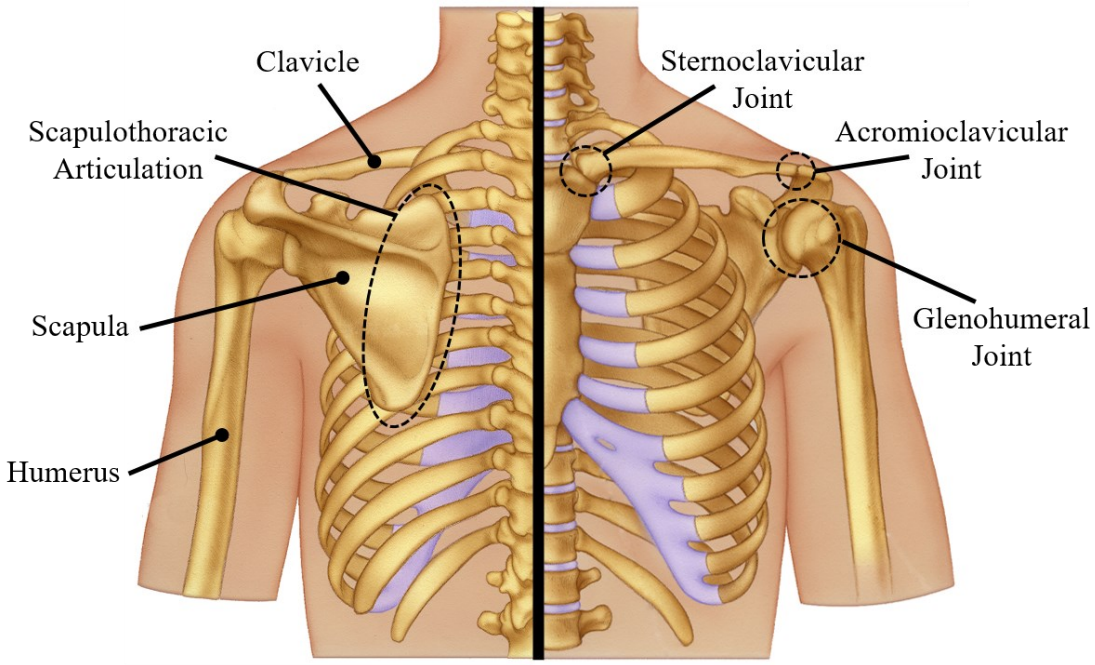

Figure 2.3: Articulating structures (bones and joints) comprising the shoulder complex. (Adapted with permission from Medical Art Library, 2017a, 2017b).

2.2.1.2 Functional Anatomy

The **sternoclavicular joint** is a synovial saddle joint composed of the superior portion of the sternum (manubrium) and the proximal end of the clavicle and is the only skeletal articulation between the upper limb and the axial skeleton (Figure 2.3). The joint surfaces are covered with hyaline cartilage, since they are relatively flat bony interfaces, they rely on surrounding ligamentous structures to provide stability to the joint. The SC joint allows for movement of the clavicle in three planes: retraction, up/down rotation, and axial rotation (Figure 2.2).

The **acromioclavicular joint** is a synovial gliding joint that joins the acromion process of the scapula with the lateral end of the clavicle (Figure 2.3). The joint is stabilized by several ligaments: conoid, trapezoid, coracoacromial, and AC. These ligaments reduce translation, shearing, and axial rotation of the clavicle at its lateral end. The AC joint functions as a strut to help with movement of the scapula and providing a greater degree of rotation to raise the arm above the head.

The **scapulothoracic joint** is the connection between the anterior surface of the scapula and the posterior chest wall (Figure 2.3; van der Helm & Pronk, 1994). Muscles wrapping the anterior and posterior of the scapula form multiple layers separated by bursa and connective tissue, which facilitate the gliding movement of the scapula across and around the rib cage (Terry & Chopp, 2000). Primary transitory motions at the ST articulation include elevation/depression, protraction / retraction, and upward/downward rotation (Figure 2.2), which add range to elevation of the arm and provide a dynamic stabilizing base for the controlled shoulder complex movements.

The **glenohumeral joint** is a synovial ball-and-socket joint formed by the articulation of the humeral head on the scapular glenoid (Figure 2.3). Two thirds of the total shoulder complex elevation occur at the GH joint, and it is predominately responsible for the large RoM in humeral flexion/extension, internal/external rotation, and abduction/adduction (Figure 2.2). While this joint is the most mobile in the human body, it is also the least stable. This high degree of freedom is achieved by two anatomical features: (1) the shallow socket of the glenoid, while made deeper by the addition of the glenoid labrum to the circumference of the fossa, is less than half the surface area of the humeral head; and (2) the opposing surfaces of the joint are incongruent, with a radius of curvature mismatch approximately 3mm greater in the glenoid surface (Iannotti *et al.*, 1992). The low simultaneous surface contact and the bony incongruence allows for a large RoM without articular impingement and for small translations of the humeral head across the glenoid fossa (Soslowsky *et al.*, 1992; Zumstein *et al.*, 2014; Bey *et al.*, 2010; Dal Maso *et al.*, 2014; Kedgley *et al.*, 2008).

Stability of the joint is provided by passive structures including the articular capsule, glenohumeral ligaments and the glenoid labrum which deepens concavity of the glenoid, as well as active rotator cuff muscles that originate from the scapula and wrap around the joint inserting near the humeral head. The rotator cuff muscles increase stability of the GH joint through concavity-compression (Itoi, Morrey & An, 2009)

2.3 SHOULDER JOINT STABILITY

Joint stability is the sum of a joint's bony congruence, the passive tension in the ligaments, and the dynamic compressive stability provided by adjacent muscles. The large mobility of the GH joint comes at

the expense of joint stability. The shoulder stability ratio (SSR) is defined by the proportion of force necessary to dislocate the humeral head from the glenoid socket to the force compressing the humeral head against the glenoid socket and is determined in part by morphology of the articulating surfaces (Lippitt *et al.*, 1993). The articulating geometry of the shallow glenoid fossa and the large humeral head means that bony congruence contributes little to stability. Thus, stability of the GH joint is produced predominately by interactions of active and passive stabilizers.

2.3.1 Passive Joint Stabilizers

Passive stabilization of the GH joint is provided by the capsuloligamentous complex, comprising the glenoid labrum, joint capsule, and glenohumeral ligaments (Itoi, Morrey & An, 2009). The GH joint capsule is a comparatively loose anatomical structure, reinforced by the glenohumeral ligaments. While the passive joint stabilizers are not the focus of this thesis, a brief description of their function is included for completeness.

The capsuloligamentous soft tissue constraints function in coordinated load sharing to resist joint translation, by contributing passive tension in the end ranges of motion yielding joint contact forces opposite the direction of displacement. The shoulder joint capsule along with the three glenohumeral ligaments (anterior, posterior, and inferior) resist joint distraction forces, increase joint compression, and create negative intraarticular pressure (Wilk, Arrigo & Andrews, 1997), contributing to GH joint stability.

The glenoid labrum is a circumferential fibro-cartilaginous structure attached to the rim of the glenoid fossa, contributing to GH stability by increasing the glenoid socket depth, and decreasing likelihood of humeral head dislocation (Matsen *et al.*, 2009). The magnitude of this contribution fluctuates based on anatomical variance and applied muscle compressive forces, with higher compressive joint loads and a deeper glenoid increasing resistance to humeral head translation. The labrum contributes about 10% to glenohumeral stability and damage to the labrum reduces joint stability predominately in the middle of the RoM, when capsuloligamentous structures are lax (Halder *et al.*, 2001).

2.3.2 Active Joint Stabilizers

In addition to passive muscle tension, active stabilization of the GH joint is provided by dynamic muscle contraction, and concavity compression. Concavity-compression refers to the pressure generated when the convex humeral head is compressed into the glenoid-labral socket through contraction of muscles surrounding the shoulder. Increasing compressive load enhances stabilization but the magnitude of this benefit varies around the circumference of the glenoid. In normal shoulders, the SSR is 45-60% in the superior-to-inferior direction and 30-36% in the anterior-to-posterior direction (Klemt *et al.*, 2017). These

differences may be attributed to labrum / glenoid depth and muscle moment arms (Klemt *et al.*, 2017; Halder *et al.*, 2001).

The muscles providing compression are the rotator cuff muscles comprising: subscapularis, supraspinatus, infraspinatus and teres minor (Figure 2.4; Itoi, Morrey & An, 2009). These muscles are able to effectively apply compressive forces to the joint and are well positioned to provide co-contraction to counteract externally produced shear forces, directing resultant GH joint force vectors into the glenoid fossa to stabilize the joint (Veeger & van der Helm, 2007). This mechanism of dynamic positioning of the humeral head so joint reaction force remains within the glenoid fossa is referred to as scapulohumeral balance (Halder *et al.*, 2001). A more detailed overview of the relevant upper limb musculature is presented in Section 2.4.

2.4 UPPER LIMB MUSCULATURE

The upper limb muscles can be divided into several important groups based on the joints over which they cross, or by their function. These are the rotator cuff, scapula stabilizers, prime movers, and arm accessory group.

2.4.1 Rotator Cuff Muscles

The four most important muscles of the GH joint are collectively known as the rotator cuff muscles: subscapularis, supraspinatus, infraspinatus, and teres minor (Figure 2.4). They are the deepest shoulder muscle layer, arising from origins on the scapula and are arranged to wrap around and insert on the humeral head, allowing them to have advantageous lines of action for increasing glenoid compression and decreasing humeral head translations (Veeger & van der Helm, 2007). The primary function of the rotator cuff is to provide dynamic stability during upper extremity movements, and they are often recruited as a group to keep the humeral head centralized within the glenoid fossa. In addition to GH stability, supraspinatus assists in abduction, subscapularis adducts and internally rotates the shoulder, in opposition to infraspinatus and teres minor, which externally rotate and adduct the shoulder (Jobe, Phipatanakul & Coen, 2009).

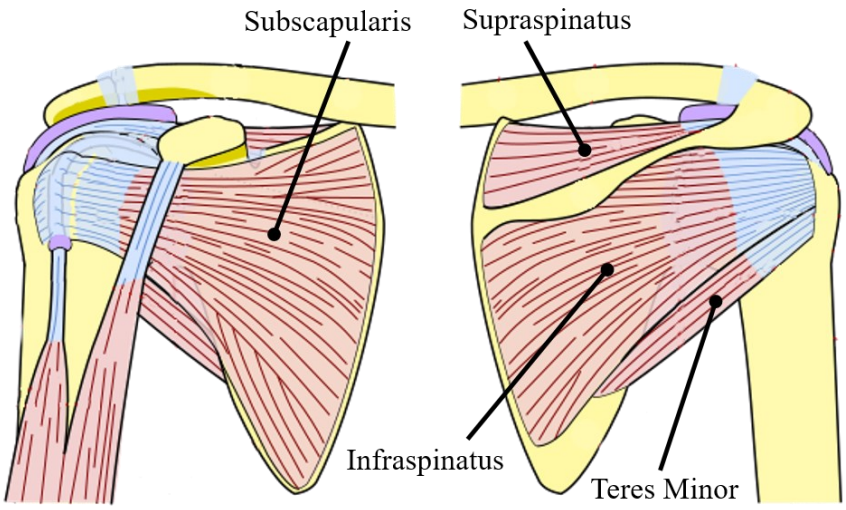

Figure 2.4: Anterior (*left*) and posterior view (*right*) of the rotator cuff musculature (Adapted from National Institute of Arthritis and Musculoskeletal and Skin Diseases (NIAMS)).

2.4.2 Scapula Stabilizers

The main stabilizers of the scapula are trapezius, serratus anterior, the rhomboids, and levator scapulae (Figure 2.5). Serratus anterior has its multiple origins on the lateral side of the first eight ribs and converges to insert on the medial border and inferior angle (AI) of the scapula. Its primary role is to stabilize the scapula during arm elevation and to protract the scapula forward and around the thoracic rib cage (Jobe, Phipatanakul & Coen, 2009). Trapezius is a very broad muscle, arising along the spine from C1 to T12 vertebrae, with insertions covering the superior scapula spine, acromion, and lateral part of the clavicle. Given the large distribution of trapezius across the back, its action is complex, and typically discussed in terms of smaller segments within the muscle. These functions include upward rotation and elevation for the upper trapezius fibers, retraction for the middle trapezius, and depression for the lower trapezius (Jobe, Phipatanakul & Coen, 2009). Rhomboid major and rhomboid minor form a sheet of muscle originating between the C7 and T5 vertebrae and inserting onto the medial border of the scapula. These muscles function to stabilize the medial border of the scapula and are very active in scapula depression and retraction (Jobe, Phipatanakul & Coen, 2009). Levator scapulae originates between the C1 and C4 vertebrae, with insertion along the medial border of the scapula. It functions to elevate the scapula and tilt the glenoid cavity inferiorly by rotating the scapula downward (Jobe, Phipatanakul & Coen, 2009).

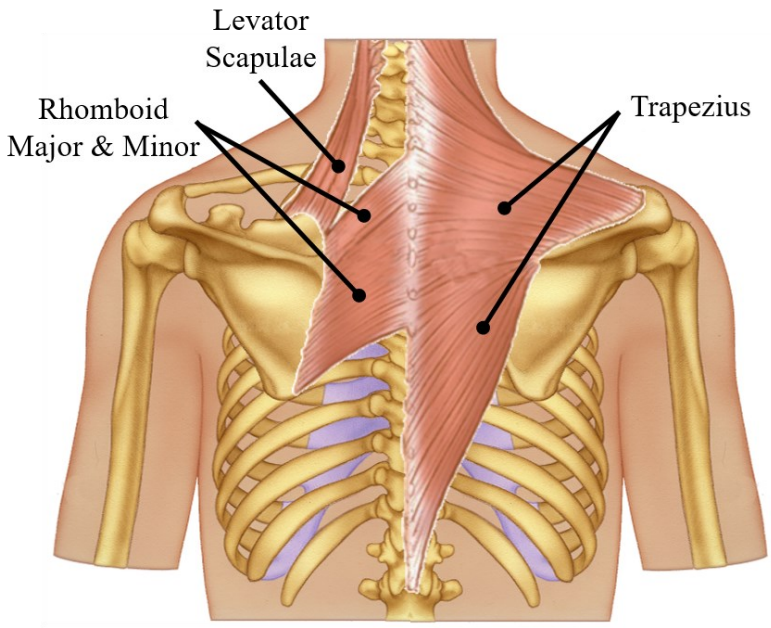

Figure 2.5: Musculature of the scapular stabilizer group (Adapted with permission from Medical Art Library, 2017a, 2017b).

2.4.3 Prime Movers / Humeral Depressors

The main muscles that produce movement of the upper limb are the deltoid, latissimus dorsi, pectoralis major and teres major (Figure 2.6). Pectoralis major originates from the clavicle and the sternum and inserts into the humerus. This muscle is a strong internal rotator and horizontal abductor of the humerus. The muscle also acts to adduct the arm in the frontal plane, whilst flexing the arm in the sagittal plane (Ackland *et al.*, 2008). Latissimus dorsi has a very broad origin – arising along the spine from the T7 vertebra to the pelvis and inserting into the intertubercular groove of the humerus. The muscle depresses and internally rotates the humerus and retracts the shoulder girdle. Teres major originates from the scapula and inserts into the humerus, alongside the insertion of latissimus dorsi. Like its neighbor, teres major can depress and internally rotate the humerus. Teres major can also act to upwardly rotate the scapula (Ackland *et al.*, 2008). Deltoid overlies the shoulder superficially and has three origins: the clavicle, the scapular spine, and the acromion, and has a singular insertion on the deltoid tuberosity of the humerus. Generally, deltoid functions to abduct the arm at the glenohumeral joint, but fibers in the anterior portion of the muscle also flex and medially rotate the humerus, while fibers in the posterior deltoid can extend and externally rotate the humerus (Itoi, Morrey & An, 2009).

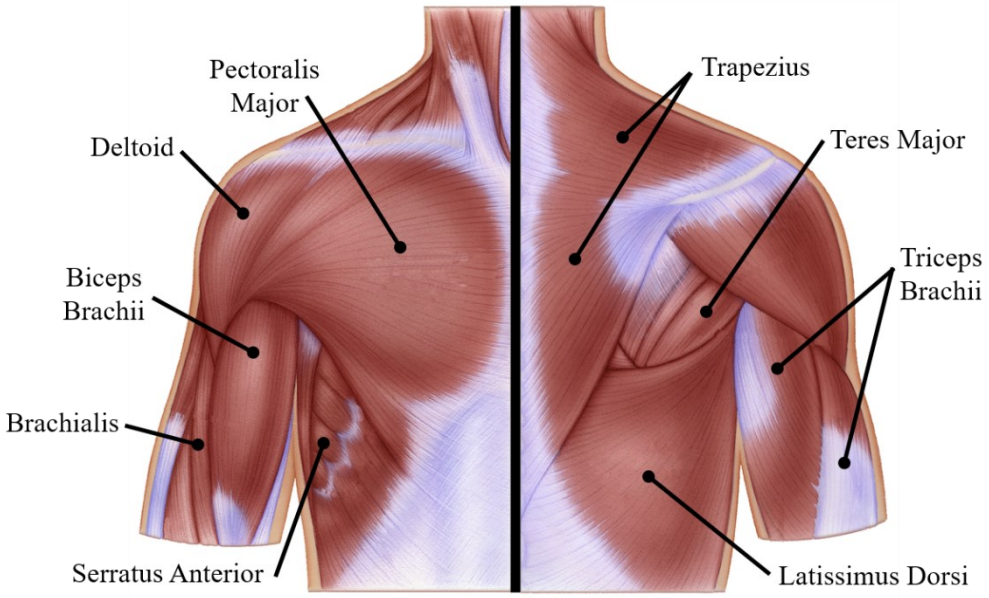

Figure 2.6: Superficial anterior (*left*) and posterior (*right*) musculature of the shoulder complex. (Adapted with permission from Medical Art Library, 2017a, 2017b).

2.4.4 Arm Accessory Muscles

This accessory group includes biceps brachii, triceps brachii, brachialis, and coracobrachialis, where biceps and triceps cross both the elbow and shoulder while brachialis acts only at the elbow joint, and coracobrachialis acts only at the shoulder (Figure 2.6). Biceps brachii has a short head and long head, the former originating from the coracoid process of the scapula and the latter originating on the supraglenoid tubercle and passing through the bicipital groove. Tendons from both heads insert on the proximal end of the radius. The biceps' primary function is flexion of the elbow and supination of the forearm. It also assists in shoulder elevation and stabilization (Itoi, Morrey & An, 2009). The long head of biceps tendon additionally 'tethers' the labrum, increasing its stabilizing effect when the biceps are activated (Klemt *et al.*, 2017). Triceps brachii has three heads: medial, lateral, and long head. The long head originates from the infra-glenoid tubercle of the scapula, while the medial and lateral heads arise from the proximal, posterior humerus. All three heads merge into the triceps common tendon which inserts on the olecranon process of the ulna. Triceps brachii predominately acts as an elbow extensor with the long head having a small role in shoulder extension (Ackland *et al.*, 2008). Brachialis originates on the distal aspect of the humerus and inserts into the coronoid process of the ulna. This muscle is a primary flexor of the elbow (Ackland & Pandy, 2009). Coracobrachialis originates from the coracoid process of the scapula and inserts

onto the medial shaft of the humerus. At the glenohumeral joint, coracobrachialis flexes and adducts the humerus, assists in internal rotation and shoulder stabilization (Ackland *et al.*, 2008).

2.5 CONCLUDING REMARKS

The muscles, joints, and ligaments of the shoulder complex are well constructed to provide extensive mobility while withstanding the loading associated with everyday activities and athletic endeavors. The rowing kinetic chain requires coordinated mechanics of all the body segments to produce a stable, effective, and efficient rowing movement. This is achieved by large, superficial upper limb muscles contributing to force production in the drive phase (Soper & Hume, 2004), while the scapula and rotator cuff are pivotal in transferring power from the legs, through the kinetic chain, and out to the hands. The high mobility provided by low congruency in the articulating structures make the shoulder joint comparatively unstable. Shoulder stability is load dependent, with increased joint forces leading to a proportional decrease in stability. In rowing, repetitive loading coupled with poor or deteriorating technique can lead to acute and chronic injuries. To further understand the mechanics which lead to shoulder injuries in rowers, it is necessary to review literature which examines kinematics, loading and muscle activity in this group.

This chapter introduced the musculoskeletal anatomy of the shoulder complex and upper limb, with some perspective on the importance of the shoulder in rowing. The following chapter contains an introduction to the fundamentals of rowing and a literature review of rowing biomechanics research on athlete kinematics and performance measures, with a focus on studies examining the upper body and shoulder complex. It will set the background and objectives for the experimental work undertaken in this thesis and help place this work in the context of the wider literature, to highlight its relevance and novelty within the broader scope of rowing biomechanics research.

3. CHAPTER 3: ROWING FUNDAMENTALS & RESEARCH PARADIGMS

3.1 THE TECHNICAL BASICS

The fundamental basis of rowing is a repetitive action called 'the stroke'. The stroke is a cyclical, closed kinetic chain movement, where the rower's feet are constrained in shoes fixed to the shell (i.e., the boat), and the rowers' hands remain at the oar handle. While the stroke is a continuous, fluid, movement, it is typically described in four distinct parts: *catch, drive, finish,* and *recovery* (Figure 3.1). The drive and recovery are kinetic phases where the handle travels in essentially a horizontal line, with the catch and finish acting as transition points. Propulsive force is generated in the drive phase, which commences at the catch. After the blade enters the water, the athlete works to extend the lower limbs, with a stable trunk and arms extended forwards (Pollock *et al.*, 2009). In mid-to-late drive phase, after full extension of the legs, the athlete rotates the trunk posteriorly and draws the arms into the body to reach the finish, where the blade exits the water. Transitioning out of the finish, the recovery phase reverses the overall athlete motion, in preparation for the next stroke. The athlete first extends the arms, flexes the trunk anteriorly, then compresses the legs back up and into the catch (Nilsen, Daigneault & Smith, 2002a), in order to start another working drive phase.

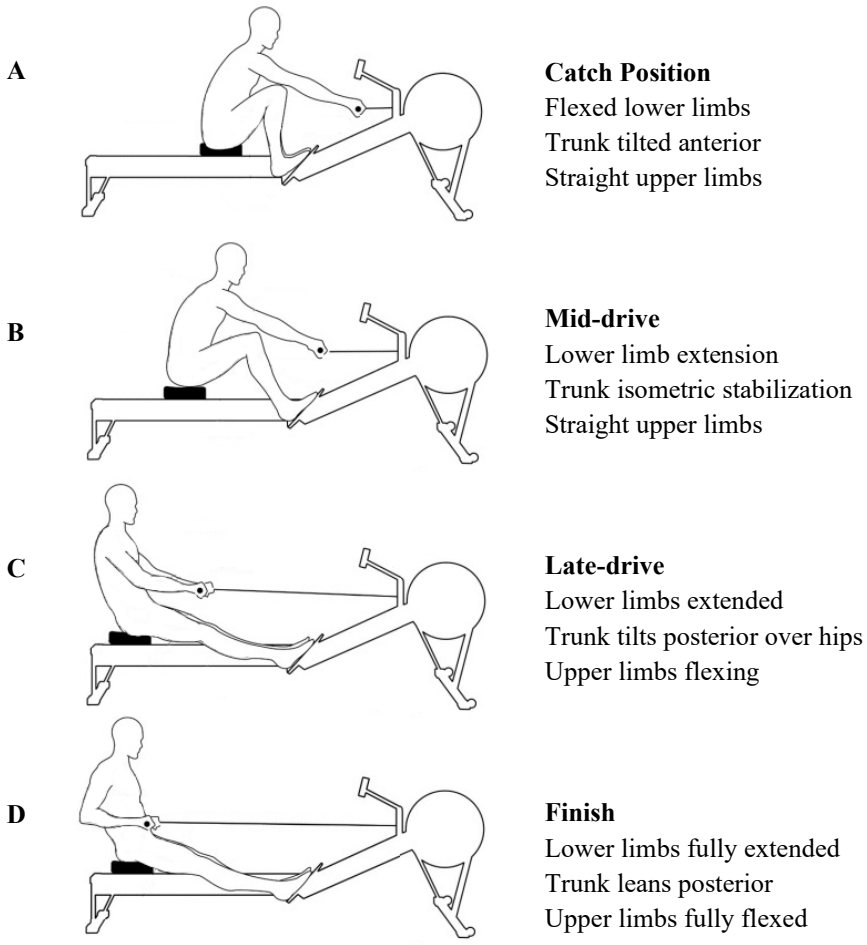

Figure 3.1: Proper ergometer rowing technique [Adapted from Concept 2 (2006)]. The drive phase (B-C) of the rowing stroke sequence is initiated at the catch (A)and is concluded at the finish (D). The recovery phase is initiated at the finish position and concludes at the catch position of the next stroke (D-A).

There are two technical classifications or modalities in on-water rowing – sweeping and sculling – which have different associated movement patterns and load distributions. Sculling uses two oars per athlete, one extending to either side of the shell (Figure 3.2). Crew size (i.e., the number of rowers in the boat) in sculling events include the single (1x), double (2x), and the quadruple (4x). The rower's mass remains centered, and motion is predominately limited to sagittal flexion/extension with minimal thoracic rotation or bending. In contrast, sweep rowing uses one oar per person, which extends out to either the athlete's right side known as stroke side (port) or their left side, bow side (starboard). Crew size in sweep events include pairs (2-), fours (4 +/- with or without coxswain), and eights (8+). Athlete movement patterns are asymmetric, and generally follow the blade's line of action through the water. This results in thoracic rotation with some lateral bending toward the oar side at the catch, and a counter rotation at the finish.

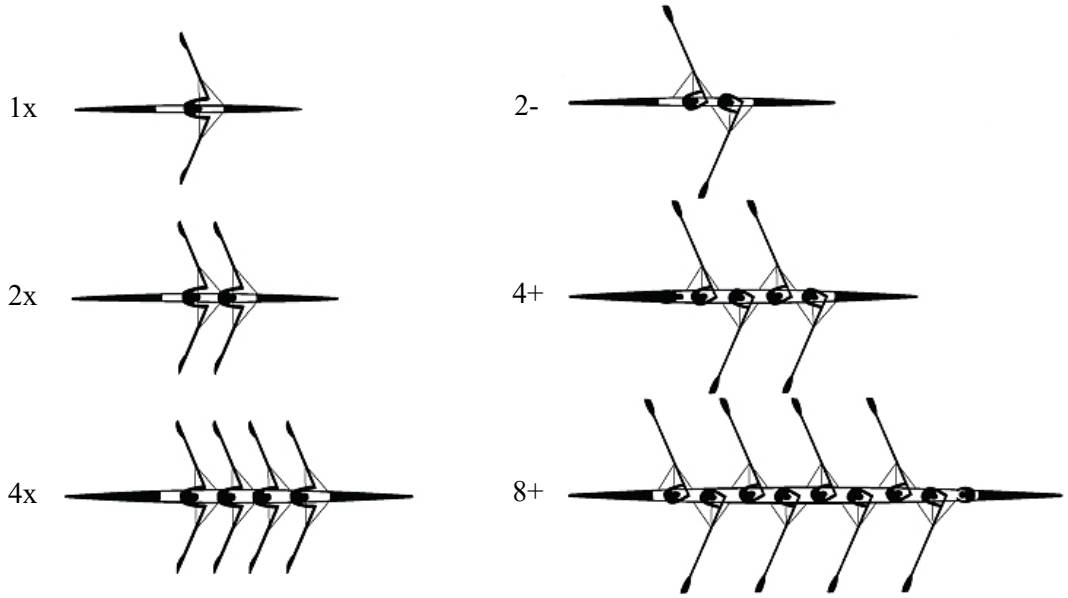

Figure 3.2: Common boat classes in sculling (*left*) and sweeping (*right*). (x) indicates a sculling boat; (-) indicates omission of a coxswain; (+) indicates inclusion of a coxswain

3.1.1 Water and Land Training

The amount of time spent in the boat is greatest during the spring and summer, but adverse weather reduces time on the water. To circumvent a loss in fitness, "land training" typically includes weight training and rowing ergometer work aimed at increasing aerobic and anaerobic endurance (Table 3.1). Ergometers are machines built to simulate the rowing motion where athletes pull a handle connected to a flywheel to generate resistance. Ergometer rowing is a cyclic movement in which the subject pulls a handle that is connected to the flywheel that generates the rowing resistance. The rowing cycle is formed by the rower sliding back and forth along a monorail.

The well documented relationship between ergometer rowing improvement and on-water progress makes them popular in teaching, training, and testing. Examining 2000 m ergometer times of elite rowers found strongly positive correlations with world championship rankings (Mikulić *et al.*, 2009). Consequently, ergometers are an effective measure of rowing performance, often used to assist crew selections as well as physiological testing in a controlled environment, thus avoiding the confounding effects seen with on-water testing.

This also makes the ergometer an important instrument for examining movement, allowing sports scientists to derive more precise information from system kinematics and force-time profiles. There are several different types of rowing ergometers, the most popular of which (for both rowers and non-rowers) is the air-braked stationary ergometer from Concept 2 (Concept 2, Vermont, USA) (Fleming, Donne &

Mahony, 2014; Kleshnev, 2005). However dynamic ergometers, such as the Row Perfect 3 (RP3 Rowing Ltd, Haaksbergen, Netherlands), have been designed to simulate the force transfer of on-water rowing more accurately (Fleming, Donne & Mahony, 2014; Jones *et al.*, 2010).

3.1.1.1 Stationary vs. Dynamic Ergometers

On a conventional stationary ergometer, the position of the foot stretcher and flywheel are fixed. The rower pushes against the fixed stretcher/flywheel, moving away from it during the drive and toward it during the recovery. This means that the rower's center of mass is translated along the central monorail during the stroke cycle.

Dynamic ergometers comprise a free-floating stretcher mechanism which also slides along the central monorail. The free mechanism includes the stretcher and the flywheel, which is pushed forward by the rower during the drive phase and pulled back during the recovery. Although the seat can slide freely, when used by a skilled rower, seat translation (and by extension, the rower's center of mass) should remain minimal during the stroke cycle.

Comparing dynamic to stationary ergometers, force profiles and stroke rates on dynamic ergometers are more in line with on-water rowing than those of static ergometers. Researchers observed decreased peak handle force, rate of force development, impulse, and drive:recovery ratio on the dynamic ergometer (Benson *et al.* 2011, Jones et al. 2010). In contrast, percent time to peak force and stroke rate increased during dynamic ergometry. Greene *et al.* (2013) also observed a faster increase in handle force and leg speed on dynamic ergometers compared to stationary ergometers and attributed these increases to differences in inertial effects at the beginning of the drive phase. It is also worth noting that not all static ergometers are created equal. Air-braked ergometers are the most common for team training (Concept 2; Nordic Track), but there are also variants that utilize magnetic resistance (Schwinn; JOROTO), and water resistance (Water Rower; Merax). Each has advantages and disadvantages, but few papers have performed side-by-side biomechanical assessments. An exception is Steer, McGregor & Bull, (2006) who compared lumbopelvic kinematics between Concept 2 and Water Rower ergometers.

3.2 PHYSIOLOGY OF ROWING

Olympic rowing sprint distance is 2000 meters. This distance can be covered in approximately 6-8 minutes, depending on the boat class/crew size. Rowing is classified as a strength-endurance sport, wherein performance requires not only explosive power but also a high level of aerobic fitness. The energy pathways utilized to complete a rowing race are approximately 75% aerobic capacity and 25% anaerobic capacity (Ingham *et al.*, 2002). A standard 2000 m race may be divided into 3 phases: the start, the body, and the sprint. The start and sprint phases involve a high stroke rate, in anaerobic metabolic zones, resulting in

accumulation of lactic acid and acute muscle pain (Maciejewski *et al.*, 2013). The body of the race sees the stroke rate lower and the athlete moves to an aerobic threshold metabolic pace for 4-6 minutes (Nilsen, Daigneault & Smith, 2002c). Historically speaking the largest driving forces behind athlete ranking and crew selection have been individual anthropometrics and cardiovascular fitness (Hagerman, 1984). A large number of research studies and continual monitoring of elite rowing populations concur that height, mass, and VO2 max are all highly correlated to 2000 m time (Volianitis & Secher, 2009; Mickelson & Hagerman, 1982). Consequently, athlete training programs cover various intensities of rowing (Table 3.1).

Table 3.1: Standard metabolic training zones in rowing with approximate stroke rates and expected relative metabolic effort for which each zone may be achieved.

Training Zone	Stroke Rate	Heart Rate
Utilization 2 (UT2)	16-20	65-75%
Utilization 1 (UT1)	20-24	75-85%
Aerobic Threshold (AT)	24-28	80-90%
Oxygen Transport (TR2)	28-32	90-100%
Anaerobic Threshold (TR1)	> 32	Max

A large proportion of training that occurs prior to the racing season is high volume, low intensity endurance work at UT1 and UT2, to develop baseline aerobic fitness. Along with high volume endurance training, muscle power and movement speed are trained at intensities corresponding to oxygen transport (TR2) and anaerobic threshold (TR1), particularly as the race season approaches. Nilsen, Daigneault & Smith (2002b) suggests that a standard yearly rowing program requires approximately 650 hours of training, although for a senior international elite rower this may be closer to 1500 hours of training per year (Nilsen, Daigneault & Smith, 2002b).

In addition to aerobic and anaerobic fitness, effective rowing also requires good flexibility, core strength and muscle co-ordination (Thompson, 2005). Muscle co-ordination is particularly important as rowing is a cyclic activity which requires a precise, fluid technique to accelerate the boat rapidly and efficiently. Large forces must be transmitted to the oars to effectively propel the boat through the water. Power is generated predominately by the lower limbs during the drive phase, and it is essential that this force is effectively transmitted through the rower's trunk which acts as a braced cantilever in the kinetic chain, transferring forces from the legs and the footplate, to the arms and the oar (Caplan & Gardner, 2010).

3.2.1 Fatigue

Fatigue is a multifaceted phenomenon with definitions emphasizing differences in quantification and interpretation of fatigue, including any exercise induced reduction in the ability to exert muscle force or power, stemming from central or peripheral mechanisms (Phillips, 2015). In training and competition, central and peripheral fatigue reduce muscle output capacity and impact performance parameters (Knicker *et al.*, 2011). For rowers specifically, fatigue can lead to a decrease in stroke rate, stroke length, muscle force, and technique execution (Holt *et al.*, 2003), and particularly induces increased variability in smoothness and consistency over many stroke cycles (Cortes, Onate & Morrison, 2014).

Physiological and biomechanical changes occur during prolonged movement, with effects setting on more rapidly at higher activity intensities. During a sixty-minute low intensity ergometer training session, Holt *et al.* (2003) observed an increase in maximal flexion of the lumbar spine at the catch, which the authors attributed to muscle fatigue in this area and suggested may have an impact on low back pain development. However, Mackenzie, Bull & McGregor (2008) found no kinematic changes in the spine or lower limb, nor in performance metrics, for the same sixty-minute protocol. In contrast to the preceding studies, which examined the impact of endurance related fatigue on kinematics, short, high intensity protocols assess strength related fatigue. Wilson *et al.* (2013) examined lumbar spine kinematics during a fatiguing ergometer step-test protocol, finding a significant increase in sagittal plane lumbar spine RoM compared to on-water rowing. Using electromyography (EMG) and kinematics to quantify fatigue over a high intensity 2000 m ("2k") ergometer test, Pollock *et al.* (2012) found changes in body segment sequencing, with peak angular velocity of trunk extension and upper extremity flexion occurring later in the drive toward the end of the 2k test, compared to the beginning. Husmann *et al.* (2017) found a significant decrease in maximal voluntary contraction of knee extensors after completion of a 2k test, which the researchers attributed to central fatigue. Wilson (2010) and Caldwell, McNair & Williams (2003) suggested that fatigue leads to decreased precision of controlled movements, decreasing the rower's sensitivity to lumbar positioning and postural control towards the end of training sessions.

3.3 BIOMECHANICS OF ROWING

Rowing is often touted as a full body workout and with good reason – throughout the rowing cycle almost every major muscle group contributes; estimates divide the workload as approximately 40% legs, 40% trunk, 20% arms (Kleshnev, 2006b). Not surprisingly, muscle coordination plays an important role in efficiently accelerating the boat or the flywheel on an ergometer. The basic biomechanics of rowing and the transmission of force from the foot plate to the handle is achieved through accurate sequencing of lower

limb, trunk, and upper limb motion. Movement of the different body segments occurs smoothly in the skilled rower.

When holding the catch position, the athlete's ankles, knees, and hips are in full flexion, the pelvis and torso are angled anteriorly, and the upper limbs are in full forward extension. Elbow extensors and shoulder protractors are all engaged, while the wrist and finger extensors actuate the small motion needed to place the blade in the water (Figure 3.3A; Nilsen, Daigneault & Smith, 2002c). In this compressed position, a great deal of potential energy may be stored in the legs, back, and arms in preparation for the drive phase of the stroke (Hosea & Hannafin, 2012).

Mechanical loading between the catch and the point of maximum handle force (MHF) is referred to as the early drive phase, which is dominated by the quadriceps and gluteal muscles, as the athlete works to rapidly extend the lower limbs, by pushing with their feet against the fixed footplate. The trunk muscles fire isometrically (Figure 3.3B) and myoelectric analysis has demonstrated that thoracic paraspinals and erector spinae stabilize the spine to manage increased lumbar compression and shear load (Hosea & Hannafin, 2012). The arms remain extended with the shoulders relaxed, while trapezius and serratus anterior stabilize the scapula and torso (Pollock *et al.*, 2009), to provide a secure platform through which force may be transferred to the oar handle.

Peak acceleration at the mid-drive (i.e., MHF) coincides with maximal, simultaneous, isometric activation of the trunk muscles. In mid-to-late drive phase, after passing MHF, the athlete rotates the trunk posteriorly over the hips through contraction of the erector spinae muscles and latissimus dorsi (Nilsen, Daigneault & Smith, 2002c). The trunk muscles extend the upper body from approximately 20° of flexion at the catch to 20° of extension at the finish (relative to vertical at 0°). The rhomboids and trapezius retract the scapula, and triceps brachii draws the arms into the body and the finish (end of the stroke) where the blade exits the water (Figure 3.3C). Posterior rotation of the trunk prior to full leg extension (i.e. ‘opening up the body too early’ or ‘taking the catch with the back’) can cause a decrease in mechanical efficiency and boat velocity (McGregor, 2017).

From the late drive phase, through the finish, the ankles are plantarflexed, the knees are fully extended, and the hips and lumbar spine are in relative extension (i.e., ‘laid-back position’) compared to the catch position. The upper body generates momentum through the humeral extensors and internal rotators, with the elbows flexing into the body at chest height (Figure 3.3D).

Transitioning out of the finish, the recovery phase reverses the overall athlete motion, and the major muscle groups used in the drive phase are relatively quiescent (Hosea & Hannafin, 2012). The elbows are quickly extended to straight arms and the oar handles moved forward over the rower’s extended knees. The

athlete then uses the abdominal muscles (rectus abdominus and external obliques) to flex the trunk anteriorly, slowly flexing the knees, hips and ankles sliding the seat along the tracks (or monorail), and compressing back up into the catch position (Nilsen, Daigneault & Smith, 2002a), to start another working drive phase.

The technical classes in rowing are more alike than different when it comes to biomechanics and muscle activation. However, there are some differences in associated movement patterns and load distributions. In sweep rowing, athlete motions are asymmetric, generally following the blade's line of action through the water. This results in thoracic rotation with some lateral bending toward the oar side at the catch, and a counter rotation at the finish via concentric force in ipsilateral internal obliques and erector spinae and eccentric force in those contralateral muscles (Wilson, 2010).

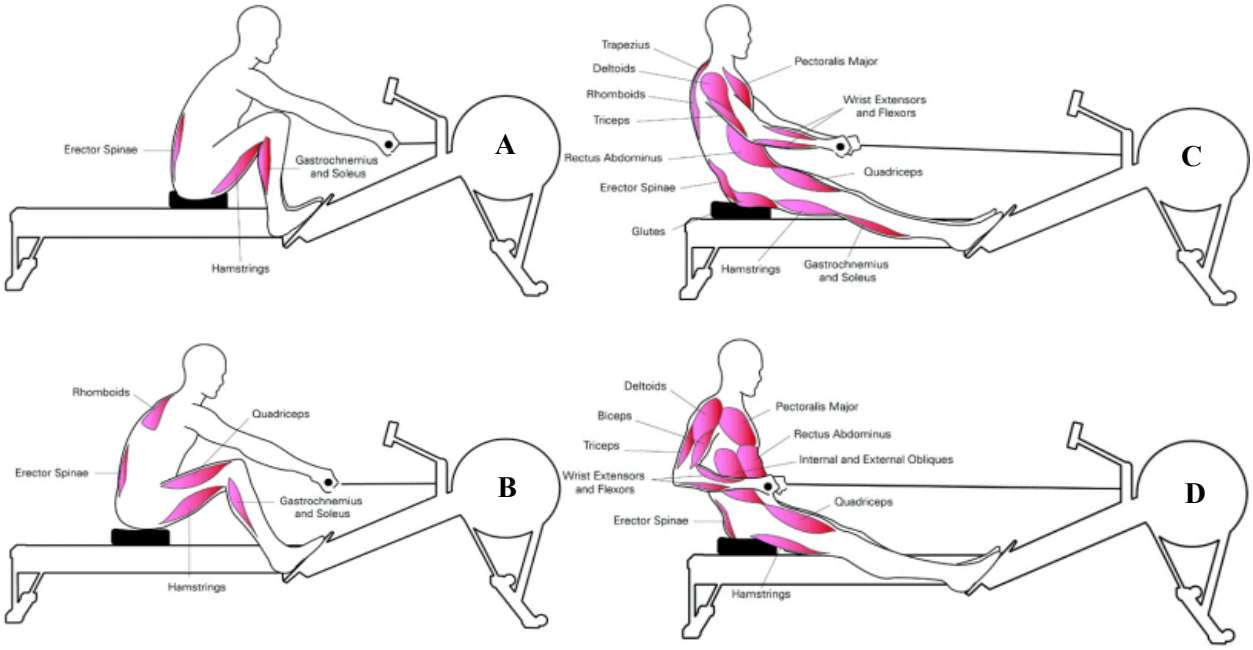

Figure 3.3: Phases of the rowing stroke and relevant activated muscles groups during each phase (A) the catch (B) early to mid-drive (C) late-drive (D) finish. (Adapted from Concept 2 (2006)).

3.3.1 Technique and the Kinetic Chain

Rowing technique influences rowing performance, and an athlete's success is dependent on their ability to execute that technique. The anthropometric variability among elite rowers implies that there is more than one optimal rowing technique, dependent upon an athlete's characteristics. Coaches have highlighted the importance of having a long stroke initiated by the legs and accelerated through the trunk and arms (Nilsen, Daigneault & Smith, 2002a). Kinematic and electromyography studies comparing rowers with varying years of experience, reinforce that more practice improves performance, and confirm that

accurate sequencing of limb and trunk motion leads to effective force transmission from the foot stretcher to the oar handle, increasing speed (Smith & Spinks, 1995).

Because rowing is a strength endurance sport, performance is associated with biomechanical efficiency, where muscle force is maximized while energy expenditure is minimized (So, Tse & Wong, 2007). This is true for experienced rowers, which show a longer stroke, better force summation on the drive, and retained momentum on the recovery. They also maintain higher stroke rates more smoothly and with greater stroke-to-stroke consistency (Smith & Spinks, 1995; Pollock *et al.*, 2009).

Having reviewed the biomechanics of the rowing motion, the role of the kinetic chain in rowing can be explored. The kinetic chain is an engineering concept used to describe human movement, often in musculoskeletal or sports medicine circles. Rowing has been classified as a closed kinetic chain exercise where the proximal and distal segments (hands and feet) are externally constrained so as to prohibit free movement (i.e. by the handle and footplate) (Karandikar & Vargas, 2011; Ellenbecker & Davies, 2001). Through all the phases of the stroke cycle, coordinated mechanics of the body segments allow the muscles and joints to produce a stable, effective, and efficient rowing movement.

The importance of the lower extremity and lumbar spine have been well studied in the rowing mechanics literature. However, there is limited research on the contributions of the thoracic spine shoulder complex, and upper limb to force generation and momentum transfer. The lower extremities are described as the primary force generating mechanism and base of support, but Baudouin & Hawkins (2002) suggest that the ability of the trunk to transfer forces through to the arms and subsequently to the handle is imperative to the resulting force on the oar. If the strong primary muscles cannot rely on accessory muscles for stability and support, then the kinetic chain loses efficiency. Thus, maintaining proper loading and control through the kinetic chain is important in producing boat velocity, improving posture and coordination. Deficits in the kinetic chain can lead to injury or decreased performance.

An inability to execute the stroke correctly, through poor technique or fatigue, affects total power output (Hofmijster, Van Soest & De Koning, 2008). Heavy training regimes and poor rowing technique are thought to be primary causes of chronic rowing injuries (Bull & McGregor, 2000). Rowers may reach forward too far into the catch and lean backward too far into the finish and studies have shown that muscle fatigue decreases the ability to maintain proper technique and increases lumbar flexion, instigating injury development (Caldwell, McNair & Williams, 2003). If the pelvis is rotated more anteriorly such that the lumbar spine maintains a less flexed position at the catch, trunk fatigue and risk of back pain decreases (McGregor, Bull & Byng-Maddick, 2004). However, limited knowledge exists about specific kinematic and biomechanical changes in response to training load and fatigue, and the impact of such changes on overall performance (Karlson, 2000; Mackenzie, Bull & McGregor, 2008).

3.4 ROWING INJURIES

Rowing is a low impact sport, with a comparatively low injury rate. Of those injuries sustained, most are categorized as repetitive or overuse in nature. The physically demanding nature of rowing, where the cyclic stroke sequence is performed thousands of times at high intensity over long periods throughout training sessions and competitions, can result in injuries that impact rowing careers.

Many epidemiological research studies have been performed in the hope of establishing an injury profile for rowers and in identifying risk factors. Broadly speaking, injuries more often result from ergometer training than from rowing ((Hosea & Hannafin, 2012)), and large increases in training volume, intensity or frequency, form a triad of risk factors, which typically precede incidents of rowing injuries (Thornton *et al.*, 2017b). Repetitive loading coupled with improper or deteriorating technique, onset of fatigue during long training sessions, can lead to injuries, both acute and chronic (McGregor, Bull & Byng-Maddick, 2004; Hannafin, 2000; Karlson, 2012). Changing boat size or technical class, are also factors associated with injuries (Evans & Redgrave, 2016). The most common injury sites are the low back (15-25%), knees (10-15%), arms (10-15%), and shoulders (7-10%) (Rumball *et al.*, 2005; Hickey, Fricker & McDonald, 1997; Hosea & Hannafin, 2012).

Most of the research cited has been done at the elite level. Hickey, Fricker & McDonald, (1997) found, for a group of 84 female and 88 male elite rowers over a ten-year period, 71.3% of 320 total injuries could be categorized as chronic in nature. Wilson *et al.*, (2010) reported a series of 44 injuries in 20 male and female international rowers, over a twelve-month period, concluding that 50% of reported injuries occurred along the spine. Smoljanovic *et al.*, (2015) surveyed 634 senior rowers at World Rowing Championships and found 71.9% of reported injuries (0.92 injuries/rower) were chronic in nature. Of all reported injuries, 8.3% were to the shoulder/upper arm. Injury severity in 32% of cases was classified as minor that did not result in loss of time from training or competition.

Understanding injury patterns among top tier athletes is important, however, as universal participation in the sport has steadily grown, particularly among women, juniors, and masters athletes, there is an imperative to describe the diversity of musculoskeletal problems and their prevalence within these groups. One survey of 526 intercollegiate athletes reported back pain prevalence was higher among rowers with higher body mass, who started rowing at an earlier age and who trained on-land more intensely than colleagues (Teitz, O'Kane & Lind, 2003). To address training effects, the authors recommended that continuous ergometer training should not exceed 30 minutes without rest (Teitz, O'Kane & Lind, 2003). To explore the impact of age on injury rates, Smoljanovic *et al.*, (2009) surveyed 398 competitors at Junior World Championships and found 73.8% of reported injuries (0.99 injuries/ rower) were overuse related. Of all reported injuries,

7.1% were to the shoulder/upper arm. Injury severity in 86.5% of cases was "incidental to minor", however rowers reporting traumatic injuries had fewer years' experience than uninjured competitors (Smoljanovic *et al.*, 2009). Masters outnumber youth and elite rowers but until recently there was no published data describing injury incidence in this group. Surveying 743 masters rowers at the World Rowing Masters Championships, Smoljanović & Bay (2018) found a lower mean injury rate (0.48 injuries/rower) per year than was previously reported for juniors and seniors, as well as reporting that 62.5% of injuries were overuse related. Of all reported injuries, 10.6% were to the shoulder/upper arm. The slight increase in upper body injury frequency reported by masters rowers noted in Smoljanović & Bay (2018) is interesting when considered in light of previously published research linking normal aging of musculoskeletal structures to increased shoulder injury prevalence and a decrease in global strength (Pribicevic, 2012).

3.4.1 Injuries of the Shoulder Girdle

Although less common than low back injuries, shoulder injuries can have serious long term impacts on an athlete's training progress, acting to impede the quality of the stroke, and carrying a potential for lost fitness and missed competition (McNally, Wilson & Seiler, 2005). Long lasting effects of chronic shoulder pain are significantly correlated with years of work, frequency of practice, and level of sport (Mohseni-Bandpei *et al.*, 2012). Several cohort studies have looked at injury rates across university and national team athletes. Literature consensus suggests about 7-10% of total sustained injuries involve the shoulder, however, team injury rates have been seen as high as 35% (Winzen *et al.*, 2011; Hickey, Fricker & McDonald, 1997; Wilson *et al.*, 2010; Boland & Hosea, 1994). The prevalence of shoulder and upper thoracic injuries is thought to be larger among the para-rowing community (Smoljanovic *et al.*, 2013; Thornton *et al.*, 2017); however, no published prevalence data is available on the topic. Postural mechanics of the spine, shoulder, and elbow examined during para-rowing experimental studies (Cutler *et al.*, 2017; Smoljanović *et al.*, 2011) currently represent the most quantifiable data in support of the para-athlete being at higher risk of upper body overuse injuries.

Shoulder pain and upper limb injuries are frequently identified as the result of tension, weakness, or muscle imbalance (Rumball *et al.*, 2005). Athletes commonly present with tightness in latissimus dorsi and upper trapezius, and may have weakness in the rotator cuff muscles (Richardson & Jull, 1995). It is suspected that overuse of rhomboid major, trapezius, levator scapulae, and serratus anterior contribute to compromised shoulder girdle positioning with decentralization of the humeral head, and stretching of the posterior capsule, (Kibler *et al.*, 2002; Page, Frank & Lardner, 2010). Significant forces cross the shoulder complex during the drive phase and if rotator cuff and scapular forces are unbalanced, shoulder girdle stability can only be achieved under high stress (Urbanczyk *et al.*, 2020). Case studies have indicated that hypermobility in the joints, leading to an extreme combination of scapular protraction, anterior tilt, and

humeral internal rotation, may yield rotator cuff tendinopathy, anterior instability, or impingement (Thornton *et al.*, 2017b). These scapular positions are commonly exaggerated in the outside arm of sweep rowers.

Treatments for upper limb injuries include ice, stretching, massage, relative rest, nonsteroidal anti-inflammatory medication, and cortisone injections (Hosea & Hannafin, 2012; Thornton *et al.*, 2017). Long-term management involves correcting muscle imbalances including strengthening ST stabilizers, postural adjustment, and technique modification. An obvious reference to this is when coaches refer to "relaxing the shoulders", an audio cue to help athletes decrease force in upper trapezius.

Unfortunately, the mechanisms for injury of the upper limbs and shoulder are less well documented and understood in the rowing biomechanics literature. This is potentially due to difficulties in modelling and evaluating forces acting on these joints. Therefore, this thesis aims to develop a kinematic and kinetic description of upper body technique in ergometer rowing using computational methods and identify biomechanical parameters influenced by the trunk and shoulder in the context of performance and injury prediction.

3.5 CURRENT ROWING RESEARCH PARADIGMS

Biomechanical assessments have been used to help predict boat velocity and analyze rowing technique, by profiling kinematics using motion capture and matching movement to force and power measured on instrumented ergometers or boats. Sports scientists have strived to develop means of enhancing rowing performance, through investigations of optimal rowing technique (Bull & McGregor, 2000; Torres-Moreno, Tanaka & Penney, 2000; Soper & Hume, 2004; Strahan *et al.*, 2011), efficiency and transfer of power from lower to upper limbs (Baudouin & Hawkins, 2002; Hofmijster, Van Soest & De Koning, 2009), minimization of injury risk (Stallard, 1980; Teitz, O'Kane & Lind, 2003; McGregor, Patankar & Bull, 2007), and the use of biofeedback tools in training (Page & Hawkins, 2003; Fothergill, 2010; McGregor, 2017). There are also numerous investigations into correlates of performance with key physiological characteristics (Fukunaga *et al.*, 1986; Ingham *et al.*, 2002; Smith, 2000).

3.5.1 Boats versus Ergometers

Recent advances in wireless technology have seen rowing shells outfitted with angle sensors, load cells, and strain gauges at oarlocks and on oars for measuring handle force, oarlock gate force and oar angle (Figure 3.4). Bespoke telemetry systems indirectly measure biomechanical variables to help coaches assess performance and provide real-time feedback on the water (Hume, 2017; Kleshnev, 2004). Perić, Ilić & Ahmetovićvić, (2019) used a BioRowTel (BioRow, Cambridge, UK) on-water data system to determine

dynamics useful in distinguishing between elite and university athlete classes. Results highlighted power output, finish angle, work per stroke, body mass and height, as discriminating parameters.

However, there are numerous challenges associated with biomechanical assessments of on-water rowing. Boat instrumentation must be lightweight, waterproof, and wireless; and even then, the additional equipment adds a non-trivial amount of weight to the shell, feedback can be convoluted by uncontrollable (i.e., environmental) variables, and data streaming is limited compared to a laboratory setting. When filming alongside a rowing shell for video analysis, parallax errors can also be introduced as relative perspective is not constant. Lamb (1989) filmed 30 international rowers on static ergometer and on-water, finding that most kinematic variables were similar throughout the drive phase, for the legs and trunk. There were significant differences in upper limb contributions during the early and late drive phases between static ergometer and on-water data.

Figure 3.4: On-water and on-ergometer data acquisition systems. Clockwise from top left: oarlock gate angle sensor (Nielsen-Kellerman, 2017); oar shaft force sensor (SmartOar, 2016); boat hull impeller/velocity sensor (Neilsen-Kellerman, 2021); flywheel rotary displacement transducer; under seat force sensors; inline handle uniaxial load cell.

Rower movement has traditionally been assessed in the laboratory because rowing machines are affordable, portable, and easy to instrument with a much wider variety and number of sensors than boats. Thoroughly instrumented ergometers have strain gauges at the foot-stretchers, position encoders on the flywheel and slide, and pressure sensors at the seat and handle (Figure 3.4). Most importantly, a laboratory setting allows much easier instrumentation of the athlete themselves and ergometers can be used in

conjunction with electromyography or motion tracking to examine physiological and biomechanical parameters (Buckeridge *et al.*, 2012; Murphy, 2009; Bull *et al.*, 2004).

There are however some biomechanical, physiological and performance differences among static-ergometer rowing, dynamic-ergometer rowing, and on-water rowing, some of which were highlighted in Section 3.1.1.1. Kleshnev (2005) showed differences in power production of body segments between on-water and on-ergometer, with foot stretcher force 30% higher than handle force on the water, while on the ergometer they are similar. Rowers also have a longer stroke on an ergometer, suggesting that ergometers favor athletes with slower leg drive and stronger upper body. Within ergometer rowing, static and dynamic machines produce kinematic differences, including a greater stroke length, with greater anterior pelvic rotation and femoral flexion in dynamic ergometry (Hislop *et al.*, 2010). The static air-braked ergometer system appears to better simulate the conditions of larger, faster boat classes than it does a single scull (de Campos Mello *et al.*, 2009). Two variants of static ergometers (air-braked and water-braked) showed a similarity in force profiles but differences in sagittal plane thigh rotation and pelvic rotation (Steer, McGregor & Bull, 2006). Despite sources of variability, ergometers remain valuable tools in testing, cross training, and monitoring, but data collected on the ergometer should interpreted with judiciousness when used for selection purposes (Kleshnev, 2005; Mikulić *et al.*, 2009).

3.5.2 Motion Analysis Technologies

There are many tools available for analysis of human motion including: inertial measurement units (IMUs), EM systems, OMC systems, digital video recording, and medical imaging techniques. Each of these tools has advantages and drawbacks.

EM tracking has been used to study sagittal kinematics of the spine and the lower extremities in ergometer rowing, assuming the limbs act with left/right leg symmetry (Bull & McGregor, 2000; McGregor, Bull & Byng-Maddick, 2004; Mackenzie, Bull & McGregor, 2008; Buckeridge *et al.*, 2012; Strahan *et al.*, 2011). EM tracking systems use six-degree-of-freedom sensors to measure low-frequency magnetic fields generated by a transmitter (Figure 3.5). Some systems, such as the Ascension Technologies Flock of Birds, used a pulsed DC update method, which transmits bursts of data at uneven intervals. The advantages of EM sensors include relatively simple digitization, ability to record and display position and orientation with little data processing, and no line-of-sight requirement between sensors and transmitter (Parent, 2012; Franz *et al.*, 2014). The drawbacks of EM systems relate to the range of accuracy of the magnetic field and any restricted movement from instrumentation (Sorriento *et al.*, 2020). EM systems may be limited by tethered cable connections causing a hindrance to subjects, a smaller total number of usable physical sensors, and a sensitivity to metal and other electronics (Murphy, Bull & McGregor, 2011; Meyer *et al.*, 2008). Although current-generation EM tracking systems are less affected by metal artifacts than

earlier ones and some new systems are wireless (Sorriento *et al.*, 2020). EM systems use a digitization and indirect-reference tracking method. Positions of digitized anatomical landmarks are defined relative to the EM sensors' local coordinate system, which when combined with an optimized common segment shape technique, are used to calculate joint centers for the lumbo-sacral, hip, knee, and ankle (Murphy, 2009; Ng *et al.*, 2009).

(A) (B)

Figure 3.5: (A) Ascension Technologies Flock of Birds® EM tracking system (Ascension Technology Corp., 2000). (B) Polhemus Liberty® EM tracking systems (Polhemus, 2015).

Optical tracking systems offer alternative solutions for non-invasively quantifying three-dimensional kinematics and are widely considered to have become a gold-standard method for motion capture (Corazza *et al.*, 2010). OMC systems consist of infrared cameras to record passive or active markers placed on anatomical landmarks (Figure 3.6). Large systems may use eight or more fast infrared cameras. OMC systems manufactured by Vicon (Oxford Metrics, Oxford, UK) and Qualisys (Qualisys AB, Göteborg, Sweden) are commonly used in functional and sporting tasks (Pueo & Jimenez-Olmedo, 2017) and have been used by research groups in Europe and Canada to assess posture and overall body movement in rowing (Price, 2016; Cerne *et al.*, 2013; Skublewska-Paszkowska *et al.*, 2016). Despite a line-of-sight requirement between markers and cameras, optical systems have the advantage of being able to image large active areas at high rate and resolution. All anatomical landmarks of interest can be directly tracked using retro-reflective markers or digitized during calibration and generated virtually for motion trials. However, because orientation cannot be directly measured, more markers are required for OMC than with EM systems (Parent, 2012). An OMC approach may not provide real-time feedback due to more complex processing of potentially noisy data (Sorriento *et al.*, 2020).

(A) **(B)**

Figure 3.6: Vicon optical motion capture system (A) Vantage® infra-red cameras (B) Vue® digital video cameras (Vicon Motion Systems Limited, 2021).

Both OMC and EM tracking systems require a laboratory-based setting, which limit their ability to monitor athletes in a field environment. Wearable technologies are an alternative approach that have the potential to overcome some of the limitations associated with lab-based motion analysis systems. IMUs typically fall into the group of microelectromechanical systems that are small, portable, lightweight, inexpensive, and low power and generally contain a combination of magnetometers, accelerometers, and gyroscopes to directly measure three dimensional linear acceleration (accelerometer), angular velocity (gyroscope), and orientation (magnetometer) (Taborri *et al.*, 2020). Other wearable sensors include flexible strain sensors, which operate by correlating joint angular motion with resistance change when a force is applied to the sensor (Adesida, Papi & McGregor, 2019). Wireless IMUs have been advantageous for studies tracking on-water rowing (Ruffaldi, Peppoloni & Filippeschi, 2015; Armstrong & Nokes, 2017; Readi *et al.*, 2015) but tend to have lower resolution and are susceptible to environmental interference, data transfer bandwidth limits, and positional drift from integration (Adesida, Papi & McGregor, 2019).

3.5.3 Electromyography

Motion analysis technologies measure the kinematics of a dynamic activity, so to assess muscular biomechanics, studies have used electromyography to examine muscle recruitment patterns during ergometer rowing. Several differences in muscle activity patterns have been observed between on-water rowing and ergometry. Results suggest that significant differences exist while comparing recruitment and kinematic patterns between on-water and static ergometer rowing, with greater muscle activation and faster onset of the knee extensors for ergometer rowing than for on-water rowing (Bazzucchi *et al.*, 2013). These differences may be due to altered acceleration and deceleration of moving masses on static ergometer versus on-water (Fleming, Donne & Mahony, 2014). Surface electromyography from various arm (e.g. brachioradialis, biceps brachii, deltoid), leg (e.g. rectus femoris, biceps femoris, vastus lateralis), and trunk (e.g. rectus abdominis, erector spinae, latissimus dorsi) muscles have been used to investigate the effects of muscle fatigue (So, Tse & Wong, 2007) and examine co-activation for spinal stabilization (Pollock *et al.*,

2009) during continuous static ergometer rowing. Rodriguez *et al.* (1990) found that arm muscles reached their maximal levels of activity at the middle of the drive phase, at approximately the same time as leg and trunk muscles, lending credence to the kinetic chain principle governing load transfer from the footplate to the handle.

3.5.4 Inverse Dynamics Modelling

In lieu of direct, invasive, internal measurement tools, intersegmental inverse dynamics analysis (IDA) has been frequently implemented to estimate joint kinetics in sports. Biomechanical models are founded on inverse rigid body dynamics - a process of calculating internal kinetic information (i.e., joint forces and moments) from anthropometric parameters (i.e., mass, height), measured kinematic information (i.e., positions, velocities, and accelerations) and measured external kinetic information (i.e., ground reaction forces).

Mathematical models, defined by a system of differential equations, represent the skeleton as a series of rigid segments (i.e. bones) connected by virtual joints (Winter, 2009). Typically, a recursive Newton-Euler method is utilized in a distal-to-proximal sequence, to derive desired model outputs at each joint from the measured experimental inputs described above (Murray & Johnson, 2004). For closed chain kinetic activities, the Newton-Euler approach combines indeterminant forces (such as muscle forces) into net forces and moments about the joints, which can be solved using linear and angular equations of motion, based on model inputs which include external reaction forces, segment position and acceleration, segment mass, segment center of mass, joint centers, and mass moment of inertia.

IDA has been used with multi-segment models of rowing (Figure 3.7) to estimate net forces and moments across the elbow, shoulder, hip, knee, ankle, and along the spine (Greene *et al.*, 2013; Consiglieri & Pires, 2009; Buckeridge, Bull & McGregor, 2016; Kornecki & Jaszczak, 2010). Studies have examined full body mechanics where the trunk is treated as a single segment connecting the shoulder to the pelvis (Hase *et al.*, 2004; Kornecki & Jaszczak, 2010). Others have quantified lumbar spine loading in the sagittal plane with half-body models that take a 'bottom-up' approach, where kinetic data is acquired from an instrumented footplate and seat (Buckeridge, Bull & McGregor, 2016; Cerne, Kamnik & Munih, 2011; Halliday, Zavatsky & Hase, 2004) or from a 'top-down' approach, where external force is applied at the handle (Morris *et al.*, 2000; Greene *et al.*, 2013).

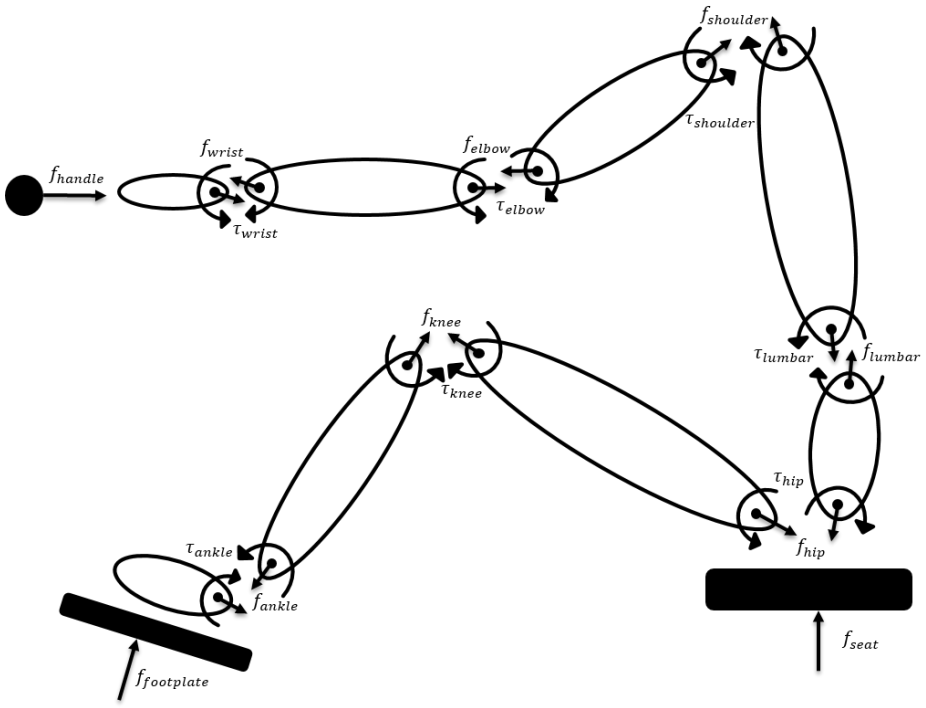

Figure 3.7: Geometric schematic free-body diagram of the rower + ergometer equipment system with external reaction forces and expected intersegmental forces and moments.

Inverse dynamics modelling of ergometer rowing provides useful information on the influence of various external factors to loads experienced by an athlete. Despite wide use of IDA in biomechanical analysis, it relies on assumptions, such as constant inertial properties, frictionless joints, and uniformly rigid segments. Errors can arise from inaccuracies from using generalized segmental parameters, surface marker movements, and estimated joint center locations (Riemer & Hsiao-Wecksler, 2008). Its largest limitation, however, lies in its inability to determine muscle activity, as muscle actions are simply represented as net moments about the joint (Winter, 2009). MSK models are a convenient way to simulate dynamic activities and examine effects of different parameters that might otherwise be too complex to assess experimentally. MSK models employ computational methods beyond rigid body inverse dynamics to study contributions of individual muscles and connective tissues during joint movement. However, because the human body is built with more muscles than there are degrees of freedom, to solve for the system's static indeterminacy, assumptions are made that the muscle forces contributing to a task are distributed according to an optimization criterion (Karlsson & Peterson, 1992; Van der Helm, 1994; Charlton & Johnson, 2006; Prinold *et al.*, 2013).

Comprehensive models of the torso and upper limb have been used to study simple activities of daily living (Klemt *et al.*, 2017; Pandis, Prinold & Bull, 2015) and dynamic athletic tasks (Persad, 2016); however there is only one that has been used to study upper body biomechanics during rowing (Juliussen, 2011).

Juliussen (2011) was a case study which utilized a single elite rower to build a rowing simulation within the AnyBody modelling program (Damsgaard *et al.*, 2006), to correlate model outputs with kinetics, kinematics, and EMG, and proposed validating predictions of chest compression forces relevant to rib stress injuries among rowers (Juliussen, 2011).

3.6 UPPER EXTREMITY ROWING RESEARCH

Researchers at Imperial College London have collaborated with British Rowing since 1998, providing feedback to coaches and athletes about rowing kinematics and biomechanics that affect rowing performance, training, and injury risk (McGregor *et al.*, 2016). Development of a custom prototype static ergometer has incorporated instrumentation into the seat, handle, and footplates to measure rowing kinetics. Combined with motion capture data, studies have characterized the effects of speed, intensity, and fatigue on lower limb (Buckeridge *et al.*, 2012) and lumbosacral spine (Holt *et al.*, 2003; Murphy, 2009) biomechanics. While these studies have helped establish a novel biomechanical assessment, they have predominately focused on two-dimensional, lumbar-pelvic, and unilateral lower limb metrics. Limited research has examined the contributions of the thoracic spine, shoulder complex, and upper limb during rowing (Price, 2016; Sforza *et al.*, 2012; Jones *et al.*, 2010; Attenborough, Smith & Sinclair, 2012). However, movement patterns following the leg drive are important because substantial mobility occurs at the shoulder complex, and significant forces are transmitted across it. This makes quantifying upper body posture and joint motion during rowing important to optimize biomechanical performance and assess injury risk.

3.6.1 Upper Limb Performance

The upper body and upper limb provide an essential link between the boat and the oar. Research suggests up to 40% of the velocity from the late drive through the finish comes from the upper limb, and subtle biomechanical factors may play important roles in rowing performance (Soper & Hume, 2004).

Kinesiology studies have confirmed core concepts about upper limb positioning that have been incorporated into rowing doctrine. Twelve studies were reviewed that analyzed upper extremity kinematics in rowers, with several types of study protocol (Table 3.2). Six of the twelve studies included national team athletes as subjects, four studies included university athletes, and the remaining used amateur or club rowers. OMC was the most popular kinematics tracking measurement system (7 studies). Video analysis was used in 3 studies and goniometers were used in 1 study, which also paired this with EMG. All studies recorded motion on either stationary or dynamic ergometers (or both), and two of those also included on-water motion tracking. Studies examining upper extremity biomechanics in rowing are summarized in Table 3.2.

Table 3.2: Studies examining upper extremity biomechanics on-water and on-ergometer. OMC: optical motion capture; EM: electromagnetic tracking; ROM: range of motion; Para-rowing setups for legs-trunk-arms (PR3), trunk-arms (PR2), and arms-shoulders (PR1) rowers. Stroke rates given in strokes per minute (spm).

Author & Year	Study type	Subject population & Protocol	Objective & Major Results
Jones et al., 2010	OMC on ergometer (Qualisys)	N=5 (female) 'amateur' athletes. 4 minutes @ 32 spm	Compared arm kinematics between stationary and dynamic rowing ergometers. Subjects on the stationary erg tend to 'jerk' the handle to achieve greater power. Dynamic ergometer is more effective for recreational users.
Attenborough, Smith & Sinclair, 2012	OMC on ergometer (Motion Analysis)	N=15 (8 female / 7 male) club, state & national athletes. 5 x 1 minute @ 18/24/30/36 spm	Quantified upper extremity joint energy contribution to total energy expenditure, joint power across sex and rate. Males generate more work through shoulder rotation than females; angular shoulder & elbow energy decreased as rate increased.
Cutler et al. 2017	OMC on ergometer (Vicon)	N=17 (8 female / 9 male) university varsity athletes. 3 x 10 strokes (LTA @ 24 spm, TA @ 30 spm, AS @ 36 spm)	Analyzing indoor ergometer para-rowing setups. PR2 and PR1 utilized more extreme ranges of motion for lumbar flexion, elbow flexion and shoulder abduction than PR3 at the catch and finish positions.
Sforza et al., 2012	OMC on ergometer (SMART BTS)	N=18 (female / male not reported) national team athletes. 3 x 30 strokes @ 28 spm	Explored limb bilateral asymmetries and sagittal ROM; upper limbs were symmetric with right-left differences up to 20 mm vertical & sagittal; thoracic and cervical spine ROM was 68° & 23° extension from catch to finish.
Tachibana et al., 2007	Video analysis on ergometer (DIAS, DHK)	N=60 (21 female / 39 male) novice to national team athletes. 1 x 6 minutes @ 20/25/30/35 spm	Used PCA to regress importance of muscle cross-sectional areas to drive power. Elbow extensor CSA best explains power contributed by the arm pull (this is only 10% of total power) and elbow flexors contribute to leg and trunk partial power.
Price, 2016	OMC on ergometer (Vicon)	N=12 (female) university varsity athletes.	Thoracic spine curvature did not change with increasing rate; transverse shoulder angle became more protracted at the catch and less retracted at the finish as rate increased; suggesting scapula stabilizer fatigue.
Bompa, 1980	Tensiometer on ergometer	N=18 (male). 2 x 6 seconds isometric contractions	Determined 'power positions' for handle pull relative to sagittal height & elbow angle; greater peak force when handle pulled into upper abdomen, not upper chest; pulling with fully extended elbows yields higher handle force.

Table 3.2 (continued)

Author & Year	Study type	Subject population & Protocol	Objective & Major Results
Bingul et al., 2014	Video analysis on ergometer (Simi Motion)	N=5 (male). national team athletes. 2000 meters test @ 28-29 spm	As distance increases, elbow angle at the catch decreases (i.e., less straight arms)
Marcolin et al., 2015	Goniometer & EMG on-water & on ergometer	N=1 (male). national team athlete. 2 x 2 minutes @ 20/32 spm	Increased elbow peak flexion at the finish on ergometer, compared to on-water and as rate increased; upper limb muscle EMG was higher on ergometer.
Halliday et al., 2001	OMC on ergometer (Vicon)	N=5 (male). university athletes. 4 x 10 strokes @ 16/20/24/28/32 spm. (random order)	Joints of the upper limb undergo motion in all three dimensions; showed large shoulder and elbow ranges of motion at 24 spm
Lamb, 1989	Video analysis on-water & on ergometer (Milliken)	N=30 (male) national team athletes. Continuous @ 30 spm (digitized 2-4 strokes)	Kinematics of the upper arm and forearm segments were significantly different between on-water & on-ergometer. differences that occurred in the arm motion at the beginning and end of the drive phase; last 60% of the drive phase showed a greater contribution from the relative hand velocity to the total linear oar velocity.

This group of kinematic and electromyography studies on rowers of varying experience levels, reinforces that effective technique relies on accurate sequencing of limb and trunk motion to maximize force transmission from the foot stretcher to the oar handle. Cross-plots of elbow flexion versus muscle activity and resultant handle force showed different coordinative patterns between ergometer and on-water rowing (Marcolin *et al.*, 2015). On-water rowing showed higher EMG activity for the pectoralis major and latissimus dorsi, but higher EMG values were collected for the biceps brachii, deltoid, and trapezius on the ergometer (Marcolin *et al.*, 2015). Movements of the upper arm and forearm segments are different on water and on ergometer, however, only at the beginning and end of the drive phase. These changes may be related to the arms compensating for slippage of the oar when being placed in the water. In contrast, the catch position in static ergometer rowing occurs around a fixed fulcrum and force of the arm segments tends to be greater than during on-water rowing (Lamb, 1989).

Ergometer vs. on-water differences notwithstanding, arm position and upper body inclination are important for force output. At the catch, it is recommended that the upper arms be perpendicular to the torso (Jones *et al.*, 2010). Qualifying a 'power position' at the catch, Bompa (1980) recommended against an extended upper body reaching action, suggesting this position was unfavorable in terms of upper body efficiency. Pulling the handle through the early drive phase with straight arms (i.e. with elbows extended

to 180°) optimized load transfer through the entire limb, yielding more consistent force production over many rowing cycles (Bompa, 1980). Bingul *et al.* (2014) suggests this may be more difficult with fatigue onset, finding that, as distance increases further into a 2k race, elbow angle at the catch decreases.

HT and ST muscles are most active in the mid-drive phase, around MHF, supporting load transfer through the kinetic chain (Pollock *et al.*, 2009, 2012). While a relatively small percentage of total rowing power is performed in the arm pull, bilateral symmetry between the upper limbs is important (Sforza *et al.*, 2012), with correlations between elbow extensor cross sectional area and power may be made covariable with the arms playing an isometric role in transmitting work of the leg drive and trunk swing to the handle (Tachibana *et al.*, 2007). Upper extremity energy contributions during the drive phase are affected by stroke rate, where percent contribution of shoulder angular energy to total energy output decreases linearly (Attenborough, Smith & Sinclair, 2012). 3D rotation of the upper arm around the shoulder joint and extension of the upper limb are also affected, finding that during a fatiguing protocol, transverse shoulder angle becomes more protracted at the catch and less retracted at the finish as rate increased (Price, 2016), and a decrease in shoulder angular energy contribution over time (Attenborough, Smith & Sinclair, 2012), suggesting scapula stabilizer fatigue.

Arm position and upper body inclination are important for force output at the finish. Peak force is greatest when the handle is pulled into the upper abdominal level (Bompa, 1980). Keeping the elbows close to the trunk and extending the humerus into the finish produces more handle force by taking advantage of a direct line of action from latissimus dorsi (Halliday *et al.*, 2001). Both Jones *et al.* (2010) and Lamb (1989) showed sharp elbow deceleration at the end of the drive phase for ergometer rowing, a more acute elbow angle at the finish, and greater relative hand velocity moving into and out of the finish position. Arm segment motion differences near the finish may be related to the need to 'feather' in on-water rowing (Lamb, 1989). Subjects using stationary ergometers appeared to 'jerk' the handle ostensibly to achieve greater power, an arm motion considered biomechanically inefficient and which may present greater injury risk (Jones *et al.*, 2010).

All these upper limb performance and injury risk management metrics are intensified when examining athletes in para-rowing classifications. Cutler *et al.* (2017) examined setups for legs-trunk-arms (PR3), trunk-arms (PR2), and arms-shoulders (PR1) rowers and found that these athletes were more susceptible to utilizing extreme ranges of motion for lumbar flexion, elbow flexion and shoulder abduction at the catch and finish positions to compensate for limitations associated with type of disability and para-rowing equipment (Cutler *et al.*, 2017). Ultimately for all rowing athletes, engraining musculoskeletal control of the finish and catch positions in particular will increase stroke efficiency for the same

physiological workload and improve consistency in horizontal acceleration of both the trunk and shoulder (McGregor *et al.*, 2016).

3.7 CONCLUDING REMARKS

This chapter covered an in-depth review of the fundamentals of rowing, with rowing technique broken down into important phases of the stroke action, highlighting key performance parameters and muscular loading. Physiology and biomechanics essential to executing the rowing action effectively and the consequences of failure to do so were discussed.

Injury prevalence studies have reported that the upper extremity is the third most frequent injury site among rowers, with slightly higher prevalence among masters rowers. Shoulder problems have been attributed to physical demands on the joint including the RoM and repetitive nature of rowing with injury disposition modulated by postural defects or poor technique. Despite availability of data on injury incidence, there are few reports that address connections between rowing biomechanics and performance reduction or injury risk. A review of the literature has been undertaken of current research paradigms and the existing body of work concerning how the upper limb, thoracic spine, and shoulder complex play essential roles in the functioning of the kinetic chain for the dynamic rowing movement.

This chapter has elucidated existing gaps in the literature including a paucity of data in biomechanics of the upper extremities during rowing, and a narrow understanding of mechanisms of injury to the upper limbs and shoulder. This background framework has also highlighted open questions around connections between shoulder and spine biomechanics and performance in ergometer rowing and implications for training and athlete health. The thesis work herein will attempt to address some of these questions through primary experimental studies, by quantifying upper body technique in ergometer rowing, utilizing sophisticated computational tools. Better understanding the influence of the trunk and shoulder to biomechanical performance may also introduce new considerations in links to injury prediction.

4. CHAPTER 4: COMPARING OPTICAL & ELECTROMAGNETIC TRACKING DURING STATIC & DYNAMIC MOTION[1]

For dynamic biomechanical analyses and motion simulation development, it is important that experimental measurements from human motion studies are derived from well-standardized methodologies. The previous chapter introduced the advantages and limitations of several motion analysis technologies in relation to current rowing research paradigms. Both EM and OMC systems have been used independently as robust means to record motion data during ergometer rowing at Imperial College London and this chapter will go into greater depth to describe the recording and data processing techniques utilized, and will specifically compare the dynamic accuracy of kinematics, simultaneously measured by an extended-range EM system (Flock of Birds) and an OMC system (Vicon) in a gait analysis laboratory.

4.1 INTRODUCTION

Non-invasive methods that use skin mounted sensors work by coordinating recorded movement of sensors to the underlying bone. Marker methodologies include EM systems (McClure *et al.*, 2001; Parkin *et al.*, 2001) and passive marker optical systems (van Andel *et al.*, 2009; Lempereur *et al.*, 2014; Shaheen, Alexander & Bull, 2011). All marker methods suffer from inaccuracies related to consistency of marker placement or soft tissue artifacts arising from relative movement between the underlying bone and the skin mounted markers (Leardini *et al.*, 2005). Anatomical landmarks of interest can be directly tracked or digitized during calibration and generated virtually for motion trials. When combined with output reaction forces and analyzed with a biomechanical model, non-invasive methods represent a powerful tool for providing insight into biomechanics during dynamic activities.

EM systems are "active" systems, requiring wires between sensors and receivers, but offer the advantage of automatically created coordinate frames, independent six degree-of-freedom measurements, simpler digitization processes and no need for direct line of sight due to cable connection. Electromagnetic devices such as the Flock of Birds (Ascension Technology, Burlington, VT, USA) are popular measurement devices for accurate recording of three-dimensional kinematics. Collaboration between Imperial College London and British Rowing has used this EM tracking system for biomechanics research on elite rowers, offering a framework to describe the execution of rowing technique and has provided quantitative feedback

[1] Accepted in part as: Urbanczyk CA, Bonfiglio A, McGregor AH, Bull AMJ. "Comparing Optical and Electromagnetic Tracking Systems to Facilitate Compatibility in Sports Kinematics" *International Biomechanics*

to help athletes improve performance and reduce injury risk (Buckeridge, Bull & Mcgregor, 2015; Bull & McGregor, 2000; McGregor, Bull & Byng-Maddick, 2004; Bull, Berkshire & Amis, 1998). However, this technology also presents drawbacks which include remaining within a fixed functional range of a magnetic field transmitter, wired connections between system components, indirect tracking of anatomical landmarks (through digitization), and a maximum frame rate of 75 Hz that is reduced as the number of sensors increases, effectively limiting the total number of body segments that can be tracked to four. Accuracy of the system can also be affected when recording near ferrous material (Ng *et al.*, 2009; Richards, 1999) such as a large metal ergometer. Murphy, Bull & McGregor (2011) verified the EM system for use in a large human performace laboratory by optimizing the layout of all of equipment within and without the capture volume. This careful attention to the experimental environment and close monitoring of distortion was essential to minimize the effects introduced by the EM systems sensitivity to metal and other electronics.

Optical technology presents advantages for analyzing complex full-body motions. OMC systems have been used by research groups in Europe and Canada to analyze gross kinematics during ergometer rowing (Price, 2016; Cerne *et al.*, 2013; Skublewska-Paszkowska *et al.*, 2016; Attenborough, Smith & Sinclair, 2012; Pollock *et al.*, 2009; Villapún Puzas, 2015), and have been employed to assess other dynamic tasks including cricket, pull-ups, and overhand throwing (Persad, 2016; Klemt, 2018; Urbanczyk *et al.*, 2020). The Vicon optical system in use at Imperial College London uses passive retro-reflective markers tracked in three dimensions by surrounding infrared cameras. The systems are extremely accurate, able to identify individual markers to a resolution of <1 mm, even in large laboratory capture volumes. OMC overcomes EM system limitations with increased framerate (functionally up to 240 Hz), greater flexibility in marker placement with direct tracking of anatomical landmarks, and the ability to simultaneously record many more body segments, as framerate and field of view are unaffected by the number of trackers. Although OMC has no wired connections between system components, OMC imposes line-of-sight requirements between cameras and markers. Dynamic subject movement may sometimes make it challenging to maintain line of sight. To overcome this, redundancy in the number of cameras is introduced and, data processing techniques are applied to ameliorate marker occlusion, but post-processing time is typically longer than for EM systems.

Few studies have simultaneously investigated the accuracy and precision of an OMC system and an EM system during dynamic motion. Hassan, Jenkyn & Dunning (2007) reported direct comparisons between OMC and EM tracking systems when reflective markers and sensors were affixed side-by-side to a robotic articulating arm, designed to emulate movements seen at the elbow joint. The study provided a concurrent assessment of each system for slow movements with small angular deviations. The authors found that, as the robot was moved through a known RoM, both systems tended to underestimate the

displacement, but the mean angular difference between each system and the robotic arm did not exceed 2°. The authors were able to reduce these differences by applying least-squares corrections during data post-processing. Hassan, Jenkyn & Dunning (2007) did not apply their experimental methods to an in-vivo model, thus were unable to address the inaccuracies native to human subject testing, such as skin motion artifact, for which rigid body corrections may be inappropriate. Few in-vivo studies have compared the performance of these systems for compound motions under dynamic conditions. In addition to assessing system accuracy and precision using a robotic manipulator system, Lugade *et al.* (2015) examined intra-day and inter-day repeatability of EM and OMC measurements during a sit-to-stand task. The authors found that the optical system demonstrated slightly higher inter-day coefficients of multiple correlation (CMC) for sagittal plane hip, knee, and ankle joint angles, and did not find any differences between systems in joint RoM. Lugade *et al.* (2015) concluded that both systems demonstrated an adequate ability to track dynamic motion and suggested that small differences may be attributable to skin motion artifact having affected the larger EM system sensors. There are no publications that simultaneously assess these technologies in more complex, higher speed, whole-body motions, such as rowing.

EM systems are a relatively older motion tracking technology and have in many applications been surpassed by OMC systems, which have become regarded as the "gold standard" in motion tracking technologies (Pueo & Jimenez-Olmedo, 2017; Glossop, 2009). The efficacy of the "Flock of Birds" EM system (Ascension Technologies, VT, USA) preferred by researchers in the Biodynamics Lab at Imperial College London was established in 1998 (Bull, Berkshire & Amis, 1998; Bull & McGregor, 2000). That EM tracking system has been used independently as a robust means to record lower extremity and lumbar spine motion data during ergometer rowing, generating important descriptions of lower body and trunk sequencing (McGregor, Bull & Byng-Maddick, 2004; Holt *et al.*, 2003), and establishing key links between biomechanics parameters and performance metrics, which continue to be used to analyze quality of elite rowing technique (Buckeridge, 2013; Murphy, 2009). Previous work on scapula and shoulder complex movement using EM tracking has precisely examined simple, well-defined movements (Meskers *et al.*, 1999; Hannah, 2015; Fayad *et al.*, 2008) but it may be less suitable for whole-body tracking of dynamic activities in large capture volumes and the UKNSM is specifically implemented to operate with inputs derived from OMC marker data (Persad, 2016; Prinold, 2012; Klemt, 2018; Charlton, 2003).

The long-standing collaboration between Imperial College and British Rowing has generated a wealth of historical biomechanics data on elite level rowers and established performance protocols and parameters still used by athletes and coaches. Demonstrating that a new OMC based tracking methodology was capable of obtaining equivalent values in relation to spine and lower limb, to those generated by the previously validated EM tracking system was important for providing reassurance to external stakeholders

and maintaining links to elite athlete recruitment. To leverage Imperial College's substantial rowing biomechanics database from previous EM studies, developing a standard of compatibility between EM and OMC system measurements was prudent. This type of compatibility can be used to preserve older data to operate with newer or alternative systems and facilitates comparison of current and future OMC measurements by contextualization in relation to historical EM rowing data (Rowlands *et al.*, 2016), effectively ensuring continuity in athlete training assessments and research outputs.

The purpose of this study was to compare the accuracy and precision of EM and OMC displacements in three dimensions during ergometer rowing to demonstrate that a new OMC based tracking methodology was minimally capable of obtaining equivalence with the previously validated EM system, in relation to spine and lower limb metrics and that OMC should be considered for use in this thesis by expanding capture capabilities, without losing the ability to compare to prior work from the group. This was achieved by quantifying the relative error in reported position of mounted sensors/markers, digitized anatomical landmarks, and calculated joint centers during (1) static apparatus tracking, (2) dynamic apparatus tracking, and (3) dynamic athlete tracking.

4.2 MATERIALS & METHODOLOGY

To meet the research goal, a protocol of EM sensor and OMC marker placement was developed considering the expected kinematics of a seated athlete and the requirements of each measurement device. Twelve healthy subjects participated in this study (Table 4.1). All subjects were club or national team athletes rowing regularly at the time of the study. Imperial College London research ethics committee granted approval, written informed consent was obtained from each participant prior to testing, and all athlete data were anonymized.

Table 4.1: Subject population demographics

	Age (years)	Mass (kg)	Height (m)	Years Rowing
Total (n = 11 female / 1 male)	25.7 ± 2.2	74.8 ± 6.0	178.6 ± 7.8	8.8 ± 3.7

4.2.1 Apparatus

All rowing trials were performed on a bespoke instrumented ergometer (Figure 4.1). External ergometer kinetics were collected by one load cell at the handle (ELHS model, Entran, Lexington, Kentucky, USA); a rotary encoder at the flywheel (ERN120, Heidenhain Ltd., Traunreut, Germany); four load cells under the seat (ELPM model, Entran, Lexington, Kentucky, USA) (Murphy, 2009); and three strain gauges under each footplate (Buckeridge, 2013).

Kinematic data were simultaneously recorded with a four receiver 'extended range' EM tracking system operating at 75Hz ('Flock of Birds', Ascension Technologies, VT, USA) and a ten camera OMC system, operating at 100Hz ('MX T-series', Vicon, Oxford, UK). The laboratory was arranged for a large OMC capture volume (54 m^3) and OMC data were streamed to Vicon Nexus 1.8.5 software (Vicon, Oxford, UK). The EM system transmitter was located 1 m to the right of the ergometer slide rail and 1.25 m above the floor atop a wooden tower (Figure 4.1). Details of the optimization of the laboratory layout for use with the EM tracking system can be found in Murphy, Bull & McGregor (2011). EM data were streamed to a custom data acquisition program (LabVIEW 2016, National Instruments, TX, USA).

The origin of the EM system axes was at the center of the transmitter cube, 1.25m above the lab floor. Positive directions of each of these axes were left (X), superior (Y), and anterior (Z). The origin of the OMC system was on the lab floor, in the center of the ergometer rail, directly underneath the handle cage (Figure 4.1). Positive directions of each of these axes were left (X), superior (Z), and posterior (Y). To create a single, laboratory coordinate frame shared by both systems, appropriate translations and rotations were applied to the EM data to align with the OMC system global coordinate frame.

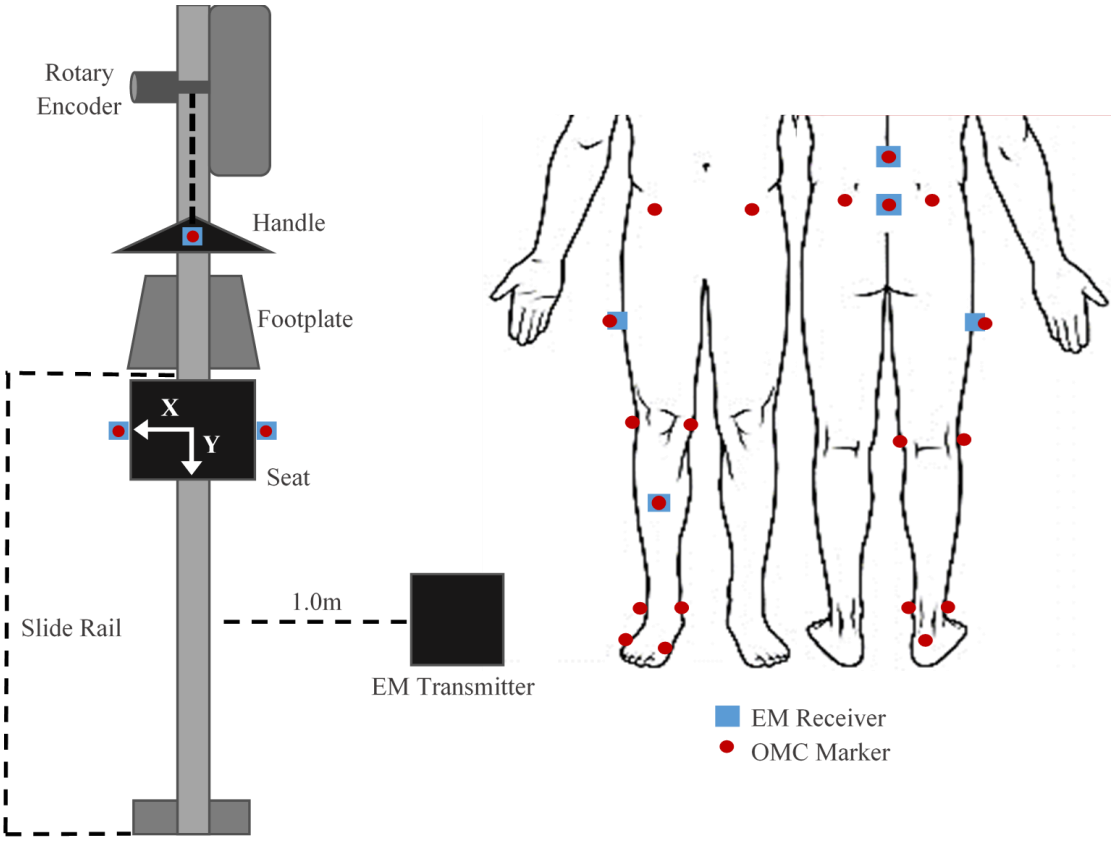

Figure 4.1: Diagram of optical motion capture (OMC) marker and electromagnetic (EM) receiver layout during rowing trials. Top-down view of sensors and markers affixed to the instrumented ergometer (*left*). Anterior and posterior views of sensors and markers as applied to subject anatomical landmarks (*right*. See Table 4.2).

4.2.2 Athlete preparation and protocol

OMC markers and EM sensors were attached to the pelvis, lumbar spine, and right leg of each subject (Figure 4.1; Table 4.2). Digitization and marker placement were performed by a single operator, an experienced sports bio-mechanist with training in landmark palpation, skin marker placement and extensive experience with methods used in the current protocol.

Four EM sensors (FoB1-FoB4) were attached to the skin at the thoracolumbar junction (FoB1: T12/L1) and lumbosacral junction (FoB2: L5/S1) using adhesive pads ('PAL Stickies', PAL Technologies, UK). The remaining sensors were attached midway along the lateral right thigh (FoB3) and to the anterior right tibia (FoB4) using fabric straps (Figure 4.2). EM system calibration followed the procedure previously described (Murphy, Bull & McGregor, 2011), which involved digitizing nine relevant bony landmarks by palpation with a stylus tip affixed to EM sensor FoB3 (Table 4.2). While the stylus tip was in contact with the landmark of interest, the EM sensor was rotated about that point to create a 3D cloud of position data. A sphere fitting procedure was used to determine a vector to the landmark from sensors FoB1, FoB2, and FoB4, already attached to the athlete (Hiniduma, Gamage & Lasenby, 2002).

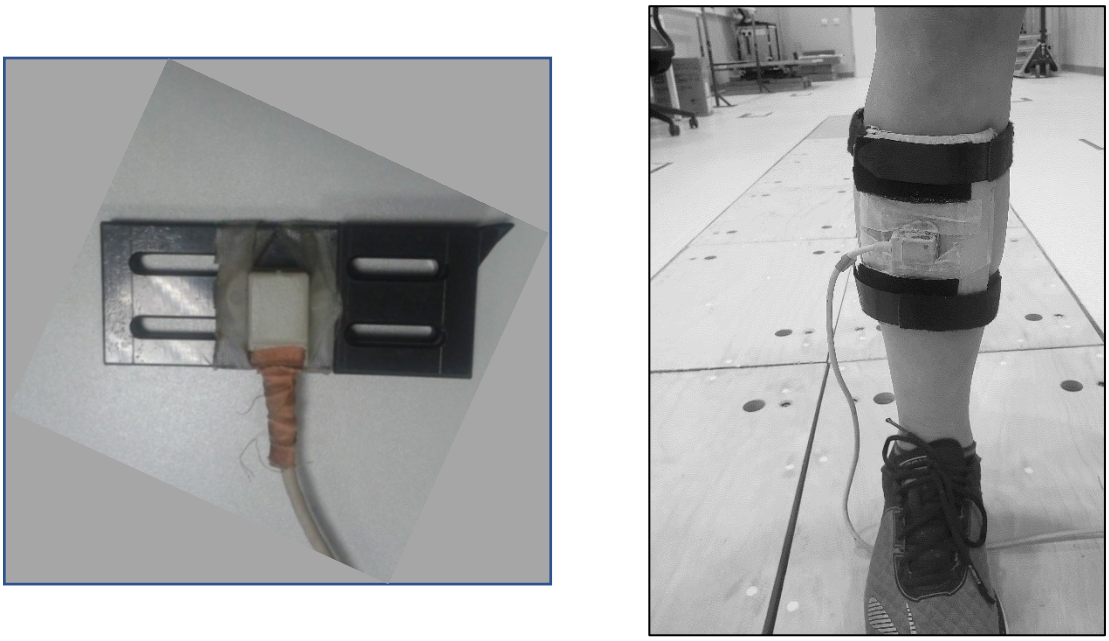

Figure 4.2: Electromagnetic (EM) sensor, FoB3, affixed to plate with stylus tip (*left*). EM sensor, FoB4, affixed to anterior tibia plate (*right*).

After digitization of each landmark, a retro-reflective OMC marker was placed on each of the locations (Table 4.2). OMC markers were also placed atop each of the four EM sensors, on the ergometer handle and on the left and right sides of the ergometer seat (Figure 4.1). A static calibration trial was collected for the OMC system, with the athlete standing at the center of the capture volume in neutral

anatomical position (i.e., arms slightly raised away from one's sides, palms facing forward). The knee joint center (KJC) was defined as the midpoint between lateral and medial epicondyles and the ankle joint center (AJC) was defined as the midpoint between the lateral and medial malleoli (Buckeridge, 2013; Murphy, 2009). The right hip joint center (HJC) was determined through a functional calibration (Camomilla *et al.*, 2006) trial where the athlete flexed their hip and knee anteriorly to 90º, then extended their hip and knee posteriorly, then circumducted their hip with their knee flexed at 90º.

Table 4.2: Anatomical landmarks digitized by electromagnetic (EM) system and markered for optical motion capture (OMC) system.

Anatomical point	Abbreviation	Notes
Right anterior superior iliac spine	RASIS	Digitized/Markered
Left anterior superior iliac spine	LASIS	Digitized/Markered
Right posterior superior iliac spine	RPSIS	Digitized/Markered
Left posterior superior iliac spine	LPSIS	Digitized/Markered
Right lateral femoral epicondyle	RLFE	Digitized/Markered
Right medial femoral epicondyle	RMFE	Digitized/Markered
Right fibula malleolus	RFM	Digitized/Markered
Right tibia malleolus	RTM	Digitized/Markered
Right calcaneus	RCC	Markered
1st metatarsal	MT1	Markered
5th metatarsal	MT5	Digitized/Markered
Hip joint center	HJC	Functionally calculated
Knee joint center	KJC	Midpoint between femoral epicondyles
Ankle joint center	AJC	Midpoint between tibial & fibular malleoli

Rowers performed three 3-minute rowing trials at low, medium, and high stroke rates (18 spm, 24 spm, and 28 spm). Participants rested for a minimum period of 3 minutes, and a maximum period as needed, to minimize any potential for fatigue effects. Real-time feedback from the ergometer and computer monitor was displayed to athletes and researchers during testing (McGregor *et al.*, 2016), which facilitated maintaining a consistent stroke rate.

4.2.3 Static and dynamic apparatus tracking

Three subjects participated in a secondary protocol which involved tracking the ergometer apparatus under static and dynamic conditions but did not include marker placement on the athletes themselves. Four

EM sensors and four OMC markers were attached to the middle of the ergometer handle, the lower right corner of the footplate, and the left and right side of the ergometer seat (Figure 4.3). OMC and EM systems simultaneously recorded sensor/marker position, which were compared to 'known positions' measured by the ergometer rotary encoder and a precision measuring tape (Figure 4.4). During static apparatus tracking, accuracy was determined at three locations along the length of the slide rail, (*catch, mid-slide, finish*; Figure 4.3). The catch position (also referred to as the origin position) was recorded while the handle was placed in its cage and the seat was at the front of the slide rail (34 cm from the origin, +Y direction). Mid-slide (i.e., half slide) occurred with both the handle and seat at 112 cm from the origin (+Y direction) and finish (i.e., rear) occurred with the handle and seat at 156 cm from the origin (+Y direction). All static apparatus testing 'known positions' and seat width were recorded using a precision tape measure (Figure 4.4). Static position data were acquired for 15 seconds at each of the three locations, with 3 repetitions per location. During dynamic trials, each subject completed three 60-second rowing trials at 18 spm, 24 spm, and 28 spm (the same stroke rates as the protocol from athlete testing in Section 4.2.2) and 'known positions' of the handle in the sagittal plane were recorded directly by the ergometer affixed rotary encoder.

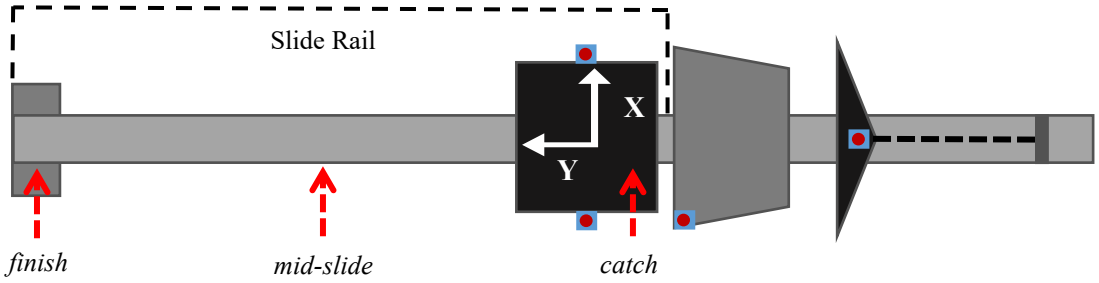

Figure 4.3: During static apparatus tracking, accuracy was checked at several +Y-positions along the length of the slide rail (catch, mid-slide, finish). These approximate positions are indicated with dashed red arrows underneath the slide rail.

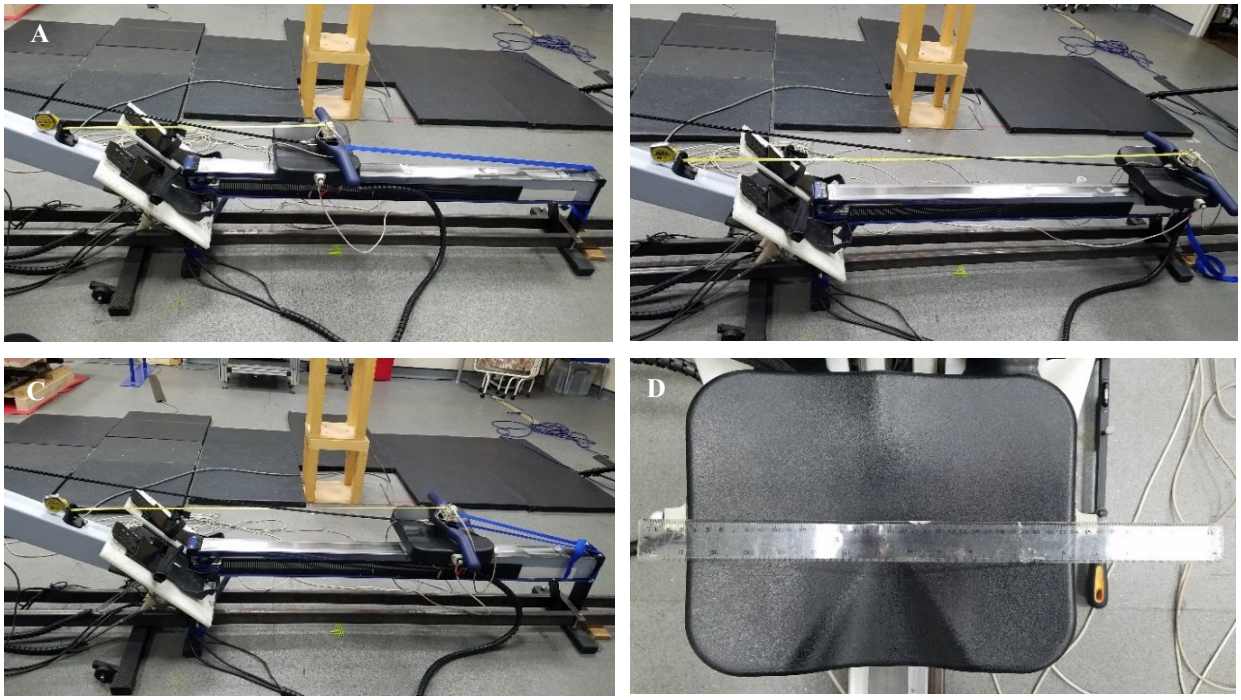

Figure 4.4: Laboratory arrangement with positioning of seat and handle relative to slide rail and electromagnetic (EM) system tower. (A) Origin/Catch position. (B) Rear/Finish position. (C) Half/Mid-slide position. (D) Measurement of seat width.

4.2.4 Data Analysis & Statistics

Kinetic data and kinematic data were synchronized and post-processed in MATLAB 2017B (MathWorks, MA, USA). All trial data were smoothed using a 4th order low-pass Butterworth filter with a 6 Hz cutoff frequency (Pollock *et al.*, 2009). Data from all systems were harmonized to share a single global coordinate frame, with its origin located at the handle cradle near the center of the ergometer frame. Data from each dynamic rowing trial was divided into individual strokes where the start of each stroke was identified as the minimum sagittal (Y-axis) handle position. The catch of each stroke was defined the first instant in which handle force surpassed 75N. The finish was defined as maximum sagittal handle displacement. Each stroke was time normalized to 201 data points using a cubic spline interpolation, such that each stroke extended from the start (0%) to a subsequent next start (100%). Each trial was referenced to initial marker/sensor position, permitting comparison of system drift between and within subjects.

All statistics were conducted with R packages in RStudio 3.6 (RStudio Team, 2016), including mean tracked position and 95% confidence intervals with a significance level of $\alpha=0.05$. Initial ANOVA analysis compared reported sensor position bias between stroke rates for each system. Where no statistical difference was found, data were pooled to reduce statistical complexity, with means and 95% confidence intervals calculated across all speeds. Body segment angles relative to horizontal and intersegmental angles between

adjacent body segments were compared between the OMC system and EM system for the thigh, shank, knee joint, and lumbosacral junction (Figure 4.5).

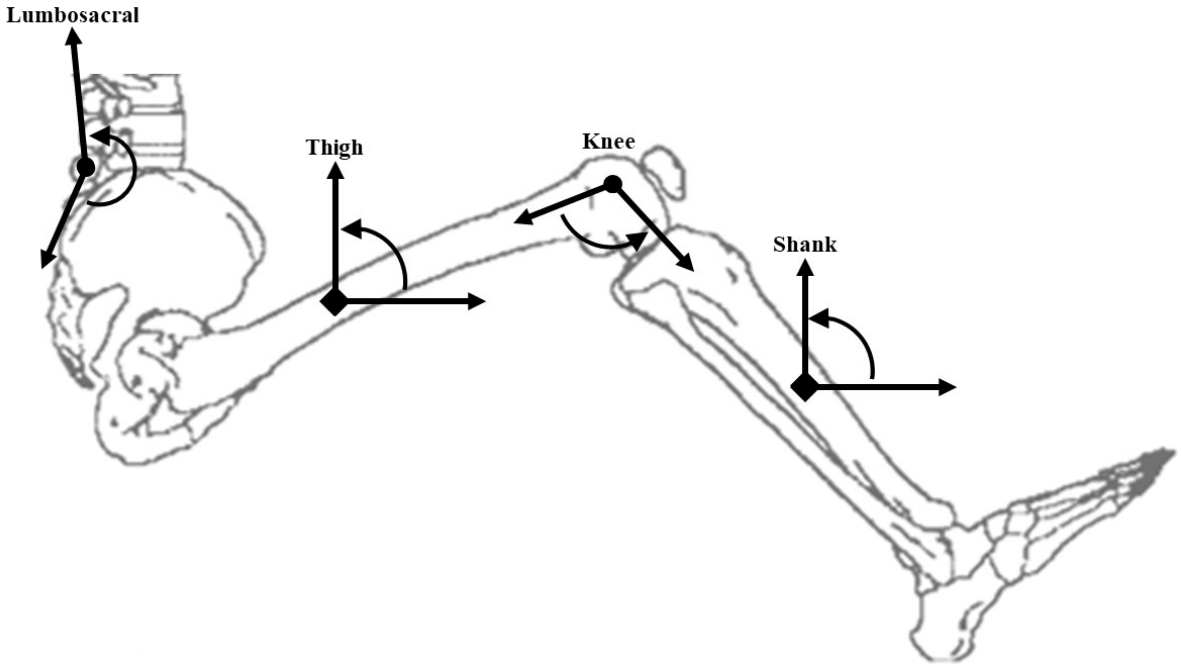

Figure 4.5: Simplified schematic of local 2D coordinate frames used to describe body segment angles and intersegmental angles in the sagittal-plane of movement (Murphy, 2009).

During dynamic apparatus testing, each measurement system reported sagittal plane handle position independently, the tracking systems through handle affixed markers/sensors, and the ergometer system through the rotary encoder stroke length. Misalignment of kinematic waveforms between the ergometer, the OMC system, and the EM system was attributed to a shift in time, which was corrected by applying a static time shift to one of the lines, in this case, the EM kinematic data. Capture latency between the ergometer and the OMC system was considered trivial and no correction was deemed necessary.

Correction of EM system capture latency used a method of data curve fitting which minimized the sum of the squares of the vertical offsets between the sagittal plane handle displacement of the EM system and the handle displacement waveforms generated by the ergometer system kinematic data. For every participant, and for each continuous 3-minute rowing trial, a single time-shift translational offset was calculated and applied to the EM system kinematic data.

For Bland-Altman analysis, data were pooled across all speeds to compare the bias and limits of agreement of each motion tracking system. Root mean square (RMS) error was used to quantify the difference in each system's tracked position to the 'known position' during static testing. Similarity of waveforms between OMC and EM data were assessed using the Sprague and Geers metric during dynamic

testing (Schwer, 2007). Geers metric can discriminate magnitude (M) and phase (P) differences in tracked position between systems, and was interpreted such that metric values at or near zero indicated excellent agreement between waveforms; less than 0.30 difference was considered good and greater than 0.50 difference was considered poor (Schwer, 2007; Klemt, 2018).

4.3 RESULTS

4.3.1 Apparatus Tracking: Accuracy and Precision

Static ergometer tracking results demonstrated that OMC positions recorded on the ergometer were consistently closer to the 'known positions', than those positions recorded by the EM system, with lower RMS errors and lower RMS standard deviations ($p < 0.001$). Across all three slide-rail locations examined, average RMS error for the OMC system was 0.08 ± 0.04 mm while EM system RMS error was 1.44 ± 2.17 mm. Recorded static positions of markers/sensors affixed to the handle, the footplate, and the seat, indicated that both the OMC system and EM system show sufficient accuracy, with little position bias (Figure 4.6). However, in comparing the variance of static measurements, the OMC system showed consistent differences across time, and was much less prone to noise ($p < 0.001$) than the EM system. As indicated by 95% confidence intervals, the OMC system precision lies well within the variation limits of the EM system (Figure 4.6).

For each of the Y-axis positions at which the seat and handle were arranged for static trial data acquisition, the variation in reported X-axis and Z-axis sensor position were noted as an indicator of system accuracy and precision. Once the sensors and markers had been affixed, the footplate sensor should maintain the same 3D spatial position throughout the study. Across all the static trials estimated footplate sensor position was similar between the OMC and EM systems, but the variance in estimated position was larger from the EM system. In X, Y, and Z axes the OMC marker was reportedly located at -208.97 ± 0.20 mm, 316.46 ± 0.45 mm, and 156.90 ± 0.25 mm, while the EM sensor was reportedly located at -201.72 ± 6.23 mm, 323.39 ± 3.96 mm, 151.52 ± 1.86 mm. The reported footplate position was consistent within each trial, but it was not consistent across trials, with large deviations in reported position as the seat and handle sensors were moved in the sagittal plane (Figure 4.7).

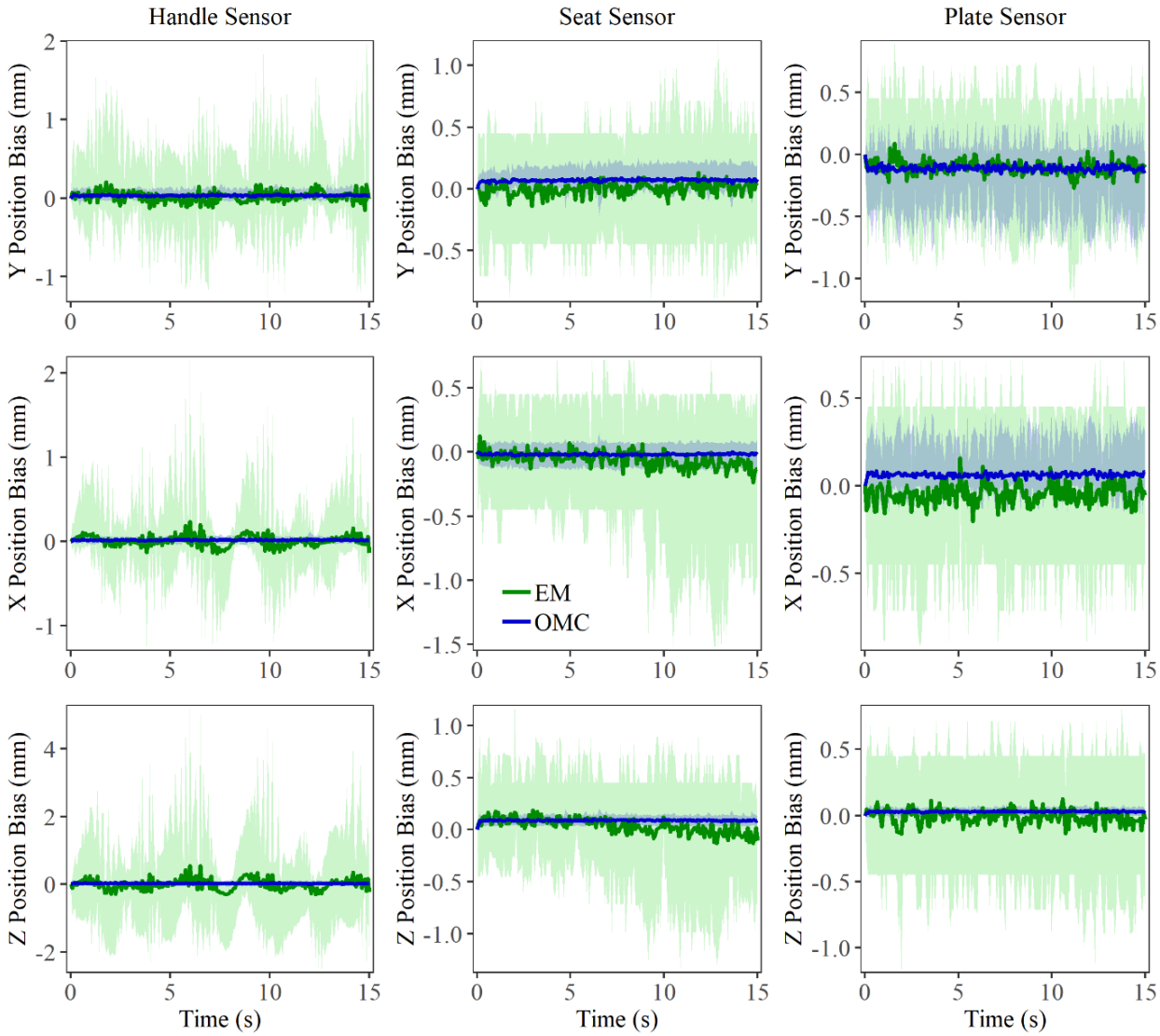

Figure 4.6: Difference in position (mean ± 95% CI) from 'known position' (recorded by tape measure) of static optical motion capture (OMC) markers and electromagnetic (EM) sensors located at the handle, right side of seat, and footplate in sagittal plane (Y, *top*), frontal plane (X, *middle*), and transverse plane (Z, *bottom*) during static apparatus tracking.

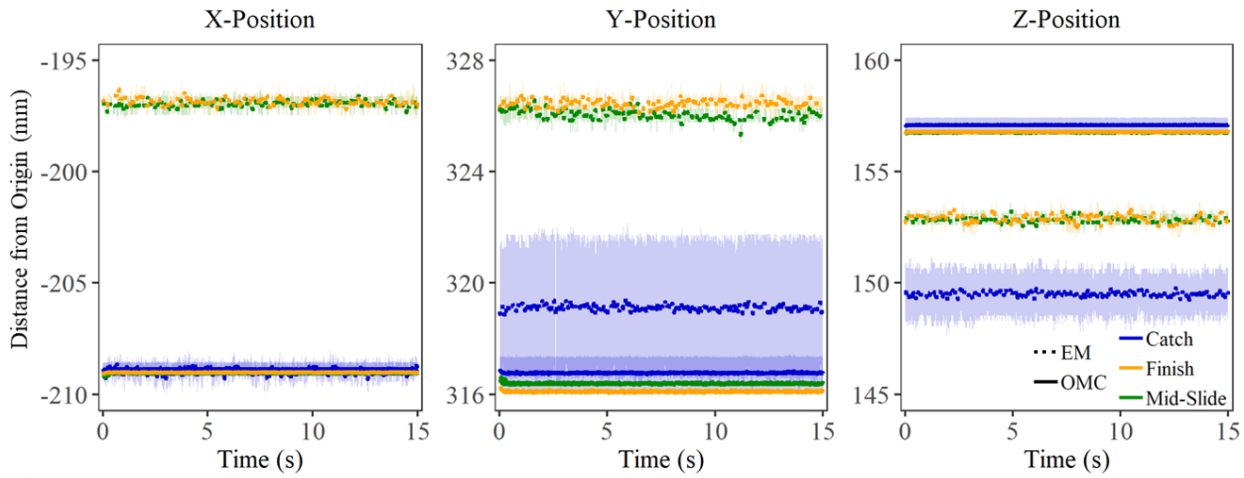

Figure 4.7: X-axis (*left*), Y-axis (*middle*), and Z-axis (*right*) distance from lab coordinate system origin (mean ± std) for sensors attached to ergometer footplate. Position estimates for each system were made near the catch, finish, and at mid-slide during static apparatus tracking.

The ergometer seat and sensors only translate along the Y-axis, and X-axis seat sensor position should remain constant across all trials. Under static tracking, sensor position reported by the EM system had large errors and between-trial variance (Figure 4.8). Comparing data spread between the right seat sensor and the left seat sensor showed differences in absolute tracked position were greater for sensors fixed further from the transmitter (Figure 4.8). A compact way of visualizing this difference was to calculate the ergometer seat width based on the X-axis distance between markers/receivers fixed to left and right sides of ergometer seat. For seat width measured during static apparatus tracking the OMC estimated seat width but was closer to the true seat width while the EM system estimated seat width was less accurate and less precise (Figure 4.9). At slide positions farther from the transmitter, seat width was underestimated (catch: 312.6 ± 0.34 mm, finish: 294.7 ± 0.01 mm), but for the mid-slide position radially closer to the transmitter, the EM system over-estimated the X-axis position (mid-slide: 340.3 ± 0.02 mm). The large 95% confidence intervals in EM estimated seat width were predominately attributed to between trial variance in reported position of the left seat sensor (Figure 4.8).

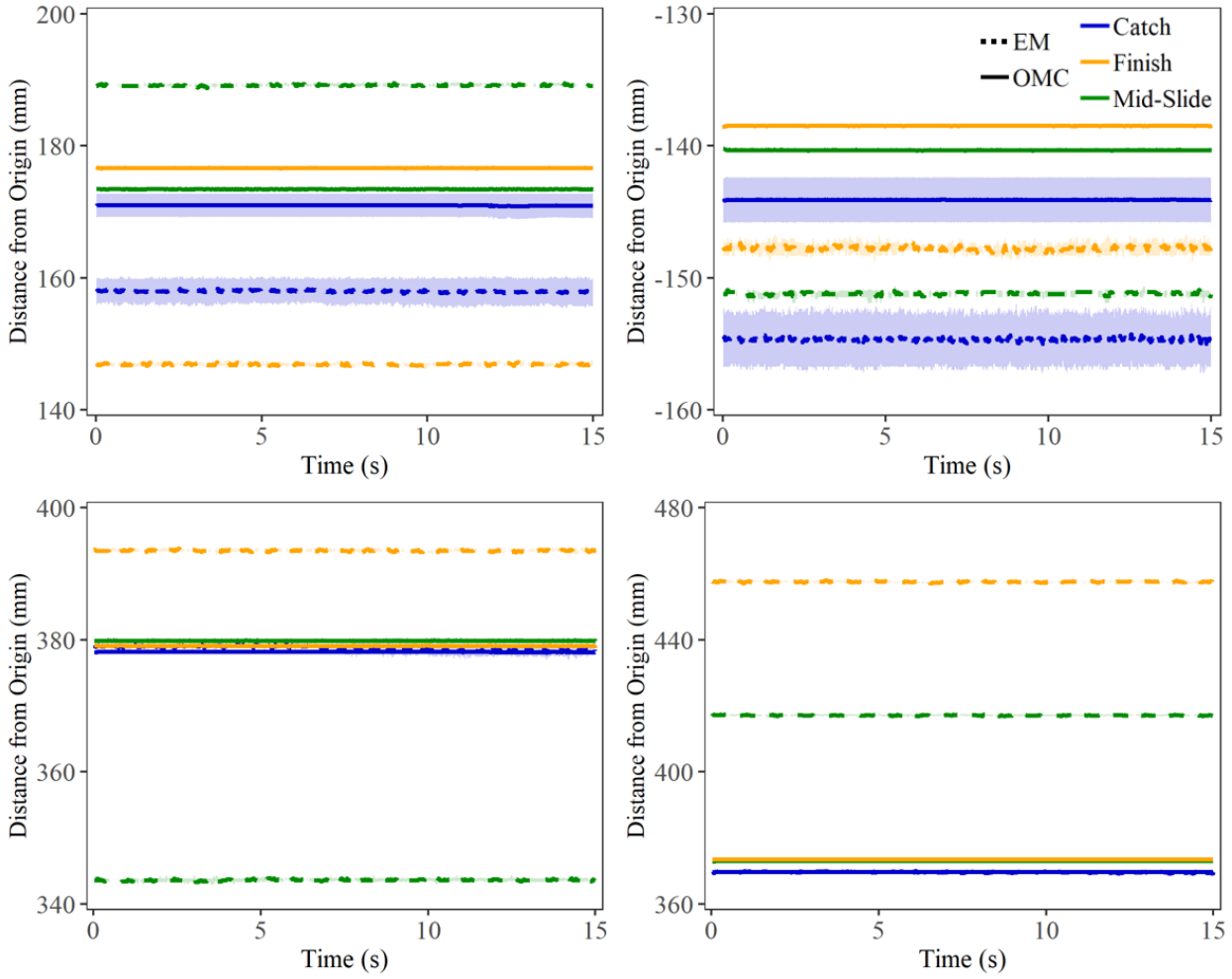

Figure 4.8: X-axis (*top*) and Z-axis (*bottom*) distance from lab coordinate system origin (mean ± std) for sensors attached to the left-side (*left*) and right-side (*right*) of the ergometer seat. Position estimates for each system were made near the catch, finish, and at mid-slide during static apparatus tracking.

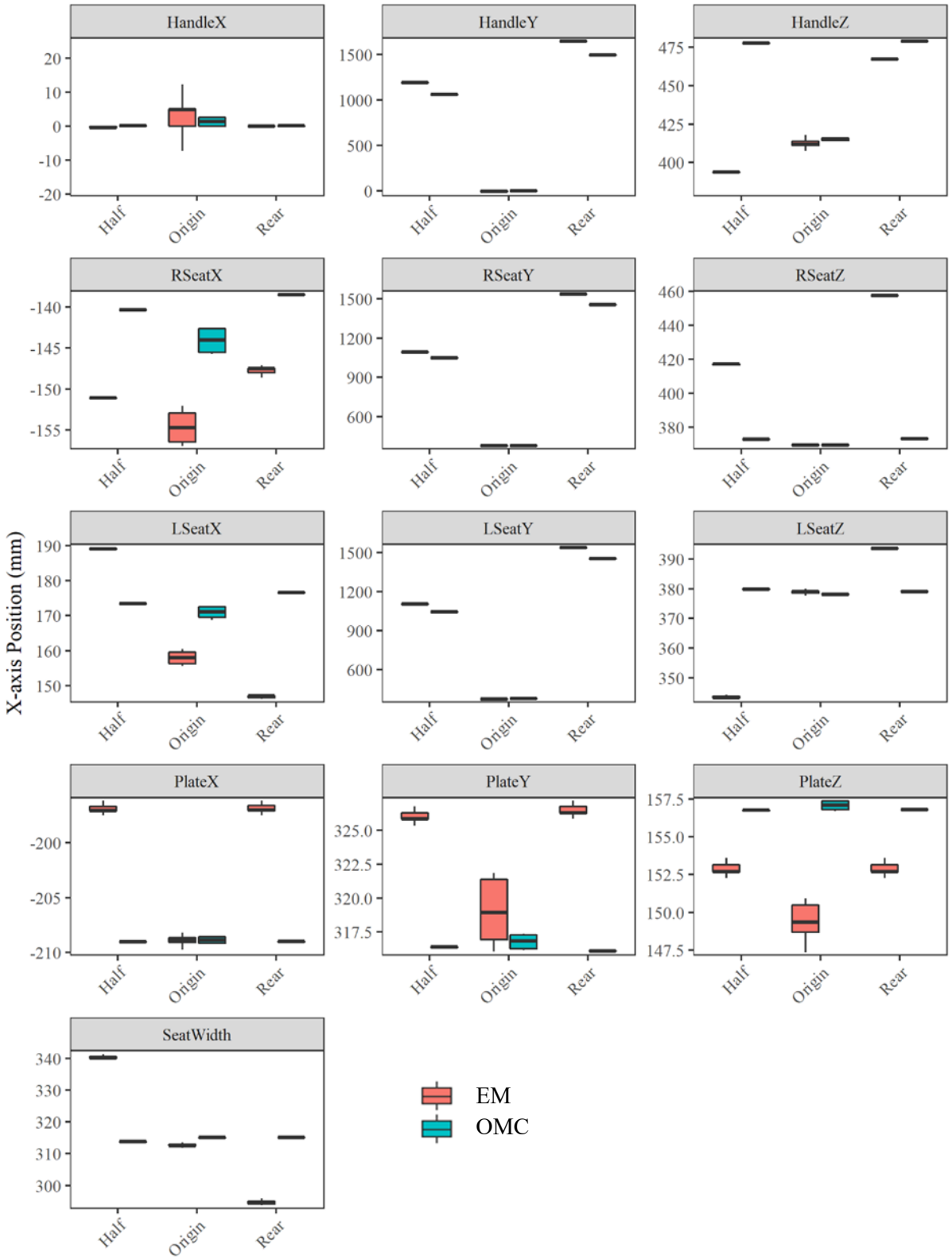

Figure 4.9: Estimated X-axis distance from lab coordinate system origin (mean ± IQR) for all ergometer affixed sensors during static apparatus tracking. Estimates for each electromagnetic (EM) and optical motion capture (OMC) systems at were made at Y-axis positions near the catch (*origin*), finish (*rear*), and mid-slide (*half*).

Under dynamic tracking conditions, there was no significant difference between estimated sensor position as stroke rate increased (Figure 4.10; $p = 0.79$). When visually comparing stroke trajectories captured by both tracking systems and the ergometer instrumentation, the EM system trajectories had a jagged appearance (Figure 4.11). This jagged tracking of smooth movements may be a result of the lower frame rate and burst transmission of data from the EM system. For both systems, smoothing the data reduced random noise, with low pass filtering methods and averaging over many strokes benefitting the EM system data (Section 4.2.4).

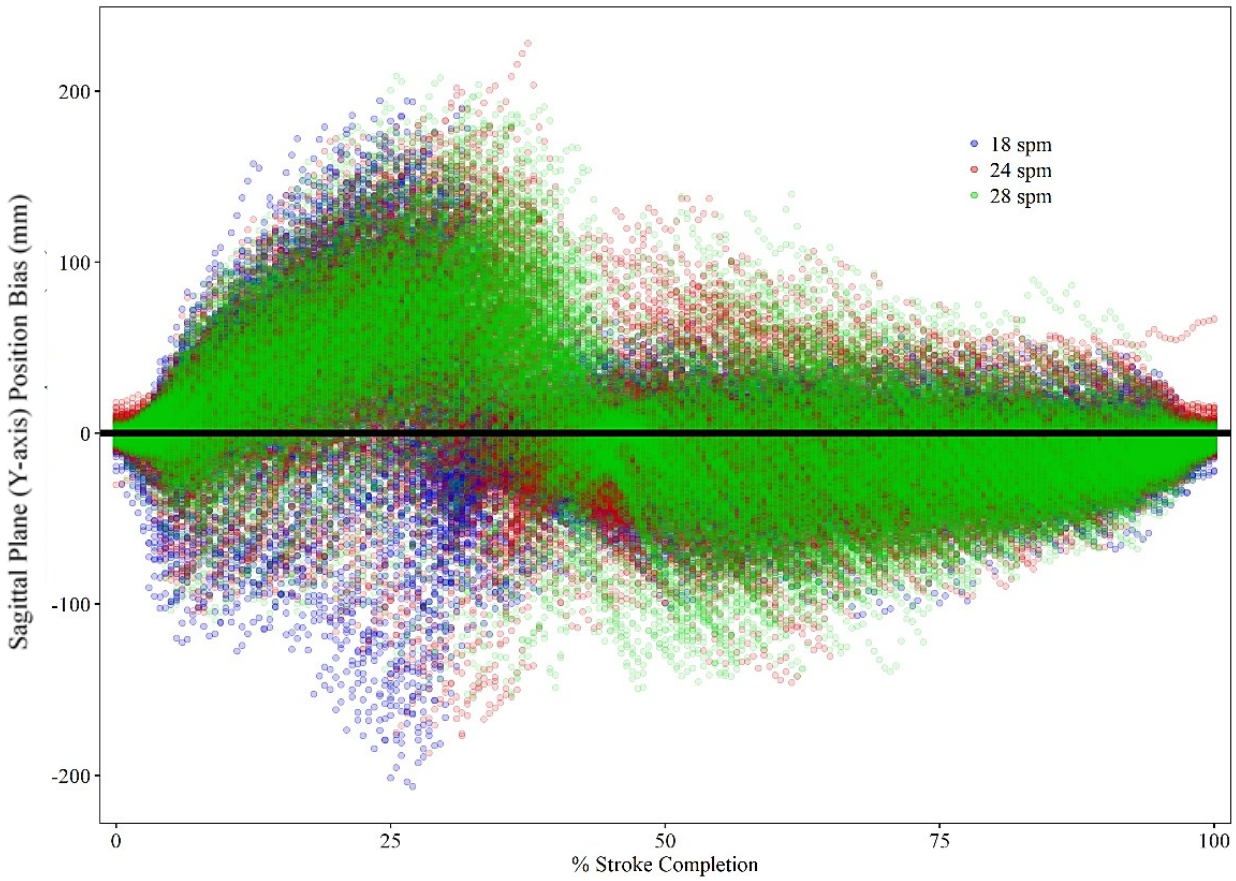

Figure 4.10: Differences in reported anterior-posterior handle sensor position between the optical motion capture (OMC) system and the electromagnetic (EM) systems at all three stroke rates.

During dynamic apparatus tracking, differences in sagittal plane handle displacements recorded by each tracking system were compared to handle position measured directly by the rotary encoder integrated into the ergometer flywheel. No significant difference was found in sagittal plane handle position between OMC and ergometer systems (RMS error = 34.3 mm; $p = 0.93$). However, the EM system showed significant differences in sagittal plane handle position from both the OMC system (RMS error = 137.6 mm; $p < 0.05$) and from the ergometer instrumentation (RMS error = 136.4 mm; $p < 0.05$). This estimated

position difference is clearly visible as a rightward shift in mean displacement for handle and seat trajectories reported by the EM system (Figure 4.11 - *left*). For the handle sensor, the average deviation or time-lag from the ergometer and the OMC system to the EM system was 6.14% of stroke completion. This deviation may be related to the lower frame rate and burst data transmission of the EM system, resulting in a capture latency. The capture latency could be corrected by applying a least squares fitting technique to the EM system data relative to known ergometer output positions, specifically the minimum handle displacement. After latency correction, quality of fit improved substantially with RMS error between the EM system reduced to 25.2 mm with the OMC system, and 34.4 mm with the ergometer (Figure 4.11 - *right*). After latency correction there was no statistical difference in estimated position between the EM and OMC systems ($p = 0.93$), nor the EM system and ergometer ($p = 0.84$).

Bland-Altman analysis was used to examine the average bias, or discrepancy between methods during dynamic apparatus tracking. Uncorrected EM trajectories and those after application of the least-squares minimization technique were compared to low-pass filtered trajectories from the OMC system and from the ergometer. In Bland-Altman analysis, if the average bias between two systems is small and the limits of agreement are narrow, the two tracking methods could be considered essentially equivalent. This was not, however, the case between the OMC and EM systems tested here. Examining sagittal plane handle displacement before capture latency correction, as mean stroke length increases, absolute value of mean bias increases, with a clear cyclic trend throughout the stroke cycle (Figure 4.12). The mean difference in stroke length was 28.1 mm (limits of agreement: -220.3 mm, 276.6 mm) between the OMC and EM systems (OMC-EM), and 31.7 (limits of agreement: -216.7 mm, 279.1 mm) between the ergometer and the EM system (Erg-EM). After correcting for the EM system capture latency, this cyclic trend disappears, variance around the bias line becomes consistently flat and the limits of agreement contract (Figure 4.13).

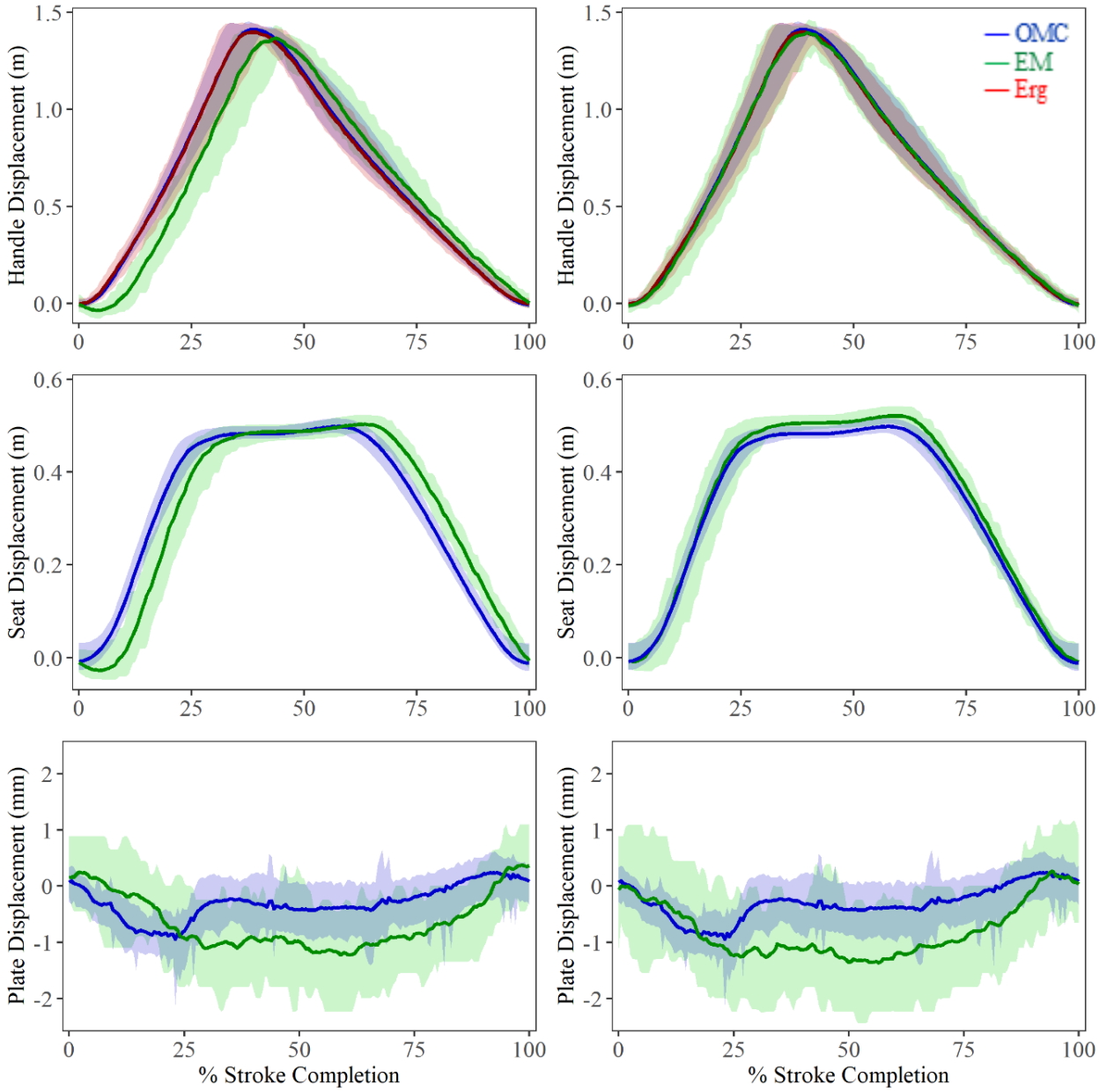

Figure 4.11: Sagittal plane displacements (mean ± 95% CI) for the ergometer (Erg), optical motion capture (OMC) and electromagnetic (EM) systems across all stroke rates. Before correction (*left*), EM system capture latency is visible as a rightward time-shift in mean displacement for handle and seat trajectories. After capture latency correction (*right*) using least-squares fitting, phase differences between systems decreased.

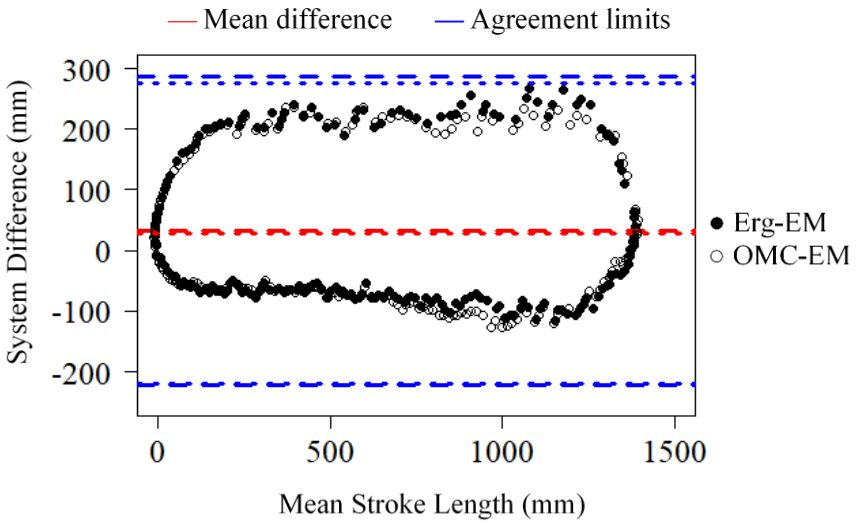

Figure 4.12: Bland-Altman comparison of mean bias and limits of agreement for anterior-posterior handle displacements between optical motion capture (OMC) and electromagnetic (EM) systems (OMC-EM) and the ergometer (Erg) and the EM system (Erg-EM) before capture latency correction during dynamic apparatus tracking.

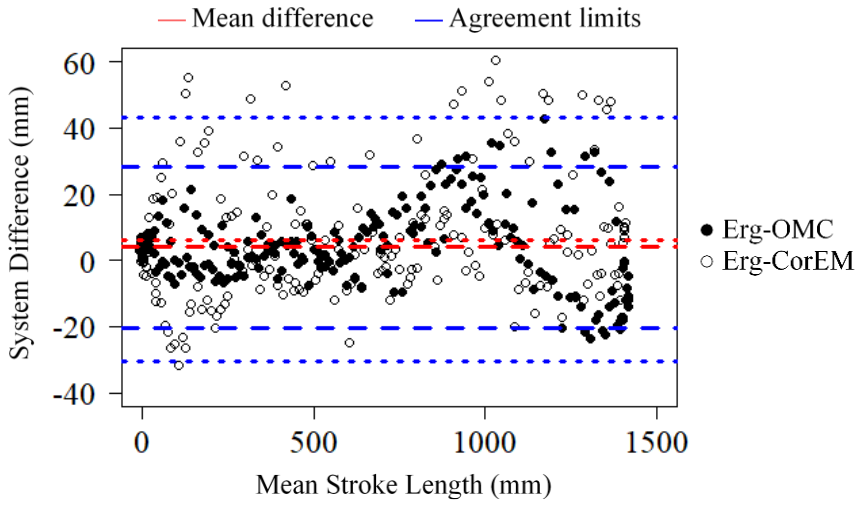

Figure 4.13: Bland-Altman comparison of mean bias and limits of agreement for anterior-posterior handle displacements between the ergometer (Erg) and optical motion capture (OMC) system (Erg-OMC), and between the Erg and EM system after capture latency correction (Erg-CorEM).

Mean bias between the erg and the corrected EM trajectories (Erg-CorEM) were 1.1 mm (limits of agreement: -23.5 mm, 25.5 mm). The mean bias between the OMC and EM systems (OMC-CorEM) was reduced to 2.2 mm (limits of agreement: -27.3 mm, 31.7 mm; Figure 4.14). The corrections brought the EM system in line with differences between the OMC system and ergometer (Erg-OMC) whose mean bias was

-5.19 mm (limits of agreement: -22.3 mm, 11.9 mm). This contraction of limits of agreement can also be seen for A/P seat displacement between OMC and EM systems before (OMC-EM) and after (OMC-CorEM) capture latency correction (Figure 4.15).

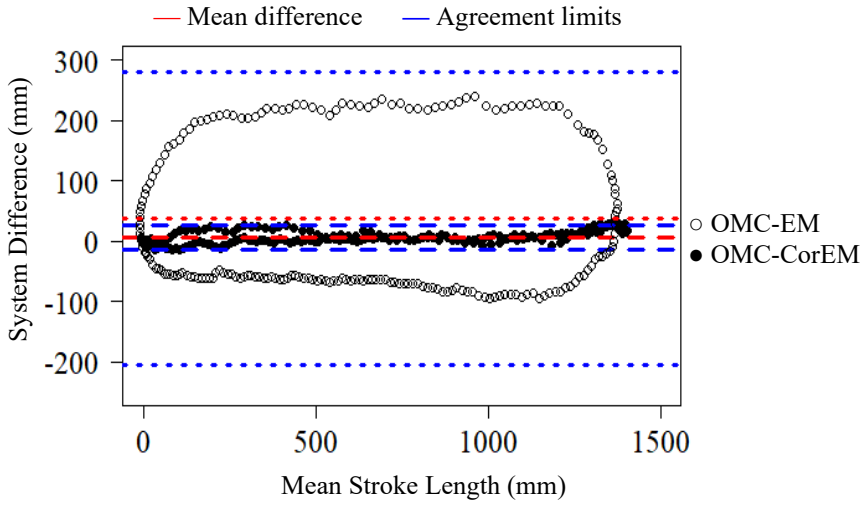

Figure 4.14: Bland-Altman comparison of bias and limits of agreement (mean ± 95% CI) during dynamic apparatus tracking for anterior-posterior handle displacements between optical motion capture (OMC) and electromagnetic (EM) systems before (OMC-EM) and after capture latency correction (OMC-CorEM).

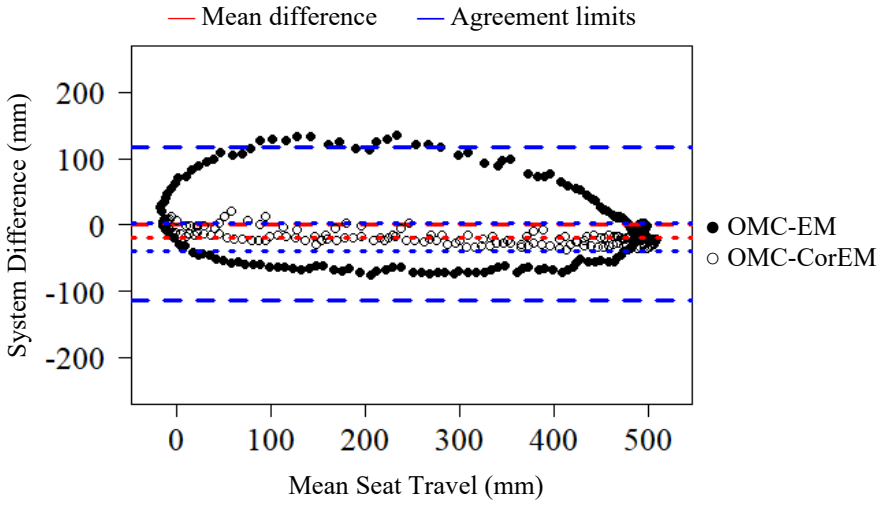

Figure 4.15: Bland-Altman comparison of bias and limits of agreement (mean ± 95% CI) during dynamic apparatus tracking for anterior-posterior seat displacement between optical motion capture (OMC) and electromagnetic (EM) systems before (OMC-EM) and after capture latency correction (OMC-CorEM).

Estimated seat width could be directly compared to the 'known' seat width (315.0 mm; measured by precision tape measure), providing an estimate of system accuracy in the medial/lateral (M/L) direction (Figure 4.16; Figure 4.17). Seat width measured during dynamic apparatus tracking (Figure 4.17) displayed similar results in X-axis position estimation as was seen in static tracking (Figure 4.16). The OMC system slightly overestimated seat width in dynamic trials (316.1 ± 0.3 mm; RMS = 1.16 mm) while the EM system was less consistent during dynamic trials (314.1 ± 2.8 mm; RMS = 2.69 mm). Similar to results seen in static tracking, during the stroke cycle, at slide positions farther from the transmitter, the EM system underestimated seat width near the catch and finish positions (catch: 312.6 ± 0.34 mm, finish: 312.7 ± 0.01 mm), but the EM system overestimated seat width through the middle of the drive and recovery phases (mid-drive: 318.3 ± 0.02 mm; mid-recovery: 317.3 ± 0.02 mm) when the receivers were closer to the transmitter (Figure 4.16; Figure 4.17). This discrepancy in seat width can be predominately attributed to between trial variance in reported position of the left seat sensor, which was much less consistent than the right seat sensor (Figure 4.8).

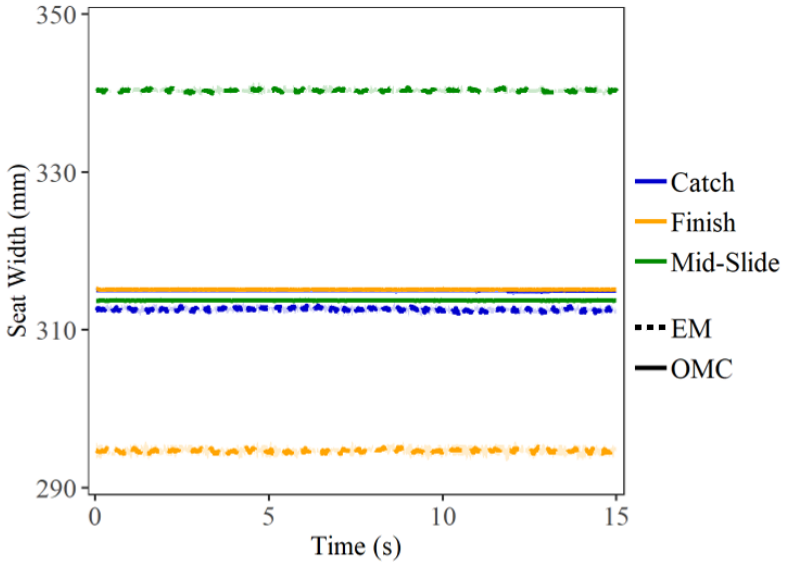

Figure 4.16: Seat width (mean ± std) was calculated as the medial-lateral distance between estimated position of optical motion capture (OMC) and electromagnetic (EM) system sensors fixed to left and right sides of the ergometer seat, during static apparatus tracking.

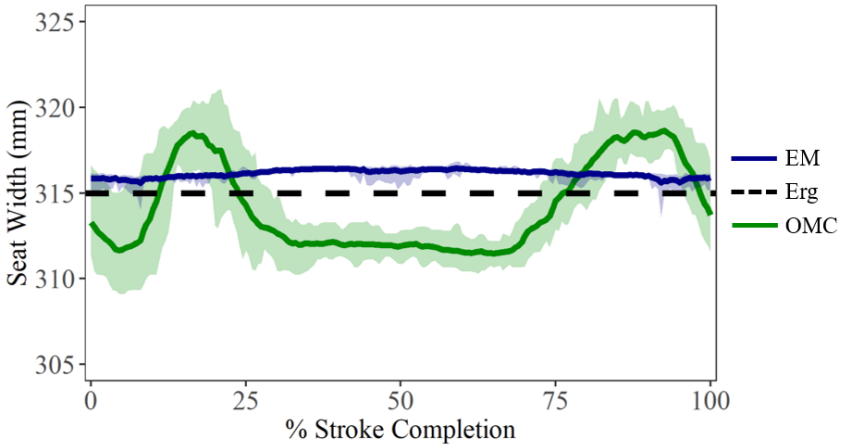

Figure 4.17: Seat width (mean ± std) was calculated as the medial-lateral distance between estimated position of optical motion capture (OMC) and electromagnetic (EM) sensors fixed to left and right sides of the ergometer seat, during dynamic apparatus tracking. Catch occurs at 0% and 100%. Finish occurs at ~40%.

4.3.2 Athlete Tracking: Co-localized Markers and Joint Centre Estimates

Dynamic tracking of athletes during an ergometer rowing step test demonstrated similar data trends to those from the dynamic apparatus tracking results. Initial repeated measures ANOVA statistical analysis compared reported sensor position difference between stroke rates for each system; however, no significant difference was found as stroke rate increased ($p = 0.56$; Figure 4.18). Therefore, data were pooled across all stroke rates to calculate descriptive statistics. Both systems still benefit from low pass filtering to reduce random noise and averaging over all recorded stroke cycles from each subject removes the burst transmission artifacts in the EM system (Figure 4.19).

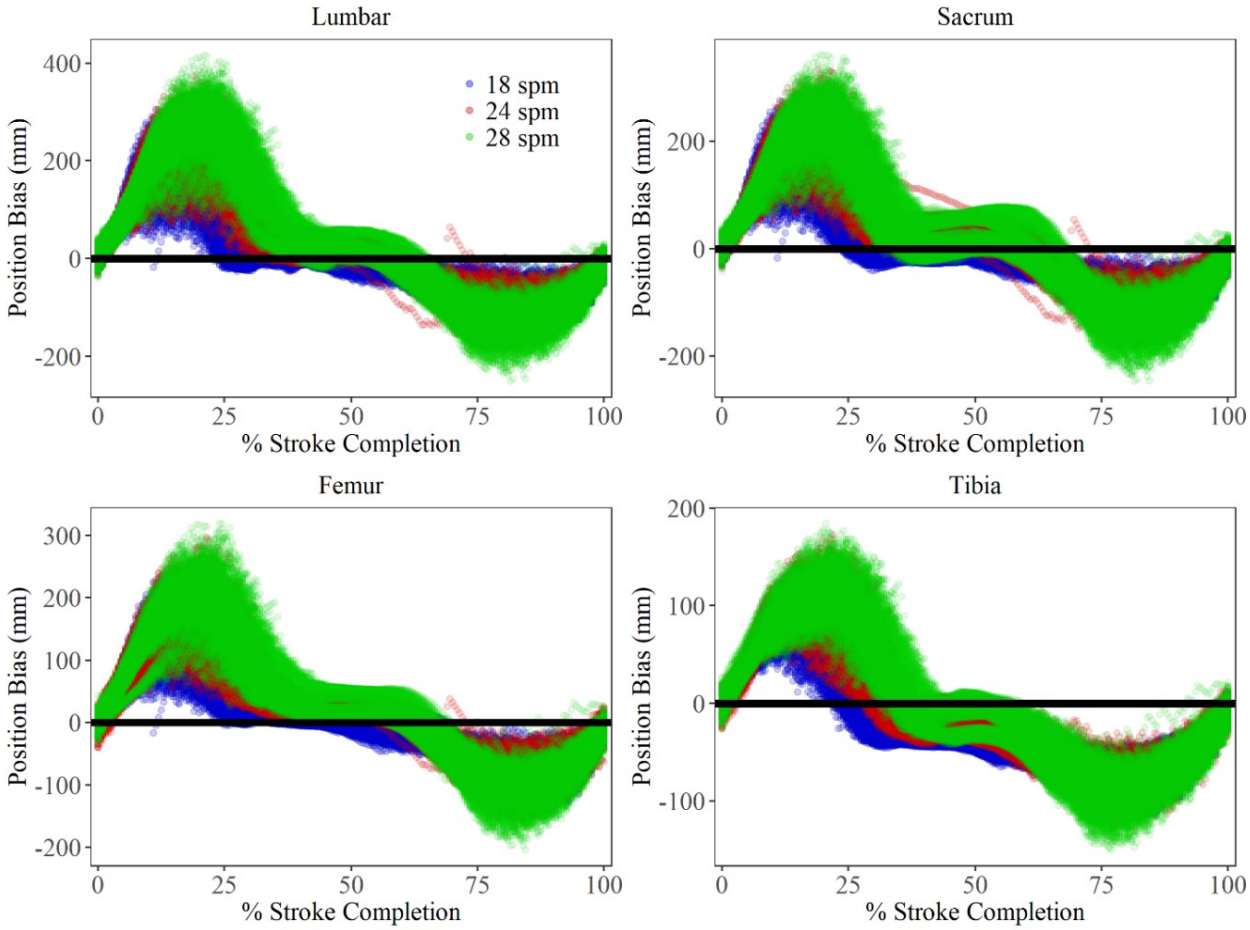

Figure 4.18: Difference in instantaneous position reported by the optical motion capture (OMC) and electromagnetic (EM) systems at all stroke rates before capture latency correction for markers & sensors affixed to the lumbar (*top-left*), sacrum (*top-right*), femur (*bottom-left*), and tibia (*bottom-right*) segments.

During dynamic athlete tracking, differences in sagittal plane sensor position recorded by each tracking system were compared. Significant differences were found between the EM system and the OMC system (Table 4.3; Table 4.4) Unfortunately, because of the limited available EM sensors, no comparison between the EM system and the ergometer stroke length could be made simultaneously. However, the abundance of retroreflective markers did allow for comparison of the OCM system to ergometer stroke length. The estimated position between the OMC and EM systems was visible as a rightward shift in mean displacement for all sensors (Figure 4.20). In the anterior/posterior direction, average deviation, or lag from the OMC system to the EM system was 4.5% before addressing the capture latency issue by applying least squares minimization to the EM system data.

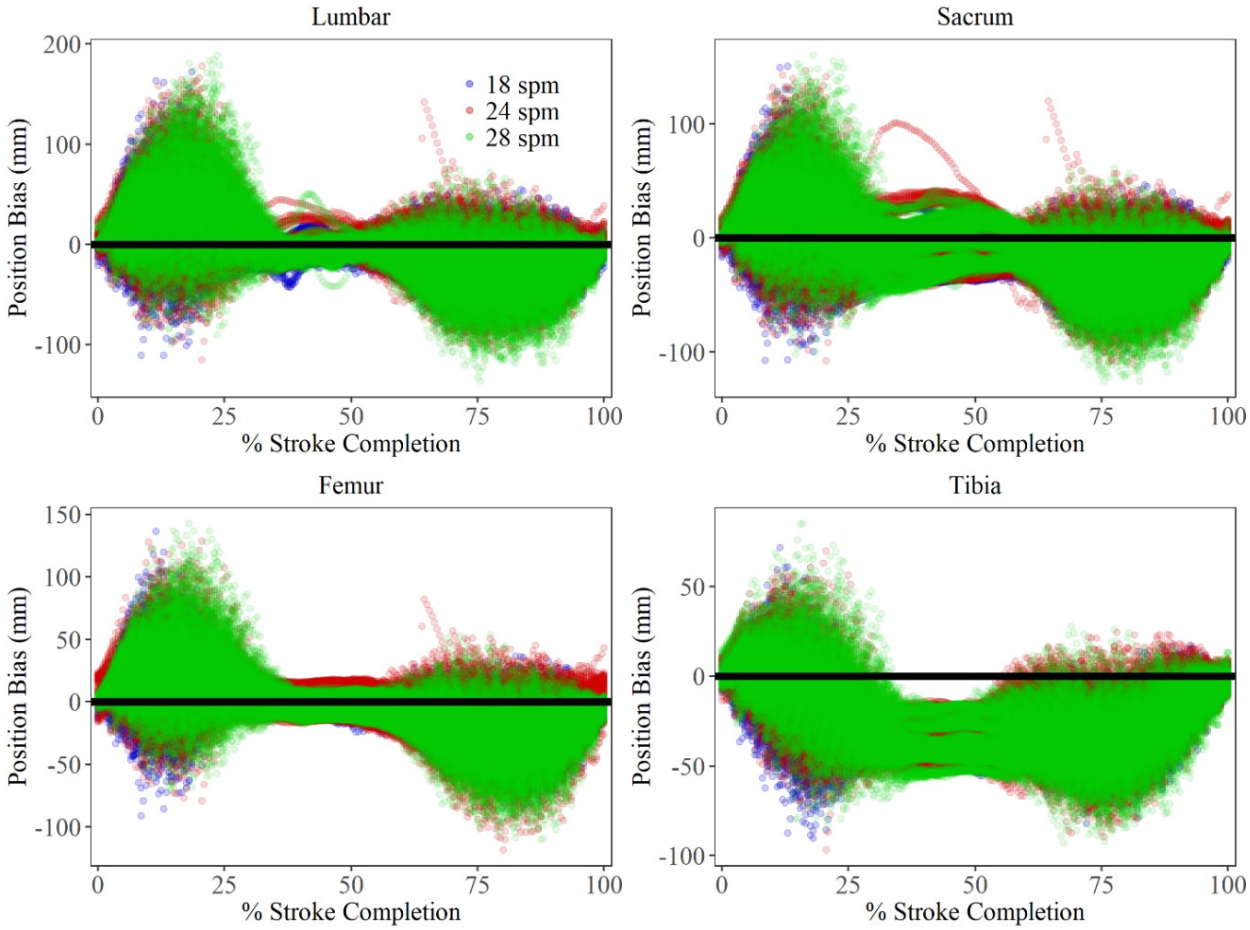

Figure 4.19: Difference in instantaneous position reported by the optical motion capture (OMC) and electromagnetic (EM) systems at all stroke rates after capture latency correction for markers & sensors affixed to the lumbar (*top-left*), sacrum (*top-right*), femur (*bottom-left*), and tibia (*bottom-right*) segments.

For both the EM and OMC systems, three-dimensional co-localized marker/sensor displacements (Figure 4.20) and predicted joint center trajectories (Figure 4.21) were highly correlated, with cross-correlation values from 0.89 - 0.97 (Table 4.3; all p-values > 0.35). However, the EM system capture latency contributed to large RMS errors (Table 4.4). Mean displacements in co-localized markers and joint centers over the entire stroke cycle, with and without phase correction, show similar trends before and after EM capture latency correction with mean trajectories for each tracking system falling within 95% confidence intervals of the other system. (Figure 4.20; Figure 4.21). Agreement between systems in sagittal plane displacements show the most improvement with capture latency correction (Table 4.3; Table 4.4). Only transverse plane hip joint movement and sagittal plane ankle joint movement show large magnitude discrepancies with confidence intervals that do not substantially overlap (Figure 4.21).

Table 4.3: Coefficients of multiple correlation (CMC) in athlete tracking sensor waveform differences between optical motion capture (OMC) and electromagnetic (EM) systems

	Medial/Lateral		Anterior/Posterior		Superior/Inferior	
Sensor Location	**Original**	**Corrected**	**Original**	**Corrected**	**Original**	**Corrected**
Lumbar	0.610	0.607	0.861	0.826	0.944	0.910
Pelvis	0.771	0.759	0.851	0.813	0.937	0.902
Femur	0.829	0.835	0.849	0.815	0.907	0.878
Tibia	0.655	0.583	0.866	0.825	0.915	0.867
Hip	0.613	0.612	0.852	0.808	0.518	0.259
Knee	0.805	0.805	0.853	0.814	0.915	0.880
Ankle	0.698	0.645	0.851	0.756	0.715	0.629

Table 4.4: Root mean square (RMS) error in athlete tracking sensor waveform differences between optical motion capture (OMC) and electromagnetic (EM) systems

	Medial/Lateral		Anterior/Posterior		Superior/Inferior	
Sensor Location	**Original**	**Corrected**	**Original**	**Corrected**	**Original**	**Corrected**
Lumbar	15.13	15.70	110.93	18.17	41.04	28.92
Pelvis	5.88	5.40	95.74	18.15	27.65	20.12
Femur	15.06	16.11	83.00	15.95	30.12	11.68
Tibia	7.30	10.60	54.85	23.53	40.28	37.31
Hip	5.20	5.38	97.19	22.07	32.82	31.42
Knee	7.55	8.51	78.40	40.02	48.41	12.54
Ankle	6.49	4.24	52.90	55.88	14.82	6.73

Rowing is predominately defined by motion in the anterior/posterior direction, with large displacements and smaller relative variance yielding a high signal-to-noise ratio. Mean ranges of sagittal plane hip, knee, and ankle joint displacements during the rowing trials were 623.3 ± 37.7 mm, 502.2 ± 38.1 mm, 19.9 ± 4.5 mm, and 593.3 ± 53.6 mm, for the OMC system and 559.8 ± 48.7 mm, 103.4 ± 11.6 mm for the EM system (Figure 4.21). Sagittal plane displacements show improvement with capture latency correction. Displacement ranges in medial/lateral and superior/inferior directions were smaller with larger relative standard deviations (Figure 4.20; Figure 4.21). Medial/lateral and superior/inferior displacements show greater apparent magnitude differences between systems, but appear to lack a clear, consistent trend in overestimation versus underestimation of one tracking system relative the other. Confidence of

agreement in medial/lateral displacements appears ambiguous due to larger relative standard deviations, particularly at the KJC (Figure 4.21).

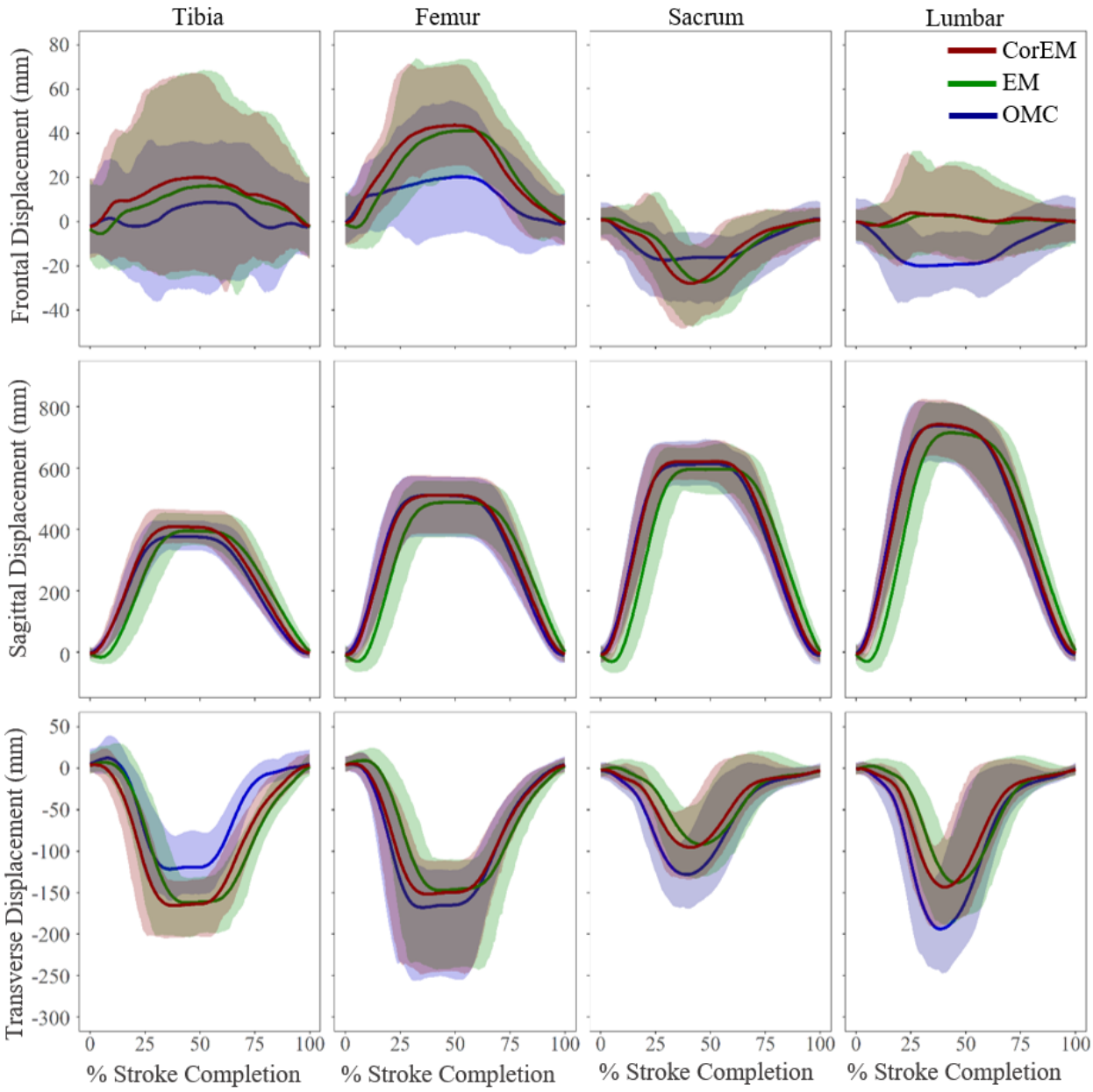

Figure 4.20: Co-localized marker tracking (mean ± 95% CI) in three dimensions with and without phase correction. Bold lines are mean tracked position, shaded ribbons are confidence intervals for the optical motion capture (OMC) system, electromagnetic (EM) system before correction, and the EM system after correction (CorEM).

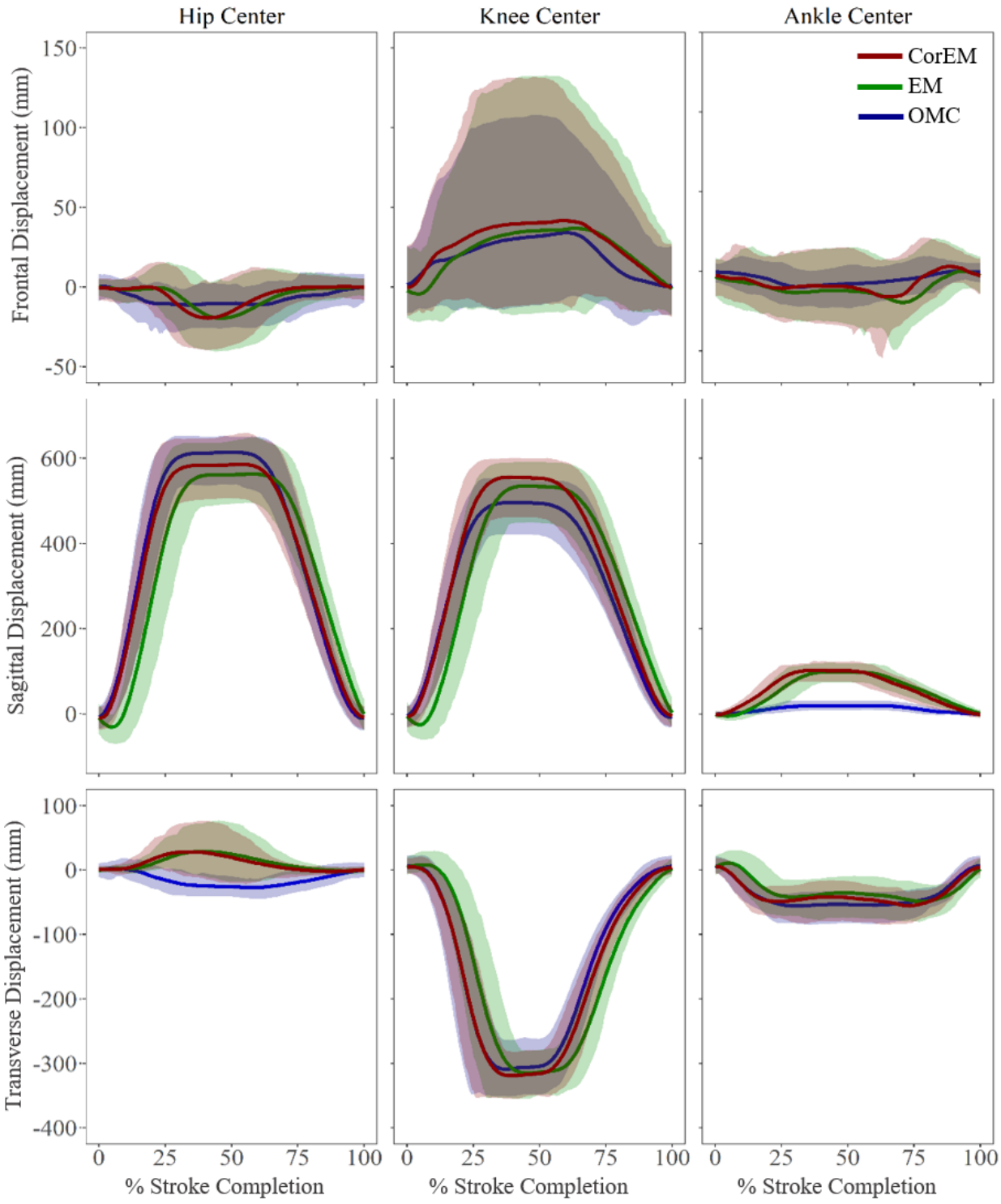

Figure 4.21: Simultaneous joint center position estimates (mean ± 95% CI) between optical motion capture (OMC) and electromagnetic (EM) systems before and after capture latency correction. Bold lines are mean tracked position, shaded ribbons are confidence intervals for the optical motion capture (OMC) system, electromagnetic (EM) system before correction, and the EM system after correction (CorEM).

Quantitative evaluation of the effect of capture latency on estimated position difference using Sprague and Geer's metric is shown in Table 4.5. Geer's metric was able to discriminate magnitude and phase differences between OMC and EM systems, across co-localized marker/sensor displacements and predicted joint center trajectories. Values were highly related in the anterior/posterior direction, while overall agreement was poorest in the medial/lateral direction. Deviations attributed to phase differences were substantially reduced by applying capture latency correction to the EM data and calculated metric values less than 0.3 were considered "good" for most trajectories (Table 4.5 – Phase), with the exception of superior/inferior movement of the HJC, for which Geers metric attributes all deviation to phase effects, despite lag correction. Referring to the hip center transverse displacement graph in Figure 4.19, indeed the OMC and EM system waveforms appear 180º out of phase with each other. The largest deviations were attributed to magnitude differences, which show only mild improvement with capture latency correction. Geer's metric values show good overall agreement in anterior/posterior and superior/inferior directions (Table 4.5 – Magnitude). However, in the medial/lateral direction, hip and ankle magnitudes improve but were still poor overall, while metric values for medial/lateral femur and knee worsen after capture latency correction. Bearing in mind the large confidence intervals present in medial/lateral KJC (Figure 4.21), femur sensor, and tibia sensor (Figure 4.20) motion, it is feasible that some of these deviations may be indistinguishable between systems or due to noise.

Table 4.5: Geer's metric for magnitude and phase differences between optical motion capture (OMC) and electromagnetic (EM) systems. Good < 0.3 (*green*); 0.3 < Moderate < 0.5 (*yellow*); Poor > 0.5 (*red*). Negative metric values indicate an under-prediction of EM displacements relative to OMC. Analytical formulations of Geers metric may be found in Schwer (2007).

	Medial/Lateral		**Anterior/Posterior**		**Superior/Inferior**	
	Magnitude					
	Original	**Corrected**	**Original**	**Corrected**	**Original**	**Corrected**
Lumbar	-0.367	-0.368	-0.040	0.003	-0.300	-0.277
Pelvis	0.266	0.266	-0.027	0.020	-0.307	-0.279
Femur	1.213	1.392	-0.045	0.007	-0.126	-0.095
Tibia	0.221	0.268	0.054	0.100	0.469	0.499
Hip	0.528	0.503	-0.056	-0.009	-0.016	-0.043
Knee	0.253	0.335	0.060	0.108	0.033	0.048
Ankle	1.482	0.998	4.335	4.557	-0.193	-0.065
	Phase					
Lumbar	0.456	0.459	0.070	0.016	0.114	0.034
Pelvis	0.172	0.147	0.071	0.016	0.107	0.039
Femur	0.215	0.172	0.073	0.018	0.090	0.024
Tibia	0.261	0.234	0.068	0.015	0.107	0.065
Hip	0.324	0.315	0.072	0.016	0.748	0.687
Knee	0.172	0.115	0.068	0.016	0.083	0.021
Ankle	0.237	0.227	0.066	0.057	0.123	0.062

Comparing average segmental kinematics through the stroke at each of the three stroke rates, there were minor changes within each system as rate increases; however, all the mean curves fall well within the 95% confidence intervals. While average joint RoM was similar across both systems, the EM system overall has wider variance than the OMC system (Figure 4.22; Figure 4.23; Figure 4.24; Figure 4.25). The EM system displays a wider RoM for all lower limb kinematic angles.

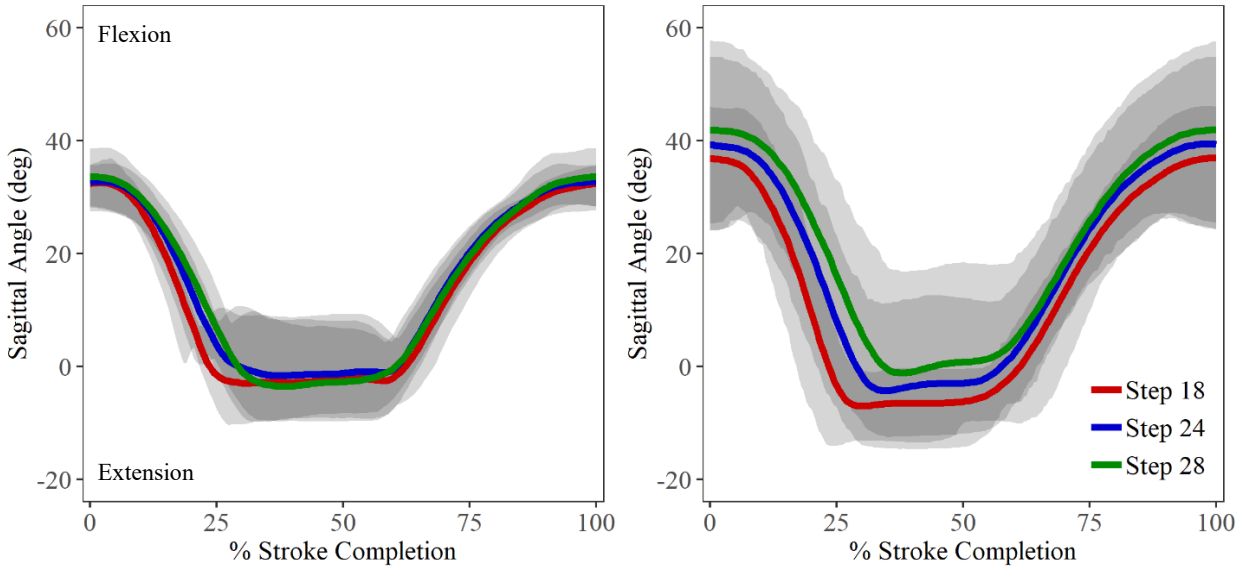

Figure 4.22: Sagittal plane angle (mean ± 95% CI) of the thigh segment above horizontal (0º), calculated in the direction from hip to knee, for optical motion capture (OMC, *left*) and electromagnetic (EM, *right*) systems. Shaded ribbons are confidence intervals for stroke rates 18 spm (*light gray*), 24 spm (*mid gray*), and 28 spm (*dark gray*).

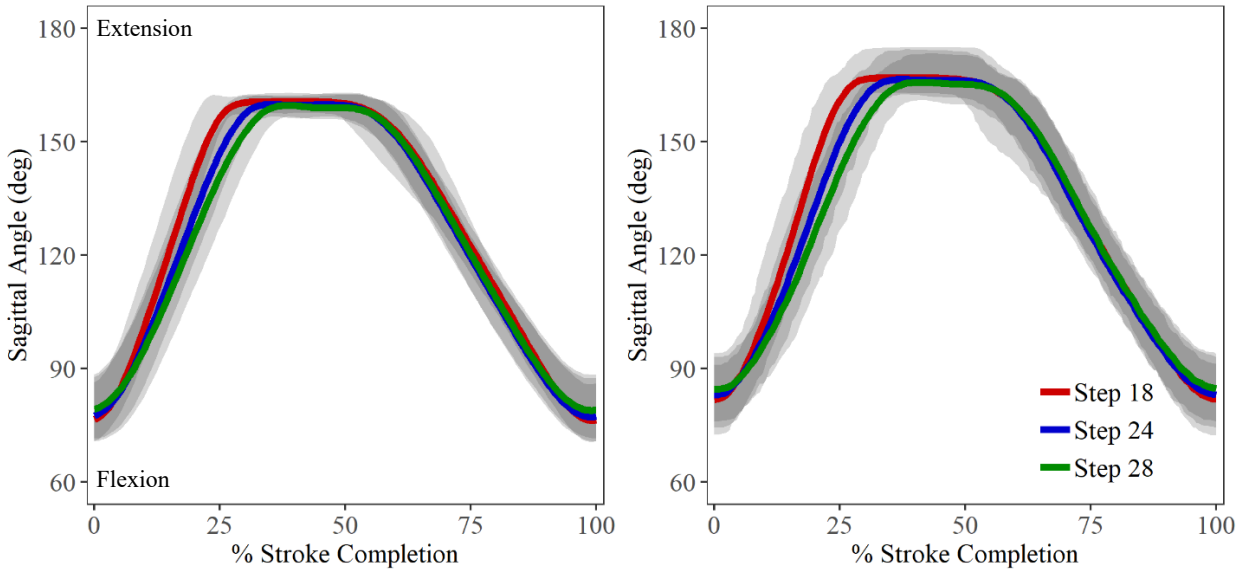

Figure 4.23: Sagittal plane angle (mean ± 95% CI) of the shank segment above horizontal (180º), calculated in the direction from ankle to knee, for optical motion capture (OMC, *left*) and electromagnetic (EM, *right*) systems. Shaded ribbons are confidence intervals for stroke rates 18 spm (*light gray*), 24 spm (*mid gray*), and 28 spm (*dark gray*).

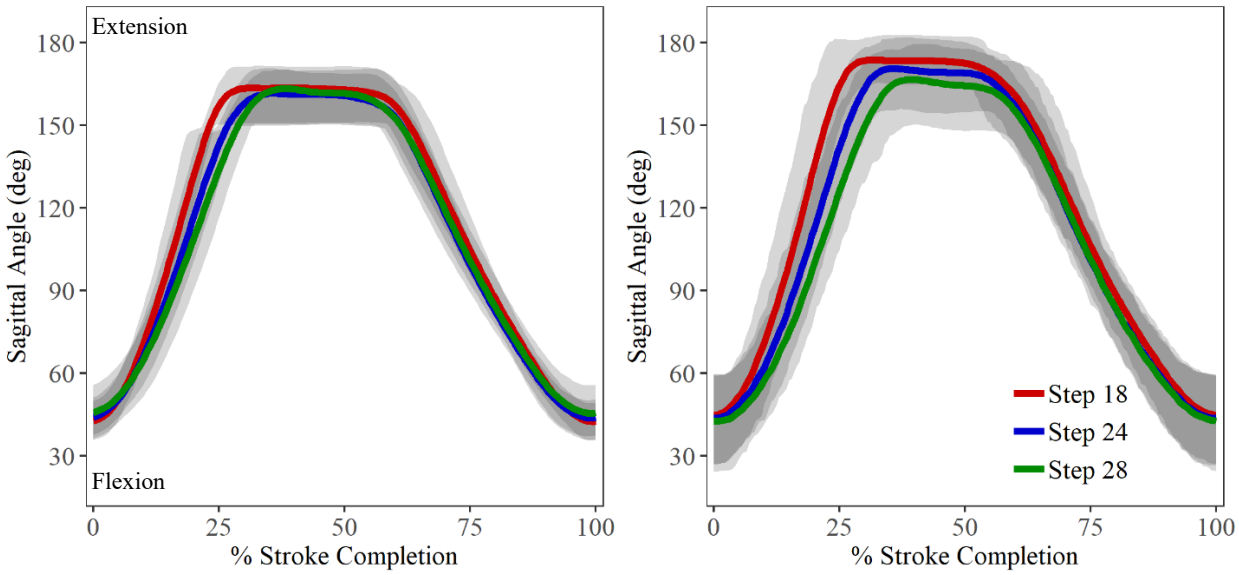

Figure 4.24: Intersegmental knee joint angle (mean ± 95% CI), calculated between the thigh and shank segments for optical motion capture (OMC, *left*) and electromagnetic (EM, *right*) systems. Shaded ribbons are confidence intervals for stroke rates 18 spm (*light gray*), 24 spm (*mid gray*), and 28 spm (*dark gray*).

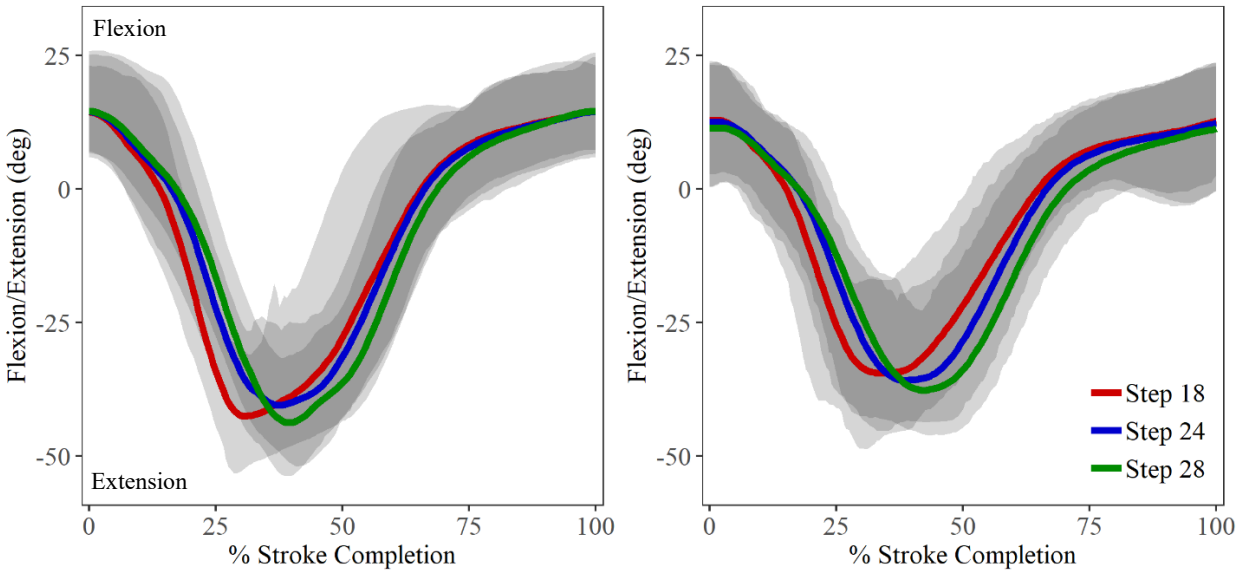

Figure 4.25: Lumbosacral angle (mean ± 95% CI) calculated in the direction from sacrum sensor to lumbar sensor and flexion (+) /extension (-) across vertical (0º) for optical motion capture (OMC, *left*) and electromagnetic (EM, *right*) systems. Shaded ribbons are confidence intervals for stroke rates 18 spm (*light gray*), 24 spm (*mid gray*), and 28 spm (*dark gray*).

Mean ranges of sagittal plane shank, knee, thigh, and lumbosacral joint angles during the rowing trials were: 82.49 º ± 4.76º, 118.79 º ± 7.04 º, 35.72 º ± 4.25 º, 55.78 º ± 7.44 º, for the OMC systems, while EM system joint ranges were: 83.16 º ± 5.82 º, 126.19 º ± 10.58 º, 43.27 º ± 7.49 º, and 66.52 º ± 11.27 º, respectively. At key locations during the stroke, OMC under-estimates EM for lumbosacral flexion at the catch and over-estimates lumbosacral extension at the finish. (Figure 4.25). Athlete foot position was not controlled between trials and unique athlete anthropometry and physiological variability will have influenced movement time, flexion, and extension angles.

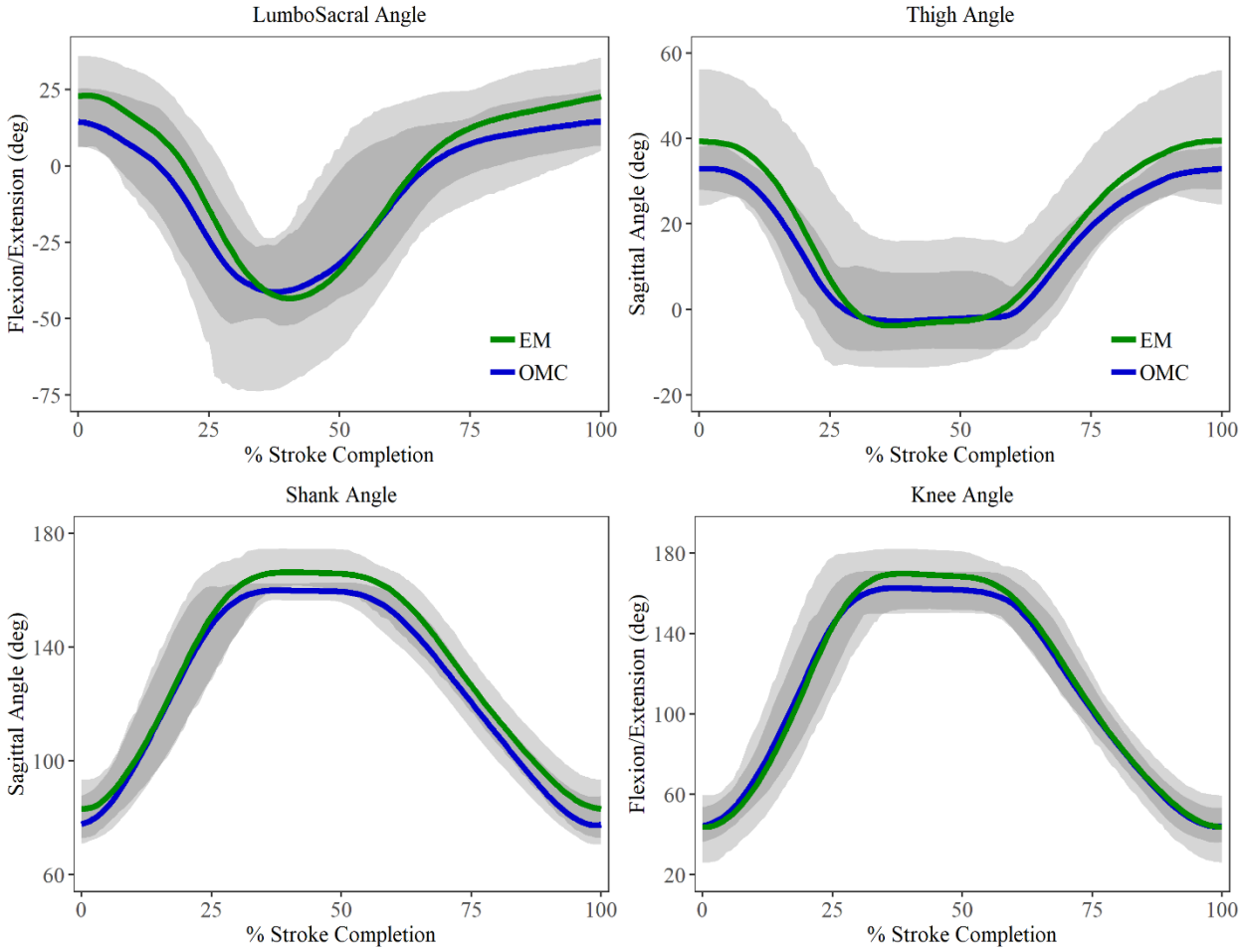

Figure 4.26: Sagittal plane angles (mean ± 95% CI) comparing optical motion capture (OMC) and electromagnetic (EM) systems after pooling data across all stroke rates. Dark gray bands are OMC 95% CI; light gray bands are EM 95% CI.

4.4 DISCUSSION

The first aim of this method comparison study was to assess the accuracy and precision of an OMC system and an EM system to estimate 3D positions during static and dynamic apparatus tracking. The

second aim was to compare the similarity in 3D kinematics derived from data recorded by each of those systems when tracking volunteer athletes performing ergometer rowing.

Assessment of motion capture in the context of rowing kinematics have been previously reported for EM systems (Bull & McGregor, 2000; Ng *et al.*, 2009) and OMC systems (Caplan & Gardner, 2010; Cerne, Kamnik & Munih, 2011) independently. However, studies comparing EM and OMC motion tracking systems have only utilized simple, well-defined movements. These have included applying markers and sensors to an articulated robotic arm which was moved through known ranges of motion at various speeds and the estimated position was compared to the known range (Hassan, Jenkyn & Dunning, 2007; Lugade *et al.*, 2015). The study by Lugade *et al.* (2015) also examined the repeatability of OMC and EM systems using an in-vivo subject model. The authors recorded sagittal hip, knee and ankle joint angles during a sit-to-stand movement and reported both systems as reasonably adequate for tracking dynamic motion. Rowing involves complex, compound motions beyond the scope addressed by either of these method comparison studies. Tracking systems are increasingly utilized for highly sensitive surgical guidance (Glossop, 2009; Koivukangas, Katisko & Koivukangas, 2013) and complicated performance analyses (Pueo & Jimenez-Olmedo, 2017) where accuracy and precision are paramount.

Accuracy in OMC systems is dependent on appropriate positioning of cameras to observe marker movement and on the quality of calibration of the capture volume. The OMC system outperformed the EM system in static apparatus tracking, demonstrating greater precision in reporting 3D positions and greater accuracy in determining distance between two points on a rigid segment, specifically the width of the ergometer seat. Despite operating within the 1.5 m extended range stated by the manufacturer, the accuracy of the EM system was affected by distance between the transmitter and sensors with greater distance increasing error. Position error may have been compounded by the equipment arrangement as the metal ergometer slide rail was located between the transmitter and the left seat sensor. Interference from ferromagnetic materials and electronics in the vicinity of the transmitter may compromise the reliability of generated data as indicated by the significant variability in estimated position found in the current study (Figure 4.9). In a study quantifying EM system accuracy, Ng *et al.*, (2009) noted that of the four sensors employed during their experiments, the sensor located farthest from the transmitter produced the largest angular error, while the sensor closest to the transmitter produced the smallest angular error. This is consistent with results from the current study's variability in reported x-axis position, z-axis position, and ergometer seat width (Figure 4.8; Figure 4.16; Figure 4.17).

A similar magnitude effect was reported by Hassan, Jenkyn & Dunning (2007), where deviations from the known position dictated by the articulated robotic arm occurred mostly at small angles and displacements. The authors concluded that both systems were acceptable for measuring simulated upper

extremity kinematics when appropriate post-hoc filtering was applied, but the authors did not assess repeatability of the tracking systems using an in-vivo subject model. Similar to dynamic tracking results in the current study, Lugade *et al.* (2015) found that compared to known positions, the optical system showed consistent differences across time, but the EM system demonstrated an "inverted U pattern" in the sagittal plane, with the largest position errors at small angles.

In addition to position estimate discrepancies along the x-axis and z-axis apparent during static apparatus tracking, y-axis stroke trajectories showed estimated position differences during dynamic tracking between both systems and compared directly to the known ergometer position. It was postulated that the lower frame rate and the sequential burst transmission of the EM sensors resulted in a substantial capture latency from the ergometer and OMC system to the EM system, visible as a rightward shift in mean displacement for handle and seat trajectories reported by the EM system (Figure 4.11 - *left*). Capture latency in an integrated tracking system potentially impacts any correlations or conclusions drawn from or about kinetic and kinematic relationships during dynamic activities. In the case of rowing, ergometer derived kinetics are linked to kinematic timings of key events throughout the stroke cycle and used as a surrogate for assessing performance metrics. For example, the time from catch to peak handle force generation, the range of thoracic and lumbar spinal motion during that period, and the coincidence of peak handle force with neutral alignment of the spine are all interconnected to evaluate postural control and technique (McGregor *et al.*, 2016).

Similar to results presented in this chapter, issues related to tracking latency and transmission/update rates in EM systems have been previously reported (LaScalza, Arico & Hughes, 2003; Franz *et al.*, 2014), but such results may be less reflective of the performance of newer commercial systems available today. The capture latency could be corrected for by applying a least squares minimization technique to the EM system data relative to known ergometer output positions, specifically the minimum handle displacement. After correction of capture latency in the EM system data, mean sensor positions reported by both systems and the ergometer tended to fall within the 95% confidence interval of each other suggesting that either system is sufficiently accurate when the expected displacements are large, relative to the inherent system noise. Results from the Bland-Altman analysis on dynamic apparatus tracking data show that, before capture latency correction, the limits of agreement were tighter for pure translations of the seat markers and sensors than for handle displacements, but both displayed a similar cyclic trend: as distance from the origin increased, bias increased. During dynamic athlete tracking trials, the limits of agreement between the two systems were even wider and the average bias was sufficient to impact assessing motion in all three directions. Ng *et al.* (2009) did suggest that ergometers modified with non-ferrous components had the potential to work with EM tracking systems for accurate real-time measurements. Fortunately, phage-lag

correction was able to substantially reduce the limits of agreement and the scatter around the average bias line in dynamic apparatus tracking (Figure 4.14; Figure 4.15), but it was not as successful for correcting the athlete tracking data (Figure 4.20).

Both EM and OMC systems demonstrated an ability to adequately track large sagittal plane movements during ergometer rowing, but both systems tended to have greater difficulty accurately tracking smaller movements such as those in the frontal and transverse planes (Figure 4.20; Figure 4.21). The EM system demonstrated greater RMS error in calculating 3D sensor positions, joint center positions, and angles between lower-limb body segments. Similar to Lugade *et al.* (2015) who reported sagittal plane lower limb joint angles during a sit-to-stand activity, finding that OMC had lower RMS errors but higher intra- and inter-day CMC values than EM. When examining compound motions, especially accounting for "off-axis" movements, interactions between segment coordinate systems may contribute to errors in corresponding transformation matrices (Hassan, Jenkyn & Dunning, 2007). Relative error works well for point-to-point comparisons, such as was applicable during static apparatus testing, However, in dynamic testing, time or spatial variation affect system agreement, necessitating a metric that accounts for both the shape of the waveform (magnitude) and time of arrival (phase).

Full validation was beyond the scope of this thesis work, but this study presented verification of a new OMC based tracking methodology for ergometer rowing with respect to an established EM based tracking methodology, which had previously been validated against MRI (Bull *et al.*, 2004). This study represented a prospective performance qualification to ensure the suitability of the OMC system and methodology to reproduce established performance metrics used by athletes and coaches. The tested characteristics of interest for each of the tracking systems, were accuracy and precision with respect to each other (i.e., dynamic apparatus testing and athlete testing), as well as with respect to externally, directly measured positions/locations (i.e., static and dynamic apparatus tracking). A retrospective validation could be carried out as future work, comparing OMC and EM system data against historical data/evidence that are documented/recorded.

Bull & McGregor (2000) demonstrated that the same EM tracking system used here was sufficiently accurate to describe common rowing movement patterns in the sagittal plane. Calculated spinal parameters were used to discern differences in rowing technique and discriminate between qualitatively 'good' and 'bad' rowing technique. Results from the current study appear to support the conclusion that the EM system is capable of discerning salient changes in sagittal plane trajectories (Figure 4.18, Figure 4.19), due to displacements during the rowing stroke being very large along the anterior/posterior axis compared to the resolution of the EM sensors. Comparing kinematics results with previously published EM derived joint angles, Buckeridge (2013) reported a knee joint RoM of 137.2º ± 13.47º which is larger than both the EM

and OMC range of motion found in this chapter. In contrast, the lumbosacral range of motion of 18.80º ± 8.62º (Buckeridge, 2013) and 21.02º ± 10.82º (Murphy, 2009) were each smaller than reported here. This may however be affected by differences in how body angles (i.e., shank, thigh, and lumbosacral) were calculated. Frontal plane and transverse plane displacements during rowing are relatively small and many of the Geer's metric magnitude values calculated here were moderate-to-poor in the medial/lateral direction. Even though Geers metric generates a quantitative value of similarity, the scale by which it is interpreted is not absolute, and Schwer (2007) references only a "rule-of-thumb" guidance. Metric values close to zero indicated excellent agreement between waveforms, less than 0.30 difference was considered good and greater than 0.50 difference was considered poor (Schwer, 2007; Klemt *et al.*, 2019a). Negative metric values indicated an under-prediction of EM displacements relative to OMC.

Given reported difficulties in analyzing small displacements and angular rotations using an EM system (Hassan, Jenkyn & Dunning, 2007), discriminating differences in spinal torsion and lateral bending may not be feasible, and re-examining published spinal flexion/extension values may be useful future research. Measurements obtained from either tracking system can be related provided appropriate scaling and coordinate frames are used. Unlike the current study's use of athletes rowing at different stroke rates to study dynamic tracking, Ng *et al.* (2009) limited their rowing study to mimicking a human spine as a static multi-hinge model being moved with constant stroke rate (22 spm) along an ergometer slide rail. The authors suggested that different velocities might elicit variations in estimated position error. While sequential data transmission of EM sensors could be detrimental to data acquisition of higher speed movements, this does not appear to have affected the current study. Despite stroke rate increasing from 18 spm to 28 spm, this did not translate into changes in mean position differences, nor in the data variance. Increasing stroke rate also did not affect the amount of capture latency, as the percentage capture latency between the EM and OMC systems remained approximately 6% across all stroke rates. In contrast to results in this chapter, Lugade *et al.* (2015) found small increases in OMC and EM system RMS error with increasing angular speed from 30° - 60° for their oscillating articular robotic arm. However, absolute displacements in that study were much smaller than those seen in ergometer rowing.

Results of this experiment may have been affected by potential sources of error, including limitations of accuracy in measurements of known positions. The standard of using a precision tape measure during static apparatus testing was selected because it did not require software processing for interpretation of data, was immediately verifiable and repeatable, and tolerance guidelines for precision tape measures up to 3 m are accurate to ± 0.8 mm. Harmonization of global coordinate frames between tracking systems also presented an opportunity for error propagation as the EM system origin located at the center of the transmitter cube could not be directly measured/markers/digitized. Capture latency correction was

performed on a per participant and per trial basis. Variation in latency across the athlete population was not a characteristic of interest in this study and was not assessed.

Steps were taken to limit possible sources of error for both systems, including adhering to the established EM system laboratory optimization (Murphy, Bull & McGregor, 2011). To minimize the effect of variance in calibration of the optical system in athlete tracking trials, digitization and marker placement were performed by a single operator, an experienced sports bio-mechanist with training in landmark palpation, skin marker placement and extensive experience with the methods used in the current protocol. An abundance of soft tissue along the thigh could affect the position of this sensor/marker during strenuous movement, but this was not assessed during the current study. Qualitatively, the EM system benefits from not requiring a line of sight between transmitter and sensors, meaning that the sensors can be tucked inside form fitting clothing (i.e., spandex shorts commonly worn by rowers). Optical tracking of OMC markers placed on the lower back at the lumbar and sacral level were prone to visual obstruction from the cameras by the athlete's body or clothes before and after the finish position. This may be rectified in post-processing by utilizing in-built OMC software "gap-filing" techniques, however it is best to mitigate the need for such processing tools by appropriately placing the OMC cameras to sufficiently cover the entirety of the capture volume. In ergometer rowing, this specifically involved ensuring that a pair of cameras were angled upward from the floor to ensure capture of lower back markers potentially hidden from high tripod or wall mounted cameras angled downward. Having to utilize gap-filling tools to overcome dropped frames may affect the reliability of kinematics generated from the optical system.

The kinematics of each limb segment were determined via local coordinate frames. As the interest in this study was in direct comparisons between OMC marker and EM sensor positions, the minimum necessary marker sets dictated simultaneous tracking of important identified anatomical landmarks (Table 4.2). However, the method for the OMC system used markers placed on the landmarks, while the EM systems digitized each of those same landmarks. The EM system stored digitized landmark positions relative to each of the four sensors attached mid-way along each of the athlete's limb segments. If possible, OMC system technical clusters would also have been attached; however, practical limitations related to available physical space on the athlete's body made attachment of both EM system sensors and OMC cluster plates infeasible.

All skin mounted marker methods suffer from inaccuracies related to soft tissue artifacts, which result from skin and muscle deformations during limb movement. Relative movement between the markers and the underlying bone may lead to overestimation or underestimation of actual segment movement (Meskers *et al.*, 1998; Karduna *et al.*, 2001). Such errors depend on the individual anthropometry, marker locations, and the type of activity being performed (Leardini *et al.*, 2005). Published literature suggest soft tissue

artifacts in the lower limb are dependent on the load applied and direct measurement of anatomical landmarks are more susceptible to motion artifact than when using technical clusters (Cappozzo *et al.*, 2005; Peters *et al.*, 2010; Lempereur *et al.*, 2014). Reported translational error ranged from 0.1-14 mm and rotational error ranged from 0.3-10° in the tibia. Translational error ranged from 22–31 mm and rotational error ranged from 12–15° in the thigh (Stagni *et al.*, 2005; Peters *et al.*, 2010; Garling *et al.*, 2007). Error magnitudes that may have varied across athletes due to differences in height and mass represent a limitation to drawing broad conclusions about more detailed measures of body segment kinematics. Future work may be required to measure skin motion artifact against medical imaging modalities (e.g., MRI); however, this kind of validation was outside the scope of the work in this thesis.

Improvements in speed and consistency of data acquisition justify transitioning to an OMC system. However, caution is warranted when analyzing small displacements and angles, as both systems had difficulty tracking narrower ranges in medial/lateral and superior/inferior directions and tended to have larger percent deviation. OMC was more sensitive to small perturbations in marker position, thus prone to noise effects, and lower update rates and resolution makes EM less sensitive to true shifts. Nevertheless, measurements obtained from either system can be related provided appropriate scaling and coordinate frames are used. This compatibility facilitates interpretation of current and future OMC data in relation to EM measures and helps ensure continuity of athlete training progression.

4.5 CONCLUDING REMARKS

This chapter specifically compared the dynamic accuracy and precision of EM and OMC displacements in three dimensions during ergometer rowing by simultaneously measuring by an extended-range EM system (Flock of Birds) and an OMC system (Vicon) in a gait analysis laboratory. While both EM and OMC systems demonstrated an ability to adequately track large dynamic compound movements in the sagittal plane during ergometer rowing, both systems struggled at times to precisely track small displacements and narrow angular ranges in medial/lateral and superior/inferior directions. It was demonstrated that a new OMC based tracking methodology could obtain equivalence with the previously validated EM system, in relation to spine and lower limb metrics. Improvements found in speed and consistency of data acquisition with the OMC system over the EM system are beneficial for dynamic human motion studies and justified further use of OMC in this thesis by expanding capture capabilities with MSK model implementation, and without losing the ability to compare to prior work from the group.

The remainder of this thesis will encompass methods and results derived from independent use of the Vicon OMC system during ergometer rowing. Chapter 5 specifically details the experimental

methodology applied to the robust data acquisition, processing, and analysis techniques for this full body dynamic rowing movement.

5. CHAPTER 5: SPATIO-TEMPORAL ANALYSIS OF ERGOMETER ROWING KINETICS AND KINEMATICS

In Chapter 4, a method-comparison study examined consistency and accuracy of kinematic measurements between tracking systems during ergometer rowing. It was shown that an OMC system methodology was sufficiently accurate and precise compared with a previously validated EM system to track lower body dynamics during ergometer rowing in the sagittal plane. Improvements in speed and consistency of data acquisition with the OMC system justified further use of OMC in this thesis by expanding capture capabilities with MSK model implementation.

The goal of this chapter is to implement the selected OMC methodology in whole body dynamic tracking of ergometer rowing for performance analysis and biomechanical feedback. This chapter describes the materials and methodology used for the main experimental study. This includes the marker model used to capture full body kinematics of rowers, a description of the motion capture process, and the details of the instrumented ergometer used to acquire external kinetics. Ergometer derived kinetic and kinematic results are presented in this chapter, prior to analysis of athlete kinematics and model derived biomechanics in subsequent chapters.

5.1 KINETIC & KINEMATIC INVESTIGATIONS OF THE ROWING STROKE

An important consideration in rowing biomechanics is examining the way in which an athlete moves, to ascertain the quality of their technique. Aspects of rowing technique can be described through kinematic and kinetic measurements. Kinematics describes the motion of rigid bodies with respect to time, without consideration of the forces and moments associated with that motion. Kinetics is the study of the forces and torques acting on, and generated by, the body internally and externally. As previously discussed in the Chapter 3 literature review (Section 3.5.1), assessment in a laboratory using an ergometer provides a repeatable method of measuring rowing performance parameters and technique in a closed, controlled environment.

Alongside the motion tracking analysis tools detailed in Chapter 3, Section 3.5.2, kinetic data derived from instrumented ergometers can generate information such as force-time profiles to identify specific components of a rower's biomechanics, with a view to enhancing performance. Performance variables can be analyzed with respect to power, smoothness and consistency (Smith & Spinks, 1995). Spatio-temporal analysis is a versatile tool to break down complex motion into a sequence of phases and sub-phases. The drive and recovery phases in the rowing stroke each have clearly defined biomechanical functions and

boundaries. Each of these phases may be additionally subdivided based on easily identified events, termed key moments or key events in this thesis.

Experimental methodologies on indoor ergometer rowing may be simple, or complex combinations of three dimensional angles, positions, orientations, magnitude, and center of pressure (CoP). Murphy (2009) parameterized variables most useful in predicting rowing performance and discrete aspects of technique that could affect these variables. The most salient features, indicative of high performance, were rapid handle force production, maintained seat suspension (SS), and larger drive-to-recovery ratios. Murphy (2009) previously showed that rowers exhibit asymmetrical CoP motion on the ergometer seat and Buckeridge (2013) found CoP asymmetry on the foot plate as well.

Practical real-time feedback has been provided to coaches, trainers, and athletes in the form of graphical representations of force and body position during the stroke when monitored on an ergometer (Smith & Loschner, 2002; McGregor *et al.*, 2016). The force developed and stroke timing have been regarded as key aspects in unique individual stroke profiles (Wing & Woodburn, 1995), and Smith & Spinks, (1995) suggested that rowers of different standards can be distinguished by certain encompassing characteristics which can aid coaches in assessing a rower's strengths and weaknesses, and in improving an individual's training.

In order to achieve the main thesis aims of developing a kinematic and kinetic description of upper body technique in ergometer rowing, and reporting parameter influence in the context of performance and injury, the objectives of this chapter were to (1) describe in detail the experimental methodology employed during the primary series of athlete performance assessment and data collection, (2) perform a spatio-temporal analysis of ergometer derived kinematic and force data, and (3) generate a comprehensive biomechanics feedback mechanism for athletes and coaches.

5.2 MATERIALS & METHODOLOGY

This study was designed to collect full body kinematics from rowers using an indoor ergometer with an optical motion tracking system. Ethical approval for all phases of the work was obtained from the Imperial College Research Joint Research Compliance Office (JRCO) (Appendix A: Ethics Approval Documentation). All research staff associated with the project partook in laboratory safety inductions to ensure competence in the use of the laboratory equipment.

5.2.1 Participant Recruitment

A total of forty-nine healthy male and female rowers between the ages of 18 and 45 were recruited from the local rowing community with a focus on boat clubs based along the Thames River in London.

Recruitment was predominantly via poster, social media, and email. Inclusion and exclusion criteria are reported in Table 5.1. Prior to participation in the study, all volunteers were required to read a participant information sheet provided and sign a consent form (Appendix A: Ethics Approval Documentation).

Table 5.1: Inclusion and Exclusion criteria for rowing study

Inclusion Criteria	Exclusion Criteria
• Healthy male and female volunteers aged 18 – 45 years. • Minimum rowing experience of two years. • No history of surgical intervention, which may limit mobility. • In fit physical condition – no injuries in the past six months and able to complete a 12-minute step test.	• Current episode of lower back pain or any other serious illnesses or injuries. • Any history of severe mobility-limiting pathologies. • Any history of surgical intervention on any joint of the upper limb that limits mobility. • Any known allergy to adhesives. • Unable to speak or read English at a sufficient level to give informed consent. • Suffers from a psychiatric illness that limits informed consent. • Any systemic inflammatory, connective tissue disorders or medical disorders that limit exercise. • Known pregnancy.

Once verified against study inclusion/exclusion criteria, volunteers were invited to a ninety-minute assessment session at the Biodynamics Lab at Charing Cross Hospital (Hammersmith, W6 8RF). Participants were asked to bring appropriate attire for rowing on an ergometer (e.g., spandex shorts, sports bra, sneakers, etc.). Consent forms were obtained prior to commencing any data collection or assessment. In addition to the consent form, all participants were asked to fill in a demographics form requesting their height, weight, sex, age, years of experience, training habits, current and historical injuries (Appendix A: Ethics Approval Documentation). Individuals were assigned a specific group classification based on the type of team/squad for which they competed: collegiate rowers for a university, club rowers for a post graduate competitive squad, elite rowers for an officially recognized national team, and masters' rowers for club teams specifically over age 27. Of the recruited participants, 22 were collegiate rowers, 7 were club level rowers, 8 were masters level rowers, and 12 were elite rowers. All athletes were distinguished by preferred rowing modality and sidedness (i.e., port vs. starboard vs. sculling). Aggregate anthropometric data for all participants and athlete cohort classification criteria are reported in Table 5.2.

Table 5.2: Population-wide anthropometric data (mean ± std) and athlete cohort classification data for age, mass, and height, as well as years of experience in rowing.

	Age (years)	Mass (kg)	Height (m)	Years Rowing
Total (n=49)	25.5 ± 6.2	76.0 ± 10.9	179.1 ± 9.5	7.9 ± 6.7
Female (n=32)	25.0 ± 5.7	71.3 ± 7.7	174.7 ± 6.9	7.5 ± 5.8
Male (n=17)	26.5 ± 6.9	85.3 ± 10.3	187.6 ± 7.9	8.6 ± 7.7
Club (n=7)	26.4 ± 2.9	75.9 ± 9.2	182.0 ± 6.1	6.6 ± 3.9
Elite (n=12)	25.8 ± 2.2	78.4 ± 5.5	184.6 ± 6.9	9.4 ± 2.8
Master (n=8)	36.1 ± 6.4	76.4 ± 15.7	172.9 ± 10.6	18.0 ± 7.8
University (n=22)	20.9 ± 1.7	74.0 ± 11.4	177.2 ± 9.4	4.4 ± 2.6
Port (n=16)	25.5 ± 5.8	77.3 ± 13.3	179.7 ± 10.7	6.6 ± 4.0
Starboard (n=23)	24.2 ± 5.4	77.2 ± 9.0	180.6 ± 7.7	6.1 ± 5.2
Sculling (n=10)	30.8 ± 7.3	71.3 ± 9.1	174.4 ± 9.6	13.2 ± 9.0

5.2.2 Equipment and Setup

All kinetic data were collected via custom instrumentation fitted and calibrated to a modified indoor ergometer (Model D, Concept 2, VT, USA) as described in Chapter 4 (Section 4.2.1) and further detailed below (Figure 5.1).

- Four uniaxial load cells (ELPM model, Entran, KY, USA) were mounted under the sliding seat to measure the magnitude of vertical forces and the center of pressure on the seat (Figure 5.1A). Each load cell had a range of 1250 N and the manufacturer's calibration stated a hysteresis and non-linearity of 0.15% each.
- A rotary encoder (ERN120, Heidenhain Ltd., Traunreut, Germany) was fitted to the ergometer flywheel (5000 increments per revolution) to measure stroke length and chain angle above horizontal (Figure 5.1B).
- Underneath each footplate three piezoelectric strain gauges (Micro-measurements, Vishay, NC, USA) were fitted to measure horizontal and vertical pushing forces and longitudinal center of pressure (Figure 5.1C).

- A uniaxial load cell (ELHS model, Entran, KY, USA) was fitted in line with the ergometer handle and chain (2.5 kN range, 0.5% combined non-linearity and hysteresis) to measure pulling force (Figure 5.1D).

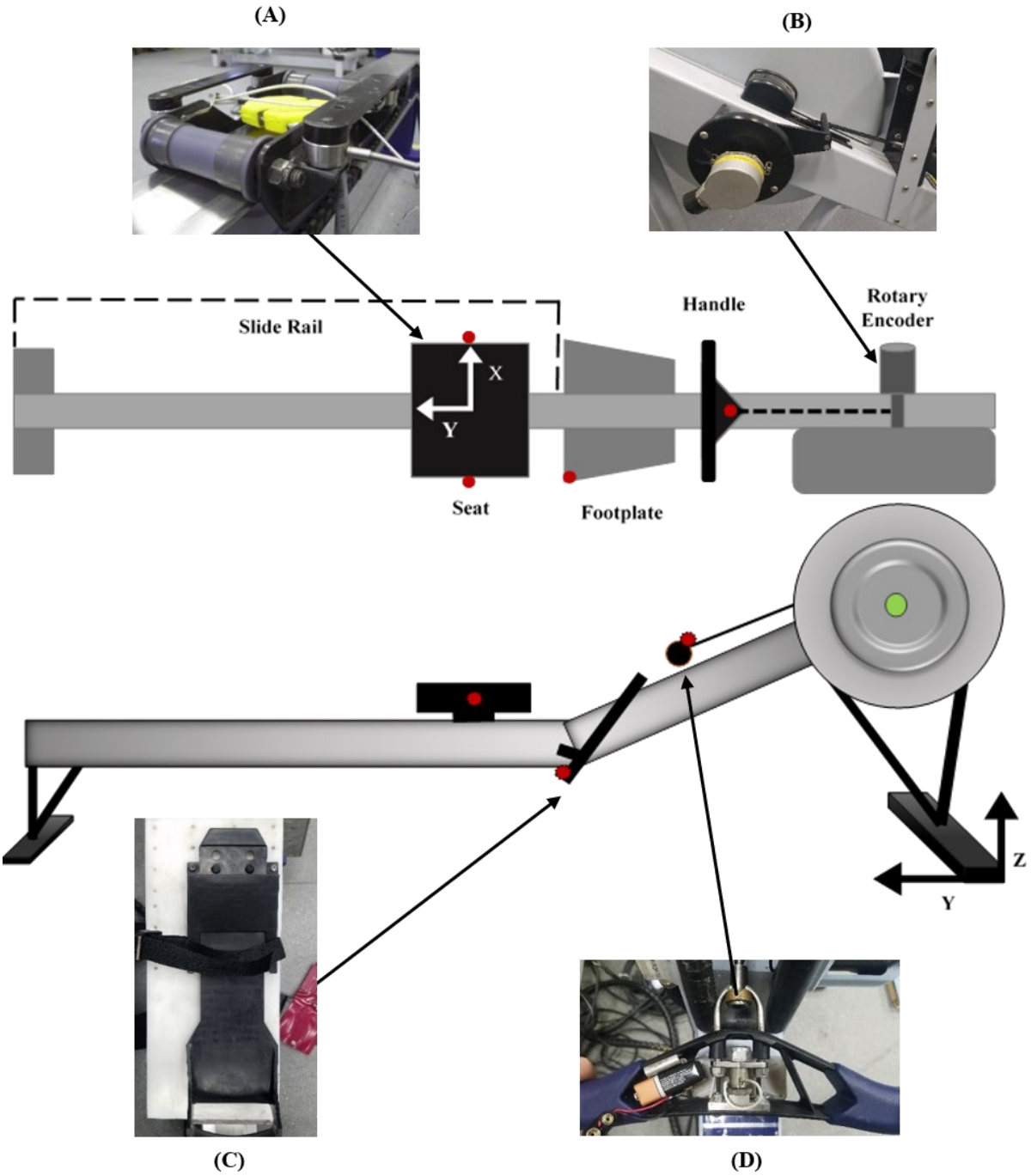

Figure 5.1: Ergometer schematic and instrumentation: (A) under seat mounted uniaxial load cells, (B) flywheel mounted rotary encoder, (C) footplate modified with longitudinal and perpendicular oriented strain gauges, (D) handle mounted uniaxial load cell.

The instrumented rowing machine was connected to a PC through a multi-channel signal conditioning unit (cDAQ-9178, National Instruments, TX, USA) and all data acquisition signals were recorded at 1000 Hz and synchronized through bespoke software (Figure 5.2, LabVIEW 2016, National Instruments, TX, USA).

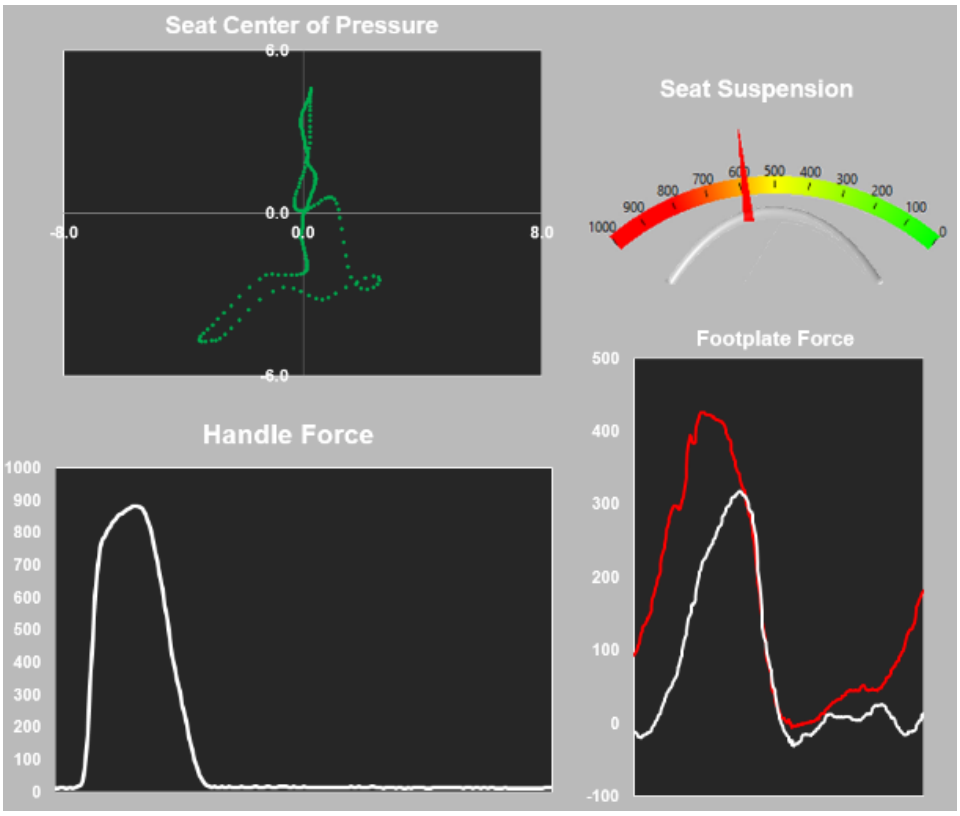

Figure 5.2: Custom LabVIEW 2016 (National Instruments, TX USA) real-time data acquisition software interface showing representative kinetic data from a single stroke cycle. Clockwise from top left: green trajectory indicates seat center of pressure (*top-left*); suspension reported as instantaneous total vertical seat force in Newtons (*top-right*); vertical (*red line*) and horizontal (*white line*) footplate force under right foot in Newtons (*bottom-right*); handle chain tension in Newtons (*bottom-left*).

Kinematic data were captured using a ten-camera optical motion tracking system (Vicon MX-T series, Oxford, UK) recording at an acquisition rate of 100 Hz. The ten cameras were arranged around the Biodynamics lab space (Figure 5.3) for capturing full body kinematics while minimizing marker occlusion. The instrumented ergometer was placed at the center of the capture volume (15 m^2) with the long axis of the slide rail aligned to +Y direction. The OMC system was calibrated prior to each testing session, according to Vicon reference guidelines (Vicon Motion Systems Limited, 2015), ensuring a camera-marker accuracy of better than 0.30 mm was always obtained. Some trials were recorded via digital video camera for reference purposes upon participant's permission. Vicon Nexus 2.7 software (Vicon, Oxford, UK) was

used to reconstruct and post-process marker trajectories, including labelling and gap filling. During gap filling, rigid body or pattern matching methods were predominately used. In the case where there was a significant gap (more than 20 frames), visual checks were done to ensure that the occluded marker predicted trajectory followed the expected path of motion. All data were exported, post-processed, and analyzed using custom MATLAB scripts (MATLAB R2017B, Math Works, Natick, MA, USA) (Appendix B: MATLAB Code for Motion Capture Kinematics & Ergometer Kinetics Data Processing).

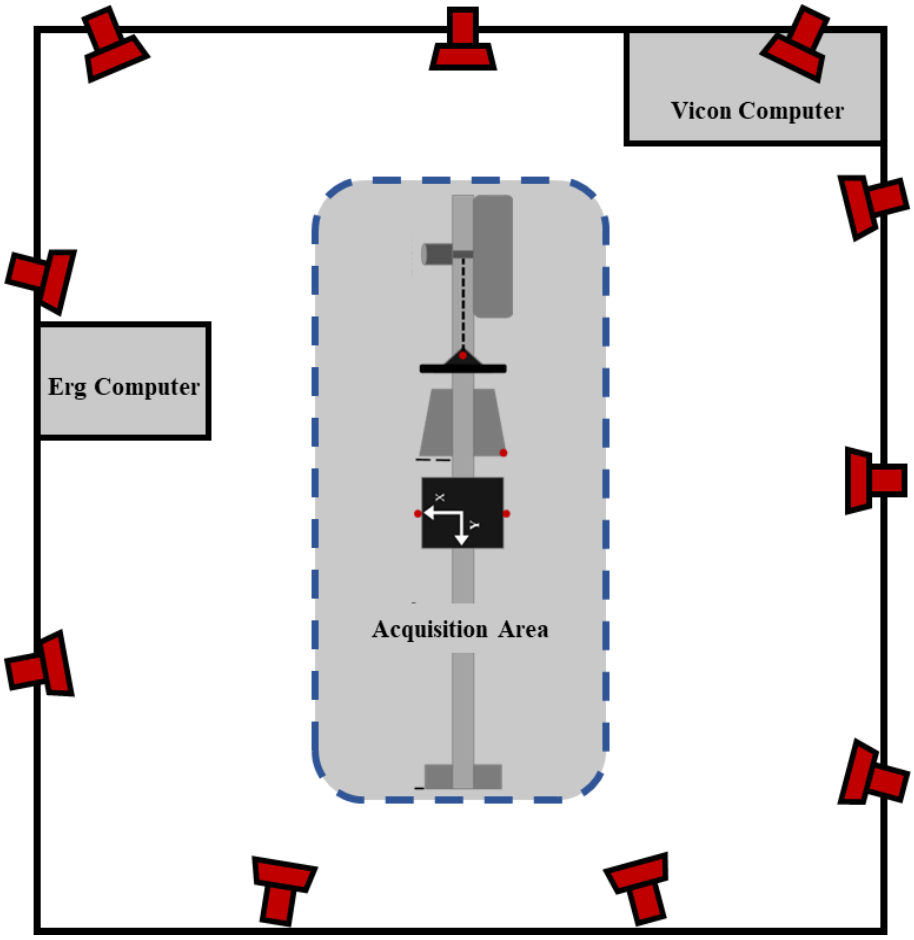

Figure 5.3: Schematic top-down view of Biodynamics laboratory arrangement with modified ergometer at the center of acquisition area, surrounded by ten Vicon MX-T infrared cameras and computer systems.

Figure 5.4: Biodynamics laboratory with modified ergometer at the center of the room surrounded by ten Vicon MX-T infrared cameras.

To track the athlete's lower limbs, upper limbs, spine and shoulder, a total of ninety-five 14mm reflective markers were affixed in clusters and on anatomical landmarks (Table 5.3). On the axial skeleton, markers were placed on the left and right acromion processes, clavicles, jugular notch (MA), Manubrial-sternal junction, and xiphoid process (XI). Six markers were placed on the pelvis at the left and right iliac crests, posterior superior iliac spines, and anterior superior iliac spines. The spine was defined with single markers on C7, T6, T12, and L5, as well as horizontal 3-marker clusters at the vertebral levels of T1, T7, L1, and a T-shaped cluster at S1 (Figure 5.5). On the appendicular skeleton, all markers were placed bilaterally. On the upper extremities, markers were placed on the medial and lateral epicondyles, radial and ulnar styloid processes, and 1st and 5th metacarpophalangeal joints (Table 5.3). Clusters of four markers, fixed to rigid nylon plates were attached along the middle of the humerus and the forearm (Figure 5.6). On the lower extremities, markers were placed on the calcaneus, medial and lateral condyles, malleoli, and 2nd and 5th metatarsophalangeal joints (Figure 5.5), with an additional set of rigid nylon cluster plates attached along the middle of the thigh and shank (Figure 5.6). A specially designed 3-marker scapula tracker was placed along the scapular spine. (Figure 5.7; Prinold, 2012). To track movement of the ergometer, single markers were placed at the center of the handle, and to the left and right sides of the ergometer seat.

Table 5.3: Athlete markered anatomical landmarks and cluster locations with number of markers per cluster (#).

SEGMENT	CLUSTER LOCATION	MARKER	MARKER LOCATION
Hand	--	MC1	2nd metacarpal tuberosity
(both)		MC5	5th metacarpal tuberosity
Forearm	On ulna bone (4)	USP	Ulnar styloid process
(both)		RSP	Radial styloid process
Upper Arm	On humerus bone (4)	HLE	Lateral humeral epicondyle
(both)		HME	Medial humeral epicondyle
Scapula	Scapular Tracker (3)	-	Left & Right scapular spine
(both)		LAC	Left acromioclavicular joint
		RAC	Right acromioclavicular joint
Chest	--	MA	Jugular notch
		STRN	Manubrial-sternal junction
		XI	Xiphoid process
		LCLAV	Left sternoclavicular joint
		RCLAV	Right sternoclavicular joint
Cervical Spine	--	C7	C7 spinous process
Upper Thoracic Spine	T1 (3)	-	T1 spinous process cluster
		T6	T6 spinous process
Lower Thoracic Spine	T7 (3)	-	T7 spinous process cluster
		T12	T12 spinous process
Lumbar Spine	L1 (3)	-	L1 spinous process cluster
		L5	L5 spinous process
Pelvis	S1 (3)		S1 pelvis cluster
		RASIS	Right anterior-superior iliac spine
		LASIS	Left anterior-superior iliac spine
		RICT	Right iliac crest
		LICT	Left iliac crest
		RPSIS	Right posterior- superior iliac spine
		LPSIS	Left posterior- superior iliac spine
Thigh	On lateral thigh (4)	-	
(both)		FLE	Lateral femoral epicondyle
		FME	Medial femoral epicondyle
Calf	On tibia bone (4)	-	
(both)		FM	Fibula malleolus
		TM	Tibia malleolus
Foot	--	CC	Calcaneus
(both)		MTF	Top of midfoot
		MT1	1st metatarsal tuberosity
		MT5	5th metatarsal tuberosity

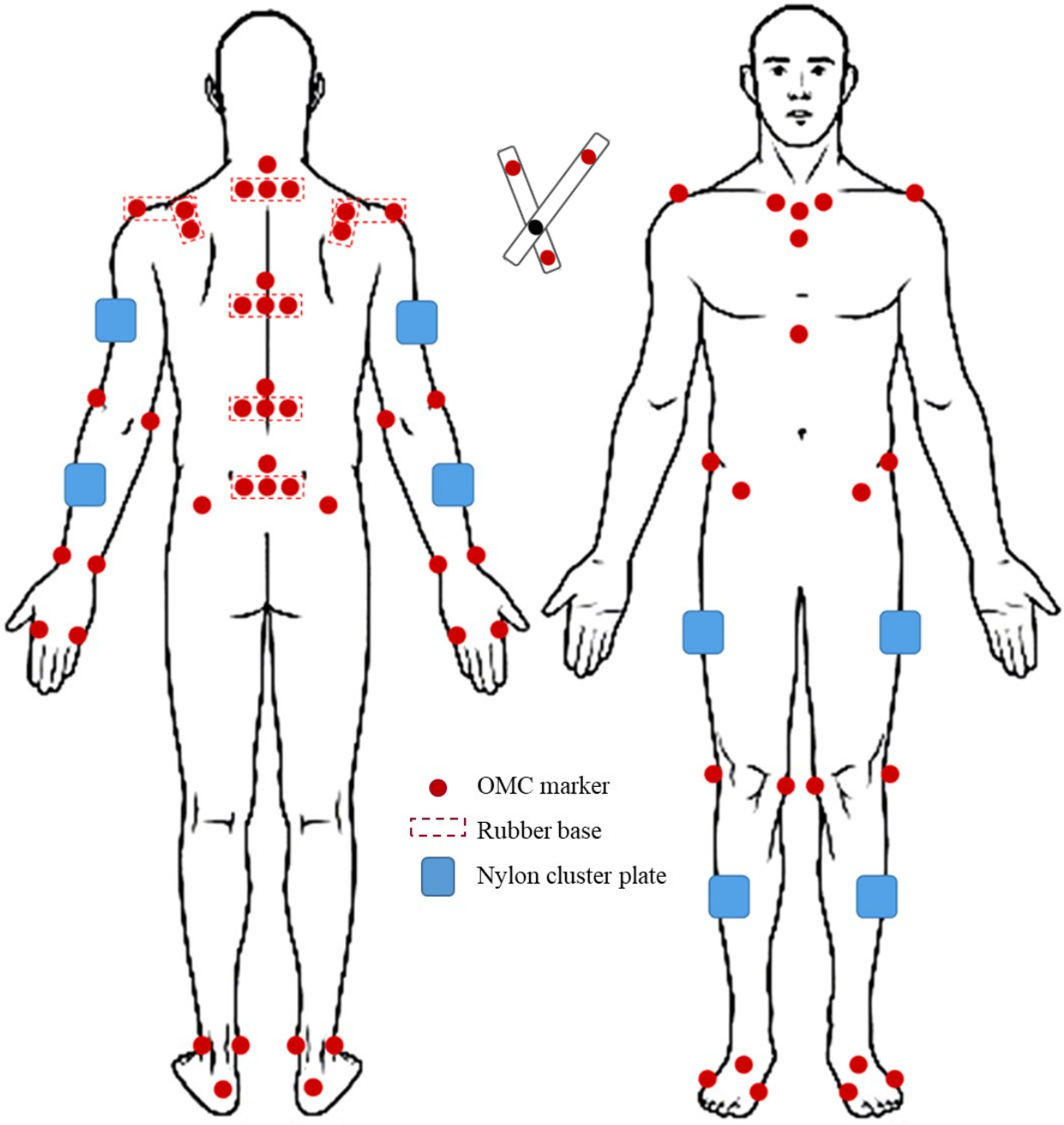

Figure 5.5: Anterior and posterior views of marker model arrangement on participant. Red dots represent individual optical motion capture (OMC) markers. Red dashed lines indicate groups of markers that shared a flexible rubber base and were affixed to athlete with hypo-allergenic double-sided tape. Blue boxes represent rigid nylon cluster plates which comprised 4 markers and were secured around body segments by elastic Velcro bands (see Figure 5.4). Central inset is of the scapula locator used in calibration (see Figure 5.6).

Figure 5.6: Custom 3D printed nylon rigid cluster plates with elastic Velcro bands for securing to body segments and four 14 mm retroreflective markers affixed per plate.

The scapula tracker consists of a rectangular base affixed along the middle of the scapular spine; an adjustable arm positioned to sit at the junction of the spine with the acromion process and incorporates a cluster of three markers (Figure 5.7). For accurate tracking of the scapula throughout the rowing stroke, a palpation device known as a scapula locator developed by Johnson, Stuart & Mitchell (1993), was used to estimate 3D scapula location in common static positions and during slow dynamic movement, by placing each of three adjustable feet on three scapula landmarks (acromial angle (AA), IA, and trigonum spinae (TS)). The scapula locator created a local anatomical coordinate frame for the scapula during calibration trials, following ISB recommendations (Wu *et al.*, 2005). The scapula tracker created a technical coordinate frame for motion trials, which was calibrated to the anatomical coordinate frame defined by the scapula locator (Figure 5.7). This combination tracking method reduces measurement error, with device repeatability for intra-subject scapula rotations within 2° - 5° (Barnett, Duncan & Johnson, 1999; Shaheen, Alexander & Bull, 2011; Johnson, Stuart & Mitchell, 1993).

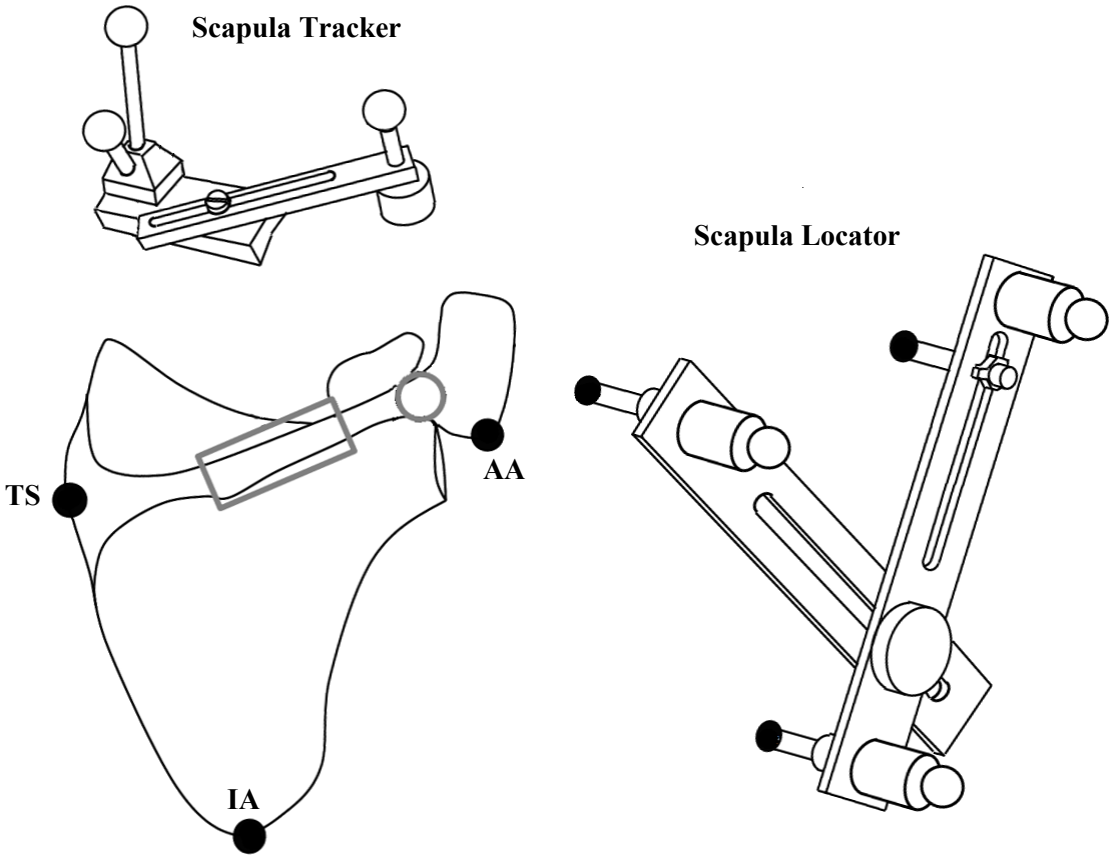

Figure 5.7: Scapula tracker (*top-left*) used during all trials and scapula locator (*right*) used in calibration trials. Black dots on the scapula (*bottom-left*) indicate landmark positions for placing each locator foot. Gray circle & rectangle indicate placement and footprint of scapula tracker. (Adapted from Prinold, 2012).

5.2.3 Experimental Protocol

Upon arrival, each athlete was asked to perform a short warm-up on the instrumented ergometer (5-10 minutes). The rowers adjusted the height of the footplate as well as the ergometer drag factor to match their use in a regular training session. Recommended drag factor is 100-130, depending on the participant's sex and weight (Rowing Australia, 2019). All drag factors used were within this range.

After warm-up two researchers attached all the markers and clusters (Table 5.3) as shown in Figure 5.5. Markers and clusters were attached using high-strength hypoallergenic double-sided tape. Four static calibration trials were collected. The first, standing at the center of the capture volume in a neutral anatomical position (i.e., arms slightly raised away from one's sides, palms facing forward). The remaining three involved using the scapula locator to palpate the anatomical landmarks: TS, AA, and IA, to digitize the scapula position in three distinct static positions, chosen to simulate scapula positions similarly seen in rowing, to increase tracking accuracy (Figure 5.8). Additionally, two dynamic calibration trials were

collected. The first, to obtain the glenohumeral joint center, used the scapula locator while the participant slowly moved their right arm along a simple movement pattern of shoulder flexion then abduction, at 90° of elbow flexion, and then horizontal circumduction (e.g., similar to stirring a large pot), starting and ending with the arm alongside the torso (Prinold & Bull, 2016; Hiniduma, Gamage & Lasenby, 2002). The second dynamic calibration trial, to obtain the functional HJC, involved the participant performing a standard "star-arc" pattern by circumduction of each leg and kicking out in each of five directions (Camomilla *et al.*, 2006).

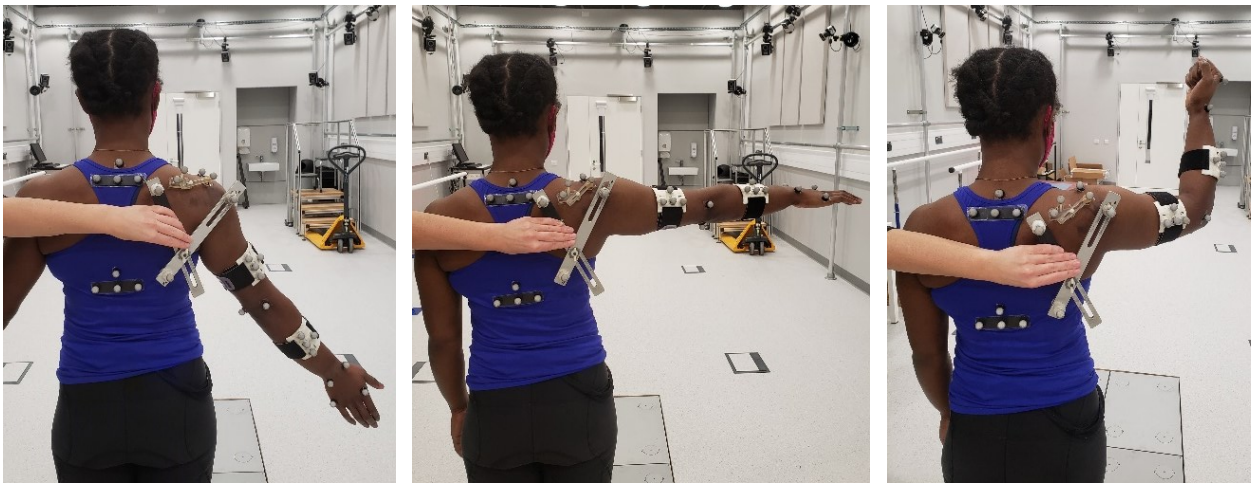

(A) **(B)** **(C)**

Figure 5.8: Three static positions for the scapula calibration with the scapula locator: (A) anatomical neutral; (B) abduction - shoulder at approximately 120° abduction in coronal plane; (C) scaption - shoulder at 90° abduction in scapular plane and elbow at 90° flexion.

After calibration, athletes performed a "step test" protocol (Table 5.4) on the instrumented ergometer, consisting of four, 3-minute rowing trials at increasing stroke rate (18/24/28/32 spm). In-built ergometer hardware measured stroke rate, average 500 m pace and total distance rowed, which was both recorded and provided as real-time feedback to the athlete during each interval. Participants were allowed time to rest between each step to recover as needed; this was for a recommended 3-5 minutes between trials. This study protocol closely reflects standard training and testing procedures, with lexicon commonly used in the rowing community (Nilsen, Daigneault & Smith, 2002b).

Table 5.4: Structure and description of ergometer 'step test' protocol. Detailed description of training zones and stroke rates can be found in Chapter 3 (Table 3.1). Utilization 2 (UT2); Utilization 1 (UT1); Aerobic Threshold (AT); Oxygen Transport (TR2); Anaerobic Threshold (TR1)

Trial	Step	Description	Duration
1	18 spm	UT2 pace (heart rate ~130-150 bpm)	3 min
2	24 spm	UT1/AT pace (heart rate ~160-170 bpm)	3 min
3	28 spm	AT/TR2 pace (heart rate ~170-180 bpm)	3 min
4	32 spm	TR1 pace (max heart rate)	3 min

5.2.4 Data Handling and Statistical Analysis

All study data were anonymized, adhering to procedures for ensuring confidentiality. Data analysis was performed at Imperial College London - South Kensington Campus, SW7 2AZ. Motion capture data were initially processed in Vicon Nexus 2.7 software (Vicon, Oxford, UK) to reconstruct marker trajectories. Markers were labelled per Table 5.3 and missing trajectory data were gap-filled by interpolating between the data immediately before and after the missing data utilizing Vicon Nexus 2.7 in-built algorithms (Figure 5.9). The marker data were low-pass filtered with a 4^{th} order, zero-shift, Butterworth filter using a 6 Hz cutoff frequency. This filter type and cut-off have previously been verified for kinematics studies in rowing, cricket bowling, pullups, and activities of daily living (Buckeridge, Bull & McGregor, 2015; Persad, 2016; Klemt *et al.*, 2018).

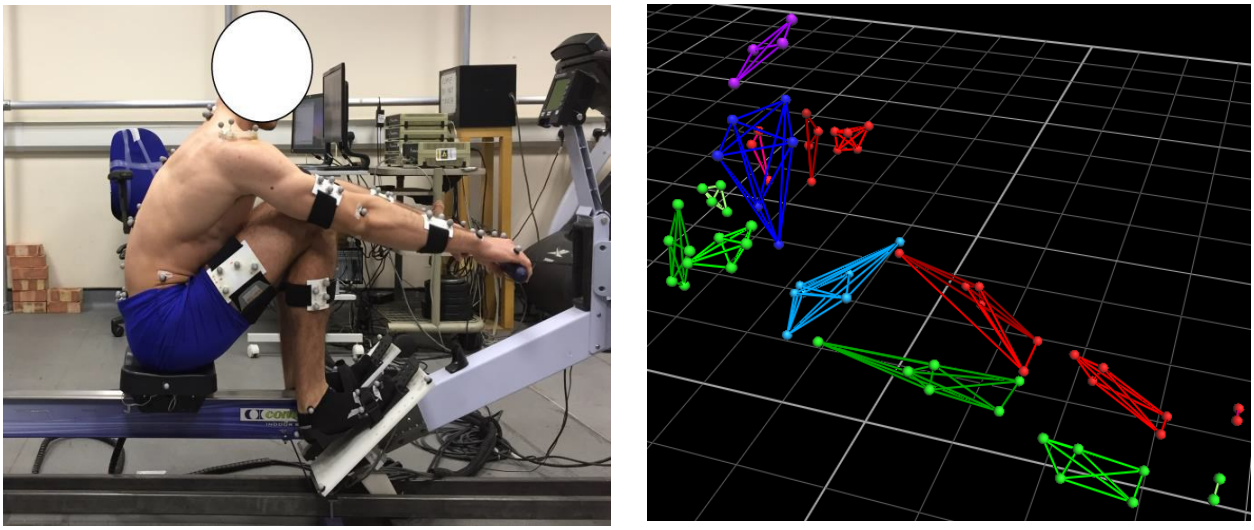

(A) **(B)**

Figure 5.9: (A) Subject at catch position wearing full marker set described above. (B) Marker trajectories of subject at finish position, reconstructed and labelled in Vicon Nexus 2.7.

External kinetic data from the instrumented ergometer was processed with a 4th order, zero-shift, Butterworth filter using a 10 Hz cutoff frequency in MATLAB R2017B (MathWorks, Natick, MA, USA) and then combined with imported kinematic data from Vicon. Synchronized motion data and external force data from continuous 3-minute rowing trials were divided into individual strokes where the start of each stroke was identified as the minimum sagittal (Y-axis) handle position. The catch was identified as the onset of handle force which exceeds a threshold of 75 N with a steep, increasing slope (Buckeridge *et al.*, 2012). The finish was defined as maximum sagittal handle displacement. The first 3 and last 3 strokes of each trial were discarded to minimize the effects of acceleration or deceleration at the beginning and end of each trial, to ensure stroke consistency. Each stroke was time normalized to 201 data points, from 0-100% of completion using a cubic spline interpolation, such that the drive time was from start (0%) to finish, and the recovery time was from finish to the next subsequent catch (100%). Time normalization allowed for comparison across rates and between athletes. Kinetic data were also body weight normalized to each individual athlete's weight.

Data were used to examine three-dimensional biomechanical parameters. Outcome measures included ergometer instrumentation derived handle force, seat force, footplate force, and pace. OMC derived measures included stroke length, seat travel and athlete affixed marker trajectories. Drive:recovery ratio was calculated as the recovery time over the drive time. Stroke length was calculated as the difference between the maximum and minimum sagittal plane (Y-axis) handle position. Vertical and horizontal components of foot force were directly measured from each footplate and bilateral resultant force was

calculated to illustrate overall magnitude of footplate force. Seat suspension (SS) represents the effective transfer of force from the feet to the handle (Murphy, 2009), and was calculated here as:

$$SS = 1 - body\ weight\ normalized\ seat\ force \quad \text{Equation 5.1}$$

Foot force asymmetry index (ASI), or the difference in resultant foot force (RFF) between the left and right feet, was calculated using a modified Robinson index (Equation 5.2; Viteckova *et al.*, 2018). Values close to zero indicate that leg drive was symmetric. Negative values favor the left leg and positive values favor right leg.

$$ASI = \frac{(RFF_{right} - RFF_{left})}{(RFF_{right} + RFF_{left})} * 100 \quad \text{Equation 5.2}$$

A correlation analysis was used to quantify the direction and strength of linear relationships among the ergometer derived variables – total seat force, resultant footplate force, and handle force – by estimating a sample correlation coefficient for maximum force across all stroke rates. Catch slip is the period between change of handle direction and start of force generation. Differences in handle-to-seat timing were quantified by the ratio of seat movement during the initial period of catch slip ($Disp_{seat}/Disp_{handle}$). Smaller ratios indicate greater handle movement versus seat movement. Larger ratios indicate greater seat movement versus handle movement.

Collected data were analyzed over the entire athlete population, and subdivided into distinct cohorts, such that comparisons were also made between (1) male vs. female athletes, (2) across experience level: university vs. club vs. elite vs. masters, and (3) by rowing modality and sidedness: port vs. starboard vs. sculling (Section 5.2.1).

Appropriate statistical analyses were conducted using R statistical packages in RStudio 3.6 (RStudio Team, 2016) and JMP Pro 14 (SAS Institute, NC, USA). Comparisons between groups for changes in movement patterns with respect to rating, force output, and fatigue were quantified by repeated measures analysis of variance (ANOVA) using a mixed linear model with Tukey HSD post-hoc corrections. Correlation analysis was used to examine linear dependencies among spatio-temporal variables generating Pearson's correlations coefficients. All rate of change (RoC) calculations utilized maximum likelihood to fit a piecewise linear regression model given *a priori* breakpoint estimates (Muggeo, 2003). The statistical significance alpha level was set at $p < 0.05$.

5.3 RESULTS

The outcome measures discussed in this chapter are kinetics and kinematics derived from ergometer instrumentation alone. These parameters include stroke length, duration, and ratio of stroke phases, handle

force, seat force and CoP, and foot stretcher force and CoP, handle, and seat trajectories. These parameters were used to generate a full description of individual stroke profiles and mean profiles for each of the previously described athlete cohorts (Section 5.2.1; Table 5.2**Error! Reference source not found.**).

In the interest of salience, of the many comparisons that were performed, results presented here focus on population-wide trends and those cohort comparisons which were statistically significant. Additional results from cohort comparisons can be found in Appendix C: Supplemental Spatio-Temporal Results.

5.3.1 Ergometer Derived Kinetics

Spatio-temporal analysis of ergometer-derived kinetic and kinematic parameters were assessed throughout the full stroke and at three key points in each stroke: the catch, MHF, and the finish (Figure 5.10).

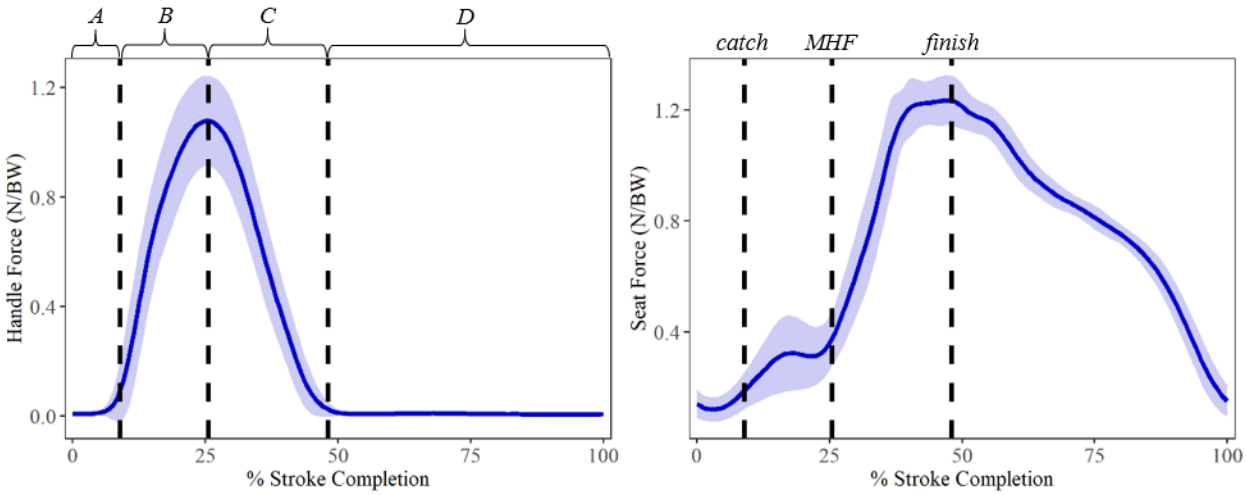

Figure 5.10: Population-wide handle force (*left*) and seat force (*right*) normalized to athlete body weight (mean ± std) in N/BW at rate 32 spm (mean ± std). Blue line is mean force, shaded ribbon is standard deviation. Dashed vertical lines on both graphs, indicate occurrence of the catch, MHF, and the finish. Stroke sub phases in the handle force graph (*left)* shows (A) catch slip period, (B) early-drive, (C) late-drive, (D) recovery.

The primary and most oft cited standard ergometer performance metric is the "split time" which describes the average time to row 500 m. Split times for all athlete groups are given in Table 5.5 and will be referenced when relating kinetic and kinematic parameters to performance output. Figure 5.11 gives the absolute time to reach key stroke events, including the time to reach MHF, the finish of the stroke, the total stroke time and ratio of time spent on the drive versus the recovery. This ratio is displayed in inverse form in Figure 5.11. Box and whisker plots include mean markers (×) and mean lines. Interquartile blocks have whiskers extending from the top and bottom to 1.5 times larger and smaller, respectively, than the

interquartile range (IQR). Values outside this range are outliers and represented by dots (Figure 5.11 & Figure 5.12).

Table 5.5: Ergometer split times (avg /500 m) for all athlete groups (mean ± std).

	18 spm	24 spm	28 spm	32 spm
Total	2:06.1 ± 0:09.8	1:54.7 ± 0:09.3	1:50.1 ± 0:09.5	1:48.3 ± 0:10.0
Female	2:13.0 ± 0:05.8	2:01.6 ± 0:04.7	1:57.3 ± 0:04.9	1:55.7 ± 0:05.4
Male	1:56.7 ± 0:05.4	1:45.2 ± 0:04.8	1:40.3 ± 0:04.1	1:38.0 ± 0:04.2
Club	2:02.7 ± 0:09.1	1:52.5 ± 0:09.1	1:48.5 ± 0:09.5	1:46.7 ± 0:08.8
Elite	1:52.8 ± 0:05.0	1:42.7 ± 0:04.9	1:38.7 ± 0:04.8	1:35.5 ± 0:04.1
Master	2:09.6 ± 0:10.6	1:55.8 ± 0:07.1	1:50.6 ± 0:07.4	1:49.6 ± 0:07.6
University	2:08.1 ± 0:08.4	1:56.7 ± 0:09.0	1:52.1 ± 0:09.4	1:50.1 ± 0:10.2
Port	2:06.0 ± 0:11.3	1:55.6 ± 0:11.6	1:50.8 ± 0:12.0	1:52.4 ± 0:12.6
Starboard	2:06.7 ± 0:10.2	1:54.6 ± 0:08.6	1:49.9 ± 0:09.0	1:48.2 ± 0:10.2
Sculling	2:02.7 ± 0:09.0	1:52.5 ± 0:07.2	1:48.3 ± 0:06.4	1:46.3 ± 0:05.7

Across the entire athlete population, total stroke time, recovery time, and drive-to-recovery ratio decreased with increasing rate ($p < 0.001$; Figure 5.11). In contrast, drive time only decreased significantly between 18 spm and 24 spm ($p < 0.01$) but did not continue to decrease for the higher rates up to 32 spm (Figure 5.11). There were significant increases in relative timing to catch, MHF, and finish ($p < 0.0001$; Figure 5.12). As rate increased, time spent in the early-drive phase (i.e., before MHF) increased ($p = 0.0002$) even though total absolute stroke time decreased. The decreases in total stroke time were largely attributable to diminished recovery time (Figure 5.11). In this broad population of athletes, the seat moved posteriorly in time with the change in handle direction, but before the start of handle force generation. Catch slip decreased slightly as rate increased ($p = 0.0256;$ Table 5.6) but because of decreased overall stroke time, this represents a significant increase in percent time between change of direction and onset of handle force ($p < 0.0001$). Percent timing to catch, MHF, and finish increase significantly at every stroke rate. ($*p < 0.01$).

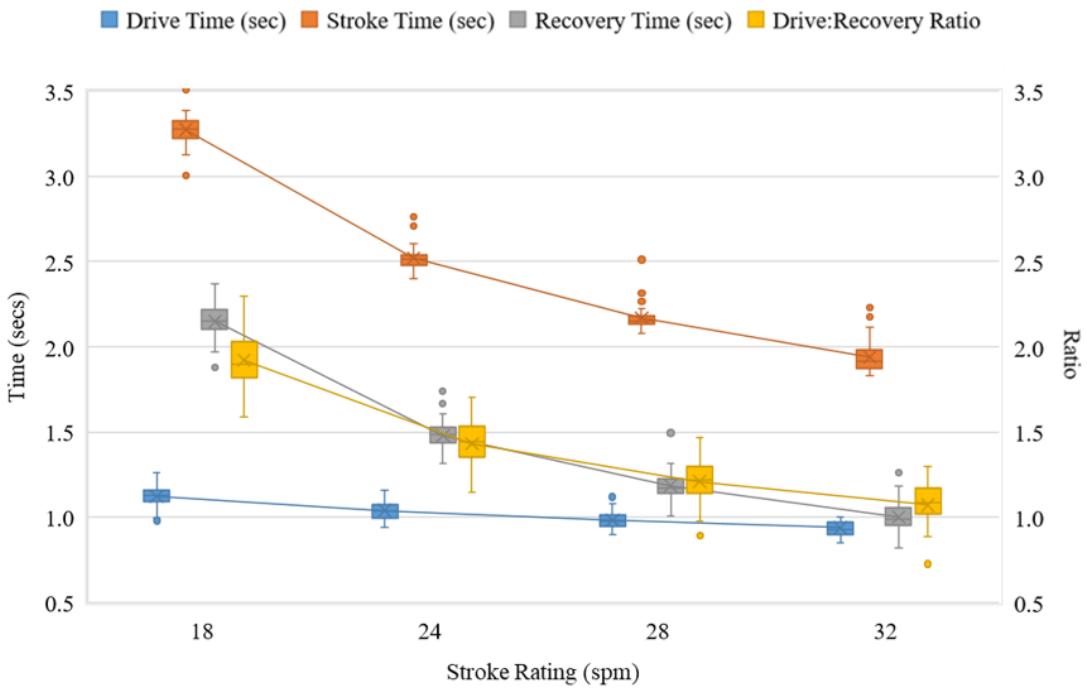

Figure 5.11: Total stroke time, drive phase time, and recovery phase time, (mean & IQR) in seconds (secs). Drive:recovery ratio is the ratio of time spent in the recovery phase versus the drive phase, plotted on right-side axis.

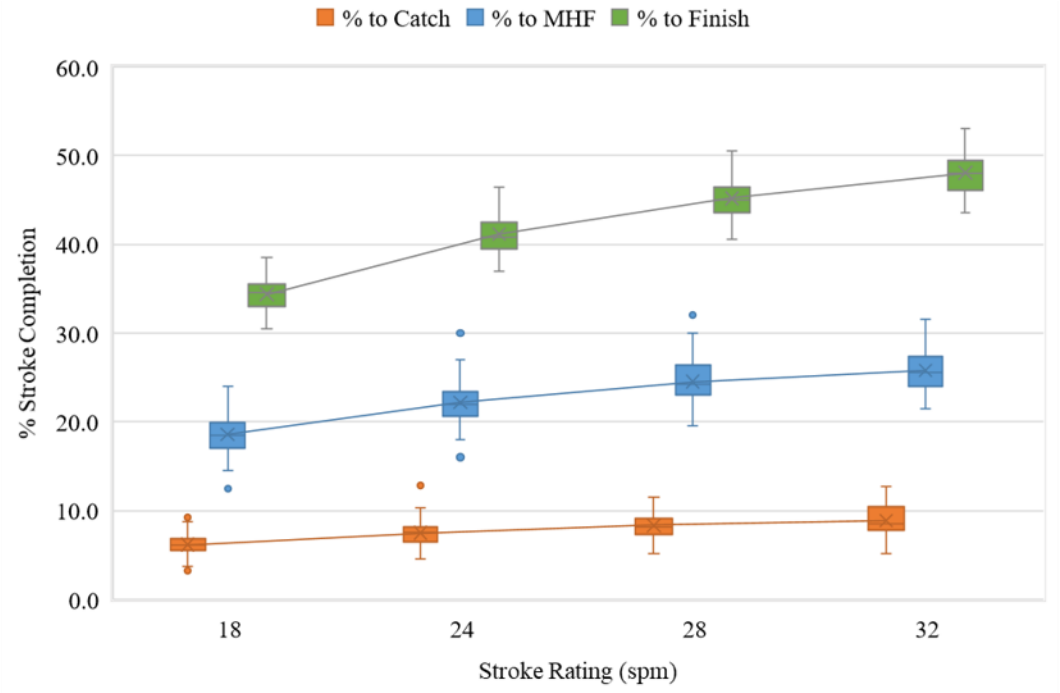

Figure 5.12: Relative timing in % of stroke completion (mean & IQR) to reach key kinematic stroke moments: catch, max handle force (MHF), & finish, at all stroke rates.

5.3.1.1 Handle Force

Throughout the drive phase, all handle force series began with an approximately symmetrical bell-shaped curve, where the time from MHF to the finish was slightly shorter than the time from the catch to MHF (Figure 5.13 - *left*). Across the entire athlete population, as stroke rate increased, there was no change in MHF ($p = 0.658$). Between each stroke rate increase, the time to reach MHF increased ($p = 0.0002$) by 3.6% from 18 spm to 24 spm, 2.3% from 24 spm to 28 spm, and 1.3% from 28 spm to 32 spm, respectively (Table 5.6). Rate of handle force development (HF-RoC) was calculated as a piecewise linear regression from the catch to MHF (Figure 5.13 - *right*). HF-RoC significantly increased with stroke rate ($p < 0.001$; Table 5.6).

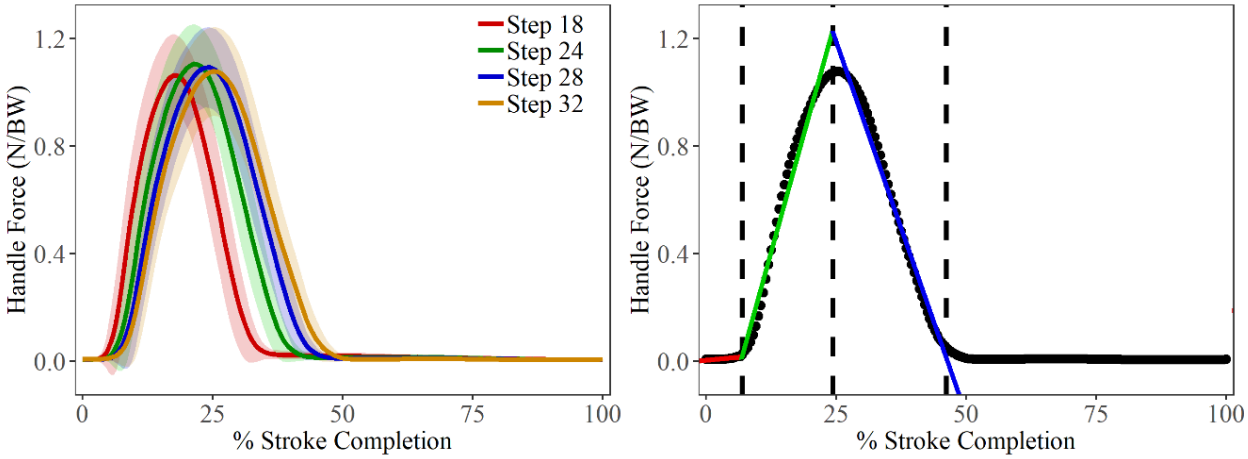

Figure 5.13: Population-wide handle force (mean ± std) at all stroke rates (*left*). Piecewise linear regressions of each handle movement phase at 32 spm delineated by dashed vertical lines at the catch, max handle force (MHF), and the finish (*right*).

Table 5.6: Descriptive statistics (mean ± std) for all athlete cohorts of max handle force (MHF) in Newtons (N), rate of handle force production (HF-RoC) in normalized force per second (N/BW/s), stroke length (SL) in meters (m), catch slip (CS) in secs (s), time to reach MHF and time to reach the finish (FIN) in secs (s). Asterisks (*) indicate ANOVA of $p < 0.05$ with respect to stroke rate across total athlete population.

		18 spm	24 spm	28 spm	32 spm	
Total	CS (s)	0.20 ± 0.04	0.19 ± 0.04	0.18 ± 0.04	0.17 ± 0.03	
	HF-RoC (N/BW/s)	2.83 ± 0.05	3.26 ± 0.05	3.39 ± 0.06	3.62 ± 0.06	*
	MHF (N)	819 ± 156	845 ± 165	838 ± 163	824 ± 168	
	MHF Time (s)	0.59 ± 0.11	0.54 ± 0.08	0.52 ± 0.07	0.49 ± 0.06	
	SL (m)	1.56 ± 0.10	1.57 ± 0.09	1.55 ± 0.10	1.51 ± 0.10	
	FIN Time (s)	1.12 ± 0.06	1.04 ± 0.05	0.98 ± 0.05	0.94 ± 0.06	*

Table 5.6 (continued)

		18 spm	24 spm	28 spm	32 spm
Female	CS	0.20 ± 0.04	0.19 ± 0.04	0.18 ± 0.04	0.17 ± 0.03
	HF-RoC	2.80 ± 0.05	3.13 ± 0.05	3.20 ± 0.05	3.38 ± 0.06
	MHF	738.4 ± 87.3	753.6 ± 90.9	749.5 ± 104.6	724.3 ± 105.4
	MHF Time	0.60 ± 0.10	0.56 ± 0.08	0.53 ± 0.07	0.50 ± 0.06
	SL	1.53 ± 0.09	1.53 ± 0.07	1.51 ± 0.08	1.46 ± 0.07
	FIN Time	1.14 ± 0.05	1.05 ± 0.05	1.00 ± 0.05	0.95 ± 0.06
Male	CS	0.198 ± 0.05	0.18 ± 0.04	0.17 ± 0.03	0.17 ± 0.03
	HF-RoC	2.89 ± 0.05	3.46 ± 0.06	3.67 ± 0.06	3.89 ± 0.07
	MHF	966.5 ± 145.5	1008 ± 142.1	999.2 ± 122.3	982.5 ± 118.9
	MHF Time	0.56 ± 0.12	0.52 ± 0.08	0.50 ± 0.07	0.48 ± 0.06
	SL	1.62 ± 0.09	1.63 ± 0.10	1.62 ± 0.10	1.58 ± 0.10
	FIN Time	1.10 ± 0.08	1.02 ± 0.06	0.96 ± 0.04	0.92 ± 0.04
Club	CS	0.18 ± 0.02	0.18 ± 0.02	0.17 ± 0.02	0.17 ± 0.02
	HF-RoC	3.54 ± 0.06	4.31 ± 0.08	4.47 ± 0.07	4.54 ± 0.07
	MHF	937.8 ± 132.2	941.7 ± 164.1	916.7 ± 165.8	912.1 ± 131.6
	MHF Time	0.51 ± 0.16	0.51 ± 0.11	0.48 ± 0.09	0.47 ± 0.08
	SL	1.55 ± 0.12	1.59 ± 0.11	1.54 ± 0.13	1.51 ± 1.06
	FIN Time	1.08 ± 0.06	1.04 ± 0.07	0.99 ± 0.08	0.96 ± 0.07
Elite	CS	0.21 ± 0.03	0.20 ± 0.04	0.19 ± 0.04	0.17 ± 0.02
	HF-RoC	2.85 ± 0.06	3.31 ± 0.06	3.45 ± 0.06	4.01 ± 0.08
	MHF	829.5 ± 100.2	874.7 ± 116.0	880.1 ± 95.9	883.9 ± 94.0
	MHF Time	0.64 ± 0.05	0.56 ± 0.05	0.55 ± 0.05	0.50 ± 0.04
	SL	1.62 ± 0.08	1.60 ± 0.09	1.59 ± 0.09	1.58 ± 0.10
	FIN Time	1.13 ± 0.03	1.02 ± 0.03	0.97 ± 0.04	0.93 ± 0.04
Master	CS	0.20 ± 0.07	0.17 ± 0.06	0.17 ± 0.05	0.17 ± 0.05
	HF-RoC	2.16 ± 0.03	2.58 ± 0.03	2.75 ± 0.03	2.84 ± 0.03
	MHF	748.7 ± 160.2	790.1 ± 115.9	808.3 ± 128.7	785.0 ± 122.6
	MHF Time	0.54 ± 0.08	0.50 ± 0.06	0.49 ± 0.05	0.48 ± 0.06

Table 5.6 (continued)

		18 spm	24 spm	28 spm	32 spm
Master	SL	1.49 ± 0.08	1.50 ± 0.07	1.50 ± 0.07	1.45 ± 0.06
	FIN Time	1.11 ± 0.09	1.03 ± 0.06	0.98 ± 0.05	0.95 ± 0.06
University	CS	0.20 ± 0.04	0.19 ± 0.04	0.18 ± 0.04	0.17 ± 0.04
	HF-RoC	2.82 ± 0.05	3.10 ± 0.05	3.17 ± 0.05	3.38 ± 0.05
	MHF	789.7 ± 163.8	805.6 ± 180.2	794.4 ± 182.2	780.9 ± 190.2
	MHF Time	0.60 ± 0.09	0.56 ± 0.08	0.53 ± 0.07	0.49 ± 0.07
	SL	1.55 ± 0.10	1.56 ± 0.09	1.55 ± 0.09	1.50 ± 0.09
	FIN Time	1.14 ± 0.06	1.05 ± 0.05	0.99 ± 0.05	0.93 ± 0.05
Port	CS	0.21 ± 0.04	0.20 ± 0.04	0.18 ± 0.04	0.17 ± 0.03
	HF-RoC	3.04 ± 0.05	3.47 ± 0.05	3.62 ± 0.06	3.86 ± 0.07
	MHF	818.6 ± 139.5	838.1 ± 175.9	839.3 ± 185.3	813.3 ± 194.6
	MHF Time	0.57 ± 0.11	0.54 ± 0.09	0.50 ± 0.08	0.49 ± 0.08
	SL	1.54 ± 0.13	1.56 ± 0.11	1.55 ± 0.19	1.49 ± 0.09
	FIN Time	1.12 ± 0.07	1.05 ± 0.05	0.98 ± 0.05	0.95 ± 0.07
Starboard	CS	0.20 ± 0.05	0.19 ± 0.04	0.18 ± 0.04	0.18 ± 0.04
	HF-RoC	2.74 ± 0.05	3.09 ± 0.05	3.17 ± 0.05	3.38 ± 0.05
	MHF	814.0 ± 172.1	842.7 ± 165.7	839.9 ± 158.2	825.1 ± 164.9
	MHF Time	0.59 ± 0.11	0.56 ± 0.08	0.54 ± 0.07	0.50 ± 0.06
	SL	1.58 ± 0.09	1.58 ± 0.08	1.56 ± 0.09	1.52 ± 0.09
	FIN Time	1.14 ± 0.06	1.04 ± 0.05	0.99 ± 0.05	0.94 ± 0.06
Sculling	CS	0.19 ± 0.04	0.17 ± 0.04	0.16 ± 0.03	0.16 ± 0.02
	HF-RoC	3.02 ± 0.05	3.44 ± 0.06	3.61 ± 0.06	4.05 ± 0.07
	MHF	866.8 ± 154.3	869.0 ± 126.6	848.3 ± 109.3	827.5 ± 87.9
	MHF Time	0.58 ± 0.09	0.53 ± 0.07	0.50 ± 0.04	0.48 ± 0.05
	SL	1.59 ± 0.10	1.56 ± 0.10	1.54 ± 0.10	1.49 ± 0.11
	FIN Time	1.09 ± 0.07	1.03 ± 0.07	0.98 ± 0.07	0.94 ± 0.08

Male versus female normalized handle force is plotted in Figure 5.14. Males produced significantly greater MHF than females at all stroke rates ($p < 0.0001$) but as stroke rate increased, MHF remained constant within male and female cohorts. From 18 to 32 spm, females decreased stroke length by 4.3% ($p = 0.006$) while males stroke length did not change (Table 5.6). There were no other statistically significant differences with respect to stroke rate between males and females.

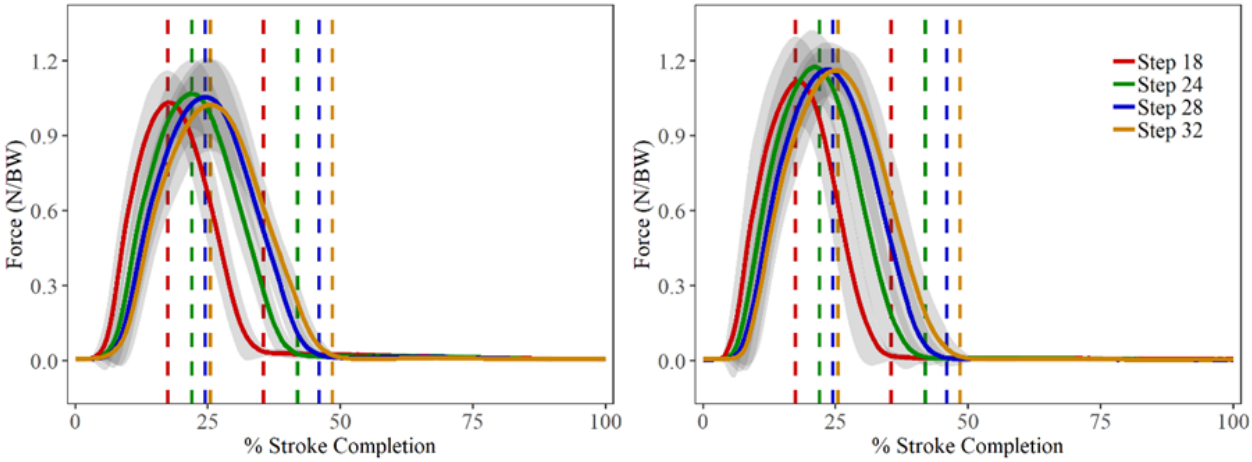

Figure 5.14: Body weight normalized handle force (mean ± std) in N/BW for female (*left*) and male (*right*) athlete cohorts. Each pair of vertical dashed lines represents the occurrence of max handle force (MHF) and the finish to match each of the four stroke rates tested.

There was a significant effect of athlete experience on MHF ($p = 0.003$), with masters athletes achieving substantially lower MHF than club ($p = 0.015$) and elite ($p = 0.0051$) rowers. From 18 to 32 spm, there was no significant change in MHF within each group, however, elites and masters showed a positive direction of change (2.2% and 1.7%, respectively) with increasing stroke rate, while club and university athletes showed a slightly negative direction of change (-0.9% and -0.4%, respectively). Differences in the shape of the force profile showed significant differences in stroke length ($p < 0.001$) among all four age/experience cohorts (Table 5.6). Elite rowers achieved greater MHF later in the stroke than masters rowers ($p = 0.031$) for all stroke rates (Figure 5.15; Table 5.6).

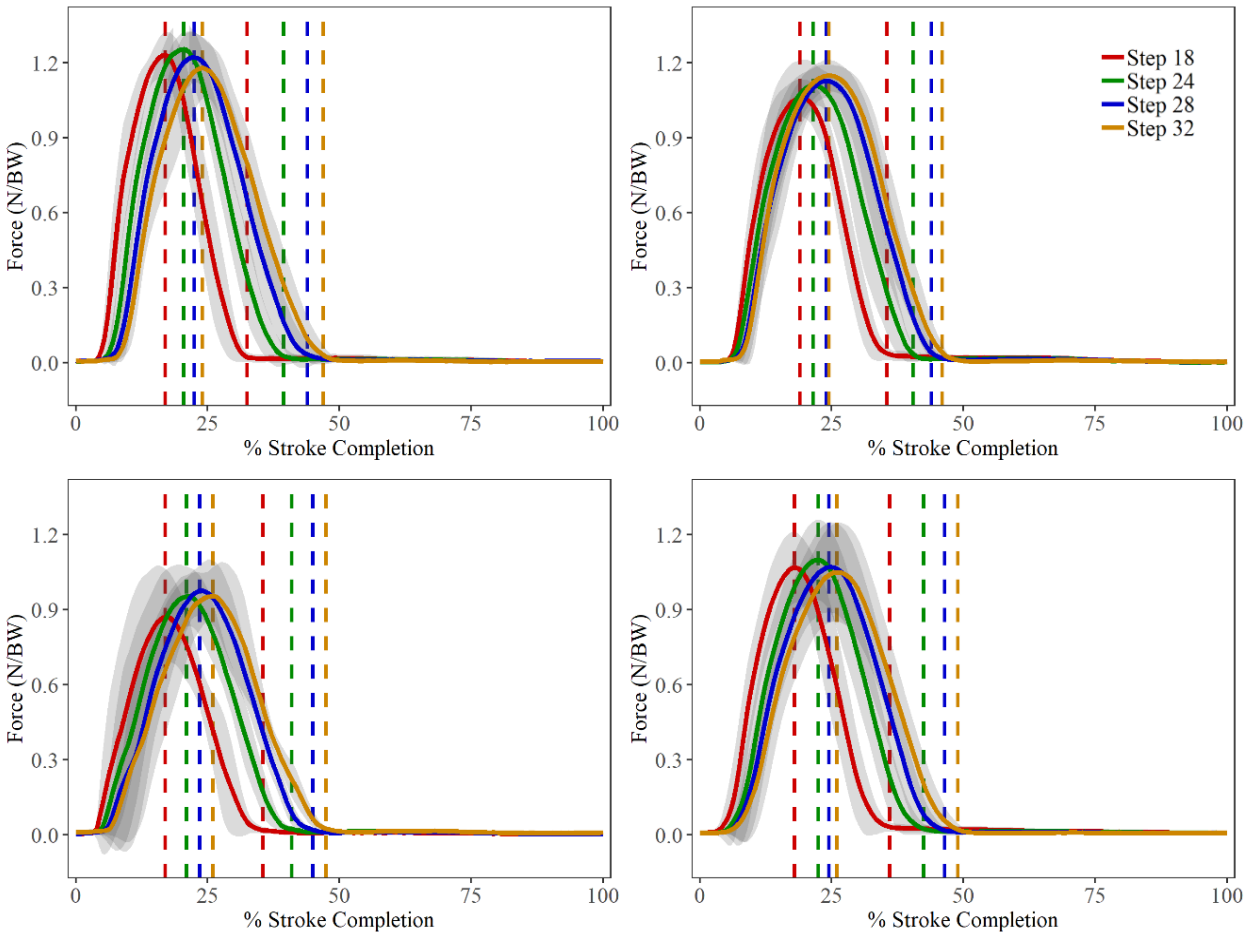

Figure 5.15: Body weight normalized handle force (mean ± std) in N/BW for club (*top-left*) and elite (*top-right*) masters (*bottom-left*) and university (*bottom-right*) athlete cohorts. Each pair of vertical dashed lines represents the occurrence of max handle force (MHF)and the finish to match each of the four stroke rates tested.

5.3.1.2 Seat Force and Center of Pressure

Population-wide pattern changes were observed as rate increased for both maximum seat force (MSF) and seat center of pressure distribution. Early-drive SS occurs from the catch to MHF, and late-drive SS occurs from MHF to MSF (which typically coincides with the finish position). As stroke rate increased from 18 spm to 32 spm, there was a significant increase in SS at the catch (17.8%, $p < 0.001$; Figure 5.17), but there was no difference in suspension at MHF (-1.3%, $p = 0.489$), and there was a significant decrease in suspension at the finish (-12.2%, $p < 0.001$; Figure 5.17).

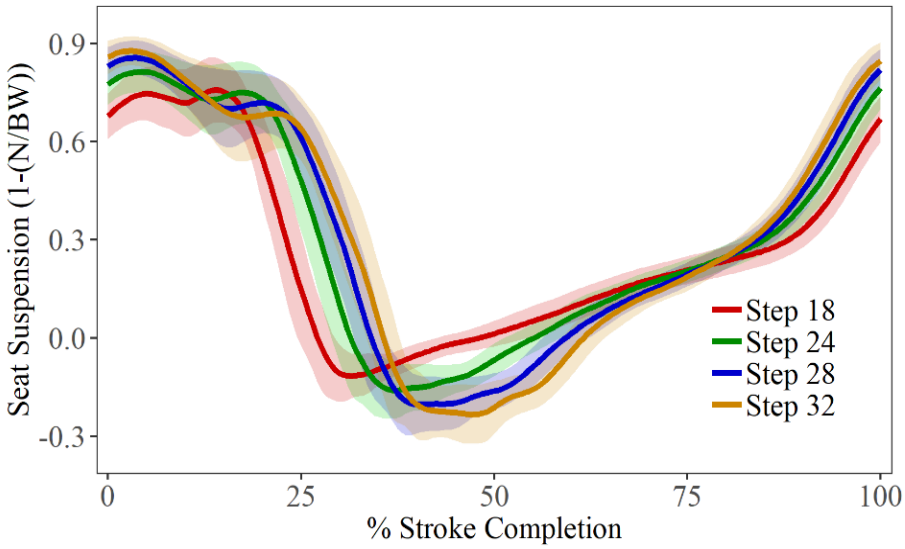

Figure 5.16: Population-wide seat suspension (*1- normalized seat force*) for all stroke rates (mean ± std).

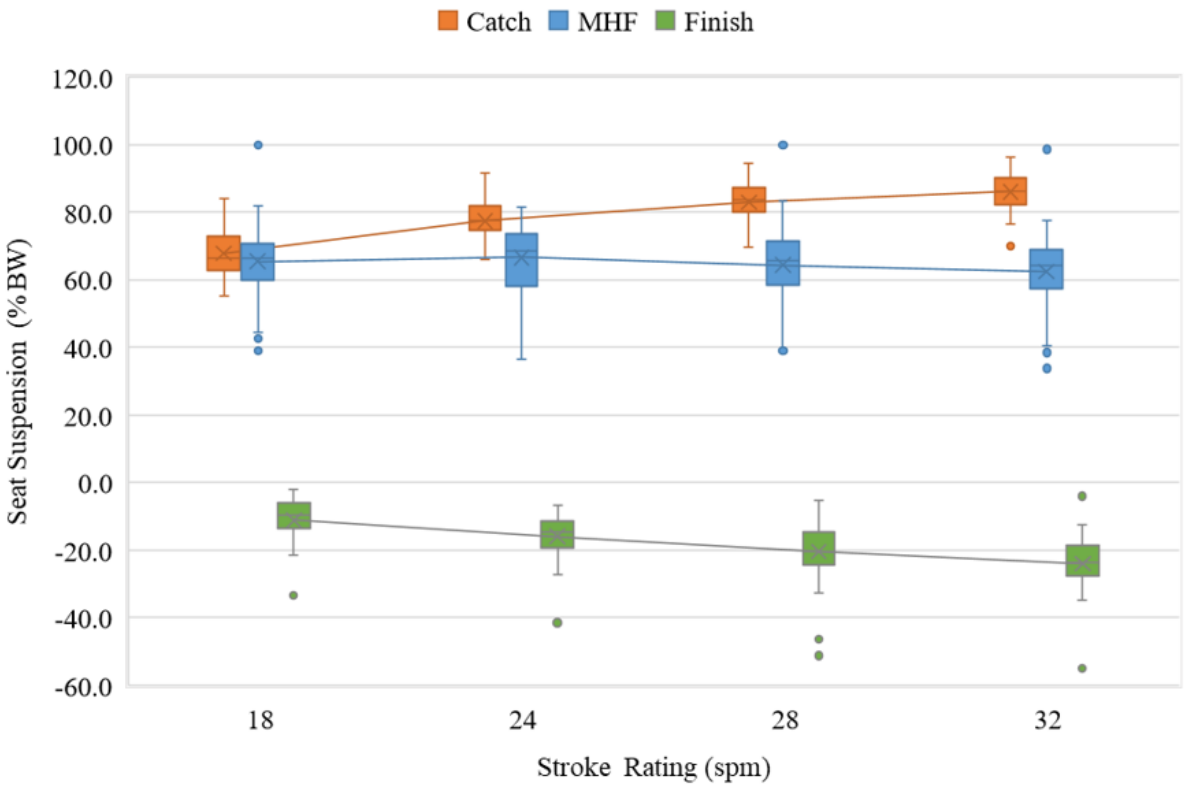

Figure 5.17: Seat suspension (mean & IQR) % body weight (%BW) at key stroke moments.

Large early-drive SS is associated with higher performance metrics and can be visualized by the gradient of seat force (SS-RoC) during this phase (*red-line,* Figure 5.18). At rate 18 spm, early-drive SS-RoC gradient was 0.22 ± 0.04% while at 32 spm it decreased to -1.08 ± 0.05% (Table 5.7). The higher the absolute value and the more horizontal the slope, the better the SS. The inflection point between the shift from early drive suspension to late drive suspension occurred near MHF (*green line*, Figure 5.18). After reaching the finish position, body weight was shifted back to the footplate in two stages indicated by their difference in slope. At first, slowly through the middle of the recovery (0.011 ± 0.003), then increasing in gradient (0.037 ± 0.001) in the final 15% preceding the next catch (Figure 5.18). Significant changes were seen in timing of MSF as rate increased ($p < 0.0001$). At the lowest rate (18 spm), MSF preceded reaching the finish position, however, at higher rates, the seat-force profile shifted relatively later, with MSF at 32 spm coinciding with the finish (Table 5.7; Figure 5.16; Figure 5.18).

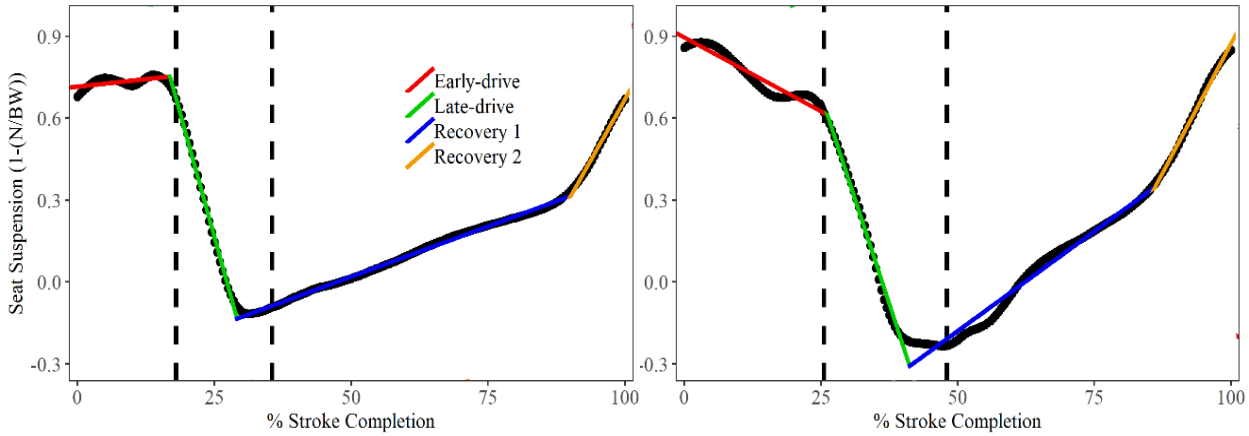

Figure 5.18: Mean seat suspension (*black dots*) for entire athlete population and calculated piecewise linear regression gradients for each salient stroke phase were compared between rate 18 spm (*left*) and 32 spm (*right*). Left and right dashed vertical lines indicate max handle force (MHF) and the finish, respectively.

Similar changes in seat force patterning were observed across both sexes as rate increased; although, males had significantly higher MSF than females ($p = 0.0001$; Table 5.7). Both males and females achieved peak SS within the first 5% of the stroke. Only at 18 spm was either group able to maintain or increase this suspension through the early-drive phase, holding good suspension for 10-15% before reaching MHF. As stroke rate increased from 24 spm to 32 spm the rate at which SS declined during the late-drive phase decreased (Table 5.7).

No differences were seen when comparing athletes by preferred rowing modality (i.e., port vs. starboard vs. sculling) for either MSF ($p = 0.915$) or SS ($p = 0.062$). When grouped by athlete age/competition level, there was no difference in MSF ($p = 0.107$), but masters rowers showed significantly less catch suspension than other groups ($p = 0.042$; Table 5.7). Across all stroke rates, elite, club, and

university athletes showed similar mean suspension away from the seat during the first 10-20% of the stroke (-0.36% to -0.58%), while masters rowers showed clearly declining SS through the early-drive phase (-0.96%) compared to the other athlete cohorts (*$p < 0.0001$*; Table 5.7). However, sharper increases in MSF and loss of SS through the late drive were displayed by elites (-7.36%) compared to club (-6.77%) and university (-6.77%) rowers (*$p = 0.0021$*; Table 5.7).

Table 5.7: Descriptive statistics (mean ± std) for all athlete cohorts of max seat force (MSF) in Newtons (N), relative time to reach MSF (% to MSF), and the seat suspension (SS) percent rate of change in early-drive phase (ED-SS RoC) and late-drive phase (LD-SS RoC). Asterisks (*) indicate ANOVA of $p < 0.05$ with respect to stroke rate across total athlete population.

		18 spm	**24 spm**	**28 spm**	**32 spm**	
Total	MSF	876.9 ± 133.2	918.3 ± 142.1	955.4 ± 153.7	981.0 ± 164.3	*
	% to MSF	31.7 ± 4.0	38.2 ± 5.5	42.2 ± 5.5	44.1 ± 5.1	*
	ED-SS RoC	0.22 ± 0.04%	-0.45 ± 0.04%	-0.85 ± 0.04%	-1.08 ± 0.05%	*
	LD-SS RoC	-7.24 ± 0.06%	-6.80 ± 0.08%	-6.46 ± 0.09%	-6.11 ± 0.12%	*
Female	MSF	817.2 ± 94.1	858.2 ± 105.0	895.3 ± 119.3	903.5 ± 122.4	
	% to MSF	32.3 ± 4.0	39.5 ± 5.3	43.1 ± 5.4	45.0 ± 4.7	
	ED-SS RoC	0.12 ± 0.04%	-0.57 ± 0.04%	-0.95 ± 0.04%	-1.19 ± 0.04%	
	LD-SS RoC	-7.42 ± 0.08%	-6.96 ± 0.10%	-6.61 ± 0.11%	-6.43 ± 0.13%	
Male	MSF	985.9 ± 124.9	1027.9 ± 135.4	1065.0 ± 148.6	1104.1 ± 146.2	
	% to MSF	30.6 ± 3.6	35.9 ± 5.3	40.6 ± 5.4	42.6 ± 5.3	
	ED-SS RoC	0.29 ± 0.04%	-0.28 ± 0.05%	-0.68 ± 0.05%	-0.88 ± 0.06%	
	LD-SS RoC	-7.48 ± 0.07%	-7.34 ± 0.09%	-6.74 ± 0.09%	-6.19 ± 0.11%	
Club	MSF	887.7 ± 111.1	928.3 ± 124.6	951.6 ± 114.8	992.7 ± 120.9	
	% to MSF	30.5 ± 3.7	38.0 ± 4.9	41.9 ± 5.3	43.8 ± 5.6	
	ED-SS RoC	0.50 ± 0.09%	-0.24 ± 0.07%	-0.71 ± 0.07%	-0.97 ± 0.07%	
	LD-SS RoC	-8.00 ± 0.14%	-7.25 ± 0.12%	-6.23 ± 0.12%	-5.61 ± 0.12%	
Elite	MSF	881.8 ± 73.6	928.5 ± 90.9	966.5 ± 86.0	984.6 ± 99.0	
	% to MSF	32.3 ± 3.4	37.3 ± 5.4	40.8 ± 4.8	42.7 ± 3.7	
	ED-SS RoC	0.07 ± 0.04%	-0.36 ± 0.04%	-0.59 ± 0.04%	-0.74 ± 0.04%	
	LD-SS RoC	-8.19 ± 0.10%	-7.12 ± 0.08%	-6.86 ± 0.10%	-7.27 ± 0.11%	

Table 5.7 (continued)

		18 spm	24 spm	28 spm	32 spm
Master	MSF	969.8 ± 195.6	1018.2 ± 197.3	1092.5 ± 216.6	1102.2 ± 219.9
	% to MSF	30.3 ± 3.4	36.3 ± 4.2	40.1 ± 4.4	43.0 ± 4.9
	ED-SS RoC	-0.28 ± 0.05%	-0.89 ± 0.05%	-1.23 ± 0.05%	-1.43 ± 0.04%
	LD-SS RoC	-6.50 ± 0.11%	-7.13 ± 0.16%	-7.71 ± 0.23%	-7.02 ± 0.21%
University	MSF	845.0 ± 132.0	881.8 ± 138.4	913.3 ± 151.4	942.3 ± 162.4
	% to MSF	32.2 ± 4.3	39.4 ± 5.9	43.7 ± 5.8	45.0 ± 5.2
	ED-SS RoC	0.25 ± 0.04%	-0.45 ± 0.04%	-0.95 ± 0.04%	-1.15 ± 0.05%
	LD-SS RoC	-7.38 ± 0.07%	-6.83 ± 0.09%	-6.58 ± 0.11%	-6.29 ± 0.13%
Port	MSF	880.2 ± 155.5	923.1 ± 177.5	966.3 ± 192.8	988.9 ± 198.4
	% to MSF	32.1 ± 4.2	39.6 ± 5.6	43.4 ± 5.1	43.9 ± 6.0
	ED-SS RoC	0.42 ± 0.04%	-0.30 ± 0.04%	-0.72 ± 0.05%	-1.00 ± 0.05%
	LD-SS RoC	-6.84 ± 0.06%	-6.03 ± 0.06%	-5.82 ± 0.08%	-5.10 ± 0.07%
Starboard	MSF	867.5 ± 106.8	911.2 ± 112.8	948.1 ± 127.8	969.3 ± 143.5
	% to MSF	31.8 ± 3.9	38.5 ± 5.2	42.5 ± 5.8	44.3 ± 5.3
	ED-SS RoC	0.07 ± 0.04%	-0.55 ± 0.04%	-0.95 ± 0.04%	-1.13 ± 0.04%
	LD-SS RoC	-7.21 ± 0.07%	-6.94 ± 0.08%	-6.80 ± 0.12%	-6.56 ± 0.12%
Sculling	MSF	910.2 ± 151.1	933.9 ± 136.1	958.9 ± 130.7	984.7 ± 135.4
	% to MSF	30.8 ± 3.6	36.6 ± 4.7	40.0 ± 4.7	42.7 ± 5.0
	ED-SS RoC	-0.48 ± 0.06%	-0.78 ± 0.06%	-0.97 ± 0.07%	0.12 ± 0.07%
	LD-SS RoC	-7.90 ± 0.02%	-7.19 ± 0.15%	-6.78 ± 0.15%	-8.37 ± 0.18%

Seat center of pressure during the stroke cycle was quantified based on the values of the seat's four load cells. Seat CoP can be calculated in anterior/posterior and medial/lateral axes. However, initial data analysis revealed that when no discernable force magnitudes were being applied to the seat, such as when an athlete approached 100% body weight suspension, reported CoP coordinates lay outside the physical borders of the ergometer seat area (30 x 25 cm^2). These erroneous CoP coordinates, outside the range of -15 to 15 cm (X) and -12.5 to 12.5 cm (Y), were excluded from further data analysis by employing a median filter based on instantaneous seat force (Murphy, 2009). Total anterior/posterior displacement of seat center of pressure (CoP) remained relatively unchanged with increasing stroke rate (4.26 ± 0.19 cm), however there was a general posterior shift in CoP as rate increased from 18 to 32 spm (Figure 5.19), at the catch (-

2.69 cm), MHF (-1.02 cm), and finish (-0.96 cm). During all steps, seat CoP shifted posteriorly during the first 10% of the stroke, then anteriorly through MHF and the finish. Seat CoP reached its most anterior coordinates partway through the recovery phase (Figure 5.20). Masters rowers were the only subgroup that displayed a statistically larger overall anterior/posterior (A/P) seat drift (6.21 ± 1.6 cm; $p = 0.034$) compared to all other cohorts (4.52 ± 0.65 cm) (Figure 5.21).

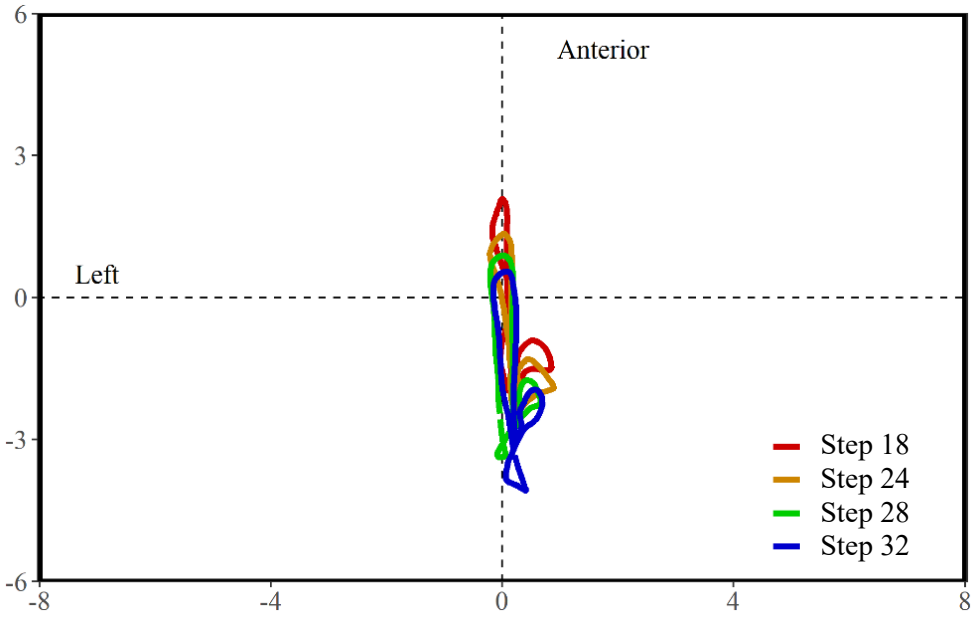

Figure 5.19: Mean curves of population-wide seat center of pressure (CoP) distribution throughout the stroke cycle at all stroke rates. Horizontal axis is left/right seat CoP (cm), and vertical axis is anterior/posterior seat CoP (cm).

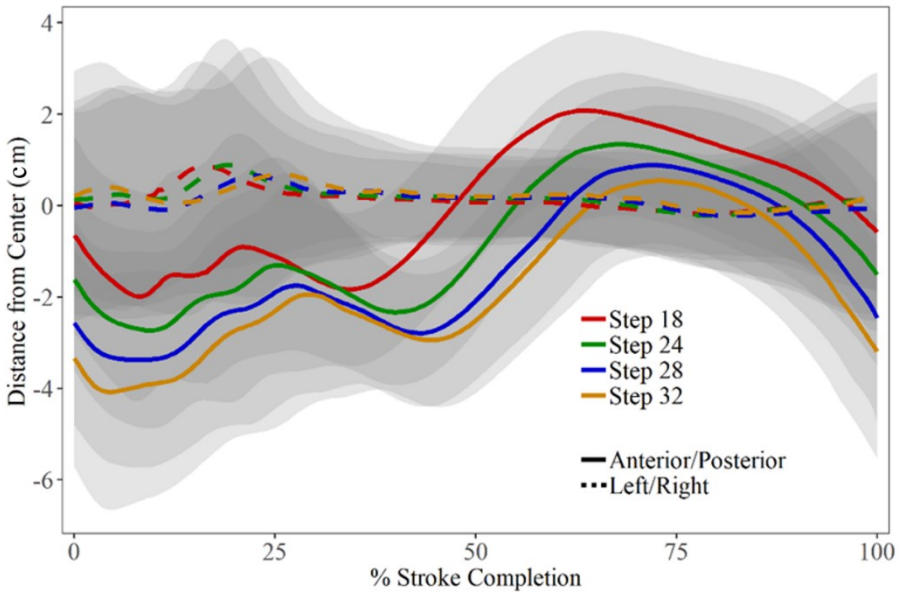

Figure 5.20: Population-wide seat center of pressure (CoP) drift (mean ± std) in anterior/posterior and left/right directions, throughout the full stroke cycle at all stroke rates.

Across the entire athlete population, there was no change in medial/lateral (ML) drift between stroke rates (0.96 ± 0.11 cm; $p = 0.54$). All athlete groups showed greater ML drift during the early-drive phase than during the recovery, with a drift of 0.73 ± 0.07 cm at MHF (Figure 5.20). When subdivided into athlete cohorts, there were no significant differences in seat CoP between males and females, nor were there any significant differences in seat CoP among athlete cohorts when grouped by preferred rowing modality However, the masters athlete group showed a dissimilar seat CoP pattern, particularly at stroke rate 18 spm (Figure 5.21), when compared to club, elite, and university rowers, although this difference was not statistically significant.

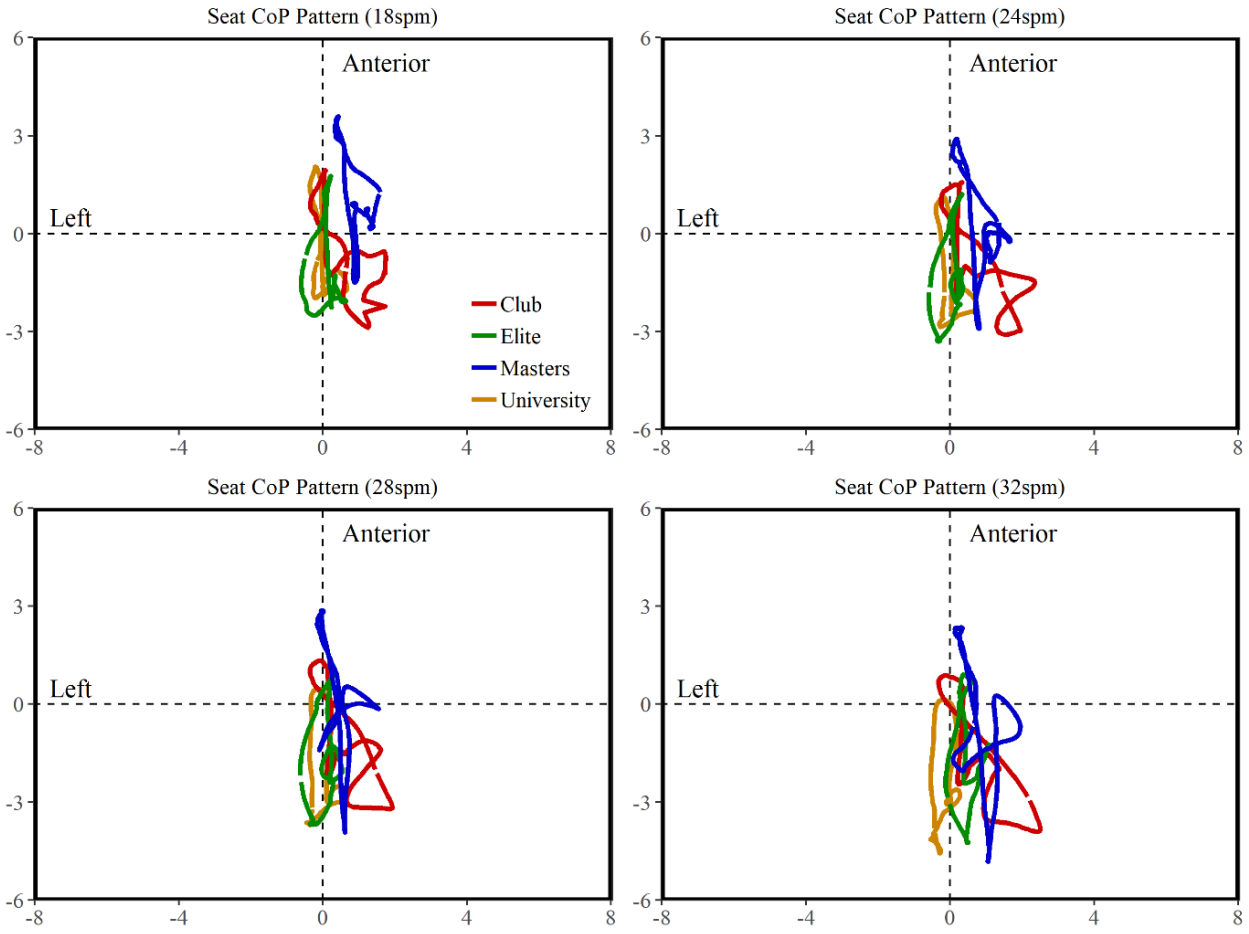

Figure 5.21: Top-down view of ergometer seat and center of pressure (CoP) (mean paths) in centimeters throughout the stroke cycle for all age/competition level cohorts. Stroke rate trials: 18 spm (*top left*), 24 spm (*top right*), 28 spm (*bottom left*), 32 spm (*bottom right*).

5.3.1.3 Footplate Force and Symmetry

Foot force around the finish position for individual athletes sometimes included negative values, indicating that the rower was pulling against the stretcher straps, potentially to compensate for trunk extension at the finish. In the recovery phase, resultant foot force increased, with a sharp rise in the last 10%, preceding the next catch, as the rower transferred weight from the seat to the footplate (Figure 5.22).

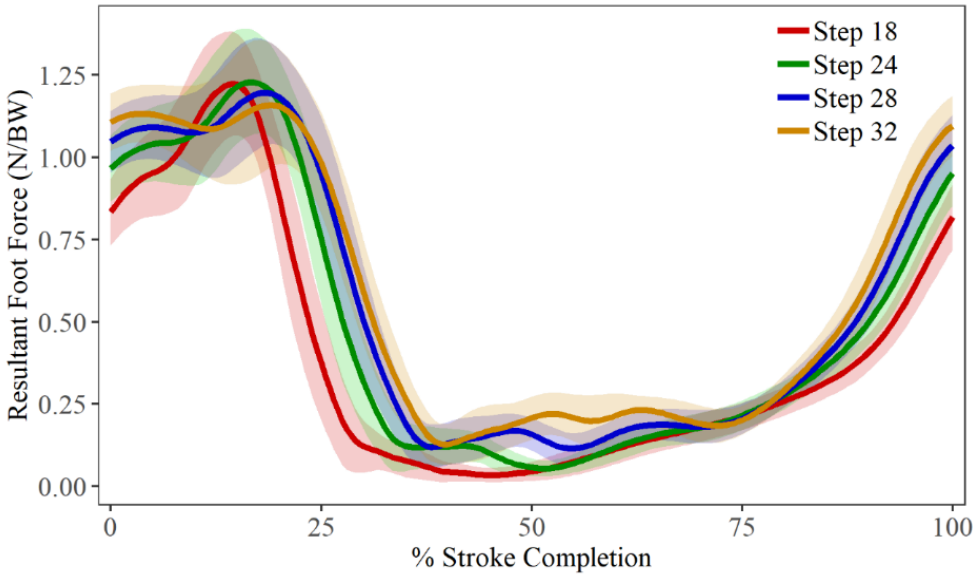

Figure 5.22: Population-wide resultant foot force (mean ± std) at all stroke rates.

Average maximum resultant footplate force (MFF) showed non-significant fluctuations as stroke rate changed (Table 5.8). Examining differences by sex, as with the handle force results, males generated a higher MFF compared to females ($p < 0.0001$; Figure 5.23; Table 5.8). Comparing across age/competition level, elite athletes displayed greater MFF than university ($p = 0.029$) and masters rowers ($p = 0.045$) but not club rowers (Table 5.8). No differences in MFF were identified when comparing athlete groups by preferred rowing modality. None of the athlete cohorts showed significant differences in timing of MFF with respect to stroke rate (Table 5.8).

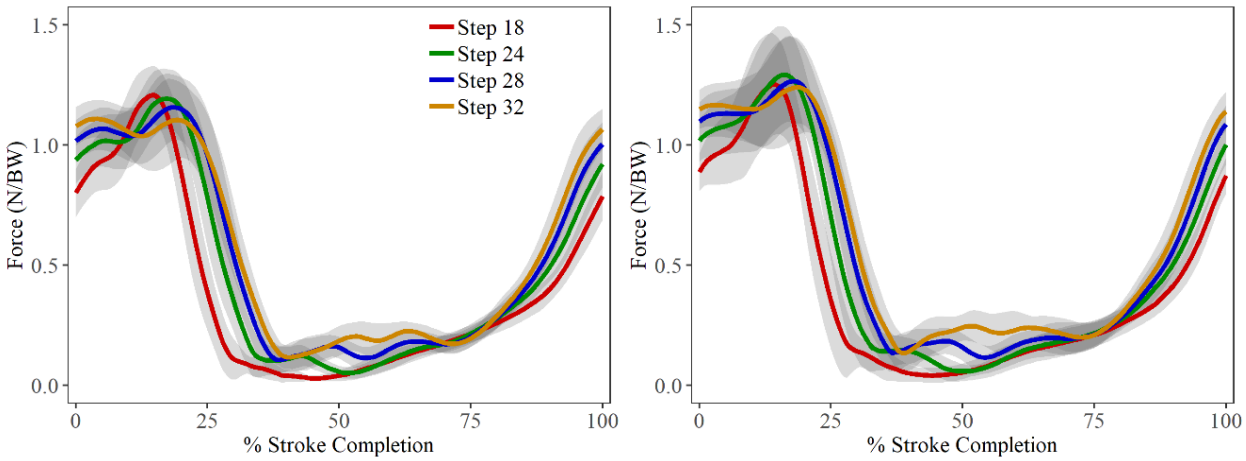

Figure 5.23: Body weight normalized resultant foot force (mean ± std) in N/BW for female (*left*) and male (*right*) athlete cohorts at all stroke rates.

ASI for resultant foot force was calculated at MFF (Table 5.8). All ASI values were close to zero and none were significantly different between any athlete cohorts or at different stroke rates. This implies that when cumulative loading was largest during the drive, pressure was relatively evenly distributed through the lower limbs. However, examining the standard deviation of the ASI for each group, university students had much greater overall variance (7.77 ± 0.25) than the masters group (3.86 ± 1.23).

Table 5.8: Descriptive statistics (mean ± std) for all athlete cohorts of max footplate force (MFF) in Newtons (N), relative time to reach MFF (% to MFF), and the overall foot force asymmetry metric at MFF (MFF-ASI).

		18 spm	**24 spm**	**28 spm**	**32 spm**
Total	MFF	937.7 ± 150.94	946.8 ± 172.8	933.4 ± 170.6	918.3 ± 174.6
	% to MFF	14.6 ± 2.14	16.02 ± 4.41	17.48 ± 13.40	17.30 ± 19.47
	MFF-ASI	-2.51 ± 7.03	-3.24 ± 6.85	-3.52 ± 6.84	-3.78 ± 7.05
Female	MFF	869.8 ± 99.4	865.8 ± 108.5	856.3 ± 120.3	830.1 ± 104.4
	% to MFF	14.6 ± 2.3	16.2 ± 4.4	18.1 ± 16.1	16.1 ± 18.1
	MFF-ASI	-1.06 ± 7.21	-1.29 ± 6.62	-1.51 ±6.27	-1.77 ± 6.20
Male	MFF	1061.6 ± 150.2	1094.2 ± 170.6	1074.0 ± 158.6	1058.3 ± 172.2
	% to MFF	14.4 ± 1.9	15.6 ± 4.3	16.3 ± 5.6	19.1 ± 21.4
	MFF-ASI	-4.99 ± 6.13	-6.56 ± 6.06	-6.94 ± 6.73	-6.80 ± 7.35

Table 5.8 (continued)

		18 spm	24 spm	28 spm	32 spm
Club	MFF	1007.7 ± 129.8	982.7 ± 180.9	951.3 ± 165.9	956.8 ± 156.8
	% to MFF	14.2 ± 2.1	17.4 ± 2.2	13.0 ± 7.9	24.1 ± 29.7
	MFF-ASI	-2.61 ± 4.02	-5.27 ± 5.28	-6.44 ± 7.20	-5.81 ± 8.42
Elite	MFF	984.7 ± 111.7	1025.8 ± 129.7	1024.4 ± 102.6	1028.1 ± 97.4
	% to MFF	15.3 ± 2.3	17.0 ± 2.8	18.0 ± 2.6	17.3 ± 1.8
	MFF-ASI	-0.11 ± 6.63	-0.50 ± 5.86	-0.89 ± 5.64	-0.92 ± 5.60
Master	MFF	907.1 ± 132.5	954.9 ± 130.9	963.0 ± 149.2	918.8 ± 167.6
	% to MFF	14.0 ± 1.9	11.8 ± 6.6	13.6 ± 7.6	12.1 ± 7.8
	MFF-ASI	0.51 ± 5.01	-1.34 ± 3.55	-1.38 ± 1.97	-1.51 ± 4.91
University	MFF	895.0 ± 164.0	888.2 ± 179.0	869.1 ± 180.7	864.2 ± 181.9
	% to MFF	14.4 ± 2.0	16.2 ± 4.3	19.9 ± 18.2	16.3 ± 19.9
	MFF-ASI	-4.48 ± 8.00	-4.51 ± 8.01	-4.50 ± 7.69	-4.63 ± 7.39
Port	MFF	960.9 ± 159.3	962.5 ± 212.6	959.2 ± 222.1	911.0 ± 221.4
	% to MFF	14.7 ± 1.8	16.6 ± 4.6	20.6 ± 20.7	18.1 ± 22.9
	MFF-ASI	-1.63 ± 5.54	-2.45 ± 5.96	-3.18 ± 5.84	-2.36 ± 6.38
Starboard	MFF	919.6 ± 155.3	933.5 ± 142.0	921.0 ± 127.8	916.7 ± 133.1
	% to MFF	14.5 ± 2.4	15.3 ± 4.7	14.7 ± 6.5	13.8 ± 7.9
	MFF-ASI	-3.08 ± 8.33	-3.85 ± 7.68	-3.94 ± 7.54	-4.94 ± 7.46
Sculling	MFF	956.1 ± 147.8	941.8 ± 148.4	911.7 ± 130.3	893.5 ± 133.7
	% to MFF	14.7 ± 1.8	17.1 ± 2.0	18.7 ± 1.4	23.3 ± 29.8
	MFF-ASI	-2.72 ± 6.41	-3.12 ± 6.79	-2.93 ± 7.25	-2.40 ± 7.04

5.3.1.4 Ergometer Derived Kinetics Correlation Analysis

If MHF and MFF exhibit a highly linear relationship, it may be possible to reduce the amount of instrumentation required in data acquisition without sacrificing the utility of the data in relation to athletic performance. MHF showed the strongest positive correlation with MFF (*r=0.757*; Figure 5.24A) and a moderate positive correlation with MSF (*r=0.582*; Figure 5.24b). MSF and MFF also showed a moderate positive correlation (*r=0.673*; Figure 5.24C). Linear regression of SS against MFF also showed moderate correlations at the catch (*r=0.497*), MHF (*r=0.648*; Figure 5.24D), and the finish (*r=0.592*). It is important

to note that computation of a correlation coefficient does not detect non-linear associations between continuous variables. Scalar values from each stroke rate trial were not correlated independently.

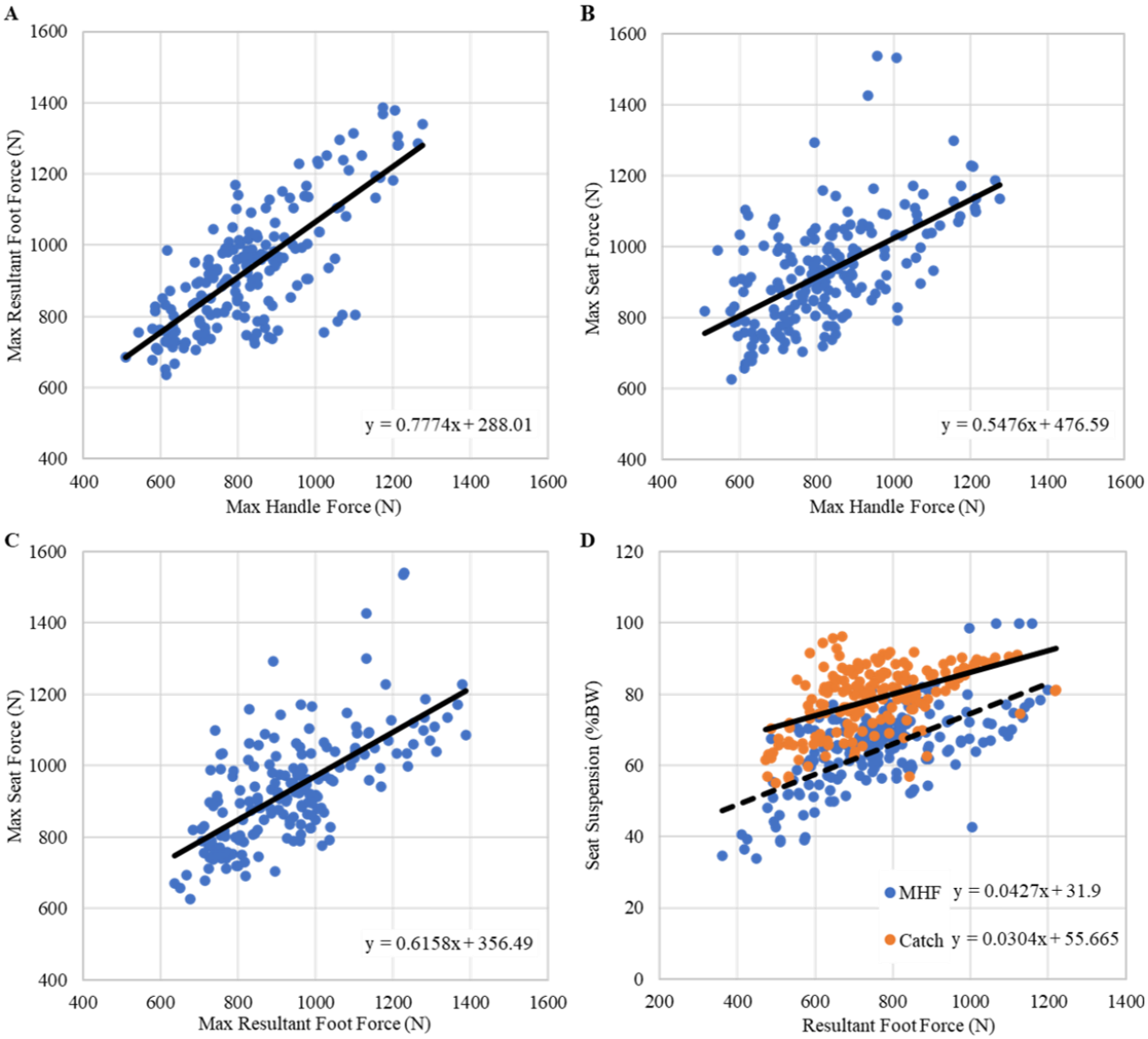

Figure 5.24: Linear regressions among observed values of ergometer derived kinetic metrics, maximum handle force, maximum seat force, and maximum resultant footplate force, pooled across all stroke rates. A) Footplate vs. Handle force. B) Seat vs. Handle force. C) Seat vs. Footplate force. D) Seat suspension vs. Footplate force at catch and maximum handle force (MHF).

5.3.2 Motion Capture Derived Ergometer Kinematics

The simplest form of stroke-time analysis can be achieved by examining timing, trajectory, velocity, and acceleration of the handle and seat.

5.3.2.1 Handle and Seat Kinematics

As discussed above, total stroke length did not significantly change with stroke rate; however, handle displacement loops generated from sagittal and vertical plane position in the global coordinate frame indicated differences in handle kinematics as stroke rate changed (Figure 5.24). Across the total athlete population, handle position loops showed a predominately flat drive with a slight upward draw into the finish. As stroke rate increased, area inside each of the loops decreased as vertical hand position on the recovery rose, while hand position on the drive remained the same. While calculated stroke length did not significantly change with stroke rate across the entire athlete population (Table 5.6), sagittal plane handle position loops show decreased mean horizontal displacement at 32 spm, specifically near the catch and finish positions (Figure 5.25).

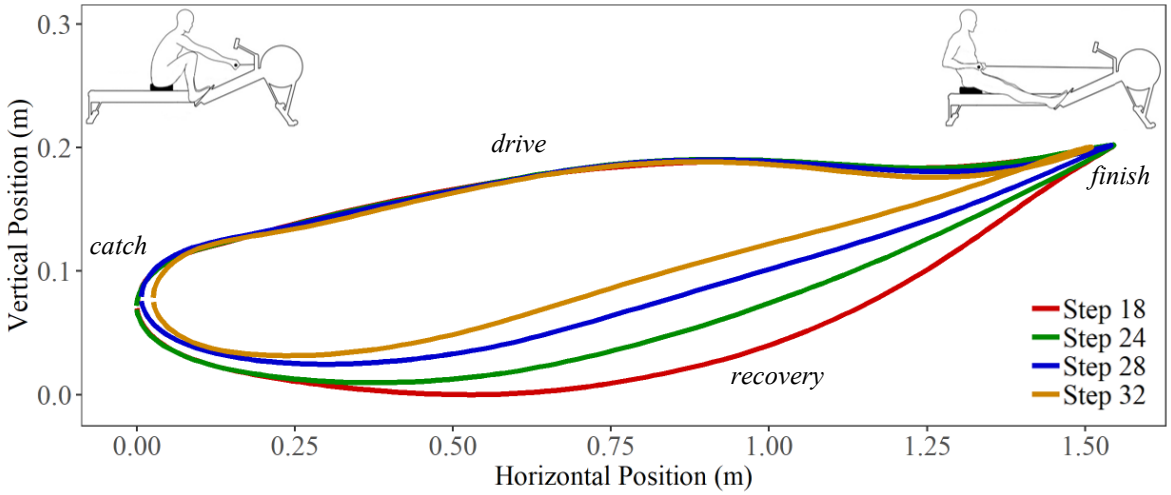

Figure 5.25: Mean sagittal plane handle position loops across whole athlete population with rowing stroke phases indicated at all stroke rates.

Movements patterns in horizontal seat travel across the entire athlete population changed little with stroke rate (Figure 5.26A). Two inflection points were observed in seat trajectory, which were used to delineate three phases of seat travel (Figure 5.26B). The first inflection (SI1) occurred near the end of the drive phase as the legs reached full extension and the second inflection (SI2) occurred part way through the recovery phase as the knees began to flex (Figure 5.26B). As stroke rate increased from 18 spm to 32 spm, the percentage time between SI1 and SI2 decreased because SI1 occurred relatively later in the stroke, while the timing of SI2 remained unchanged (Figure 5.26). As the stroke duration spent between SI1 and SI2

approximates full lower limb extension, minimal A/P seat movement should occur between SI1 and SI2; however, if A/P seat movement occurs it can be visualized as a dip below the linear regression through that phase (*green line;* Figure 5.26B).

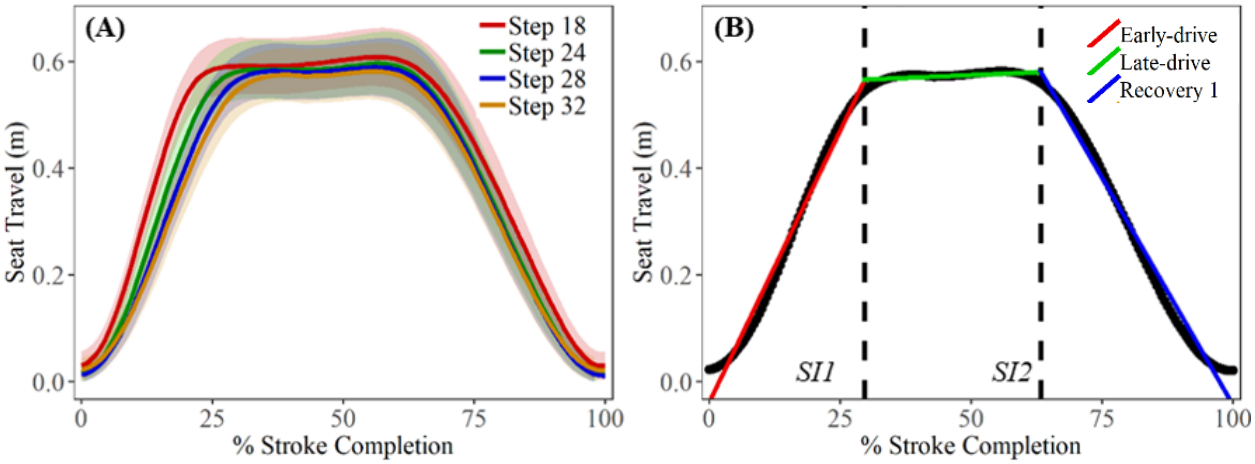

Figure 5.26: (A) Population-wide sagittal seat travel (mean ± std) at all stroke rates. (B) Piecewise linear regressions of each seat movement phase delineated by first seat travel inflection (SI1) and second seat travel inflection (SI2) for seat travel at 32 spm.

Neither handle velocity nor acceleration increased significantly between 18 spm and 32 spm. Handle velocity and acceleration were quasi symmetric between the drive phase and the recovery phase, and the amount of relative stroke time spent near maximal positive velocity increased with stroke rate, while the amount of relative stroke time spent near maximum negative velocity generation decreased with stroke rate (Figure 5.27A). Two inflection points were observed in handle velocity, which delineated three phases of handle acceleration (Figure 5.26B). The first (HI1) occurred near the transition out of catch-slip, as the handle force threshold was passed, and the second (HI2) occurred part way through the late-drive phase, prior to the finish (Figure 5.26B). As stroke rate increased from 18 spm to 32 spm, the percentage time between HI1 and HI2 increased from 21.1% to 32.0% ($p < 0.001$; Table 5.9). Across all stroke rates, when applied handle force crossed MHF, handle acceleration (HA2) was close to zero (*green-line*; Figure 5.27B; Table 5.10).

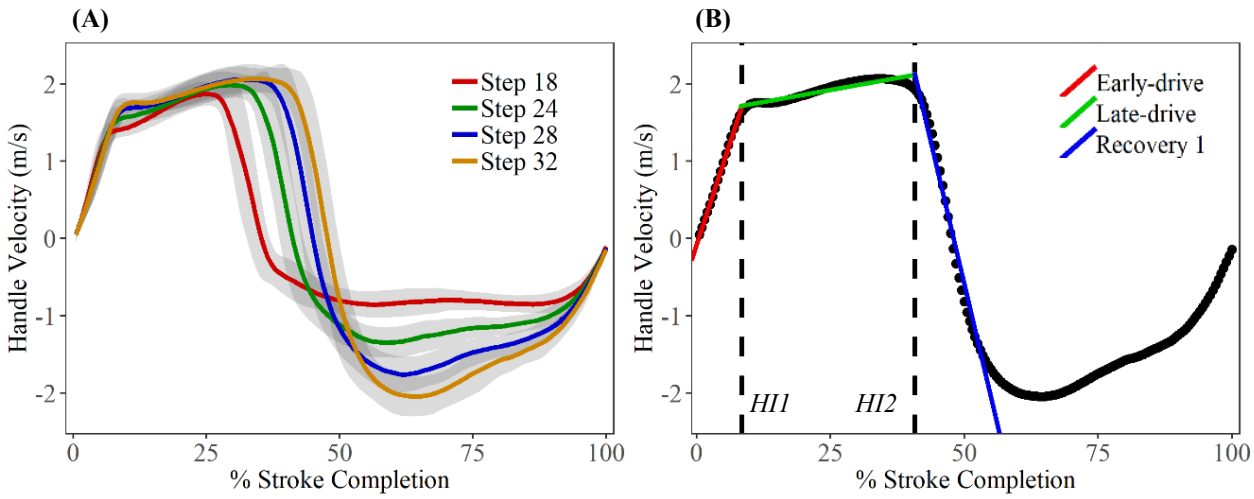

Figure 5.27: (A) Population-wide sagittal handle velocity (mean ± std) at all stroke rates. (B) Piecewise linear regressions of early and late drive handle movement phases delineated by first handle velocity inflection (HI1) and second handle velocity inflection (HI2) for handle velocity at 32 spm.

Table 5.9: Descriptive statistics (mean ± std) for all athlete cohorts in % of stroke completion to reach first and second seat travel inflection points (SI1 & SI2) and first and second handle velocity inflection points (HI1 & HI2), as determined by piecewise linear regression. Asterisks (*) indicate ANOVA of $p < 0.05$ with respect to stroke rate across total athlete population.

		18 spm	24 spm	28 spm	32 spm	
Total	HI1	6.09 ± 2.63	7.28 ± 3.06	8.13 ± 3.13	8.58 ± 3.00	
	HI2	27.27 ± 1.68	33.25 ± 1.81	37.42 ± 1.75	40.62 ± 1.64	*
	SI1	21.86 ± 1.35	25.67 ± 1.73	28.26 ± 2.00	29.70 ± 2.18	*
	SI2	65.36 ± 1.73	64.10 ± 2.07	63.80 ± 2.24	63.35 ± 2.36	
Female	HI1	6.25 ± 2.93	7.53 ± 3.09	8.30 ± 3.23	8.78 ± 3.15	
	HI2	28.62 ± 1.81	35.01 ± 1.87	38.62 ± 1.75	41.64 ± 1.62	
	SI1	21.90 ± 1.35	25.90 ± 1.76	28.56 ± 1.97	29.75 ± 2.14	
	SI2	65.38 ± 1.73	64.15 ± 2.08	64.22 ± 2.22	63.84 ± 2.27	
Male	HI1	5.67 ± 2.46	6.80 ± 2.94	7.69 ± 3.13	8.11 ± 2.98	
	HI2	26.07 ± 1.50	31.63 ± 1.68	36.38 ± 1.68	39.38 ± 1.61	
	SI1	21.80 ± 1.36	25.14 ± 1.70	27.82 ± 2.05	29.63 ± 2.27	
	SI2	65.33 ± 1.76	63.84 ± 2.05	63.20 ± 2.32	62.67 ± 2.52	

Table 5.9 (continued)

		18 spm	24 spm	28 spm	32 spm
Club	HI1	5.37 ± 2.42	6.78 ± 3.11	7.78 ± 3.16	8.41 ± 3.06
	HI2	26.16 ± 1.31	32.08 ± 1.89	36.24 ± 1.75	39.90 ± 01.52
	SI1	19.69 ± 1.28	23.42 ± 1.74	26.38 ± 2.07	27.93 ± 2.19
	SI2	65.17 ± 1.74	63.38 ± 2.19	62.35 ± 2.52	62.24 ± 2.55
Elite	HI1	6.49 ± 3.67	7.09 ± 3.29	7.73 ± 3.24	7.85 ± 3.21
	HI2	29.30 ± 1.85	33.21 ± 2.03	36.69 ± 1.83	39.06 ± 1.75
	SI1	22.55 ± 1.42	25.18 ± 1.70	27.07 ± 1.91	27.66 ± 2.03
	SI2	64.32 ± 1.80	63.66 ± 2.02	63.62 ± 2.15	63.66 ± 2.20
Master	HI1	5.78 ± 2.04	7.29 ± 2.79	8.33 ± 3.30	8.18 ± 3.03
	HI2	27.14 ± 1.18	33.87 ± 1.38	38.36 ± 1.48	41.65 ± 1.48
	SI1	22.35 ± 1.27	26.58 ± 1.53	28.82 ± 1.89	30.16 ± 2.17
	SI2	64.34 ± 1.81	64.40 ± 1.96	64.16 ± 2.19	63.35 ± 2.43
University	HI1	6.05 ± 2.69	7.66 ± 3.11	8.41 ± 3.49	8.88 ± 3.33
	HI2	27.69 ± 1.77	34.22 ± 1.84	38.81 ± 1.79	41.82 ± 1.63
	SI1	22.08 ± 1.36	26.28 ± 1.82	29.32 ± 2.06	30.87 ± 2.27
	SI2	66.34 ± 1.74	64.35 ± 2.11	64.32 ± 2.28	63.69 ± 2.41
Port	HI1	6.36 ± 3.18	7.72 ± 3.26	8.60 ± 3.35	8.38 ± 3.14
	HI2	27.36 ± 1.87	33.23 ± 1.99	37.74 ± 1.86	40.13 ± 1.80
	SI1	21.82 ± 1.39	25.58 ± 1.81	27.69 ± 2.02	28.37 ± 2.12
	SI2	65.65 ± 1.79	64.82 ± 2.10	64.43 ± 2.23	64.85 ± 2.26
Starboard	HI1	5.81 ± 2.72	7.09 ± 3.02	7.92 ± 3.30	8.68 ± 3.07
	HI2	27.21 ± 1.72	33.23 ± 1.87	37.33 ± 1.78	40.88 ± 1.55
	SI1	22.13 ± 1.34	25.72 ± 1.70	28.68 ± 2.00	30.37 ± 2.26
	SI2	65.33 ± 1.79	63.84 ± 2.02	63.93 ± 2.22	63.11 ± 2.24
Sculling	HI1	5.88 ± 2.27	7.12 ± 2.35	7.77 ± 2.75	8.27 ± 3.05
	HI2	27.15 ± 1.32	33.23 ± 1.36	37.38 ± 1.49	40.30 ± 1.58
	SI1	21.57 ± 1.28	25.61 ± 1.67	28.16 ± 2.00	29.25 ± 2.12
	SI2	65.21 ± 1.71	62.66 ± 2.13	61.86 ± 2.38	61.77 ± 2.39

Comparing the position of the seat and handle at the catch, MHF and finish (Figure 5.28A), as well as the ratio of handle-to-seat velocity (Figure 5.28B), can help quantify the relative movement of the athlete's body segments and coordination between the lower and upper body. Across the whole athlete population, as stroke rate increased, the ratio decreased from 0.72 to 0.59, suggesting that at higher stroke rates rowers were more likely to lead with their upper body (Figure 5.25). Smaller ratios indicated greater handle movement versus seat movement and would imply a higher relative use of the upper body. Conversely, larger ratios indicated greater seat movement versus handle movement and implies a higher relative use of the lower body.

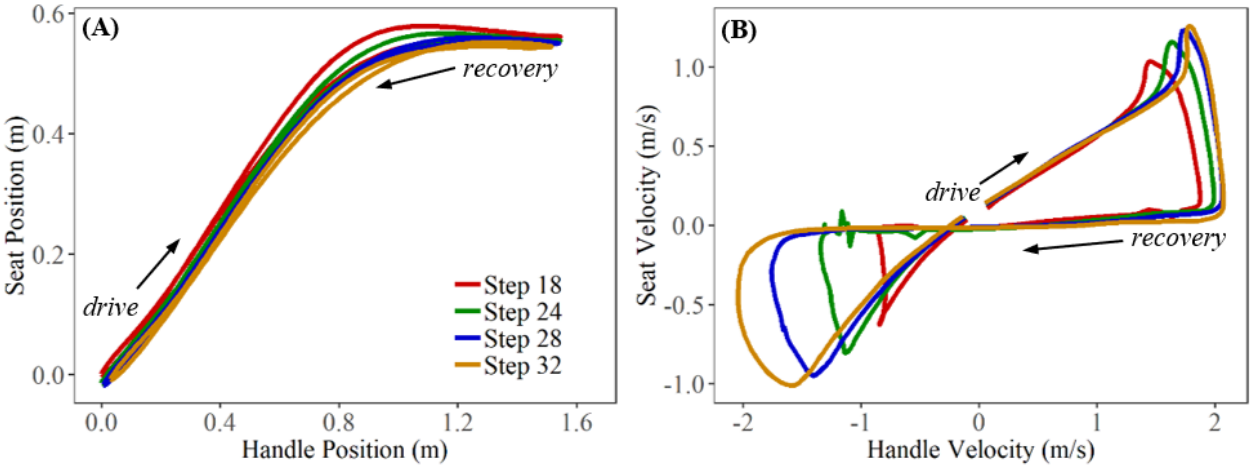

Figure 5.28: (A) Mean relative displacement of the seat versus the handle and (B) Mean relative velocity of the seat versus the handle for all stroke rates. Arrows indicate direction of curve into the drive and recovery phases.

Drive phase seat velocity, or the RoC in seat position before SI1, could be used to approximate leg extension velocity, whilst handle acceleration may be directly related to stroke force and power. As such, relative position and velocity of the seat and handle are both metrics that may be useful in quantifying coordination of upper and lower body movements in the drive phase.

Across the entire athlete population, as stroke rate increased, early-drive handle acceleration increased ($p < 0.001$) while late-drive handle acceleration decreased ($p = 0.024$) and drive-phase seat velocity decreased ($p < 0.001$; Table 5.10). There was no difference in drive phase seat velocity between sexes ($p = 0.26$), but males showed greater late-drive handle acceleration than females ($p = 0.004$), although no difference was observed in early-drive handle acceleration ($p = 0.091$). Comparing athletes by age/competition level revealed that masters had significantly slower seat velocity ($p = 0.0005$) during the drive phase than the other three cohorts. There were no differences in either HA1 ($p = 0.138$) nor HA2 ($p = 0.321$) among any of the age/competition level cohorts (Table 5.10). There were also no significant differences found among cohorts of preferred rowing modality in either HA1 ($p = 0.5871$) or HA2 ($p =$

0.8778), but scullers showed significantly slower seat velocity during the drive phase than their sweep rowing counterparts ($p = 0.0028$; Table 5.10).

Table 5.10: Descriptive statistics (mean ± std) for all athlete cohorts of handle acceleration (m/s^2) during early-drive phase (HA1) and late-drive phase (HA2) and seat velocity (m/s) from stroke start to the first seat travel inflection point (SV1). Asterisks (*) indicate ANOVA of $p < 0.05$ with respect to stroke rate across total athlete population.

		18 spm	24 spm	28 spm	32 spm	
Total	HA1	7.09 ± 0.32	8.78 ± 0.45	9.77 ± 0.48	10.82 ± 0.52	*
	HA2	0.86 ± 0.05	0.81 ± 0.06	0.74 ± 0.07	0.61 ± 0.07	*
	SV1	0.85 ± 0.01	0.74 ± 0.01	0.67 ± 0.01	0.62 ± 0.01	*
Female	HA1	6.95 ± 0.39	8.45 ± 0.46	9.44 ± 0.49	10.22 ± 0.49	
	HA2	0.76 ± 0.05	0.72 ± 0.06	0.68 ± 0.06	0.52 ± 0.06	
	SV1	0.84 ± 0.01	0.74 ± 0.01	0.67 ± 0.01	0.62 ± 0.01	
Male	HA1	7.61 ± 0.31	9.44 ± 0.43	10.62 ± 0.51	12.03 ± 0.57	
	HA2	1.08 ± 0.04	1.04 ± 0.06	0.87 ± 0.06	0.77 ± 0.07	
	SV1	0.87 ± 0.01	0.75 ± 0.01	0.68 ± 0.01	0.620 ± 0.01	
Club	HA1	8.31 ± 0.44	10.01 ± 0.64	10.79 ± 0.64	11.57 ± 0.63	
	HA2	0.98 ± 0.05	0.88 ± 0.08	0.82 ± 0.08	0.68 ± 0.08	
	SV1	0.90 ± 0.01	0.77 ± 0.01	0.69 ± 0.01	0.64 ± 0.01	
Elite	HA1	7.19 ± 0.39	9.31 ± 0.61	10.29 ± 0.59	11.93 ± 0.62	
	HA2	0.85 ± 0.06	0.87 ± 0.08	0.81 ± 0.07	0.71 ± 0.07	
	SV1	0.88 ± 0.01	0.79 ± 0.01	0.72 ± 0.01	0.67 ± 0.01	
Master	HA1	6.62 ± 0.22	7.88 ± 0.29	8.82 ± 0.33	10.33 ± 0.38	
	HA2	0.88 ± 0.03	0.81 ± 0.04	0.72 ± 0.04	0.62 ± 0.04	
	SV1	0.78 ± 0.01	0.69 ± 0.01	0.65 ± 0.01	0.58 ± 0.01	
University	HA1	7.15 ± 0.35	8.25 ± 0.38	9.36 ± 0.46	10.47 ± 0.53	
	HA2	0.83 ± 0.04	0.70 ± 0.06	0.62 ± 0.07	0.57 ± 0.07	
	SV1	0.84 ± 0.01	0.73 ± 0.01	0.65 ± 0.01	0.61 ± 0.01	

Table 5.10 (continued)

		18 spm	24 spm	28 spm	32 spm	
Port	HA1	6.75 ± 0.39	8.31 ± 0.45	9.42 ± 0.49	11.15 ± 0.54	
	HA2	0.89 ± 0.06	0.81 ± 0.07	0.69 ± 0.08	0.51 ± 0.07	
	SV1	0.90 ± 0.01	0.78 ± 0.01	0.71 ± 0.01	0.64 ± 0.01	
Starboard	HA1	7.40 ± 0.37	8.91 ± 0.48	9.72 ± 0.48	10.52 ± 0.51	
	HA2	0.87 ± 0.05	0.79 ± 0.06	0.74 ± 0.07	0.62 ± 0.07	
	SV1	0.84 ± 0.01	0.74 ± 0.01	0.67 ± 0.01	0.63 ± 0.01	
Sculling	HA1	7.59 ± 0.25	9.15 ± 0.28	10.42 ± 0.43	11.41 ± 0.49	
	HA2	0.90 ± 0.03	0.83 ± 0.04	0.72 ± 0.05	0.65 ± 0.06	
	SV1	0.80 ± 0.01	0.69 ± 0.01	0.62 ± 0.01	0.57 ± 0.01	

5.4 DISCUSSION

This chapter detailed the experimental methodology employed during the primary series of athlete performance assessment and explored ergometer derived kinetic and kinematic results through spatio-temporal analysis with a view to generating a comprehensive feedback mechanism for athletes and coaches, as well as generating hypotheses on ergometer instrumentation-derived surrogates of athlete kinematics, which will be further examined in Chapters 6 and 7.

Scalar ergometer split times do not correlate with good rowing technique or effectual ergometer training (Torres-Moreno, Tanaka & Penney, 2000). A key coaching principle in rowing, and one which has been documented in rowing biomechanics research, is for an athlete to suspend their body weight between their feet and hands. This is important to maximize the transfer of load from the foot plate to the handle, without energy loss through the seat. Maintaining proper loading and coordinated mechanics through the kinetic chain is important to produce stable, efficient rowing. During the drive phase, as the legs exert pressure on the foot stretcher, activation of the trunk muscles facilitate suspension by providing stability through the upper extremities (Thompson, 2005). Results in this chapter showed that increased rating, and relative increases in drive time correlated with lower split times but achieving higher stroke rates was mainly attributed to substantially decreasing recovery time. Drive time only decreased significantly from 18 spm to 24 spm and not at higher rates, suggesting that there is a limit to the possible speed of the drive (Figure 5.11). Murphy, (2009) previously identified that later timing of the finish of the stroke, as well as greater SS during the drive, less medio-lateral seat drift, and faster rate of handle force development were all highly correlated with better performance outputs. Deficits on the drive phase of the stroke cycle can

lead to reduced total propulsive force applied to the handle and reduced suspension from the seat (Warmenhoven *et al.*, 2018). As the limit of an individual's drive speed is approached, in order to achieve a desired stroke rate, the recovery phase is rushed, indicated by the significant decrease in recovery time and stroke time (Figure 5.11). These temporal variations may be linked to handle and seat force profile changes (Figure 5.13; Figure 5.16). Differences in magnitude of SS at the catch, MHF, and the finish may suggest that as stroke rate goes up, rowers increasingly use momentum to achieve suspension at the catch, but fatigue or habituation suggests they were unable to maintain that position through to MHF and consequently "collapse" more heavily down onto the seat at the finish (Figure 5.16; Figure 5.17; Figure 5.18). Declining early-drive SS among masters athletes (Table 5.7) suggests some deficits in core rowing muscle's strength, which will be examined more closely in Chapter 8. Reasons for larger MSF and sharper loss of SS during the late drive shown by elite and club athletes are probably different and would require further investigation and research (Table 5.7). Footplate force was relatively evenly distributed between the left and right the lower limbs for all groups, but ASI values for university students had much greater variance than the masters group, which may suggest that bilateral foot force consistency is related to years of rowing experience.

Essential drive coordination begins from the moment the handle and seat change direction at the catch. Catch slip can be attributed in part to the ergometer equipment, specifically the slack between the handle chain, the shock cords, and the flywheel. However, larger handle travel before the catch (i.e. larger catch-slip) indicated less favorable performance outputs overall (Table 5.5; Table 5.6). Thompson (2005) suggests that simultaneous movement of the handle and the seat out of the catch position maximizes force production and energy efficiency. In both ergometer rowing and on-water rower, Smith *et al.*, (2015) and Kleshnev (2009) identified an early drive "microphase" within the first 5% of stroke completion, similar to this study's catch-slip, wherein the rower's mass accelerates but the boat system does not, stating that "ineffective crews" may entirely lack the initial boat acceleration microphase that occurs from 0.8 – 0.12 secs (Kleshnev, 2010). Handle and seat kinematics throughout the stroke cycle have potential value as surrogates for estimating athlete kinematics in lieu of direct measurements. Although total stroke length did not significantly change with stroke rate, sagittal plane handle position loops show shortening in mean horizontal displacement at 32 spm (Figure 5.25). This suggests that rowers achieve slightly less forward reach into the catch, and slightly less lean back into the finish (Ng *et al.*, 2015; Alijanpour *et al.*, 2021), and this may be a mechanism related to the rushed recovery phase at higher stroke rates discussed above (Figure 5.11; Table 5.5). Seat velocity (SV1) from the catch to SI1 can potentially be used as a surrogate for leg extension velocity and correlated to drive time to compare relative time of leg extension to trunk extension. However, consideration must be made for overlap of these movements (Kleshnev, 2010). The percentage of stroke completion spent between seat inflection points SI1 and SI2 may occur simultaneously with a full

leg extension phase (Figure 5.26B), where the movement is from the athlete using their hips to rotate the trunk into and out of the finish position. Ideally this should be accomplished with minimal seat movement, and any excess anterior motion during this phase suggests the athlete is posteriorly over-rotating their hips and implies decreased postural trunk control (McGregor, Patankar & Bull, 2005). Extraneous seat velocity oscillations around the finish position or during the catch slip period could be indicative of unexpected knee and hip joint oscillations, which compromise stroke efficiency and consistency.

McGregor, Bull & Byng-Maddick (2004) compared different common technical errors during ergometer rowing and discussed their potential influence on performance and injury risk. One such error, where the seat moves posteriorly out of the catch with little productive movement of the handle (i.e., "shooting the slide"), results in decreased cumulative force through the stroke. In contrast, when the direction of the handle changes before the seat, initiation of the drive occurs through early extension of the upper body or posterior rotation of the pelvis (i.e., "leading with the shoulders"), and is also associated with lower total power output and less stroke-to-stroke consistency. In either instance, the performance result was a lower handle force, shorter force duration, and less athlete suspension (Table 5.6; Table 5.7). These specific errors could be classified based on relative timing of handle and seat movement. Results in this chapter showed that across the whole athlete population, as stroke rate increased, the ratio of handle-to-seat displacement during the catch-slip period decreased, suggesting that at higher rates, rowers are more likely to lead with their upper body. This finding was interesting given that stroke length slightly decreased with potentially less forward reach into the catch at higher rate (Figure 5.25). To ascribe differences to specific combinations of upper body movements, athlete instrumentation and further kinematic analysis is necessary, which will be discussed in Chapter 6.

A major coaching objective in improving technique is to reduce variation in boat velocity (Nilsen, Daigneault & Smith, 2002a). Handle velocity is necessary for calculating stroke power but is valid alone only when assuming a perfectly connected kinetic chain. Seat velocity (Figure 5.26; Table 5.10) and acceleration have previously been used to approximate the rower's center of mass (Baudouin & Hawkins, 2004; Hofmijster *et al.*, 2007), but this simplified measure neglects any non-sagittal plane motion which would introduce fluctuations in boat velocity. Paired with handle velocity and acceleration (Figure 5.27; Table 5.10), which includes vertical motions, different body segment movement patterns can and have been used to distinguish and classify sequential and simultaneous rowing styles (Kleshnev, 2000). As ergometer-derived surrogates of joint movement, the timings and overlap in segment motion phases combine to give an overview of gross athlete kinematics and a granular view of body segment momentum interactions (Kleshnev, 2006b).

McGregor, Bull & Byng-Maddick (2004) suggested these types of movement patterns carry a secondary effect on hip and lumbar joint flexion, producing spinal kinematic variations associated with increased injury risk. Similarly, Buckeridge *et al.* (2012) noted that elite rowers exhibited a high level of consistency in foot force production, independent of stroke rate but suggested that when initiating the drive phase with asymmetric lower limb force, compensatory moments at the pelvis and lumbar spine may be created, to maintain a straight-line handle trajectory. This potentially reflects some differences seen in when comparing seat center of pressure between sweep rowers and scullers. Unfortunately, because the existing ergometer setup utilizes only a single uniaxial load cell mounted in line with the handle chain, it was not possible to discern loading differences through each of the hands. A future hardware advancement may be to modify the handle setup to include multiple load sensors to assess hand pressure distribution (Pudlo, Pinti & Lepoutre, 2005).

Quantifiable relationships exist among the three major kinetic ergometer outputs (i.e., handle force, seat force, and footplate force). Determining a mathematical transfer function between one or more of these metrics may allow instrumentation requirements to be reduced for others to use this analysis without sacrificing scope of performance assessment. All kinetic and kinematic data presented in this thesis was collected in a laboratory setting where there were fewer limitations to the instrumentation that could be employed and the biomechanical data that could be acquired (Chapter 3, Section 3.5.1). Ergometers are considered an effective training tool that satisfactorily reproduce on-water kinematics (Lamb, 1989; Hawkins, 2000; Page & Hawkins, 2003). While data acquisition in a laboratory setting has the luxury of being extensive, data derived from ergometer rowing cannot be directly translated to on-water rowing performance. Transitioning data collection to an on-water environment highly favors equipment which is wireless, minimizes added boat weight, and maximizes available bandwidth. With moderately strong, positive linear correlations reported in this chapter (Section 5.3.1.4) - between MHF, MSF, and MFF (Figure 5.24) – and continuing developments in wireless telemetry systems, it may be possible for limited instrumentation to be transferred to boats, which may subsequently be correlated to more detailed data acquired in the laboratory, in order to achieve a similarly robust measure of rowing performance on the water.

Qualitative visual analysis of rowing technique by coaches involves observation of continuous kinematic variables. Technology that provides objective feedback during training sessions can be beneficial in assessing an athlete's technical ability to supplement a coach's qualitative feedback or to support athletes without access to coaching (Page & Hawkins, 2003). Rowing instrumentation systems have been used to quantify kinetic variables and through application of biomechanics principles, develop hypotheses on the influence of spatio-temporal characteristics of movement patterns and force profiles relative to aspects of

rowing technique and correlated to performance metrics. Coordination of body segments and force exertion after the catch is important, as better synchronization may contribute to consistently smooth, efficient rowing performance. Murphy (2009) defined several predictors of higher performance including rapid handle force production, longer stroke length, and greater SS, which were affected by lumbar flexion at the catch, knee compression at the catch, and leg extension at the finish (Murphy, 2009). In the absence of complex human motion tracking equipment, kinetic and kinematic measurements of the system may predict the influence of rowing technique, when relationships can be established with kinematics measured directly from athletes. Results in this chapter suggest that instrumentation of a rowing ergometer alone could be used as a simplified biofeedback tool to improve quality of rowing stroke movement. M/L seat drift may predict off-axis forces affecting boat stability. Left/right foot force asymmetries may predict torsional forces in the boat (Buckeridge, 2013). Handle and seat kinematics may be surrogates of joint movement, with seat velocity as a surrogate for leg extension velocity, handle velocity as a surrogate for shoulder or trunk velocity. Relative movements and timing of the seat and handle may indicate transfer of propulsive force from the feet to the handle.

Applications and implications of the work presented in this chapter are that instrumentation-driven spatio-temporal biofeedback offers a tool for quantifying and visually displaying performance information. Knowledge of the relationships between kinetic, kinematic, and performance factors developed within this thesis and derived from previously published literature allow for assessment of athlete technique with less complex equipment, increasing accessibility to technique quantification and simplifying feedback for improving motor skills and rowing performance (Smith & Loschner, 2002).

5.5 CONCLUSIONS

The goal of this chapter was to implement OMC for use in whole body dynamic tracking of ergometer rowing. Spatio-temporal analysis of ergometer derived kinetics and kinematics were presented and discussed in the context of biomechanical feedback for performance analysis. Converting complex captured data into simple representations of physical parameters can enhance an athletes' ability to understand their body segment motion and help coaches better communicate its relationship to performance.

In this chapter, the influence of the upper body on ergometer derived performance metrics has only been inferred from relative movement between the seat and handle and comparing external force at each of the footplate, seat, and handle. Kinematics of the upper limb, shoulder complex, and upper spine would further the understanding of whole-body factors in rowing technique. Thus, changes in joint kinematics and the underlying muscular changes from which altered kinematics arise are further examined in Chapters 6 and 7, where modelling of scapular biomechanics for the enhancement of interpreting performance data is

examined, the fidelity of ergometer derived kinetic and kinematic variables as surrogates of athlete kinematics is discussed, and insight into mitigating injury risk and guiding training periodization is proposed.

6. CHAPTER 6: FATIGUE LEADS TO ALTERED SHOULDER AND SPINE KINEMATICS DURING HIGH PERFORMANCE ERGOMETER ROWING[2]

In Chapter 5 experimental materials and methodologies central to completing this thesis work were described, and key results from spatio-temporal analysis of ergometer instrumentation derived kinetics were discussed, including measures of handle force, seat force, footplate force, and stroke length. This enabled real-time visualization and detailed biomechanical feedback of rowing technique and performance for athletes and coaches. This chapter presents kinematic data on the shoulder complex during ergometer rowing, suitable for input into an inverse dynamics MSK model.

Analyzing and understanding human movement involves reconstruction of bone position and orientation in 3-D space at each instant in time throughout the entire motion. Steps involved in the processing and analysis from the kinematic model are presented in this chapter. Alterations in joint kinematics presented include scapulothoracic and glenohumeral data for all subjects as well as between cohorts distinguished by athlete demographic differences.

6.1 INTRODUCTION

As previously discussed in Chapter 3 (Section 3.1), the rowing stroke is a continuous fluid movement typically described in four parts: *catch, drive, finish,* and *recovery*. At the catch, the lower extremities, trunk, and shoulders are in full flexion and elbows are in full extension. During the propulsive drive phase, the athlete extends the lower limbs and shoulders, posteriorly rotates the trunk, and flexes and abducts the elbows until reaching the finish position. During the early-drive phase, the shoulders remain in full flexion and elbows in full extension. During the late-drive phase the shoulders extend and the elbows 'break' and flex, reaching maxima near the finish position. The recovery phase reverses overall motion, first extending the elbows, then flexing the shoulders, anteriorly rotating the trunk, and flexing the lower extremities. Sweep rowing can also add asymmetric axial rotation and lateral bending of the upper body.

In rowing, the first of two fundamentally different coaching styles extrapolates that longer stroke length is proportional to higher power output and advocates for more excursion of more recruited muscles. A contrasting style extols that the means of attaining extra length by adding strain to smaller stabilizing

[2] Published in part as: Urbanczyk, C.A., Miller, E., McGregor, A.H. and Bull, A.M. (2020). Fatigue leads to altered spinal kinematics during high performance ergometer rowing. *ISBS Conference Proceedings Archive*, 38(1): 256-259.

muscles is not worth the cost since, as these muscles fatigue, injury risk increases (Kleshnev, 2006a; Cookson *et al.*, 2017).

The importance of the lower extremity and lumbar spine have been well studied in the rowing mechanics literature. Previously published kinematic studies have quantified simple metrics including lumbo-pelvic and lumbo-thoracic rotation in the sagittal plane (McGregor, Patankar & Bull, 2007) and reinforced that accurate sequencing of limb and trunk motion leads to effective force transmission (Smith & Spinks, 1995). However, there is limited research on the contributions of the thoracic spine, shoulder complex, and upper limb to force generation and momentum transfer. In a "closed chain" activity such as rowing, where the movement pattern is predictable, studying athlete kinematics enables specific identification of technique that is lacking or incorrect, and can be used to refine skills to improve athlete performance, while minimizing risk of injury. Injuries to the spine are the most commonly reported amongst rowers, followed by the knees and arms (Smoljanovic *et al.*, 2009; Wilson *et al.*, 2010). This has been attributed to intense, repetitive, flexion/extension and compressive forces, often stemming from high training volumes on the ergometer and poor technique (Thornton *et al.*, 2017b; Buckeridge, Bull & McGregor, 2016).

The four major curves of the spine: cervical, thoracic, lumbar, and sacral are optimized for high flexibility and strength in compressive loading. However, rowing can be a source of excessive spinal loading, where the back acts as a brace to transmit load from the legs through to the handle. Several studies have identified the catch as the position of greatest injury risk to the rower and suggested that hyperflexion of the torso is a precipitating factor. It has been recommended that the spine should be flexed by as much as 45° to maximize force generation potential (Nilsen, Daigneault & Smith, 2002b), but this creates large moments at the vertebrae, which with high repetition, muscle fatigue, and deterioration in posture can leave the spine susceptible to injury. Wilson (2010) and Caldwell, McNair & Williams (2003) suggested that fatigue leads to decreased precision of controlled movements, decreasing the rower's postural control towards the end of training sessions.

Excessive flexion and extension of the back have been implicated as mechanisms of low back injury (Tanaka, Ide & Moreno, 2007; Wilson *et al.*, 2013). While sagittal plane mechanics are the most prominent effectors, out of plane asymmetries can contribute to decreased efficiency and spinal injury (McGregor, 2002; Buckeridge, Bull & Mcgregor, 2015). The nature of rowing as a whole-body activity connected throughout by the kinetic chain means that altered spinal kinematics may propagate proximally to affect thoracic mobility, and shoulder and elbow stability. Restricted lower body mobility may be compensated for elsewhere to achieve longer stroke length. This typically comes from lumbar and thoracic flexion, and

scapular protraction. Increased shoulder flexion angle at the catch was associated with rib stress fractures but using more extreme joint ranges did not translate to increased force production (Cutler *et al.*, 2017).

Building a kinematic map of upper body movement patterns in multiple planes is fundamental for developing a complete biomechanical model of the body in rowing. This chapter examines upper body kinematics in the sagittal, frontal, and transverse planes, throughout the rowing stroke before and after fatigue onset. Motion of the upper limb, shoulder complex and spine were described by three-dimensional joint angles, joint positions, segment velocities and segment orientations. Intersegmental differences at critical points during the rowing stroke were examined to assess whether a straight (neutral) or a flexed overall spinal posture provides more efficient load transfer.

6.2 METHODS

Materials and methodology were described in Chapter 5, Section 5.2. Data from a subset of the total athlete population were utilized in each of the following kinematic analyses. Lower participant numbers were a combination of accessibility of national team (i.e., elite) athletes (n=9) and subjects excluded from further analysis due to systematic experimental errors or model non-convergence (n=4). For spinal kinematics analysis, time intensive marker reconstruction and data processing limited total subject inclusion. Demographics of those athletes used in kinematic analysis of the upper extremity (Table 6.1) and kinematic analysis of the spine (Table 6.2) are reported in brief here.

Table 6.1: Anthropometric data (mean ± std) for age, mass, and height, as well as years of experience in rowing, specific to athletes whose data were used in upper extremity kinematic analysis.

	Age (years)	Mass (kg)	Height (m)	Years Rowing
Total (n=36)	25.5 ± 7.1	76.9 ± 10.2	179.4 ± 10.2	8.1 ± 7.0
Female (n=20)	24.7 ± 7.1	69.7 ± 8.1	172.6 ± 5.5	7.5 ± 6.2
Male (n=16)	26.6 ± 7.1	86.0 ± 10.3	187.9 ± 8.1	8.8 ± 8.0
Club (n=6)	27.4 ± 3.2	80.2 ± 9.0	186.3 ± 8.8	8.3 ± 4.2
Elite (n=3)	26.4 ± 3.1	82.0 ± 8.5	192.3 ± 10.2	10.3 ± 3.3
Master (n=6)	39.0 ± 4.3	80.8 ± 15.9	176.6 ± 9.5	20.3 ± 7.1
University (n=21)	20.9 ± 1.7	74.4 ± 11.5	177.3 ± 9.4	4.5 ± 2.6
Port (n=12)	23.8 ± 5.4	77.3 ± 15.6	179.4 ± 12.5	6.6 ± 4.3
Starboard (n=16)	23.9 ± 6.2	78.5 ± 10.1	180.4 ± 9.1	6.3 ± 5.5
Sculling (n=8)	31.6 ± 7.8	73.3 ± 9.1	177.5 ± 7.9	13.7 ± 9.7

Table 6.2: Anthropometric data (mean ± std) for age, mass, and height, as well as years of experience in rowing, specific to athletes whose data were used in spinal kinematic analysis.

	Age (years)	Mass (kg)	Height (cm)	Years Rowing
Total (n=16)	26.7 ± 5.5	79.8 ± 13.6	182.6 ± 11.7	8.7 ± 5.4
Female (n=6)	28.3 ± 5.3	68.3 ± 5.2	172.3 ± 7.1	11.2 ± 5.6
Male (n=10)	25.8 ± 5.4	86.7 ± 12.4	188.8 ± 9.4	7.2 ± 4.6
Port (n=5)	28.0 ± 5.9	92.5 ± 14.2	189.0 ± 8.2	7.9 ± 5.3
Starboard (n=7)	23.8 ± 5.0	79.0 ± 9.5	183.2 ± 8.8	6.8 ± 5.5
Sculling (n=4)	31.4 ± 1.3	66.1 ± 3.3	170.6 ± 8.7	13.5 ± 1.8

Twenty-two retro reflective markers along the spine and six pelvis markers were used to create four segments: upper thoracic (vertebral levels C7 – T1), lower thoracic (T6 – T7), lumbar (T12 – L1), and pelvis (L5 – S1 & hip markers). Additionally, twenty-four markers placed on the chest and upper extremities were used to create forearm, humerus, scapula, and clavicle segments (Figure 6.1). These markers were a subset of the whole-body marker set previously described in Chapter 5, Section 5.2.2.

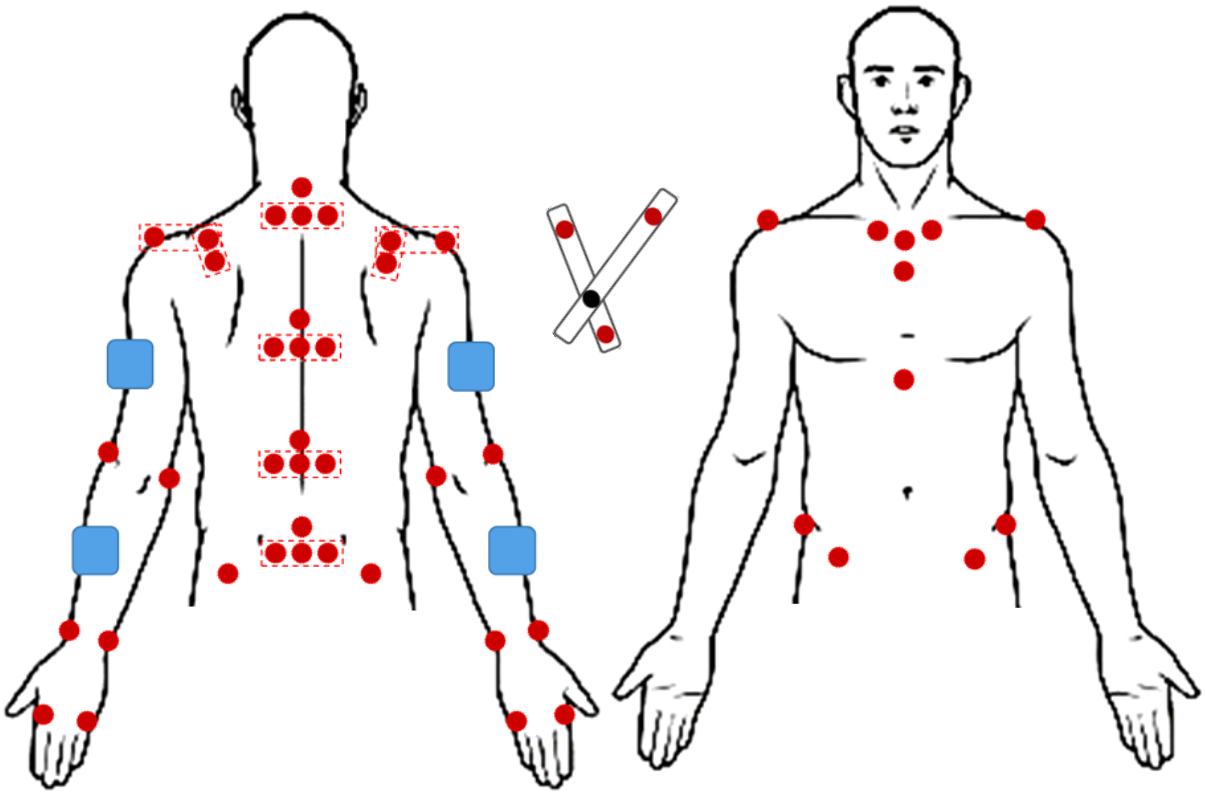

Figure 6.1: Anterior and posterior views of spinal and upper extremity marker sub-sets. Red dots represent individual retro-reflective markers. Red dashed lines indicate groups of markers that share a flexible rubber base, affixed to athlete with hypo-allergenic double-sided tape. Blue boxes represent rigid nylon marker cluster plates, secured around body segments by elastic Velcro bands. Central inset is of the scapula locator used in calibration.

6.2.1 Data Processing and Analysis

Captured motion data and external forces were processed and analyzed in MATLAB 2017B (MathWorks Inc., Natick, MA, USA) utilizing two separate processing pipelines designated by the body segments/region of interest. Spinal marker data were analyzed using a custom inverse kinematics model built in MATLAB 2017B. Upper extremity data served as inputs into UKNSM computational model, comprehensive details of which are described in Chapter 7.

6.2.1.1 Upper Limb Kinematics

The UKNSM was used to calculate inverse kinematics across the right shoulder and arm. Local coordinate frames for each body segment were defined based on anatomical landmarks following ISB standards (Wu *et al.*, 2005). A description of the anatomical frames of each body segment were given in Chapter 2 (Section 2.2.1; Figure 2.2) and calculations of the Euler sequences used for joint kinematics are summarized in Table 6.3. Body segment coordinate frames were defined as the superior oriented Y, lateral

oriented X, and posterior oriented Z axes. Rotations of the distal coordinate system have been described with respect to the proximal coordinate system. Detailed information on the local coordinate frames for the thorax, clavicle, humerus, forearm and scapula employed by the UKNSM were characterized in Charlton (2003) and (Charlton & Johnson, 2006). Positive elbow rotations were assigned as flexion, pronation, and adduction. Zero alignment at the elbow occurred when the forearm was fully extended and supinated relative to the upper arm. Positive glenohumeral rotations were assigned as flexion, adduction, and internal rotation and positive scapulothoracic rotations were assigned as internal rotation, upward rotation, and posterior tilt (Table 6.3). Non-ISB standard Euler rotation sequences utilized by the UKNSM for the GH joint were selected to generate joint angles that are clinically relevant, by aligning the rotation about the x-axis (i.e., flexion/extension) with the largest movements occurring in the sagittal plane during ergometer rowing.

Table 6.3: Euler rotation sequences for joint angle calculations between United Kingdom national shoulder model (UKNSM) body segments, and clinical/ anatomical description of those rotations.

Articulation	Euler Sequence	Clinical Description
Glenohumeral (GH)	x -z'-y"	(+) Flexion – Adduction – Internal Rotation
Elbow	x-z'-y"	(+) Flexion – Adduction – Pronation
Scapulothoracic (ST)	y-z'-x"	(+) Internal Rotation – Upward Rotation – Posterior Tilt

Statistical significance was set at $p < 0.05$ and appropriate statistical analyses were conducted using R packages in RStudio 3.6 (RStudio Team, 2016) and JMP Pro 14 (SAS Institute, NC, USA). Statistical parametric mapping toolboxes (spm1d; Pataky, 2016) were used to determine significant differences between the athlete cohorts and across stroke rates in MATLAB 2017B (MathWorks, MA, USA). Each stroke rate and percentage of stroke completion (0 - 100%) were defined as the within subject factors and joint rotations as the dependent variables. Tukey HSD post-hoc tests were used to perform pair-wise comparisons. Piecewise linear regression with *a priori* breakpoint estimates was used to estimate the RoC in elbow, GH, and ST joint angles during the early-drive, late-drive, and recovery phases at each stroke rate (Muggeo, 2003).

6.2.1.2 Spinal Kinematics

Vertebral angles between adjacent spinal segments (i.e., pelvic, lumbar, and thoracic) were calculated such that $\boldsymbol{\alpha}$ was the angle of flexion/extension in the global sagittal plane, $\boldsymbol{\beta}$ was the angle of lateral bending in the global frontal plane, and $\boldsymbol{\gamma}$ was the angle of rotation in the global transverse plane (Figure 6.2). Sagittal plane lumbar-pelvic and lumbar-thoracic ratios were calculated at each frame between each of the adjacent spine segments by dividing the $\boldsymbol{\alpha}$ angle of the upper segment by the $\boldsymbol{\alpha}$ angle of the lower segment

(McGregor, Patankar & Bull, 2007). To examine the effect of the fatiguing step protocol on postural control, flexion/extension of the thoracic and lumbar spine at the catch was correlated with stroke number within each trial and between stroke rates.

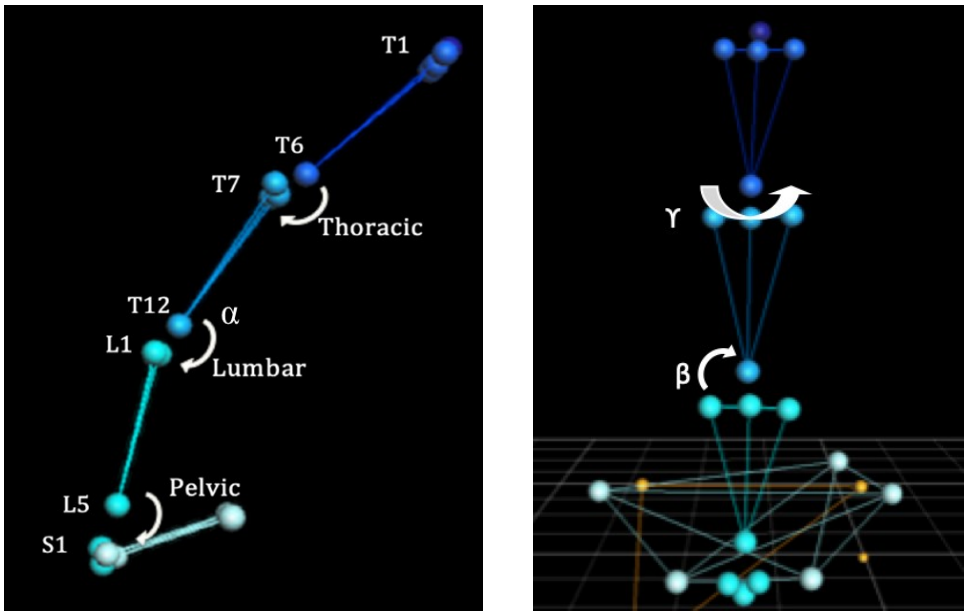

Figure 6.2: Spinal marker and segment labelling, with local coordinate frame rotation axes (α, β, γ).

Statistical significance was set at $p < 0.05$ and appropriate statistical analyses were conducted using R packages in RStudio 3.6 (RStudio Team, 2016) and JMP Pro 14 (SAS Institute, NC, USA). Linear regression analysis, including Pearson correlation, was used to quantify changes in spinal angles through the fatiguing protocol as a function of stroke number within each stroke rate trial. Fisher's r-to-z comparison was used to determine the significance of the difference between correlation coefficients.

6.3 RESULTS

Average kinematics of the upper limb and shoulder for the entire subject population were compared across stroke rate and statistically significant differences were highlighted between different athlete cohort groups (Section 6.3.1). Average kinematics of the lumbar and thoracic spine were compared across stroke rates and among preferred rowing modalities (Section 6.3.2).

6.3.1 Upper Limb Joint Angles

6.3.1.1 Population-wide results

Ergometer rowing shows marked transitions in elbow and shoulder kinematics between the drive and recovery phases. As stroke rate increased, maximum elbow flexion did not change (Table 6.4). However, relative timing of joint flexion did change with stroke rate, having occurred before the finish at 18 spm and

having occurred after the finish at 32 spm (Figure 6.3). Elbow flexion RoC in the early-drive and the late-drive decreased with increasing stroke rate (Figure 6.3; Figure 6.4; Table 6.4). Elbow flexion RoC was close to zero (0.37 ± 0.06 º per %) during the early-drive phase and greatest during the late-drive phase (6.43 ± 0.09 º per %), with the inflection between the phases occurring after MHF and indicating the point at which the elbows first break (Figure 6.3; Figure 6.4; Table 6.4). An elbow flexion RoC that was close to zero during the early drive, with a relatively later occurring inflection point indicated better maintenance of upper arm extension.

At all stroke rates, maximum GH extension and GH abduction coincided with the finish, and maximum GH internal rotation occurred immediately after the finish (Figure 6.6Table 6.4). No statistically significant differences were found in maximum GH extension, abduction, internal rotation, and RoM as stroke rate increased (Figure 6.6; Table 6.4). Averaged across all stroke rates, GH RoM was 101.7 ± 0.2º in flexion/extension, 71.6 ± 0.6º in adduction/abduction, and 44.7 ± 0.3º in internal/external rotation (Table 6.4). Statistically significant differences were found in extension, abduction, internal rotation, and Figure 6.6GH extension RoC during the late-drive phase as stroke rate increased ($p < 0.001$; Table 6.4; Figure 6.5), but there were no significant differences in GH extension RoC during the early-drive phase. No statistically significant differences were found in either GH joint angle or ST joint angle at the catch and finish positions (Figure 6.6; Figure 6.7).

No statistically significant differences were seen in maximum scapular internal/external rotation, up/down rotation, or anterior/posterior tilt as rate increases from 18 to 32 spm (Figure 6.7).

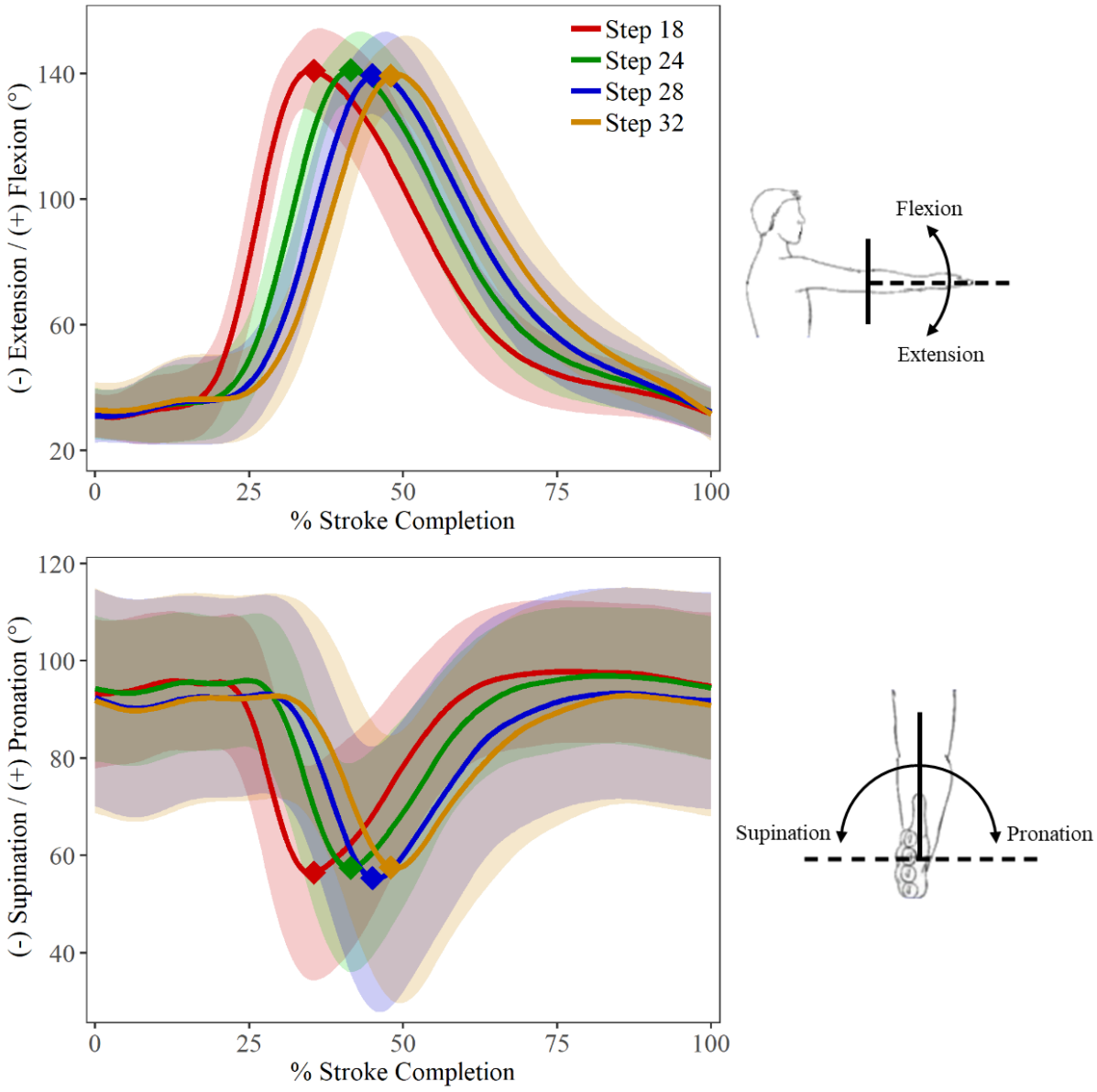

Figure 6.3: Population-wide (n=36) elbow kinematics (mean ± std) at all stroke rates (*left*). Flexion/extension (*top*), pronation/supination (*bottom*), with illustration of related limb movements (*right*). Diamond markers indicate occurrence of the finish at each of the correspondingly colored stroke rates.

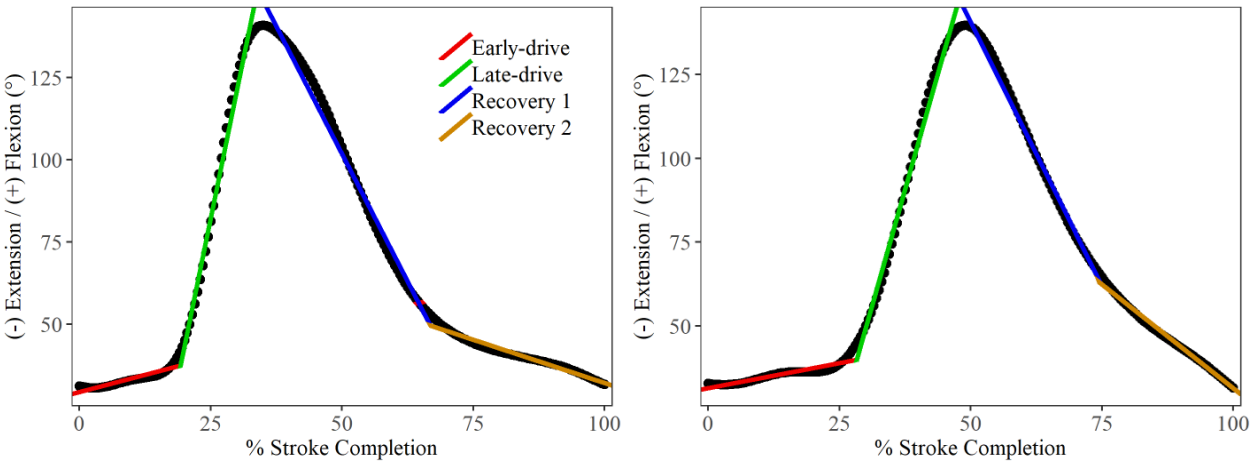

Figure 6.4: Mean elbow joint angle (black dots) for entire athlete population and piecewise linear regression gradient estimates for early drive, late-drive, and recovery phases, at stroke rate 18 spm (*left*) and 32 spm (*right*).

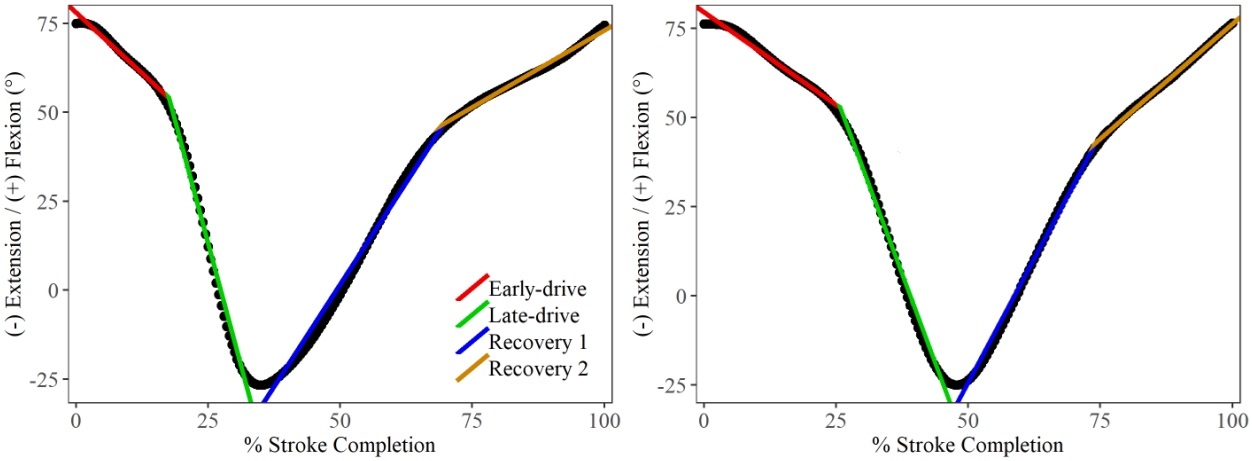

Figure 6.5: Mean glenohumeral joint angle (black dots) for entire athlete population and piecewise linear regression gradient estimates for early drive, late-drive, and recovery phases, at stroke rate 18 spm (*left*) and 32 spm (*right*).

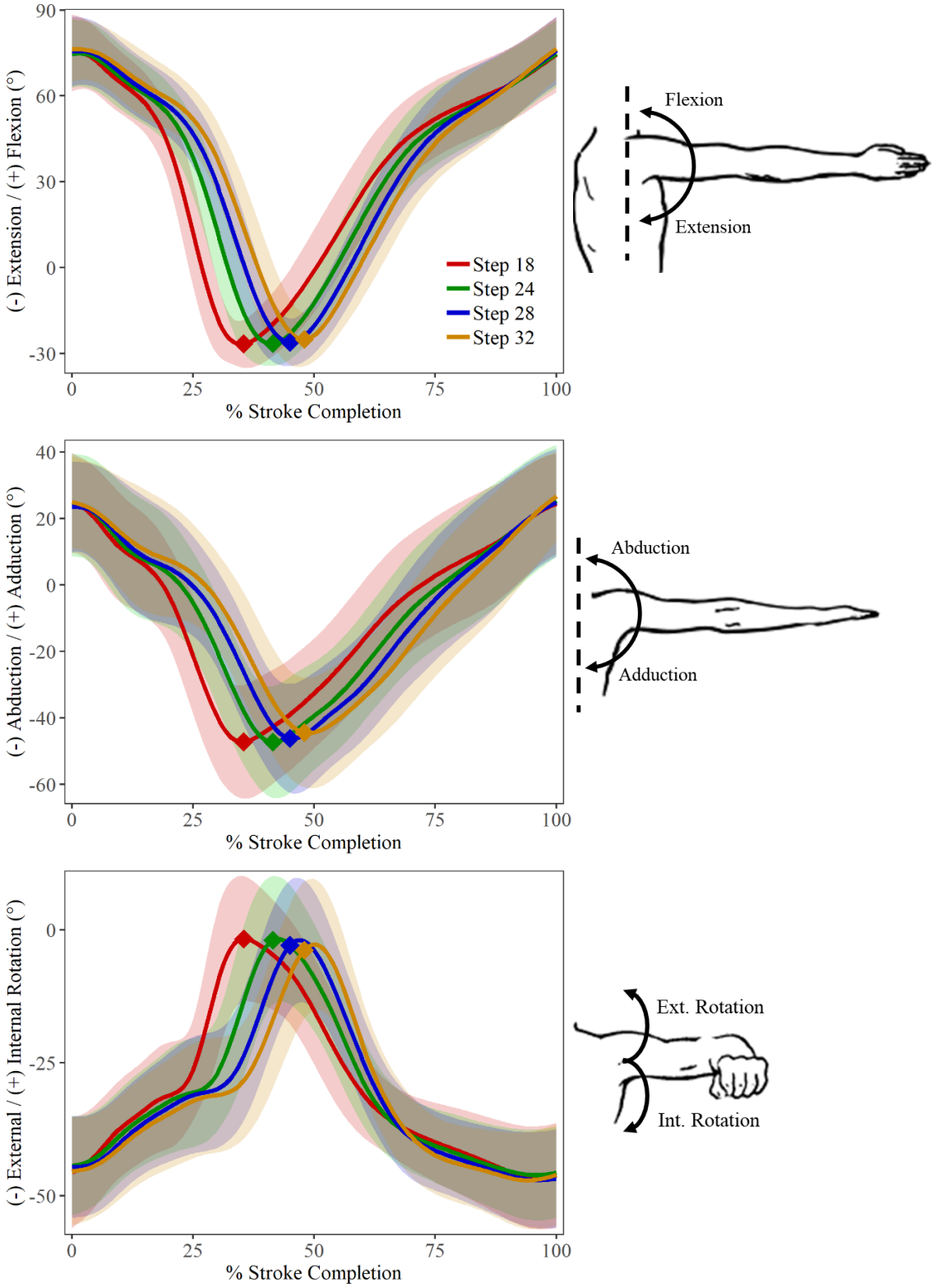

Figure 6.6: Population-wide glenohumeral kinematics (mean ± std) at all stroke rates. Flexion/extension (*top*), abduction/adduction (*middle*), internal/external rotation (*bottom*), with illustration of related limb movements (*right*). Diamond markers indicate occurrence of the finish at each of the correspondingly colored stroke rates.

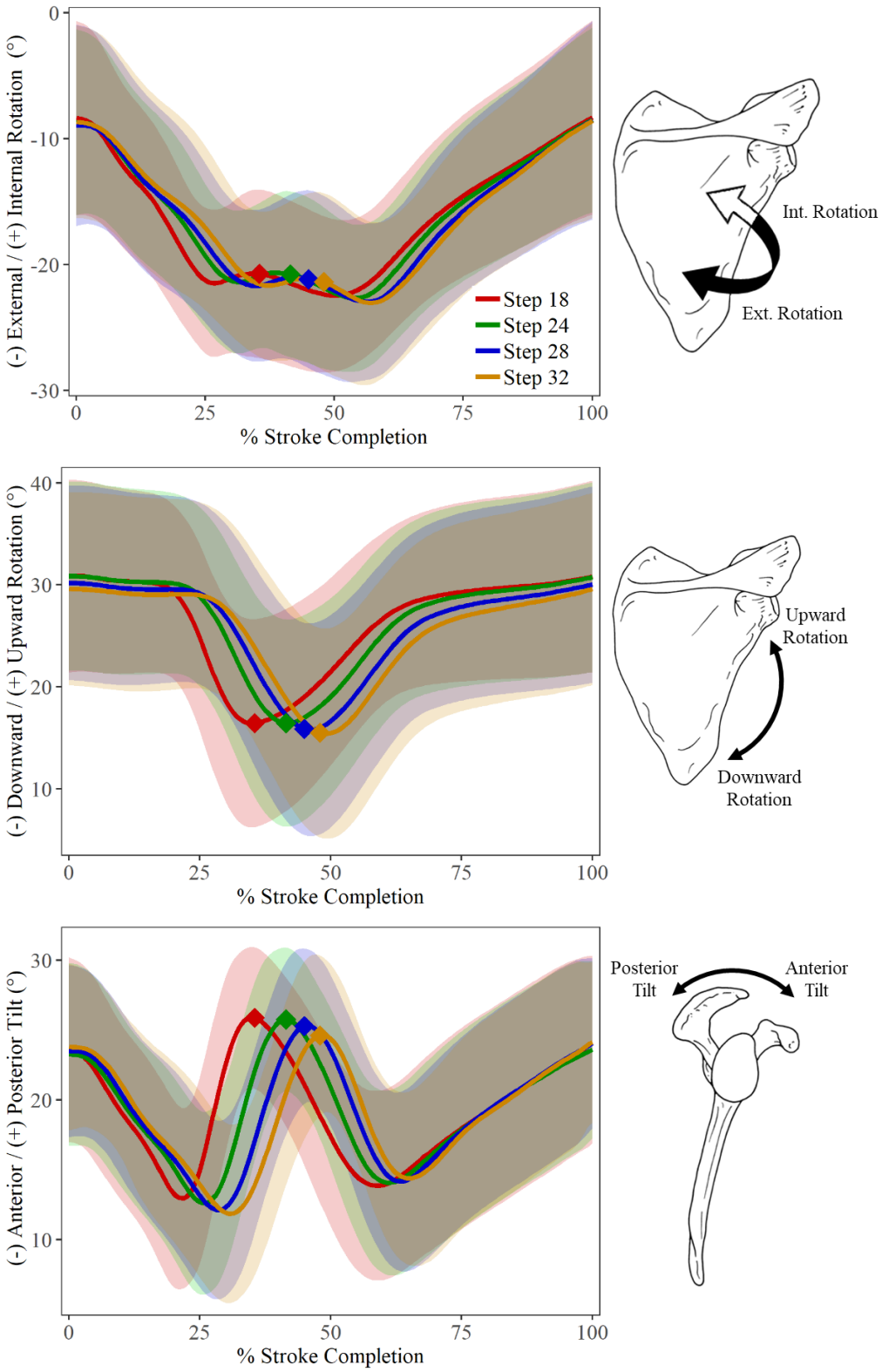

Figure 6.7: Population-wide scapulothoracic kinematics (mean ± std) at all stroke rates. Internal/external rotation (*top*), upward/downward rotation (*middle*), anterior/posterior tilt (*bottom*), with illustration of related movements (*right*). Diamond markers indicate occurrence of the finish at each of the correspondingly colored stroke rates.

Table 6.4: Maximum joint angle (mean ± std), timing of max joint angle in % of stroke completion, and rate of change (RoC) in degrees per stroke % at the glenohumeral (GH), elbow (ELB), and scapulothoracic (ST) joints. Asterisks (*) indicate ANOVA difference ($p < 0.05$) with respect to stroke rate.

		18 spm	24 spm	28 spm	32 spm	
GH	Max Extension	-26.7 ± 10.8	-26.6 ± 10.8	-26.1 ± 10.7	-25.0 ± 10.6	
	Max Abduction	-47.2 ± 14.9	-47.3 ± 16.5	-46.2 ± 16.1	-44.5 ± 15.4	
	Max Internal Rotation	-1.7 ± 9.7	-1.7 ± 9.9	-1.9 ± 10.7	-2.7 ± 10.8	
	Early-drive Extension RoC	-1.37 ± 0.39	-1.18 ± 0.26	-1.14 ± 0.21	-1.04 ± 0.17	
	Late-drive Extension RoC	-5.54 ± 0.47	-4.70 ± 0.34	-4.25 ± 0.28	-3.99 ± 0.22	*
ELB	Max Flexion	141.0 ± 5.8	141.1 ± 5.6	139.7 ± 6.1	139.7 ± 6.1	
	Max Supination	56.4 ± 8.7	57.5 ± 8.8	55.3 ± 9.0	57.4 ± 9.2	
	Early-drive Flexion RoC	0.42 ± 0.43	0.38 ± 0.28	0.38 ± 0.21	0.30 ± 0.61	
	Late-drive Flexion RoC	7.81 ± 0.66	6.48 ± 0.44	5.90 ± 0.36	5.53 ± 0.63	
ST	Max External Rotation	-22.5 ± 6.6	-22.7 ± 6.5	-22.9 ± 6.5	-23.1 ± 6.6	
	Max Up Rotation	16.4 ± 12.0	16.4 ± 12.7	15.8 ± 14.3	15.4 ± 14.4	
	Max Posterior Tilt	25.9 ± 13.9	25.8 ± 13.8	25.3 ± 20.4	24.6 ± 21.1	

6.3.1.2 Effect of Sex

An effect of sex was observed in shoulder joint kinematics for GH joint flexion/extension ($p = 0.031$), abduction/adduction ($p = 0.011$), and internal/external rotation ($p < 0.001$). At all stroke rates, females displayed significantly greater external shoulder rotation at the catch ($p = 0.046$; Figure 6.8; Table 6.5). While there were no statistically significant differences between males and females for maximum GH joint extension or abduction, males showed faster GH extension during the early-drive ($p < 0.001$), slower extension in the late-drive phase ($p = 0.005$), and faster GH adduction on the recovery ($p = 0.031$) than their female counterparts (Figure 6.8; Table 6.5).

At the elbow joint, differences in flexion/extension kinematics were observed ($p = 0.011$), but no differences in pronation/supination (Figure 6.9). Males showed faster elbow flexion RoC during the early-drive phase ($p = 0.0002$) than females, but no statistically significant difference in elbow flexion RoC was seen during the late-drive phase ($p = 0.093$; Table 6.5). Based on linear regression analysis and the estimated inflection point between early and late drive elbow flexion, it was found that male rowers break their elbows earlier (23.4%) than female rowers (25.7%) during the drive phase ($p < 0.001$; Table 6.5).

At the ST joint, no statistically significant differences were observed between males and females in either scapular internal/external rotation or in anterior/posterior tilt (Figure 6.10). However, throughout the entire stroke cycle and at every stroke rate, female rowers displayed greater scapular upward rotation than male rowers ($p < 0.001$; Figure 6.10; Table 6.5).

Table 6.5: Maximum joint angles in degrees (mean ± std) and rate of change (RoC) in degrees per stroke % at the glenohumeral (GH), elbow (ELB), and scapulothoracic (ST) joints for female and male athlete cohorts.

			18 spm	**24 spm**	**28 spm**	**32 spm**
ELB	Early-drive Flexion RoC	Female	0.31 ± 0.31	0.26 ± 0.20	0.29 ± 0.14	0.17 ± 0.13
		Male	0.52 ± 0.32	0.57 ± 0.19	0.54 ± 0.15	0.48 ± 0.12
ST	Max Up Rotation	Female	19.3 ± 9.1	19.3 ± 9.2	18.0 ± 9.9	17.5 ± 10.2
		Male	13.0 ± 7.1	12.7 ± 7.2	12.8 ± 7.1	12.6 ± 7.1
GH	Max Extension	Female	-28.5 ± 9.9	-28.7 ± 9.7	-27.7 ± 9.8	-26.6 ± 9.4
		Male	-24.6 ± 11.2	-25.4 ± 11.0	-25.6 ± 10.6	-24.2 ± 10.4
	Max Abduction	Female	-49.5 ± 14.1	-49.3 ± 16.0	-47.7 ± 16.1	-46.0 ± 14.6
		Male	-44.7 ± 15.9	-45.8 ± 16.8	-45.0 ± 15.7	-43.3 ± 16.4
	Max External Rotation	Female	-50.3 ± 9.8	-49.3 ± 10.1	-50.5 ± 10.2	-50.1 ± 12.3
		Male	-42.3 ± 10.3	-42.3 ± 10.9	-43.0 ± 13.0	-43.5 ± 14.6
	Early-drive Extension RoC	Female	-1.20 ± 0.30	-0.99 ± 0.18	-1.00 ± 0.15	-0.85 ± 0.13
		Male	-1.54 ± 0.28	-1.39 ± 0.19	-1.31 ± 0.14	-1.28 ± 0.10
	Late-drive Extension RoC	Female	-5.71 ± 0.34	-4.86 ± 0.24	-4.38 ± 0.20	-4.13 ± 0.17
		Male	-5.33 ± 0.32	-4.67 ± 0.23	-4.23 ± 0.19	-3.93 ± 0.15
	Recovery Adduction RoC	Female	1.13 ± 0.08	1.26 ± 0.09	1.33 ± 0.10	1.47 ± 0.10
		Male	1.24 ± 0.08	1.42 ± 0.09	1.55 ± 0.11	1.62 ± 0.13

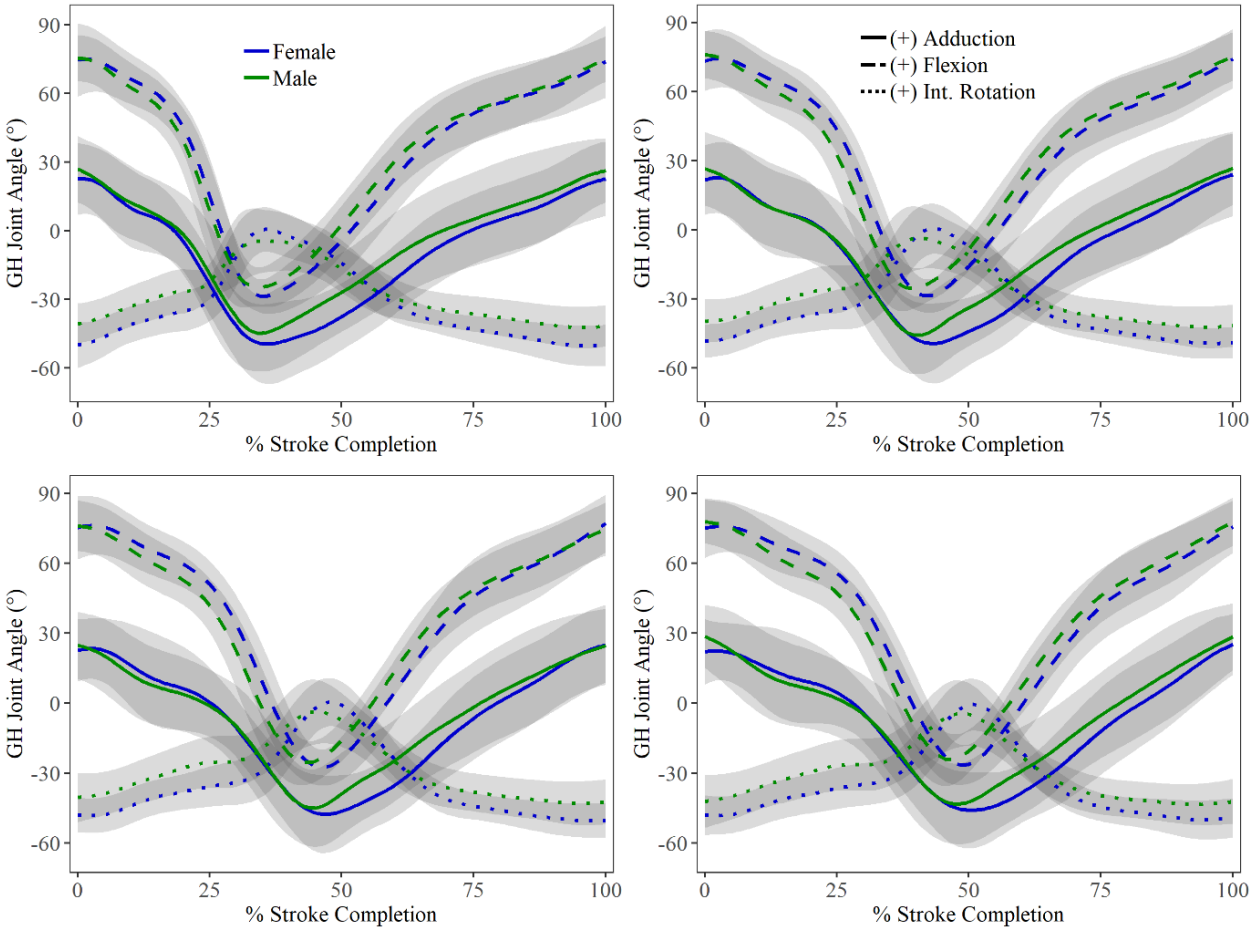

Figure 6.8: Male (n=16) versus female (n=20) glenohumeral (GH) joint angles (mean ± std). Stroke rate trials: 18 spm (*top left*), 24 spm (*top right*), 28 spm (*bottom left*), 32 spm (*bottom right*).

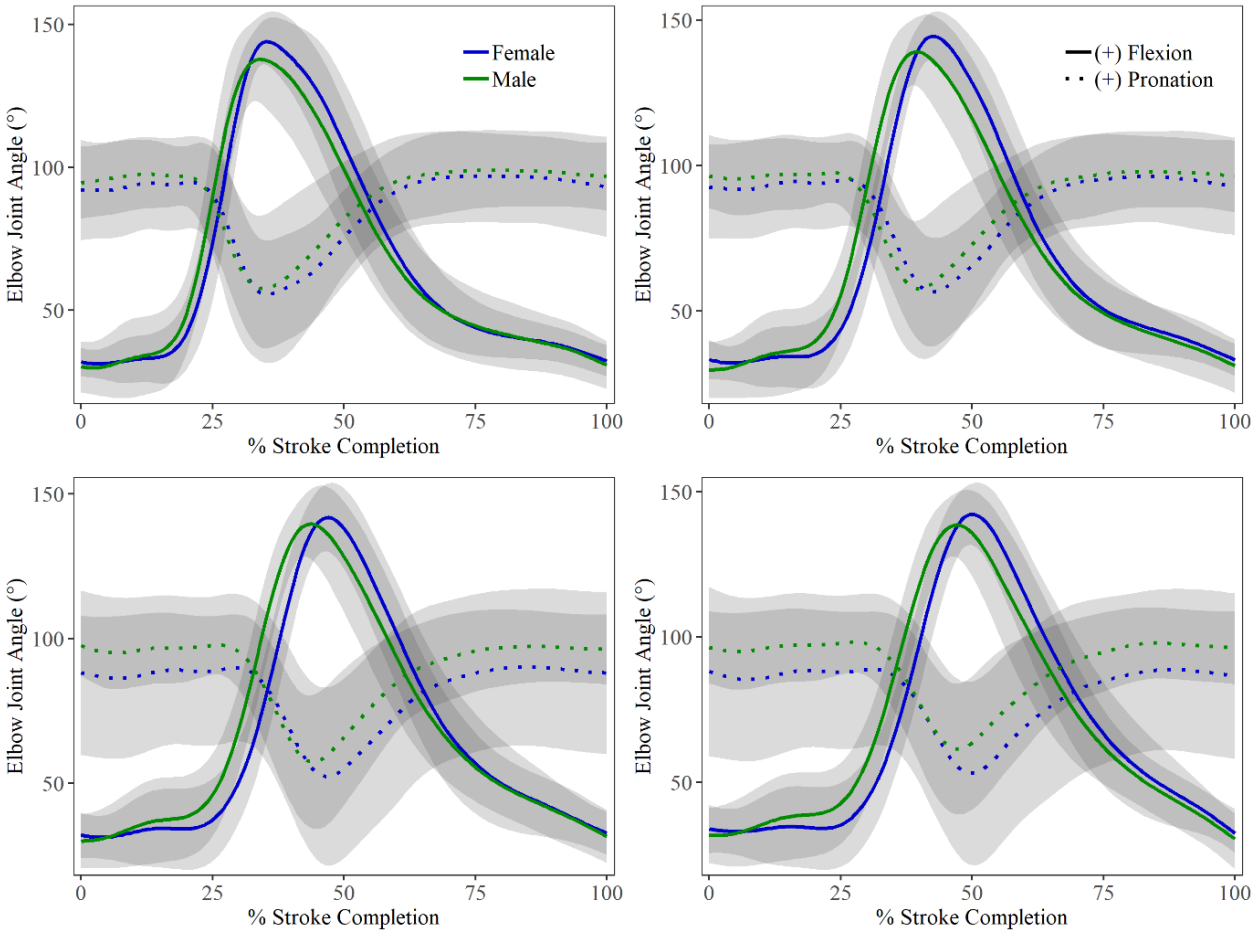

Figure 6.9: Male versus female elbow joint angles (mean ± std). Stroke rate trials: 18 spm (*top left*), 24 spm (*top right*), 28 spm (*bottom left*), 32 spm (*bottom right*).

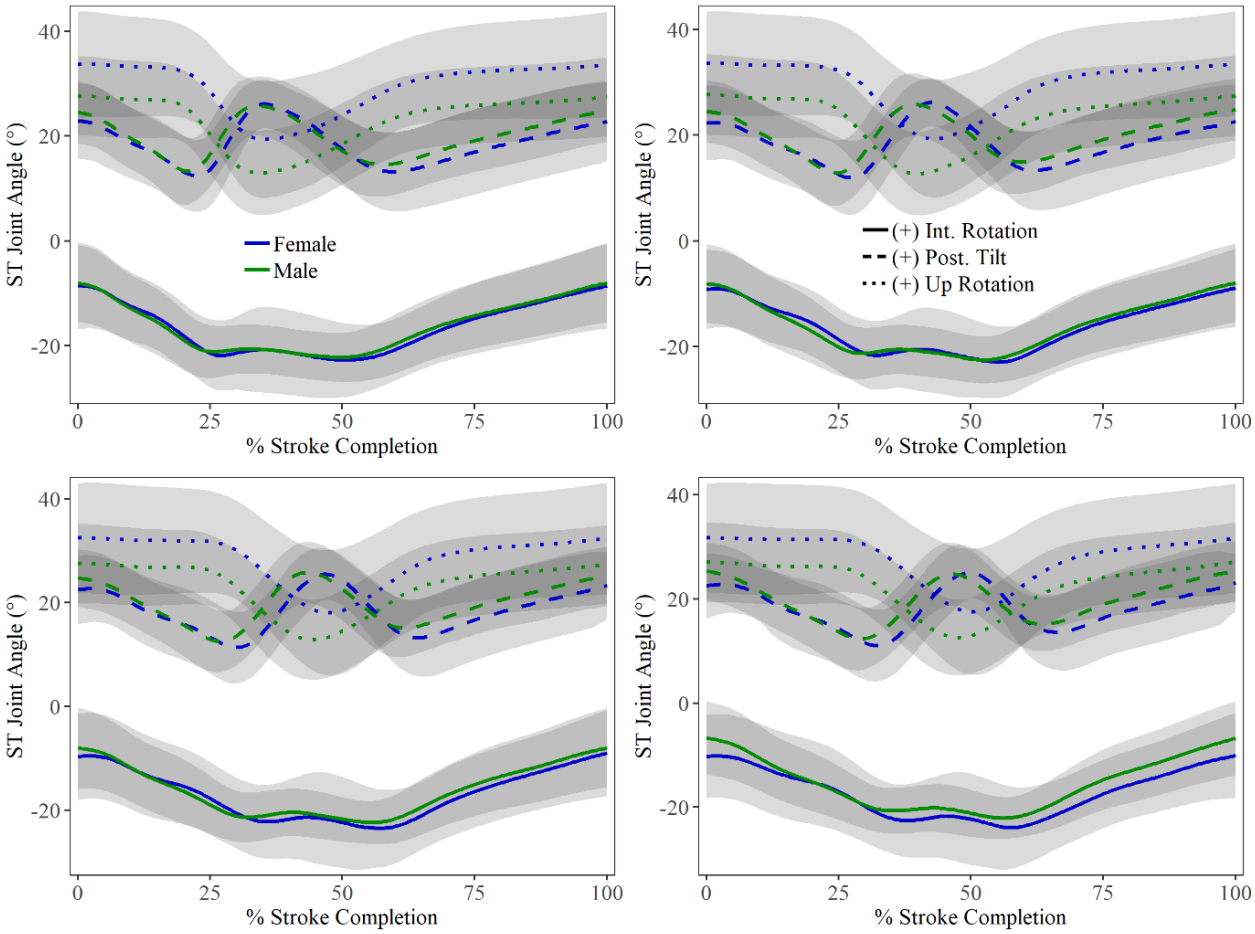

Figure 6.10: Male versus female scapulothoracic (ST) joint angles (mean ± std). Stroke rate trials: 18 spm (*top left*), 24 spm (*top right*), 28 spm (*bottom left*), 32 spm (*bottom right*).

6.3.1.3 Effect of Competitive Level

Statistically significant effects of competition level were observed in GH flexion/extension range of motion ($p = 0.0463$; Figure 6.11) and in GH abduction/adduction range of motion ($p = 0.019$; Figure 6.11). These differences were most noteworthy in the masters group, where range of motion was significantly reduced, by approximately 15-20º compared to the other competition level cohorts (Figure 6.11; Table 6.6). There were no statistically significant differences among athletes of varying competition level for GH internal/external rotation (Figure 6.11). Club and university rowers shared the most similar movement patterns in GH flexion/extension and abduction/adduction ($p = 0.56$; Figure 6.11). While there were no statistical differences between cohorts for any GH joint maxima or minima, elite rowers showed the fastest GH extension during the early-drive ($p = 0.004$) and late-drive phase ($p < 0.001$), and fastest GH flexion on the recovery ($p < 0.001$) compared with the other cohorts (Table 6.6; Figure 6.11). There were also significant differences in GH abduction/adduction RoC, with masters consistently slower than the other

cohorts in drive phase GH abduction ($p < 0.001$) and recovery GH adduction ($p < 0.014$; Table 6.6; Figure 6.11).

At the elbow joint, there were significant differences between cohorts in joint flexion/extension motion patterns ($p = 0.044$; Figure 6.12) but no differences between cohorts in elbow joint pronation/supination. Maximum elbow joint flexion near the finish was similar across all cohorts (Table 6.6). However, elbow flexion RoC during the early-drive phase was faster among elites ($p < 0.012$; Table 6.6; Figure 6.11; Figure 6.12) but linear regression showed similar elbow flexion RoC during the late-drive between elite and club rowers (7.19 ± 0.08 %), which were statistically different from university ($p < 0.001$) and masters rowers ($p = 0.028$; Table 6.6; Figure 6.12).

At the ST joint, no differences in scapular internal/external rotation were observed for any age/competition level cohorts (Figure 6.13). There were small differences in patterns of scapular anterior/posterior tilt, with club rowers showing greater anterior tilt throughout the recovery phase ($p = 0.016$) than the other athlete cohorts (Figure 6.13). Throughout the entire stroke cycle, masters rowers showed significantly greater scapular upward rotation (35.12 ± 4.02°) than the other athlete cohorts ($p = 0.032$; Figure 6.13).

Table 6.6: Joint angle range of motion (RoM) in degrees (mean ± std) and rate of change (RoC) in degrees per stroke % at the glenohumeral (GH), elbow (ELB), and scapulothoracic (ST) joints for age/competition level cohorts.

			18 spm	24 spm	28 spm	32 spm
GH	Flexion / Extension RoM	Masters	94.15 ± 6.86	96.85 ± 6.69	93.44 ± 8.40	95.78 ± 7.31
		Club	104.1 ± 10.8	104.7 ± 10.5	105.7 ± 10.5	103.0 ± 8.6
		Elite	113.8 ± 5.92	115.6 ± 6.71	114.7 ± 7.19	116.2 ± 7.48
		University	101.7 ± 13.4	100.6 ± 11.3	102.1 ± 10.7	100.9 ± 10.9
	Abduction / Adduction RoM	Masters	55.01 ± 14.86	58.62 ± 10.37	53.25 ± 9.58	54.60 ± 11.95
		Club	74.57 ± 17.23	72.26 ± 14.38	75.37 ± 12.34	75.82 ± 11.98
		Elite	71.77 ± 2.87	73.40 ± 4.34	72.85 ± 5.12	69.39 ± 6.04
		University	76.91 ± 17.20	76.99 ± 17.39	75.53 ± 17.22	74.72 ± 17.17
	Early-drive Extension RoC	Masters	-1.19 ± 0.10	-1.07 ± 0.07	-0.86 ± 0.06	-0.83 ± 0.06
		Club	-1.54 ± 0.19	-1.33 ± 0.12	-1.30 ± 0.11	-1.19 ± 0.08
		Elite	-1.53 ± 0.10	-1.44 ± 0.09	-1.45 ± 0.07	-1.44 ± 0.06
		University	-1.30 ± 0.39	-1.10 ± 0.22	-1.12 ± 0.17	-0.98 ± 0.14

Table 6.6 (continued)

			18 spm	24 spm	28 spm	32 spm
GH	Late-drive Extension RoC	Masters	-5.54 ± 0.17	-4.85 ± 0.13	-4.50 ± 0.12	-4.29 ± 0.11
		Club	-5.78 ± 0.18	-4.78 ± 0.13	-4.38 ± 0.12	-4.06 ± 0.10
		Elite	-6.35 ± 0.13	-5.58 ± 0.11	-5.07 ± 0.10	-4.77 ± 0.09
		University	-5.40 ± 0.43	-4.56 ± 0.27	-4.15 ± 0.23	-3.90 ± 0.18
	Recovery Flexion RoC	Masters	2.33 ± 0.05	2.62 ± 0.06	2.79 ± 0.07	2.80 ± 0.08
		Club	2.30 ± 0.05	2.67 ± 0.06	2.87 ± 0.08	2.92 ± 0.07
		Elite	3.27 ± 0.13	3.23 ± 0.11	2.98 ± 0.10	2.93 ± 0.09
		University	2.26 ± 0.13	2.59 ± 0.13	2.78 ± 0.13	2.80 ± 0.13
	Early-drive Abduction RoC	Masters	-1.65 ± 0.05	-1.44 ± 0.04	-1.26 ± 0.04	-1.21 ± 0.05
		Club	-2.54 ± 0.17	-1.99 ± 0.11	-1.83 ± 0.09	-1.69 ± 0.09
		Elite	-2.28 ± 0.14	-2.02 ± 0.09	-1.81 ± 0.05	-1.63 ± 0.04
		University	-2.31 ± 0.19	-1.90 ± 0.15	-1.66 ± 0.13	-1.51 ± 0.12
	Recovery Adduction RoC	Masters	0.92 ± 0.02	1.09 ± 0.03	1.12 ± 0.04	1.29 ± 0.06
		Club	1 .11 ± 0.05	1.24 ± 0.06	1.39 ± 0.07	1.48 ± 0.08
		Elite	1.18 ± 0.05	1.31 ± 0.05	1.39 ± 0.04	1.37 ± 0.03
		University	1.29 ± 0.09	1.44 ± 0.11	1.55 ± 0.13	1.65 ± 0.12
ELB	Early-drive Flexion RoC	Masters	0.24 ± 0.15	0.34 ± 0.11	0.31 ± 0.08	0.13 ± 0.07
		Club	0.26 ± 0.18	0.28 ± 0.12	0.22 ± 0.09	0.18 ± 0.08
		Elite	0.47 ± 0.12	0.71 ± 0.09	0.72 ± 0.07	0.74 ± 0.05
		University	0.47 ± 0.39	0.38 ± 0.22	0.43 ± 0.16	0.31 ± 0.13
	Late-drive Flexion RoC	Masters	7.57 ± 0.25	6.70 ± 0.21	6.44 ± 0.18	5.90 ± 0.15
		University	7.64 ± 0.55	6.41 ± 0.34	5.85 ± 0.29	5.41 ± 0.23
		Club	8.80 ± 0.29	7.35 ± 0.22	6.45 ± 0.17	5.97 ± 0.14
		Elite	8.46 ± 0.20	7.34 ± 0.16	6.86 ± 0.14	6.30 ± 0.11
ST	Average Up / Down Rotation	Masters	34.72 ± 4.08	34.76 ± 4.08	34.83 ± 4.05	36.16 ± 3.91
		Club	23.44 ±9.76	23.50 ± 10.04	23.60 ± 9.89	23.66 ± 9.75
		Elite	23.86 ± 3.95	23.57 ± 3.80	23.18 ± 3.69	23.07 ± 3.58
		University	25.50 ± 9.51	25.76 ± 9.59	24.72 ± 10.02	24.08 ± 9.72

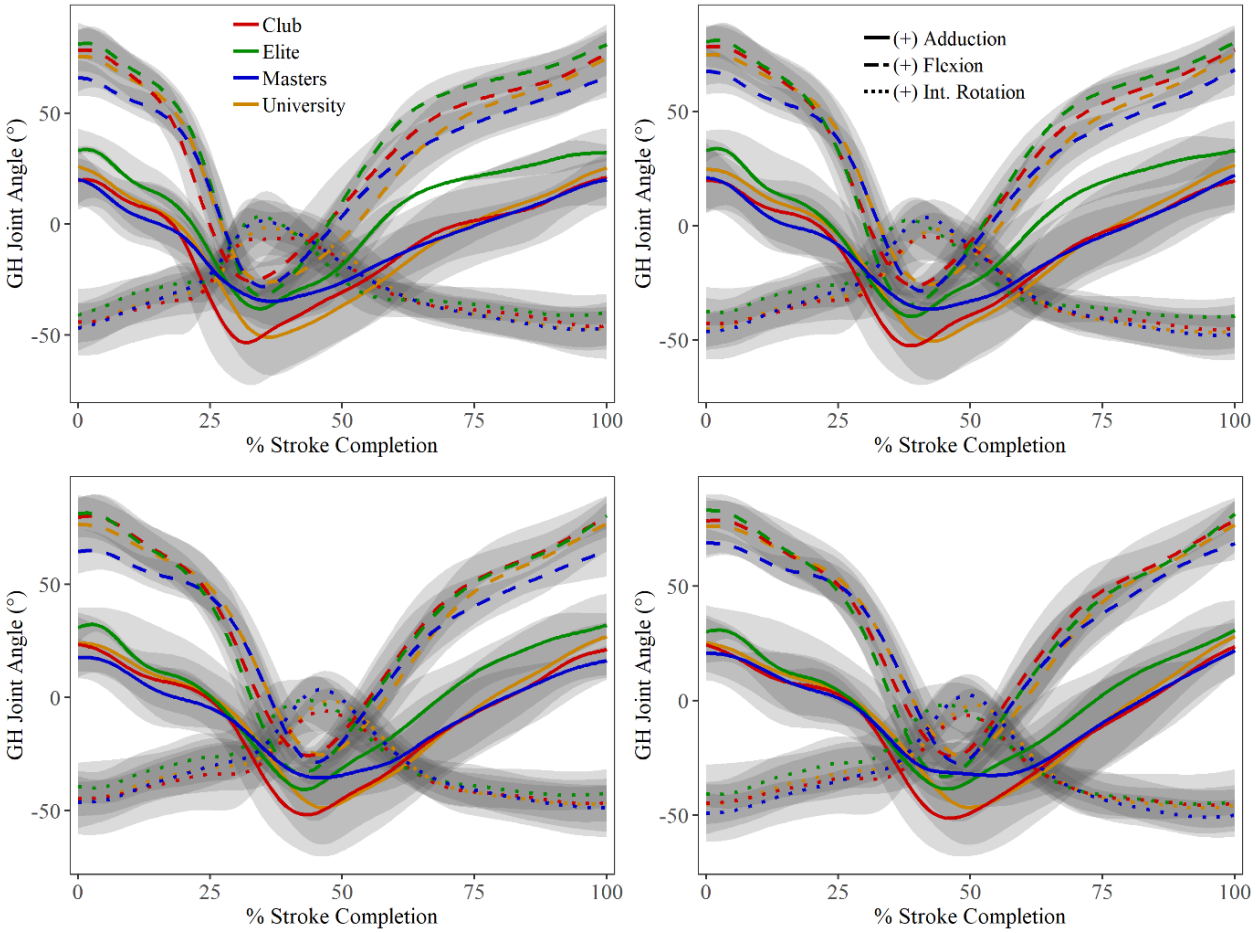

Figure 6.11: Glenohumeral (GH) joint angles (mean ± std) (Euler rotations) for each age/competition level cohort: club (n=6), elite (n=3), masters (n=6), university (n=21). Stroke rate trials: 18 spm (*top left*), 24 spm (*top right*), 28 spm (*bottom left*), 32 spm (*bottom right*).

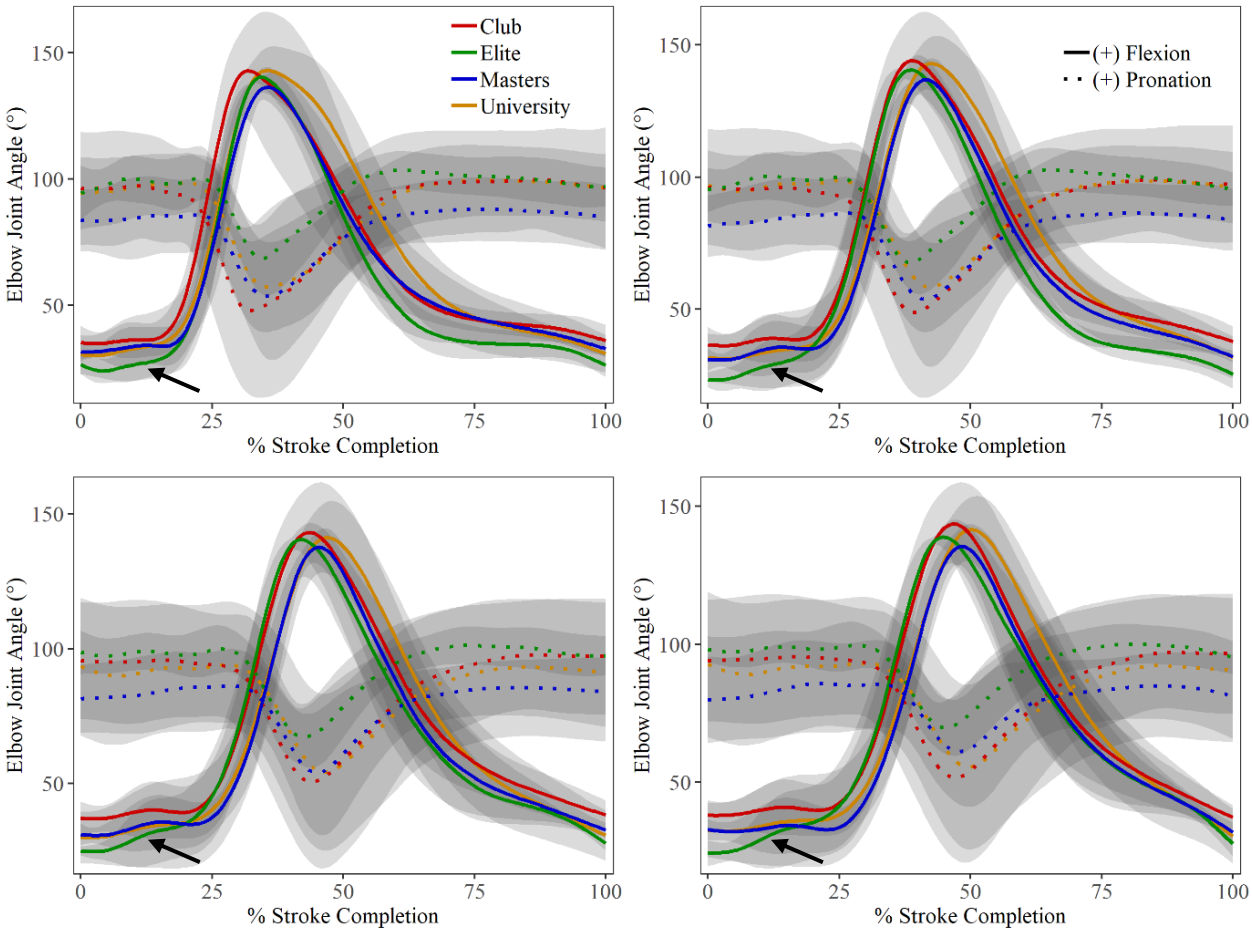

Figure 6.12: Elbow joint angles (mean ± std) (Euler rotations) for each age/competition level cohort. Stroke rate trials: 18 spm (*top left*), 24 spm (*top right*), 28 spm (*bottom left*), 32 spm (*bottom right*). Arrows indicate difference in early-drive flexion RoC ($p < 0.05$).

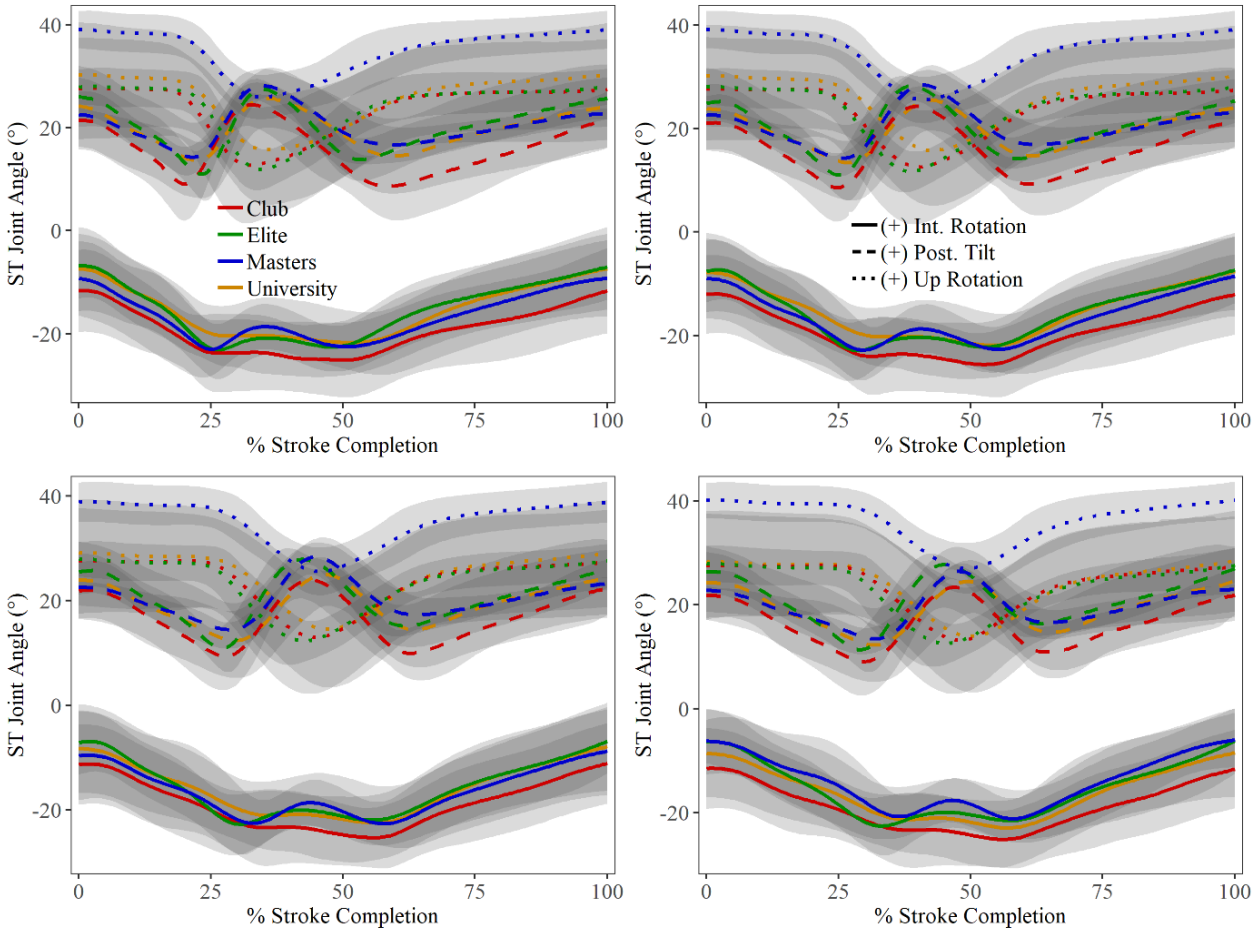

Figure 6.13: Scapulothoracic (ST) joint angles (mean ± std) for each age/competition level cohort. Stroke rate trials: 18 spm (*top left*), 24 spm (*top right*), 28 spm (*bottom left*), 32 spm (*bottom right*).

6.3.1.4 Effect of Rowing Modality

Statistically significant effects of preferred rowing modality (i.e. port, starboard, sculling) were observed at the GH joint, with scullers displaying greater external shoulder rotation at the catch than either the port ($p = 0.021$) or starboard sweep rowing cohort ($p = 0.022$; Figure 6.14; Table 6.7). No significant differences in GH joint flexion/extension or GH joint abduction/adduction were observed for any of the rowing modality cohorts.

At the elbow joint, there were significant differences in joint flexion/extension motion patterns, with starboard sweep rowers showing greater elbow extension at the catch than scullers and port sweep rowers ($p = 0.05$; Figure 6.15; Table 6.7). During the early-drive phase, both scullers and starboard rowers showed an elbow joint flexion RoC that was close to zero (Figure 6.15; Table 6.7), suggesting that both groups maintain better arm extension than port rowers ($p = 0.036$) who have a much faster elbow flexion RoC.

At the ST joint, differences in scapular internal/external rotation and upward/downward rotation were observed between preferred rowing modality cohorts. Port rowers have significantly lower upward scapular rotation than either scullers or starboard sweep rowers ($p < 0.001$; Figure 6.16; Table 6.7). Starboard rowers have significantly greater maximum scapular internal rotation angle ($p = 0.05$) and throughout the whole stroke cycle, starboards showed consistently more internally rotated positioning of their right scapula than the port cohort ($p = 0.011$; Figure 6.16; Table 6.7).

Table 6.7: Joint angles in degrees (mean ± std) and rate of change (RoC) in degrees per stroke % at the glenohumeral (GH), elbow (ELB), and scapulothoracic (ST) joints for preferred rowing modality cohorts.

			18 spm	24 spm	28 spm	32 spm
GH	Max Ext. Rotation	Starboard	-42.17 ± 8.96	-41.42 ± 6.99	-42.44 ± 7.51	-43.21 ± 8.06
		Sculling	-52.30 ± 10.51	-50.55 ± 10.62	-51.38 ± 10.20	-50.11 ± 12.41
		Port	-40.14 ± 8.23	-41.40 ± 8.69	-41.63 ± 9.64	-43.77 ± 10.71
ELB	Catch Extension	Starboard	27.50 ± 9.63	28.10 ± 10.11	28.17 ± 10.29	29.23 ± 10.86
		Sculling	34.01 ± 4.71	34.36 ± 5.45	35.28 ± 5.94	36.47 ± 6.45
		Port	32.50 ± 5.51	33.37 ± 5.89	32.35 ± 5.89	35.28 ± 6.07
	Early Drive Flexion RoC	Starboard	0.24 ± 0.30	0.26 ± 0.19	0.23 ± 0.15	0.18 ± 0.12
		Sculling	0.30 ± 0.22	0.32 ± 0.13	0.28 ± 0.10	0.16 ± 0.09
		Port	0.67 ± 0.26	0.60 ± 0.16	0.69 ± 0.12	0.58 ± 0.10
	Late Drive Flexion RoC	Starboard	8.01 ± 0.42	6.87 ± 0.31	6.18 ± 0.26	5.73 ± 0.21
		Sculling	7.89 ± 0.33	6.98 ± 0.25	6.29 ± 0.20	5.97 ± 0.17
		Port	7.21 ± 0.38	5.95 ± 0.26	5.32 ± 0.21	4.93 ± 0.18
ST	Max Internal Rotation	Starboard	-5.11 ± 4.20	-5.42 ± 4.22	-6.40 ± 6.53	-6.10 ± 6.50
		Sculling	-8.23 ± 6.55	-8.38 ± 6.56	-8.04 ± 4.03	-10.41 ± 3.01
		Port	-12.32 ± 8.49	-12.38 ± 8.59	-11.98 ± 9.24	-10.82 ± 9.86
	Max Down Rotation	Starboard	19.01 ± 8.51	19.03 ± 8.57	17.73 ± 9.21	17.98 ± 9.51
		Sculling	18.82 ± 7.43	18.65 ± 7.53	18.76 ± 7.36	17.21 ± 6.92
		Port	11.56 ± 8.98	11.67 ± 9.08	10.77 ± 8.74	9.97 ± 8.63

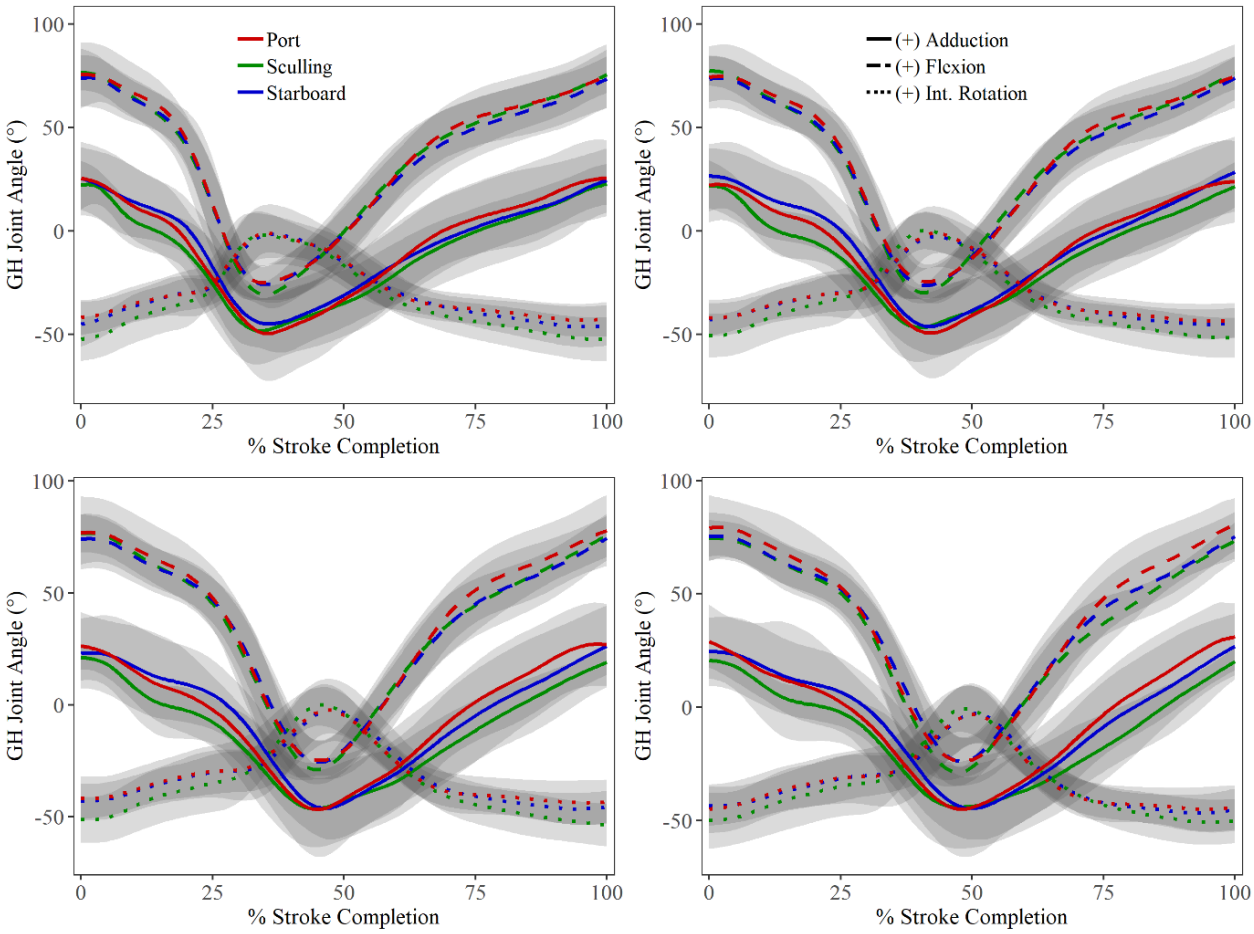

Figure 6.14: Glenohumeral (GT) joint angles (mean ± std) for each preferred rowing modality cohort: port (n=12), starboard (n=16), sculling (n=8). Stroke rate trials: 18 spm (*top left*), 24 spm (*top right*), 28 spm (*bottom left*), 32 spm (*bottom right*).

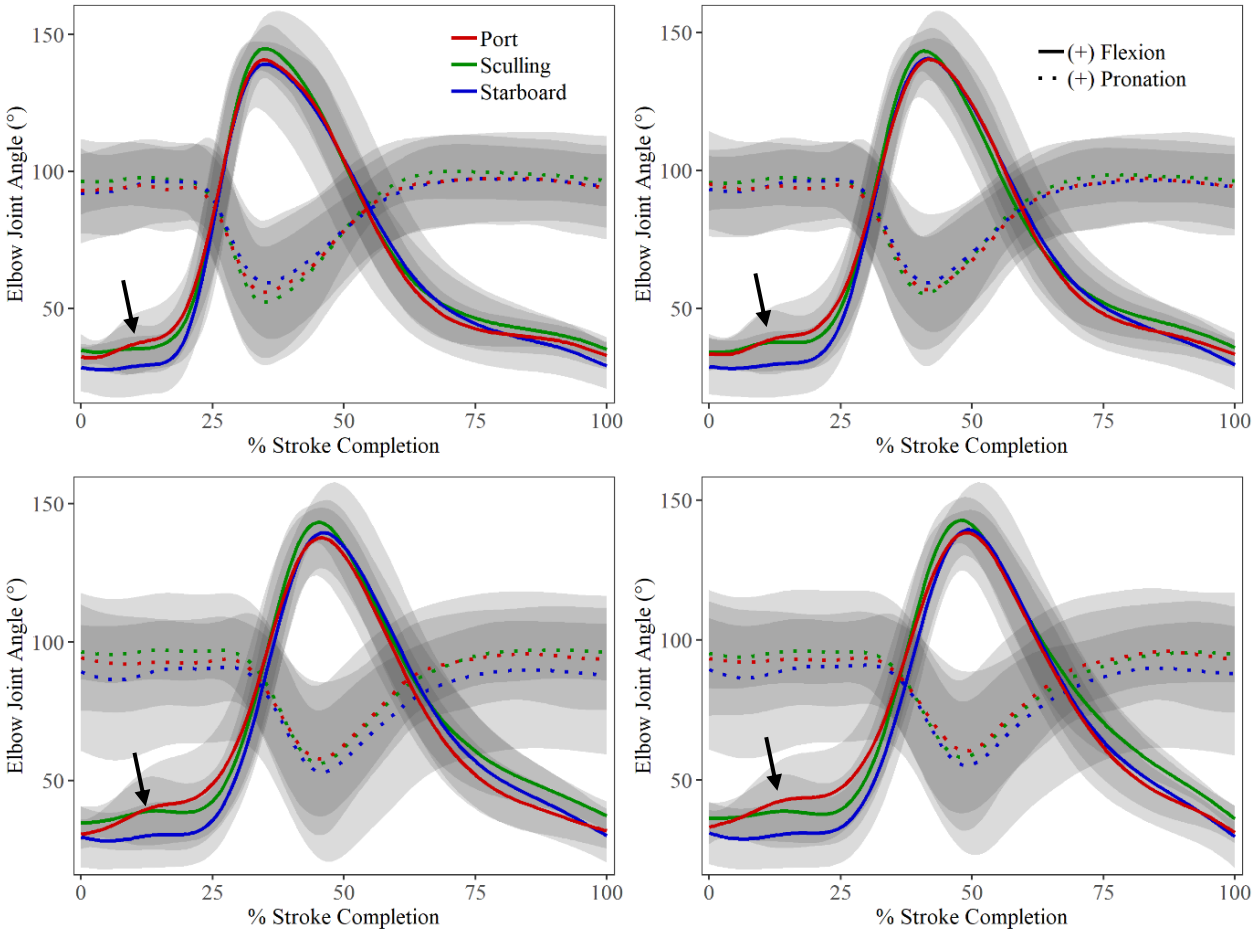

Figure 6.15: Elbow joint angles (mean ± std) for each preferred rowing modality cohort. Stroke rate trials: 18 spm (*top left*), 24 spm (*top right*), 28 spm (*bottom left*), 32 spm (*bottom right*). Arrows indicate significant difference in early-drive flexion RoC ($p < 0.05$).

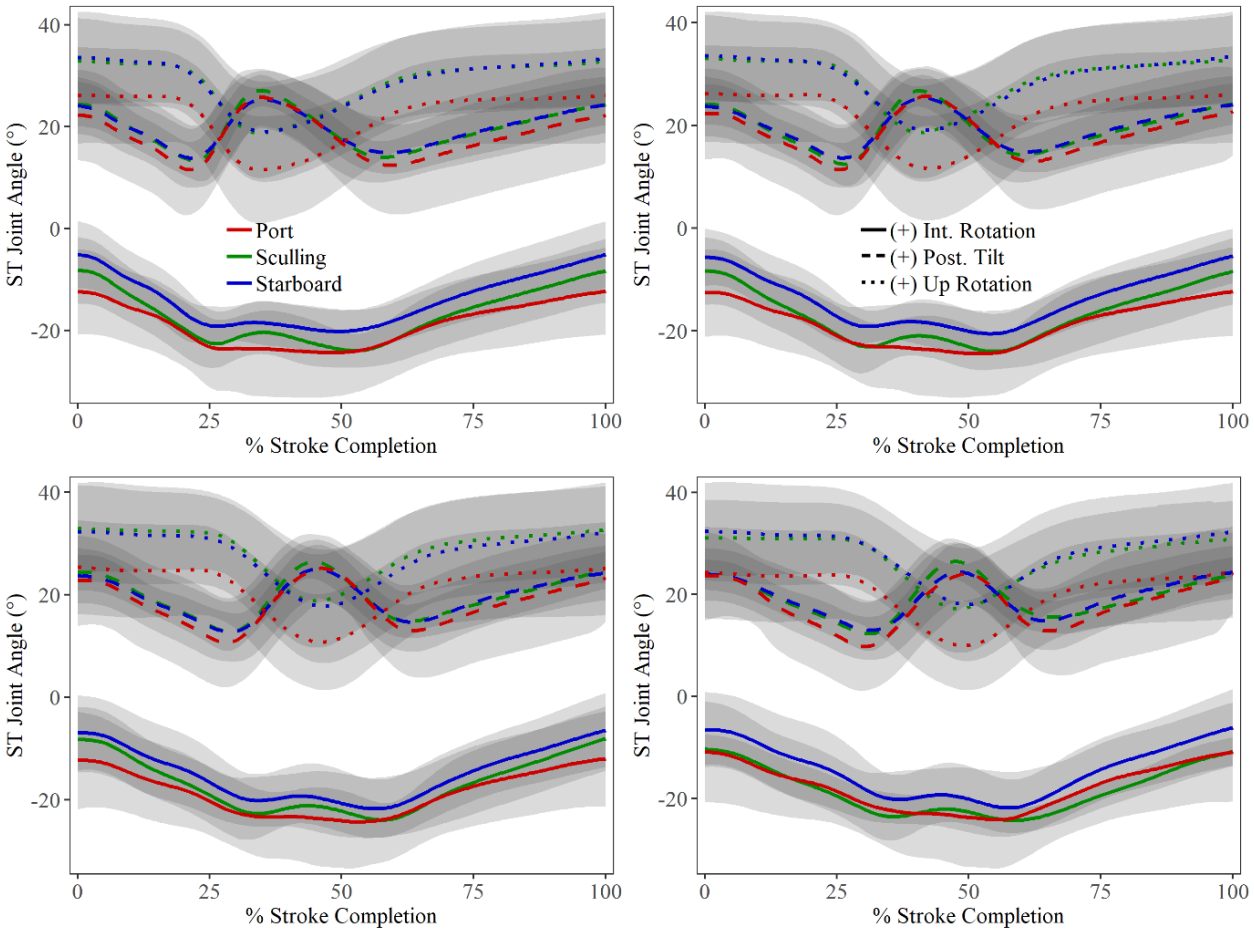

Figure 6.16: Scapulothoracic (ST) joint angles (mean ± std) for preferred rowing modality cohort. Stroke rate trials: 18 spm (*top left*), 24 spm (*top right*), 28 spm (*bottom left*), 32 spm (*bottom right)*.

6.3.2 Spinal Segment Angles and Ratios

Mean segment flexion/extension (α) angles for the lumbar and thoracic spine segments and pelvis followed similar movement patterns through the stroke cycle with maximum flexion occurring at the catch and maximum extension at the finish, with slight increases in both as rate increased (Figure 6.17; Table 6.8). At 32 spm, the thoracic segment showed decreased maximum extension at the finish ($p = 0.048$). Although no other spinal segment kinematics showed statistically significant changes, there was a tendency toward increased pelvic extension at the finish and decreased lumbar flexion at the catch with increasing stroke rate (Table 6.8). When MHF was reached, pelvic and lumbar flexion/extension angles were close to zero, indicating that the lower spine was nearly vertically aligned when loading was at its highest (Table 6.8). Patterns in lateral bending (β) and spinal torsion (ϒ) showed only small angular variation through the stroke and showed no statistically significant changes with stroke rate (Table 6.8).

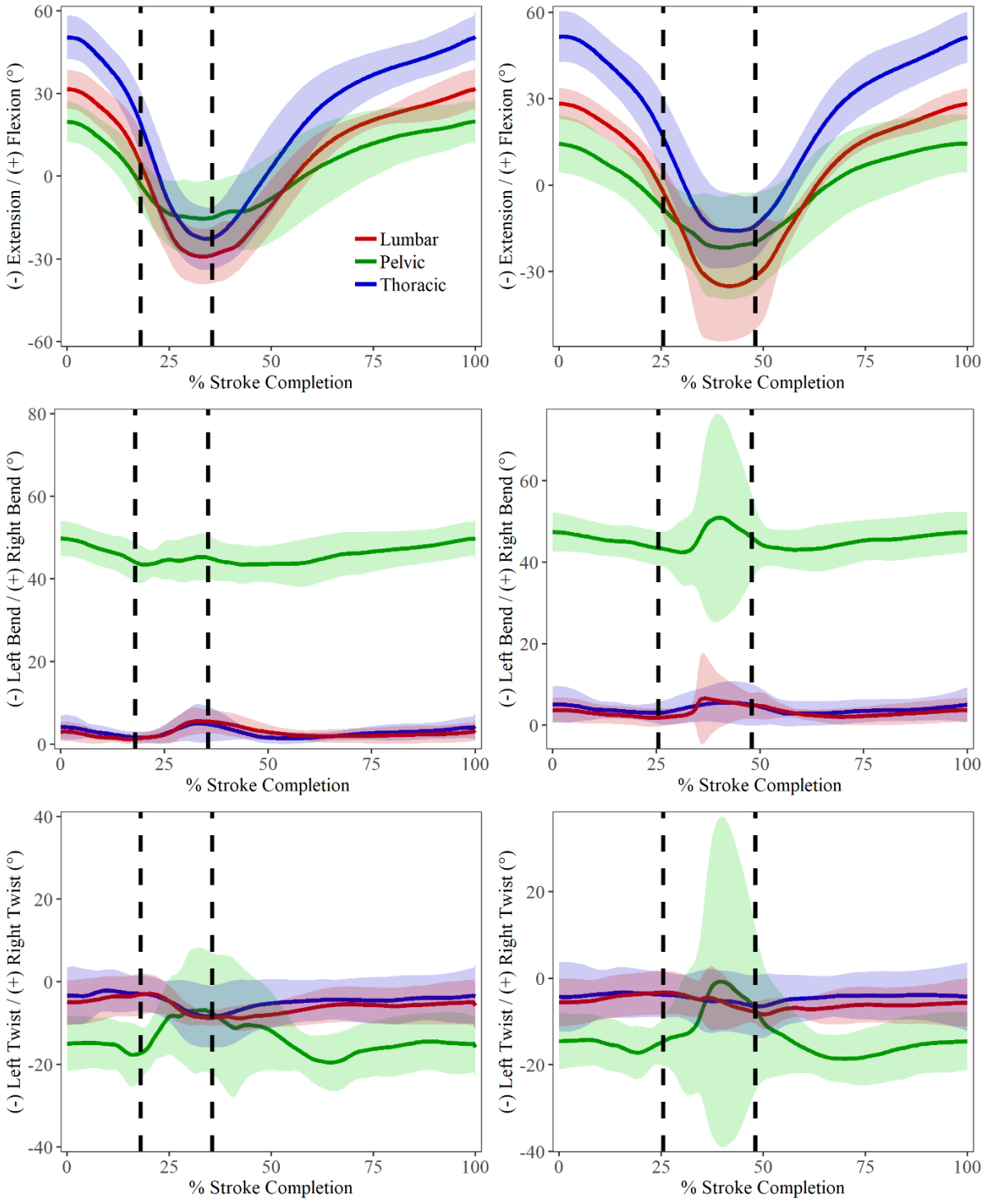

Figure 6.17: Population-wide (n=16) spinal segment angles (mean ± std) through the stroke cycle at 18 spm (*left*) and 32 spm (*right*) for sagittal plane α angle (*top*), frontal plane β angle (*middle*) and transverse plane ϒ angle (*bottom*). Vertical dashed lines indicate timing of max handle forces (MHF) and the finish.

Table 6.8: Population-wide (n=16) thoracic, lumbar, and pelvis spinal joint angles in degrees (mean ± std) achieved at the catch, max handle force (MHF), and the finish positions.

			18 spm	24 spm	28 spm	32 spm
Thoracic	Flexion / Extension	Catch	50.37 ± 5.18	51.11 ± 5.37	51.66 ± 5.41	51.60 ± 5.75
		MHF	19.26 ± 7.62	17.04 ± 8.40	15.61 ± 8.86	16.78 ± 9.10
		Finish	-22.47 ± 7.32	-22.64 ± 6.89	-20.71 ± 6.67	-14.10 ± 7.27
	Lateral Bending	Catch	4.11 ± 1.85	4.41 ± 1.94	4.38 ± 2.01	5.08 ± 2.84
		MHF	1.65 ± 0.92	1.75 ± 0.81	2.13 ± 0.73	3.04 ± 1.77
		Finish	4.88 ± 2.82	4.82 ± 2.67	5.25 ± 3.17	5.01 ± 3.32
	Transverse Twisting	Catch	-3.35 ± 4.47	-3.95 ± 4.83	-3.55 ± 5.02	-4.25 ± 5.19
		MHF	-2.92 ± 2.78	-3.59 ± 3.18	-3.25 ± 3.04	-3.78 ± 3.43
		Finish	-8.40 ± 4.88	-7.90 ± 5.02	-7.21 ± 5.15	-6.44 ± 4.65
Lumbar	Flexion / Extension	Catch	31.59 ± 4.60	31.18 ± 4.64	29.61 ± 3.87	28.36 ± 3.47
		MHF	4.62 ± 7.71	1.43 ± 7.08	-1.65 ± 6.52	-2.27 ± 5.59
		Finish	-28.63 ± 6.63	-33.24 ± 10.53	-29.88 ± 5.90	-31.55 ± 12.10
	Lateral Bending	Catch	3.06 ± 1.48	4.58 ± 2.00	4.06 ± 1.82	3.76 ± 1.93
		MHF	1.33 ± 0.85	1.97 ± 1.37	1.82 ± 1.24	1.87 ± 1.42
		Finish	5.51 ± 1.91	5.90 ± 3.17	4.92 ± 1.56	4.83 ± 2.05
	Transverse Twisting	Catch	-4.97 ± 3.55	-5.93 ± 4.03	-5.76 ± 3.84	-5.59 ± 3.58
		MHF	-3.08 ± 3.29	-3.80 ± 3.61	-3.64 ± 3.39	-3.27 ± 3.28
		Finish	31.59 ± 1.23	31.18 ± 2.95	29.61 ± 1.33	28.36 ± 1.69
Pelvis	Flexion / Extension	Catch	-8.73 ± 4.81	-9.44 ± 4.87	-8.03 ± 5.85	-7.82 ± 6.43
		MHF	19.84 ± 6.17	19.36 ± 5.53	16.86 ± 7.03	14.45 ± 7.17
		Finish	-2.93 ± 8.84	-4.84 ± 9.39	-6.94 ± 11.03	-8.15 ± 11.28
	Lateral Bending	Catch	-15.02 ± 2.74	-16.98 ± 2.70	-19.58 ± 2.90	-19.76 ± 3.17
		MHF	49.80 ± 3.09	49.05 ± 3.03	48.19 ± 2.74	47.38 ± 2.70
		Finish	44.06 ± 3.57	43.38 ± 2.25	43.32 ± 2.93	43.47 ± 6.78
	Transverse Twisting	Catch	45.17 ± 4.37	45.05 ± 4.63	44.42 ± 4.33	46.11 ± 4.24
		MHF	-14.98 ± 4.14	-14.36 ± 5.12	-13.83 ± 3.65	-14.50 ± 3.61
		Finish	-17.31 ± 9.58	-15.67 ± 7.03	-15.08 ± 8.90	-14.57 ± 12.48

Ratios of angle change provide a concise way of quantifying relative movement between spinal segments. Overall, the lumbo-thoracic ratio was lower than the lumbo-pelvic ratio, primarily because the torso remains "straighter" compared to the lumbar spine (Figure 6.18; Figure 6.19). While Figure 6.18 suggests increasing lumbo-thoracic ratio at MHF and decreasing lumbo-thoracic ratio at the catch, there were no significant differences related to increasing stroke rate at either the catch ($p > 0.868$), the finish ($p > 0.059$), or at MHF ($p > 0.388$). However, lumbo-thoracic ratios were largest at MHF, being significantly greater than at the catch ($p < 0.0429$) at all stroke rates, suggesting an increased flexion of the middle back during the heavily loaded drive phase. At the finish, lumbo-thoracic ratios were lower than at the catch and MHF, indicating that thoracic rotation was increased compared to lumbar rotation (Figure 6.18) but only the finish lumbo-thoracic ratio at 32 spm was statistically different from either the catch ($p < 0.0058$) or MHF ($p < 0.0004$) at all stroke rates. This was due to large standard deviations at the finish, which may be attributed to variation in the technical style of each rower.

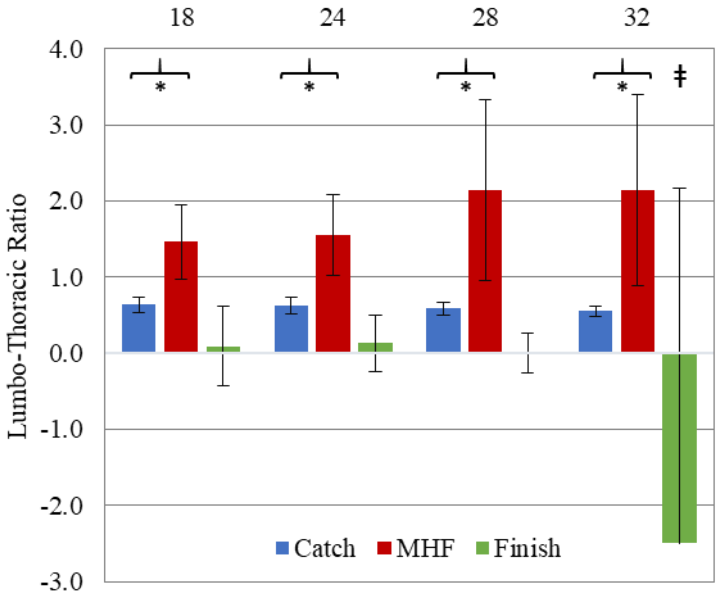

Figure 6.18: Population-wide sagittal plane lumbo-thoracic ratios (mean ± std) at catch, max handle force (MHF), and finish position at all stroke rates. Significant differences ($p < 0.05$) in ratio were found at the finish with respect to stroke rate (ǂ) and between catch and MHF stroke positions (*****) at all stroke rates.

When considering population-wide sagittal plane lumbo-pelvic, as stroke rate increases, the ratio at the catch increases. However, there were no significant differences in lumbo-pelvic ratio related to increasing stroke rate at either the catch ($p = 0.683$), the finish ($p = 0.084$), or at MHF ($p = 0.098$). Despite large standard deviations, lumbo-pelvic ratios were significantly greater at the catch, than at MHF ($p = 0.017$), at all stroke rates except 24 spm ($p = 0.748$). Movement patterns suggest that lumbar rotation was

increased compared to pelvic rotation at least in the early drive phase (Figure 6.19). Across all stroke rates, there were no significant differences in lumbo-pelvic ratios between the catch and the finish ($p = 0.225$) or MHF and the finish ($p = 0.076$). Lumbo-pelvic ratios generally had larger standard deviations than lumbo-thoracic ratios. This may be due to smaller lumbar and pelvis range of sagittal plane movement throughout the stroke cycle.

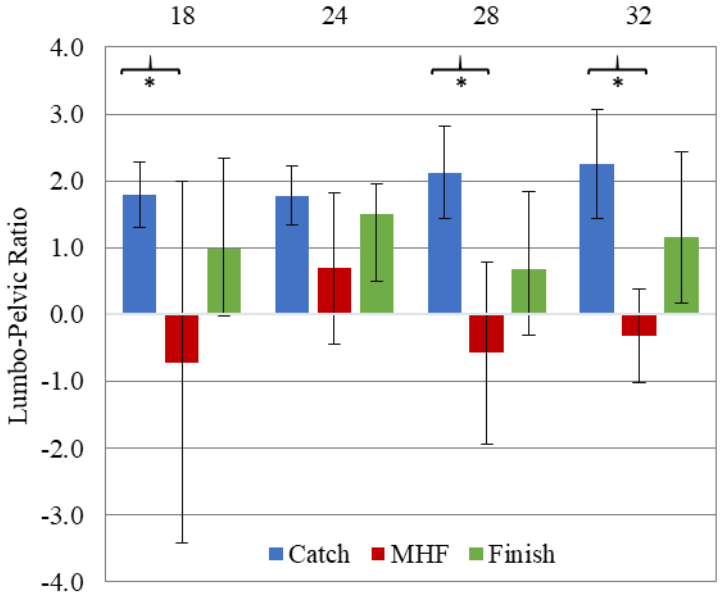

Figure 6.19: Population-wide sagittal plane lumbo-pelvic ratios (mean ± std) at catch, max handle force (MHF), and finish positions at all stroke rates. Significant differences ($p < 0.05$) in ratio were found between catch and MHF stroke positions (*****) at 18 spm, 28 spm, & 32 spm.

To explore whether preferred rowing modality and athlete sidedness affected spinal kinematics, mean lumbar and thoracic angles in the transverse and frontal plane were compared among scullers, starboard sweep rowers, and port sweep rowers. Statistical differences were found in left/right lumbar spinal torsion between port and starboard sweep rowers at the catch ($p = 0.004$; Figure 6.20). There was a trend for the sculling group to display less bending and twisting kinematics, than either port or starboard sweep cohort, at the thoracic spine level (Figure 6.20; Figure 6.21). However, no statistical differences were found among scullers, port rowers or starboard rowers in lateral bending at either the lumbar ($p = 0.224$) or thoracic ($p = 0.228$) level to suggest preferred rowing modality correlated with bilateral spinal asymmetry (Figure 6.21).

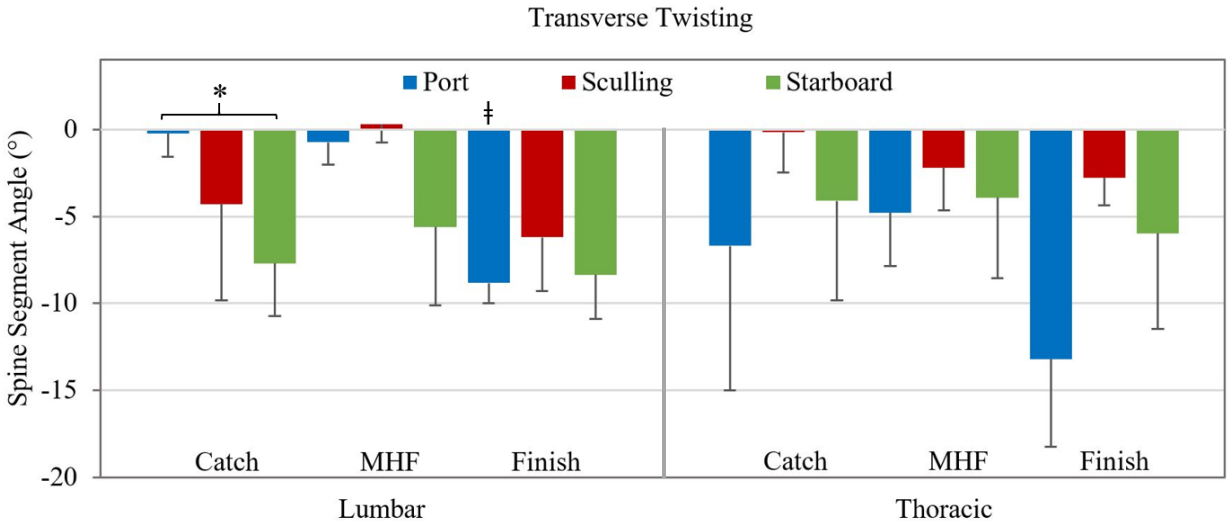

Figure 6.20: Differences in spinal torsion (mean ± std) for lumbar (*left*) and thoracic (*right*) segments between scullers (n=4), port rowers (n=5), and starboard rowers (n=7) averaged across all stroke rates. Significant differences ($p < 0.05$) in lumbar angle were found between all modality cohorts at the catch (*****) and within port rowers at the finish positions (ǂ).

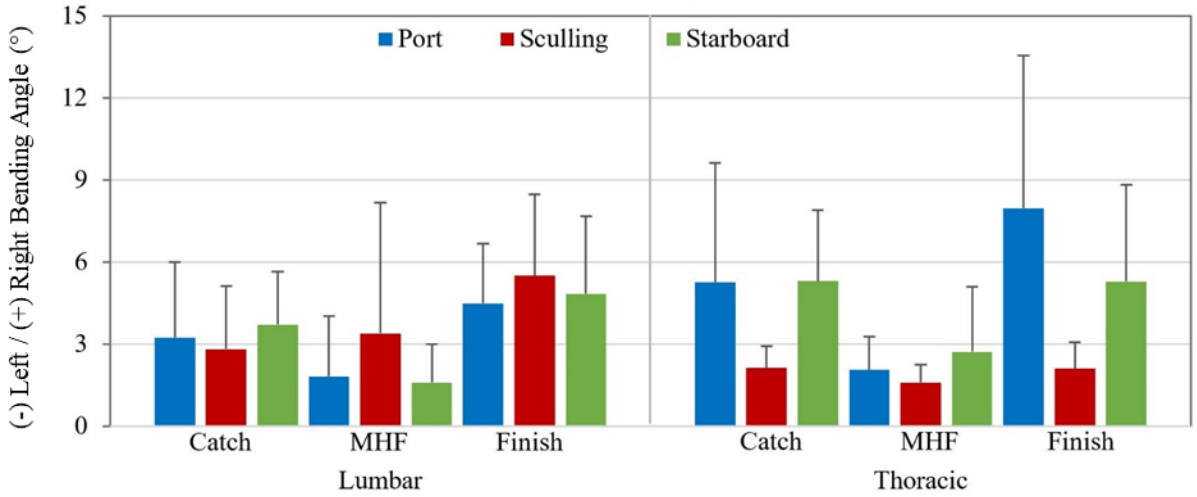

Figure 6.21: Differences in lateral bending (mean ± std) for lumbar (*left*) and thoracic (*right*) segments between scullers, port rowers, and starboard rowers averaged across all stroke rates.

6.3.3 Fatigue and Postural Control

The fatiguing step test elicited changes in spinal posture with increasing stroke rate. Linear regression was used to examine the effect of fatigue by comparing the relationship of stroke number to sagittal plane flexion angle at the catch for the lowest (18 spm) and highest (32 spm) stroke rates (Figure 6.22). Demonstrated by the slope ('b') of the linear regression, subjects were more capable of maintaining the same spinal angles at low rate, compared to high rate (Figure 6.22). At 18 spm, flexion angles did not

change for thoracic (b = 0.0377; $p = 0.065$), lumbar (b = 0.003; $p = 0.859$), or pelvic (b = 0.0103; $p = 0.582$) spine segments. Rate of postural decline increased as stroke rate increased (Figure 6.22). At 32 spm flexion angles decreased significantly at lumbar (b = -0.075; $p < 0.0001$) and thoracic (b = -0.032; $p = 0.012$) segments, but not at the pelvis (b = -0.016; $p = 0.582$). A significant interaction of stroke rate was also found in the relationships of stroke number to flexion angle for the lumbar segment ($p < 0.0001$) and the thoracic segment ($p = 0.005$). No significant interaction of stroke rate to stroke number and flexion angle was found for the pelvis ($p = 0.353$). A Fisher's r-to-z comparison indicated that at the thoracic segment the Pearson correlation for 18 spm (r = 0.085) was significantly greater ($p < 0.0001$) than at 32 spm (r = -0.100). At the lumbar segment, the correlation for 18 spm (r = 0.008) was significantly greater ($p < 0.0001$) than at 32 spm (r = -0.372) but at the pelvis, the correlation for 18 spm (r = 0.025) was not significantly different ($p = 0.13$) from 32 spm (r = -0.040).

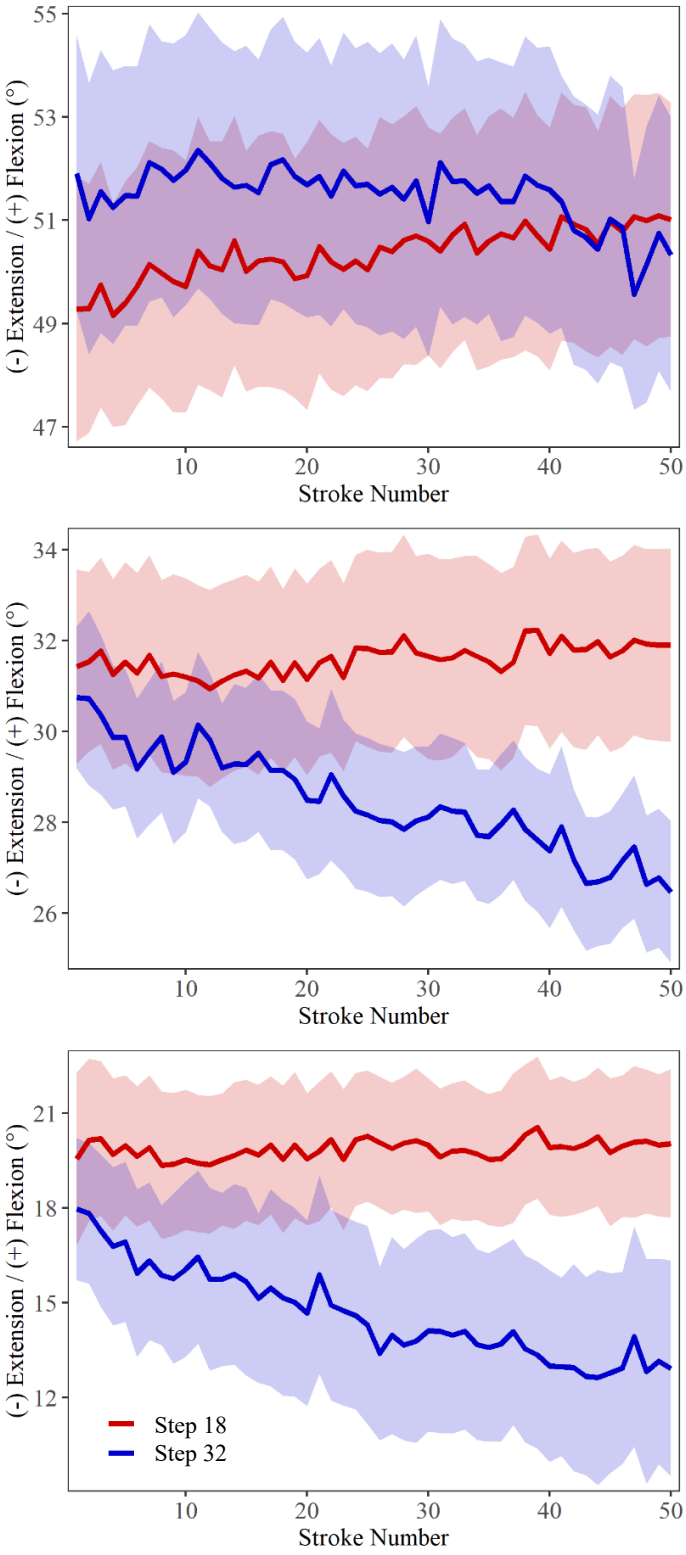

Figure 6.22: Population-wide sagittal plane flexion angle (mean ± ste) at the catch, for thoracic spinal segment (*top*), lumbar spinal segment (*middle*), and pelvis (*bottom*) varies with stroke number within each stroke rate trial. Flexion angle RoC was statistically different ($p < 0.001$) between 18 spm and 32 spm for thoracic and lumbar segments.

Linear regression analysis of scapulothoracic kinematics as a function of the fatiguing step test protocol produced no statistically significant changes in scapular internal / external rotation (Figure 6.23). Within each stroke rate trial there was no effect of increasing stroke number ($p = 0.875$). Similar scapular internal / external rotation angles were found for 18 spm (b = 0.028), 24 spm (b = 0.024), 28 spm (b = 0.018), and 32 spm (b = 0.026). There were also no statistically significant interactions between stroke number and stroke rate ($p = 0.925$).

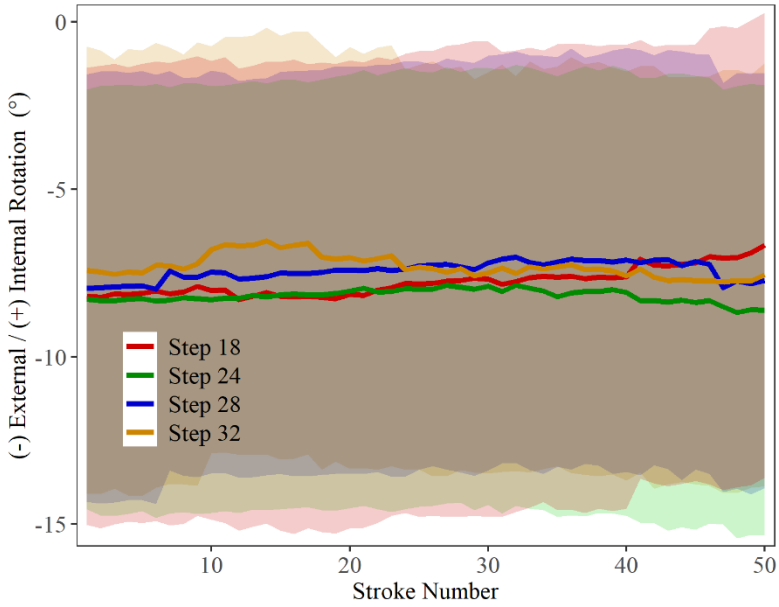

Figure 6.23: Population-wide scapulothoracic internal/external rotation (mean ± std) at the catch. No statistical differences with stroke number within or between stroke rate trials.

6.4 Discussion

In the closed chain rowing activity, studying athlete kinematics enables specific identification of technique to refine skills and improve performance. This chapter examined kinematic contributions of the thoracic spine, shoulder complex, and upper limb in the sagittal, frontal, and transverse planes, throughout the stroke cycle and at varying rowing intensity (i.e., stroke rate). Results presented in this chapter suggest that rowers achieve different positions and "stroke length" through a combination of pelvic rotation and thoracic spinal flexion, but not changes in scapular internal rotation or anterior tilt. Patterns of lumbo-pelvic motion have previously been identified in elite rowers (McGregor, Patankar & Bull, 2007), where deviations from these patterns were attributed to fatigue or aberrant rowing technique. Lumbo-thoracic motion and scapulothoracic motion have not previously been assessed in detail.

The catch, finish, and MHF each represent vulnerable positions in the stroke, as the spine is loaded in a flexed position, or must quickly change directions out of a highly loaded extension movement

(McGregor et al., 2004; Pollock et al., 2009). The results presented in this chapter found altered sagittal plane thoracic and lumbar spine kinematics between each stroke rate, and within stroke rates due to fatigue.

Chapter 5 introduced the concept of catch-slip and discussed the importance of drive coordination from the moment the handle and seat change direction at the catch (Section 5.4). Average catch-slip, whose duration (in seconds) decreases slightly with stroke rate (Section 5.3.1; Table 5.6), was attributed in part to the "slack" or "give" inherent in the ergometer handle chain system. However, catch-slip could also be attributed to flexion of the thoracic spine as leg extension initiates the drive phase. Spinal kinematic results presented in this chapter show that average thoracic flexion angle at the catch does not change with stroke rate but that a significant interaction of stroke rate was found in the relationship of increasing stroke number to increasing thoracic flexion angle at the catch (Section 6.3.2; Section 6.3.3; Table 6.8; Figure 6.22). It is possible that catch-slip is a mixture of handle chain slack and changes in timing of body kinematics due to fatigue onset. This could be further explored with the currently available dataset, or in the future with a modified fatiguing protocol (i.e., longer trial duration, similar to Holt *et al.*, (2003)) better suited to separating catch-slip influences inherent in the ergometer system versus those arising from changes in athlete kinematics.

The lumbo-thoracic ratio allows comparisons between the upper spine and lower spine and how they interact, particularly at the catch. In line with previous studies, it has been shown that at higher stroke rates anterior pelvic tilt decreases and that this is compensated by increased lumbar and thoracic flexion at the catch (McGregor, Bull & Byng-Maddick, 2004). When MHF was reached, alpha angles, and lumbo-thoracic ratio were near zero, indicating that the thoracic and lumbar spine were vertically aligned when loading was at its highest (Figure 6.18). Spinal alignment is important for efficient load transfer and MHF is the point at which spinal load is highest as force is transferred from the legs to the handle, suggesting that a straight or neutral alignment is important from a performance perspective. Price (2016) found that rowers were able to maintain a constant thoracic flexion angle through approximately 40% of the drive phase, but the author found no consistent change in spinal flexion as target power level (e.g., stroke rate) increased. Cerne *et al.*, (2013) found similar average trunk inclination angles between elite rowers and junior rowers, at the catch and at the finish, as well as no changes in trunk inclination with respect to stroke rate (Cerne *et al.*, 2013).

With respect to out of plane motion, this study found little change within and between rates for patterns of spinal lateral bending (β) and spinal torsion (ϒ), with only small angular variation through the stroke and no statistically significant changes with rate (Figure 6.17). This was in contrast to Wilson (2010), who found a 5° mean frontal plane lumbar spine angulation with 4.1 ± 1.9° increase with rate during a similar step test protocol. While results presented in this chapter display a trend for scullers to have lower

bending and twisting kinematics, no statistical differences were found ($p = 0.075$). Results on bending and torsion with respect to bilateral spinal asymmetry may not be generalizable to a single large cohort because small numerical values and large standard deviations make percentage differences difficult to quantify but may also connote that bending and torsion are more dependent upon individual athlete technique than are generalizable to a single broad cohort (Figure 6.20; Figure 6.21). Previous research has also concluded that out-of-plane rotations have a low impact on technique, with only 0.53% of out-of-plane rotations demonstrating significant changes with respect to rowing intensity (Murphy, 2009). However, measurement error may play a factor here, as spinal segment angles in the frontal and transverse plane have been notoriously difficult to measure with either electromagnetic or optoelectronic tracking systems (Buckeridge, 2013; Murphy, 2009). Consequently, recommending training interventions based on movement in the frontal and transverse planes would be difficult.

Negative changes in lumbar-pelvic kinematics and reductions in range of motion have been connected to low back pain (McGregor, Patankar & Bull, 2007; Wilson *et al.*, 2013). Visualizing sagittal plane postural decline allows athletes to gauge how they are affected by fatigue and the implications of this fatigue on performance over time. Results presented in this chapter show that fatigue significantly affected spinal postural control at the catch for the higher stroke rating, with decreases in sagittal plane spinal flexion correlated to increasing stroke number within each stroke rate trial (Figure 6.22). This decline may be loss of postural control and consistent movement patterning due to muscular fatigue. Additionally, the rate at which a fatigue induced decline occurs, may be modulated by the baseline muscular strength, endurance, and motor control displayed by an individual athlete. This corroborates published work biomechanically distinguishing novice from elite rowers (Smith & Spinks, 1995). Bell *et al.*, (2013) discusses the effect of different trunk positions at the finish, correlating greater "lean-back" with greater elbow joint range of motion, a more acute elbow angle at the finish, and an increased power output of ~18%. However, the authors provide only a qualitative definition of "lean-back" positioning and concede that the technique of an extended spinal position demands more work of trunk musculature. Results presented in this chapter have shown that during ergometer rowing kinematic changes may set in quickly at the highest stroke rates (Figure 6.22), suggesting ramifications of a "greater lean-back" technique. While fatigue has been referred to several times, it is a limitation of this study that "fatigue" by its physiological definition (Chapter 3, Section 3.2.1) was not evaluated. The "step test" is a fatiguing protocol and while biomechanical changes seen in this chapter are linked to fatigue (McGregor, Patankar & Bull, 2005; Montusiewicz *et al.*, 2016; Price, 2016) there are likely other factors at play as well, including athlete exercise habituation.

Athletes with limited joint range of motion in the lumbar spine have been observed to gain stroke length by compensating through increased thoracic spinal flexion. Results in this chapter, for mean sagittal

plane (α) angles, show decreased thoracic maximum extension at the finish, with increased stroke rate, while pelvic extension increases at the finish and lumbar flexion decreases at the catch (Figure 6.17; Table 6.8). This result can be linked to sagittal plane handle kinematics presented in Chapter 5, Section 5.3.2.1 where a slight decrease in total stroke length was observed, which was initially attributed as rowers achieving slightly less forward reach into the catch, and slightly less lean back into the finish (Chapter 5, Section 5.3.2.1; Figure 5.25), and now appears associated with spinal kinematics, specifically. Although sex differences in spinal kinematics were not specifically examined within the scope of this thesis, unlike differences found in spatio-temporal analysis results from Chapter 5 (Section 5.3.1; Table 5.6), McGregor, Patankar & Bull, (2008) found that there was no difference in stroke length between sexes but that females demonstrated greater anterior pelvic rotation than males. Any such increasing spinal curvature suggests an increasingly hunched position of the spine with increased stroke rate and fatigue onset. It has been shown that kyphosis of the thoracic spine can negatively impact lung function and rib cage mobility (Lorbergs *et al.*, 2017). Findings from this chapter suggest that declining biomechanical technique may be associated with other metrics of declining overall athletic performance, including decreased physiological output.

Upper limb patterns of motion presented in this chapter were comparable to previously published two-dimensional (Kaya *et al.*, 1995; Pudlo, Pinti & Lepoutre, 2005) and three-dimensional (Halliday *et al.*, 2001) kinematics studies of ergometer rowing. However, previously published sagittal range of motion for the elbow and GH joints tended to be smaller in internal/external rotation and larger in flexion/extension than reported here, which may have contributed to reported differences of kinematics at varying stroke rates. This could be due to two-dimensional motion analysis assumptions underestimating actual joint motion. Using the UK national shoulder model with the calibration method of the scapula locator and scapula tracker for anatomical and technical frames is currently the best way of accurately measuring shoulder motion. The model has previously been validated against bone pin derived kinematics (Karduna *et al.*, 2001) and verified for other extreme athletic activities including pull-ups (Prinold & Bull, 2016; Urbanczyk *et al.*, 2020) and cricket bowling (Persad, 2016).

Kinematic relationships derived from ergometer outputs are not ideal for predicting on-water rowing performance, however, they are a close approximation. Lamb (1989) found that the only statistically significant differences between the two rowing forms were the movement patterns of the upper extremities at the catch and finish. Across the whole athlete population, neither minimum joint angle, nor maximum joint angle, nor joint range of motion changed with stroke rate for any of the three upper limb joints examined (GH, ST, elbow). However, relative time to reach maximum shoulder extension, abduction, and rotation increased with stroke rate. Relative time spent during the drive with maximally extended elbows increased as rate increased, with maximum flexion also occurring relatively later in the drive (Figure 6.3).

Unlike the findings reported by Halliday *et al.* (2001), GH joint rotation shows a qualitative change in peak timing of angle-profile between 18 spm and 32 spm (Figure 6.6). However, observations about timings of maxima and minima in joint kinematics should be interpreted conservatively, as differences may be due to changes in drive and recovery phase duration in the normalized stroke cycle. Core concepts about upper limb positioning derived from previous research and observational data of expert coaches attribute increased force production to pulling the handle through the early drive phase with straight arms (i.e. elbows extended to 180°), keeping the elbows close to the trunk through the late drive (Bompa, 1980; Bompa, Borms & Hebbelinck, 1990), and extending the humerus so as to achieve an acute elbow angle at the finish (Halliday *et al.*, 2001). Results in this chapter showed that both the elbow joint and GH joint were slightly flexed (Figure 6.3; Figure 6.6) and suggest that at the catch the arms need not be perpendicular to the torso. The fact that the arms were not fully extended may reduce strain on the arms by avoiding hyperextension. Although, Jones *et al.* (2010) goes so far as to suggest that for "less-able" rowers it may be easier to apply power with slightly bent arms. This may be a lever arm effect related to muscle force outputs, a concept that will be explored in Chapter 7.

Excessive scapular protraction during rowing has been hypothesized to result from declining postural control or fatigue (McDonnell, Hume & Nolte, 2011; McGregor, Bull & Byng-Maddick, 2004; Price, 2016). Rotator cuff impingement has been associated with a protracted and a relatively anteriorly tilted scapula, which can decrease the subacromial space (Ludewig & Reynolds, 2009; Kibler & Sciascia, 2010). Significant changes were noted in scapular anterior/posterior tilt between 18 spm and all other stroke rates (Figure 6.7), however no changes in scapular internal / external rotation were found to result from the fatiguing step test protocol used in this experimental series (Figure 6.23). Scapulothoracic joint angle outputs from the UKNSM are a complex means of quantifying the range of internal and external rotation of the scapula, and do not exactly reproduce the compound protraction and retraction motion that the athlete moves their shoulders through during the rowing stroke. A simplified variation of this measurement may be contrived from Price (2016) which quantified bilateral shoulder protraction as the transverse shoulder angle between vectors linking the left acromion marker to a T1 marker, and then to the right acromion marker. This metric presumed that any movement of the acromion in the transverse plane indicated a change in scapular position. This may be a viable option when considering data acquisition and instrumentation reduction and recommending biomechanical surrogates for biofeedback. In depth data, over a broad population can facilitate creation of a database of descriptions and classifications of several rowing techniques based on observed postures and forces in rowing set-ups. This will allow for reflections upon how movement strategies may differ by age, experience, and sex in rowing athletes.

6.5 CONCLUSIONS

Results presented in this chapter highlight the spatiotemporal relationship between timing of key stroke moments and kinematic metrics, showing that spinal motion in the transverse and frontal planes have little influence, while alterations in sagittal plane spinal rotations may indicate declining postural control at the catch that deteriorates at higher stroke rates. Relative movement between spine segments at critical points during the stroke show greater lumbar flexion (compared to thoracic) at the catch and neutral alignment during MHF. Providing an accurate representation of spinal movement in all planes through each stroke, enables assessment of form differences across athletes.

Kinematic motion of the upper limb, shoulder complex and upper spine furthers understanding of whole-body factors in rowing technique. The preferred movement path selected by each athlete is based on individual constraints, such as strength, injury, or fatigue. Having examined athlete kinematics, linking this and the previously discussed spatio-temporal analysis to underlying muscular changes are further examined in Chapter 8, where modelling of scapular biomechanics for the enhancement of interpreting performance data is discussed to determine the best possible posture for individuals to achieve specific performance outputs, row more effectively, and in a way that prevents potential spinal injury.

7. CHAPTER 7: MUSCULOSKELETAL FORCES AT THE SHOULDER DURING ERGOMETER ROWING[3]

Understanding shoulder loading during rowing and ergometer rowing is a major step toward improving performance coordination, tailoring individual athlete training programs, and investigating pathomechanics of injuries. This chapter reviews fundamentals of computational modelling for the shoulder complex and introduces the UKNSM, describing its functionality, advantages, and limitations, and briefly outlines the processing steps used in simulating musculoskeletal dynamics of ergometer rowing. This chapter presents muscle and joint forces in the upper extremity and GH contact patterns. Contributions of the surrounding musculature to shoulder stability during ergometer rowing are discussed across the entire population and contrasted among athlete cohorts, including by sex, preferred modality, and competition level.

7.1 INTRODUCTION

The forces in the shoulder complex during rowing are frequently dismissed as being small compared to loads at the knee and hip joint. This is because shoulder injuries are less common than low back and knee injuries (McNally, Wilson & Seiler, 2005); although their significance should not be downplayed, as shoulder injuries have been linked to lost fitness, missed competition, impact on stroke quality and long term chronic shoulder pain (Mohseni-Bandpei *et al.*, 2012). Various cohort studies have reported that the upper extremity is the third most frequent injury site among rowers, comprising approximately 7-10% of all sustained injuries; however, national team injury rates have been seen as high as 35% (Winzen *et al.*, 2011; Hickey, Fricker & McDonald, 1997; Wilson *et al.*, 2010; Boland & Hosea, 1994), and upper extremity injuries are reported as having slightly higher prevalence among masters rowers (Smoljanović *et al.*, 2018) and among the para-rowing community (Cutler *et al.*, 2017).

Shoulder pain and upper limb injuries are frequently identified as the result of tension, weakness, or muscle imbalance (Rumball *et al.*, 2005). Athletes commonly present with tightness in latissimus dorsi and upper trapezius, and may have weakness in the rotator cuff muscles (Richardson & Jull, 1995). It is suspected that overuse of rhomboid major, trapezius, levator scapulae, and serratus anterior contribute to compromised shoulder girdle positioning with decentralization of the humeral head, and stretching of the

[3] Published in part as: Urbanczyk, C.A., McGregor, A.H. and Bull, A.M. (2019). Modelling scapular biomechanics to enhance interpretation of kinematics and performance data in rowing. *ISBS Conference Proceedings Archive*, 37(1): 133-136.

posterior capsule, (Kibler *et al.*, 2002; Page, Frank & Lardner, 2010). Unfortunately, mechanisms of injury in the upper limbs and shoulder are less well documented in the rowing biomechanics literature. This is due to difficulties in evaluating forces acting on these joints. However, case studies have indicated that hypermobility in the joints may yield rotator cuff tendinopathy, anterior instability, or impingement (Thornton *et al.*, 2017b). Kinematic factors that have been identified in assessing shoulder injury risk include scapular positions commonly exaggerated in the outside arm of sweep rowers, including large scapular protraction, anterior tilt, and humeral internal rotation (Ludewig & Reynolds, 2009).

In vivo measurements of biomechanical factors can be technically and ethically challenging to obtain as they typically involve recruiting human subjects, are often restricted to a laboratory setting, and can be highly invasive. MSK models have been developed to simulate and analyze the mechanics of movement on a broad spectrum of loading conditions that might otherwise be too complicated or ethically unviable to carry out experimentally. MSK models provide in vivo information such as muscle forces and joint contact forces, that can be used to quantify occupational and functional activities (Pandis, Prinold & Bull, 2015; Klemt *et al.*, 2018), and to optimize surgical or rehabilitation techniques (Klemt *et al.*, 2019b; Kontaxis & Johnson, 2008). Most multi-body dynamics models are built on IDA foundations, which use observed kinematics and external kinetics as primary inputs to quantify soft tissue loading and muscle force (Prinold *et al.*, 2013). As was discussed in Chapter 3 (Section 3.5.4), IDA has been used with multi-segment models to estimate joints forces and moments during rowing, and comprehensive MSK models of the torso and upper limb have been used to study dynamic athletic tasks (Persad, 2016; Urbanczyk *et al.*, 2020; Langholz, Westman & Karlsteen, 2016), including ergometer rowing (Juliussen, 2011).

This thesis utilized the UKNSM for computational modelling because it is considered anatomically complete as it contains all necessary muscle lines to include elbow and scapula kinematics and the model is implemented to run in the MATLAB environment. Recent updates to the UKNSM have incorporated a validated scapular tracking method (Prinold, Shaheen & Bull, 2011) and have integrated the labrum and capsuloligamentous structures (Klemt *et al.*, 2017). Published literature utilizing the UKNSM have investigated GH joint loading during activities of daily living (Klemt *et al.*, 2018), occupational tasks (Smith, Reilly & Bull, 2020; Pandis, Prinold & Bull, 2015; Ismail, 2016), and dynamic athletic movements including cricket bowling (Persad, 2016), pull-ups (Urbanczyk *et al.*, 2020; Prinold & Bull, 2016), and overhead throwing (Klemt, 2018).

Muscle coordination plays an important role in efficiently accelerating the boat or the flywheel on an ergometer, with up to 40% of the velocity from the late drive through to the finish coming from the upper limb (Soper & Hume, 2004; Kleshnev, 2006a). The upper body and upper limb provide an essential link between the boat and the oar. At the catch position, the elbow extensors and scapular protractors are

engaged, while fine motor work in the wrist and finger extensors place the blade in the water (Nilsen, Daigneault & Smith, 2002c). Mechanical loading in the early drive phase involves the isometric firing of the trunk muscles. Deep paraspinals, abdominals, and erector spinae muscles stabilize the spine, while trapezius and serratus anterior stabilize the scapula (Pollock *et al.*, 2009). Peak acceleration at MHF coincides with maximal force in the trunk muscles. Through the late drive phase, the trunk muscles extend the upper body from approximately 20° flexion to 20° extension (Nilsen, Daigneault & Smith, 2002c). The upper body generates momentum through the humeral extensors and internal rotators, by concentric contraction of latissimus dorsi and teres major. The rhomboids retract the scapula, biceps brachii flexes the elbow, and triceps brachii draws the arms into the body and the finish position. Sharp deceleration into and acceleration out of the finish position are supported by contraction of the rotator cuff musculature surrounding the shoulder. Biceps long head and subscapularis create stability within the GH joint by resisting anterosuperior translation and centralizing the humeral head on the glenoid fossa through concavity compression (Itoi, Morrey & An, 2009; Lippitt *et al.*, 1993).

Muscle forces drive the variation seen in external movement patterns, impacting the joint forces and contact patterns. The GH joint is an important link in maintaining stable and efficient load transfer through the kinetic chain. GH joint reaction forces may be decomposed into three components: compressive force, anterior-posterior shear force and superior-inferior shear force (Lee, Suter & Herzog, 2000). The compressive force component acts to press the humeral head into the glenoid socket, while the shear force components act to translate the humeral head across the glenoid surface and load the glenoid labrum. The ratio of the shear force components to compression quantifies loading of the capsuloligamentous labral complex and succinctly describes the risk of joint luxation (Nishinaka *et al.*, 2008). Differences in shoulder loading have been demonstrated for various overhead actions (Prinold, 2012; Persad, 2016; Klemt, 2018), with larger shoulder shear forces being associated with increased likelihood of joint instability.

The magnitude of GH joint reaction forces is an important factor in assessing high-risk positions of GH joint instability but so too is the locus of that force against the glenoid fossa. A glenoid contact pattern visualizes the way in which the resultant shear force vector causes humeral head translation across the glenoid surface. This information can be useful in program planning for strength & conditioning and rehabilitation, as off-center humeral head loading in the GH joint may be a cause of rotator cuff injury in athletic, occupational, and functional tasks (Klemt, 2018).

The aim of this chapter is to reveal the sensitivity with which internal biomechanics may be mapped to external kinematics and discuss how computational modelling can enhance our interpretation of performance data in the context of rowing. This includes presenting the musculoskeletal shoulder loads in rowers and exploring potential relationships to risk of shoulder injuries during ergometer rowing.

7.2 COMPUTATIONAL MODELLING WITH THE UKNSM

The UKNSM is a three-dimensional inverse dynamics model of the right-sided upper limb consisting of five rigid bone segments, 87 muscle lines of action (29 functional regions of 22 muscles), and 3 glenohumeral ligaments, crossing 5 joints (**Error! Reference source not found.**). The UKNSM model was developed using skeletal geometry derived from the Visible Human (VH) dataset (Spitzer & Whitlock, 1998), while muscle morphology data were obtained from three cadaveric studies (van der Helm *et al.*, 1992; Johnson *et al.*, 1996; Veeger *et al.*, 1997).

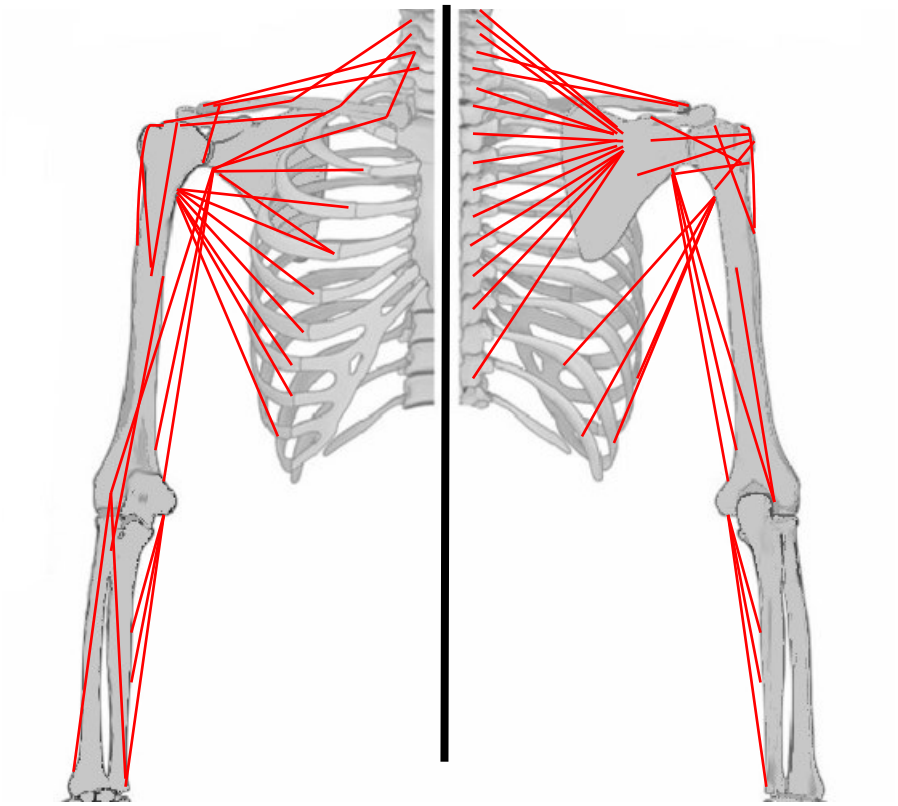

Figure 7.1: Anterior (*left*) and posterior (*right*) views of the bony structures comprising the United Kingdom national shoulder model (UKNSM), and illustrative muscle lines of action (*red lines*). Adapted from (Persad, 2016).

Outputs from the UKNSM have been validated against measurements from instrumented shoulder implants (Nikooyan *et al.*, 2010; Prinold, 2012) and further verified through comparison of predicted muscle moment arms with cadaveric measurements (Gatti *et al.*, 2007) and electromyographic muscle activations (Johnson & Pandyan, 2005; Pandis, Prinold & Bull, 2015). All calculations in this validated MSK model were completed in MATLAB Runtime v9.0 (MATLAB 2017b, MathWorks Inc., Natick, USA). Kinematic data in the form of marker trajectories from motion capture trials, external kinetics from force plates, and subject specific anthropometrics provided primary model inputs. Scaled body parameters

including segment masses, center of mass and moment of inertia, were obtained from regression equations (de Leva, 1996) using each subject's height and weight.

An overview of the processing steps involved in the UKNSM calculations to predict muscle and joint loading during shoulder motion is shown below:

1. **Subject scaling**
   Input: Anatomical dataset, anthropometric measurements, kinematic calibration data
   Output: Body segment parameters, scaling factors
2. **Inverse kinematics**
   Input: Scaling factors, local coordinate systems. kinematic trial data
   Output: Upper limb joint angles
3. **Inverse dynamics**
   Input: Body segment parameters, scaling factors, joint angles, external kinetic data
   Output: Intersegmental forces and moments
4. **Muscle wrapping**
   Input: Anatomical dataset, joint angles, scaling factors, body segment parameters
   Output: Muscle lines of action, muscle moment arms
5. **Load-sharing optimization**
   Input: Intersegmental forces and moments, muscle lines of action, muscle moment arms, muscle force boundaries, ligament boundaries

Output: Joint forces, contact patterns, muscle forces.

7.2.1 Subject Scaling

Scaling has been shown to greatly affect model predictions (Karduna *et al.*, 2001), so all body segments and intersegmental distances in the UKNSM were scaled to each experimental subject for bespoke bone size, muscle origins and insertions. Bone geometries, muscle architecture, and physiological cross-sectional area for initial scaling in the UKNSM were derived from the Visible Human Project anatomical dataset (Spitzer & Whitlock, 1998). The clavicle, humerus, radius and ulna were scaled linearly by the distance between the joint centers. For each body segment, respectively, this was from SC to AC joint for the clavicle, GH to ELB for the humerus, and ELB to wrist for the forearm. The scapula was scaled linearly from AI to AA. The torso was scaled non-homogenously in three dimensions with the height from XI to the midpoint between the jugular notch (MA) and 7th cervical vertebra (C7), with the width from MA to

the right AC joint, and with depth from C7 to the midpoint between XI and MA (**Error! Reference source not found.**). Muscle origin and insertion sites were scaled to their corresponding segments, however physiological cross-sectional area of each muscle remain unscaled.

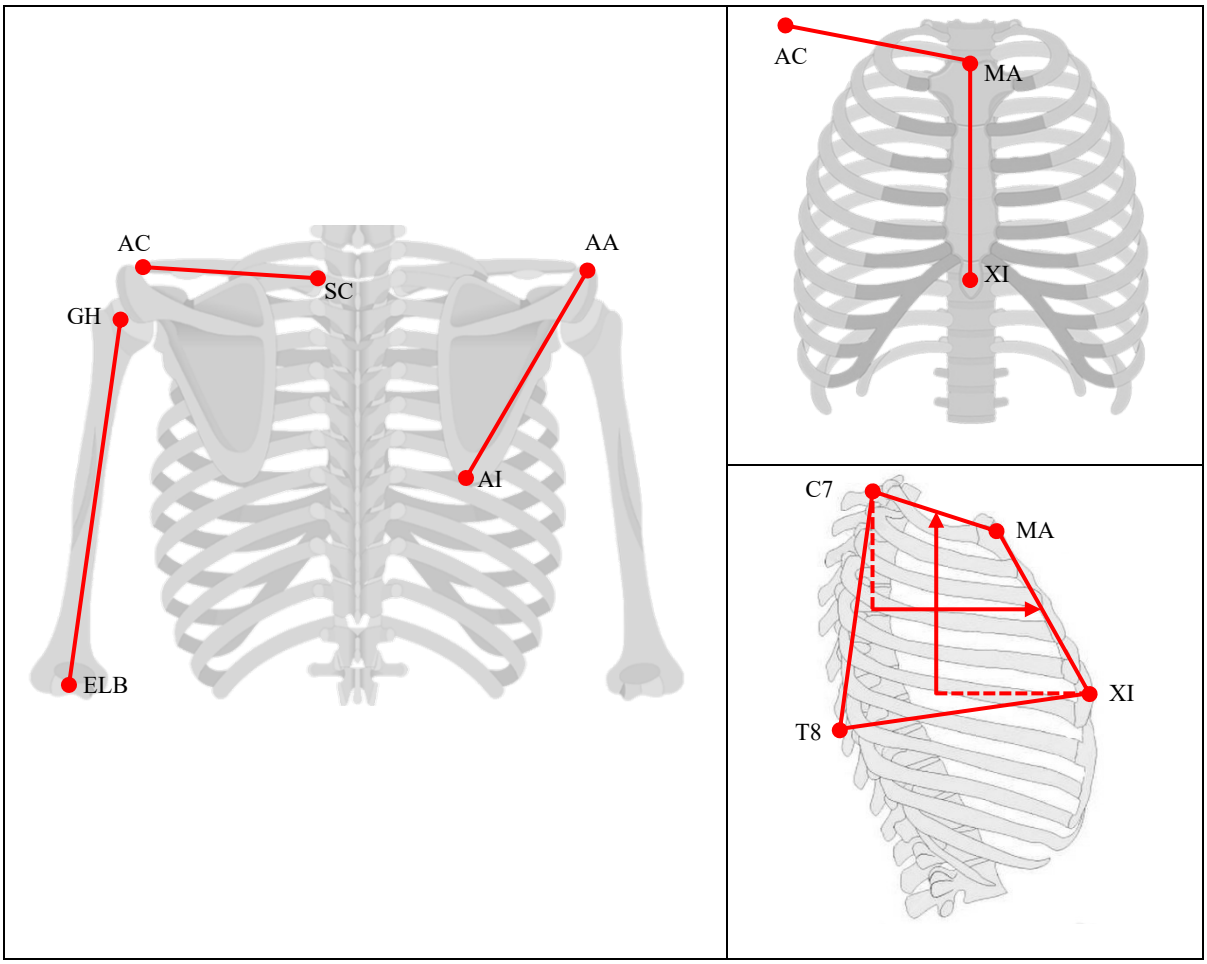

Figure 7.2: Segment lengths used in homogenous scaling (*left*): clavicle length (SC-AC), humerus length (GH-ELB), scapula length (AI-AA). Torso was scaled non-homogenously in width by MA-AC (*top-right*) and in depth by XI, MA, and C7 (*bottom-right*). Adapted from (Persad, 2016; Get Body Smart, 2021)

7.2.2 Inverse Kinematics

Once the scaled anatomical model for each subject has been created, measured marker trajectories were used to define local coordinate frames for each body segment, as defined by anatomical landmarks (Wu et al. 2005),) and calculate joint kinematics between segments. The UKNSM models upper limb articulations with 13 rotational degrees of freedom (DOF): 3 DOF at the SC joint, 3 DOF at the SC joint, 2 DOF at the ST joint, 3 DOF at the GH joint, and 2 DOF at the elbow (Prinold, 2012). Segment coordinate frame axes were oriented as lateral X, superior Y, and posterior Z. Joint angles between adjacent body

segments were calculated by extracting Euler angles from the transformation matrix between two local coordinate frames, according to Euler rotation sequences indicated in Table 7.1.

Table 7.1: Euler rotation sequences used by the United Kingdom national shoulder model (UKNSM) for joint angle calculations between body segments.

Articulation	Sequence used by model
Sternoclavicular (SC)	y-z'-x"
Acromioclavicular (AC)	y-z'-x"
Glenohumeral (GH)	x-z'-y"
Elbow	x-z'-y"
Scapulothoracic (ST)	y-z'-x"
Humerothoracic (HT)	y-z'-y"

Euler angles are used to represent joint angles in biomechanics because they can describe the rotation about each axis of one frame relative to another, in static or moving reference frames. There are twelve possible Euler angle sequences as the resulting outputs are order dependent. An example of one such Euler sequence is outlined in **Error! Reference source not found.**, where a rotation of α° about the X-axis is followed by a rotation of β° about the new Y-axis, and finally a rotation of γ° about the twice-changed Z-axis.

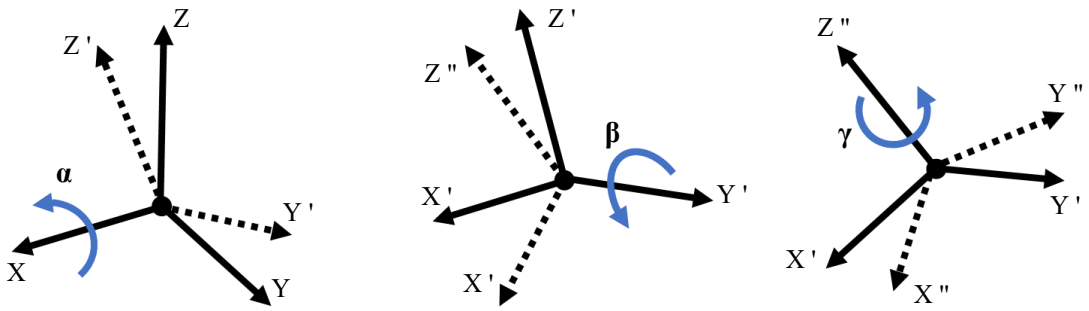

Figure 7.3: Example X Y' Z" Euler sequence. Adapted from (Persad, 2016)

Additionally, the modelling framework of the UKNSM includes a kinematic optimization that determines the position of the scapula based on tracking a rigid technical cluster during motion trials, and with respect to a scapular anatomical frame established during calibration trials (Prinold, Shaheen & Bull, 2011; Shaheen, Alexander & Bull, 2011). The kinematic optimization algorithm makes use of MATLAB's built-in constrained minimization function (*fmincon*), which calculates a least-squares difference minimization between modelled and measured kinematics, while applying constraints to avoid non-

physiological positions and orientations of the scapula and humerus (Prinold & Bull, 2014; Persad, 2016). The scapulothoracic joint was approximated using an ellipsoid fit to the right half of the rib cage, where TS and AI were constrained to lie outside the STGP, preventing the scapula from penetrating the thorax but allowing translation across the outside of the STGP ellipsoid. The glenohumeral joint rotation center was computed using a spherical fitting method (Hiniduma, Gamage & Lasenby, 2002); however, translations of the humeral head against the glenoid fossa are not considered by the UKNSM.

7.2.3 Inverse Dynamics

Intersegmental joint forces and moments were calculated based on Newton's equations of motion through derivations of joint angles, accelerations, and externally applied forces. The Newton-Euler equations for force (F) and moment (M) are:

$$\sum F = m * \ddot{x} \qquad \text{Equation 7.1}$$

$$\sum M = I * \ddot{\theta} \qquad \text{Equation 7.2}$$

The equations can be simply illustrated with a two-dimensional free body diagram of a generic rigid body (**Error! Reference source not found.**), where F is the force and M is the moment acting at the proximal (p) and distal (d) joints of the segment in x and y directions. Force is dictated by the segment weight ($m * g$), linear accelerations ($\ddot{x}$), and reaction forces (R), while moment is defined by the moment of inertia (I) and the angular acceleration ($\ddot{\theta}$).

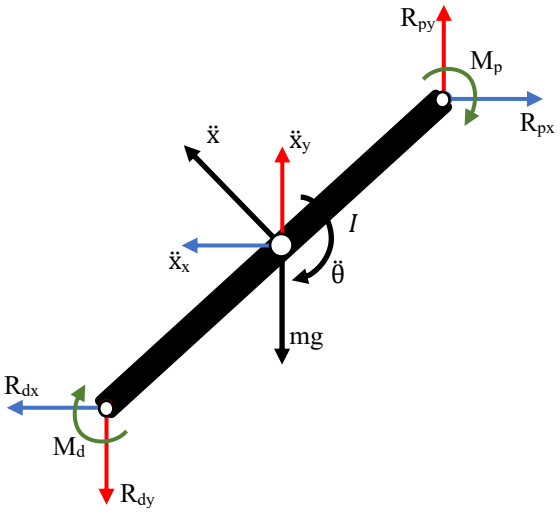

Figure 7.4: 2D free body diagram of a generic beam segment. Segment accelerations (m*g; $\ddot{x}$), relevant forces (F) and relevant moments (M) are labelled along X & Y axes for proximal (p) & distal (d) ends of the beam segment.

7.2.3.1 Handle Force Implementation

The inverse dynamics subroutine of the UKNSM can accept an external force vector at the hand. Handle force recorded from the ergometer instrumentation was accounted for during the inverse dynamics model calculation as a tensile reaction force, transformed directly into the forearm coordinate frame. In the ergometer setup, where handle force was measured with a single in line load cell (Section 5.2.2), the force at each hand was indeterminate. The handle force was, therefore, assumed to be evenly distributed to each hand and to act perpendicularly to the handle. Handle motion was assumed to occur only in the sagittal plane, allowing the horizontal and vertical force components to be calculated based on chain angle recorded by the rotary encoder (Section 5.2.2), while lateral handle force remained zero.

7.2.4 Muscle Wrapping

Once intersegmental dynamics have been calculated, muscle wrapping, and load sharing determine final model outputs. The UKNSM represents bones as solid geometric objects, around which muscle lines are wrapped. The UKNSM contains 13 wrapping objects: the torso and scapulothoracic gliding plane were modelled as ellipsoids. The humeral head was represented as two spheres around which the rotator cuff and long head bicep muscles wrap; three cylinders were aligned along the long axes of the humerus, radius, and ulna; two cylinders cross the elbow joint; and four cylinders for wrapping the remaining shoulder muscles (Charlton & Johnson, 2006). The muscle wrapping algorithm computes a best-fit path for each muscle line of action as the shortest distance between origin and insertion around any relevant geometric wrapping objects. A muscle's wrapping path is defined by a straight line from muscle origin to effective origin (i.e., where the muscle line first meets the wrapping object). It then wraps around the geometric object surface to an effective insertion after which it forms a straight line to the anatomic muscle insertion. Modelling details of each of the UKNSM muscles are in **Error! Reference source not found.**2.

A limitation of employing wrapping objects is that they may predict erroneous muscle paths under certain kinematic scenarios, such as high abduction angles. Via points (Horsman *et al.*, 2007) were introduced into the UKNSM (Persad, 2016) to increase muscle moment arms, to constrain muscle paths, and resolve wrapping issues at extreme ranges of motion, which might otherwise result in 'flipping' of muscle paths through non-physiological positions. An example of which is shown in **Error! Reference source not found.**.

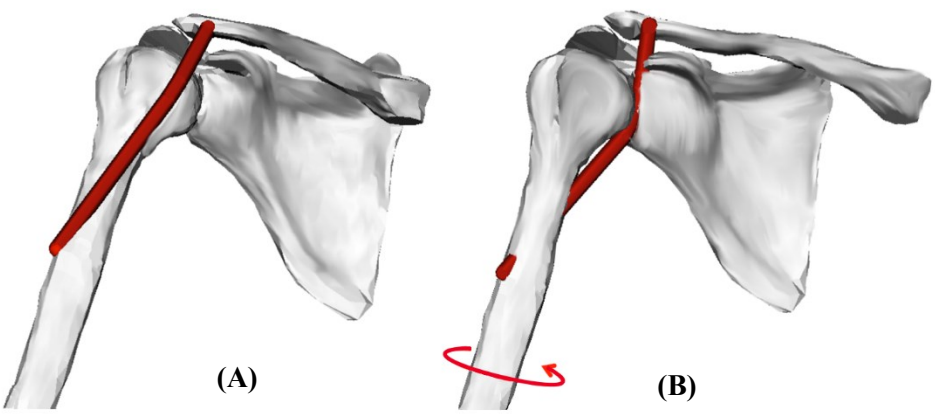

Figure 7.5: The shortest distance between muscle origin and insertion around a spherical wrapping object representing the humeral head can result in (A) a deltoid muscle path correctly computed at a low abduction angle (B) or a deltoid muscle path incorrectly computed after internal humeral rotation and resulting in a non-physiological position due to 'flipping'. Adapted from (Prinold, 2012).

Table 7.2: United Kingdom national shoulder model (UKNSM) muscle elements, associated excursions, wrapping objects and the bone segments to which they are fitted. (E: ellipsoid, S: sphere, C: cylinder, 0: no wrapping).

Muscle	Origin	Insertion	Number of Divisions	PCSA (cm^2)	Wrapping Object	Segment
Trapezius (clavicular)	Thorax	Clavicle	3	3.3	0	-
Trapezius (scapular)	Thorax	Scapula	13	9.7	E	Scapula
Levator Scapulae	Thorax	Scapula	4	2.3	E	Scapula
Rhomboid Minor	Thorax	Scapula	2	1.3	0	-
Rhomboid Major	Thorax	Scapula	5	4.4	0	-
Serratus Anterior	Thorax	Scapula	9	10.5	E	Scapula
Pectoralis minor	Thorax	Scapula	3	3.3	0	-
Pectoralis Major	Thorax	Humerus	10	19	E	Thorax
Latissimus Dorsi	Thorax	Humerus	5	6.6	E	Thorax
Deltoid	Scapula	Humerus	5	12.2	S	Humerus
Supraspinatus	Scapula	Humerus	1	3	S	Humerus
Infraspinatus	Scapula	Humerus	3	6	S	Humerus
Subscapularis	Scapula	Humerus	3	7.8	S	Humerus
Teres Minor	Scapula	Humerus	1	2.1	S	Humerus
Teres Major	Scapula	Humerus	1	4.1	S	Humerus
Coracobrachialis	Scapula	Humerus	2	2.04	0	-
Biceps short head	Scapula	Radius	1	2.83	C	Ulna
Biceps long head	Scapula	Radius	1	2.97	S	Humerus
Triceps	Humerus	Ulna	6	13.42	C	Radius
Brachialis	Humerus	Ulna	2	5.24	C	Radius
Anconeus	Humerus	Ulna	2	1.6	0	-
Brachioradialis	Humerus	Radius	2	2.14	C	Ulna
Supinator humerus	Ulna	Radius	1	1.51	C	Ulna
Pronator humerus	Humerus	Radius	2	1.04	0	-
Costoclavicular ligament	Thorax	Clavicle	1	0.2	0	-
Conoid ligament	Clavicle	Scapula	1	0.49	0	-
Trapezoid ligament	Clavicle	Scapula	1	1.7	0	-

7.2.5 Load Sharing Optimization

The last UKNSM processing step involves determining the moment arms of each muscle and distributing muscle forces across all lines of action, while ensuring that the torque generated about each joint remains in equilibrium with previously calculated intersegmental joint moments. Due to static indeterminacy, a numerical approach was taken to resolve the biomechanical analysis. A muscle load-sharing solution was found, wherein an optimization algorithm resolves a set of equilibrium equations quantifying muscle forces by minimizing an energy cost function within determined physiological constraints.

Mathematical constraints for muscle and ligament forces define the solution space for optimizing the strength distribution profile and usually consist of a lower stress boundary (0 N/cm^2) and an upper boundary defined as the product of the maximum muscle fascicle stress (1000 N/cm^2) and each muscle's physiological cross-sectional area (PCSA; Charlton & Johnson, 2006). Muscle force upper boundaries describe the largest amount of tension that each muscle may produce. Standard modeling approaches previously optimized for functional movements were insufficient for heavily loaded or athletic activities (Prinold, 2012; Persad, 2016). Similar to several studies which preceded it, this thesis utilized integer multipliers to alter muscle force upper boundary constraints applied in the UKNSM (Prinold, 2012; Persad; 2016; Southgate, 2012; Smith 2017). An appropriate muscle force upper boundary must be sufficiently high to ensure convergence of the model while remaining representative of physiologically available muscle strength. The muscle force upper boundary multiplier used for all participants in this study was 10x.

Additionally, the UKNSM modelling framework constrains the humeral head joint contact force vector within a 2D ellipsoid fitted to the surface of the glenoid fossa (**Error! Reference source not found.**). This constraint is designed to emulate shoulder stability, maintaining a coherent joint, while allowing for some co-contraction.

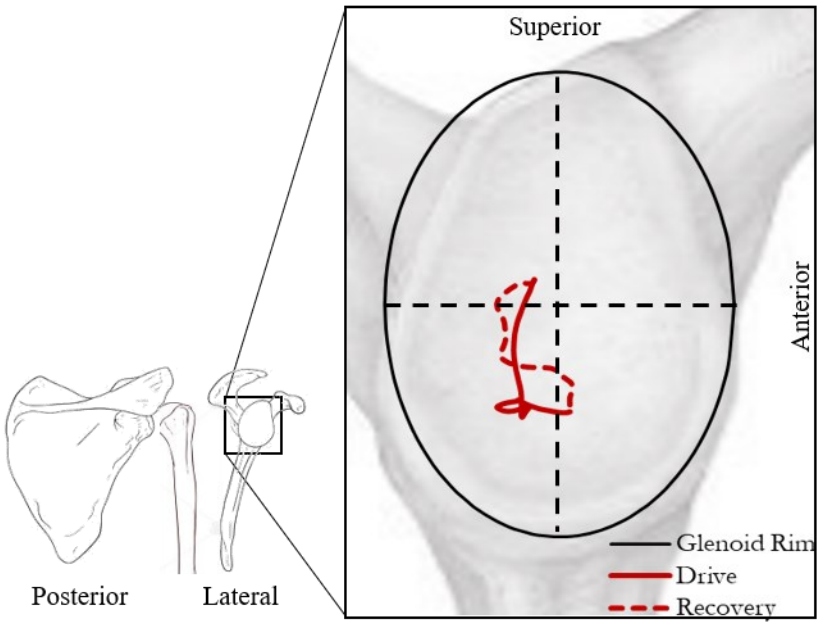

Figure 7.6: Glenohumeral (GH) joint contact pattern contained with the glenoid rim ellipse by imposing muscle force boundary constraints to the United Kingdom national shoulder model (UKNSM). The red line within the ellipse represents contact force at the GH joint during one ergometer rowing stroke cycle.

Given the above boundaries for the solution space, the UKNSM optimization algorithm minimizes the sum of squared muscle stresses according to **Error! Reference source not found.**, where i is the muscle element of interest, F_i is the estimated muscle element force, and $PCSA_i$ is the physiological cross-sectional area for each muscle element.

$$F = \sum_{i=1}^{87} \left(\frac{Fi}{PCSAi}\right)^2 \qquad \text{Equation 7.3}$$

$$\left[\left(\frac{GHx - Mx}{Ax}\right) + \left(\frac{GHy - My}{Ay}\right) - 1\right] > 0 \qquad \text{Equation 7.4}$$

The muscle load-sharing solution should represent physiologically accurate and meaningful resultant muscle forces, which may then be used to calculate components of the joint reaction forces. The constraint maintaining the GH joint reaction force within the glenoid ellipse is given by **Error! Reference source not found.**, where *GHx, GHy* are the 2D coordinates of the projected GH reaction force, *Mx, My* are the ellipse centroid coordinates, and *Ax, Ay* are ellipse axis vectors.

It is worth clarifying the distinction between intersegmental forces which were generated from joint angles through the inverse dynamics calculation (Section 7.2.3), joint forces which were generated after the load-sharing optimization and account for muscle force distribution (Section 7.2.5), and glenohumeral

contact forces which were contributed by the translational components of the humeral head against the glenoid surface (**Error! Reference source not found.**).

7.3 DATA HANDLING AND STATISTICAL ANALYSIS

Materials and methodology were presented in Chapter 5 (Section 5.2) and details of the thirty-six subjects and their cohort groupings used in computational modelling were presented in Chapter 6 (Section 6.2). Twenty-four markers placed on the chest and upper extremities were used to create forearm, humerus, scapula, clavicle, and torso segments as previously described in Chapter 6, Section 6.2. Although bilateral, whole-body kinematic data were collected for all participants, only right-side upper extremity data were analyzed using the UKNSM.

Within subject means were calculated across all strokes within each stroke rate trial. Population-wide means were calculated across all subjects and cohort means were calculated among subjects within each of the previously defined athlete groups (Chapter 5, Section 5.2.1, Section 5.2.4). Muscle and joint forces were calculated subject to the load-sharing optimization and accounting for intersegmental moments (Section 7.2.5). Joint forces are described in the local, distal coordinate segment frame. All joint and muscle forces are presented as normalized to subject body weight. GH joint reaction forces calculated by the UKNSM are represented in the anatomical coordinate frame of the glenoid plane (**Error! Reference source not found.**Figure 7.7; Lee & Lee, 2010). The GH joint reaction force components are presented as: (+) compression force, (+) posterior / (-) anterior shear (A/P shear), and (+) superior / (-) inferior shear (S/I shsear) (Figure 7.7). The UKNSM constrains the glenoid contact pattern and resultant force vector to be within the glenoid rim, to avoid dislocation. Upper muscle force bounds were set to 10 times the default model value to remove the occurance of model non-convergence for any motion frames. This follows the approach implemented for other fast or heavily loaded, athletic activities (Urbanczyk *et al.*, 2020; Prinold, 2012; Persad, 2016).

Statistical significance was set at $p < 0.05$ and appropriate statistical analyses were conducted using R packages in RStudio 3.6 (RStudio Team, 2016) and JMP Pro 14 (SAS Institute, NC, USA). Statistical parametric mapping toolboxes (spm1d; Pataky, 2016) were used to determine significant differences between the athlete cohorts and across stroke rates in MATLAB 2017B (MathWorks, MA, USA). Each stroke rate and percentage of stroke completion (0 - 100%) was defined as the within subject factors and dependent variables included joint forces and muscle forces. Scalar values of force minima and maxima were compared by repeated measures ANOVA with Tukey HSD post-hoc tests used to perform pair-wise comparisons. Fréchet distance was used to measure the similarity between glenoid contact pattern paths (Eiter & Mannila, 1994; Mechmeche *et al.*, 2016).

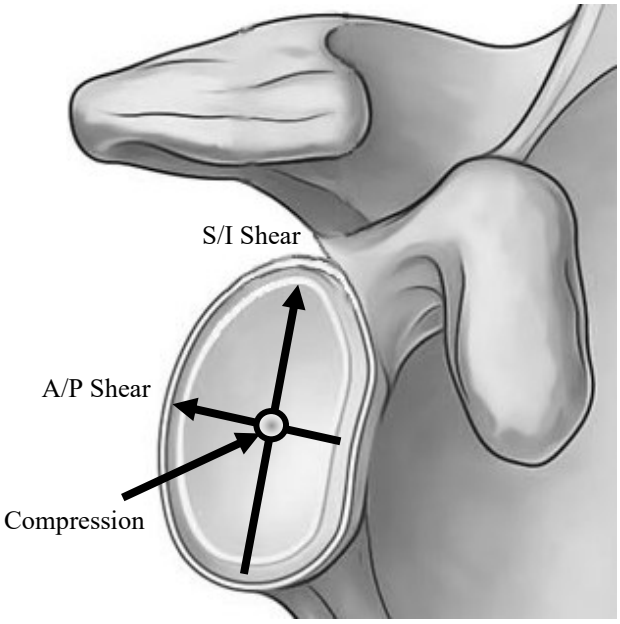

Figure 7.7: Local glenohumeral joint coordinate system for glenoid fossa contact pattern and joint reaction forces, superimposed onto an antero-medial orthoganal view of the scapula. Arrows indicate positive force directionality: (+) compression / (-) distraction; (+) posterior / (-) anterior (A/P); (+) superior / (-) inferior (S/I).

7.4 RESULTS

Population-wide group averages allow us to look for global trends in joint and muscle mechanics across entire athlete populations. All joint and muscle force results are presented as normalized to athlete body weight. Additional results can be found in Appendix D: Supplemental Biomechanics Results.

Distributed joint reaction forces indicate the level of loading sustained during a motion. Population-wide joint forces across all stroke rates reached a maximum near MHF with peak resultant elbow joint reaction forces ranging from 2.84 ± 0.70 times body weight (xBW) at 18 spm to 2.99 ± 0.67 xBW at 28 spm (Figure 7.8; Table 7.3). Peak GH joint compression forces also coincided closely with MHF, but joint force magnitudes ranged from 5.60 ± 1.40 xBW at 18 spm to 5.86 ± 1.39 xBW at 28 spm (Figure 7.9). Peak GH compression was 3.34 times greater and 4.74 times greater than either A/P shear or S/I shear force components, respectively (Table 7.3). Compared to each other, the average ratio of A/P shear to S/I shear across all stroke rates was 1.41. No statistically significant differences in maximum force were observed as stroke rate increased for elbow resultant joint force ($p = 0.43$; Figure 7.8), GH joint compression ($p = 0.44$) GH joint A/P shear force ($p = 0.46$), GH joint S/I shear force ($p = 0.49$; Figure 7.9).

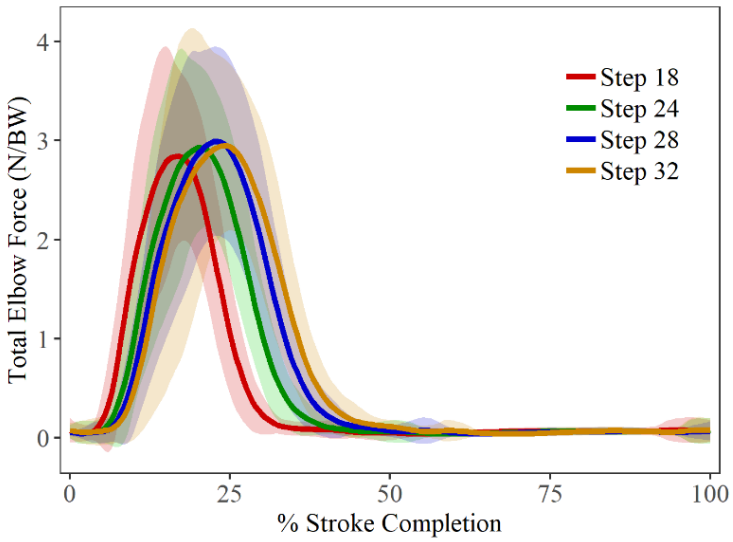

Figure 7.8: Population-wide resultant total elbow joint force (mean ± std) at all stroke rates. No statistical differences in force magnitudes.

Table 7.3: Maximum values (mean ± std) of glenohumeral (GH) joint compression, anterior-posterior (A/P) shear superior-inferior (S/I) shear, and total elbow (ELB) joint force, in N/BW; shoulder stability ratio (SSR) and total glenoid contact pattern path length (mm) at all stroke rates across entire athlete population.

		18 spm	24 spm	28 spm	32 spm
GH	Compression	5.60 ± 1.40	5.84 ± 1.34	5.86 ± 1.39	5.74 ± 1.67
	S/I Shear	1.19 ± 0.40	1.21 ± 0.41	1.21 ± 0.38	1.25 ± 0.35
	A/P Shear	-1.68 ± 1.00	-1.75 ± 0.97	-1.75 ± 1.02	-1.71 ± 0.93
	SSR	0.51 ± 0.23	0.51 ± 0.22	0.52 ± 0.21	0.53 ± 0.21
	Glenoid Path Length	81.2 ± 2.40	80.3 ± 2.41	76.2 ± 2.42	76.1 ± 2.50
ELB	Total Force	2.84 ± 0.69	2.93 ± 0.66	2.99 ± 0.67	2.95 ± 0.76

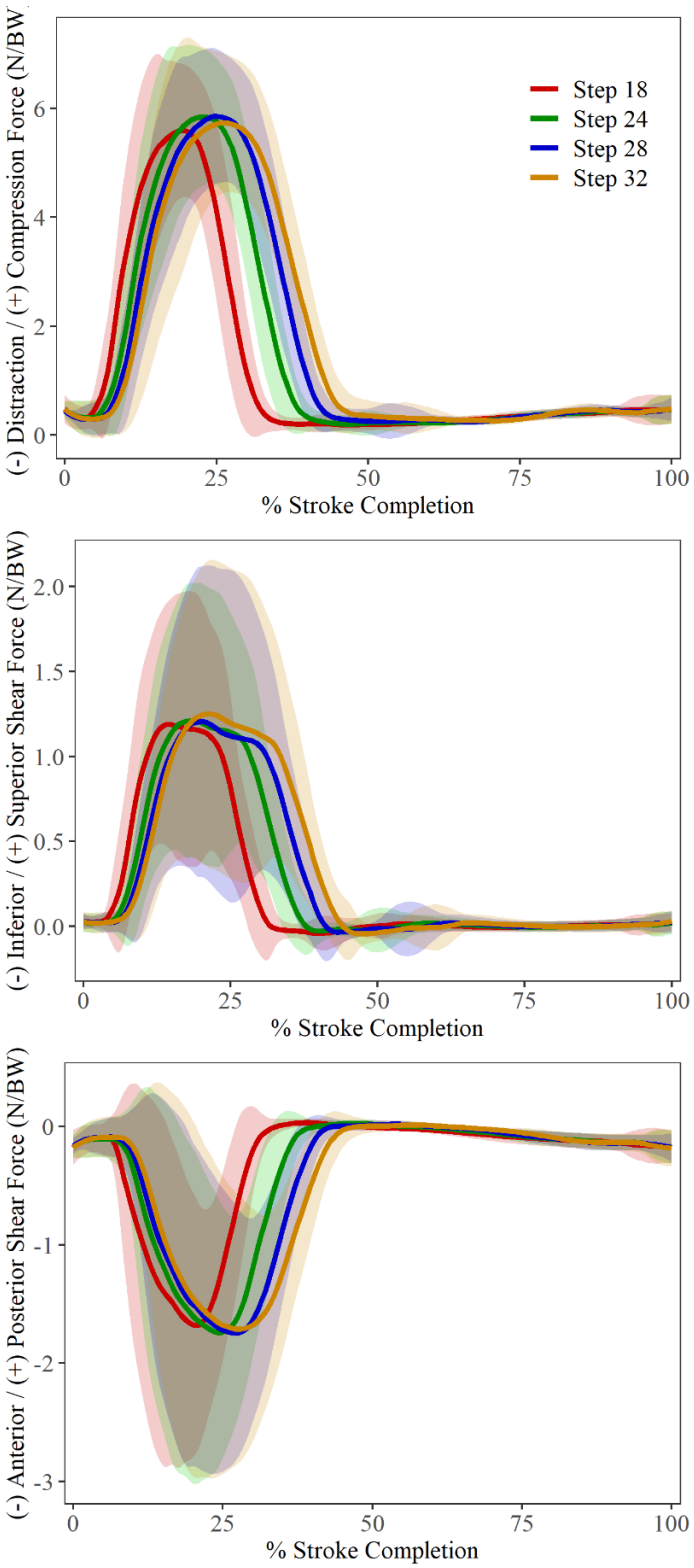

Figure 7.9: Population-wide glenohumeral joint force components (mean ± std) for humeral head (+) compression (*top*), (+) superior / (-) inferior shear (*middle*) and (+) posterior / (-) anterior shear (*bottom*), across all stroke rates. No statistical differences in force magnitudes.

In addition to the magnitude of the GH joint reaction force, an important factor in assessing positions of GH joint instability was the location of this force on the glenoid. The glenoid surface can be divided into 4 quadrants, surrounded by the glenoid rim. A contact pattern that passes close to the glenoid rim indicates an increasingly unstable position. The location of GH contact force vectors being applied by the humeral head against the glenoid fossa, throughout the rowing stroke are presented in Figure 7.10. Following the mean contact pattern through the stroke, the center of pressure moves posteriorly from the catch during early drive, then translates superiorly through late drive into the finish. Center of pressure was predominately constrained to the posterior half of the glenoid socket and does not pass close to the glenoid rim. As stroke rate increased, contact patterns showed a decreasing total path length (Table 7.3), but this was not statistically significant ($p = 0.290$). Fréchet distance was calculated between average contact patterns for each cohort and stroke rate and used to compare contact pattern similarity. The largest Fréchet distance occurred between 18 spm and 32 spm (3.91 mm) and the smallest distance between 28 spm and 32 spm (0.71 mm).

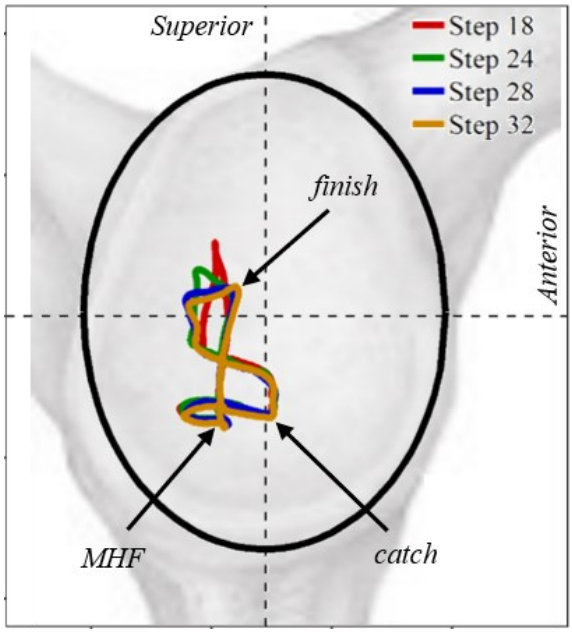

Figure 7.10: Population-wide glenoid contact patterns across all stroke rates (mean paths), with arrows indicating the instantaneous force locus at the catch, max handle force (MHF), and the finish. Glenoid rim indicated as black ellipse.

Combining information from the glenoid contact pattern and GH joint forces, SSR was calculated as the ratio of shear to compressive force acting at the GH joint and this metric is sometimes used by clinicians to describe potential shoulder pathology risk. Across all stroke rates, population wide average SSR varies between a low of 0.20 ± 0.19 and a high of 0.53 ± 0.21 (Table 7.3), with the widest range at 32 spm and smallest at 18 spm. The higher the SSR, the higher the relative effect of shear force, and so is most unstable. SSR patterns throughout the stroke cycle differed significantly among all the stroke rates ($p<0.001$). The GH joint was least stable during the drive phase and most stable near the finish position, with a steady increase in SSR throughout the recovery phase (Figure 7.11).

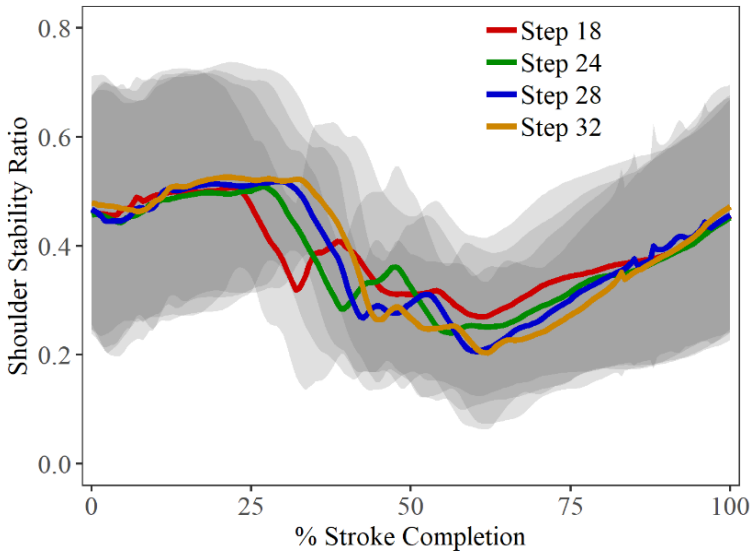

Figure 7.11: Population-wide glenohumeral joint shoulder stability ratio (mean ± std), across all stroke rates, where a higher ratio reflects increasing instability.

Mechanical loading in the early drive phase involves the isometric firing of the trunk muscles. Those muscles most active before MHF were pectoralis major, trapezius, deltoid, and brachialis (Table 7.4). Maximum force in several muscles in each muscle group coincided with MHF, including prime movers - latissimus dorsi and teres major, scapula stabilizers - serratus anterior and rhomboid major, and arm accessory muscles - biceps and triceps brachii (Table 7.4). Subscapularis, which reaches maximal force during the late drive supports acceleration into and out of the finish position (Table 7.4). The only muscle that attains maximal force during the recovery was infraspinatus (Table 7.4), when the arm was in full forward extension and lifting into the catch.

Table 7.4: Population-wide relative maximum force timing as a % of stroke completion for largest 12 force contributors as defined by maximum force generation. Percent of stroke completion is given to reach max handle force (MHF) and the finish for comparison. Green highlights muscles that reach max force prior to MHF. Yellow indicates max force at or near MHF. Red indicates max force in late-drive or the recovery phase.

Stroke Rate	18 spm	24 spm	28 spm	32 spm
MHF	**18.0**	**21.5**	**24.0**	**25.5**
FINISH	**35.5**	**41.5**	**45.0**	**48.0**
Trapezius	14.0	17.5	19.5	20.5
Deltoid	15.5	19.5	22.0	23.0
Brachialis	15.5	19.0	21.5	23.0
Pectoralis Major	16.0	19.5	22.0	23.5
Biceps Brachii	18.0	21.5	24.5	25.5
Triceps Brachii	18.0	21.5	24.0	25.0
Teres Major	18.5	22.0	24.5	25.5
Latissimus Dorsi	18.5	22.0	24.5	25.0
Serratus Anterior	18.5	22.0	24.0	25.5
Rhomboid Major	18.5	21.5	23.0	24.5
Subscapularis	23.5	28.0	31.0	33.5
Infraspinatus	91.0	89.5	88.0	86.0

Mean muscle force and standard deviation are presented for prime movers, scapula stabilizers, rotator cuff, and arm accessory muscles, which have a peak force output of greater than one xBW (Figure 7.12). No statistically significant difference in maximal muscle force output was found with respect to increasing stroke rate (*all p-values > 0.56*; Table 7.5). The largest contributing muscles are, as might be expected, the prime movers. The muscles, latissimus dorsi, teres major, and pectoralis major all work to maintain momentum for the upper body through abduction, extension, and internal rotation of the humerus at the shoulder joint (Chapter 6; Section 6.3.1.1). Averaging across all stroke rates, the highest body weight normalized force outputs were generated by teres major (2.44 ± 0.64 xBW), pectoralis major (1.78 ± 0.52 xBW), and latissimus dorsi (1.42 ± 0.36 xBW) (Figure 7.12). The most active scapula stabilizer was serratus anterior, with a peak force of 1.59 ± 0.41 xBW (Figure 7.12). Triceps brachii was the most active of the arm accessory muscles, generating a peak force of 1.43 ± 0.39 xBW (Figure 7.12). Most active during the middle of the drive, triceps brachii keeps the elbow joint extended, acting as an antagonist to biceps and brachialis, to facilitate efficient load transfer along the upper extremity. As a group, the rotator cuff muscles

stabilize the GH joint. Specifically, late in the drive phase, it was subscapularis that contracts most strongly (2.03 ± 0.49 xBW) (Figure 7.12; Table 7.5).

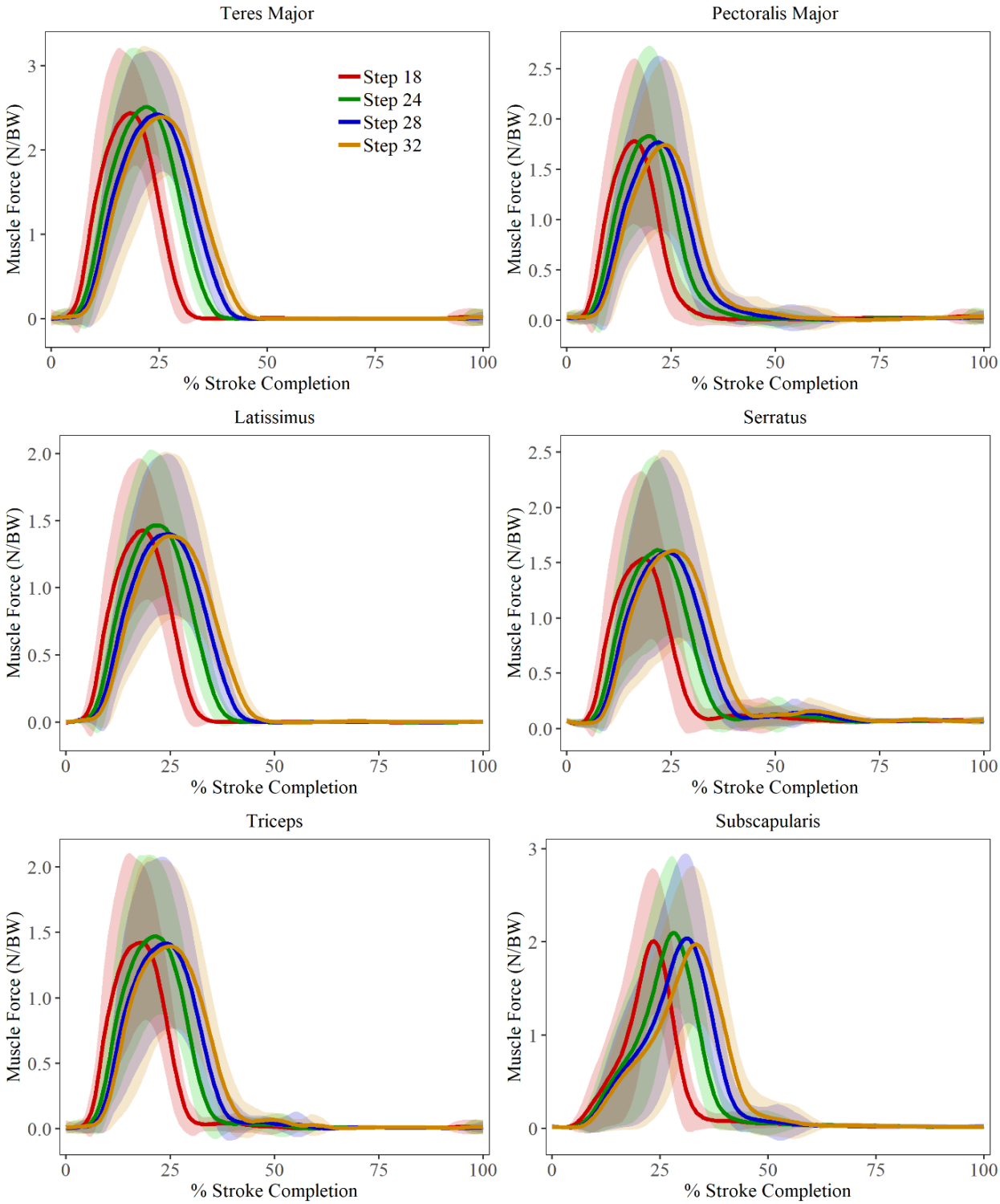

Figure 7.12: Population-wide body weight normalized muscle forces (mean ± std) at the glenohumeral joint for six largest contributing muscles across all stroke rates.

Aside from the major force contributing muscles discussed above and shown in Figure 7.12, two additional muscles were noteworthy for their distinct force patterns. Deltoid and infraspinatus were the only two muscles recorded that show a steadily increasing force throughout the recovery phase (Figure 7.13). While the total force output was small compared to other muscles during the drive phase, infraspinatus reaches a max force of 0.14 ± 0.04 xBW, and deltoid attains a force output of 0.29 ± 0.12 xBW in the final 10-15% of stroke completion (Table 7.5). Given functional anatomy, anterior deltoid can assist pectoralis major in flexing the arm, and at the end of the recovery, with the shoulder fully flexed and adducted, this would suggest that anterior deltoid was elevating the handle into the catch. Both deltoid and infraspinatus stabilize the GH joint, with lateral deltoid impeding inferior humeral head displacement and infraspinatus preventing anterior displacement.

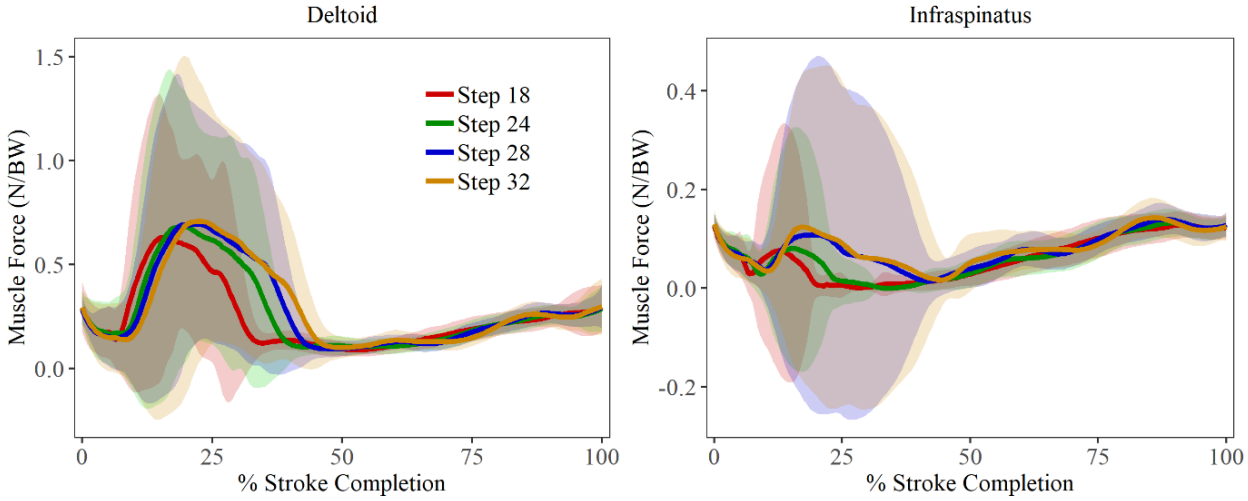

Figure 7.13: Population-wide body weight normalized muscle forces (mean ± std) at the glenohumeral joint for muscles active during the recovery phase, across all stroke rates.

Table 7.5: Population-wide maximum body weight normalized muscle force (mean ± std) in N/BW of various muscles at all stroke rates. No statistical interaction was found with respect to stroke rate.

	18 spm	24 spm	28 spm	32 spm
Teres Major	2.44 ± 0.61	2.51 ± 0.64	2.42 ± 0.63	2.39 ± 0.70
Latissimus	1.43 ± 0.39	1.47 ± 0.38	1.40 ± 0.35	1.39 ± 0.32
Pectoralis Major	1.78 ± 0.56	1.83 ± 0.54	1.77 ± 0.51	1.74 ± 0.46
Deltoid	0.63 ± 0.16	0.68 ± 0.26	0.69 ± 0.34	0.71 ± 0.34
Trapezius	0.79 ± 0.23	0.79 ± 0.21	0.80 ± 0.19	0.80 ± 0.16
Rhomboid Major	0.50 ± 0.14	0.51 ± 0.14	0.50 ± 0.13	0.47 ± 0.11
Serratus Anterior	1.54 ± 0.44	1.62 ± 0.43	1.59 ± 0.39	1.61 ± 0.39
Levator Scapulae	0.26 ± 0.09	0.26 ± 0.10	0.25 ± 0.10	0.24 ± 0.10
Subscapularis	2.01 ± 0.40	2.10 ± 0.49	2.04 ± 0.53	1.97 ± 0.56
Infraspinatus	0.13 ± 0.02	0.13 ± 0.02	0.14 ± 0.04	0.14 ± 0.10
Supraspinatus	0.37 ± 0.42	0.38 ± 0.40	0.37 ± 0.34	0.42 ± 0.45
Triceps Brachii	1.42 ± 0.45	1.47 ± 0.34	1.42 ± 0.37	1.40 ± 0.40
Coracobrachialis	0.13 ± 0.14	0.14 ± 0.14	0.14 ± 0.15	0.14 ± 0.14
Biceps Brachii	0.72 ± 0.29	0.76 ± 0.25	0.84 ± 0.25	0.78 ± 0.23
Brachialis	0.72 ± 0.24	0.72 ± 0.24	0.77 ± 0.23	0.78 ± 0.30

7.5 Evaluating Demographic Differences in Rowing Biomechanics

7.5.1 Sex Differences in Rowing Biomechanics

It is well documented that men have faster race times than women across weight classes (Keenan, Senefeld & Hunter, 2018). This has largely been attributed to greater height and mass of male rowers. When comparing body weight normalized joint reaction forces between male and female cohorts, across all stroke rates, males display greater maximum compression force ($p = 0.013$) and a greater absolute value of maximum A/P shear force ($p = 0.004$) than females. However, no significant differences were found in maximum S/I shear force ($p = 0.91$) and there were no statistically significant interactions between sex and stroke rate (Figure 7.14; Table 7.6) The average ratio of peak A/P shear force to peak S/I shear force across all stroke rates was 1.68 ± 0.06 for males and 1.15 ± 0.03 for females. Maximum total joint force at the elbow did not show statistically significant differences between males and females at any stroke rates ($p = 0.521$; Table 7.6).

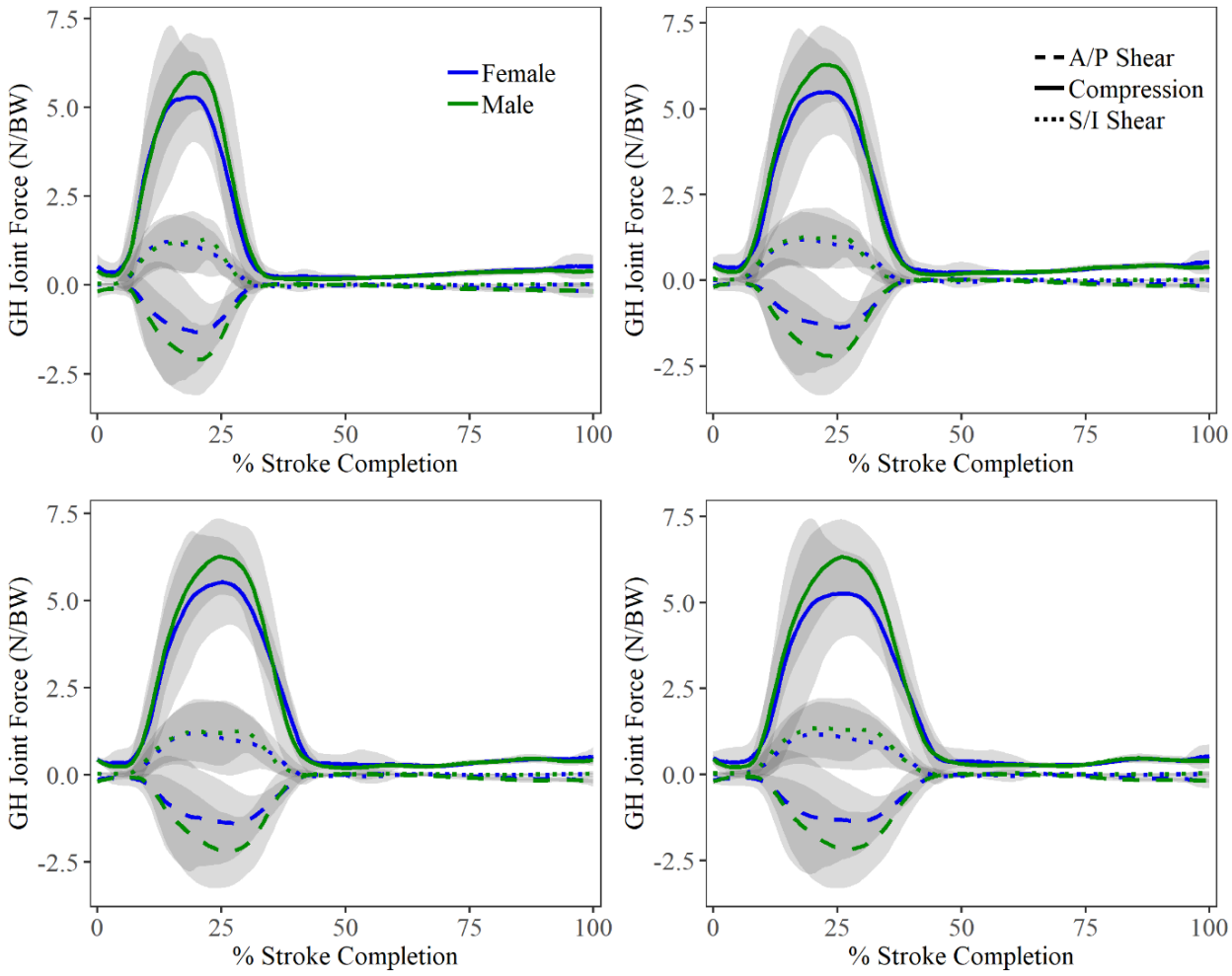

Figure 7.14: Male versus female glenohumeral (GH) joint force components (mean ± std), (+) compression, (+) superior shear (S/I) and (+) posterior shear (A/P). Stroke rate trials: 18 spm (*top left*), 24 spm (*top right*), 28 spm (*bottom left*), 32 spm (*bottom right*).

Table 7.6: Maximum values (mean ± std) of glenohumeral (GH) joint compression, anterior-posterior (A/P) shear superior-inferior (S/I) shear, and total elbow (ELB) joint force, in N/BW; shoulder stability ratio (SSR) and total glenoid contact pattern path length (mm) at all stroke rates for male and female rowers.

			18 spm	24 spm	28 spm	32 spm
GH	Compression	Female	5.29 ± 1.40	5.48 ± 1.51	5.52 ± 1.51	5.25 ± 2.01
		Male	5.97 ± 1.44	6.28 ± 1.39	6.26 ± 1.29	6.32 ± 1.18
	S/I Shear	Female	1.22 ± 0.34	1.18 ± 0.33	1.18 ± 0.36	1.17 ± 0.37
		Male	1.29 ± 0.59	1.26 ± 0.64	1.25 ± 0.60	1.35 ± 0.34
	A/P Shear	Female	-1.33 ± 1.06	-1.37 ± 1.20	-1.39 ± 1.18	-1.35 ± 1.39
		Male	-2.10 ± 0.94	-2.20 ± 0.85	-2.17 ± 0.81	-2.17 ± 0.57
	Shoulder Stability	Female	0.46 ± 0.22	0.48 ± 0.21	0.49 ± 0.21	0.50 ± 0.20
		Male	0.57 ± 0.21	0.56 ± 0.24	0.56 ± 0.22	0.58 ± 0.23
	Glenoid Path Length	Female	82.2 ± 3.28	78.9 ± 3.28	74.5 ± 3.28	75.7 ± 3.37
		Male	80.0 ± 3.57	81.9 ± 3.57	78.2 ± 3.57	76.6 ± 3.57
ELB	Total Force	Female	2.88 ± 0.52	2.88 ± 0.63	3.04 ± 0.77	2.98 ± 0.87
		Male	2.83 ± 0.85	2.98 ± 0.77	2.95 ± 0.68	2.89 ± 0.59

Across all stroke rates, males displayed higher average SSRs ($p = 0.003$) than females throughout the stroke cycle, with the largest differences in SSR occurring during the early-drive phase. At the catch specifically, SSR was higher among men (0.56 ± 0.22) than among women (0.39 ± 0.19; $p < 0.001$). At MHF males achieved a maximum SSR of 0.57 ± 0.22 and females reached a maximum SSR of 0.48 ± 0.21, which were also statistically different ($p = 0.012$; Table 7.6). Figure 7.15 also shows a rise in stability ratio for both cohorts through the last 30% of the recovery phase.

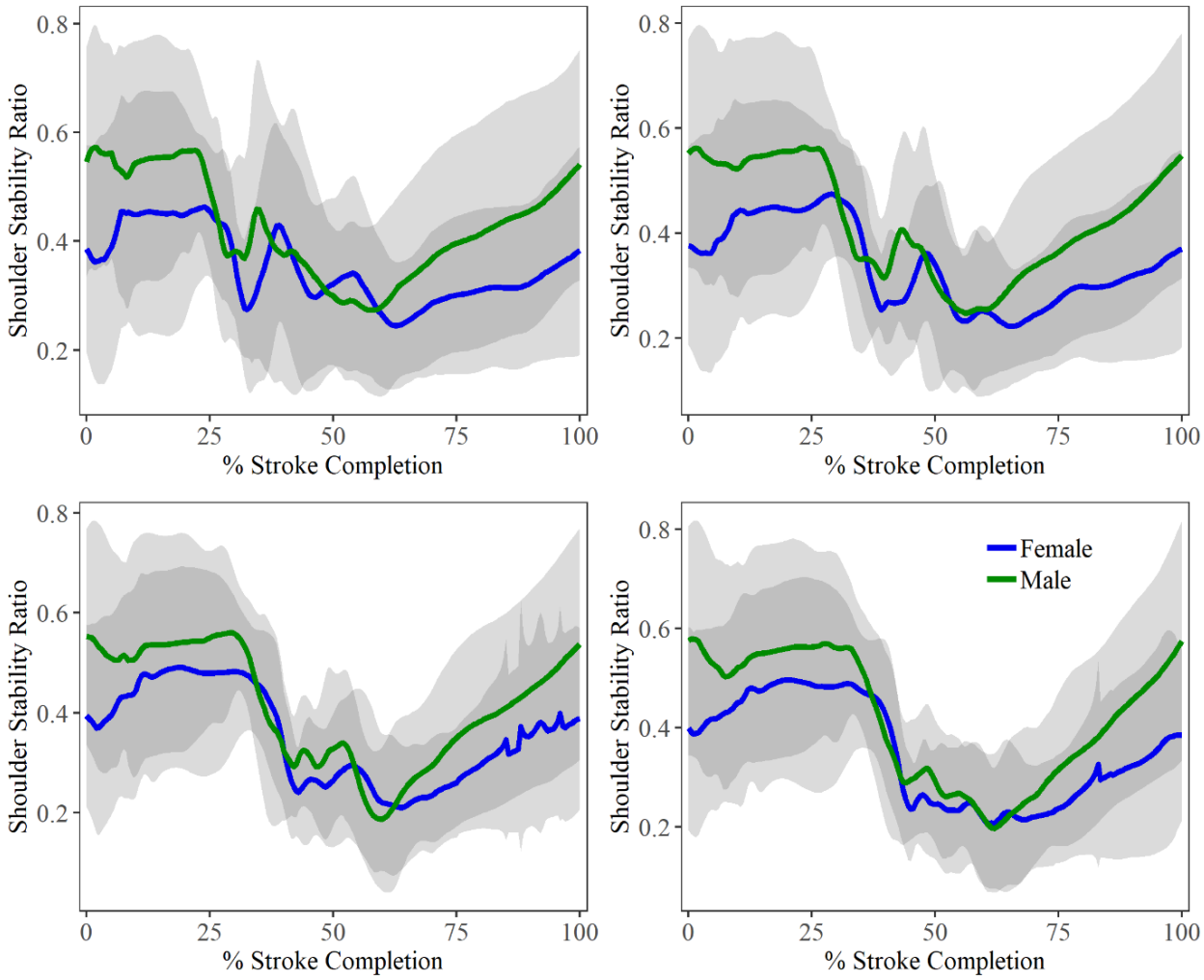

Figure 7.15: Male versus female shoulder stability ratio (mean ± std). Stroke rate trials: 18 spm (*top left*), 24 spm (*top right*), 28 spm (*bottom left*), 32 spm (*bottom right*).

Figure 7.16 shows the glenoid joint force locus for males and females at the lowest stroke rate, 18 spm (*left*) and the highest stroke rate, 32 spm (*right*). Key moments in the rowing stroke are highlighted, including the catch, MHF, and the finish. Male glenoid contact patterns tended to be more inferior than females, particularly at the catch. Center of pressure was mostly constrained to the posterior half of the glenoid socket and does not pass close to the glenoid rim (Figure 7.16). Across all stroke rate increases, glenoid contact patterns show similar total path length between males and females ($p = 0.576$). Fréchet distances calculated between average male and female contact patterns were similar for all stroke rates, ranging from 3.69 mm (*28 spm*) to 3.94 mm (*24 spm*), with the largest spatial location difference occurring at the catch (Figure 7.16).

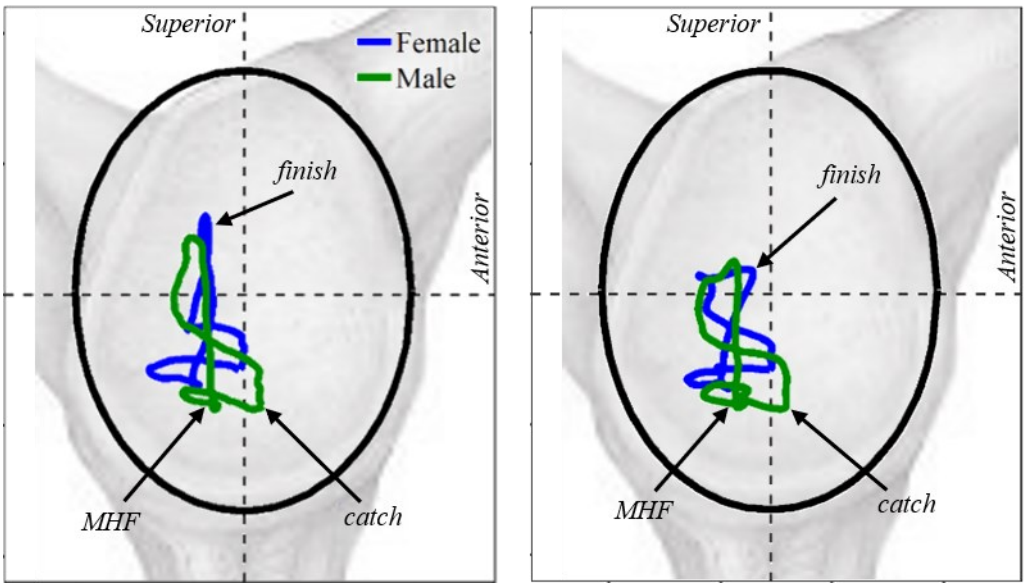

Figure 7.16: Male versus female glenoid contact patterns (mean paths), at 18 spm (*left*) and 32 spm (*right*) overlaid on a medial view of the scapula. Arrows indicate instantaneous force locus at the catch, max handle force (MHF), and the finish. Black ellipse indicates glenoid rim.

Mean force and standard deviation are presented for muscles showing statistically significant differences between male and female athlete cohorts (Figure 7.17; Figure 7.18). Examining average muscle force patterns, males appear to generate force primarily through the prime shoulder movers and select scapula stabilizers, prioritizing the larger back muscles important in humeral extension and internal rotation (i.e., latissimus dorsi, teres major). Averaging across all stroke rates, males generated higher maximum muscle force than females in teres major ($p = 0.028$), latissimus dorsi ($p = 0.0008$), and serratus anterior ($p = 0.007$; Figure 7.17; Table 7.7). Males also displayed higher force output than females among the rotator cuff muscles, subscapularis ($p < 0.0001$) and supraspinatus ($p = 0.016$; Table 7.7).

However, women appear to have a wider, more even distribution of mean and maximal muscle force output. Females displayed higher maximum muscle force than males in pectoralis major (Figure 7.17) and trapezius ($p = 0.009$; Table 7.7). Females also appeared to prioritize recruitment of arm accessory muscles for shoulder extension and abduction (Figure 7.18), with higher maximum muscles forces than males in biceps brachii, brachialis, and coracobrachialis (Figure 7.18); however, these trends were not statistically significant ($p > 0.14$; Table 7.7).

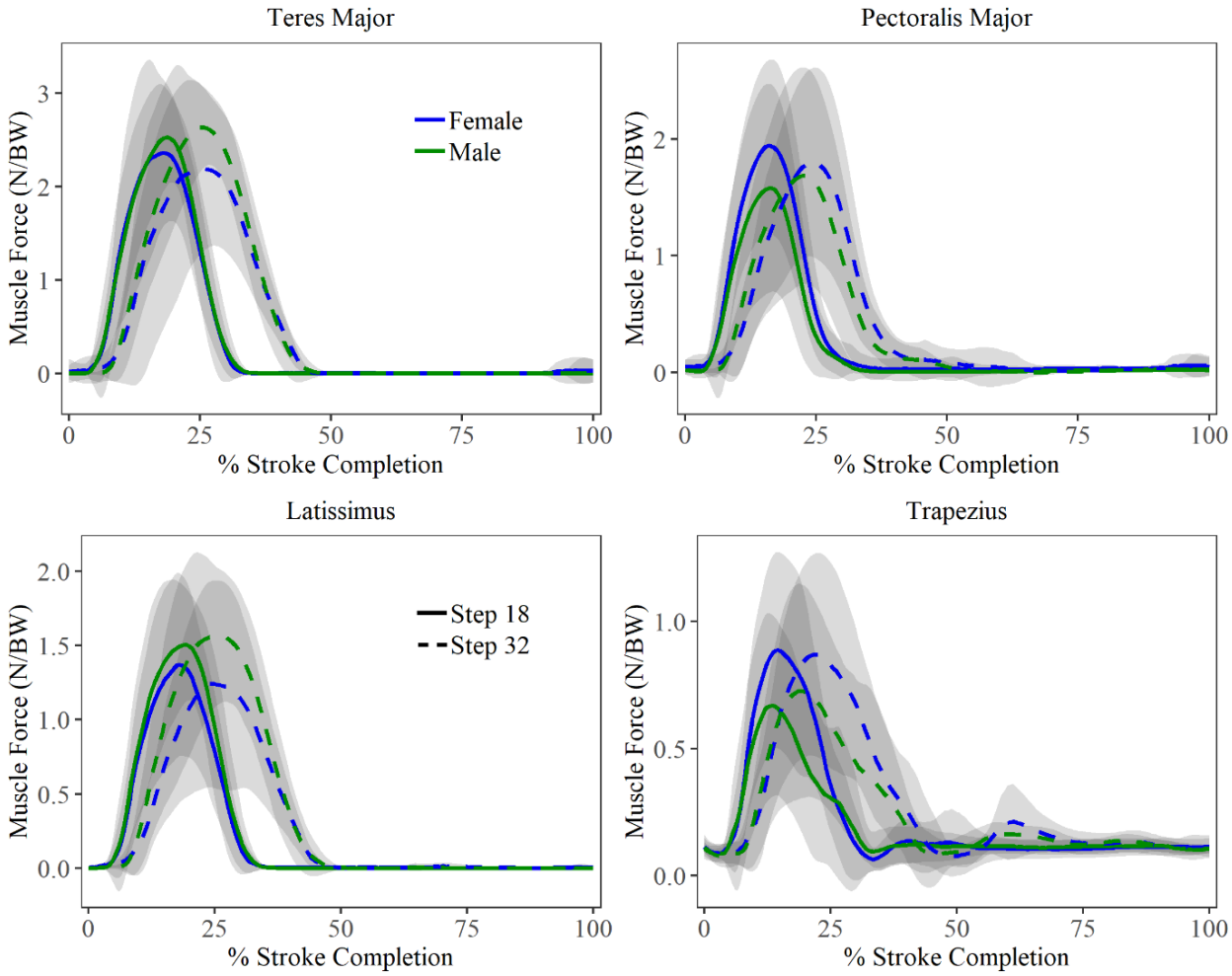

Figure 7.17: Male versus female body weight normalized muscle forces (mean ± std) in N/BW generated by prime movers and scapula stabilizer muscles. Stroke rate trials: 18 spm (*solid lines*), 32 spm (*dashed lines*).

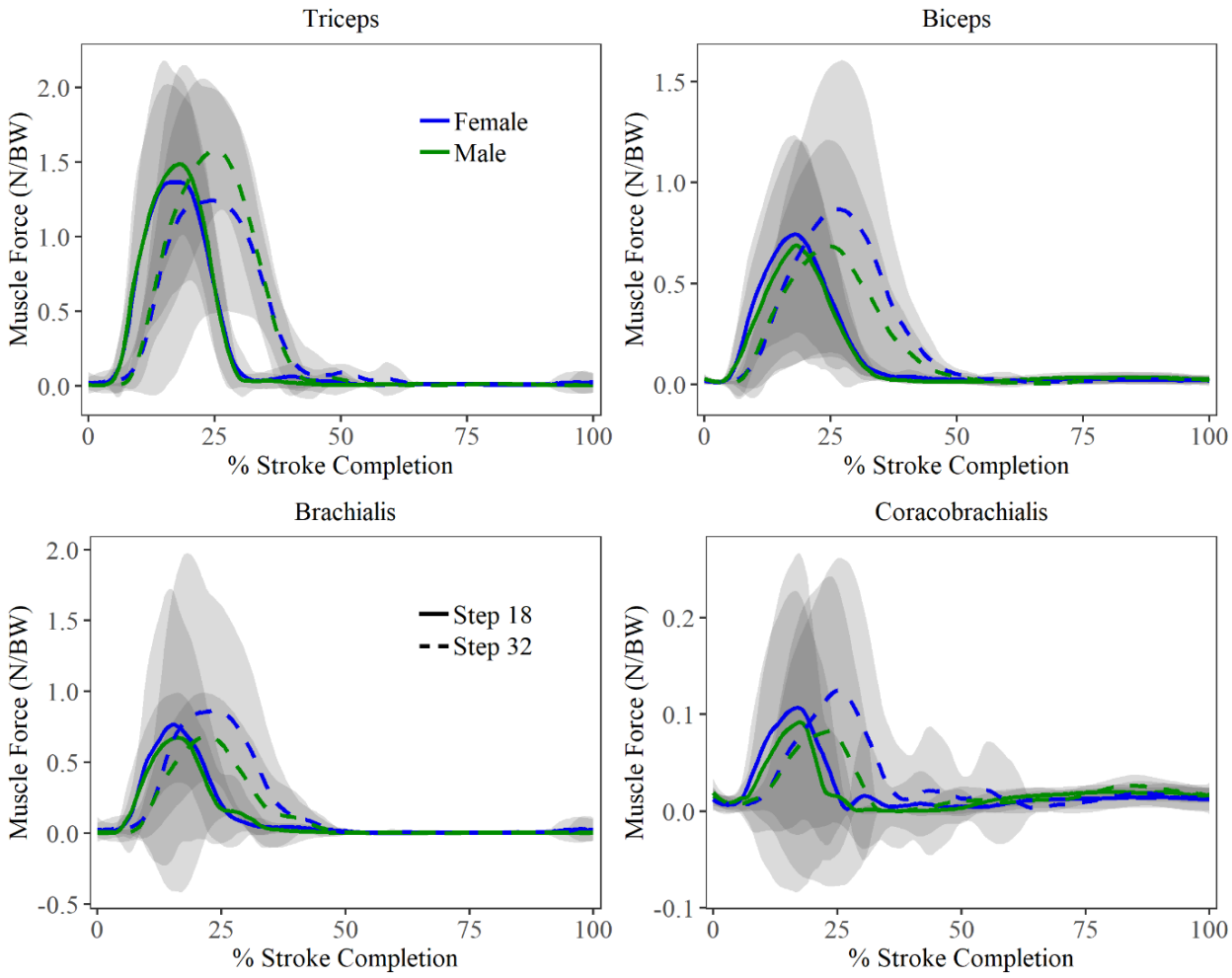

Figure 7.18: Male versus female body weight normalized muscle forces (mean ± std) in N/BW generated by arm accessory muscles. Stroke rate trials: 18 spm (*solid lines*), 32 spm (*dashed lines*).

Table 7.7: Maximum body weight normalized muscle force (mean ± std) in N/BW of various muscles at all stroke rates, for male and female cohorts.

		18 spm	24 spm	28 spm	32 spm
Teres Major	Female	2.36 ± 0.51	2.39 ± 0.56	2.25 ± 0.74	2.19 ± 0.79
	Male	2.53 ± 0.75	2.66 ± 0.71	2.64 ± 0.62	2.63 ± 0.58
Latissimus	Female	1.37 ± 0.34	1.37 ± 0.26	1.27 ± 0.30	1.24 ± 0.24
	Male	1.51 ± 0.49	1.59 ± 0.47	1.56 ± 0.41	1.56 ± 0.41
Serratus	Female	1.42 ± 0.34	1.47 ± 0.29	1.42 ± 0.28	1.39 ± 0.34
	Male	1.69 ± 0.53	1.79 ± 0.50	1.80 ± 0.43	1.88 ± 0.43
Pectoralis Major	Female	1.95 ± 0.50	2.00 ± 0.47	1.85 ± 0.41	1.80 ± 0.35
	Male	1.58 ± 0.64	1.66 ± 0.64	1.69 ± 0.58	1.69 ± 0.51
Trapezius	Female	0.89 ± 0.18	0.90 ± 0.20	0.91 ± 0.21	0.87 ± 0.20
	Male	0.67 ± 0.24	0.69 ± 0.21	0.67 ± 0.18	0.73 ± 0.13
Biceps Brachii	Female	0.74 ± 0.31	0.80 ± 0.27	0.93 ± 0.29	0.87 ± 0.23
	Male	0.69 ± 0.27	0.73 ± 0.26	0.73 ± 0.25	0.68 ± 0.25
Brachialis	Female	0.77 ± 0.19	0.72 ± 0.21	0.84 ± 0.28	0.87 ± 0.36
	Male	0.68 ± 0.30	0.72 ± 0.28	0.70 ± 0.21	0.69 ± 0.19
Coracobrachialis	Female	0.11 ± 0.06	0.12 ± 0.04	0.12 ± 0.04	0.12 ± 0.03
	Male	0.09 ± 0.05	0.10 ± 0.04	0.10 ± 0.03	0.08 ± 0.04
Subscapularis	Female	1.68 ± 0.39	1.78 ± 0.50	1.66 ± 0.53	1.63 ± 0.58
	Male	2.43 ± 0.42	2.55 ± 0.47	2.54 ± 0.51	2.43 ± 0.52
Supraspinatus	Female	0.13 ± 0.04	0.16 ± 0.09	0.14 ± 0.08	0.19 ± 0.06
	Male	0.35 ± 0.27	0.35 ± 0.27	0.35 ± 0.33	0.33 ± 0.40

7.5.2 Age & Competition Level Differences in Rowing Biomechanics

In the literature, both sexes have faster race times across years of competition (Keenan, Senefeld & Hunter, 2018) and kinematic and electromyography studies comparing rowers with varying levels of experience, reinforce that more practice improves performance (Smith & Spinks, 1995). However, age-related decline in skeletal muscle mass and aerobic fitness (Arumugam *et al.*, 2020) manifest in biomechanical changes in ergometer rowing. Comparing body weight normalized GH joint forces among university, club, elite, and masters cohorts, several differences were noted across all stroke rates. There were statistically significant differences in maximum GH joint compression force ($p = 0.0245$) and in

maximum absolute A/P shear force ($p = 0.001$) across all four athlete cohorts (Figure 7.19). Masters rowers displayed substantially lower maximum GH compression force than club ($p = 0.001$), elite ($p = 0.007$), and university athletes ($p = 0.009$; Table 7.8). Masters rowers also showed significantly lower absolute A/P shear force than club ($p = 0.001$), elite ($p = 0.033$), and university athletes ($p = 0.005$; Table 7.8). There were no significant differences in maximum GH compression or A/P shear force among the other three athlete cohorts ($p < 0.135$). There were also no statistically significant differences in S/I shear force ($p = 0.164$), with the maximum component force being similar across all groups (Figure 7.19). The average ratio of peak A/P shear to peak S/I shear across all stroke rates was 1.61 for elites, 1.56 for university rowers, 1.15 for club athletes, and 0.99 for masters rowers. Total joint force at the elbow joint did not show any statistically significant differences among the groups ($p = 0.956$).

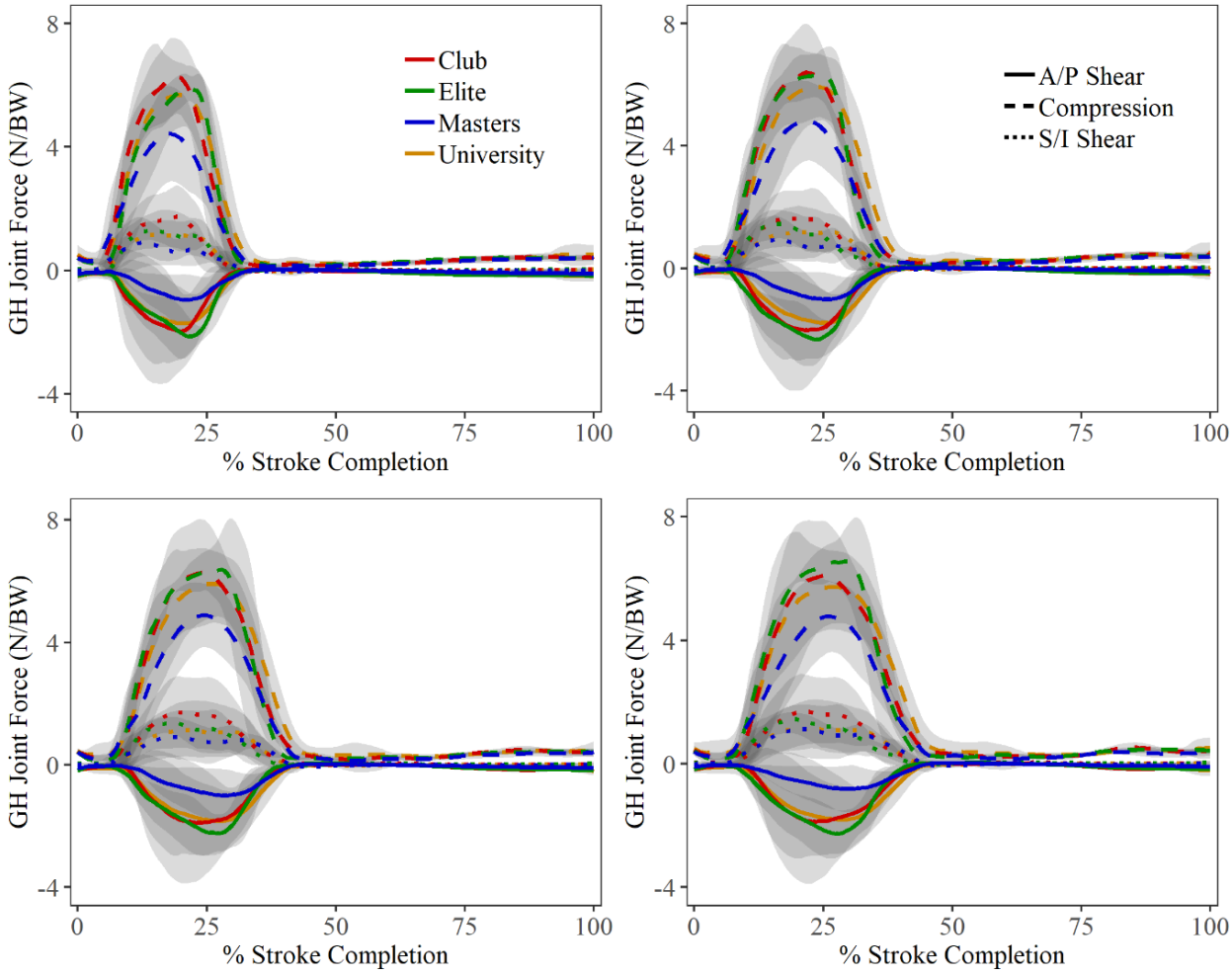

Figure 7.19: Age/ competition level cohort glenohumeral joint forces (mean ± std), (+) compression, (+) superior shear and (+) posterior shear. Stroke rate trials: 18 spm (*top left*), 24 spm (*top right*), 28 spm (*bottom left*), 32 spm (*bottom right*).

Table 7.8: Maximum values (mean ± std) of glenohumeral (GH) joint compression, anterior-posterior (A/P) shear superior-inferior (S/I) shear, and total elbow (ELB) joint force, in N/BW; shoulder stability ratio (SSR) and total glenoid contact pattern path length (mm) at all stroke rates, for each age/competition level cohort.

			18 spm	24 spm	28 spm	32 spm
GH	Compression	Club	6.29 ± 0.94	6.40 ± 0.82	6.28 ± 0.87	6.09 ± 0.94
		Elite	5.91 ± 0.26	6.32 ± 0.77	6.37 ± 0.68	6.55 ± 0.56
		Master	4.43 ± 1.76	4.82 ± 1.67	4.88 ± 1.48	4.77 ± 1.47
		University	5.69 ± 1.67	5.91 ± 1.72	5.91 ± 1.65	5.72 ± 2.16
	S/I Shear	Club	1.74 ± 0.52	1.62 ± 0.52	1.72 ± 0.33	1.69 ± 0.28
		Elite	1.29 ± 0.10	1.45 ± 0.22	1.38 ± 0.27	1.44 ± 0.24
		Master	0.90 ± 0.54	0.94 ± 0.53	0.90 ± 0.52	1.12 ± 0.53
		University	1.14 ± 0.39	1.18 ± 0.59	1.12 ± 0.36	1.13 ± 0.38
	A/P Shear	Club	-1.97 ± 1.61	-2.02 ± 0.95	-1.89 ± 0.52	-1.87 ± 0.30
		Elite	-2.13 ± 0.38	-2.32 ± 0.57	-2.23 ± 0.50	-2.27 ± 0.53
		Master	-0.96 ± 0.29	-1.01 ± 0.24	-1.00 ± 0.24	-0.82 ± 0.24
		University	-1.72 ± 1.11	-1.78 ± 1.12	-1.84 ± 1.12	-1.81 ± 1.21
	Shoulder Stability	Club	0.61 ± 0.32	0.60 ± 0.31	0.60 ± 0.29	0.60 ± 0.25
		Elite	0.58 ± 0.08	0.57 ± 0.09	0.54 ± 0.07	0.55 ± 0.08
		Master	0.62 ± 0.11	0.50 ± 0.11	0.52 ± 0.07	0.54 ± 0.09
		University	0.52 ± 0.23	0.53 ± 0.23	0.54 ± 0.21	0.55 ± 0.21
	Glenoid Path Length	Club	81.2 ± 5.7	83.9 ± 5.7	82.4 ± 5.7	78.5 ± 5.7
		Elite	75.5 ± 8.1	82.9 ± 8.1	83.8 ± 8.1	82.6 ± 8.1
		Master	85.4 ± 5.70	87.3 ± 5.70	85.3 ± 5.70	82.6 ± 6.2
		University	80.8 ± 3.1	76.8 ± 3.1	70.4 ± 3.1	72.6 ± 3.2
ELB	Total Force	Club	3.19 ± 0.72	3.27 ± 0.57	3.16 ± 0.48	3.05 ± 0.41
		Elite	3.03 ± 0.34	3.24 ± 0.66	3.19 ± 0.55	3.18 ± 0.65
		Master	2.77 ± 1.14	2.96 ± 1.14	3.02 ± 1.02	2.89 ± 0.99
		University	2.76 ± 0.49	2.81 ± 0.64	2.95 ± 0.68	2.92 ± 0.86

Across all stroke rates, club rowers displayed higher average SSRs ($p = 0.007$) throughout the stroke cycle. Maximum SSR was significantly higher for club rowers than the elites ($p = 0.003$), masters ($p = 0.023$), and university athletes ($p = 0.002$; Table 7.8). At the catch specifically, masters displayed the lowest average SSR (0.36 ± 0.11; Figure 7.20), which was significantly lower than club (0.56 ± 0.27; $p = 0.001$), elite (0.52 ± 0.15; $p = 0.009$), and university (0.49 ± 0.23; $p = 0.003$). However, at the finish, average SSR was significantly increased among masters athletes (0.44 ± 0.19), in contrast to club (0.29 ± 0.16; $p = 0.022$), elite (0.26 ± 0.14; $p = 0.001$), and university (0.29 ± 0.13; $p = 0.024$) rowers, all of whom showed decreases in SSR at the finish position (Figure 7.20). Functionally this implies that masters rowers have the greatest shoulder instability through the deceleration into and acceleration out of, the finish but were most stable throughout the rest of the stroke.

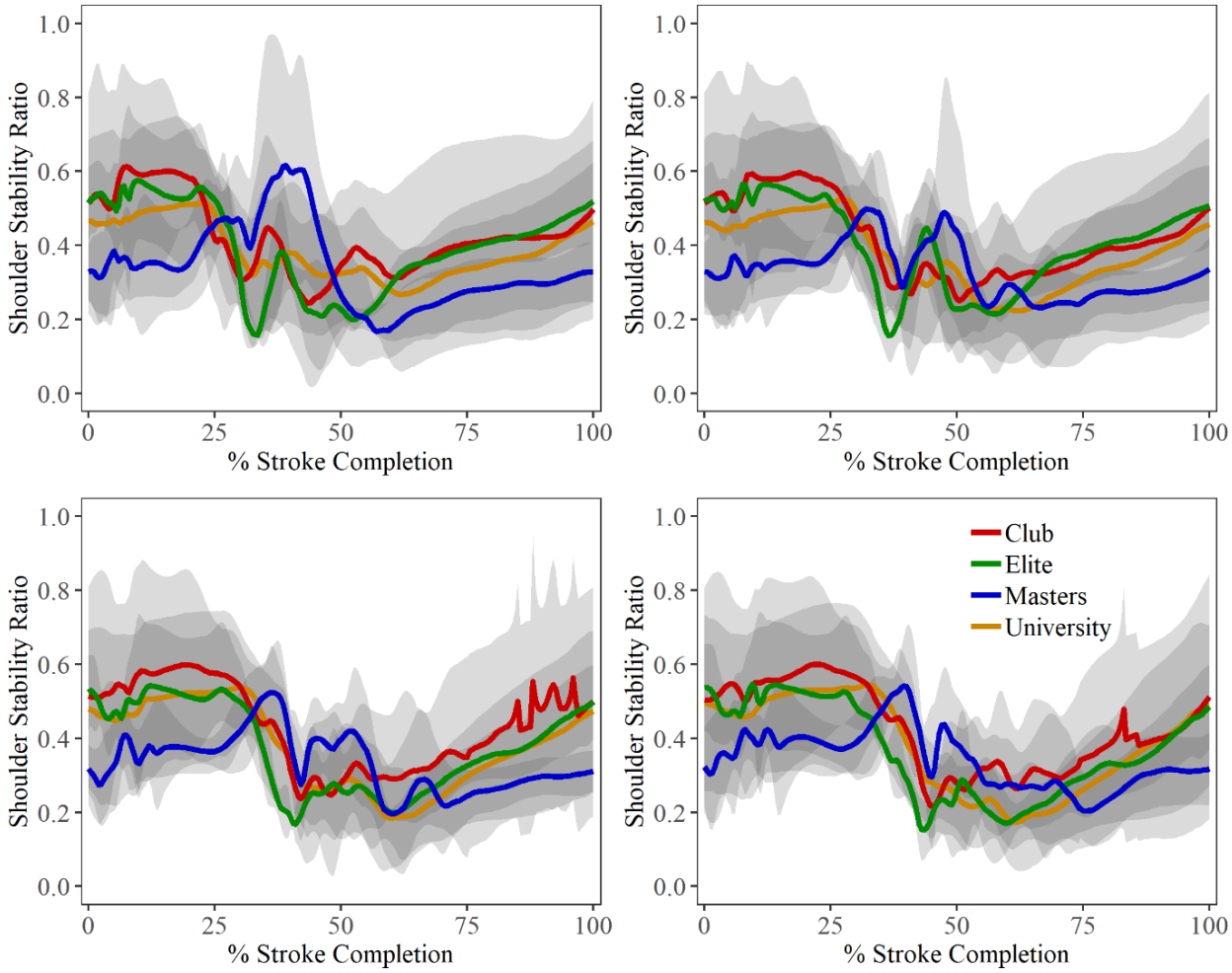

Figure 7.20: Shoulder stability ratio (mean ± std) for age/competition level cohorts. Stroke rate trials: 18 spm (*top left*), 24 spm (*top right*), 28 spm (*bottom left*), 32 spm (*bottom right*).

Figure 7.21 shows the average glenoid contact pattern for each of the age/competition level cohorts at the lowest (*left*) and highest (*right*) stroke rates tested. Glenoid contact patterns of masters rowers were positioned more superior at the catch and MHF than the other athlete cohorts and appeared to have the sharpest S/I direction change at the finish. Center of pressure was mostly constrained to the posterior half of the glenoid socket and does not pass close to the glenoid rim (Figure 7.21). Across all rates, glenoid contact patterns in masters rowers showed the longest total path length (Table 7.8); however, the difference in total path length was only significant between masters and university athletes ($p = 0.003$). Fréchet distances between average contact patterns calculated at each stroke rate were largest between masters and elite rowers at 24 spm (6.79 mm) and smallest between club and university rowers at 18 spm (2.95 mm). When averaged across all stroke rates, this trend remained, with masters rowers having larger Fréchet distances to elite (6.05 ± 0.45 mm), university (5.61 ± 0.41 mm), and club athletes (5.27 ± 0.41 mm) than the other three cohorts had among each other (club/elite: 4.71 ± 0.56 mm; club/university: 3.39 ± 0.30 mm; elite/university: 3.77 ± 0.86 mm).

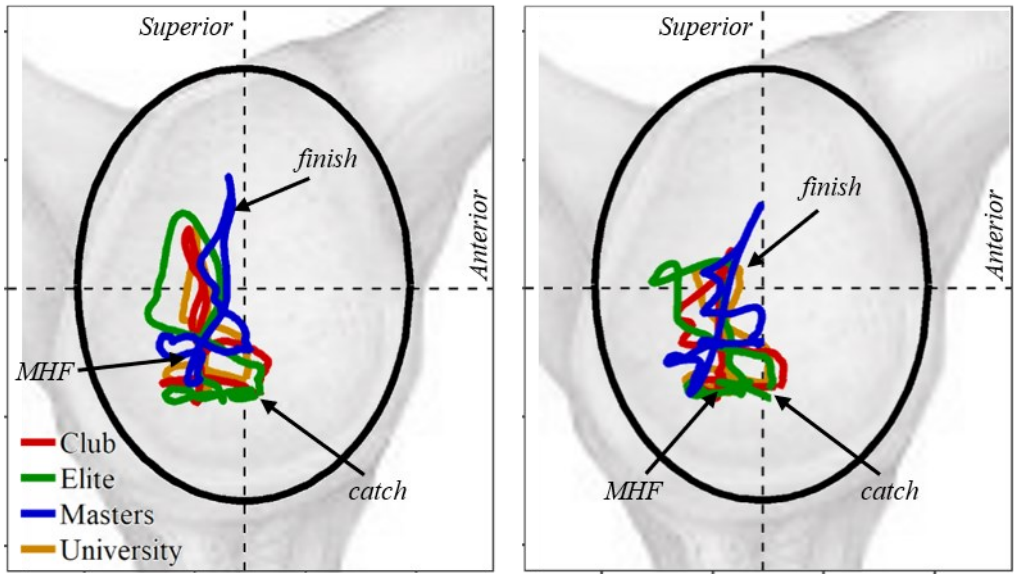

Figure 7.21: Glenoid contact patterns (mean paths) for age/competition level cohorts, at 18 spm (*left*) and 32 spm (*right*) overlaid on a medial view of the scapula. Arrows indicate instantaneous force locus at the catch, max handle force (MHF), and the finish. Black ellipse indicates glenoid rim.

Mean force and standard deviation are presented for muscles showing statistically significant differences among cohorts distinguished by age/competition level (Figure 7.22; Figure 7.23). Examining average muscle force, patterns generated through the prime shoulder movers closely resemble the handle force output examined in Chapter 5 (Section 5.3.1.1). Descriptive statistics for maximum muscle force output, are shown in Table 7.9. There were no significant differences in maximum muscle force output

among the prime movers: latissimus dorsi ($p = 0.158$), teres major ($p = 0.058$), deltoid ($p = 0.153$), pectoralis major ($p = 0.254$), or for trapezius ($p = 0.732$; Figure 7.22).

Among the other scapula stabilizer muscles, club athletes displayed significantly greater maximum force in serratus anterior (2.36 ± 0.43 xBW) than the other three athlete cohorts ($p < 0.009$; Figure 7.22; Table 7.9). Elite rowers showed significantly greater maximum force in levator scapulae (0.34 ± 0.05 xBW) than the other three athlete cohorts ($p < 0.004$). Significantly greater maximum force in rhomboid major was found among elite rowers (0.61 ± 0.12 xBW) than club and masters athletes ($p < 0.022$; Table 7.9).

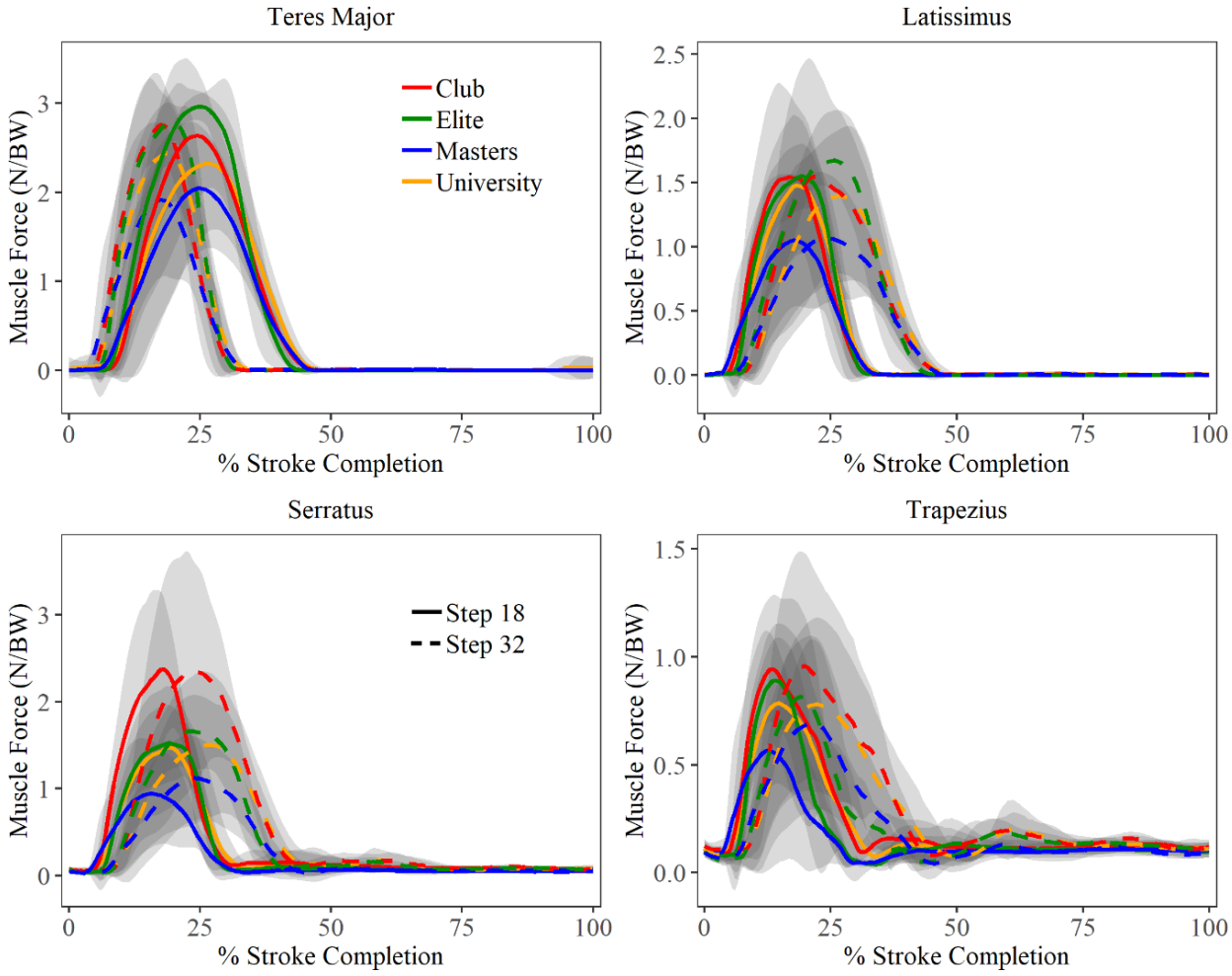

Figure 7.22: Body weight normalized muscles forces (mean ± std) in N/BW, per age/competition level cohorts, generated by prime movers and scapula stabilizer muscles. Stroke rate trials: 18 spm (*solid lines*), 32 spm (*dashed lines*).

Triceps brachii shows significantly lower maximum force output among master rowers (1.03 ± 0.42 xBW) than the three other athlete cohorts ($p < 0.006$). In contrast, masters rowers show higher maximum recruitment of the arm accessory muscles: biceps brachii and coracobrachialis (Figure 7.23; Table 7.9); however, this trend was only statistically significant between masters and club athletes for coracobrachialis ($p = 0.015$) and university athletes for biceps brachii ($p = 0.024$).

In the rotator cuff muscles, masters rowers showed significantly lower maximum muscle force in subscapularis than both elite ($p = 0.004$) and club athletes ($p = 0.012$), as well as significantly lower maximum muscle force in supraspinatus than club ($p = 0.001$) and university athletes ($p = 0.001$).

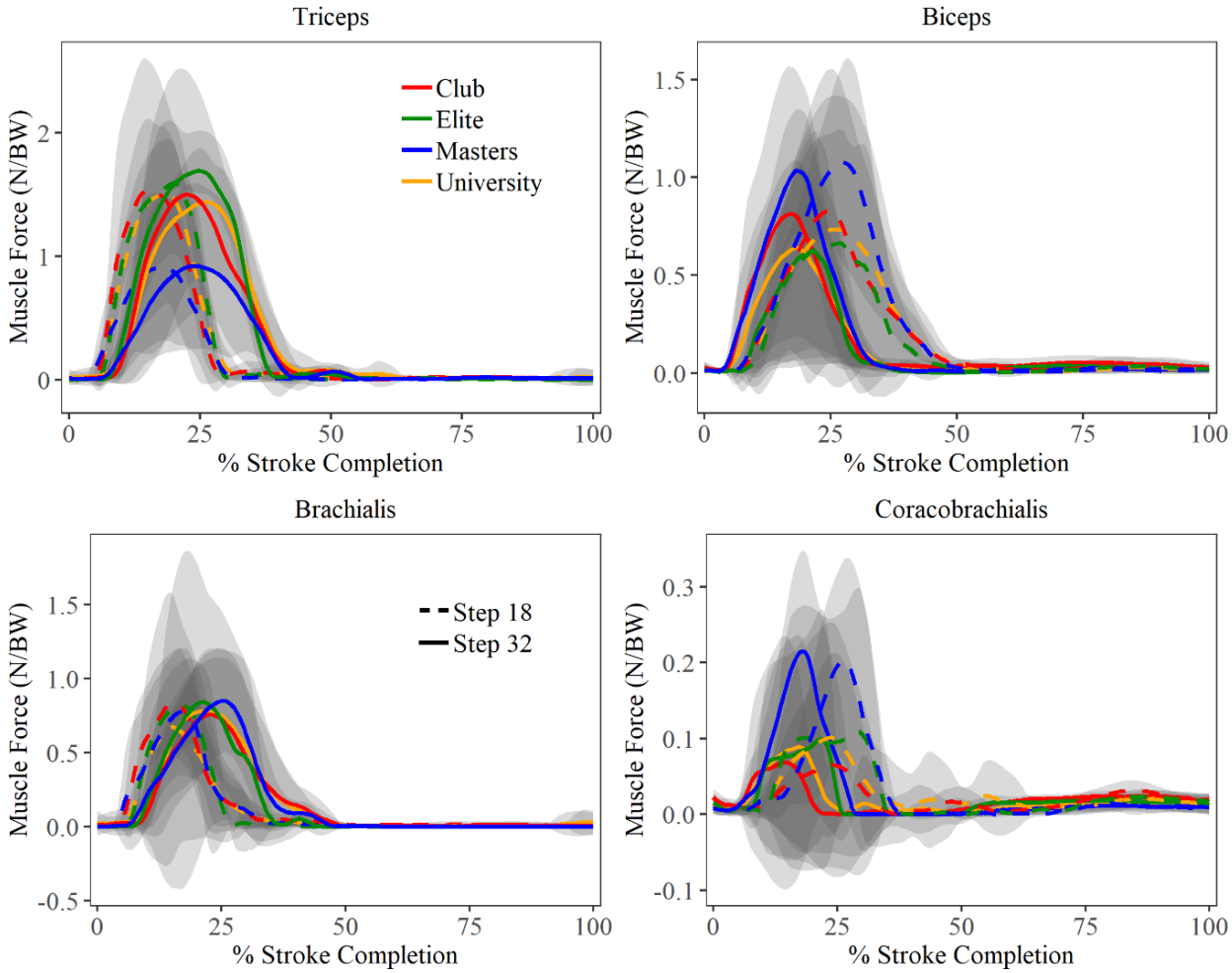

Figure 7.23: Body weight normalized muscles forces (mean ± std) in N/BW, per age/competition level cohorts, generated by the arm accessory muscles. Stroke rate trials: 18 spm (*solid lines*), 32 spm (*dashed lines*).

Table 7.9: Maximum body weight normalized force (mean ± std) in N/BW of various muscles at all stroke rates, for each age/competition level cohort.

		18 spm	24 spm	28 spm	32 spm
Teres Major	Club	2.76 ± 0.58	2.77 ± 0.54	2.69 ± 0.50	2.63 ± 0.43
	Elite	2.79 ± 0.37	2.99 ± 0.75	2.94 ± 0.38	2.96 ± 0.60
	Masters	1.91 ± 0.91	2.06 ± 0.90	2.08 ± 0.83	2.04 ± 0.83
	University	2.44 ± 0.65	2.50 ± 0.66	2.37 ± 0.72	2.32 ± 0.98
Latissimus Dorsi	Club	1.54 ± 0.48	1.54 ± 0.35	1.53 ± 0.25	1.54 ± 0.15
	Elite	1.55 ± 0.29	1.68 ± 0.52	1.63 ± 0.34	1.67 ± 0.43
	Masters	1.05 ± 0.54	1.14 ± 0.50	1.15 ± 0.47	1.07 ± 0.47
	University	1.47 ± 0.34	1.52 ± 0.33	1.42 ± 0.33	1.39 ± 0.28
Pectoralis Major	Club	1.69 ± 0.70	1.78 ± 0.51	1.67 ± 0.47	1.61 ± 0.40
	Elite	2.03 ± 0.14	2.20 ± 0.30	2.20 ± 0.36	2.26 ± 0.46
	Masters	1.76 ± 0.78	1.93 ± 0.85	1.97 ± 0.74	1.97 ± 0.63
	University	1.78 ± 0.47	1.80 ± 0.50	1.71 ± 0.49	1.69 ± 0.48
Serratus Anterior	Club	2.37 ± 0.49	2.39 ± 0.45	2.34 ± 0.43	2.34 ± 0.34
	Elite	1.52 ± 0.26	1.65 ± 0.42	1.62 ± 0.24	1.66 ± 0.35
	Masters	0.94 ± 0.48	1.02 ± 0.48	1.04 ± 0.45	1.12 ± 0.43
	University	1.47 ± 0.42	1.55 ± 0.35	1.53 ± 0.37	1.50 ± 0.38
Trapezius	Club	0.94 ± 0.21	0.92 ± 0.19	0.95 ± 0.12	0.96 ± 0.06
	Elite	0.89 ± 0.02	0.90 ± 0.10	0.84 ± 0.12	0.82 ± 0.10
	Masters	0.57 ± 0.32	0.58 ± 0.32	0.58 ± 0.31	0.69 ± 0.29
	University	0.78 ± 0.18	0.82 ± 0.21	0.81 ± 0.21	0.78 ± 0.19
Rhomboid Major	Club	0.47 ± 0.15	0.46 ± 0.11	0.46 ± 0.07	0.45 ± 0.05
	Elite	0.60 ± 0.10	0.64 ± 0.12	0.60 ± 0.14	0.61 ± 0.13
	Masters	0.36 ± 0.20	0.40 ± 0.20	0.41 ± 0.18	0.37 ± 0.16
	University	0.55 ± 0.13	0.57 ± 0.11	0.53 ± 0.12	0.51 ± 0.10

Table 7.9 (continued)

		18 spm	24 spm	28 spm	32 spm
Triceps Brachii	Club	1.54 ± 0.31	1.58 ± 0.22	1.54 ± 0.17	1.50 ± 0.14
	Elite	1.60 ± 0.26	1.71 ± 0.49	1.67 ± 0.13	1.69 ± 0.29
	Masters	0.91 ± 0.39	0.99 ± 0.38	0.98 ± 0.35	0.92 ± 0.33
	University	1.51 ± 0.36	1.55 ± 0.35	1.48 ± 0.44	1.44 ± 0.52
Biceps Brachii	Club	0.81 ± 0.45	0.90 ± 0.25	0.83 ± 0.21	0.83 ± 0.21
	Elite	0.62 ± 0.29	0.64 ± 0.19	0.65 ± 0.25	0.66 ± 0.23
	Masters	1.03 ± 0.27	1.14 ± 0.28	1.18 ± 0.21	1.08 ± 0.19
	University	0.64 ± 0.24	0.66 ± 0.23	0.79 ± 0.28	0.73 ± 0.27
Coracobrachialis	Club	0.07 ± 0.05	0.07 ± 0.02	0.07 ± 0.03	0.07 ± 0.03
	Elite	0.10 ± 0.10	0.11 ± 0.12	0.10 ± 0.13	0.11 ± 0.13
	Masters	0.22 ± 0.05	0.24 ± 0.06	0.25 ± 0.04	0.20 ± 0.03
	University	0.09 ± 0.05	0.10 ± 0.03	0.10 ± 0.03	0.10 ± 0.03
Subscapularis	Club	2.40 ± 0.24	2.33 ± 0.38	2.27 ± 0.44	2.11 ± 0.51
	Elite	2.39 ± 0.34	2.55 ± 0.51	2.67 ± 0.57	2.61 ± 0.61
	Masters	1.48 ± 0.43	1.63 ± 0.50	1.66 ± 0.45	1.58 ± 0.44
	University	2.06 ± 0.46	2.15 ± 0.54	2.03 ± 0.61	1.96 ± 0.62
Supraspinatus	Club	0.27 ± 0.39	0.22 ± 0.01	0.28 ± 0.01	0.31 ± 0.01
	Elite	0.25 ± 0.00	0.32 ± 0.00	0.32 ± 0.00	0.34 ± 0.00
	Masters	0.06 ± 0.00	0.05 ± 0.00	0.06 ± 0.00	0.07 ± 0.00
	University	0.23 ± 0.39	0.27 ± 0.37	0.27 ± 0.27	0.26 ± 0.50

7.5.3 Effect of Preferred Rowing Modality on Rowing Biomechanics

The effects of preferred rowing modality or sidedness are more difficult to discern when using ergometer rowing, as this exemplar movement was in lieu of a more representative sweep rowing simulation. However, published studies have found upper limb right-left differences in otherwise symmetric ergometer rowing (Sforza *et al.*, 2012), and asymmetric low back muscle EMG amplitudes in sweep rowers during indoor rowing (Readi *et al.*, 2015).

Comparing body weight normalized GH joint forces among athletes grouped by preferred rowing modality (i.e., sculling, port sweep, starboard sweep), several differences were noted across all stroke rates.

There was no significant difference in GH compression force across the groups ($p = 0.19$; Table 7.10). However, there were statistically significant differences in maximum absolute A/P shear force ($p = 0.029$) and in maximum S/I shear force ($p = 0.003$) across all three athlete cohorts (Figure 7.24). Scullers displayed substantially higher maximum S/I shear force (1.88 ± 0.12) than both port rowers ($p = 0.021$) and starboard rowers ($p = 0.001$; Table 7.10), while port rowers showed significantly higher maximum absolute A/P shear force (2.54 ± 0.22) than starboard sweep rowers ($p = 0.049$) and scullers ($p = 0.012$; Table 7.10). There were no statistically significant differences in total elbow joint force found among the preferred rowing modality cohorts ($p = 0.353$).

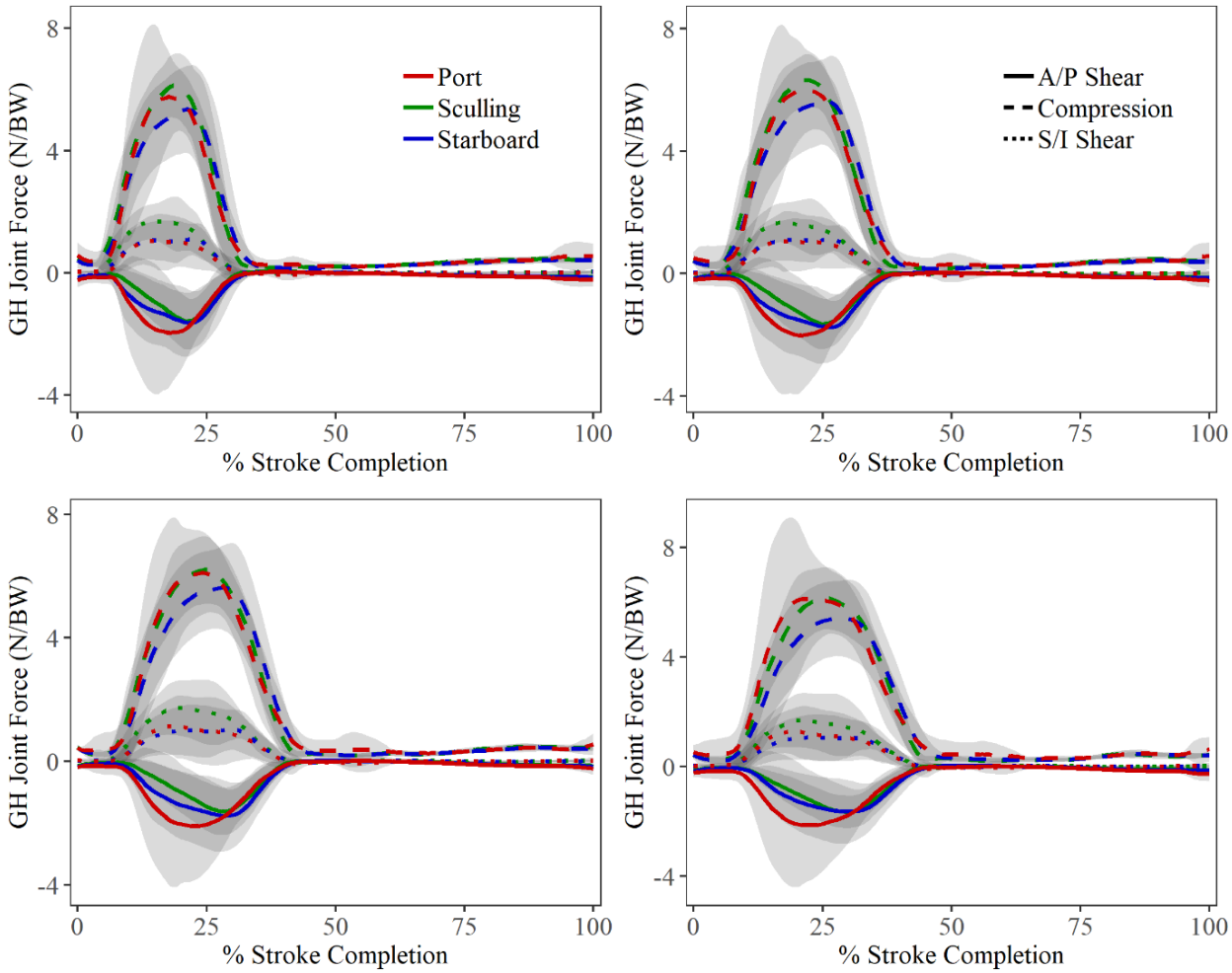

Figure 7.24: Preferred rowing modality/side cohort glenohumeral joint forces (mean ± std), (+) compression, (+) superior shear (S/I) and (+) posterior shear (A/P). Stroke rate trials: 18 spm (*top left*), 24 spm (*top right*), 28 spm (*bottom left*), 32 spm (*bottom right*).

Table 7.10: Maximum values (mean ± std) of glenohumeral (GH) joint compression, anterior-posterior (A/P) shear superior-inferior (S/I) shear, and total elbow (ELB) joint force, in N/BW; shoulder stability ratio (SSR) and total glenoid contact pattern path length (mm) at all stroke rates, for preferred rowing modality cohorts.

			18 spm	**24 spm**	**28 spm**	**32 spm**
GH	Compression	Port	5.75 ± 0.91	5.99 ± 1.30	6.11 ± 1.66	6.12 ± 1.20
		Starboard	5.35 ± 1.34	5.62 ± 1.43	5.62 ± 1.28	5.42 ± 1.20
		Sculling	6.13 ± 1.18	6.32 ± 1.06	6.20 ± 0.93	6.15 ± 1.10
	S/I Shear	Port	1.05 ± 0.12	1.07 ± 0.26	1.14 ± 0.24	1.28 ± 0.32
		Starboard	1.09 ± 0.53	1.12 ± 0.55	1.03 ± 0.61	1.07 ± 0.39
		Sculling	1.67 ± 0.57	1.67 ± 0.53	1.73 ± 0.44	1.69 ± 0.41
	A/P Shear	Port	-1.97 ± 0.85	-2.02 ± 0.63	-2.10 ± 0.87	-2.14 ± 0.83
		Starboard	-1.63 ± 0.97	-1.76 ± 0.99	-1.76 ± 0.85	-1.64 ± 0.71
		Sculling	-1.58 ± 0.39	-1.64 ± 0.40	-1.61 ± 0.39	-1.65 ± 0.34
	Max Stability	Port	0.52 ± 0.29	0.52 ± 0.32	0.55 ± 0.30	0.57 ± 0.29
		Starboard	0.51 ± 0.27	0.51 ± 0.27	0.51 ± 0.25	0.52 ± 0.20
		Sculling	0.51 ± 0.09	0.52 ± 0.08	0.53 ± 0.09	0.55 ± 0.10
	Glenoid Path Length	Port	83.4 ± 4.1	81.2 ± 4.2	79.6 ± 4.3	79.9 ± 4.5
		Starboard	81.2 ± 3.7	80.2 ± 3.7	73.2 ± 3.6	73.2 ± 3.6
		Sculling	78.0 ± 5.1	79.2 ± 5.1	77.4 ± 5.1	77.4 ± 5.4
ELB	Total Force	Port	2.97 ± 0.43	3.04 ± 0.50	3.05 ± 0.69	3.03 ± 0.52
		Starboard	2.70 ± 0.67	2.77 ± 0.62	2.95 ± 0.56	2.88 ± 0.50
		Sculling	2.98 ± 0.90	3.08 ± 0.84	3.03 ± 0.69	3.16 ± 0.69

Little difference was found in shoulder stability between athletes of varying preferred rowing modality (Figure 7.25). Across all stroke rates, the cohorts displayed similar average SSRs ($p = 0.181$) throughout the stroke cycle. Only at the catch, was SSR significantly lower among scullers than port rowers ($p = 0.026$) or starboard rowers ($p = 0.024$; Table 7.10). There were no statistical differences among the groups at either MHF ($p = 0.304$) or at the finish ($p = 0.309$; Figure 7.25). This suggests that the small differences in GH compression force and shear force components, among groups were not enough to elicit change in the clinical SSR metric.

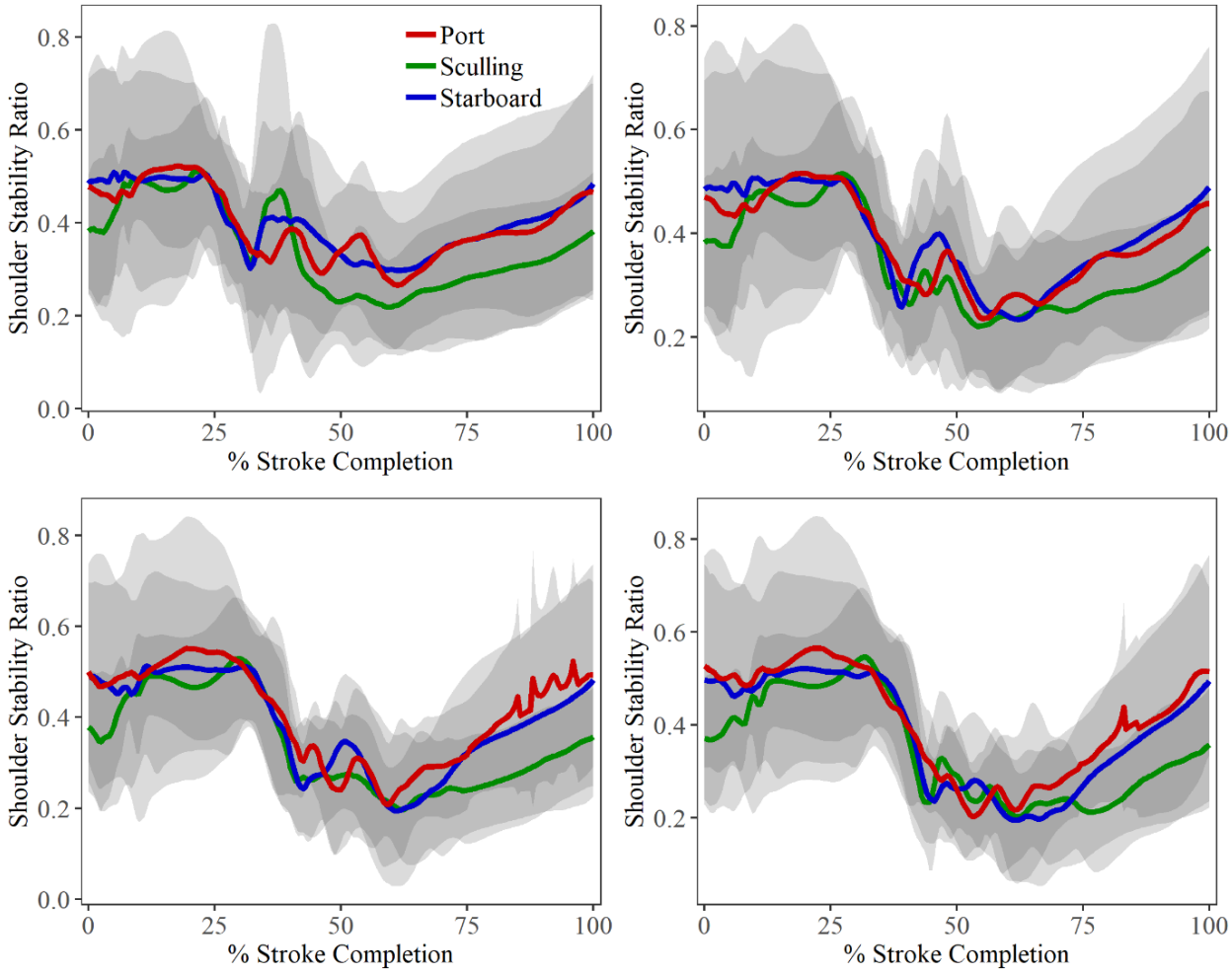

Figure 7.25: Shoulder stability ratio (mean ± std) for each preferred rowing modality/side cohort. Stroke rate trials: 18 spm (*top left*), 24 spm (*top right*), 28 spm (*bottom left*), 32 spm (*bottom right*).

Glenoid contact patterns for each of the preferred rowing modalities are shown at the lowest (18 spm) and highest (32 spm) stroke rates (Figure 7.26). Across all rates, there were no significant differences in total path length amongst the three athlete cohorts ($p = 0.342$; Table 7.10). Center of pressure was mostly constrained to the posterior half of the glenoid socket and does not pass close to the glenoid rim (Figure 7.26). During the early drive phase, the sculling mean contact pattern displaces further posterior between the catch and MHF than do the contact patterns of the sweep athlete cohorts (Figure 7.26). Fréchet distances between average contact patterns calculated at each stroke rate were largest between scullers and port rowers at 18 spm (4.78 mm) and smallest between port and starboard rowers at 18 spm (2.33 mm). When averaged across all stroke rates, this trend remained, with scullers having larger Fréchet distances to port rowers (4.26 ± 0.51 mm) and starboard rowers (4.15 ± 0.68 mm) than the sweep rowing cohorts had between each other (port/starboard: 2.48 ± 0.22 mm).

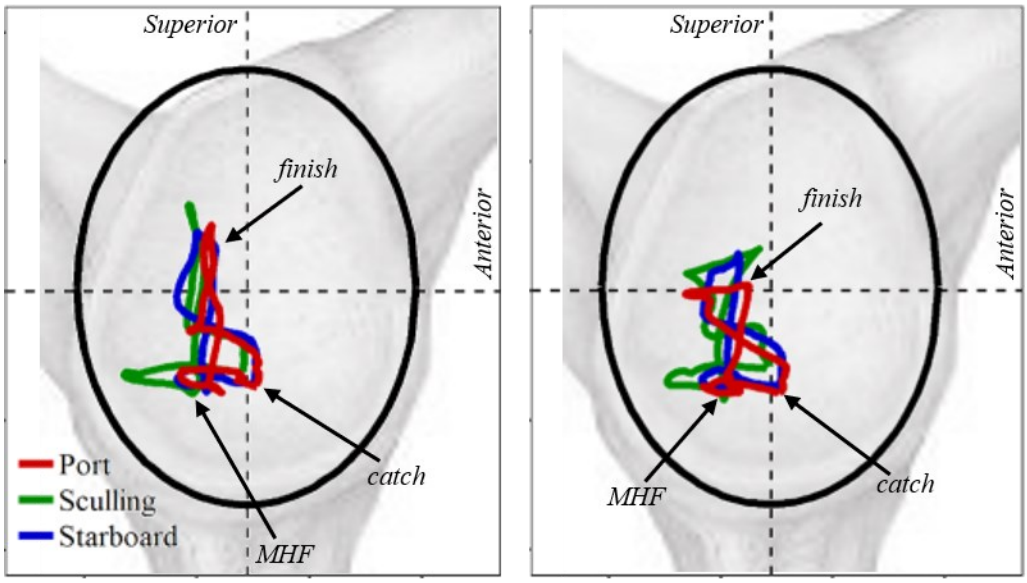

Figure 7.26: Glenoid contact patterns (mean paths) for each preferred rowing modality/side cohort, at 18 spm (*left*) and 32 spm (*right*) overlaid on a medial view of the scapula. Arrows indicate instantaneous force locus at the catch, max handle force (MHF), and the finish. Black ellipse indicates glenoid rim.

Mean force and standard deviation are presented for muscles showing statistically significant differences among cohorts distinguished by preferred rowing modality / side (Figure 7.27). Descriptive statistics for maximum muscle force output, are shown in Table 7.11.

There were significant differences among the three athlete cohorts in maximum muscle force output of the prime movers and scapula stabilizers, but not in any of the arm accessory muscles or rotator cuff muscles. Starboard rowers showed significantly lower maximal force output in teres major than port rowers ($p = 0.028$) and scullers ($p = 0.05$; Table 7.11). Scullers displayed significantly greater maximal force output in pectoralis major (Figure 7.27) than both port ($p = 0.016$) and starboard rowers ($p = 0.004$).

Among the scapula stabilizer muscles, scullers displayed significantly greater force output than either sweep cohort in trapezius ($p = 0.001$) and levator scapulae ($p < 0.001$; Table 7.11; Figure 7.27). Higher maximum force output in levator scapulae, which functionally works with the rhomboids to elevate and downwardly rotate the scapula, suggests a broader distribution of scapula stabilizer force in scullers compared to the sweep cohorts (Table 7.11; Figure 7.27).

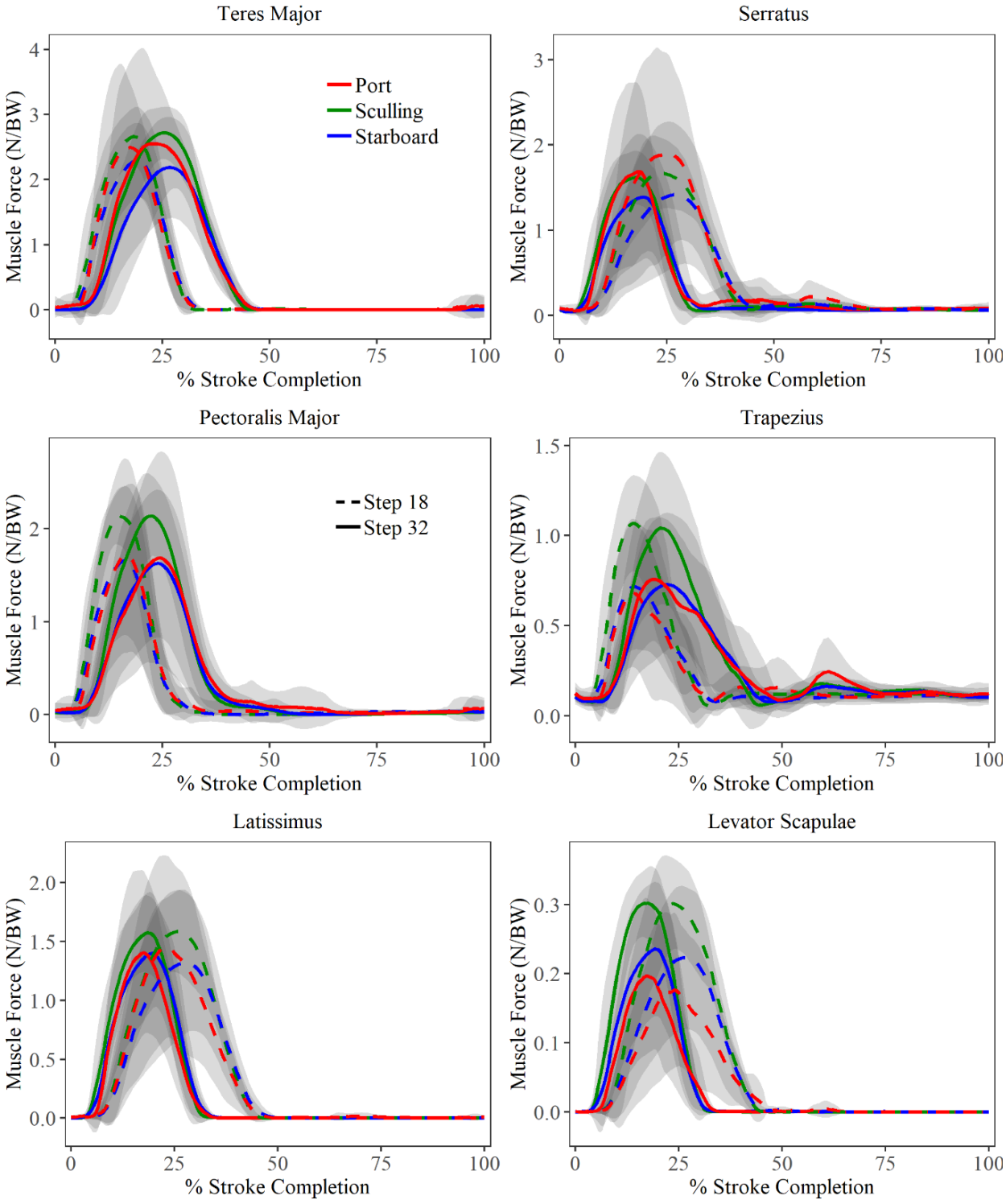

Figure 7.27: Body weight normalized muscle forces (mean ± std) in N/BW, for each preferred rowing modality/side cohort, generated by prime movers and scapula stabilizers. Stroke rate trials: 18 spm (*solid lines*), 32 spm (*dashed lines*).

Table 7.11: Maximum body weight normalized muscle force (mean ± std) in N/BW of various muscles at all stroke rates, for each preferred rowing modality cohort.

		18 spm	24 spm	28 spm	32 spm
Teres Major	Port	2.49 ± 0.40	2.55 ± 0.61	2.53 ± 0.70	2.55 ± 0.72
	Starboard	2.30 ± 0.63	2.39 ± 0.58	2.24 ± 0.54	2.19 ± 0.50
	Sculling	2.66 ± 0.71	2.71 ± 0.62	2.69 ± 0.54	2.72 ± 0.56
Latissimus	Port	1.41 ± 0.28	1.46 ± 0.27	1.41 ± 0.27	1.46 ± 0.30
	Starboard	1.40 ± 0.43	1.47 ± 0.44	1.37 ± 0.42	1.32 ± 0.39
	Sculling	1.58 ± 0.43	1.57 ± 0.39	1.57 ± 0.32	1.58 ± 0.36
Serratus	Port	1.69 ± 0.44	1.78 ± 0.34	1.77 ± 0.33	1.91 ± 0.44
	Starboard	1.39 ± 0.47	1.48 ± 0.45	1.46 ± 0.43	1.41 ± 0.38
	Sculling	1.62 ± 0.48	1.65 ± 0.47	1.65 ± 0.39	1.67 ± 0.36
Trapezius	Port	0.68 ± 0.06	0.68 ± 0.10	0.68 ± 0.12	0.76 ± 0.16
	Starboard	0.72 ± 0.21	0.76 ± 0.19	0.76 ± 0.21	0.73 ± 0.18
	Sculling	1.07 ± 0.35	1.04 ± 0.32	1.07 ± 0.26	1.04 ± 0.20
Levator Scapulae	Port	0.20 ± 0.04	0.20 ± 0.05	0.19 ± 0.06	0.18 ± 0.06
	Starboard	0.24 ± 0.08	0.25 ± 0.08	0.23 ± 0.07	0.22 ± 0.06
	Sculling	0.30 ± 0.10	0.30 ± 0.10	0.30 ± 0.08	0.30 ± 0.07
Pectoralis Major	Port	1.71 ± 0.47	1.76 ± 0.35	1.68 ± 0.35	1.69 ± 0.43
	Starboard	1.66 ± 0.60	1.65 ± 0.64	1.63 ± 0.59	1.63 ± 0.55
	Sculling	2.13 ± 0.62	2.31 ± 0.58	2.20 ± 0.47	2.14 ± 0.41

7.6 DISCUSSION

Rowing performance is largely influenced by anthropometry (Barrett & Manning, 2004) and aerobic capacity (Ingham *et al.*, 2002). However, these variables cannot entirely explain performance variation across different athlete classes. Much focus in rowing performance literature has been paid to contributions from the lower extremity and their effects on the lumbar spine. Objectives of this chapter were to analyze muscle force patterns in the upper extremity, compare GH joint compression and shear force components, and clarify contributions of the surrounding musculature to joint stability during ergometer rowing. Population-wide group averages allow us to look for global trends in joint and muscle mechanics across entire athlete populations. These biomechanical parameters were discussed within the broad rowing subject

population and contrasted across distinct sub-cohorts of athletes, including by sex, age/level of competition, and preferred rowing modality/side.

7.6.1 Joint Force & Stability

Distributed joint reaction forces indicate the level of loading sustained during a movement. Changes in joint loading patterns related to stroke rate were not expected given the findings from Chapter 5, where it was observed that handle force did not change with rate. Comparing body weight normalized forces across the entire athlete population, neither resultant elbow joint force, nor component GH joint forces varied significantly with stroke rate (Figure 7.8; Figure 7.9). As SSR was calculated as the instantaneous ratio of shear to compressive GH joint force, it also varied little with stroke rate; however, it was affected by position within the stroke. The highest SSRs were observed during the drive phase, when cumulative loading was largest and lowest SSRs observed partway through the recovery phase (Figure 7.11). The findings of this study demonstrate substantial shear forces on the glenoid during ergometer rowing. The largest ratios of GH shear force to compression presented in this study were comparable to activities of daily living involving an outstretched arm, such as picking and placing an object, albeit lower than pushing and pulling movements (Klemt *et al.*, 2018). This initially unintuitive result may be a function of significant muscular co-contraction in the trunk and upper extremity, and/or a proprioceptive response to stabilize the GH joint during heavy load transfer in the drive.

Statistically significant differences in maximum joint forces between male and female athlete cohorts were anticipated, but a stroke rate related interaction was not found. Males displayed higher maximum compressive GH joint force, higher A/P shear force, and a higher ratio of A/P to S/I shear than females (Figure 7.14). This result was logical as males generate significantly larger MHF than females (Chapter 5, Section 5.3.1.1). Higher A/P shear forces as a result of males pulling harder on the handle in the sagittal plane, necessitate higher compression forces to maintain GH stability during the drive phase. Attenborough, Smith & Sinclair (2012) observed lower upper extremity energy contribution in females than males across stroke rates and inferred that male rowers generate greater work through shoulder rotation than females. Results in this chapter support this finding, as males displayed higher average shoulder stability ratios at the catch and through the last 20% of the recovery phase (Figure 7.15). Variability in muscle mass, morphology, and GH joint laxity may also be related to this difference.

Age related musculoskeletal declines manifest in biomechanical changes in ergometer rowing. Chronic shoulder pain in rowers results from compromised shoulder positioning, instability under high load and acceleration (Thornton *et al.*, 2017b) and will probably deteriorate further with age. Masters rowers displayed the lowest average shoulder stability ratios through the early drive but SSR distinctly increased at the finish (Figure 7.20). Functionally this implies that masters rowers have the greatest shoulder

instability when accelerating out of the finish but were most stable throughout the rest of the stroke. While it is not clear why, one possibility is that increased joint stiffness, more common in older adults (Borgia, Radzak & Freedman Silvernail, 2021), may confer some inherent stability. Results from this chapter show that, compared to university, club, and elite rowers, masters athletes (*>27yrs*) have less GH compression, less A/P shear force (Figure 7.19), and longer total glenoid contact pattern lengths (Figure 7.21). Rotator cuff damage can be caused by exposure to repetitive high loads and is more common in older athletes and compensation may evoke kinematic changes (McMahon, Prasad & Francis, 2014). Differences in GH joint force and shoulder stability results for masters rowers, (Section 7.5.2) align with the upper extremity movement pattern differences seen in Chapter 6 (Section 6.3.1.3), which show that masters athletes have significantly reduced GH and ST range of motion (Figure 6.11; Figure 6.13; Table 6.6).

Although all three preferred rowing modality cohorts shared similar levels of GH joint compression (Figure 7.24), in a somewhat unexpected result, scullers showed significantly higher S/I shear force than their sweep counterparts, while port rowers showed significantly higher absolute A/P shear force than starboard rowers and scullers (Table 7.10). On the water, a port rowers right shoulder is inside, closer to the oarlock and center of oar rotation, while a starboard rowers right shoulder is outside, farther from the oarlock and follows a larger arc around the oar center of rotation (Chapter 3; Section 3.1). Using right sided shoulder data for comparison between port and starboard rowers may highlight differences between inside versus outside shoulder stability in sweep rowers, despite ergometer rowing being deemed an essentially symmetric motion. A kinematic difference linked to this inside / outside arm concept and presented in Chapter 6 (Section 6.3.1.4), was that during the early-drive phase, elbow joint flexion RoC was closer to zero among starboard rowers than port rowers, suggesting starboard rowers maintain better arm extension than port rowers (Figure 6.15; Table 6.7). Scullers also displayed lower SSRs during the recovery and at the catch, but this was not significant (Figure 7.25). However, this result suggests that there may be a basic difference in the approaches of sweep rowers and scullers to power application during ergometer rowing, that was not necessarily reflected in gross joint kinematics presented in Chapter 6 (Section 6.3.1.4). Unfortunately, there is little published research comparing biomechanics of sweeping and sculling, save for differences in the anatomic location of stress-induced rib fractures, which are commonly associated with bending and torsional forces applied to the trunk (McDonnell, Hume & Nolte, 2011).

7.6.2 Glenoid Contact Patterns

The stability of the GH joint is linked to the direction of the reaction force at the joint. This was represented by a glenoid contact pattern and illustrates the translation of the humeral head across the glenoid surface, caused by shear forces. For mean glenoid contact patterns for a single stroke cycle *(~2-3 seconds*) across the entire athlete population and all stroke rates, the center of pressure remained mostly constrained

to the posterior half of the glenoid socket and does not pass close to the glenoid rim (Figure 7.10). Both factors suggest a more stable shoulder position and it is reasonable to conclude that humeral head contact with the glenoid labrum is unlikely, particularly in the anterior direction. GH instability is most common in the anterior-inferior direction (Reilly, 2011), and contact patterns that show greater S/I translation or a predominantly anterior center of pressure, are considered positions at greater risk of shoulder subluxation (Klemt *et al.*, 2019b).

The pattern in the population-wide group was similar to those seen in activities of daily living that involve an outstretched arm, such as picking and placing objects (Klemt *et al.*, 2018; Charlton, 2003), but it is important to remember that the drive phase of the rowing stroke is more heavily loaded than most functional activities. There are also implications from the fact that the stroke cycle, and this contact pattern, may be repeated thousands of times in on-water and land training sessions. This type of repetitive motion has ramifications for how joint force contact patterns are relevant to long term shoulder health and incidence of overuse injuries.

Across all rates, glenoid contact patterns of males and females showed similar total path length, but male contact patterns tended to be more inferior and more posterior than females, particularly at the catch (Figure 7.16). While generalized laxity is more common in females, this does not necessarily correlate with shoulder laxity specifically (Tang & Simpson, 2016). It has been suggested that larger glenoid contact patterns could be indicative of greater GH laxity which is a predisposing factor in the development of impingement syndrome (Hannafin, 2000). Total glenoid contact pattern path length was largely similar among the preferred rowing modalities; however, scullers had larger Fréchet distances to port and starboard mean contacts patterns, than the two sweep cohorts had to each other (Figure 7.26). Glenoid contact patterns of masters rowers were positioned more superior at the catch and MHF than the other athlete cohorts (Figure 7.21), and masters rowers showed the longest total contact pattern path length. However, this difference was only significant between masters and university athletes (Table 7.8). Contact patterns that show greater S/I translation are considered at higher shoulder injury risk (Klemt *et al.*, 2019b), but in line with muscle force results from this chapter (Section 7.5.2; Table 7.9), weakness in supraspinatus could result in a more superiorly positioned glenoid center of pressure (Figure 7.21), as the muscle would otherwise act to depress the humeral head against the upward pull of deltoid (Itoi, Morrey & An, 2009).

Anatomical variability of the glenoid fossa in this subject population represents a limitation to interpreting glenoid contact pattern results in this thesis. The UKNSM leverages the Visible Human male dataset skeletal geometries (Spitzer & Whitlock, 1998) and is not currently implemented for subject specific modelling; however, this application is in development (Klemt, 2018). Adult glenoid fossa morphology includes variations in size, shape, and angulation with respect to the scapular plane (Saha, 1971).

Morphological variation of the glenoid has been implicated as a risk factor in the development of shoulder joint pathologies including glenohumeral instability and recurrent dislocation (Wilk, Arrigo & Andrews, 1997; De Wilde *et al.*, 2004; Eichinger *et al.*, 2016; Saha & Vasudeva, 2020). But in vivo measurements of glenoid variation can be difficult to determine without MRI and were beyond the scope of this thesis. Thus, glenoid contact patterns should be interpreted conservatively, as individual variation may affect potential injury risk.

7.6.3 Muscle Forces

Magnitude and timing of maximum force output for each of the largest contributing muscles help establish a muscle recruitment order throughout the stroke. Pectoralis major, trapezius, deltoid, and brachialis were most active in the early-drive phase. Maximum force in prime movers - latissimus dorsi and teres major, scapula stabilizers - serratus anterior and rhomboid major, and arm accessory muscles - biceps brachii and triceps brachii, coincide with MHF (Table 7.4). During the drive phase, triceps brachii acts as an antagonist to biceps short head to maintain extension of the elbow and support efficient load transfer through a straight arm (Bompa, Borms & Hebbelinck, 1990). This idea is supported by Tachibana *et al.*, (2007) who concluded from principal component analysis of surface EMG, that physiological cross-sectional area of the elbow extensor muscles best explained power contributed by the arm pull. While the scapula is retracting, serratus anterior actively keeps the medial border close to the thoracic wall (Paine & Voight, 1993) and stabilizes the rib cage during forced respiration (Warden *et al.*, 2002). Abbot & Hannafin (2001) have previously implicated contraction of serratus anterior in the occurrence of rib stress fractures among rowers. The current study noted that serratus anterior contributed the largest force outputs of the scapula stabilizers during the mid-drive phase (Table 7.4; Table 7.5), which concurs with the concept that forceful contraction of serratus anterior, over thousands of strokes could lead to stress fractures (Rumball *et al.*, 2005; Karlson, 2000). Results in this chapter showing differences in force outputs between serratus anterior and the scapula retractors (i.e., trapezius and rhomboid major) (Table 7.5; Figure 7.12) may also lend merit to a muscle imbalance or antagonistic co-contraction theory of rib stress fractures (Vinther *et al.*, 2006). Through the late drive phase, the upper body generates momentum through the humeral extensors and internal rotators, by concentric contraction of latissimus dorsi and teres major. Coaches have highlighted the importance of having a long stroke initiated by the legs and accelerated through the trunk and arms (Nilsen, Daigneault & Smith, 2002a), but differ on whether adding extra length by protracting the scapula, may result in decreased latissimus dorsi connection and greater load transfer through upper trapezius. Contraction of the rotator cuff musculature surrounding the shoulder lends stability to the GH joint by centralizing the humeral head on the glenoid fossa. However, the variation in maximum force timing suggests different roles for each of them. Subscapularis contraction during the late drive supports

humeral deceleration into the finish position, a sharp change in direction of arm movement, and humeral acceleration out onto the recovery (Figure 7.12). Late-recovery maximum force in infraspinatus suggests that its main role is to support the arm when it is in full forward extension and lifting into the catch (Figure 7.13). The infraspinatus line of action works to restrain the humeral head from sliding anterosuperior on the glenoid fossa. On the recovery, infraspinatus works in tandem with anterior deltoid as it elevates the handle into the catch position (Figure 7.13). These actions help set up the rower up for a relaxed but sharp catch with a stable scapular position (Price, 2016).

Both Jones *et al.* (2010) and Lamb (1989) showed sharp elbow deceleration at the end of the drive phase for ergometer rowing, a more acute elbow angle at the finish, and greater relative hand velocity moving into and out of the finish position, which dove tails with the finding presented in this chapter of maximum supraspinatus force in the late drive. Compared to on-water rowing, Marcolin *et al.* (2015) found higher upper limb muscle EMG in ergometer rowing and distinct muscle activation patterns between the two training types. On-water rowing showed higher EMG activity in pectoralis major and latissimus dorsi, but higher EMG values for the biceps brachii, deltoid, and trapezius when on the ergometer (Marcolin *et al.*, 2015). This runs counter to findings from this chapter, where latissimus dorsi and pectoralis major both show substantially higher force outputs than trapezius, biceps brachii, and deltoid (Figure 7.12; Figure 7.13; Table 7.5). However, the strength of a comparison with Marcolin *et al.*, (2015) is limited since EMG results are presented as a percentage of maximum voluntary contraction, while the model-derived results in this chapter were presented as body weight normalized muscle force, in N/BW or xBW.

Sex differences seen in rowing performance are not fully explained by anthropometry. In a functional activity, males and females were found to use different muscle recruitment strategies to improve endurance during a repetitive shoulder task (Fedorowich *et al.*, 2013). In ergometer rowing, examining body weight normalized forces, males were found to generate force primarily through large trunk muscles, like latissimus dorsi, teres major and serratus anterior, focusing on rate of humeral extension (Chapter 6; Section 6.3.1.2; Figure 6.8; Table 6.5) with decreased co-activation in antagonists (Figure 7.17). Women showed a wider distribution of muscle force across prime movers, scapula stabilizers, and arm accessory muscles. This included higher max force than males in trapezius, pectoralis major, biceps brachii, brachialis, and coracobrachialis (Figure 7.18; Table 7.7), which suggests a more global approach to isometric stabilization of the upper extremity during the drive phase. The kinematic effect of higher force output in trapezius among female rowers was specifically reflected in greater scapular upward rotation than male rowers (Chapter 6; Section 6.3.1.2; Figure 6.10; Table 6.5). Having previously found higher "muscularity" among male rowers than female rowers, Soper & Hume (2004) correlated that to competitive margins, concluding that a male's "physique" (e.g., greater biceps brachii volume) was a more important determinant of success

at the elite level than for females. From the muscle force results presented in this chapter, males show preferential recruitment of large superficial muscles during the drive phase, which would support this idea (Table 7.7; Figure 7.17). In contrast, females of differing performance ability were found to have similar anthropometric characteristics (Soper & Hume, 2004). More detailed biomechanical profiles, such as those generated by the UKNSM, could be utilized to identify influential physiological characteristics, and better distinguish performance outcomes among female rowers.

While outwardly, stroke shape and timing may be coachable, rowing expertise has been correlated with variation in muscle synergies which adjust mechanical output (Turpin *et al.*, 2011). Experienced athletes selectively recruited muscle groups that propel the boat while relaxing muscles that do not. Elite and club rowers showed higher maximum force in serratus anterior, levator scapulae, and rhomboid major than university or masters rowers (Figure 7.22; Table 7.9). While sharing similar muscle force output in the prime movers as club and elite rowers, university athletes displayed wider variances than both cohorts in teres major, subscapularis, and triceps brachii (Table 7.9). It has been suggested that among athletes of varying age or competition level, differences in performance metrics are driven by differences in muscular coordination, with novices showing less muscular coordination, higher rate of fatigue onset, and as a result, less stroke efficiency (Green & Wilson, 2000). Club athletes showed higher serratus anterior force than other groups (Figure 7.22). Coordination of respiration with contraction of serratus anterior during the stroke cycle has been implicated as a precipitating mechanism of rib stress fractures in rowers (Abbot & Hannafin, 2001). The high serratus anterior force results presented in this chapter among club athletes support the rib cage compression theory, that after MHF, co-contraction of scapular muscles create a compression force on the rib cage. This highlights the importance of trunk muscle strength and conditioning for young, highly competitive athletes.

Regular rowing, continued in advancing age, has a favorable influence on muscular morphology and has been attributed to attenuating age-related reduction in aerobic fitness and skeletal muscle mass, (Arumugam *et al.*, 2020; Boland & Hosea, 1994). However, this is not the case for muscle power (Volianitis, Yoshiga & Secher, 2020). Masters rowers had the lowest maximum force output among the prime movers and scapula stabilizers (Figure 7.22; Table 7.9) but showed the highest peak muscle forces in the arm accessory muscles, biceps brachii and coracobrachialis (Figure 7.23). This emphasis on the recruitment of smaller muscles suggests that masters rowers change their rowing technique, to more pronounced use of the upper extremity. This may be simply better muscle load sharing developed through age and greater experience or a reflection of compensation for reduced global strength, such as loss of muscle strength in large trunk muscles and the lower extremity. Indeed, it was noted in Chapter 6 (Section 6.3.1.3) that masters rowers display significantly smaller GH flexion / extension RoM and abduction /

adduction RoM (Table 6.6). Smoljanović & Bay (2018) hypothesized that such a kinematic change could have elicited their finding of a higher frequency of overuse injuries among competitive masters rowers than among elite and junior rowers (Smoljanovic *et al.*, 2009, 2015). Unfortunately, because of the small athlete sample size in each of the elite, club, and masters cohorts, achieved statistical power was low. The muscle force results in this chapter (Section 7.5.2) indicate that testing additional athletes in those cohorts could improve the effect size for discriminating differences among age/competition level cohorts.

The effects of sidedness are more difficult to discern when using ergometer rowing as the exemplar movement in lieu of a more representative sweep rowing simulation. However, published studies have found upper limb right-left differences in otherwise symmetric ergometer rowing (Sforza *et al.*, 2012), and asymmetric low back muscle EMG amplitudes in sweep rowers during indoor rowing (Readi *et al.*, 2015). Scullers displayed greater maximum force in pectoralis major and trapezius than the sweep cohorts (Figure 7.27; Table 7.11). Scullers also showed greater force output than either sweep cohort in levator scapulae, which functionally works with the rhomboids to elevate and downwardly rotate the scapula (Table 7.11; Figure 7.27). These results imply a broader distribution of muscle forces, particularly across all the scapula stabilizers. While a relatively small percentage of total rowing power is generated in the arm pull, bilateral symmetry between the upper limbs is important (Sforza *et al.*, 2012). Despite finding significant differences in GH joint forces between port and starboard rowers (Table 7.11), at the muscle load-sharing level, only teres major produced significantly greater maximum force output in port rowers than in starboard rowers (Figure 7.27; Table 7.11).

7.7 INJURY ASSESSMENT AND MITIGATION

Computational modelling can sensitively delineate the effects of rowing dynamics, making it valuable to athletes, coaches, and trainers, for technique optimization, training impact, and strength and conditioning balance. UKNSM modifications, such as inclusion of the glenoid labrum (Klemt, 2018), and small alterations to muscle force limiting, have improved model reliability for dynamic, higher speed, athletic movements (Persad, 2016). Handle force output (and by extension ergometer performance) was strongly related to muscle force magnitude and timing of the prime movers latissimus dorsi, teres major, and pectoralis major, during the early-to-mid drive phase (Figure 7.12; Chapter 5, Section 5.3.1.1; Figure 5.13). The trunk and arm muscles spend much of this time in eccentric or isometric contraction, with the shoulders in forward flexion and adduction. Applied strain and strain rate while a muscle is lengthening have been identified as factors in muscle damage (Lieber & Fridén, 1993; Proske & Morgan, 2001). Eccentric loading during scapular retraction, produced high force in serratus anterior, suggesting a large increase in antagonistic co-contraction, as trapezius and rhomboid major contract concentrically (Figure

7.13; Table 7.5). These findings also fit with the forceful contraction theory of rib stress fractures in rowing (Rumball *et al.*, 2005; Karlson, 2000) and may be a factor in scapular dyskinesia (Noguchi *et al.*, 2013).

Similar to elbow muscle injuries highlighted in tennis (Riek, Chapman & Milner, 1999), epicondylitis can arise in rowers due to improper initiation of the drive phase by flexing the elbows with pronated forearms, (Bompa, Hebbelinck & Van Gheluwe, 1985). When performed correctly, full extension of the upper limb should be maintained through the early drive, giving triceps brachii an advantageous line of action, and which results in substantial loading through the muscle (Table 7.5; Figure 7.12). If, at the catch, the elbow is slightly bent in flexion, biceps brachii can potentially overpower the triceps, decreasing load transfer efficiency (Cookson *et al.*, 2017). Strengthening triceps brachii and anconeus to stabilize the elbow during the drive phase and de-emphasizing early contraction of the elbow flexors (i.e., biceps brachii and brachialis) can help mitigate elbow injury development. High humeral elevation, internal rotation, and reduced scapular posterior tilt, are thought to contribute to impingement injuries (Persad, 2016; Prinold, 2012). Substantial force in subscapularis during the late drive, and relative quiescence of middle deltoid (Figure 7.12; Figure 7.13) function to depress and retract the scapula, and centralize the humeral head, implying an inherent impingement mitigation strategy in rowing in this cohort of athletes.

Predisposing mechanical factors of various pathologies, including labral injuries, scapular dyskinesia, rib stress injury, and impingement syndrome, are precipitated along the continuum from the spine, through the scapula, the shoulder, and the arm, compounding pathomechanics along the way. Results on the influence of postural control of the spine shown in Chapter 6 (Section 6.3.3; Figure 6.22) were described as a potential result of insufficient strengthening or onset of fatigue and have been linked to a kyphotic curvature of the thoracic spine (Koopmann *et al.*, 2018). One proposed compensatory mechanism includes increasing scapular protraction, specifically at the catch. However, no changes in scapular internal / external rotation were noted with increasing stroke rate (Section 6.3.1.1; Figure 6.7), nor were there any changes in muscle force output among the scapula stabilizers as a function of stroke rate (Figure 7.12; Table 7.7). Nonetheless, poor scapular mechanics appear as a common technical error referred to as 'over-reaching' or 'lunging' at the catch (Nugent *et al.*, 2020). This particular position of the arms and shoulder complex potentially increases compressive forces around the rib cage and may impinge on soft tissue structures (Thornton *et al.*, 2017b). Such altered shoulder mechanics can be exacerbated by pre-existing glenohumeral laxity or instability, leading to increased shear of the humeral head in the glenoid socket and compromised shoulder positioning affects transmission of force to the oar handle (Arumugam *et al.*, 2020). This would suggest that to decrease risk of injury (and simultaneously improve performance), an important emphasis should be placed on increasing the strength and stability of the shoulder, including appropriate

training for scapula-thoracic musculature, to avoid development of muscular imbalances and ensure postural alignment.

Strength training plays a crucial role in building and maintaining power for rowing. Implementation of strength and conditioning programs that include a special training focus on shoulder muscular endurance can help minimize effects of fatigue and engrain positive postural coordination. Alternate pushing and pulling exercises, performed over a full range of motion, build shoulder stability and anterior/posterior muscular balance (Urbanczyk *et al.*, 2020). Additional focus on muscles involved in shoulder rotation would be particularly beneficial to female athletes (Attenborough, Smith & Sinclair, 2012), as intensive training has shown improvements in effective work, attributed to better sequencing of main muscle groups (Soper & Hume, 2004). Regular strength and conditioning of serratus, latissimus and rotator cuff muscles will most benefit masters athletes, to mitigate generalized muscle strength decrease and ensure glenohumeral stability as symptomatic and asymptomatic rotator cuff tear prevalence increases with age (Teunis *et al.*, 2014).

7.8 CONCLUDING REMARKS

This chapter reveals the sensitivity with which internal biomechanics may be mapped to external kinematics and discusses how computational modelling can enhance our interpretation of performance data in the context of rowing. Population averages allowed us to identify global trends in joint and muscle mechanics. Comparing averages among athlete cohorts (by age, sex, level of competition, boat class) demonstrated the way in which computational modelling can be specifically valuable to coaches and trainers for technique optimization, training impact, options for strength and conditioning tailored to muscle balance work.

The thesis work presented herein attempted to address questions around connections between shoulder and spine biomechanics and performance in ergometer rowing and implications for training and athlete health by laying the foundational work of quantifying upper body technique in ergometer rowing, utilizing sophisticated computational tools. The rowing stroke cycle was broken down into important moments and phases, highlighting joint and muscular loading. It was found that muscle forces drive the variation seen in external movement patterns, which impact joint forces and GH contact patterns. These musculoskeletal shoulder loads have implications for biomechanical performance and may introduce new considerations in predicting injury during ergometer rowing. For all rowing athletes, engraining musculoskeletal control of the finish and catch positions in particular will increase stroke efficiency for the same physiological workload and improve consistency in horizontal acceleration of both the trunk and

shoulder (McGregor *et al.*, 2016). Biomechanics is essential to executing the rowing action effectively and the consequences of failure to do so were discussed.

The next chapter presents an athlete case study, which serves to illustrate the depth and utility of computational modelling to enhance interpretation of and individual's performance data, relative to population averages, by stepping from superficial kinematics into deeper biomechanics.

8. CHAPTER 8: ENHANCING ATHLETE FEEDBACK WITH BIOMECHANICS: A CASE STUDY

The previous chapters presented results of spatio-temporal and kinetic metrics (Chapter 5), athlete kinematics and dynamics (Chapter 6), and musculoskeletal biomechanics (Chapter 7) during ergometer rowing. These analyses illustrate the effects of glenohumeral compression and shear force on joint stability and identify recruitment strategies of the surrounding musculature, which contribute to joint contact patterns and body segment positioning. Results were discussed across the broader athlete population and contrasted among distinct sub-cohorts of rowers, including by sex, age, competition level, and modality. Understanding shoulder loading during rowing and ergometer rowing is a major step toward improving performance coordination and investigating pathomechanics of injuries across the athlete spectrum but computational modelling can be specifically valuable for coaches and trainers to tailor individual athlete programs for technique optimization, training impact, and strength & conditioning balance. This chapter presents a case study that explores the utility of detailed biomechanical analysis for an individual athlete.

8.1 INTRODUCTION

Assessing the quality of an athlete's performance and facilitating improvement are fundamental coaching paradigms. Coaches and trainers rely on years of experience to visually assess athlete movement and posture in relation to the adoption of aesthetic characteristics that are perceived to represent an idealized style or technique (Kleshnev, 2006b). When athlete movement patterns deviate from the circumscribed style, coaches attempt to manipulate rower technique, through visual and audio cues, to improve performance characteristics such as force magnitude and stroke timing and as such performance. Expert opinion, observational data and qualitative visual analysis are powerful and beneficial in their own rights. However, each lack sufficient information to rigorously quantify and analyze the rowing stroke. Technologies that deliver biofeedback on an athlete's technical ability can lend objective support to supplement the coach's qualitative assessment. Ergometers display limited real-time quantitative feedback such as projected split times (i.e., time per 500 m interval) and power output to the user and while we know that these metrics directly represent higher rowing performance, the quantitative assessment methods described and discussed throughout this thesis sought to answer the question: what biomechanically characterizes a high level of rowing skill.

The UKNSM computational model used in this thesis generated several core outputs for individual athlete assessment, including joint angles, joint forces, contact patterns and muscle forces across the shoulder complex during the rowing stroke. The aim of the work presented in this chapter is to explore the

utility of subject specific biomechanical parameters and translate that into a foundation from which to recommend means to improve an individual's rowing performance.

8.2 ATHLETE BIOFEEDBACK

The most cited standard ergometer performance metric is the "split time", which describes the average time to row 500 meters. It is an immensely important metric in crew selection and team ranking but this singular scalar value fails to capture the "how" and "why" of any ergometer rowing experience. Mechanical power output may be an objective measure, but biomechanical analysis provides much broader and deeper quantitative data that can be incorporated into a biofeedback process intended to assist individual athletes to refine motor skills by linking specific muscle work to movement patterns and timing of force development, to achieve beneficial technique changes.

A translational research objective of this thesis, and a valuable deliverable to external stakeholders, was to generate a performance summary and biofeedback report that was sufficiently detailed yet not overly complex, which could be disseminated to every individual study participant. A summary report was produced following each testing session that could be shared with the athlete (and their coaching staff). The summary report comprised all key performance parameters and was separated into 3 main sections: ergometer scores, performance scores, and biomechanics scores (Figure 8.1). A detailed comments section was included explaining how certain scores were calculated and interpreted, highlighting areas of the athlete's strength and weakness with respect to their technique and performance.

Figure 8.1 is a representative performance report for an individual study participant (male, masters, sculling cohort). The ergometer scores section is comprised solely of data available via the monitoring system built into the Concept 2 ergometer by the manufacturer. For each of the four 3-minute rowing trials during the testing session, average split-time, stroke rate, and distance rowed were recorded (Figure 8.1: Ergometer Scores). A diminishing return in split time and meters rowed as stroke rate increases up to 32 spm was observed, in line with the population means documented in Chapter 5 (Section 5.3.1; Figure 5.11; Table 5.5).

Performance Scores

Step	Catch Slip (sec)	% to Force Generation	Time to Max HF (sec)	% to Max Handle Force	Max Handle Force (N)	% to Max Foot Force	Max Resultant Foot Force (N)	% to Max Seat Force	Max Seat Force (N)	Stroke Length (mm)	% to Finish	Drive Time (sec)	Stroke Time (sec)	Drive:Recovery Ratio
18	0.13	4.2	0.40	12.5	792.4	11.5	1169.1	28.5	941.9	1456.7	31.0	1.00	3.22	2.23
24	0.13	5.3	0.40	16.0	799.7	15.0	1139.6	37.0	960.5	1472.9	38.0	0.94	2.48	1.63
28	0.13	6.4	0.41	19.5	795.6	17.5	1101.6	42.5	1020.7	1474.9	43.0	0.91	2.11	1.33
32	0.14	7.4	0.40	21.5	786.4	17.0	1049.8	46.0	1039.1	1425.4	46.5	0.87	1.87	1.15

Biomechanics Scores

		Seat Force (N)	Suspension (%BW)	Vertical Foot Force (N)	Horizontal Foot Force (N)	Foot Force Asymmetry Vertical	Foot Force Asymmetry Horizontal
Catch	18	224.9	66.3	659.0	143.4	2.6	61.2
	24	136.4	79.6	732.1	255.7	4.4	42.3
	28	99.2	85.1	757.1	302.8	5.3	44.6
	32	81.1	87.8	766.2	343.1	6.1	39.6
MHF	18	0.30	100.0	972.0	632.3	8.3	18.0
	24	0.33	99.9	934.6	626.9	7.5	12.9
	28	0.31	100.0	877.6	603.5	6.6	14.8
	32	9.12	98.6	796.0	600.5	7.5	13.6
Finish	18	887.4	-33.0	-74.5	-112.9	-28.5	-12.1
	24	944.3	-41.6	-90.1	-104.9	-13.7	-5.0
	28	1009.1	-51.3	-97.2	-131.3	-13.8	-2.8
	32	1034.4	-55.1	-108.7	-157.6	-14.9	-6.7

Height 167.6 cm
Weight 667.1 N

Ergometer Scores

Erg Piece	Time	Rate	Meters	Split
Step 18	1:00	18	242	02:03.9
Step 18	2:00	19	250	02:00.0
Step 18	3:00	19	251	01:59.5
Avg/Total		18	742	02:01.2
Step 24	1:00	24	266	01:52.7
Step 24	2:00	24	272	01:50.2
Step 24	3:00	25	273	01:49.8
Avg/Total		24	809	01:51.2
Step 28	1:00	28	281	01:46.7
Step 28	2:00	28	281	01:46.7
Step 28	3:00	28	282	01:46.3
Avg/Total		28	844	01:46.6
Step 32	1:00	31	285	01:45.2
Step 32	2:00	32	288	01:44.1
Step 32	3:00	32	284	01:45.6
Avg/Total		31	857	01:45.0

Comments

Foot force asymmetry values close to zero indicate leg drive is symmetric. Negative values favor left leg and positive values favor right leg. Negative foot force at the finish represent pulling against the shoe restraints, potentially indicating minor loss of connection to the footplate. Catch slip (i.e. the time between change of handle direction and start of force generation) remains the same as rate increases. Suspension above the seat as a percentage of body weight increases with rating at the catch, stays consistent at MHF and weight deposition onto the seat increases at the finish. Center of pressure on the seat is midline on the drive and the recovery, and does not shift as rate increases. Handle position loops show a flat drive and downward draw at the finish. Vertical handle position on the recovery rises as hands move away more quickly and directly with increasing rating. Stroke length decreases at the highest rating as reach into the catch and lean back into the finish decrease. Seat force steadily increases with rating, while handle force output remains consistent. Seat travel (distance from the footplate) has a distinct decrease while the legs are fully extended (i.e. from late-drive, through finish to knees up).

Figure 8.1: Example representative subject performance summary report with specific sections on ergometer monitored scores (*right*), ergometer instrumentation derived performance scores (*top*), biomechanics scores (*left*), and a feedback comments sections (*bottom*) explaining and interpreting various scores.

The performance scores section reports spatio-temporal metrics including maximum values of specific power outputs, displacements, and the relative timing (in % of stroke completion) to reach key stroke moments. Catch slip, or the time between change of handle direction (i.e., stroke start) and beginning of force generation remains the same as rate increases, as does time to reach MHF, but because total stroke time decreases, this represents a relative increase. MHF remains consistent with stroke rate, but MFF decreases, and MSF steadily increases with stroke rate. Total stroke length (i.e., horizontal handle displacement) increases from 18 spm to 28 spm, then decreases to 32 spm (Figure 8.1: Performance Scores).

The biomechanics scores section specifies kinetic values at each of the three key stroke moments: catch, MHF, and the finish. Foot force asymmetry was reported for both vertical and horizontal components. Values close to zero indicate leg drive was symmetric, while negative values favor left leg and positive values favor the right leg. At the finish, negative foot force values indicate pulling against the shoe restraints, potentially indicating a small loss of connection to the footplate. Suspension above the seat as a percentage of body weight increases with rating at the catch and weight deposition onto the seat increases at the finish. The near 100% body weight suspension at MHF is exceptional for any rower. This indicates that this athlete was transferring all their force directly from footplate to handle, with no energy loss into the seat/boat from the catch through MHF (Figure 8.1: Biomechanics Scores). This suspension was maintained until the athlete reaches the late-drive and finish where body weight was quickly returned to the seat applying force that works against horizontal momentum of the boat (Figure 8.1: Biomechanics Scores).

Additional graphs were provided to aid each athlete in visualizing their kinematics and force output. The inverse relationship between total handle force and seat force shows how the athlete develops power and maintains SS through the drive phase (Figure 8.2 - *top*). Maximizing SS (i.e., minimizing seat force) during the early-drive phase is important to achieving an optimal stroke profile (McGregor, Bull & Byng-Maddick, 2004; Cookson *et al.*, 2017). On the recovery, the rate of seat force decline shows how the athlete transfers body weight from the seat back onto the footplate (Figure 8.2 - *top*). Handle position loops show a flat drive and downward draw at the finish (Figure 8.2 - *bottom*). Vertical handle position on the recovery rises as stroke rate increases. The hands move away from the body more quickly and directly at higher speeds, keeping them out of the way of rapid knee flexion occurring. While the performance summary found that total stroke length decreased at the highest rating, the handle position loops show that this was specifically a result of the athlete achieving less reach into the catch and less lean back into the finish (Figure 8.2 - *bottom*).

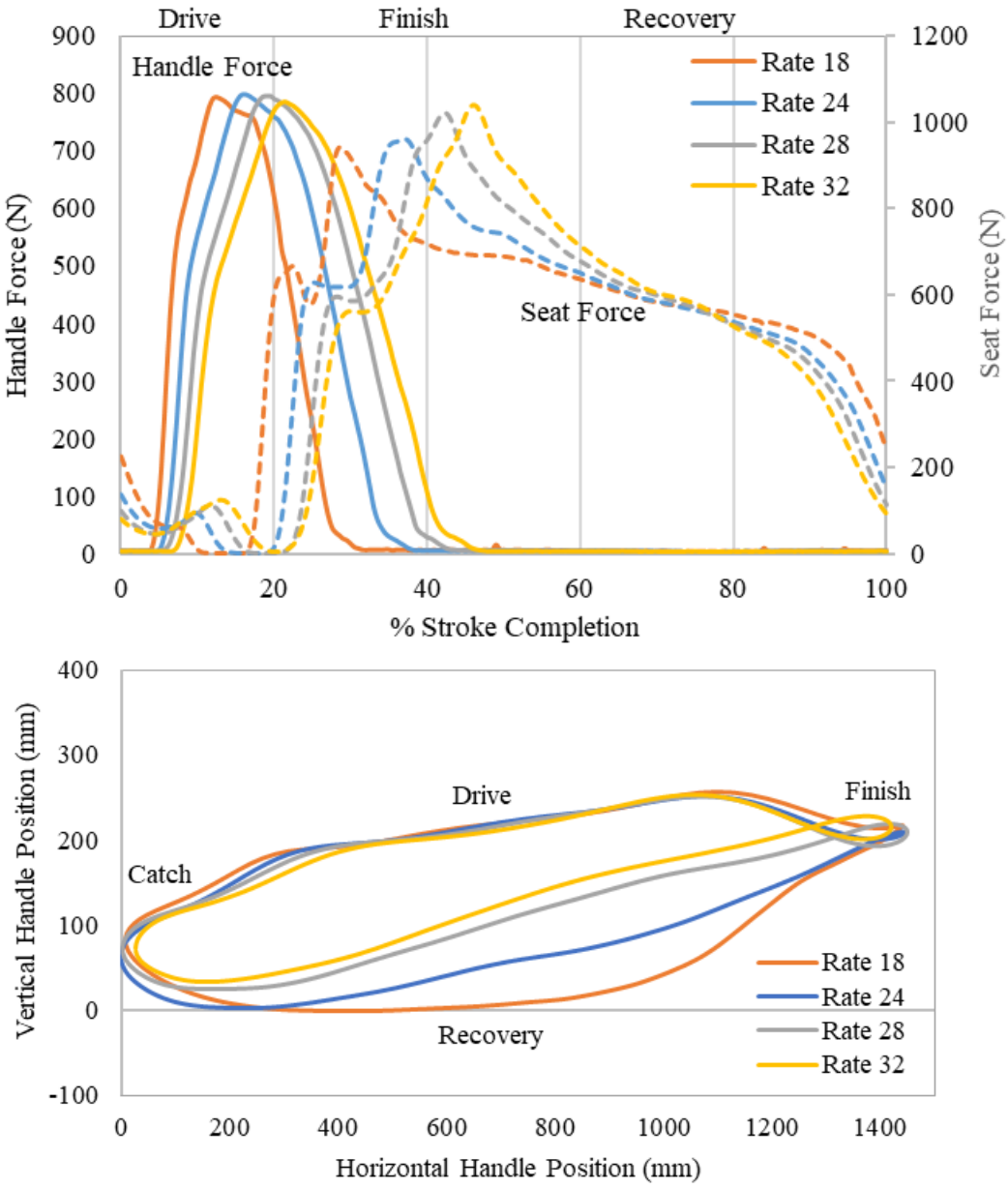

Figure 8.2: Representative athlete's mean handle force and seat force plotted together (*top*) and mean sagittal plane handle position (*bottom*), for each stroke rate with data labels indicating corresponding phase of stroke cycle (*catch, drive, finish, recovery*).

Footplate forces are presented for left and right sides to illustrate bilateral asymmetries in the vertical and horizontal force components (Figure 8.3). This athlete displays very even left/right foot force distribution from the late drive through the entire recovery phase (~ 30-100%). However, from the catch through MHF, this athlete displays both vertical and horizontal force components and foot force ASI that favor their left leg (Figure 8.1: Biomechanics Scores).

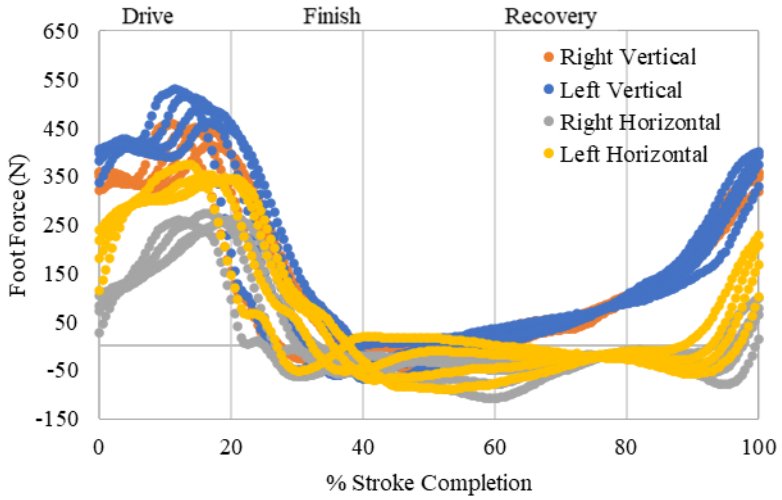

Figure 8.3: Vertical and horizontal foot plate force metrics from a representative subject for their left foot (*orange & gray lines*) and right foot (*blue & yellow lines*).

Seat kinetics and kinematics show that for each trial, center of pressure was well maintained in the middle of the ergometer seat through the drive and recovery phases (Figure 8.4 - *left*), implying that the athlete does not shift their weight side-to-side or favor one side over the other. Nor does the seat center of pressure (CoP) shift posteriorly as stroke rate increases, in contrast to the population average seat CoP shown in Chapter 5 (Section 5.3.1.2; Figure 5.19). Total seat travel (i.e., horizontal distance from the footplate) should reach a maximum when the legs become fully extended and remain plateaued until the knees flex during the middle of the recovery, as seen in the Chapter 5 population average (Section 5.3.1.2; Figure 5.26). However, this athlete shows a distinct decrease in displacement while the legs were fully extended, before reaching the finish, suggesting that as the athlete posteriorly rotates the trunk on the late drive the pelvis over rotates, causing the seat to roll slightly anteriorly (Figure 8.4 - *right*).

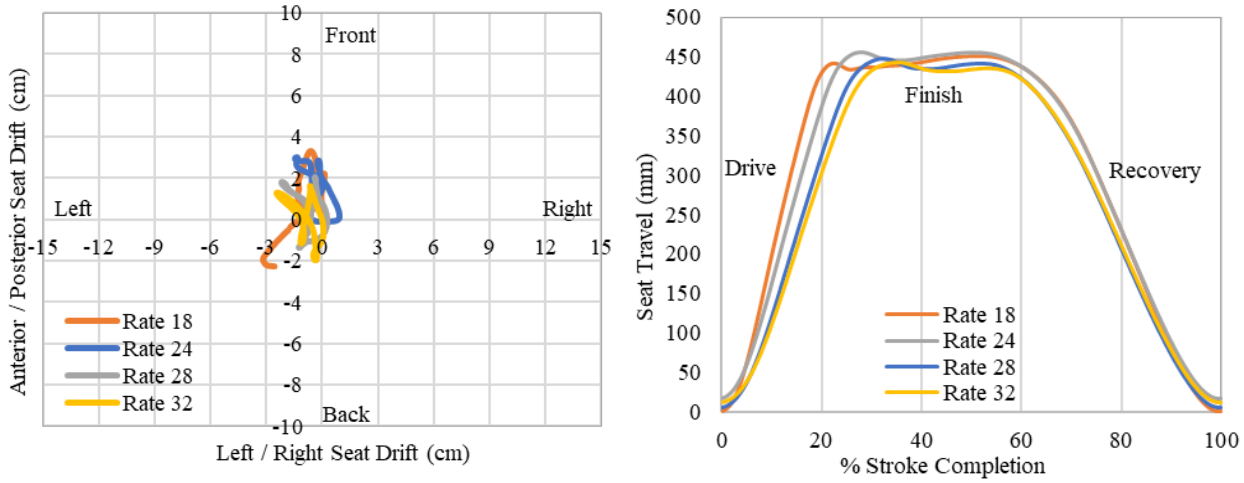

Figure 8.4: Representative athlete's mean seat center of pressure (*left*) and mean sagittal plane seat position (*right*) for each stroke rate, with data labels indicating corresponding phase of stroke cycle (*drive, finish, recovery*).

8.3 Case Study

Illustrating the depth with which computational modelling can enhance interpretation of performance data, is most readily approached in the form of a case study. Here, the case study athlete was a female, club rower with 3 years of experience, a preference for port sided sweep rowing and history of mild back muscle soreness. This athlete was selected as an outlier that deviated from the previously established cross-case population, demonstrating visually observable kinematic asymmetries. As the specific function of this comparison was diagnostic, to better illustrate differences in kinetic and kinematics variables of interest, it was important that the case study athlete and the comparator group subjects share one or more demographic characteristics. Sex differences are a confounding, covariable factor among rowing performance outcomes, therefore male subjects were excluded from the comparator group. All female study subjects for whom computational modelling outputs were generated (n=20), were used to form the comparator group. It was resolved that this comparator group provided a representative cross-section of the total study population and would provide the broadest overall context against which to evaluate performance quality of the case study athlete. Figures presented throughout this section will step from superficial kinematics into deeper biomechanics. Case study athlete biomechanics data will be displayed on the right-hand side of each figure and compared to female population means (± std) displayed on the left-hand side of each figure.

Performance data collected by ergometer instrumentation show several differences between the case study and the female population means (Figure 8.5). Across all stroke rates, the case study athlete displayed a shorter total stroke length (1.35 ± 0.01m vs. 1.50 ± 0.07m), higher MSF (1.31 ± 0.09 N/BW vs. 1.17 ± 0.08 N/BW), and a briefer late-drive duration (15.4 % vs. 20.6% of stroke completion). While the handle force profile has a more triangular shape, the MHF was comparable between the case study athlete (1.02 ±

0.09 N/BW) and the female cohort (1.05 ± 0.18 N/BW). Research has shown that MHF and impulse are related to increased power maintenance on the *drive* and to increased performance (McGregor *et al.*, 2016). While more informative than scalar metrics, force-time profiles alone are unsuited to inferring technique differences.

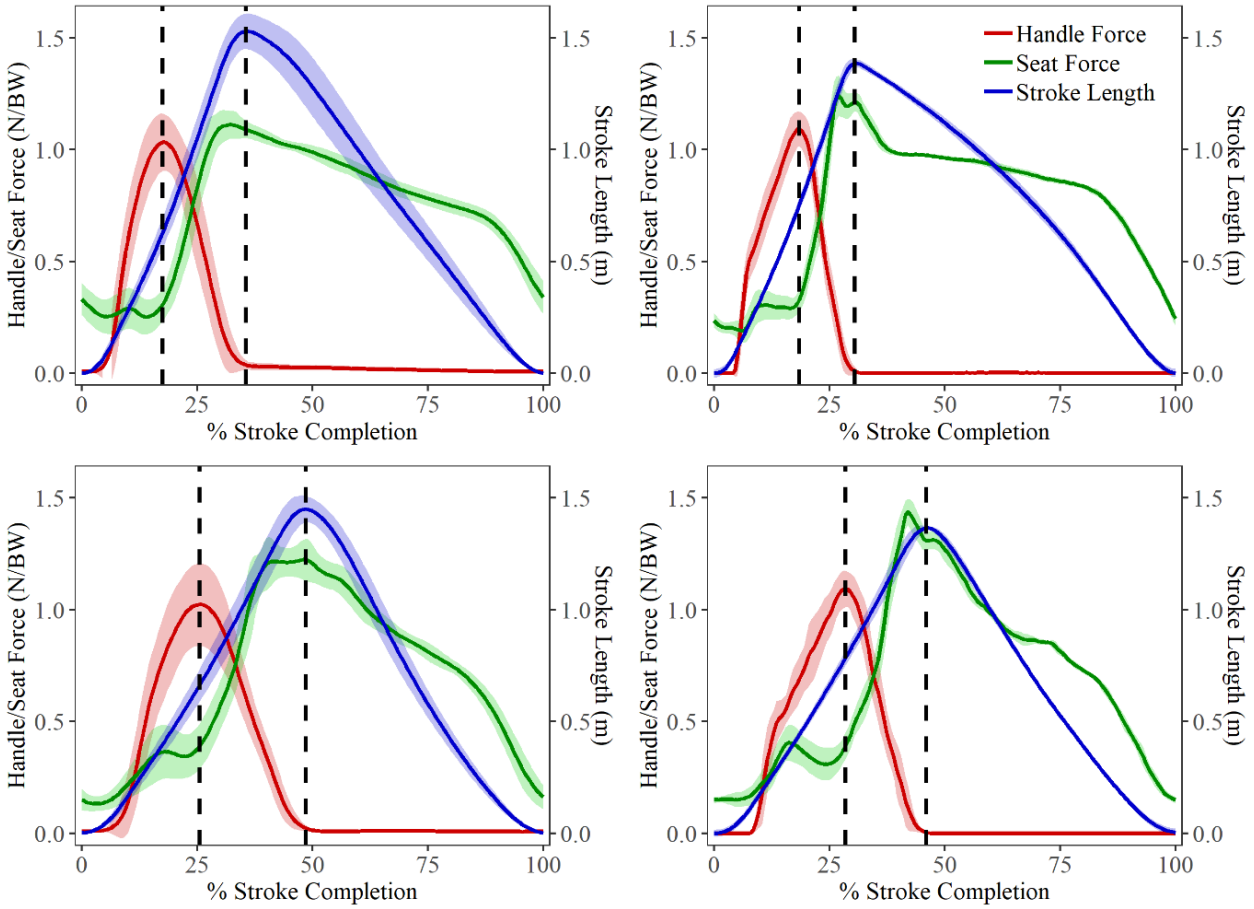

Figure 8.5: Ergometer instrument derived kinetic and kinematic spatio-temporal profiles (mean ± std) at 18 spm (*top row*) and at 32 spm (*bottom row*) for all female study participants (*left*) and case study athlete (*right*).

Inspecting whole-body or body-segment kinematics from virtually reconstructed marker trajectories, qualitative differences can be seen in the case study's movement pattern. This is visualized in Figure 8.6 in comparison to the virtual reconstruction of a representative female athlete (club, 11 years' experience). At the finish position, the case study displays lateral bend of the lumbar and thoracic spine toward the right-side and greater abduction of the right humerus compared to their contralateral (left) arm. In contrast, the representative athlete displays a vertically aligned spine and bilaterally asymmetric abduction of the upper extremities.

Due to the complexity and density of Vicon marker placement during the experimental study series, real-time visualization was limited to unlabeled marker trajectories. However, post-processed video of reconstructed athlete kinematics was provided alongside each performance summary report.

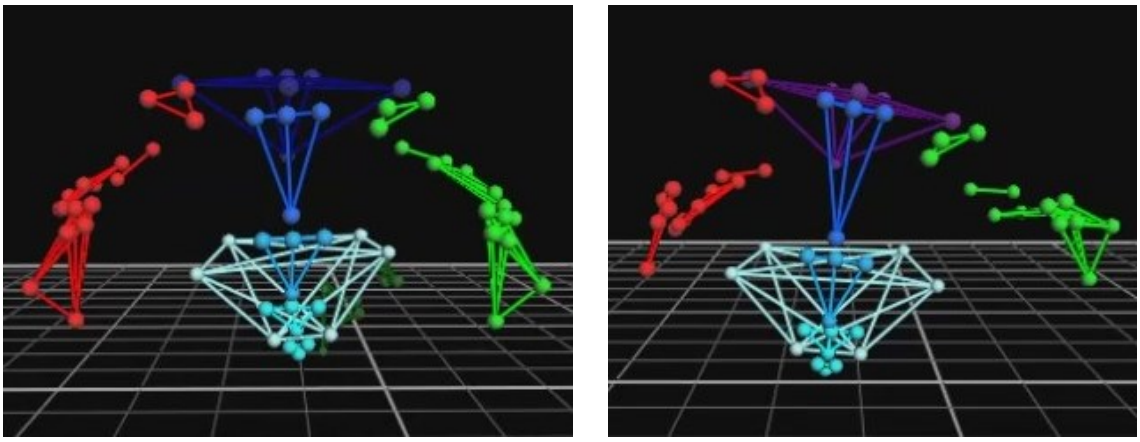

Figure 8.6: Reconstructed Vicon marker kinematics of a representative subject (*left*) and the case study subject (*right*). This illustrates qualitative differences in trunk and upper extremity positioning at the finish position.

The UKNSM computational model can be utilized to delve into body segment dynamics and muscular biomechanics. Qualitative differences in the movement patterns seen above in Figure 8.6, were quantified as disparities in joint motion and range. At the glenohumeral joint, angle profile characteristics were similar, but total range of motion was decreased (Figure 8.7). The case study athlete displays less shoulder flexion at the catch, less internal rotation, and less abduction of the shoulder into and out of the finish. In the wider female athlete population, maximum GH extension, abduction and internal rotation coincide near the finish position (i.e., maximum stroke length), but in the case study, max GH extension and abduction occur after the finish and max GH internal rotation occurs substantially after the finish (Figure 8.7). This may suggest that the athlete can improve trunk and upper extremity sequencing through the late drive.

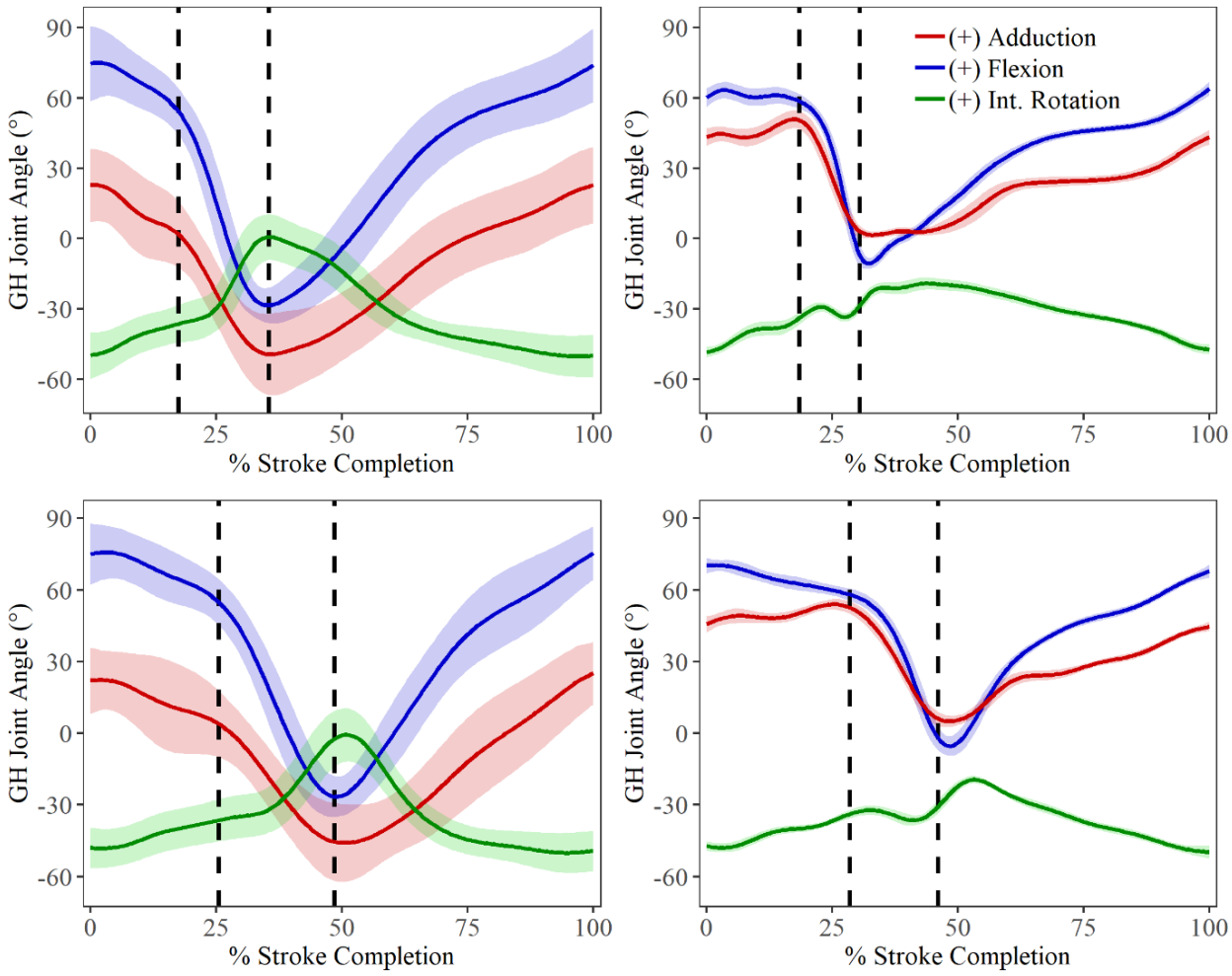

Figure 8.7: Glenohumeral (GH) joint angle kinematics (mean ± std) in the distal reference frame, illustrate kinematic technique variation at 18 spm (*top row*) and at 32 spm (*bottom row*) for all female study participants (*left*) and case study athlete (*right*).

Examining joint contact forces being applied at the shoulder during a single rowing cycle, in neither the case study nor the female cohort, does the contact pattern pass close to glenoid rim (Figure 8.8). In the female cohort, mean center of pressure was mostly constrained to the posterior half of the glenoid socket. The contact pattern moves posterior out of the catch position until MHF, then translates superiorly through the late drive into the finish position. In contrast, the case study athlete displays a more erratic contact pattern with substantially longer total path length at 18 spm (134.0 mm vs. 100.7 mm) and 32 spm (149.6 m vs. 86.2 mm) and (Figure 8.8). Their center of pressure was predominantly oriented in the anterior half of the glenoid socket (Figure 8.8) and at 32 spm showed greater superior/inferior translation (40.5 mm vs. 22.9 mm), demonstrating substantial shear force effects on the glenoid. Both features are considered positions at greater risk of shoulder subluxation (Klemt, 2018). Glenohumeral joint laxity may be a factor,

but this suggests that attention should be paid to training glenohumeral stabilizers for mitigating overuse injuries and ensuring long term shoulder health.

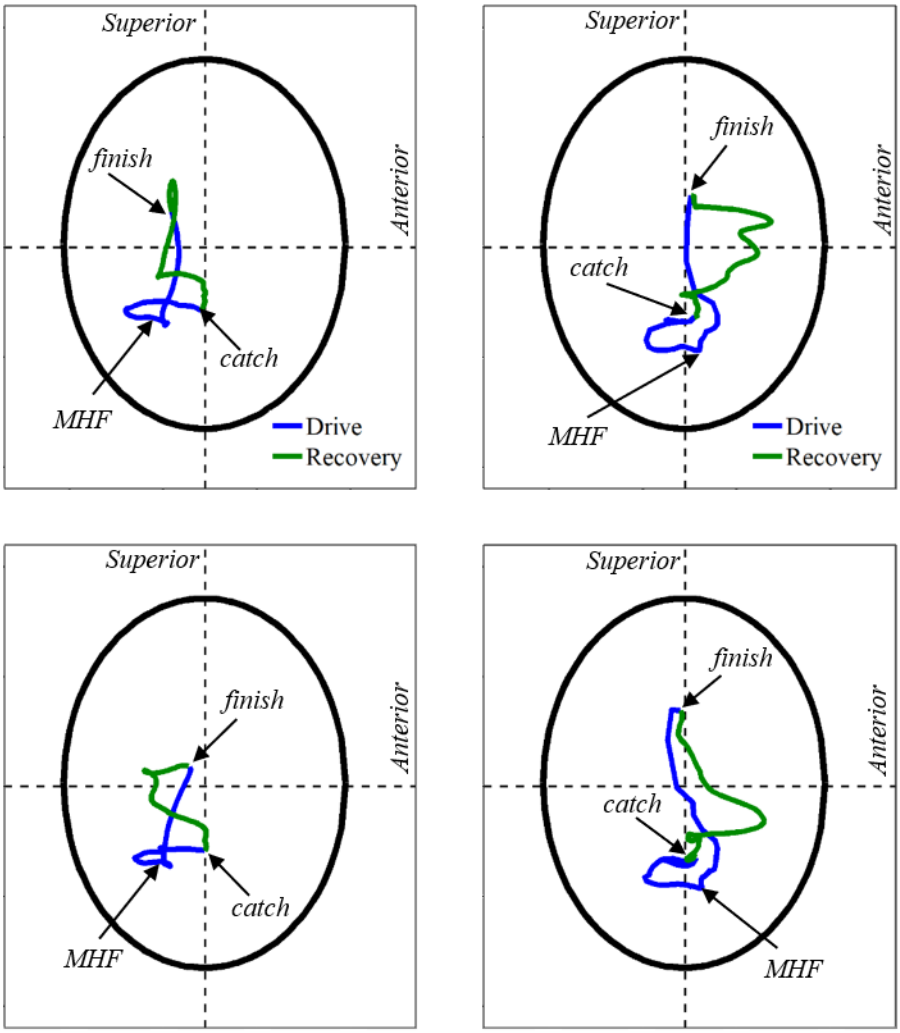

Figure 8.8: Mean glenohumeral contact patterns showing humeral head position against the glenoid fossa at 18 spm (*top row*) and at 32 spm (*bottom row*) for all female study participants (*left*) and case study athlete (*right*). Arrows indicate instantaneous force locus at the catch, max handle force (MHF), and the finish. Black ellipse indicates glenoid rim.

The shoulder stability ratio (SSR) compares shear to compressive forces in the glenohumeral joint and is used by clinicians to describe shoulder pathology risk (Figure 8.9). The case study athlete's stability ratio during the drive phase (0.59 ± 0.02) was quite high but falls within the standard deviation of SSR for the whole female cohort (0.46 ± 0.21). However, it was found that during the recovery phase, where the lowest SSRs are typically observed, the case study athlete reached a maximum SSR of 0.66 ± 0.02, approximately 10% after the finish, substantially higher than the female cohort (Figure 8.9), where a higher ratio signifies less stability (Figure 8.9).

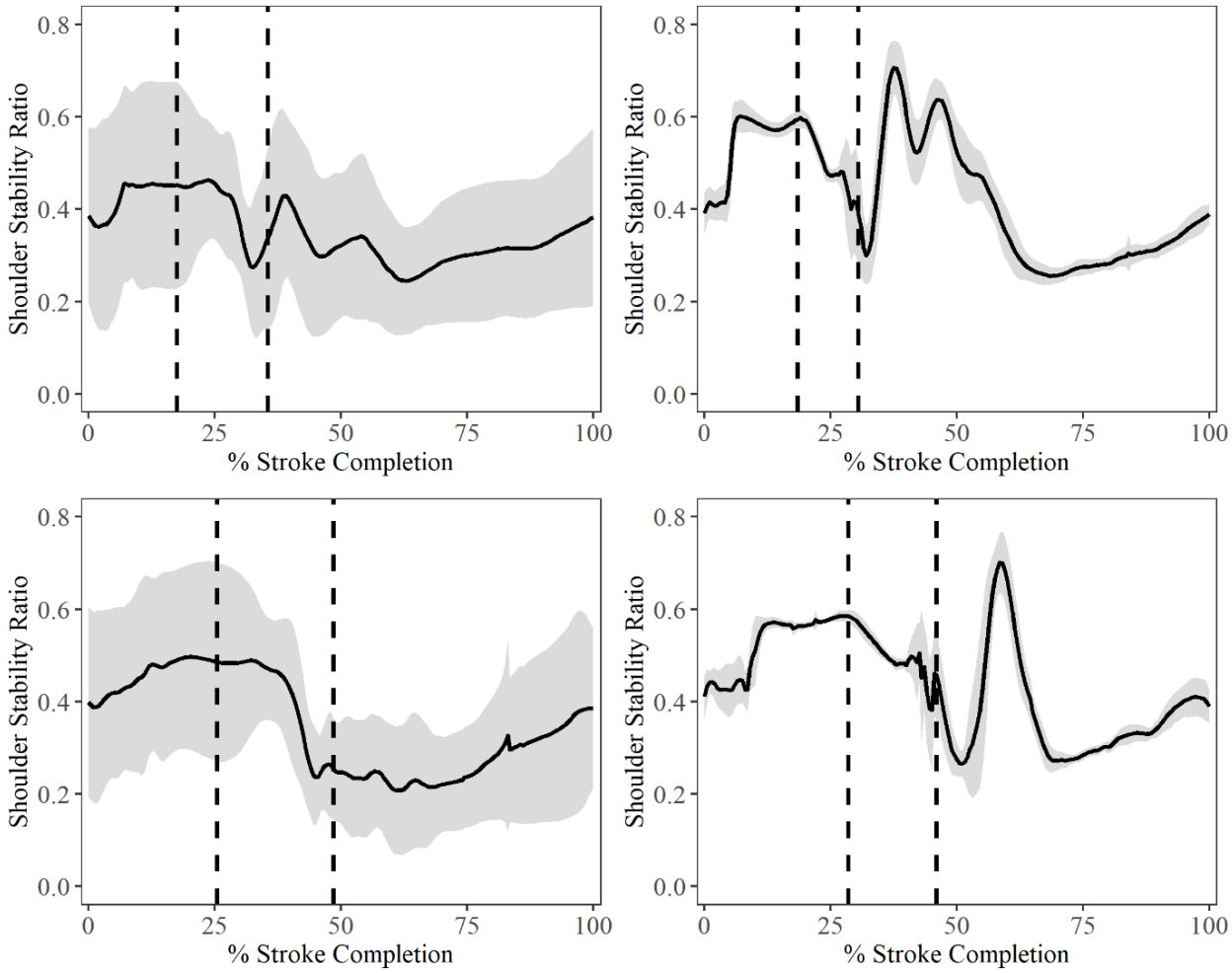

Figure 8.9: Shoulder stability ratio (mean ± std) was similar during the drive phase in the case study (*right*) and female cohort (*left*) but reaches a maximum on the recovery when a low ratio is expected at 18 spm (*top*) and 32 spm (*bottom*).

Looking directly at the components of the glenohumeral joint force (Figure 8.10) that contribute to the shoulder stability ratio and have implications on the glenoid contact pattern, the case study athlete displayed significantly higher maximum compressive GH joint force (9.84 ± 0.87 N/BW) and A/P shear force (-4.71 ± 0.39 N/BW) than the broader female cohort, suggesting that this athlete was working much harder to maintain a similar level of shoulder stability (Figure 8.9). Such forces combined with a variable contact pattern may be indicative of instability that afford a high acute injury risk and have implications for long-term shoulder health.

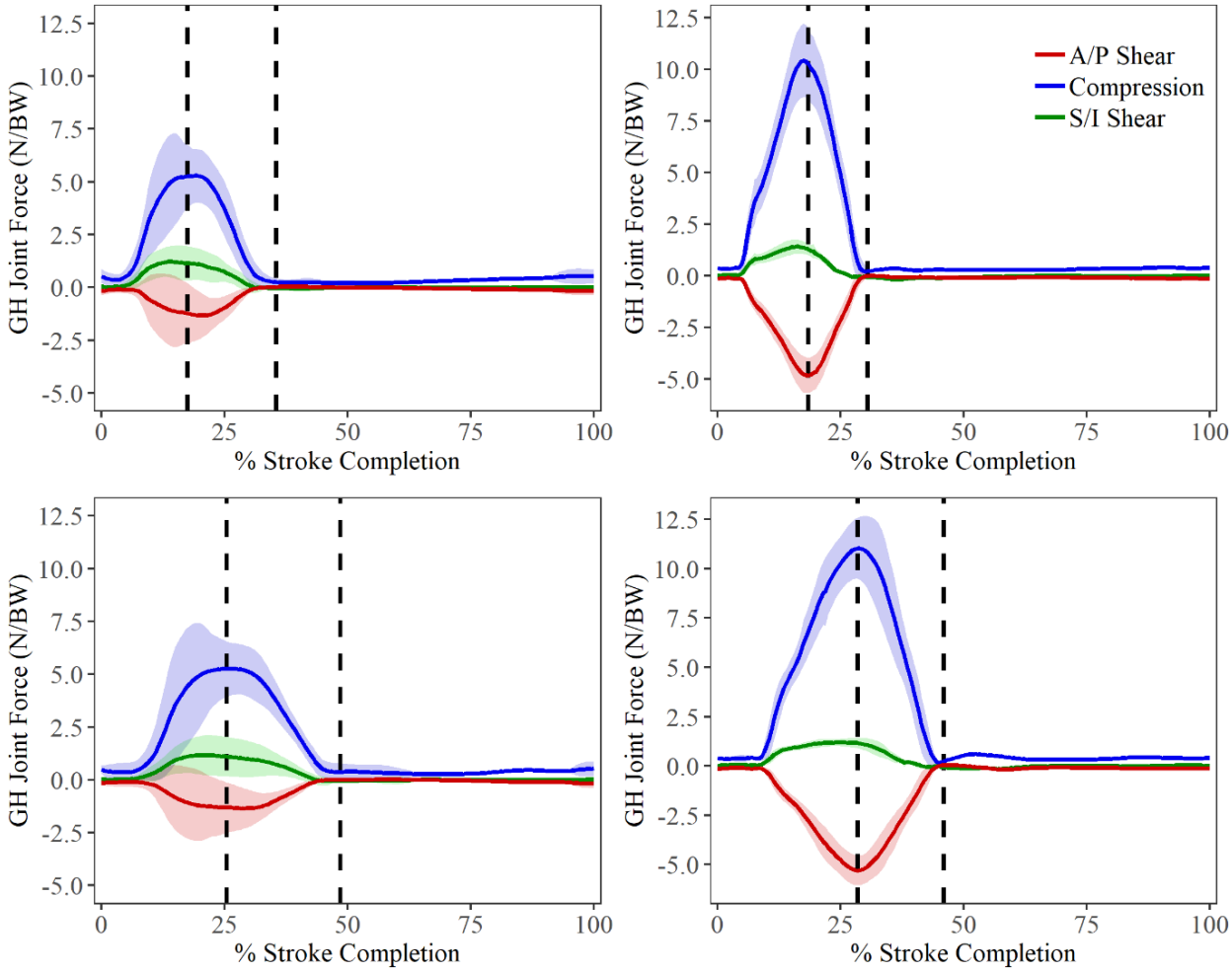

Figure 8.10: Glenohumeral (GH) joint force components in anterior-posterior (A/P) shear, superior-inferior (S/I) shear, and compression (mean ± std) for the female cohort (*left*) and the case study athlete (*right*) at 18 spm (*top*) and 32 spm (*bottom*).

Finally, muscular force differences were examined. In the broad female cohort, when cumulative force was largest, latissimus dorsi and teres major act as prime movers for the upper extremity extension and internal rotation, while deltoid plays a smaller role in abduction and stabilization (Figure 8.11). The rotator cuff muscles in Figure 8.12 show strong force in subscapularis during the late drive phase and relatively quiescent supraspinatus and infraspinatus across the female cohort. The force profiles of the case study athlete show a similar relationship between latissimus dorsi and teres major, but with a much stronger force in deltoid, relative to the larger prime movers (Figure 8.11). Given deltoid's primary function as a humeral abductor, it was unsurprising that the case study also produces higher-than-average force in supraspinatus, which typically works in tandem with deltoid (Figure 8.12). This combination may contribute to the large S/I translation seen in the case study athlete's glenoid contact pattern (Figure 8.8). As was discussed in Chapter 7 (Section 7.4), strong subscapularis contraction is important for centralizing the humeral head and in stabilization during arm acceleration around the finish position. Such a contraction was not seen in the muscle force profile of the case study athlete, which may explain the large A/P translation seen in the case study athlete's glenoid contact pattern (Figure 8.8). Higher-than-average force in infraspinatus during the late drive also reinforces that the rotator cuff muscle was working to prevent anterior humeral head displacement and compensate for reduced force in subscapularis. This could represent a core training focus for this athlete with the scope to enhance both performance and shoulder health, however, such studies are beyond the scope of this thesis.

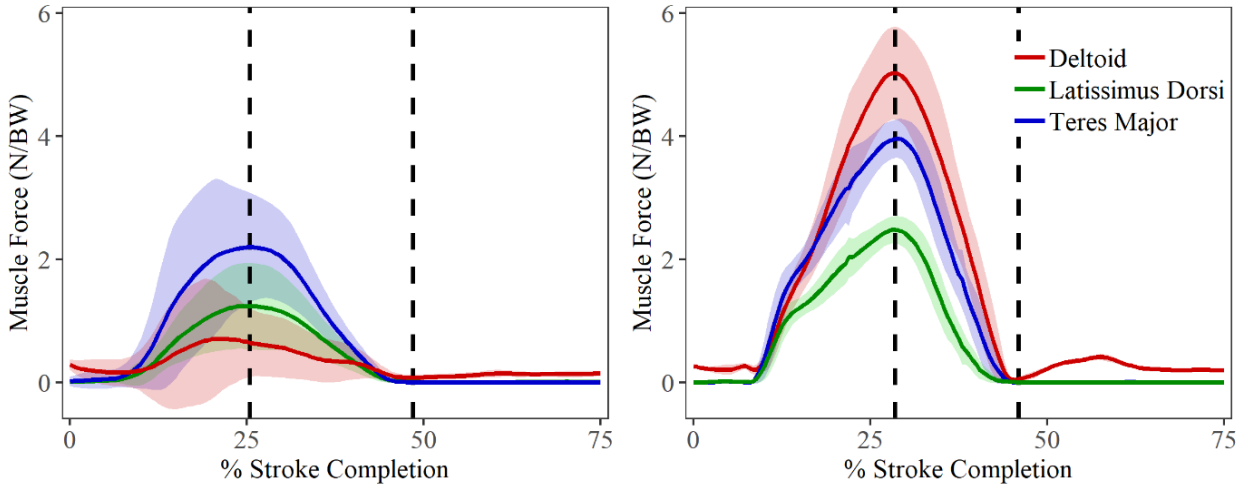

Figure 8.11: Bodyweight normalized muscle force (mean ± std) in trunk and shoulder prime movers at 32 spm for the female cohort (*left*) and case study athlete (*right*). Vertical dashed lines represent relative timing of max handle force (MHF) and the finish, respectively.

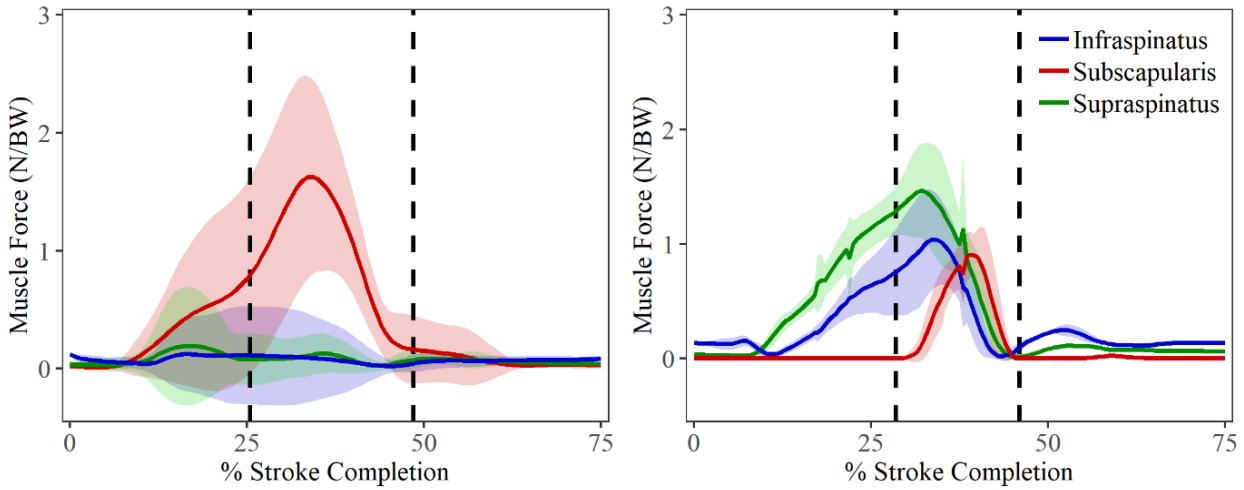

Figure 8.12: Bodyweight normalized force (mean ± std) in rotator cuff muscles at 32 spm for the female cohort (*left*) and case study athlete (*right*). Vertical dashed lines represent relative timing of mac handle force (MHF) and the finish, respectively.

The kinematic inefficiencies observed in this case study arose from variations in muscle mechanics. Higher-than-average force in deltoid and the rotator cuff muscles in the late drive suggest that the athlete was working to compensate for weakness or imbalance in the scapular stabilizers. Although the case study athlete's peak shoulder stability ratio was similar to that of the female cohort, examined in light of their much higher glenohumeral joint compression and anterior/posterior shear forces, this suggests that this athlete was working harder to maintain the same level of shoulder stability. Having identified this athlete's muscle recruitment patterns and linked them to their external kinematics, a strength & conditioning program can be tailored to meet this individual athlete's needs to optimize training impact. Attention should be paid to scapular stabilization and balance in horizontal pulling, to de-emphasize shoulder abduction. This could represent a core training focus for this athlete with the scope to enhance both performance and shoulder health. Such interventions would be difficult to target with the analytical pipeline outlined, highlighting a clear translation of this work to performance and athlete well-being.

8.4 Concluding Remarks

At every level, computational modelling can discriminate differences between athletes; and from kinematics, to dynamics, to muscle load sharing, the more apparent those differences become. Muscle forces drive the variation seen in external movement patterns, impacting joint forces and contact patterns, which have implications for performance and injury risk. This chapter explored the utility of subject specific biomechanical parameters and a database comparison approach to performance evaluation. The preferred movement path selected by each athlete is based on individual constraints, such as strength, injury, or

fatigue. The ability to entrain good habits from a muscular level (i.e., where the athlete should feel the action) can promote consistently higher performance and long-term health.

All athletes could benefit from regular physiological and biomechanical assessments including 3D motion capture methods in tandem with instrumented ergometer or on-water tools. Computational modelling methods are specifically valuable to coaches and trainers when working with teams or individual athletes on technique optimization. There are many contributing factors throughout the kinetic chain and as the rowing biomechanics database grows, it becomes a more robust reflection of athlete populations at large. This establishes a foundation from which to assess the impact of technique choices, to compare against tailored cohort averages, to recommend training schemes, and to provide deeper insights into an individual's performance, particularly ones that cannot be obtained from observation alone.

The value of such extensive athlete biofeedback may be further enhanced when information can be communicated in real-time for the athlete to make training adjustments in the moment. Chapter 10 will provide an overview of the findings of this thesis and recommend applications of MSK modelling broadly to sports biomechanics and discuss future research directions in relation to the specific thesis topic of using biomechanics to define the role of the upper extremity in rowing performance.

9. CHAPTER 9: CONCLUSIONS AND FUTURE DIRECTIONS

The overarching hypothesis for this thesis work was that the upper extremity has a significant role in rowing performance, rowing technique and propensity for injury. This thesis analyzed three-dimensional shoulder biomechanics using computational modelling to develop a kinematic and kinetic description of upper body technique in ergometer rowing. The contributions of the upper extremity to quality of rowing performance were quantified across a wide range of athlete ages and skill levels and biomechanics were used to inform performance benefits and predict injury risk. This chapter summarizes the methodologies and key findings of this thesis and highlights the practical implications and implementations of the work within the broader context of sports performance research. Strengths and limitations of the thesis work are discussed and suggestions for future research directions are proposed.

9.1 SUMMARY OF WORK

An appropriate upper extremity motion capture system was identified and a methodology for whole-body tracking during ergometer rowing was developed using OMC and bespoke ergometer instrumentation. Kinetic and kinematic data were captured for different levels of rowing athletes at various rowing intensities using a progressive fatiguing exercise protocol and used to drive the computational multibody inverse dynamics UKNSM which quantified muscle and joint forces in the upper extremity during ergometer rowing. Biomechanical parameters of the upper extremity that influence whole body movement patterns were identified and interpreted with respect to predicting performance quality and highlighting potential injury risk.

Optical and electromagnetic systems in static and dynamic tracking (Chapter 4) identified the most appropriate motion tracking technology for the measurement of the upper limb and introduced the advantages and limitations of this motion analysis technology when compared to an EM system, commonly used in rowing research. This work demonstrated that OMC could measure established, objective, kinematic and accepted performance metrics used by coaches and athletes related to the spine and lower extremity, and thus will provide backwards and forwards compatibility with EM-derived measures. An extended-range EM system and an OMC system were used to simultaneously record ergometer apparatus and athlete movements during a series of indoor rowing trials. Accuracy and precision of data were compared across systems for static and dynamic kinematics. Both EM and OMC systems demonstrated an ability to track large sagittal plane movements during ergometer rowing. Both, but both systems showed high variance when analyzing small displacements and angles in the frontal and transverse planes. The EM system showed greater RMS error than the OMC system in estimating 3D sensor positions, joint center positions, and angles between lower-limb body segments. Results suggested that lower frame rate and burst

transmission of the EM sensors caused a capture latency between the ergometer and the EM system. However, this capture latency could be corrected for by applying a least squares minimization technique to the recorded data. OMC allows movements of a greater number of body segments to be monitored and analyzed, which suits the proposed study into upper limb kinematics and is thus the more appropriate system to achieve the goal of whole-body kinematic tracking.

Continuing performance analysis and biomechanical feedback in further rowing studies, Chapter 5 detailed the experimental materials and methods for **optical motion tracking of whole-body athlete kinematics and kinetics during ergometer rowing**, including updating essential hardware and software, development of a suitable marker model and optimization of a laboratory camera setup. Spatio-temporal analysis of parameters derived from ergometer instrumentation and paired with kinematic OMC tracking, provide relatively simple but substantial quantitative feedback to athletes and coaches. Outcome measures generated a full description of individual stroke profiles and averages at the catch, MHF, and the finish. Total stroke time, recovery time, and drive-to-recovery ratio all decreased with increasing rate. However, drive time did not change, suggesting there may be a limit to leg extension speed. Catch slip also remained unchanged, representing a larger percentage of stroke completion and a greater factor in energy loss, as rate increases. Significant changes to shape and timing of seat force profiles were found, with increased SS at the catch and decrease at the finish. Changes in relative lower and upper body coordination (based on handle-to-seat displacement) suggested that rowers were more likely to lead with their upper body at higher speeds. Strong correlations among ergometer derived performance parameters such as handle force, footplate force, and seat force create opportunities for instrumentation reduction when considering on-water applications and as simplified surrogates of directly measured athlete kinematics.

In assessing relative motion between athlete body segments at key stroke moments, it was found that **fatigue leads to altered kinematics during high performance ergometer rowing** (Chapter 6). Spinal motion in the transverse and frontal planes had little influence on force output, but changes in sagittal plane spinal rotation suggested deteriorating postural control at the catch as time and stroke rate increased. Relative movement between lumbar and thoracic spine segments showed greater flexion at the catch and neutral alignment at MHF. Decreased stroke length or sagittal handle displacement was associated with alterations in thoracic spinal flexion and lumbar extension, suggesting that increasing fatigue or habituation changes spinal posture. None of the upper limb joints examined (glenohumeral, scapulothoracic, elbow) showed changes in minimum, maximum, or range of joint angle, with increasing stroke rate. However, as stroke rate increased, joint rotations showed changes in timing, relative to the finish, to reach maximum humeral extension, humeral abduction, elbow flexion, scapular external rotation, and scapular posterior tilt. During the drive phase, relative time spent with maximally extended elbows increased with stroke rate and

at the catch, both the elbow joint and glenohumeral joint were slightly flexed, suggesting that the arms need not be fully straightened or strictly perpendicular to the torso during initial loading. This may reduce strain on the arms by avoiding hyperextension. Utilization of a smaller shoulder RoM and maintaining muscular balance of the shoulder stabilizers is more important than striving for increased excursion or stroke length and scapular upward rotation is tied to lower performance output metrics. Quantifying upper extremity kinematics and linking this to underlying muscular sequencing furthers understanding of biomechanical influence in rowing technique and performance.

Comprehensive musculoskeletal **modelling of scapular biomechanics can be used to enhance interpretation of performance data in rowing** (Chapter 7). Muscle forces, joint loading and shoulder stability were compared across stroke rates and athlete sub-populations. Detailed analysis allowed the influence of upper body rowing technique to be determined, by identifying which muscles were important, the timing of their loading, and how force patterns affect joint forces and stability. Ergometer rowing demonstrated substantial shear forces at the glenohumeral joint during the drive phase, with scullers showing significantly higher peak S/I shear than their sweep counterparts and male rowers showing higher A/P shear force and GH compressive force than females. As a function of the joint force components, SSR was affected by position within the stroke but not by stroke rate. Despite the heavy loading, muscular co-contraction and/or GH proprioception during the drive phase, contribute to SSRs comparable to activities of daily living involving an outstretched arm (Klemt, 2018). GH joint stability was linked to translation of the humeral head across the glenoid, caused by shear forces. The resulting contact pattern suggests a stable shoulder position during the rowing stroke, constrained to the posterior half of the glenoid socket and not passing close to the glenoid rim. GH joint force and glenoid contact patterns are quantifiable indicators of risk, to which trainers did not previously have access. The largest muscle forces occur during the drive phase with highest loading of teres major, latissimus dorsi, pectoralis major, serratus anterior, triceps brachii, and subscapularis. Muscle force patterns highlight the importance of the rotator cuff muscles in supporting load transfer across the glenohumeral joint, with infraspinatus supporting the upper limb in forward flexion on the recovery and subscapularis stabilizing the humeral head, in the late drive. Muscle load sharing analysis indicated differential prioritization of scapula stabilizers and prime movers between male and female rowers as well as age-related differences in muscle force distribution, with elite and club athletes recruiting the large trunk muscles, while masters rowers additionally recruited arm accessory muscles. Magnitude and timing of muscle forces influence variation in external movement patterns among athlete cohorts. Understanding shoulder loading during rowing and ergometer rowing is a major step toward improving performance coordination, tailoring individual athlete training programs, and investigating pathomechanics of injuries.

To demonstrate the utility of computational modelling, in performance evaluation, **a case study of athlete feedback with biomechanics** (Chapter 8) presented an example of the quantitative feedback structure that was created and delivered to participating athletes and coaches. The detailed biofeedback provided a fuller picture of rowing technique and allowed enhanced interpretation of an individual athlete's performance data. Visualizing performance helps athletes optimize their technique or achieve specific goals, and understanding biomechanical factors helps coaches assess training program efficacy or implement balanced strength and conditioning. Assessing quality of an athlete's performance and facilitating improvement are fundamental coaching paradigms. As illustrated by the case study, this thesis work has implications for influencing best practices in successful athlete development by using objective biofeedback to link biomechanical performance quality to injury potential and to guide technique optimization.

9.2 STRENGTHS AND LIMITATIONS

The work in this thesis has contributed to our understanding of upper extremity contributions to rowing biomechanics with respect to ergometer performance, injury, and coaching feedback. Strengths of the thesis work stem from the depth and breadth of data collected and the large and diverse athlete population, from which conclusions are generalizable to the broader rowing athlete community. The work quantitatively advances our understanding of complex biomechanical relationships and allows for the prediction of causal links among the parameters measured and the implications with respect to performance quality and injury potential. While this thesis work is specifically applicable to rowing athletes and coaches, it is translatable to trainers and biomechanists studying other athletic activities or working with specialized athlete populations.

However, this thesis work is also limited by experimental choices and recruitment shortcomings. It focused on biomechanical contributions to rowing performance and has not taken into consideration physiological or psychological effects, all of which are fundamental, interrelated components.

Some interesting results were found comparing among athlete cohorts of varying age and competition level. Unfortunately, because of the small sample size in each of the elite, club, and masters cohorts, achieved statistical power was low. Additional athlete testing (particularly for elite rowers) would improve effect size to discriminate differences among cohorts.

Data were collected in a laboratory setting where there were fewer limitations to the instrumentation that could be employed and the biomechanical data that could be acquired than would be the case for on-water rowing. Ergometers are considered an effective training tool that reproduce on-water kinematics to a good degree (Lamb, 1989; Hawkins, 2000; Page & Hawkins, 2003), and are regularly used in training and

performance testing. However, data derived from ergometer rowing cannot be directly translated to on-water rowing performance. Continuing developments in wireless telemetry systems, permitting limited instrumentation to be transferred to boats, may subsequently be correlated to more detailed data acquired in the laboratory.

9.3 FUTURE WORK AND DIRECTIONS

Because the OMC system does not limit the number of body segments monitored simultaneously, the experimental series included kinematic data collection of the whole body. Although most of the work presented in this thesis focused on the upper extremity, an accurate description of bilateral asymmetry of the lower limbs can be pursued (Buckeridge, 2013). Such kinematic measures can be synchronized with footplate and seat kinetic data to drive a lower body MSK model, such as Freebody (Ding *et al.*, 2019) to examine joint and muscle loading asymmetries.

The experimental studies comprising this thesis work were not longitudinal in nature. However, it has been shown in elite athlete cohorts (Murphy, 2009; McGregor, Patankar & Bull, 2007) that specific aspects of elite rowers' technique and performance change with longitudinal training. Yearly periodization typically focuses first on improving strength and cardiovascular fitness, then moves on to technical development and physiological maintenance closer to competition season. Further data collection in repeat assessment sessions from each athlete who participated in the original study could provide longitudinal feedback on coaching interventions and training program efficacy across a much broader range of athletes, outside the international competitive circle.

9.3.1 Hardware and Software Development

The current data acquisition systems for ergometer kinetics and athlete kinematics were manually synchronized but function independently from one another. Important future work would be seamless integration of the data acquisition systems through Vicon DataStream software and directly out to LabVIEW or MATLAB structures (Figure 9.1). System integration paves the way for the possibility of real-time on-screen feedback for athletes and coaches during testing as well as expedient report generation after testing. Extensive athlete biofeedback can be enhanced when information is communicated in real-time for the athlete to make training adjustments in the moment. However, it would necessitate simplifying and reducing the potentially overwhelming amount of data presented.

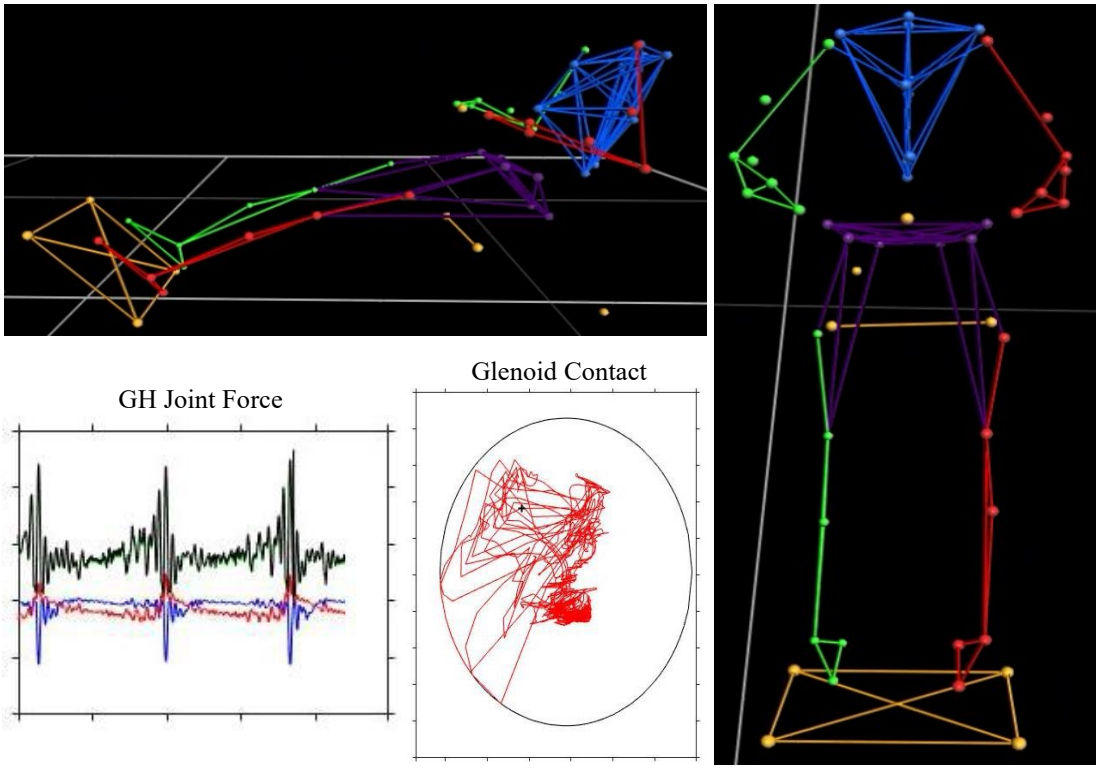

Figure 9.1: Plug-In gait Vicon marker model for potential use in real-time kinematic visualization (*top & right*). Computational modelling output feedback for glenohumeral joint force and glenoid contact pattern (*bottom left*).

While information obtained from traditional ergometer assessments made with high resolution motion tracking systems and high precision force measuring devices should theoretically result in improvements on-water, limitations should be heeded in the translation of research findings. Narrowing the gap between ergometer testing and on-water rowing measurements is an important step in addressing how specific biomechanical relationships observed in the lab change on-water. In the sweep rower, movement patterns are asymmetric, with thoracic rotation and lateral bending. In the upper limb, an anteriorly placed shoulder girdle is exaggerated in the outside arm. To better detail the effects of kinematic asymmetries introduced in sweep rowing, requires the development of an instrumented sweep rowing simulation system and acquisition of athlete kinetics and kinematics (Figure 9.2).

Figure 9.2: Sweep rowing simulation system without bespoke instrumentation (Rowing Innovations© 2018).

9.3.2 Athlete Cohort Expansion

For all rowing athletes, engraining musculoskeletal control improves stroke efficiency and consistency in both the trunk and shoulder (McGregor *et al.*, 2016). Numerous studies, including the work presented in this thesis, have investigated biomechanics of able-bodied rowers, but few have examined adaptive rowing athletes. Adaptive rowing utilizes equipment specially designed to support athletes who may only make use of their trunk and upper extremity to create boat velocity (Figure 9.3). A side-effect of adaptive rowing set-up constraints, which may include a waist or chest strap, is that athletes have higher rates of shoulder injuries (Smoljanovic *et al.*, 2013; Thornton *et al.*, 2017b). Research has found that able-bodied athletes using the PR2 and PR1 adaptive rowing set-ups were more prone to extreme ranges of motion for lumbar flexion, elbow flexion and shoulder abduction at the catch and finish positions (Cutler *et al.*, 2017). Upper limb performance and injury risk metrics may be intensified in para-rowing classifications. Investigating relevant biomechanical parameters in adaptive rowing athletes is an important step in identifying mechanisms of injury and can help promote implementing the safest training programs for these athletes and their coaches.

Figure 9.3: Trunk-arms (PR1) para-rowing athlete at the catch position during a competitive sprint race.

9.4 CONCLUSIONS & RESEARCH CONTRIBUTIONS

The upper extremity plays a significant role in rowing performance, rowing technique and propensity for injury. Understanding how muscle and joint forces correspond to traditional kinematic and power metrics offers a deeper context for optimizing rowing technique. Muscle forces drive the variation that we see in external movement patterns, indicated by differences in glenohumeral joint forces, contact patterns, and shoulder stability ratio. Over many cycles, these force production differences may have implications for performance and injury risk. When evaluated alongside ergometer-derived power metrics, biomechanics parameters derived from computational modelling have value in allowing us to look for trends across athlete cohorts, and at an individual level offers insight to evaluate and improve performance. Detailed quantitative feedback that translates what a dynamic movement should feel and look like can help athletes achieve a specific performance output or engrain a beneficial technique modification. Key contributions of the work contained in this thesis include:

- Development of a methodology using computational modelling, OMC, and ergometer instrumentation, backwards compatible with other EM rowing studies, to build a biomechanical model of the upper extremity during rowing, which was used to quantify its performance contributions in a large population of rowing athletes.
- Descriptions of kinematic parameters of the upper extremity which influence whole body movement patterns, and how these parameters change in response to variation in rowing speed and intensity, which has the potential to inform performance benefits and predict injury risk.
- Descriptions of the muscle and joint forces experienced in the upper extremity during ergometer rowing, and how these forces differ amongst different groups of rowing athletes, which can influence athlete development and guide technique optimization.
- Delivery of a quantitative biofeedback structure to athletes and coaches addressing influential parameters identified from computational modelling to enhance interpretation of performance metrics in biomechanical context and provide future translation of this work to sport.

There are many ways in which remaining research questions and newly presented research questions arising from the work in this thesis can be answered: through epidemiological studies, more detailed case study series, descriptive laboratory studies using invasive measures such as fine wire EMG to directly examine muscle activation during ergometer rowing. All of these are exciting and valuable potential future research directions that further cement a place for the research findings in this thesis within the broader context of rowing performance.

REFERENCES

Abbot, A. & Hannafin, J. (2001) Stress Fracture of the Clavicle in a Female Lightweight Rower A Case Report and Review of the Literature. *The American journal of sports medicine*. [Online] 29 (3), 370–372. Available from: doi:10.1177/03635465010290032001.

Ackland, D.C., Pak, P., Richardson, M. & Pandy, M.G. (2008) Moment arms of the muscles crossing the anatomical shoulder. *Journal of Anatomy*. [Online] 213 (4), 383–390. Available from: doi:10.1111/j.1469-7580.2008.00965.x.

Ackland, D.C. & Pandy, M.G. (2009) Lines of action and stabilizing potential of the shoulder musculature. *Journal of Anatomy*. [Online] 215 (2), 184–197. Available from: doi:10.1111/j.1469-7580.2009.01090.x.

Adesida, Y., Papi, E. & McGregor, A.H. (2019) Exploring the Role of Wearable Technology in Sport Kinematics and Kinetics: A Systematic Review. *Sensors*. [Online] 19 (7). Available from: doi:10.3390/s19071597.

Alijanpour, E., Abbasi, A., Needham, R.A. & Naemi, R. (2021) Spine and pelvis coordination variability in rowers with and without chronic low back pain during rowing. *Journal of Biomechanics*. [Online] 120, 110356. Available from: doi:10.1016/j.jbiomech.2021.110356.

van Andel, C., van Hutten, K., Eversdijk, M., Veeger, D., et al. (2009) Recording scapular motion using an acromion marker cluster. *Gait and Posture*. [Online] 29 (1), 123–128. Available from: doi:10.1016/j.gaitpost.2008.07.012.

Armstrong, S. & Nokes, L.D. (2017) Sensor node acceleration signatures and electromyography in synchronisation and sequencing analysis in sports: A rowing perspective. *Proceedings of the Institution of Mechanical Engineers, Part P: Journal of Sports Engineering and Technology*. [Online] 231 (4), 253–261. Available from: doi:10.1177/1754337116667204.

Arumugam, S., Ayyadurai, P., Perumal, S., Janani, G., et al. (2020) Rowing Injuries in Elite Athletes: A Review of Incidence with Risk Factors and the Role of Biomechanics in Its Management. *Indian Journal of Orthopaedics*. [Online] 54 (3), 246–255. Available from: doi:10.1007/s43465-020-00044-3.

Ascension Technology Corp. (2000) *Flock of Birds Real-time Motion Tracking*.

Attenborough, A.S., Smith, R.M. & Sinclair, P.J. (2012) Effect of gender and stroke rate on joint power characteristics of the upper extremity during simulated rowing. *Journal of Sports Sciences*. [Online]

30 (5), 449–458. Available from: doi:10.1080/02640414.2011.616949.

Barnett, N.D., Duncan, R.D. & Johnson, G.R. (1999) The measurement of three dimensional scapulohumeral kinematics--a study of reliability. *Clinical Biomechanics*. [Online] 14 (4), 287–290. Available from: doi:10.1016/S0268-0033(98)00106-5.

Barrett, R.S. & Manning, J.M. (2004) Rowing: Relationships between rigging set-up, Anthropometry, physical capacity, Rowing kinematics and Rowing performance. *Sports Biomechanics*. [Online] 3 (2), 221–235. Available from: doi:10.1080/14763140408522842.

Baudouin, A. & Hawkins, D. (2004) Investigation of biomechanical factors affecting rowing performance. *Journal of Biomechanics*. [Online] 37 (7), 969–976. Available from: doi:10.1016/j.jbiomech.2003.11.011.

Baudouin, A. & Hawkins, D.A. (2002) A biomechanical review of factors affecting rowing performance. *British Journal of Sports Medicine*. [Online] 36 (6), 396–402. Available from: doi:10.1136/bjsm.36.6.396.

Bazzucchi, I., Sbriccoli, P., Nicolò, A., Passerini, A., et al. (2013) Cardio-respiratory and electromyographic responses to ergometer and on-water rowing in elite rowers. *European Journal of Applied Physiology*. [Online] 113 (5), 1271–1277. Available from: doi:10.1007/s00421-012-2550-2.

Bell, G., Bennett, J., Reynolds, W., Syrotuik, D., et al. (2013) A Physiological and Kinematic Comparison of two Different Lean Back Positions During Stationary Rowing on a Concept II Machine. *Journal of human kinetics*. [Online] 37 (June), 99–108. Available from: doi:10.2478/hukin-2013-0030.

Benson, A., Abendroth, J., King, D. & Swensen, T. (2011) Comparison of rowing on a concept 2 stationary and dynamic ergometer. *Journal of Sports Science and Medicine*. 10 (2), 267–273.

Bey, M.J., Kline, S.K., Zauel, R., Kolowich, P.A., et al. (2010) In vivo measurement of glenohumeral joint contact patterns. *EURASIP Journal of Advanced Signal Processing*. [Online] Available from: doi:10.1155/2010/162136.In.

Bingul, B.M., Bulgan, C., Aydin, M., Buyukderirtis, T., et al. (2014) Two-Dimensional Kinematic Analysis of Catch and Finish Positions During a 2000M Rowing Ergometer Time Trial. *South African Journal for Research in Sport, Physical Education & Recreation*. 36 (3), 1–10.

Boland, A.L. & Hosea, T.M. (1994) Injuries in rowing. *Clinical Practice of Sports Injury Prevention and Care*. 5, 624–632.

Bompa, T. (1980) Technique and muscle force. *Canadien Journal of Applied Sports Science*. 5 (4), 245–

249.

Bompa, T.O., Borms, J. & Hebbelinck, M. (1990) Mechanical efficiency of the elbow flexors in rowing. *American Journal of Physical Medicine and Rehabilitation*. [Online] 69 (3), 140–143. Available from: doi:10.1097/00002060-199006000-00008.

Bompa, T.O., Hebbelinck, M. & Van Gheluwe, B. (1985) Force analysis of the rowing stroke employing two differing oar grips. *Canadian Journal of Applied Sport Sciences*. [Online] 10 (2), 64–67. Available from: http://europepmc.org/abstract/MED/4017153.

Borgia, B., Radzak, K.N. & Freedman Silvernail, J. (2021) Similarities in joint stiffness across footwear conditions in younger and masters-aged runners. *Footwear Science*. [Online] 1–11. Available from: doi:10.1080/19424280.2021.1906331.

British Rowing (2016) *Why Row?* [Online]. 2016. Available from: https://www.britishrowing.org/go-rowing/why-row/ [Accessed: 1 February 2018].

Buckeridge, E. (2013) *Biomechanical asymmetries and joint loading in elite rowers*. PhD Thesis. [Online] Imperial College London. Available from: https://doi.org/10.25560/28699

Buckeridge, E., Hislop, S., Bull, A. & McGregor, A. (2012) Kinematic asymmetries of the lower limbs during ergometer rowing. *Medicine and Science in Sports and Exercise*. [Online] 44 (11), 2147–2153. Available from: doi:10.1249/MSS.0b013e3182625231.

Buckeridge, E.M., Bull, A.M.J. & Mcgregor, A.H. (2015) Biomechanical determinants of elite rowing technique and performance. *Scandinavian Journal of Medicine and Science in Sports*. [Online] 25 (2), e176–e183. Available from: doi:10.1111/sms.12264.

Buckeridge, E.M., Bull, A.M.J. & McGregor, A.H. (2016) Incremental training intensities increases loads on the lower back of elite female rowers. *Journal of sports sciences*. [Online] 34 (4), 369–378. Available from: doi:10.1080/02640414.2015.1056821.

Bull, A.M., Berkshire, F.H. & Amis, A.A. (1998) Accuracy of an electromagnetic measurement device and application to the measurement and description of knee joint motion. *Proc Inst Mech Eng [H]*. [Online] 212 (5), 347–355. Available from: doi:10.1243/0954411981534123.

Bull, A.M.J., Holt, P.J., Wragg, P. & McGregor, A.H. (2004) Validation of the Use of a Skin-Mounted Device To Measure Out-of-Plane Rotations of the Spine for a Rowing Activity. *Journal of Musculoskeletal Research*. [Online] 8 (2/3), 129–132. Available from: doi:10.1142/S0218957704001296.

Bull, A.M.J. & McGregor, A.H. (2000) Measuring spinal motion in rowers: The use of an

electromagnetic device. *Clinical Biomechanics*. [Online] 15 (10), 772–776. Available from: doi:10.1016/S0268-0033(00)00043-7.

Caldwell, J.S., McNair, P.J. & Williams, M. (2003) The effects of repetitive motion on lumbar flexion and erector spinae muscle activity in rowers. *Clinical Biomechanics*. [Online] 18 (8), 704–711. Available from: doi:10.1016/S0268-0033(03)00117-7.

Camomilla, V., Cereatti, A., Vannozzi, G. & Cappozzo, A. (2006) An optimized protocol for hip joint centre determination using the functional method. *Journal of Biomechanics*. [Online] 39 (6), 1096–1106. Available from: doi:10.1016/j.jbiomech.2005.02.008.

de Campos Mello, F., de Moraes Bertuzzi, R.C., Grangeiro, P.M. & Franchini, E. (2009) Energy systems contributions in 2,000 m race simulation: a comparison among rowing ergometers and water. *European Journal of Applied Physiology*. [Online] 107 (5), 615. Available from: doi:10.1007/s00421-009-1172-9.

Caplan, N. & Gardner, T. (2010) The influence of stretcher height on posture in ergometer rowing. *European Journal of Sport Science*. [Online] 10 (4), 263–268. Available from: doi:10.1080/17461390903487545.

Cappozzo, A., Della Croce, U., Leardini, A. & Chiari, L. (2005) Human movement analysis using stereophotogrammetry. Part 1: Theoretical background. *Gait and Posture*. [Online] 21 (2), 186–196. Available from: doi:10.1016/j.gaitpost.2004.01.010.

Cerne, T., Kamnik, R. & Munih, M. (2011) The measurement setup for real-time biomechanical analysis of rowing on an ergometer. *Journal of the International Measurement Confederation*. [Online] 44 (10), 1819–1827. Available from: doi:10.1016/j.measurement.2011.09.006.

Cerne, T., Kamnik, R., Vesnicer, B., Žganec Gros, J., et al. (2013) Differences between elite, junior and non-rowers in kinematic and kinetic parameters during ergometer rowing. *Human Movement Science*. [Online] 32 (4), 691–707. Available from: doi:10.1016/j.humov.2012.11.006.

CFCF (2014) *Anatomical planes*. [Online]. Available from: https://commons.wikimedia.org/wiki/File:Anatomical_Planes.svg.

Charlton, I.W. (2003) *Musculoskeletal modelling of the shoulder*. PhD Thesis. Newcastle Univiersity.

Charlton, I.W. & Johnson, G.R. (2006) A model for the prediction of the forces at the glenohumeral joint. *Proceedings of the Institution of Mechanical Engineers, Part H: Journal of Engineering in Medicine*. [Online] 220 (8), 801–812. Available from: doi:10.1243/09544119JEIM147.

Concept 2 (2006) *Indoor Rower Product Manual*. p.32.

Consiglieri, L. & Pires, E.B. (2009) An analytical model for the ergometer rowing: Inverse multibody dynamics analysis. *Computer Methods in Biomechanics and Biomedical Engineering*. [Online] 12 (4), 469–479. Available from: doi:10.1080/10255840802687400.

Cookson, P., Morrow, A., Nolte, V. & Spracklen, M. (2017) *Rowing technique: Movement patterns in sweep and sculling technique in canada*. [Online] Available from: https://rowingcanada.org/uploads/2020/11/Canadian-Rowing-Model-Technique_FINAL.pdf

Corazza, S., Mündermann, L., Gambaretto, E., Ferrigno, G., et al. (2010) Markerless Motion Capture through Visual Hull, Articulated ICP and Subject Specific Model Generation. *International Journal of Computer Vision*. [Online] 87 (1–2), 156–169. Available from: doi:10.1007/s11263-009-0284-3.

Cortes, N., Onate, J. & Morrison, S. (2014) Differential effects of fatigue on movement variability. *Gait and Posture*. [Online] 39 (3), 888–893. Available from: doi:10.1016/j.gaitpost.2013.11.020.

Cutler, B., Eger, T., Merritt, T. & Godwin, A. (2017) Comparing para-rowing set-ups on an ergometer using kinematic movement patterns of able-bodied rowers. *Journal of Sports Sciences*. [Online] 35 (8), 777–783. Available from: doi:10.1080/02640414.2016.1189587.

Dal Maso, F., Raison, M., Lundberg, A., Arndt, A., et al. (2014) Coupling between 3D displacements and rotations at the glenohumeral joint during dynamic tasks in healthy participants. *Clinical Biomechanics*. [Online] 29 (9), 1048–1055. Available from: doi:10.1016/j.clinbiomech.2014.08.006.

Damsgaard, M., Rasmussen, J., Christensen, S.T., Surma, E., et al. (2006) Analysis of musculoskeletal systems in the AnyBody Modeling System. *Simulation Modelling Practice and Theory*. [Online] 14 (8), 1100–1111. Available from: doi:10.1016/j.simpat.2006.09.001.

Ding, Z., Tsang, C.K., Nolte, D., Kedgley, A.E., et al. (2019) Improving Musculoskeletal Model Scaling Using an Anatomical Atlas: The Importance of Gender and Anthropometric Similarity to Quantify Joint Reaction Forces. *IEEE Transactions on Biomedical Engineering*. [Online] 66 (12), 3444–3456. Available from: doi:10.1109/TBME.2019.2905956.

Eichinger, J.K., Massimini, D.F., Kim, J. & Higgins, L.D. (2016) Biomechanical Evaluation of Glenoid Version and Dislocation Direction on the Influence of Anterior Shoulder Instability and Development of Hill-Sachs Lesions. *The American journal of sports medicine*. [Online] 44 (11), 2792–2799. Available from: doi:10.1177/0363546516659281.

Eiter, T. & Mannila, H. (1994) Computing discrete Fréchet distance. *CD-TR 94/64*. [Online]. Available from: http://citeseerx.ist.psu.edu/viewdoc/download?doi=10.1.1.90.937&rep=rep1&type=pdf.

Ellenbecker, T.S. & Davies, G.J. (2001) *Closed Kinetic Chain Exercise: A Comprehensive Guide to*

Multiple Joint Exercise. Leeds. Human Kinetics.

Evans, G. & Redgrave, A. (2016) Great Britain Rowing Team Guideline for Diagnosis and Management of Rib Stress Injury: Part 2 – The Guideline itself. *British Journal of Sports Medicine*. [Online] 50 (5), 270–272. Available from: doi:10.1136/bjsports-2015-095928.

Fayad, F., Roby-Brami, A., Yazbeck, C., Hanneton, S., et al. (2008) Three-dimensional scapular kinematics and scapulohumeral rhythm in patients with glenohumeral osteoarthritis or frozen shoulder. *Journal of Biomechanics*. [Online] 41 (2), 326–332. Available from: doi:10.1016/j.jbiomech.2007.09.004.

Fedorowich, L., Emery, K., Gervasi, B. & Côté, J.N. (2013) Gender differences in neck/shoulder muscular patterns in response to repetitive motion induced fatigue. *Journal of Electromyography and Kinesiology*. [Online] 23 (5), 1183–1189. Available from: doi:10.1016/j.jelekin.2013.06.005.

Fleming, N., Donne, B. & Mahony, N. (2014) A comparison of electromyography and stroke kinematics during ergometer and on-water rowing. *Journal of Sports Sciences*. [Online] 32 (12), 1127–1138. Available from: doi:10.1080/02640414.2014.886128.

Fothergill, S. (2010) Examining the effect of real-time visual feedback on the quality of rowing technique. *Procedia Engineering*. [Online] 2 (2), 3083–3088. Available from: doi:10.1016/j.proeng.2010.04.115.

Franz, A.M., Haidegger, T., Birkfellner, W., Cleary, K., et al. (2014) Electromagnetic tracking in medicine -A review of technology, validation, and applications. *IEEE Transactions on Medical Imaging*. [Online] 33 (8), 1702–1725. Available from: doi:10.1109/TMI.2014.2321777.

Fukunaga, T., Matsuo, A., Yamamoto, K. & Asami, T. (1986) Applied Physiology Mechanical efficiency in rowing. *European Journal of Applied Physiology*. 55, 471–475.

Garling, E.H., Kaptein, B.L., Mertens, B., Barendregt, W., et al. (2007) Soft-tissue artefact assessment during step-up using fluoroscopy and skin-mounted markers. *Journal of Biomechanics*. [Online] 40 (SUPPL. 1), 18–24. Available from: doi:10.1016/j.jbiomech.2007.03.003.

Gatti, C.J., Dickerson, C.R., Chadwick, E.K., Mell, A.G., et al. (2007) Comparison of model-predicted and measured moment arms for the rotator cuff muscles. *Clinical Biomechanics*. [Online] 22 (6), 639–644. Available from: doi:doi:10.1016/j.clinbiomech.2007.02.001.

Get Body Smart (2021) *Upper Limb Bones*. [Online]. Available from: https://www.getbodysmart.com/upper-limb-bones.

Glossop, N.D. (2009) Advantages of optical compared with electromagnetic tracking. *Journal of Bone*

and Joint Surgery - Series A. [Online] 91 (SUPPL. 1), 23–28. Available from: doi:10.2106/JBJS.H.01362.

Green, R.A.R. & Wilson, D.J. (2000) A pilot study using magnetic resonance imaging to determine the pattern of muscle group recruitment by rowers with different levels of experience. *Skeletal Radiology*. [Online] 29 (4), 196–203. Available from: doi:10.1007/s002560050593.

Greene, A.J., Sinclair, P.J., Dickson, M.H., Colloud, F., et al. (2013) The effect of ergometer design on rowing stroke mechanics. *Scandinavian Journal of Medicine and Science in Sports*. [Online] 23 (4), 468–477. Available from: doi:10.1111/j.1600-0838.2011.01404.x.

Hagerman, F.C. (1984) Applied Physiology of Rowing. *Sports Medicine: An International Journal of Applied Medicine and Science in Sport and Exercise*. [Online]. 1 (4) pp.303–326. Available from: doi:10.2165/00007256-198401040-00005.

Halder, A.M., Kuhl, S.G., Zobitz, M.E., Larson, D., et al. (2001) Effects of the glenoid labrum and glenohumeral abduction on stability of the shoulder joint through concavity-compression: An in vitro study. *Journal of Bone and Joint Surgery - Series A*. [Online] 83 (7), 1062–1069. Available from: doi:10.2106/00004623-200107000-00013.

Halliday, S.E., Zavatsky, A.B., Andrews, B.J. & Hase, K. (2001) Kinematics of the upper and lower extremities in three-dimensions during ergometer rowing. In: *Proceedings of 18th Congress of the International Society of Biomechanics*. [Online]. 2001 pp. 52–54. Available from: https://isbweb.org/images/conf/2001/Longabstracts/PDF/0500_0599/0525.pdf.

Halliday, S.E., Zavatsky, A.B. & Hase, K. (2004) Can functional electric stimulation-assisted rowing reproduce a race-winning rowing stroke? *Archives of Physical Medicine and Rehabilitation*. [Online] 85 (8), 1265–1272. Available from: doi:10.1016/j.apmr.2003.11.025.

Hannafin, J.A. (2000) Rowing. In: Barbara L. Drinkwater (ed.). *Women in sport*. Oxford, Blackwell Science. pp. 486–493.

Hannah, D.C. (2015) Collecting shoulder kinematics with electromagnetic tracking systems and digital inclinometers: A review. *World Journal of Orthopedics*. [Online] 6 (10), 783. Available from: doi:10.5312/wjo.v6.i10.783.

Hase, K., Kaya, M., Zavatsky, A.B. & Halliday, S.E. (2004) Musculoskeletal Loads in Ergometer Rowing. *Journal of Applied Biomechanics*. [Online] 20 (3), 317–323. Available from: doi:10.1123/jab.20.3.317.

Hassan, E.A., Jenkyn, T.R. & Dunning, C.E. (2007) Direct comparison of kinematic data collected using

an electromagnetic tracking system versus a digital optical system. *Journal of Biomechanics*. [Online] 40 (4), 930–935. Available from: doi:10.1016/j.jbiomech.2006.03.019.

Hawkins, D. (2000) A new instrumentation system for training rowers. *Journal of Biomechanics*. [Online] 33 (2), 241–245. Available from: doi:10.1016/S0021-9290(99)00139-6.

Van der Helm, F. (1994) A Finite Element Musculoskeletal the Shoulder Mechanism. *Journal of Biomechanics*. [Online] 27 (5), 551–559. Available from: doi: 10.1016/0021-9290(94)90065-5

van der Helm, F.C.T. & Pronk, G.M. (1994) Loading of shoulder girdle muscles in consequence of a glenohumeral arthrodesis. *Clinical Biomechanics*. [Online] 9 (3), 139–148. Available from: doi:10.1016/0268-0033(94)90013-2.

van der Helm, F.C.T., Veeger, H.E.J., Pronk, G.M., van der Woude, L.H.V., et al. (1992) Geometry parameters for musculoskeletal modelling of the shoulder system. *Journal of Biomechanics*. [Online] 25 (2), 129–144. Available from: doi:10.1016/0021-9290(92)90270-B.

Hickey, G.J., Fricker, P.A. & McDonald, W.A. (1997) Injuries to elite rowers over a 10-yr period. *Medicine and Science in Sports and Exercise*. [Online] 29 (12), 1567–1572. Available from: doi:10.1097/00005768-199712000-00004.

Hiniduma, S.S., Gamage, U. & Lasenby, J. (2002) New least squares solutions for estimating the average centre of rotation and the axis of rotation. *Journal of Biomechanics*. [Online] 35 (1), 87–93. Available from: doi:10.1016/S0021-9290(01)00160-9.

Hislop, S., Cummins, K., Bull, A.M.J. & McGregor, A.H. (2010) Significant influence of the design of the rowing ergometer on elite athlete kinematics. *Proceedings of the Institution of Mechanical Engineers, Part P: Journal of Sports Engineering and Technology*. [Online] 224 (1), 101–107. Available from: doi:10.1243/17543371JSET54.

Hofmijster, M.J., Landman, E.H., Smith, R.M. & Van Soest, A.J.K. (2007) Effect of stroke rate on the distribution of net mechanical power in rowing. *Journal of Sports Sciences*. [Online] 25 (4), 403–411. Available from: doi:10.1080/02640410600718046.

Hofmijster, M.J., Van Soest, A.J. & De Koning, J.J. (2009) Gross efficiency during rowing is not affected by stroke rate. *Medicine and Science in Sports and Exercise*. [Online] 41 (5), 1088–1095. Available from: doi:10.1249/MSS.0b013e3181912272.

Hofmijster, M.J., Van Soest, A.J. & De Koning, J.J. (2008) Rowing skill affects power loss on a modified rowing ergometer. *Medicine and Science in Sports and Exercise*. [Online] 40 (6), 1101–1110. Available from: doi:10.1249/MSS.0b013e3181668671.

Holt, P.J.E., Bull, A.M.J., Cashman, P.M.M. & McGregor, A.H. (2003) Kinematics of Spinal Motion during Prolonged Rowing. *International Journal of Sports Medicine*. [Online] 24 (8), 597–602. Available from: doi:10.1055/s-2003-43273.

Horsman, K., Oopman, H.F.J.M., van der Helm, F.C.T., Prosé, L.P., et al. (2007) Morphological muscle and joint parameters for musculoskeletal modelling of the lower extremity. *Clinical Biomechanics*. [Online] 22 (2), 239–247. Available from: doi:10.1016/j.clinbiomech.2006.10.003.

Hosea, T.M. & Hannafin, J.A. (2012) Rowing Injuries. *Sports Health: A Multidisciplinary Approach*. [Online] 4 (3), 236–245. Available from: doi:10.1177/1941738112442484.

Hume, P.A. (2017) Movement Analysis of Scull and Oar Rowing. In: Bertram Müller, Sebastian I Wolf, Gert-Peter Brueggemann, Zhigang Deng, et al. (eds.). *Handbook of Human Motion*. [Online]. Cham, Springer International Publishing. pp. 1–21. Available from: doi:10.1007/978-3-319-30808-1_133-1.

Husmann, F., Gube, M., Felser, S., Weippert, M., et al. (2017) Central Factors Contribute to Knee Extensor Strength Loss after 2000-m Rowing in Elite Male and Female Rowers. *Medicine and Science in Sports and Exercise*. [Online] 49 (3), 440–449. Available from: doi:10.1249/MSS.0000000000001133.

Iannotti, J.P., Gabriel, J.P., Schneck, S.L., Evans, B.G., et al. (1992) The normal glenohumeral relationships. An anatomical study of one hundred and forty shoulders. *The Journal of bone and joint surgery. American volume*. [Online] 74 (4), 491–500. Available from: http://www.ncbi.nlm.nih.gov/pubmed/1583043.

Ingham, S.A., Whyte, G.P., Jones, K. & Nevill, A.M. (2002) Determinants of 2,000 m rowing ergometer performance in elite rowers. *European Journal of Applied Physiology*. [Online] 88 (3), 243–246. Available from: doi:10.1007/s00421-002-0699-9.

Ismail, S.H.B. (2016) *Musculoskeletal Modelling for Ergonomics: Shoulder & Low Back Loading in Bricklaying*. PhD Thesis. [Online]. Imperial College London. Available from: doi:https://doi.org/10.25560/68516.

Itoi, E., Morrey, B.F. & An, K.-N. (2009) Biomechanics of the Shoulder Joint. In: Charles A. Rockwood, Frederick A. Matsen, Michael A. Wirth, & Steven B. Lippitt (eds.). *The Shoulder*. 4th edition. [Online]. Elsevier Inc. pp. 213–265. Available from: doi:10.1001/archsurg.1973.01350210061018.

Jobe, C., Phipatanakul, W. & Coen, M. (2009) Gross Anatomy of the Shoulder. In: Charles A. Rockwood, Frederick A. Matsen, Michael A. Wirth, & Steven B. Lippitt (eds.). *The Shoulder*. 4th

edition. [Online]. Elsevier Inc. pp. 33–100. Available from: doi:10.1016/B978-1-4160-3427-8.50008-8.

Johnson, G.R. & Pandyan, A.D. (2005) The activity in the three regions of the trapezius under controlled loading conditions - An experimental and modelling study. *Clinical Biomechanics*. [Online] 20 (2), 155–161. Available from: doi:10.1016/j.clinbiomech.2004.10.005.

Johnson, G.R., Spalding, D., Nowitzke, A. & Bogduk, N. (1996) Modelling the muscles of the scapula morphometric and coordinate data and functional implications. *Journal of Biomechanics*. [Online] 29 (8), 1039–1051. Available from: doi:10.1016/0021-9290(95)00176-X.

Johnson, G.R., Stuart, P.R. & Mitchell, S. (1993) A method for the measurement of three-dimensional scapular movement. *Clinical Biomechanics*. [Online] 8 (5), 269–273. Available from: doi:10.1016/0268-0033(93)90037-I.

Jones, J.A., Allanson-Bailey, L., Jones, M.D. & Holt, C.A. (2010) An ergometer based study of the role of the upper limbs in the female rowing stroke. *Procedia Engineering*. [Online] 2 (2), 2555–2561. Available from: doi:10.1016/j.proeng.2010.04.031.

Juliussen, B.R.V. (2011) *Development of computer model for analysis of rowing*. Masters Thesis. [Online] Technical University of Denmark. Available from: http://www.anybodytech.com/resources/publications/

Karandikar, N. & Vargas, O.O.O. (2011) Kinetic Chains: A Review of the Concept and Its Clinical Applications. *PM&R*. [Online] 3 (8), 739–745. Available from: doi:10.1109/IEMBS.1995.579682.

Karduna, A.R., McClure, P.W., Michener, L.A. & Sennett, B. (2001) Dynamic Measurements of Three-Dimensional Scapular Kinematics: A Validation Study. *Journal of Biomechanical Engineering*. [Online] 123 (2), 184. Available from: doi:10.1115/1.1351892.

Karlson, K. (2000) Rowing Injuries. *Seminars in Musculoskeletal Radiology*. [Online] 28 (4). Available from: doi:10.1055/s-2005-923381.

Karlson, K.A. (2012) Rowing: Sport-specific concerns for the team physician. *Current Sports Medicine Reports*. [Online] 11 (5), 257–261. Available from: doi:10.1249/JSR.0b013e3182699154.

Karlsson, D. & Peterson, B. (1992) Towards a model for force predictions in the human shoulder. *Journal of Biomechanics*. [Online] 25 (2), 189–199. Available from: doi:10.1016/0021-9290(92)90275-6

Kaya, M., Minamitani, H., Hase, K. & Yamazaki, N. (1995) Motion analysis of optimal rowing form by using biomechanical model. In: *Proceedings of 17th International Conference of the Engineering in Medicine and Biology Society*. [Online]. 1995 IEEE. pp. 1281–1282. Available from:

doi:10.1109/IEMBS.1995.579682.

Kedgley, A.E., Mackenzie, G.A., Ferreira, L.M., Drosdowech, D.S., et al. (2008) Humeral head translation decreases with muscle loading. *Journal of Shoulder and Elbow Surgery*. [Online] 17 (1), 132–138. Available from: doi:10.1016/j.jse.2007.03.021.

Keenan, K.G., Senefeld, J.W. & Hunter, S.K. (2018) Girls in the boat: Sex differences in rowing performance and participation. *PLoS ONE*. [Online] 13 (1), 1–14. Available from: doi:10.1371/journal.pone.0191504.

Kibler, B.W. (1998) The Role of the Scapula in Athletic Shoulder Function. *The American Journal of Sports Medicine*. [Online] 26 (2), 325–337. Available from: doi:10.1177/0363546598026002801.

Kibler, B.W., Uhl, T.L., Maddux, J.W.Q., Brooks, P. V., et al. (2002) Qualitative clinical evaluation of scapular dysfunction: A reliability study. *Journal of Shoulder and Elbow Surgery*. [Online] 11 (6), 550–556. Available from: doi:10.1067/mse.2002.126766.

Kibler, B.W. & Sciascia, A. (2010) Current concepts: scapular dyskinesis. *British Journal of Sports Medicine*. [Online] 44 (5), 300–305. Available from: doi:10.1136/bjsm.2009.058834.

Klemt, C. (2018) *Musculoskeletal Shoulder Modelling for Clinical Applications*. PhD Thesis. Imperial College London. [Online] Available from: doi:https://doi.org/10.25560/75529.

Klemt, C., Nolte, D., Ding, Z., Rane, L., et al. (2019a) Anthropometric Scaling of Anatomical Datasets for Subject-Specific Musculoskeletal Modelling of the Shoulder. *Annals of Biomedical Engineering*. [Online] 47 (4), 924–936. Available from: doi:10.1007/s10439-019-02207-2.

Klemt, C., Nolte, D., Grigoriadis, G., Di Federico, E., et al. (2017) The contribution of the glenoid labrum to glenohumeral stability under physiological joint loading using finite element analysis. *Computer Methods in Biomechanics and Biomedical Engineering*. [Online] 20 (15), 1613–1622. Available from: doi:10.1080/10255842.2017.1399262.

Klemt, C., Prinold, S., Morgans, S., Smith, S.H.L., et al. (2018) Analysis of shoulder compressive and shear forces during functional activities of daily life. *Clinical biomechanics*. [Online] 54, 34–41. Available from: doi:10.1016/j.clinbiomech.2018.03.006.

Klemt, C., Toderita, D., Nolte, D., Di Federico, E., et al. (2019b) The critical size of a defect in the glenoid causing anterior instability of the shoulder after a Bankart repair, under physiological joint loading. *The Bone & Joint Journal*. [Online] 101-B (1), 68–74. Available from: doi:10.1302/0301-620X.101B1.BJJ-2018-0974.R1.

Kleshnev, V. (2010) Boat acceleration, temporal structure of the stroke cycle, and effectiveness in

rowing. *Proceedings of the Institution of Mechanical Engineers, Part P: Journal of Sports Engineering and Technology*. [Online] 224 (1), 63–74. Available from: doi:10.1243/17543371JSET40.

Kleshnev, V. (2005) Comparison of on water rowing with its simulation on concept 2 and rowperfect machines. In: *ISBS - Conference Proceedings Archive*. [Online]. 2005 Bejing, China. pp. 130–133. Available from: https://ojs.ub.uni-konstanz.de/cpa/article/view/853.

Kleshnev, V. (2006a) Method of analysis of speed, stroke rate and stroke distance in aquatic locomotions. In: *ISBS - Conference Proceedings Archive*. [Online]. 2006 Salzburg, Austria. pp. 104–107. Available from: https://ojs.ub.uni-konstanz.de/cpa/article/view/104.

Kleshnev, V. (2000) Power in Rowing. In: *ISBS - Conference Proceedings Archive*. [Online]. 2000 Hong Kong, China. pp. 2–5. Available from: https://ojs.ub.uni-konstanz.de/cpa/article/view/2258.

Kleshnev, V. (2004) Rowing Biomechanics : Technology and Technique Information. *Rowing Biomechanics Newsletter*. [Online]. Available from: http://www.biorow.com/Papers_files/2004 Rowing Technology and Technique.pdf.

Kleshnev, V. (2006b) *Rowing Biomechanics*. [Online]. 10 (106). Available from: http://www.biorow.com/Papers_files/2006 Rowing Biomechanics.pdf.

Knicker, A.J., Renshaw, I., Oldham, A.R.H. & Cairns, S.P. (2011) Interactive processes link the multiple symptoms of fatigue in sport competition. *Sports Medicine*. [Online] 41 (4), 307–328. Available from: doi:10.2165/11586070-000000000-00000.

Koivukangas, T., Katisko, J.P.A. & Koivukangas, J.P. (2013) Technical accuracy of optical and the electromagnetic tracking systems. *SpringerPlus*. [Online] 2 (1), 90–97. Available from: doi:10.1186/2193-1801-2-90.

Kontaxis, A. & Johnson, G.R. (2008) Adaptation of scapula lateral rotation after reverse anatomy shoulder replacement. *Computer Methods in Biomechanics and Biomedical Engineering*. [Online] 11 (1), 73–80. Available from: doi:10.1080/10255840701552069.

Koopmann, T., Dill, S., Brüggemann, G.-P. & Willwacher, S. (2018) Back muscle fatigue might lead to altered spine loading in recreational ergometer rowing. *ISBS Conference Proceedings Archive*. [Online] 36 (1). Available from: https://commons.nmu.edu/isbs/vol36/iss1/114.

Kornecki, S. & Jaszczak, M. (2010) Dynamic analysis of rowing on concept II type c ergometer. *Biology of Sport*. [Online] 27 (3), 187–194. Available from: doi:10.5604/20831862.919338.

Lamb, D.H. (1989) A kinematic comparison of ergometer and on-water rowing. *The American Journal of*

Sports Medicine. [Online] 17 (3), 367–373. Available from: doi:10.1177/036354658901700310.

Langholz, J.B., Westman, G. & Karlsteen, M. (2016) Musculoskeletal Modelling in Sports-Evaluation of Different Software Tools with Focus on Swimming. *Procedia Engineering*. [Online] 147, 281–287. Available from: doi:10.1016/j.proeng.2016.06.278.

LaScalza, S., Arico, J. & Hughes, R. (2003) Effect of metal and sampling rate on accuracy of Flock of Birds electromagnetic tracking system. *Journal of Biomechanics*. [Online] 36 (1), 141–144. Available from: doi:10.1016/S0021-9290(02)00322-6.

Leardini, A., Chiari, A., Della Croce, U. & Cappozzo, A. (2005) Human movement analysis using stereophotogrammetry Part 3. Soft tissue artifact assessment and compensation. *Gait and Posture*. [Online] 21 (2), 212–225. Available from: doi:10.1016/j.gaitpost.2004.05.002.

Lee, H.D., Suter, E. & Herzog, W. (2000) Effects of speed and distance of muscle shortening on force depression during voluntary contractions. *Journal of Biomechanics*. [Online] 33 (8), 917–923. Available from: doi:10.1016/S0021-9290(00)00070-1.

Lee, Y.S. & Lee, T.Q. (2010) Specimen-specific method for quantifying glenohumeral joint kinematics. *Annals of Biomedical Engineering*. [Online] 38 (10), 3226–3236. Available from: doi:10.1007/s10439-010-0074-7.

Lempereur, M., Brochard, S., Leboeuf, F. & Rémy-Néris, O. (2014) Validity and reliability of 3D marker based scapular motion analysis: A systematic review. *Journal of Biomechanics*. [Online] 47 (10), 2219–2230. Available from: doi:10.1016/j.jbiomech.2014.04.028.

de Leva, P. (1996) Adjustments to Zatsiorsky-Seluyanov's segment inertia parameters. *Journal of Biomechanics*. [Online] 29 (9), 1223–1230. Available from: doi:10.1016/0021-9290(95)00178-6.

Lieber, R.L. & Fridén, J. (1993) Muscle damage is not a function of muscle force but active muscle strain. *Journal of Applied Physiology*. [Online] 74 (2), 520–526. Available from: doi:10.1093/cvr/cvq369.

Lippitt, S.B., Vanderhooft, J.E., Harris, S.L., Sidles, J.A., et al. (1993) Glenohumeral stability from concavity-compression: A quantitative analysis. *Journal of Shoulder and Elbow Surgery*. [Online] 2 (1), 27–35. Available from: doi:https://doi.org/10.1016/S1058-2746(09)80134-1.

Lorbergs, A.L., O'Connor, G.T., Zhou, Y., Travison, T.G., et al. (2017) Severity of kyphosis and decline in lung function: The framingham study. *Journals of Gerontology - Series A Biological Sciences and Medical Sciences*. [Online] 72 (5), 689–694. Available from: doi:10.1093/gerona/glw124.

Ludewig, P.M. & Cook, T.M. (2000) Alterations in shoulder kinematics and associated muscle activity in people with symptoms of shoulder impingement. *Physical therapy*. [Online] 80 (3), 276–291.

Available from: doi:10.2519/jospt.1993.17.5.212.

Ludewig, P.M. & Reynolds, J.F. (2009) The Association of Scapular Kinematics and Glenohumeral Joint Pathologies. *Journal of Orthopaedic & Sports Physical Therapy*. [Online] 39 (2), 90–104. Available from: doi:10.2519/jospt.2009.2808.The.

Lugade, V., Chen, T., Erickson, C., Fujimoto, M., et al. (2015) Comparison of an Electromagnetic and Optical System During Dynamic Motion. *Biomedical Engineering: Applications, Basis and Communications*. [Online] 27 (05), 1550041. Available from: doi:10.4015/s1016237215500416.

Maciejewski, H., Bourdin, M., Lacour, J.R., Denis, C., et al. (2013) Lactate accumulation in response to supramaximal exercise in rowers. *Scandinavian Journal of Medicine and Science in Sports*. [Online] 23 (5), 585–592. Available from: doi:10.1111/j.1600-0838.2011.01423.x.

Mackenzie, H.A.M., Bull, A.M.J. & McGregor, A.H. (2008) Changes in rowing technique over a routine one hour low intensity high volume training session. *Journal of sports science & medicine*. [Online] 7 (4), 486–491. Available from: http://www.ncbi.nlm.nih.gov/pubmed/24149955.

Marcolin, G., Lentola, A., Paoli, A. & Petrone, N. (2015) Rowing on a boat versus rowing on an ergo-meter: A biomechanical and electromyographycal preliminary study. *Procedia Engineering*. [Online] 112, 461–466. Available from: doi:10.1016/j.proeng.2015.07.225.

Matsen, F.A., Lippitt, S.B., Bertlesen, A., Rockwood, C.A., et al. (2009) Glenohumeral Instability. In: Charles A. Rockwood, Frederick A. Matsen, Michael A. Wirth, & Steven B. Lippitt (eds.). *The Shoulder*. 4th edition. [Online]. Elsevier Inc. pp. 617–770. Available from: doi:10.1016/B978-1-4160-3427-8.50022-2.

Mazzone, T. (1988) Kinesiology of the rowing stroke. *National Strength & Conditioning Association Journal*. [Online] 10 (2), 4–11. Available from: https://journals.lww.com/nsca-scj/Citation/1988/04000/SPORTS_PERFORMANCE_SERIES__Kinesiology_of_the.1.aspx.

McClure, P.W., Michener, L.A., Sennett, B.J. & Karduna, A.R. (2001) Direct 3-dimensional measurement of scapular kinematics during dynamic movements in vivo. *Journal of Shoulder and Elbow Surgery*. [Online] 10 (3), 269–277. Available from: doi:10.1067/mse.2001.112954.

McDonnell, L.K., Hume, P.A. & Nolte, V. (2011) Rib Stress Fractures Among Rowers. *Sports Med*. [Online] 41 (11), 883–901. Available from: doi:10.2165/11593170-000000000-00000.

McGregor, A.H. (2017) Injury prevention, performance and return to sport: How can science help? *Chinese Journal of Traumatology - English Edition*. [Online] 20 (2), 63–66. Available from: doi:10.1016/j.cjtee.2016.11.005.

McGregor, A.H. (2002) The trunk muscles of elite oarsmen. *British Journal of Sports Medicine*. [Online] 36 (3), 214–216. Available from: doi:10.1136/bjsm.36.3.214.

McGregor, A.H., Buckeridge, E., Murphy, A.J. & Bull, A.M. (2016) Communicating and using biomechanical measures through visual cues to optimise safe and effective rowing. *Proceedings of the Institution of Mechanical Engineers, Part P: Journal of Sports Engineering and Technology*. [Online] 230 (4), 246–252. Available from: doi:10.1177/1754337115618552.

McGregor, A.H., Bull, A.M.J. & Byng-Maddick, R. (2004) A comparison of rowing technique at different stroke rates: A description of sequencing, force production and kinematics. *International Journal of Sports Medicine*. [Online] 25 (6), 465–470. Available from: doi:10.1055/s-2004-820936.

McGregor, A.H., Patankar, Z.S. & Bull, A.M.J. (2008) Do men and women row differently? a spinal kinematic and force perspective. *Proceedings of the Institution of Mechanical Engineers, Part P: Journal of Sports Engineering and Technology*. [Online] 222 (2), 77–83. Available from: doi:10.1243/17543371JSET22.

McGregor, A.H., Patankar, Z.S. & Bull, A.M.J. (2007) Longitudinal changes in the spinal kinematics of oarswomen during step testing. *Journal of sports science & medicine*. [Online] 6 (1), 29–35. Available from: http://www.ncbi.nlm.nih.gov/pubmed/24149221.

McGregor, A.H., Patankar, Z.S. & Bull, A.M.J. (2005) Spinal kinematics in elite oarswomen during a routine physiological 'step test'. *Medicine and Science in Sports and Exercise*. [Online] 37 (6), 1014–1020. Available from: doi:10.1249/01.mss.0000171618.22263.58.

McMahon, P.J., Prasad, A. & Francis, K.A. (2014) What is the prevalence of senior-athlete rotator cuff injuries and are they associated with pain and dysfunction? *Clinical Orthopaedics and Related Research*. [Online] 472 (8), 2427–2432. Available from: doi:10.1007/s11999-014-3560-7.

McNally, E., Wilson, D. & Seiler, S. (2005) Rowing Injuries. *Seminars in Musculoskeletal Radiology*. [Online] 9 (4), 379–396. Available from: doi:10.1055/s-2005-923381.

Mechmeche, I., Mitiche, A., Ouakrim, Y., De Guise, J.A., et al. (2016) Data correction to determine a representative pattern of a set of 3D knee kinematic measurements. In: *Proceedings of the Annual International Conference of the IEEE Engineering in Medicine and Biology Society*. [Online]. 2016 IEEE. pp. 884–887. Available from: doi:10.1109/EMBC.2016.7590842.

Medical Art Library (2017a) *Shoulder Anatomy KF5003*. [Online]. Available from: https://medicalartlibrary.com/shoulder-anatomy/.

Medical Art Library (2017b) *Upper Back Muscles KF5004*. [Online]. Available from:

https://medicalartlibrary.com/back-muscles/.

Meskers, C.G.M., Fraterman, H., Van Der Helm, F.C.T., Vermeulen, H.M., et al. (1999) Calibration of the 'Flock of Birds' electromagnetic tracking device and its application in shoulder motion studies. *Journal of Biomechanics*. [Online] 32 (6), 629–633. Available from: doi:10.1016/S0021-9290(99)00011-1.

Meskers, C.G.M., Vermeulen, H.M., De Groot, J.H., Van Der Helm, F.C.T., et al. (1998) 3D shoulder position measurements using a six-degree-of-freedom electromagnetic tracking device. *Clinical Biomechanics*. [Online] 13 (4–5), 280–292. Available from: doi:10.1016/S0268-0033(98)00095-3.

Meyer, K.E., Saether, E.E., Soiney, E.K., Shebeck, M.S., et al. (2008) Three-dimensional scapular kinematics during the throwing motion. *Journal of Applied Biomechanics*. [Online] 24 (1), 24–34. Available from: doi:10.1123/jab.24.1.24.

Mickelson, T.C. & Hagerman, F.C. (1982) Anaerobic threshold measurements of elite oarsmen. *Medicine and Science in Sports and Exercise*. [Online] 14 (6), 440–444. Available from: doi:10.1249/00005768-198214060-00006.

Mikulić, P., Smoljanović, T., Bojanić, I., Hannafin, J.A., et al. (2009) Relationship between 2000-m rowing ergometer performance times and World Rowing Championships rankings in elite-standard rowers. *Journal of Sports Sciences*. [Online] 27 (9), 907–913. Available from: doi:10.1080/02640410902911950.

Mohseni-Bandpei, M.A., Keshavarz, R., Minoonejhad, H., Mohsenifar, H., et al. (2012) Shoulder pain in iranian elite athletes: The prevalence and risk factors. *Journal of Manipulative and Physiological Therapeutics*. [Online] 35 (7), 541–548. Available from: doi:10.1016/j.jmpt.2012.07.011.

Montusiewicz, J., Smolka, J., Skublewska-paszkowska, M., Lukasik, E., et al. (2016) *Information and Software Technologies*. Communications in Computer and Information Science. Giedre Dregvaite & Robertas Damasevicius (eds.). [Online]. Cham, Springer International Publishing. Available from: doi:10.1007/978-3-319-46254-7.

Morris, F.L., Smith, R.M., Payne, W.R., Galloway, M.A., et al. (2000) Compressive and shear force generated in the lumbar spine of female rowers. *International Journal of Sports Medicine*. [Online] 21 (7), 518–523. Available from: doi:10.1055/s-2000-7409.

Muggeo, V.M.R. (2003) Estimating regression models with unknown break-points. *Statistics in Medicine*. [Online] 22 (19), 3055–3071. Available from: doi:10.1002/sim.1545.

Murphy, A.J. (2009) *Elite Rowing: Technique and Performance*. PhD Thesis. [Online] Imperial College

London.Available from: http://hdl.handle.net/10044/1/74671

Murphy, A.J., Bull, A.M.J. & McGregor, A.H. (2011) Optimizing and validating an electromagnetic tracker in a human performance laboratory. *Proceedings of the Institution of Mechanical Engineers, Part H: Journal of Engineering in Medicine*. [Online] 225 (4), 343–351. Available from: doi:10.1177/2041303310393231.

Murray, I.A. & Johnson, G.R. (2004) A study of the external forces and moments at the shoulder and elbow while performing every day tasks. *Clinical Biomechanics*. [Online] 19 (6), 586–594. Available from: doi:10.1016/j.clinbiomech.2004.03.004.

Neilsen-Kellerman (2021) *NK Impeller*. [Online]. 2021. Available from: https://nksports.com/speedcoach-impeller_1.

Ng, L., Burnett, A., Campbell, A. & O'Sullivan, P. (2009) Caution: The use of an electromagnetic device to measure trunk kinematics on rowing ergometers. *Sports Biomechanics*. [Online] 8 (3), 255–259. Available from: doi:10.1080/14763140903229492.

Ng, L., Campbell, A., Burnett, A., Smith, A., et al. (2015) Spinal kinematics of adolescent male rowers with back pain in comparison with matched controls during ergometer rowing. *Journal of Applied Biomechanics*. [Online] 31 (6), 459–468. Available from: doi:10.1123/jab.2015-0012.

Nielsen-Kellerman (2017) *Empower Oarlock*. [Online]. 2017. Available from: https://nksports.com/empower-oarlock#mageworx_product_attachments.

Nikooyan, A.A., Veeger, H.E.J., Westerhoff, P., Graichen, F., et al. (2010) Validation of the Delft Shoulder and Elbow Model using in-vivo glenohumeral joint contact forces. *Journal of Biomechanics*. [Online] 43 (15), 3007–3014. Available from: doi:10.1016/j.jbiomech.2010.06.015.

Nilsen, T., Daigneault, T. & Smith, M. (2002a) Basic Rowing Technique. In: *FISA coaching development program*. [Online] World Rowing. pp. 45–55. Available from: https://worldrowing.com/technical/coaching/training/

Nilsen, T., Daigneault, T. & Smith, M. (2002b) Basic Training Methodology. In: Thor Nilsen, Ted Daigneault, & Matt Smith (eds.). *FISA Coaching Development Program*. [Online] World Rowing. pp. 59–91. Available from: https://worldrowing.com/technical/coaching/training/

Nilsen, T.S., Daigneault, T. & Smith, M. (2002c) Basic Rowing Physiology. In: Thor S. Nilsen, Ted Daigneault, & Matt Smith (eds.). *FISA Coaching Development Program*. [Online] World Rowing. pp. 27–43. Available from: https://worldrowing.com/technical/coaching/training/

Nishinaka, N., Tsutsui, H., Mihara, K., Suzuki, K., et al. (2008) Determination of in vivo glenohumeral

translation using fluoroscopy and shape-matching techniques. *Journal of Shoulder and Elbow Surgery*. [Online] 17 (2), 319–322. Available from: doi:10.1016/j.jse.2007.05.018.

Noguchi, M., Chopp, J.N., Borgs, S.P. & Dickerson, C.R. (2013) Scapular orientation following repetitive prone rowing: Implications for potential subacromial impingement mechanisms. *Journal of Electromyography and Kinesiology*. [Online] 23 (6), 1356–1361. Available from: doi:10.1016/j.jelekin.2013.08.007.

Nugent, F.J., Flanagan, E.P., Wilson, F. & Warrington, G.D. (2020) Strength and Conditioning for Competitive Rowers. *Strength & Conditioning Journal*. [Online] 42 (3), 6–21. Available from: doi:10.1519/ssc.0000000000000531.

Page, P., Frank, C. & Lardner, R. (2010) Pathomechanics of musculoskeletal pain and muscle imbalances. In: P Page, C Frank, & R Lardner (eds.). *Assessment and Treatment of Muscle Imbalances: The Janda Approach.* Champaign, Human Kinetics. pp. 43–55.

Page, P.N. & Hawkins, D.A. (2003) A real-time biomechanical feedback system for training rowers. *Sports Engineering*. [Online] 6 (2), 67–79. Available from: doi:10.1007/BF02903529.

Paine, R.M. & Voight, M. (1993) The Role of the Scapula. *Journal of Orthopaedic & Sports Physical Therapy*. [Online] 18 (1), 386–391. Available from: doi:10.2519/jospt.1993.18.1.386.

Pandis, P., Prinold, J.A.I. & Bull, A.M.J. (2015) Shoulder muscle forces during driving: Sudden steering can load the rotator cuff beyond its repair limit. *Clinical Biomechanics*. [Online] 30 (8), 839–846. Available from: doi:10.1016/j.clinbiomech.2015.06.004.

Parent, R. (2012) Motion Capture. In: Rick B T - Computer Animation (Third Edition) Parent (ed.). *Computer Animation*. 3rd edition. [Online]. Boston, Morgan Kaufmann. pp. 187–198. Available from: doi:https://doi.org/10.1016/B978-0-12-415842-9.00006-X.

Parkin, S., Nowicky, A. V, Rutherford, O.M. & McGregor, A.H. (2001) Do oarsmen have asymmetries in the strength of their back and leg muscles? *Journal of Sports Sciences*. [Online] 19 (7), 521–526. Available from: doi:10.1080/026404101750238971.

Pataky, T.C. (2016) rft1d: Smooth one-dimensional random field upcrossing probabilities in Python. *Journal of Statistical Software*. [Online] 71 (7). Available from: doi:10.18637/jss.v071.i07.

Perić, D., Ilić, N. & Ahmetovićvić, Z. (2019) Kinematic and dynamic stroke variables of elite and sub-elite rowers. *International Journal of Performance Analysis in Sport*. [Online] 19 (1), 65–75. Available from: doi:10.1080/24748668.2018.1563857.

Persad, L.S. (2016) *Musculoskeletal modelling of the shoulder during cricket bowling*. PhD Thesis.

[Online] Imperial College London. Available from: https://doi.org/10.25560/75529

Peters, A., Galna, B., Sangeux, M., Morris, M., et al. (2010) Quantification of soft tissue artifact in lower limb human motion analysis: A systematic review. *Gait & Posture*. [Online] 31 (1), 1–8. Available from: doi:10.1016/j.gaitpost.2009.09.004.

Phillips, S. (2015) *Fatigue in Sport and Exercise*. [Online]. London, Routledge. Available from: doi:10.4324/9781315814858.

Polhemus (2015) *Liberty brochure*. [Online]. p.1. Available from: doi:10.1007/1-4020-0613-6_8889.

Pollock, C.L., Jenkyn, T.R., Jones, I.C., Ivanova, T.D., et al. (2009) Electromyography and kinematics of the trunk during rowing in elite female rowers. *Medicine and Science in Sports and Exercise*. [Online] 41 (3), 628–636. Available from: doi:10.1249/MSS.0b013e31818c1300.

Pollock, C.L., Jones, I.C., Jenkyn, T.R., Ivanova, T.D., et al. (2012) Changes in kinematics and trunk electromyography during a 2000m race simulation in elite female rowers. *Scandinavian Journal of Medicine and Science in Sports*. [Online] 22 (4), 478–487. Available from: doi:10.1111/j.1600-0838.2010.01249.x.

Pribicevic, M. (2012) The Epidemiology of Shoulder Pain: A Narrative Review of the Literature. In: Subhamay Ghosh (ed.). *Pain in Perspective*. 1st edition. [Online]. London, IntechOpen. pp. 147–186. Available from: doi:http://dx.doi.org/10.5772/52931.

Price, E. (2016) *Rowing Biomechanics: Technique Changes With an Increase of Power Demand*. Queen's University.

Prinold, J.A., Masjedi, M., Johnson, G.R. & Bull, A.M. (2013) Musculoskeletal shoulder models: A technical review and proposals for research foci. *Proceedings of the Institution of Mechanical Engineers, Part H: Journal of Engineering in Medicine*. [Online] 227 (10), 1041–1057. Available from: doi:10.1177/0954411913492303.

Prinold, J.A.I. (2012) *The Scapula in Musculoskeletal Modelling of Extreme Activities*. PhD Thesis. [Online] Imperial College London. Available from: https://doi.org/10.25560/11103

Prinold, J.A.I. & Bull, A.M.J. (2014) Scaling and kinematics optimisation of the scapula and thorax in upper limb musculoskeletal models. *Journal of Biomechanics*. [Online] 47 (11), 2813–2819. Available from: doi:10.1016/j.jbiomech.2014.05.015.

Prinold, J.A.I. & Bull, A.M.J. (2016) Scapula kinematics of pull-up techniques: Avoiding impingement risk with training changes. *Journal of Science and Medicine in Sport*. [Online] 19 (8), 629–635. Available from: doi:10.1016/j.jsams.2015.08.002.

Prinold, J.A.I., Shaheen, A.F. & Bull, A.M.J. (2011) Skin-fixed scapula trackers: A comparison of two dynamic methods across a range of calibration positions. *Journal of Biomechanics*. [Online] 44 (10), 2004–2007. Available from: doi:10.1016/j.jbiomech.2011.05.010.

Proske, U. & Morgan, D.L. (2001) Muscle damage from eccentric exercise: Mechanism, mechanical signs, adaptation and clinical applications. *Journal of Physiology*. [Online] 537 (2), 333–345. Available from: doi:10.1111/j.1469-7793.2001.00333.x.

Pudlo, P., Pinti, A. & Lepoutre, F.X. (2005) Experimental laboratory apparatus to analyze kinematics and 3D kinetics in rowing. *Sports Engineering*. [Online] 8 (1), 39–46. Available from: doi:10.1007/BF02844130.

Pueo, B. & Jimenez-Olmedo, J.M. (2017) Application of motion capture technology for sport performance analysis (El uso de la tecnología de captura de movimiento para el análisis del rendimiento deportivo). *Retos*. [Online] 2041 (32), 241–247. Available from: doi:10.47197/retos.v0i32.56072.

Readi, N.G., Rosso, V., Rainoldi, A. & Vieira, T.M.M. (2015) Do sweep rowers symmetrically activate their low back muscles during indoor rowing? *Scandinavian Journal of Medicine and Science in Sports*. [Online] 25 (4), e339–e352. Available from: doi:10.1111/sms.12319.

Reilly, P. (2011) Pathology of Cuff Tears. In: Christopher Bulstrode, James Wilson-MacDonald, Deborah M. Eastwood, John McMaster, et al. (eds.). *Oxford Textbook of Trauma and Orthopaedics*. 2nd edition. [Online]. Oxford, Oxford University Press. pp. 236–237. Available from: doi:10.1093/med/9780199550647.001.0001.

Richards, J.G. (1999) The measurement of human motion: A comparison of commercially available systems. *Human Movement Science*. [Online] 18 (5), 589–602. Available from: doi:10.1016/S0167-9457(99)00023-8.

Richardson, C.A. & Jull, G.A. (1995) Muscle control–pain control. What exercises would you prescribe? *Manual Therapy*. [Online]. 1 (1) pp.2–10. Available from: doi:10.1054/math.1995.0243.

Riek, S., Chapman, A.E. & Milner, T. (1999) A simulation of muscle force and internal kinematics of extensor carpi radialis brevis during backhand tennis stroke: Implications for injury. *Clinical Biomechanics*. [Online] 14 (7), 477–483. Available from: doi:10.1016/S0268-0033(98)90097-3.

Riemer, R. & Hsiao-Wecksler, E.T. (2008) Improving joint torque calculations: Optimization-based inverse dynamics to reduce the effect of motion errors. *Journal of Biomechanics*. [Online] 41 (7), 1503–1509. Available from: doi:10.1016/j.jbiomech.2008.02.011.

Rodriguez, R.J., Rogriguez, R.P., Cook, S.D. & Sandborn, P.M. (1990) Electromyographic analysis of rowing stroke biomechanics. *Journal of Sports Medicine and Physical Fitness*. 30 (1), 103–108.

Rowing Australia (2019) *Finding your optimal drag factor and damper setting*. [Online] Available from: https://rowingaustralia.com.au/2019/06/06/finding-your-optimal-drag-factor-and-damper-setting/.

Rowlands, A. V., Cliff, D.P., Fairclough, S.J., Boddy, L.M., et al. (2016) Moving forward with backward compatibility: Translating wrist accelerometer data. *Medicine and Science in Sports and Exercise*. [Online] 48 (11), 2142–2149. Available from: doi:10.1249/MSS.0000000000001015.

RStudio Team (2016) *RStudio: Integrated Development for R*. 1.1.456. [Online]. Boston, RStudio, Inc. Available from: http://www.rstudio.com/.

Ruffaldi, E., Peppoloni, L. & Filippeschi, a. (2015) Sensor fusion for complex articulated body tracking applied in rowing. *Proceedings of the Institution of Mechanical Engineers, Part P: Journal of Sports Engineering and Technology*. [Online] 229 (2), 92–102. Available from: doi:10.1177/1754337115583199.

Rumball, J., Lebrun, C., Di Ciacca, S. & Orlando, K. (2005) Rowing Injuries. *Sports Medicine*. [Online] 35 (6), 358–555. Available from: doi:10.1055/s-2005-923381.

Saha, A.K. (1971) Dynamic stability of the glenohumeral joint. *Acta Orthopaedica Scandinavica*. [Online] 42 (6), 491–505. Available from: doi:10.3109/17453677108989066.

Saha, S. & Vasudeva, N. (2020) Morphological Variations of Glenoid Cavity of Human Scapulae: an Anatomical Study With Clinical Relevance. *International Journal of Anatomy and Research*. [Online] 8 (1.2), 7288–7293. Available from: doi:10.16965/ijar.2019.358.

Schwer, L.E. (2007) Validation metrics for response histories: Perspectives and case studies. *Engineering with Computers*. [Online] 23 (4), 295–309. Available from: doi:10.1007/s00366-007-0070-1.

Sforza, C., Casiraghi, E., Lovecchio, N., Galante, D., et al. (2012) A Three-Dimensional Study of Body Motion During Ergometer Rowing. *The Open Sports Medicine Journal*. [Online] 6 (1), 22–28. Available from: doi:10.2174/1874387001206010022.

Shaheen, A.F., Alexander, C.M. & Bull, A.M.J. (2011) Tracking the scapula using the scapula locator with and without feedback from pressure-sensors: A comparative study. *Journal of Biomechanics*. [Online] 44 (8), 1633–1636. Available from: doi:10.1016/j.jbiomech.2011.02.139.

Skublewska-Paszkowska, M., Montusiewicz, J., Łukasik, E., Pszczoła-Pasierbiewicz, I., et al. (2016) Motion capture as a modern technology for analysing ergometer rowing. *Advances in Science and Technology Research Journal*. [Online] 10 (29), 132–140. Available from:

doi:10.12913/22998624/61941.

SmartOar (2016) *Instrumented Oar Gate Angle Sensor Accelerometer*. [Online]. 2016. Available from: https://www.smartoar.com/oars/.

Smith, H.K. (2000) Ergometer sprint performance and recovery with variations in training load in elite rowers. *International Journal of Sports Medicine*. [Online] 21 (8), 573–578. Available from: doi:10.1055/s-2000-8476.

Smith, R., Draper, C., Ng, L., Lardy, J., et al. (2015) Improving rowing performance and minimising injury. In: *ISBS Conference Proceedings Archive*. [Online]. 2015 Poitiers, France. pp. 1374–1375. Available from: https://ojs.ub.uni-konstanz.de/cpa/article/view/6679.

Smith, R.M. & Loschner, C. (2002) Biomechanics feedback for rowing. *Journal of Sports Sciences*. [Online] 20 (10), 783–791. Available from: doi:10.1080/026404102320675639.

Smith, R.M. & Spinks, W.L. (1995) Discriminant analysis of biomechanical differences between novice, good and elite rowers. *Journal of Sports Sciences*. [Online] 13 (5), 377–385. Available from: doi:10.1080/02640419508732253.

Smith, S.H.L., Reilly, P. & Bull, A.M.J. (2020) A musculoskeletal modelling approach to explain sit-to-stand difficulties in older people due to changes in muscle recruitment and movement strategies. *Journal of Biomechanics*. [Online] 98, 109451. Available from: doi:10.1016/j.jbiomech.2019.109451.

Smoljanović, T., Bohaček, I., Hannafin, J., Nielsen, H.B., et al. (2018) Sport injuries in international masters rowers: a cross-sectional study. *Croatian Medical Journal*. [Online] 59 (5), 258–266. Available from: doi:10.3325/cmj.2018.59.258.

Smoljanovic, T., Bohacek, I., Hannafin, J.A., Terborg, O., et al. (2015) Acute and chronic injuries among senior international rowers: a cross-sectional study. *International Orthopaedics*. [Online] 39 (8), 1623–1630. Available from: doi:10.1007/s00264-014-2665-7.

Smoljanovic, T., Bojanic, I., Hannafin, J.A., Hren, D., et al. (2009) Traumatic and Overuse Injuries Among International Elite Junior Rowers. *The American Journal of Sports Medicine*. [Online] 37 (6), 1193–1199. Available from: doi:10.1177/0363546508331205.

Smoljanovic, T., Bojanic, I., Hannafin, J.A., Urhausen, A., et al. (2013) Complete inclusion of adaptive rowing only 1000 m ahead. *British Journal of Sports Medicine*. [Online] 47 (13), 819–825. Available from: doi:10.1136/bjsports-2013-092157.

Smoljanović, T., Bojanić, I., Pollock, C.L. & Radonić, R. (2011) Rib stress fracture in a male adaptive

rower from the arms and shoulders sport class: case report. *Croatian Medical Journal*. [Online] 52 (5), 644–647. Available from: doi:10.3325/cmj.2011.52.644.

So, R.C.H., Tse, M.A. & Wong, S.C.W. (2007) Application of Surface Electromyography in Assessing Muscle Recruitment Patterns in a Six-Minute Continuous Rowing Effort. *The Journal of Strength and Conditioning Research*. [Online] 21 (3), 724. Available from: doi:10.1519/R-19985.1.

Soper, C. & Hume, P.A. (2004) Towards an ideal rowing technique for performance: The contributions from biomechanics. *Sports Medicine*. [Online] 34 (12), 825–848. Available from: doi:10.2165/00007256-200434120-00003.

Soper, C., Reid, D. & Hume, P.A. (2004) Reliable passive ankle range of motion measures correlate to ankle motion achieved during ergometer rowing. *Physical Therapy in Sport*. [Online] 5 (2), 75–83. Available from: doi:10.1016/j.ptsp.2003.11.006.

Sorriento, A., Porfido, M.B., Mazzoleni, S., Calvosa, G., et al. (2020) Optical and Electromagnetic Tracking Systems for Biomedical Applications: A Critical Review on Potentialities and Limitations. *IEEE Reviews in Biomedical Engineering*. [Online] 13, 212–232. Available from: doi:10.1109/RBME.2019.2939091.

Soslowsky, L.J., Flatow, E.L., Bigliani, L.U., Pawluk, R.J., et al. (1992) Quantitation of in situ contact areas at the glenohumeral joint: A biomechanical study. *Journal of Orthopaedic Research*. [Online] 10 (4), 524–534. Available from: doi:10.1002/jor.1100100407.

Spitzer, V.M. & Whitlock, D.G. (1998) The visible human dataset: The anatomical platform for human simulation. *The Anatomical Record*. [Online] 253 (2), 49–57. Available from: doi:10.1002/(SICI)1097-0185(199804)253:2<49::AID-AR8>3.0.CO;2-9.

Stagni, R., Fantozzi, S., Cappello, A. & Leardini, A. (2005) Quantification of soft tissue artefact in motion analysis by combining 3D fluoroscopy and stereophotogrammetry: A study on two subjects. *Clinical Biomechanics*. [Online] 20 (3), 320–329. Available from: doi:10.1016/j.clinbiomech.2004.11.012.

Stallard, M.C. (1980) Backache in oarsmen. *British Journal of Sports Medicine*. [Online] 14 (2–3), 105–108. Available from: doi:10.1136/bjsm.14.2-3.105.

Steer, R.R., McGregor, A.H. & Bull, A.M.J. (2006) A comparison of kinematics and performance measures of two rowing ergometers. *Journal of Sports Science and Medicine*. 5 (1), 52–59. PMID: 24198681.

Strahan, A.D., Burnett, A.F., Caneiro, J.P., Doyle, M.M., et al. (2011) Differences in Spinopelvic

Kinematics in Sweep and Scull Ergometer Rowing. *Clinical Journal of Sport Medicine*. [Online] 21 (4), 330–336. Available from: doi:10.1097/JSM.0b013e31821a6465.

Taborri, J., Keogh, J., Kos, A., Santuz, A., et al. (2020) Sport biomechanics applications using inertial, force, and EMG sensors: A literature overview. *Applied Bionics and Biomechanics*. [Online] 2020. Available from: doi:10.1155/2020/2041549.

Tachibana, K., Yashiro, K., Miyzaki, J., Ikegami, Y., et al. (2007) Muscle cross-sectional areas and performance power of limbs and trunk in the rowing motion. *Sports Biomechanics*. [Online] 6 (1), 44–58. Available from: doi:10.1080/14763140601058516.

Tanaka, C., Ide, M.R. & Moreno, R.T. (2007) Quantitative Analysis of Head and Trunk Posture in Rowers During Ergometry Training. *Salusvita*. 26 (1), 53–64.

Tang, C.-T. & Simpson, S. (2016) Shoulder. In: Ellen Casey, Monica Rho, & Joel Press (eds.). *Sex Differences in Sports Medicine*. 1st edition. [Online]. New York, Springer Publishing Company. p. 300. Available from: doi:10.1891/9781617052491.0002.

Teitz, C.C., O'Kane, J.W. & Lind, B.K. (2003) Back Pain in Former Intercollegiate Rowers. *The American Journal of Sports Medicine*. [Online] 31 (4), 590–595. Available from: doi:10.1177/03635465030310041901.

Terry, G.C. & Chopp, T.M. (2000) Functional anatomy of the shoulder. *Journal of athletic training*. [Online] 35 (3), 248–255. Available from: http://www.ncbi.nlm.nih.gov/pubmed/16558636.

Teunis, T., Lubberts, B., Reilly, B.T. & Ring, D. (2014) A systematic review and pooled analysis of the prevalence of rotator cuff disease with increasing age. *Journal of Shoulder and Elbow Surgery*. [Online] 23 (12), 1913–1921. Available from: doi:10.1016/j.jse.2014.08.001.

Thompson, P. (2005) *Sculling: Training, technique and performance*. Ramsbury, Crowood Press.

Thornton, J.S., Vinther, A., Wilson, F., Lebrun, C.M., et al. (2017a) Rowing Injuries: An Updated Review. *Sports Medicine*. [Online] 47 (4), 641–661. Available from: doi:10.1007/s40279-016-0613-y.

Thornton, J.S., Vinther, A., Wilson, F., Lebrun, C.M., et al. (2017b) Rowing Injuries: An Updated Review. *Sports Medicine*. [Online] 47 (4), 641–661. Available from: doi:10.1007/s40279-016-0613-y.

Torres-Moreno, R., Tanaka, C. & Penney, K.L. (2000) Joint excursion, handle velocity, and applied force: A biomechanical analysis of ergonometric rowing. *International Journal of Sports Medicine*. [Online] 21 (1), 41–44. Available from: doi:10.1055/s-2000-8850.

Turpin, N.A., Guével, A., Durand, S. & Hug, F. (2011) No evidence of expertise-related changes in muscle synergies during rowing. *Journal of Electromyography and Kinesiology*. [Online] 21 (6), 1030–1040. Available from: doi:10.1016/j.jelekin.2011.07.013.

Urbanczyk, C.A., Prinold, J.A.I., Reilly, P. & Bull, A.M.J. (2020) Avoiding High Risk Rotator Cuff Loading: Muscle Force During Three Pull-Up Techniques. *Scandinavian Journal of Medicine & Science in Sports*. [Online] n/a (n/a). Available from: doi:10.1111/sms.13780.

US Rowing (2018) *Rowing is growing*. [Online]. 2018. Available from: https://usrowing.org/documents/2019/6/19//usrowing-5c-20m_38277873-1.pdf?id=2023 [Accessed: 1 February 2018].

Veeger, H.E.J. & van der Helm, F.C.T. (2007) Shoulder function: The perfect compromise between mobility and stability. *Journal of Biomechanics*. [Online] 40 (10), 2119–2129. Available from: doi:10.1016/j.jbiomech.2006.10.016.

Veeger, H.E.J., Yu, B., An, K.N. & Rozendal, R.H. (1997) Parameters for modeling the upper extremity. *Journal of Biomechanics*. [Online] 30 (6), 647–652. Available from: doi:10.1016/S0021-9290(97)00011-0.

Vicon Motion Systems Limited (2021) *Cameras*. [Online]. 2021. Available from: https://www.vicon.com/hardware/cameras/.

Vicon Motion Systems Limited (2015) *Vicon Nexus Product Guide*. [Online] 1–362. Available from: http://documentation.vicon.com/nexus/v2.2/Nexus1_8Guide.pdf.

Villapún Puzas, V.M. (2015) *Lumbar spine biomechanics whilst rowing on a non-static concept 2 ergometer*. Masters Thesis. [Online] Imperial College London.

Vinther, A., Kanstrup, I.L., Christiansen, E., Alkjær, T., et al. (2006) Exercise-induced rib stress fractures: Potential risk factors related to thoracic muscle co-contraction and movement pattern. *Scandinavian Journal of Medicine and Science in Sports*. [Online] 16 (3), 188–196. Available from: doi:10.1111/j.1600-0838.2005.00473.x.

Viteckova, S., Kutilek, P., Svoboda, Z., Krupicka, R., et al. (2018) Gait symmetry measures: A review of current and prospective methods. *Biomedical Signal Processing and Control*. [Online] 42, 89–100. Available from: doi:10.1016/j.bspc.2018.01.013.

Volianitis, S. & Secher, N.H. (2009) Rowing, the ultimate challenge to the human body - Implications for physiological variables. *Clinical Physiology and Functional Imaging*. [Online] 29 (4), 241–244. Available from: doi:10.1111/j.1475-097X.2009.00867.x.

Volianitis, S., Yoshiga, C.C. & Secher, N.H. (2020) The physiology of rowing with perspective on training and health. *European Journal of Applied Physiology*. [Online]. 120 (9) pp.1943–1963. Available from: doi:10.1007/s00421-020-04429-y.

Warden, S.J., Gutschlag, F.R., Wajswelner, H. & Crossley, K.M. (2002) Aetiology of Rib Stress Fractures in Rowers. *Sports Medicine*. [Online] 32 (13), 819–836. Available from: doi:10.2165/00007256-200232130-00002.

Warmenhoven, J., Cobley, S., Draper, C. & Smith, R. (2018) Over 50 Years of Researching Force Profiles in Rowing: What Do We Know? *Sports Medicine*. [Online] Available from: doi:10.1007/s40279-018-0992-3.

De Wilde, L.F., Berghs, B.M., Audenaert, E., Sys, G., et al. (2004) About the variability of the shape of the glenoid cavity. *Surgical and Radiologic Anatomy*. [Online] 26 (1), 54–59. Available from: doi:10.1007/s00276-003-0167-1.

Wilk, K.E., Arrigo, C.A. & Andrews, J.R. (1997) Current concepts: the stabilizing structures of the glenohumeral joint. *The Journal of orthopaedic and sports physical therapy*. [Online] 25 (6), 364–379. Available from: doi:10.2519/jospt.1997.25.6.364.

Wilson, F. (2010) *Lumbar spine injury in rowing: influence of spinal kinematics, rowing mode and fatigue*. PhD Thesis. [Online] University of Dublin, Trinity College. Available from: http://hdl.handle.net/2262/85440.

Wilson, F., Gissane, C., Gormley, J. & Simms, C. (2010) A 12-month prospective cohort study of injury in international rowers. *British Journal of Sports Medicine*. [Online] 44 (3), 207–214. Available from: doi:10.1136/bjsm.2008.048561.

Wilson, F., Gissane, C., Gormley, J. & Simms, C. (2013) Sagittal plane motion of the lumbar spine during ergometer and single scull rowing. *Sports Biomechanics*. [Online] 12 (2), 132–142. Available from: doi:10.1080/14763141.2012.726640.

Wing, A.M. & Woodburn, C. (1995) The coordination and consistency of rowers in a racing eight. *Journal of Sports Sciences*. [Online] 13 (3), 187–197. Available from: doi:10.1080/02640419508732227.

Winter, D.A. (2009) *Biomechanics and Motor Control of Human Movement*. [Online]. Hoboken, NJ, USA, John Wiley & Sons, Inc. Available from: doi:10.1002/9780470549148.

Winzen, M., Voigt, H.-F., Hinrichs, T. & Platen, P. (2011) Injuries of the Musculoskeletal System in German Elite Rowers. *Sportverletz Sportschaden*. [Online] 25 (03), 153–158. Available from:

doi:10.1055/s-0031-1273299.

Wu, G., Van Der Helm, F.C.T., Veeger, H.E.J., Makhsous, M., et al. (2005) ISB recommendation on definitions of joint coordinate systems of various joints for the reporting of human joint motion - Part II: Shoulder, elbow, wrist and hand. *Journal of Biomechanics*. [Online] 38 (5), 981–992. Available from: doi:10.1016/j.jbiomech.2004.05.042.

Zumstein, V., Kraljević, M., Conzen, A., Hoechel, S., et al. (2014) Thickness distribution of the glenohumeral joint cartilage: A quantitative study using computed tomography. *Surgical and Radiologic Anatomy*. [Online] 36 (4), 327–331. Available from: doi:10.1007/s00276-013-1221-2.

APPENDIX A: ETHICS APPROVAL DOCUMENTATION

Biodynamics Laboratory
7th Floor, Charing Cross Hospital
Department of Surgery & Cancer
Imperial College London
Fulham Palace Road
London, W6 8RF
c.urbanczyk17@imperial.ac.uk
Tel: +44 (0)20 7594 2836

Investigators: Prof. Alison McGregor
Prof. Anthony MJ Bull
Caryn Urbanczyk

Participant Reference Number: _____

Evaluation of shoulder complex and upper limb kinematics in rowing for performance and injury prevention

Participant Consent Form
Version 2, 05 Jan 2018

Please initial boxes

1. I confirm that I have read and understand the Participant Information Sheet V2dated 05 Jan 2018 for the above study. I have considered the presented information, had the opportunity to ask questions, and have had my questions satisfactorily answered. ☐
2. I understand that my participation is voluntary and that I am free to withdraw at any time without giving any reason, and without my medical care, education, employment, or legal rights being affected. ☐
3. I agree to my data, including personally identifiable information, being anonymized, and stored on a password protected Imperial College computer system. ☐
4. I agree that videos may be recorded while I am performing assessment activities. ☐
5. I understand that sections of my research notes and data may be accessed by responsible persons from the research team, from Imperial College London or from regulatory authorities where it is relevant to the research and conduct. ☐

6. I understand that I can be provided with a summary report of individual findings at the conclusion of the study, at my request. ☐

7. I agree to take part in the above study. ☐

_____	_____	_____
Name of subject	Date	Signature
_____	_____	_____
Name of person taking consent	Date	Signature

Biodynamics Laboratory
7th Floor, Charing Cross Hospital
Department of Surgery & Cancer
Imperial College London
Fulham Palace Road
London, W6 8RF
c.urbanczyk17@imperial.ac.uk
Tel: +44 (0)20 7594 2836

Investigators: Prof. Alison McGregor
Prof. Anthony MJ Bull
Caryn Urbanczyk

Evaluation of shoulder complex and upper limb kinematics in rowing for performance and injury prevention

Participant Information Sheet

Version 2, 05 January 2018

The study investigators would like to invite you to join a research study. Before you decide, it is important for you to understand why the research is being done and what it will involve. This form gives detailed information about the research study and is yours to keep. Please take time to read the following information carefully and feel free to discuss it with others before you decide whether you wish to take part. Ask us if there is anything that is not clear or if you would like more information.

What is the purpose of the study?

The goals of this study are to examine movement of body segments and muscle activation while rowing on an indoor ergometer. This will help us virtually model the rowing stroke to understand aspects of technique that affect why some rowers perform better than others and why some rowers are more prone to injury.

Why have I been invited?

The study investigators would like you to consider participating in this study as you are a healthy person between the ages of 18 and 45, who has been rowing for at least two years. Other qualifying criteria include being in fit physical condition, no injuries in the past six months and able to complete a 12-minute step test, with no history of surgical intervention on any joint of the upper limb which may limit mobility. The investigators are inviting 30 volunteers to take part in this study.

Do I have to take part?

No. Participation is entirely up to you. Should you decide to take part, you will be asked to sign a consent form. Bear in mind that even after you have signed this consent form and agreed to join the study, you are free to withdraw from the study at any time. A decision to withdraw at any time, or a decision not to take part, will not affect any future interactions (e.g., care, education) that you may have with Imperial College London. If you chose to withdraw from the study at any time, the information collected up until that point

will be retained and used in the study; however, no further data will be collected. Please inform any member of the research team if you no longer wish to participate in the study.

What will be my role if I take part?

Once you have decided to take part in this research, you will be invited to attend up to four 90-minute assessment sessions (over the course of two years, with at least three months between sessions) at either the Biodynamics Lab at Charing Cross Hospital (Hammersmith, W6 8RF) or Motion Analysis Lab at Imperial College London (South Kensington, SW7 2AZ), where a member of our research team will discuss the study with you and answer any questions you may have. If you are still happy to take part, the study investigators will ask you to sign the consent form. While not mandatory, Participants are highly encouraged to attend all four sessions to assess long-term training adaptations.

Assessment steps to take place at the Biodynamics Lab:

- Your height, weight, gender, and age will be recorded at each visit to the Lab.
- The following assessments will be the same for both sessions.
    - Small reflective markers and clusters will be positioned on the skin for the VICON motion capture system to record movements.
    - Electromyography sensors will be placed on your arms, shoulders, and torso to measure muscle activity.
    - You will be asked to complete a step test on the rowing machine: 4x3 minutes at increasing stroke rates (r18, r24, r28, r32 strokes per minute [spm]). The actual rate, average 500m pace and distance covered will be recorded for each interval. You will be encouraged to rest between each interval and recover as needed.
    - Digital video footage may be recorded of you conducting the movements for reference.

**** Please note that participants should arrive with appropriate attire for the combined ergometer and motion capture systems which includes lycra shorts, trainers, and a sports bra (female participants only). ****

What are the side effects, and are there any risks in taking part?

All assessment techniques are safe and non-invasive, and all tests will be performed within your own fitness limits. Care will be taken to ensure your comfort throughout marker placement and removal.

Hypoallergenic skin adhesive used to attach reflective markers and electromyography sensors may cause some redness. If you have any allergies or skin conditions (e.g., eczema, dermatitis, etc.), please inform the researchers and alternative attachment methods can be arranged. If you notice any irritation during or immediately following the study, please inform the researcher and a first aider will be called to assist. If irritation persists for more than 24 hours, please contact us and you may be advised to consult your local medical clinic.

If you experience any joint pain and/or discomfort during the session, please inform the researcher. You may also suffer from delayed onset muscle soreness after testing.

What if something goes wrong?

Imperial College holds Public Liability ("negligent harm") and Clinical Trial ("non-negligent harm") insurance policies which apply to this trial. If you can demonstrate that you experienced harm or injury as a result of your participation in this trial, you will be eligible to claim compensation without having to prove that Imperial College is at fault. If the injury resulted from any procedure which is not part of the

trial, Imperial College will not be required to compensate you in this way. Your legal rights to claim compensation for injury where you can prove negligence are not affected. Regardless of this, if you wish to complain, or have any concerns about any aspect of the way you have been treated during the course of this study, immediately inform the Investigator (Prof. Alison McGregor a.mcgregor@imperial.ac.uk). If you are still not satisfied with the response, you may contact the Imperial AHSC Joint Research Compliance Office (http://www.imperial.ac.uk/joint-research-compliance-office/).

What are the possible benefits of taking part?
There are no direct benefits to research participants, aside from contributing to biomechanics research, and an individual summary of data provided at the close of study. However, this project will provide you with an interesting insight into how you row which may help you to improve your performance and prevent an injury.

Will my taking part in this study be kept confidential?
Any information given to us during the course of the research will be kept confidential and anonymous. If the findings of this study are published in a scientific journal, no individual will be identified in any way at any stage. Personal details and study data (demographic information regarding age, sex, height, weight, and data collected during trial) will be stored - in accordance with the Data Protection Act - on a password protected computer and paper forms will be kept in a secure filling cabinet at Imperial College London, accessible only by the principal investigators and co-investigators named on this application. Data will be held for 10 years after completion of the study.

What will happen to the results of the research study?
Results of this study will be analysed by the research team and presented at academic conferences and published in peer-reviewed journals. No participant will be identified in any report or presentation arising from the research. The study investigators will be able to provide you with an individual summary report of findings at the end of the study, upon request.

Will I be paid for taking part in the study?
You will not be paid for your participation in the study.

Who has reviewed the study?
This study was reviewed by the head of the department and the Imperial College Joint Research Compliance Office (JRCO) researchethicscommittee@imperial.ac.uk

Contacts for further information:
If you would like to consider this study further before you make your decision, please take your time to do so. For questions and concerns, or to request further information please contact Ms. Caryn Urbanczyk, who may be reached by email at c.urbanczyk17@imperial.ac.uk or by phone at +44 (0)20 7594 2836.

Thank you.

We would like to thank you for taking the time to read through this information sheet and for your consideration in participating in this study.

Biodynamics Laboratory
7th Floor, Charing Cross Hospital
Department of Surgery & Cancer
Imperial College London
Fulham Palace Road
London, W6 8RF
c.urbanczyk17@imperial.ac.uk
Tel: +44 (0)20 7594 2836

Investigators: Prof. Alison McGregor
Prof. Anthony MJ Bull
Caryn Urbanczyk

Evaluation of shoulder complex and upper limb kinematics in rowing for performance and injury prevention

Participant Data Sheet

Version 1, December 2017

Participant Reference #: _____

Date & Test Session: _____

Birthdate / Age: _____

Sex: _____

Height (m): _____

Weight (kg): _____

Side rowed: _____

Dominant hand: _____

Skill level: _____

Years rowing: _____

History of any joint pain or injury:

Imperial College Research Ethics Committee
Imperial College London
Room 221
Medical School Building
St Marys Campus
London
W2 1PG
Tel: +44 (0)207 594 9484

researchethicscommittee@imperial.ac.uk

Alison McGregor
Department of Surgery and Cancer
Room 7L16, Charing Cross Road Hospital
Fulham Palace Road
London, W6 8RF

12th January 2018

Dear Professor McGregor

Study Title:. Evaluation of shoulder complex and upper limb kinematics in rowing for performance and injury prevention

ICREC reference: 17IC4308

The above study was approved by your Head of Department on date and by the Joint Research Compliance Office on 12th January 2018.

Under the Imperial College Research Ethics Committee process, a study that has been reviewed by the Joint Research Compliance Office and Head of Division/Department (or Principal), where no significant ethical issues have been identified in the protocol or ethics application, can be approved without requiring it to go to full committee.

Documents
The documents reviewed were:

- ICREC Application form (6/12/17)
- Protocol (v2 5/01/18)
- Participant Information Sheet (v2 5/01/18)
- Participant Consent Form (v2 5/01/18)
- Poster advert (v2 5/01/18)
- Email advert (v2 5/01/18)
- JRCO Sponsorship and Insurance Request (06/12/17)

Yours sincerely,

Gary Roper,
Head of Regulatory Compliance,
Imperial College London

APPENDIX B: MATLAB CODE FOR MOTION CAPTURE KINEMATICS & ERGOMETER KINETICS DATA PROCESSING

```
%%%%%%%%%%%%%%%%%%%%%%%%%%%%%%%%%%%%%%%%%%%%%%%%%%%%%%%%%%%%%%%%%%%%%%%%%%%%%%%
%% Nexus-Matlab Session setup and Vicon Trajectory extraction
SDK=ViconNexus();
% Start Nexus-Matlab Session

%% EDIT THESE VALUES HERE BEFORE RUNNING BELOW SECTIONS %
close all; clc
% CHANGE NEXUS TRIAL %
clearvars -except SDK VB5678Step18 VB5678Step24 VB5678Step28 VB5678Step32
subject = 'ErgVB5678';
% Enter subject as is named in loaded Nexus trial
Erg = VB5678Step18;
% imports erg data file as a table (in order to use table index notation)
fileout = 'VB5678Step28.xlsx';
% STOP EDITING HERE %

%% Vicon Data Import and Processing
disp('Importing Vicon Data...')
% Export handle and seat marker positions
[X1, Y1, Z1, E1] = SDK.GetTrajectory(subject, 'Handle');
[X2, Y2, Z2, E2] = SDK.GetTrajectory(subject, 'SeatRight');
[X3, Y3, Z3, E3] = SDK.GetTrajectory(subject, 'PlateBottomRight');
[X4, Y4, Z4, E4] = SDK.GetTrajectory(subject, 'FrontTop');

[startframe, endframe] = SDK.GetTrialRegionOfInterest;
% Isolate your region of interest from the Nexus trial
ROIframes = double(startframe:endframe)';
% Make sure that your marker trajectories are completely gapfilled
framecount = length(ROIframes);
% Count the frames in your ROI and map it to a time vector (where Fs=100hz)
time=(0:.01:((framecount-1)/100))';

% Crop marker trajectories down to just the ROI and combine in data table
Handle = [X1;Y1;Z1]'; Handle=Handle(ROIframes,:);
Seat = [X2;Y2;Z2]';   Seat=Seat(ROIframes,:);
Plate = [X3;Y3;Z3]';  Plate=Plate(ROIframes,:);
Cage = [X4;Y4;Z4]';  Cage=Cage(ROIframes,:);
Vicon = [ROIframes,time,Handle,Seat,Plate,Cage];

%% Automatically find catch point for every stroke from Vicon handle
%% trajectory
Vicon_handle_pos = Vicon(:,4);
% extract handle position into separate vector
Vicon_idx = 1:1:length(Vicon_handle_pos);
% Create an index of sample count
VTF = islocalmin(Vicon_handle_pos,'MinSeparation',100,'MinProminence',100);
% This section picks out the catch frame based on minimum handle y-position
Vicon_strokeIndex = find(VTF);
% counts the number of strokes and the frames per stroke
Vicon_strokeStart = Vicon_handle_pos(VTF);
Vicon_numstrokes = length(Vicon_strokeIndex);
```

```
Vicon_strokecount = Vicon_numstrokes-1;
figure();
subplot(2,1,1);
plot(Vicon_idx,Vicon_handle_pos,Vicon_strokeIndex,Vicon_strokeStart,'r*');
title('Vicon Handle Trajectory');

%% ERG DATA IMPORT AND PROCESSING %%
% Import the relevant columns from the instrumented ergometer data excel
% files as a table
clear Stroke X Matrix idx
disp('Importing Ergometer Data...')
Erg_handle_force = Erg.Handleforce;
% make certain that any dropped data points in the raw erg files are removed
% or are set to NaN for import
% Automatically find catch point for every stroke from Ergometer handle
% position
Erg_handle_pos = Erg.AntPosthandleposition;
% extract handle force into separate vector
Erg_idx = 1:1:length(Erg_handle_pos);
% extract stroke length in cm into separate vector

ETF = islocalmin(Erg_handle_pos,'MinSeparation',100,'MinProminence',100);
Erg_strokeIndex=find(ETF);
Erg_strokeStart=Erg_handle_pos(ETF);

Erg_numstrokes = length(Erg_strokeIndex);
Erg_strokecount = Erg_numstrokes-1;
subplot(2,1,2);
plot(Erg_idx,Erg_handle_pos,Erg_strokeIndex,Erg_strokeStart,'r*');
title('Erg Handle Position');
% Check the plot for any stray infinite/zero/NaN values they may have been
% accidently left into to corrupt the data
Vicon_strokecount
Erg_strokecount

%% PLOT ERG HANDLE FORCE %%
figure();
plot(Erg_idx,Erg_handle_force,Erg_strokeIndex,Erg_strokeStart,'r*');

%%%%%%%%%%%%%%%%%%%%%%%%%%%%%%%%%%%%%%%%%%%%%%%%%%%%%%%%%%%%%%%%%%%%%%%%%%%%%%%
% STOP - CHECK GRAPHS HERE FOR MATCHING STROKE COUNTS
% Edit data tables as needed here to get same strokes
Vicon=Vicon((Vicon_strokeIndex(3):Vicon_strokeIndex(end)),:);
Erg=Erg((Erg_strokeIndex(3):Erg_strokeIndex(end-1)),:);
% Re-run above sections to update

%%%%%%%%%%%%%%%%%%%%%%%%%%%%%%%%%%%%%%%%%%%%%%%%%%%%%%%%%%%%%%%%%%%%%%%%%%%%%%%
% Crop the Vicon trial data from the first catch point to the last catch
% point
disp('Cropping Vicon Data to Stroke Start...')
Stroke=[];
X = [];
Matrix = [];
Frames = [];
for m = 1:Vicon_strokecount
     x = (1:(Vicon_strokeIndex(m+1)-Vicon_strokeIndex(m)))';
     % gives the number of samples between sequential catch indices
```

```
    X=[X;x];
    % builds a padded matrix of the number of samples in each stroke
    stroke=true(length(x),1);
    % writes a logical column of ones equal to the length of number of
    % samples between catch indices
    stroke=stroke*m;
    % converts the logical to a numerated stroke number
    Stroke=[Stroke;stroke];
    % builds a padded column of stroke count
    matrix = (Vicon(Vicon_strokeIndex(m):(Vicon_strokeIndex(m+1)-1),:));
    % extracts all remaining sensor data and groups it into subsets based on
    % stroke number
    Matrix = [Matrix; matrix];
    % builds up a padded matrix of all sensor data variables by vertically
    % concatenating each stroke
    frames = [m, matrix(1,1), matrix(end,1), size(matrix,1)];
    Frames = [Frames; frames];
end
X = array2table(X);
% NOTICE - 100% of first stroke and 0% of second stroke are the same value -
% this is ok,
Stroke = array2table(Stroke);
% but pay attention to your vector lengths or you will get dimension mismatch
% errors
Matrix = array2table(Matrix);
Frames = array2table(Frames);
Frames.Properties.VariableNames = {'Stroke','Start','End','Count'};
ReducedVicon=[Stroke, X, Matrix];
ReducedVicon.Properties.VariableNames =
{'Stroke','Sample','Frame','Time','HandleX','HandleY','HandleZ','SeatX','Seat
Y','SeatZ','PlateX','PlateY','PlateZ','CageX','CageY','CageZ'};

% Crop Erg data from the first catch point to the last catch point %
disp('Cropping Erg Data to Stroke Start...')
Stroke=[];
X = [];
Matrix = [];
for m = 1:Erg_strokecount
    x = (1:(Erg_strokeIndex(m+1)-Erg_strokeIndex(m)))';
    % gives the number of samples between sequential catch indices
    X=[X;x];
    % builds a padded matrix of the number of samples in each stroke
    stroke = m*true(length(x),1);
    % writes a logical column of ones equal to the length of number of
    % samples between catch indices and converts the logical to a numerated
    % stroke number
    Stroke = [Stroke;stroke];
    % builds a padded column of stroke count
    matrix = (Erg(Erg_strokeIndex(m):(Erg_strokeIndex(m+1)-1),:));
    % extracts all remaining sensor data and groups it into subsets based on
    % stroke number
    Matrix = [Matrix; matrix];
    % builds up a padded matrix of all sensor data variables by vertically
    % concatenating each stroke
end
X = array2table(X);
Stroke = array2table(Stroke);
```

```
ReducedErg=[Stroke, X, Matrix];
ReducedErg.Properties.VariableNames([1 2]) = {'Stroke','Sample'};

%%%%%%%%%%%%%%%%%%%%%%%%%%%%%%%%%%%%%%%%%%%%%%%%%%%%%%%%%%%%%%%%%%%%%%%%%%%%%%%
% Extrapolate - ERG data samples to match the VICON frame count for each
% individual stroke
disp('Extrapolating Erg Data to Match Vicon Frames...')
Stroke=[];
Xq = [];
Xr = [];
Vq = [];
W = [];
for m = 1:Erg_strokecount
     j=length(find(ReducedErg.Stroke==m));
     % the number of samples per stroke from the erg data
     i=(find(ReducedErg.Stroke==m,1,'first')):(find(ReducedErg.Stroke==m,1,'la
     st'));
     % index the number of samples within each stroke from the erg data
     k=length(find(ReducedVicon.Stroke==m));
     % the number of frames per stroke from the Vicon data
     w=(1:k)';
     x=(1:j)';
     % erg data sample x values input to interpolate
     v=table2array(ReducedErg(i,1:end));
     % erg data sample y values input to interpolate
     xq = (linspace(1,j,k))';
     % erg data x values/times/points to query output from interpolation
     xr = linspace(0,100,k)';
     % create stroke percent complete vector
     vq = interp1(x,v,xq,'linear');
     % erg data y values to query output from interpolation
     stroke=m*(true(length(xr),1));
     % assign stroke number to new sample outputs
     Stroke=[Stroke;stroke];
     W = [W; w];
     Xq = [Xq; xq];
     Xr = [Xr; xr];
     Vq = [Vq; vq];
end
ExtrapErg = array2table([Stroke, Xr, W, Vq(:,2:end)]);
ExtrapErg.Properties.VariableNames([1 2 3]) = {'Stroke','Percent','Frames'};
ExtrapErg.Properties.VariableNames(4:end) =
ReducedErg.Properties.VariableNames(2:end);

%% CATCH LATENCY CALCULATIONS %%
Lags = CatchLatency(ExtrapErg,Erg_strokeIndex);
Frames=[Frames,Lags];

%% FILTER HANDLE FORCE FOR UKNSM HANDLOADS %%
disp('Calculate filtered handloads...')
n = 4;
fs = 100;
fc = 10;
[b,a] = butter(n,2*fc/fs,'low');
force = ExtrapErg.Handleforce;
angle = ExtrapErg.ChainAngle;
smoothforce = filtfilt(b,a,force);
```

```
handloadx = zeros(length(smoothforce),1);
handloady = (smoothforce.*cosd(angle))/2;
handloadz = (smoothforce.*sind(angle))/2;

HandLoads = array2table([ExtrapErg.Stroke, ExtrapErg.Frames,
ExtrapErg.ChainAngle, smoothforce, handloadx, handloady, handloadz]);
HandLoads.Properties.VariableNames =
{'Stroke','Frame','ChainAngle','FiltHandleForce','HandLoadX','HandLoadY','Han
dLoadZ'};

%%%%%%%%%%%%%%%%%%%%%%%%%%%%%%%%%%%%%%%%%%%%%%%%%%%%%%%%%%%%%%%%%%%%%%%%%%%
%% Normalize Erg data to percent stroke completion - 200 data points %%
disp('Normalizing Erg Data to 201 percentage points...')
Stroke=[];
Wq = [];
Wr = [];
Zq = [];
for m = 1:Erg_strokecount
     k=length(find(ExtrapErg.Stroke==m));
     % the number of frames per stroke from the Fob data
     w=(1:k)';
     % the number of samples per stroke from the erg data
     i=(find(ExtrapErg.Stroke==m,1,'first')):(find(ExtrapErg.Stroke==m,1,'last
     '));
     % index the number of samples within each stroke from the erg data
     z=table2array(ExtrapErg(i,1:end));
     % erg data sample y values input to interpolate
     wq = (linspace(1,k,201))';
     % erg data x values/times/points to query output from interpolation
     wr = linspace(0,100,201)';
     % create stroke percent complete vector
     zq = interp1(w,z,wq,'linear');
     % erg data y values to query output from interpolation
     stroke=m*(true(length(wr),1));
     % assign stroke number to new sample outputs
     Stroke=[Stroke;stroke];
     Wq = [Wq; wq];
     Wr = [Wr; wr];
     Zq = [Zq; zq];
end
NormErg = array2table([Stroke, Wr, Zq(:,3:end)]);
NormErg.Properties.VariableNames([1 2]) = {'Stroke','Time'};
NormErg.Properties.VariableNames(3:end) =
ExtrapErg.Properties.VariableNames(3:end);

% Normalize Vicon data to percent stroke completion - 200 data points
disp('Normalizing Vicon Data to 201 percentage points...')
Stroke=[];
Xq = [];
Xr = [];
Vq = [];
for m = 1:Vicon_strokecount
     j=length(find(ReducedVicon.Stroke==m));
     % the number of samples per stroke from the erg data
     i=(find(ReducedVicon.Stroke==m,1,'first')):(find(ReducedVicon.Stroke==m,1
     ,'last'));
     % index the number of samples within each stroke from the erg data
```

```
    x=(1:j)';
    % erg data sample x values input to interpolate
    v=table2array(ReducedVicon(i,1:end));
    % erg data sample y values input to interpolate
    xq = (linspace(1,j,201))';
    % erg data x values/times/points to query output from interpolation
    xr = linspace(0,100,201)';
    % create stroke percent complete vector
    vq = interp1(x,v,xq,'linear');
    % erg data y values to query output from interpolation
    stroke=m*(true(length(xr),1));
    % assign stroke number to new sample outputs
    Stroke=[Stroke;stroke];
    Xq = [Xq; xq];
    Xr = [Xr; xr];
    Vq = [Vq; vq];
end
NormVicon = array2table([Stroke, Xr, Vq(:,2:end)]);
NormVicon.Properties.VariableNames([1 2]) = {'Stroke','Percent'};
NormVicon.Properties.VariableNames(3:end) =
ReducedVicon.Properties.VariableNames(2:end);

%%%%%%%%%%%%%%%%%%%%%%%%%%%%%%%%%%%%%%%%%%%%%%%%%%%%%%%%%%%%%%%%%%%%%%%%%%%%%%%
% ONLY RUN THIS SECTION IF THE VICON AND ERG VECTORS ARE 201 POINTS %%
% Average - Trims out stroke numbers 1-2 and last two strokes
% creates a cell array with each cell containing one stroke

disp('Averaging normalized Erg data...')
for m = 1:Erg_strokecount
    k=length(find(NormErg.Stroke==m));
    % the number of samples per stroke from the erg data
    l=(find(NormErg.Stroke==m,1,'first')):(find(NormErg.Stroke==m,1,'last'));
    % index the number of samples within each stroke from the erg data
    vv=table2array(NormErg(l,1:end));
    ErgStrokes(m) = {vv};
end

% this averages the matched values across all the cells
ErgSum = zeros(k,size(NormErg,2));
for m = 1:Erg_strokecount
    ErgSum = ErgSum + ErgStrokes{m};
end
ErgMean = ErgSum ./(Erg_strokecount);
AvgErg = array2table(ErgMean);
AvgErg.Properties.VariableNames = NormErg.Properties.VariableNames;

% Vicon Data Averaging
disp('Averaging normalized Vicon data...')
for m = 1:Vicon_strokecount
    i=length(find(NormVicon.Stroke==m));
    % the number of samples per stroke from the Vicon data

    j=(find(NormVicon.Stroke==m,1,'first')):(find(NormVicon.Stroke==m,1,'last
    '));
    uu=table2array(NormVicon(j,1:end));
    ViconStrokes(m) = {uu};
end
```

```
% this averages the matched values across all the cells, excluding the first
and last strokes.
ViconSum = zeros(i,size(NormVicon,2));
for m = 1:Vicon_strokecount
    ViconSum = ViconSum + ViconStrokes{m};
end
ViconMean = ViconSum ./ (Vicon_strokecount);
AvgVicon = array2table(ViconMean);
AvgVicon.Properties.VariableNames = NormVicon.Properties.VariableNames;

%% WRITE OUT A MULTI SHEET COMBINED EXCEL WORKBOOK OF VICON AND ERG DATA
disp('Exporting Erg and Vicon Data to Excel...')
writetable(Frames,fileout,'Sheet','Frames');
writetable(ReducedErg,fileout,'Sheet','Cropped Erg');
writetable(ExtrapErg,fileout,'Sheet','Extrapolated Erg');
writetable(NormErg,fileout,'Sheet','Normalized Erg');
writetable(AvgErg,fileout,'Sheet','Average Erg');
writetable(ReducedVicon,fileout,'Sheet','Vicon');
writetable(NormVicon,fileout,'Sheet','Normalized Vicon');
writetable(AvgVicon,fileout,'Sheet','Average Vicon');
writetable(HandLoads,fileout,'Sheet','HandLoads');


%%%%%%%%%%%%%%%%%%%%%%%%%%%%%%%%%%%%%%%%%%%%%%%%%%%%%%%%%%%%%%%%%%%%%%%%%%%%
function Lags = CatchLatency(ExtrapErg)
    %%
    handle_force=ExtrapErg.Handleforce;
    handle_pos=ExtrapErg.AntPosthandleposition;
    idx=1:length(handle_force);
    ETF = islocalmin(handle_pos,'MinSeparation',100,'MinProminence',100);
    strokeIndex=[1;find(ETF)];
    strokeStart=handle_pos(strokeIndex);

    % CREATE A LOGICAL VECTOR TO FIND CATCH POINTS FOR ALL STROKES WITHIN
    % THE TIME SERIES %%
    % there is probably a more elegant/robust way to do this that does not
    % involve hard-coding force values as integers, like with diff function
    for n = 4:length(handle_force)
        catchpoints (n-3) = ((handle_force(n-3)-handle_force(n-2)<10) && ...
            (handle_force(n-2)-handle_force(n-1)<10) && ...
            (handle_force(n-1)-handle_force(n)<10) && ...
            (handle_force(n)>75) && ...
            (handle_force(n-3)<50));
    end

    % EXTRACT THE INDICES OF THE CATCH POINTS FROM THE HANDLE FORCE %%
    % Check for clusters of indices and retain only the first index of the
    % cluster as the true catch index
    catchIndex = find(catchpoints);
    % extracts the catch start indices for each stroke
    for j = 2:length(catchIndex)
        if (catchIndex(j)-catchIndex(j-1)==1)
            catchpoints(catchIndex(j))=0;
        end
    end
    catchIndex = find(catchpoints)';
```

```
    % relabels the catch start indices for each stroke to handle clusters
    catchStart = handle_force(catchIndex);
    % indexes the catch start indices into the handle force vector
    plot(idx,handle_force,catchIndex,catchStart,'r*'); axis tight

% Calculate the latency between the strokeStart index and the catchStart
% index
% Must run this section separately - need to look at the plot for any
% discrepancies or hiccups in catch/stroke point selection. Look
% specifically for the horizontal distance between the indices - this is
% your frame lag (i.e., the time lag between the minimum handle position and
% the start of handle force generation).
latency_idx = padcat(strokeIndex,catchIndex);
figure; plot(latency_idx(:,1),'c*'); hold on; plot(latency_idx(:,2),'r*');
legend('strokeIndex','catchIndex','location','southeast');
latency_idx(:,3) = latency_idx(:,2)-latency_idx(:,1);

%%
strokeIndex=latency_idx(:,1);
catchIndex=latency_idx(:,2);
framelag=latency_idx(:,3);
percentlag = ExtrapErg.Percent(catchIndex);

Lags=[latency_idx,percentlag];
Lags=array2table(Lags);
Lags.Properties.VariableNames =
{'StrokeStart','ForceStart','FrameLag','PercentLag'};
```

APPENDIX C: SUPPLEMENTAL SPATIO-TEMPORAL RESULTS

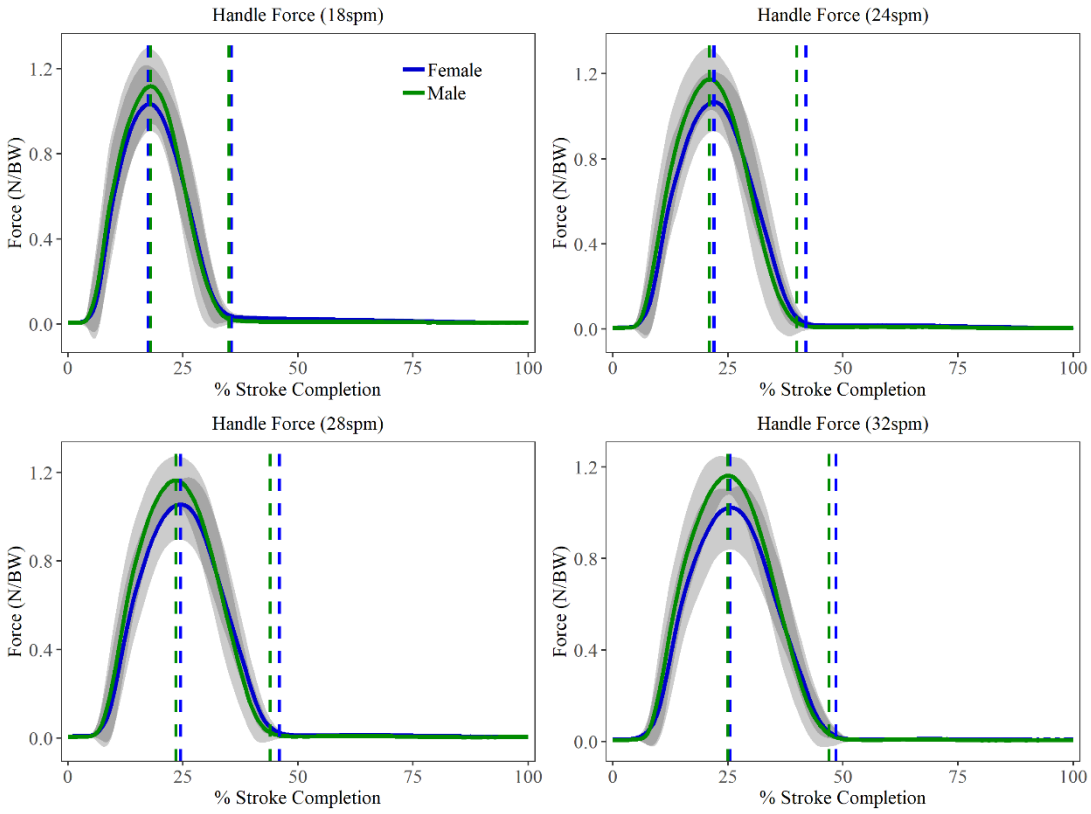

Figure 0.1: Body weight normalized handle force (mean ± std) for female and male rowers at all stroke rates.

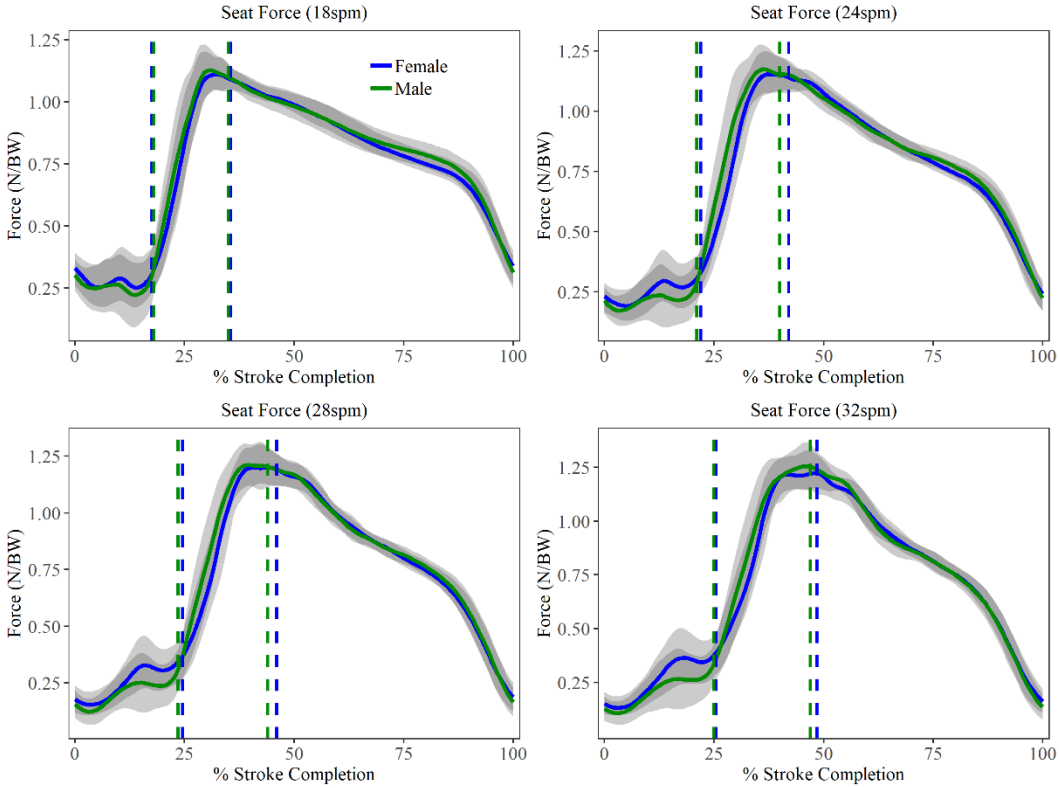

Figure 0.2: Body weight normalized seat force (mean ± std) for female and male rowers at all stroke rates.

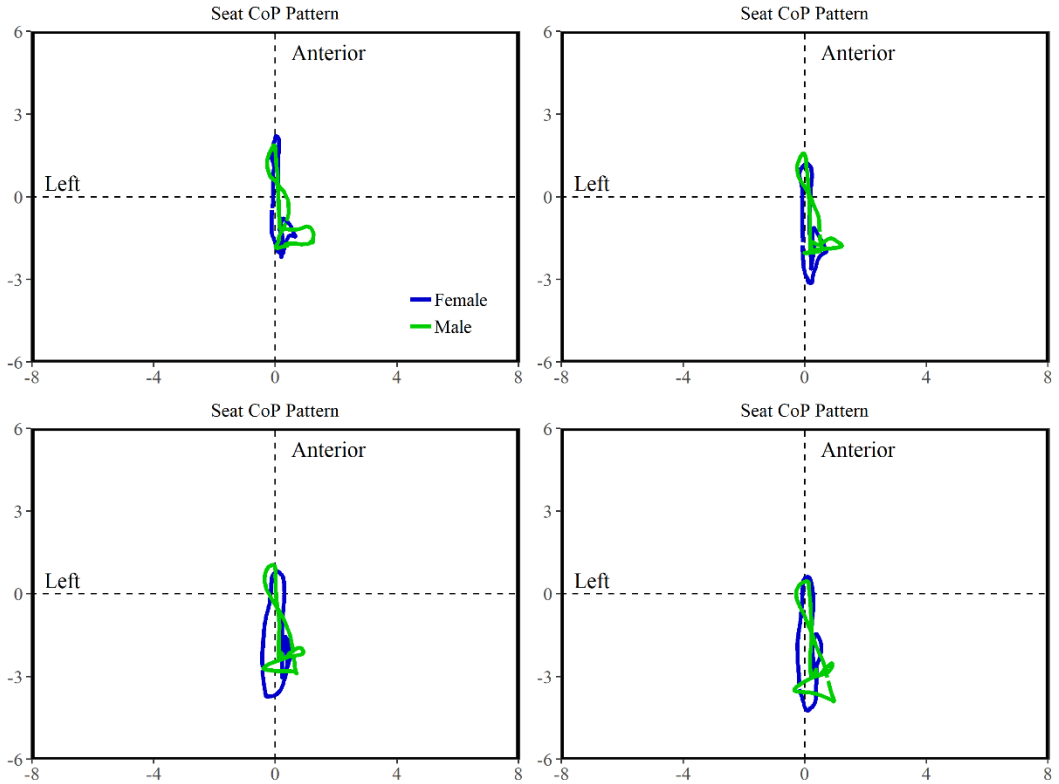

Figure 0.3: Top-down view of ergometer seat CoP (mean paths) in centimeters through the stroke cycle for males versus females at 18 spm (*top left*), 24 spm (*top right*), 28 spm (*bottom left*), 32 spm (*bottom right*).

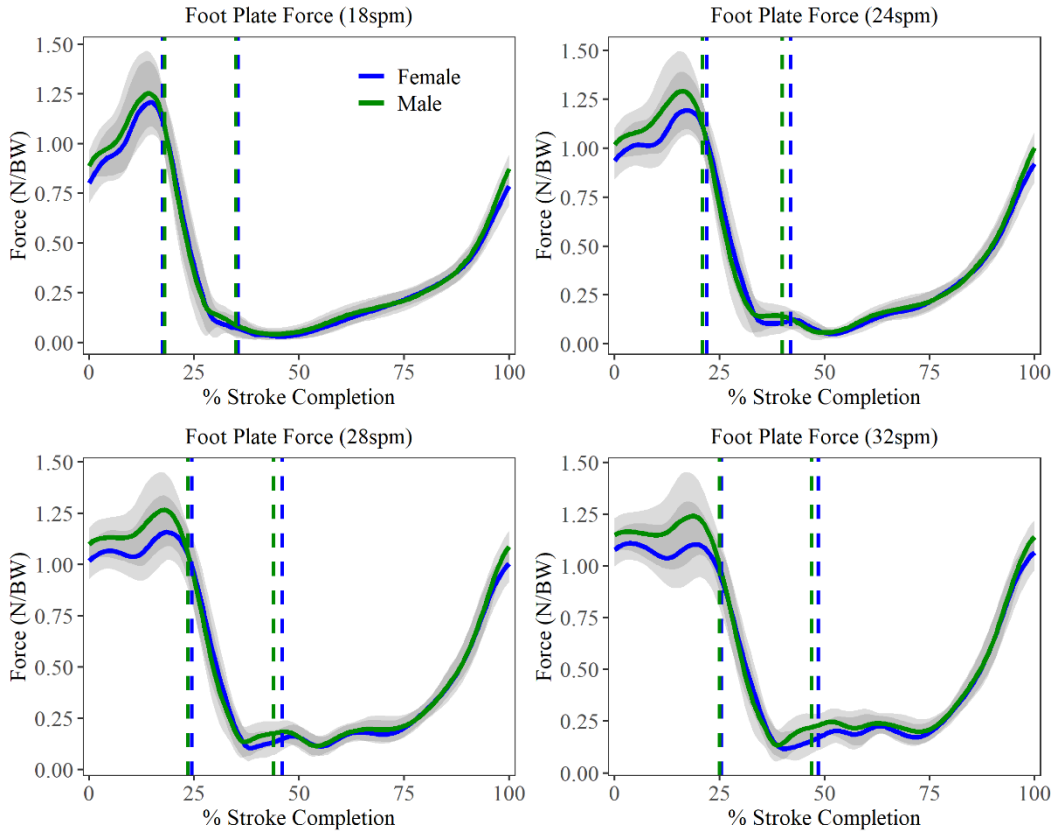

Figure 0.4: Body weight normalized footplate force (mean ± std) for female and male rowers at all stroke rates.

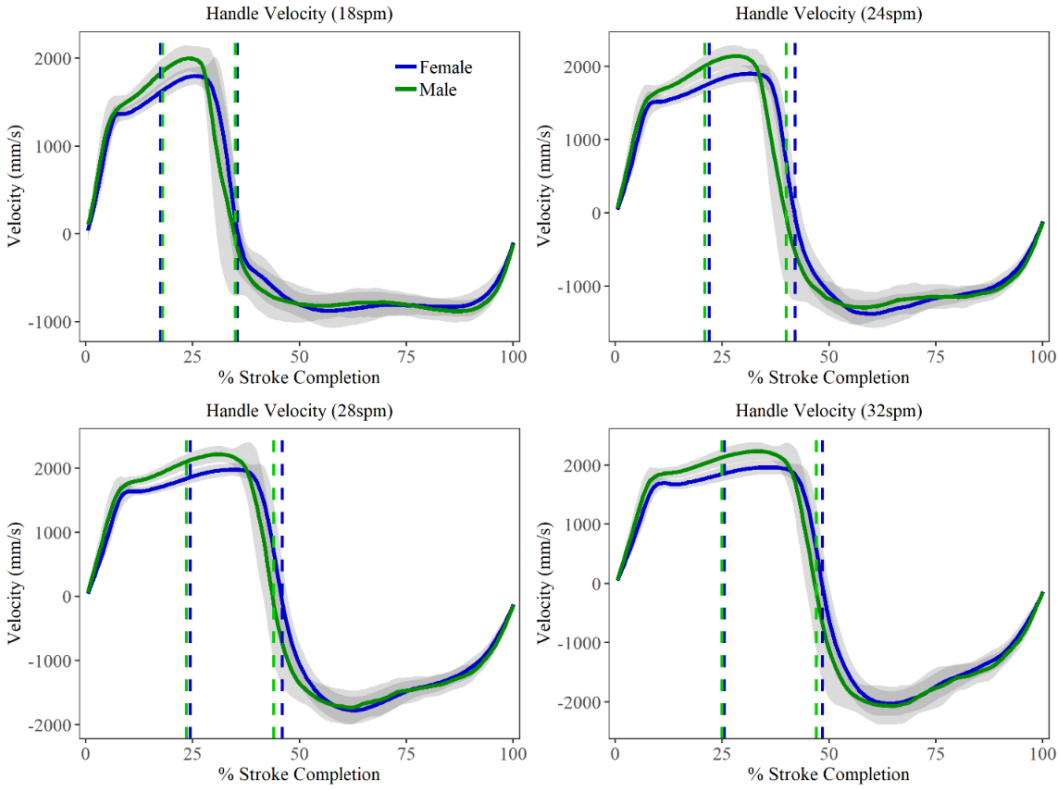

Figure 0.5: Handle velocity (mean ± std) for female and male rowers at all stroke rates.

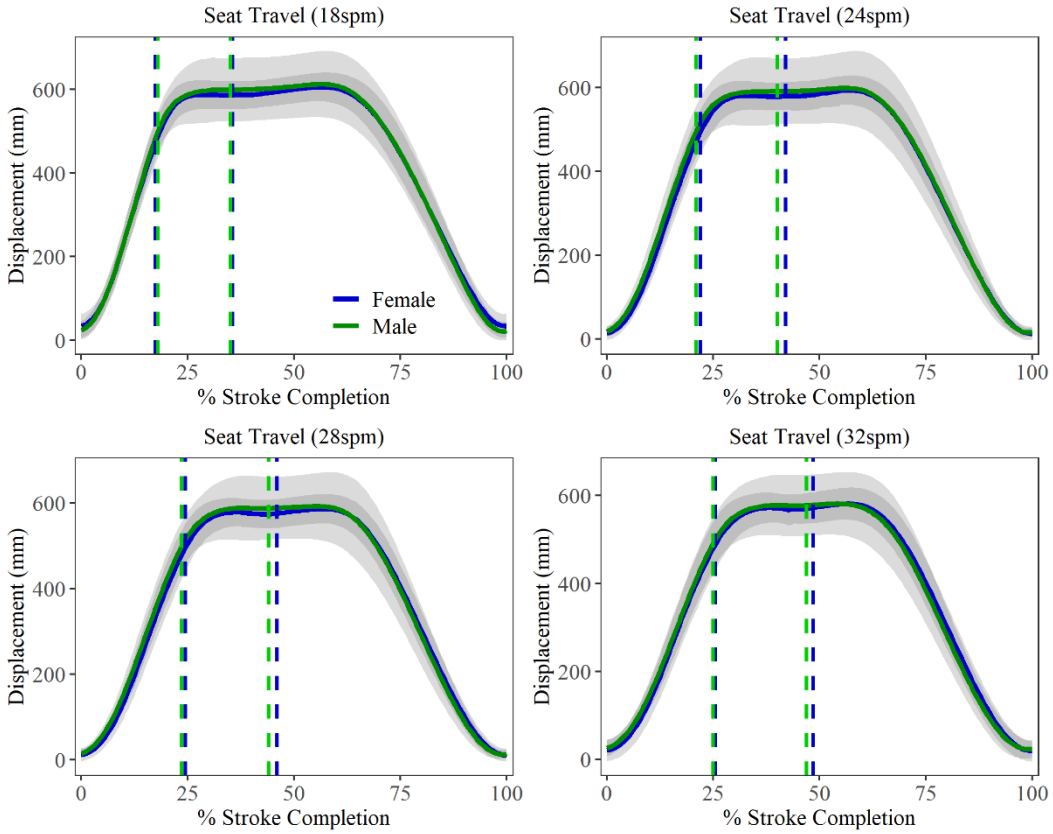

Figure 0.6: Seat displacement (mean ± std) for female and male rowers at all stroke rates.

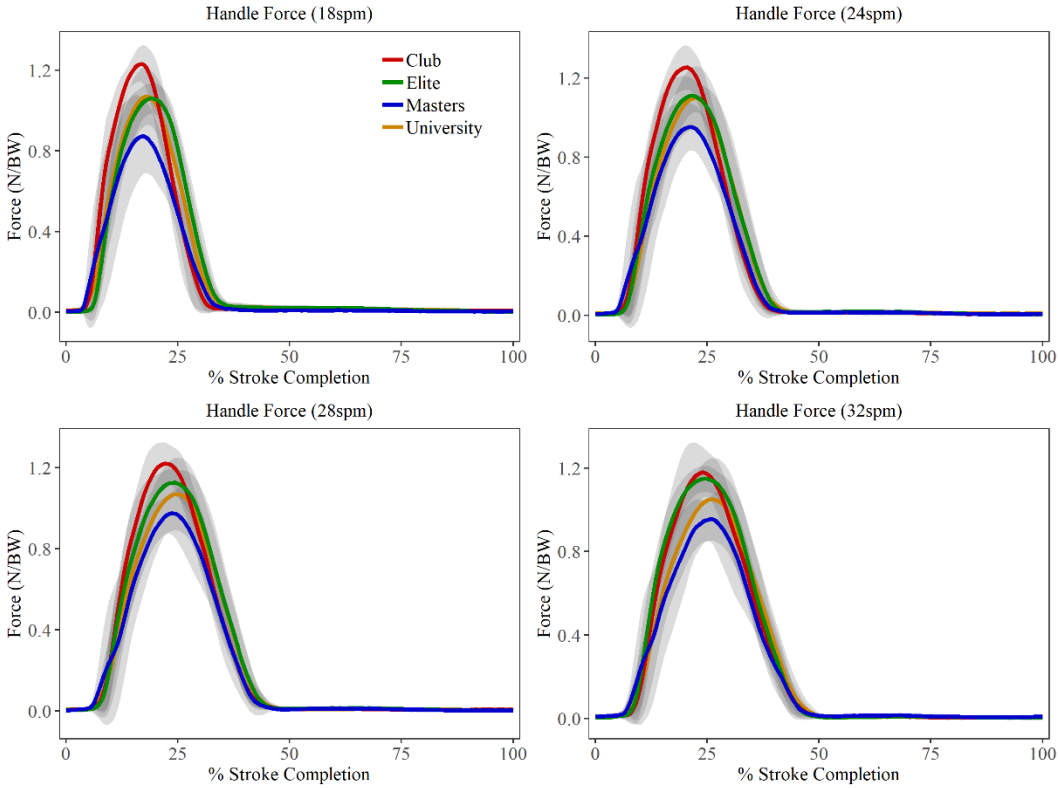

Figure 0.7: Body weight normalized handle force (mean ± std) for age/competition level cohorts at all stroke rates.

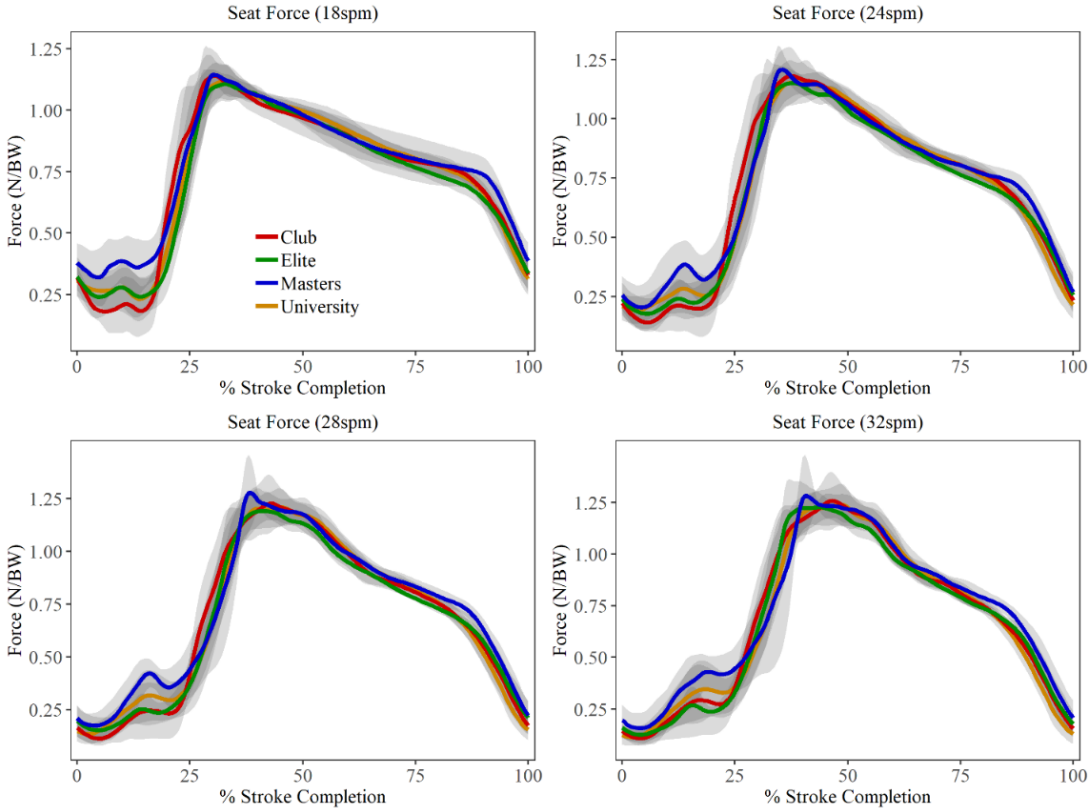

Figure 0.8: Body weight normalized seat force (mean ± std) for age/competition level cohorts at all stroke rates.

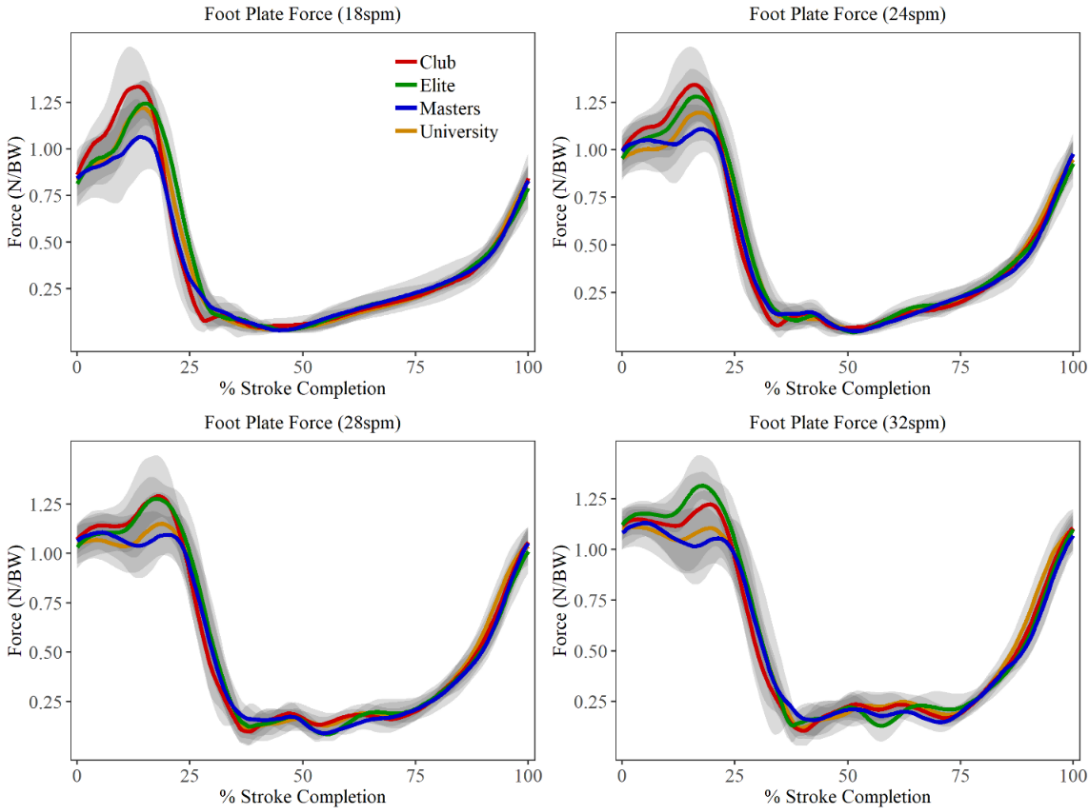

Figure 0.9: Body weight normalized foot force (mean ± std) for age/competition level cohorts at all stroke rates.

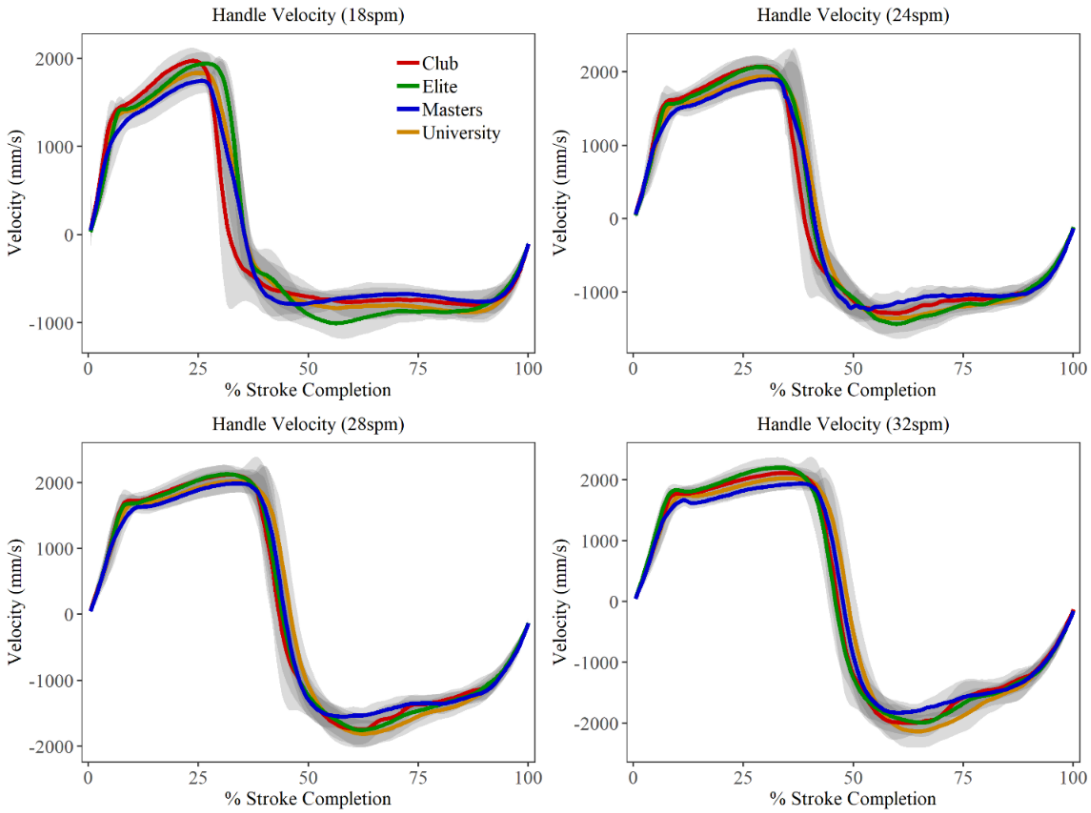

Figure 0.10: Handle velocity (mean ± std) for age/competition level cohorts at all stroke rates.

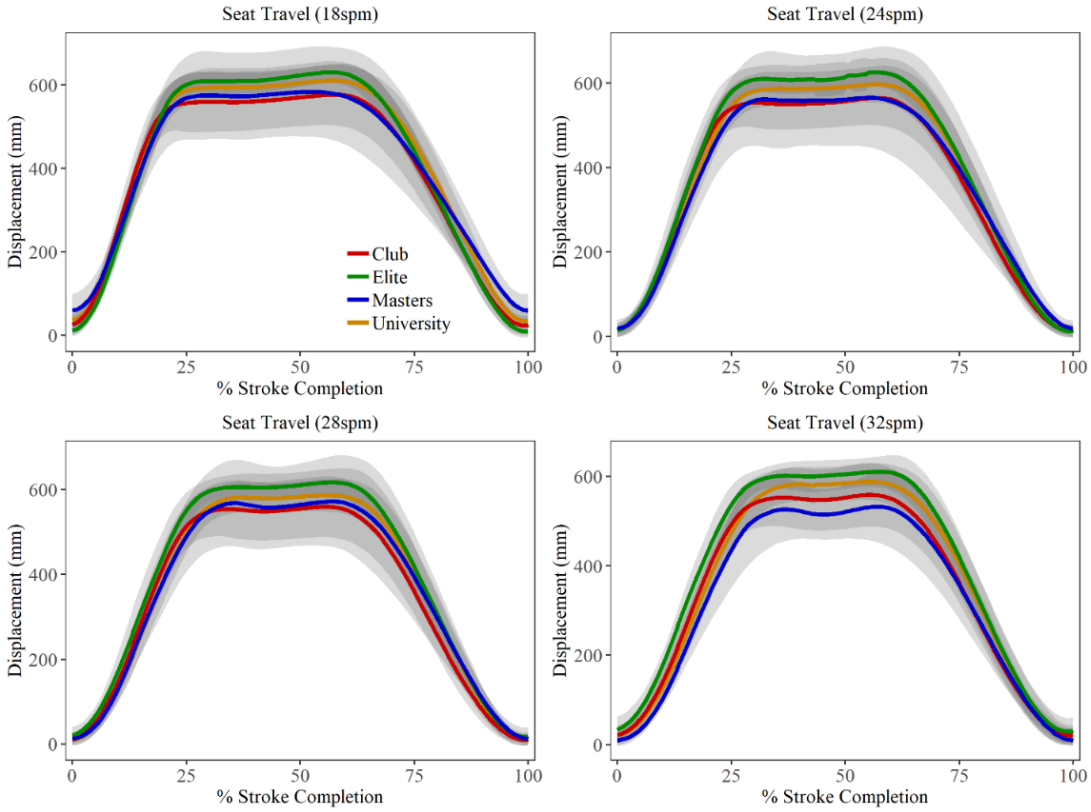

Figure 0.11: Seat displacement (mean ± std) for age/competition level cohorts at all stroke rates.

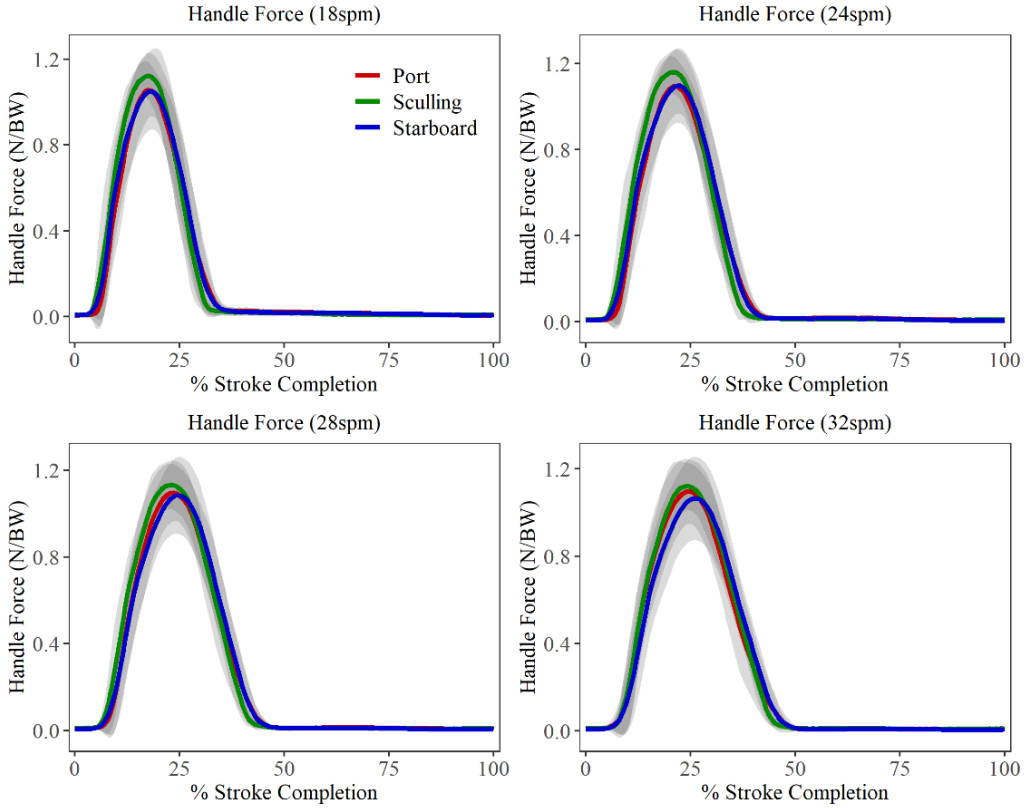

Figure 0.12: Body weight normalized handle force (mean ± std) by preferred rowing modality at all stroke rates.

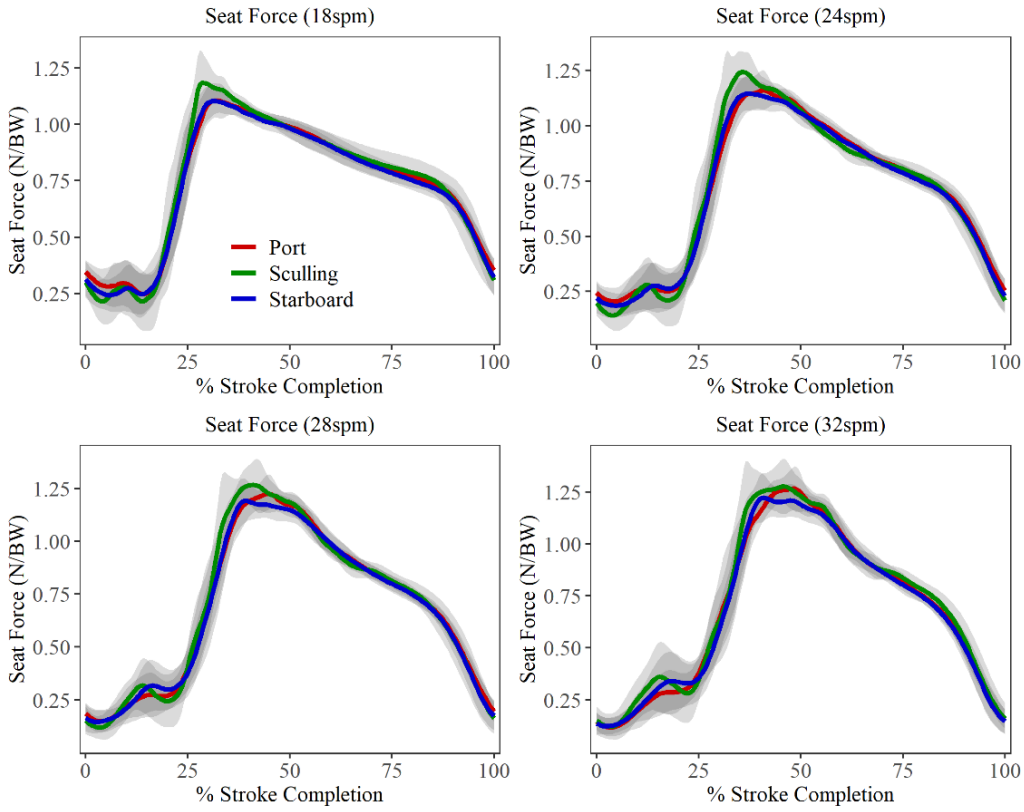

Figure 0.13: Body weight normalized seat force (mean ± std) by preferred rowing modality at all stroke rates.

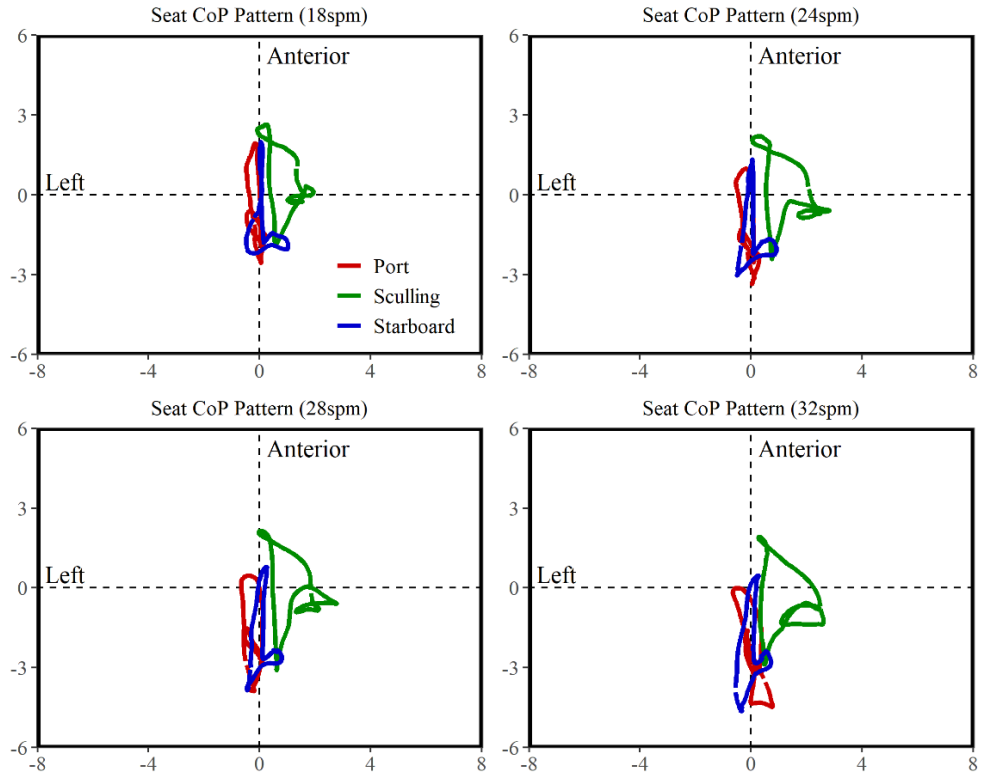

Figure 0.14: Top-down view of ergometer seat CoP (mean paths) in centimeters through the stroke cycle by preferred rowing modality at all stroke rates.

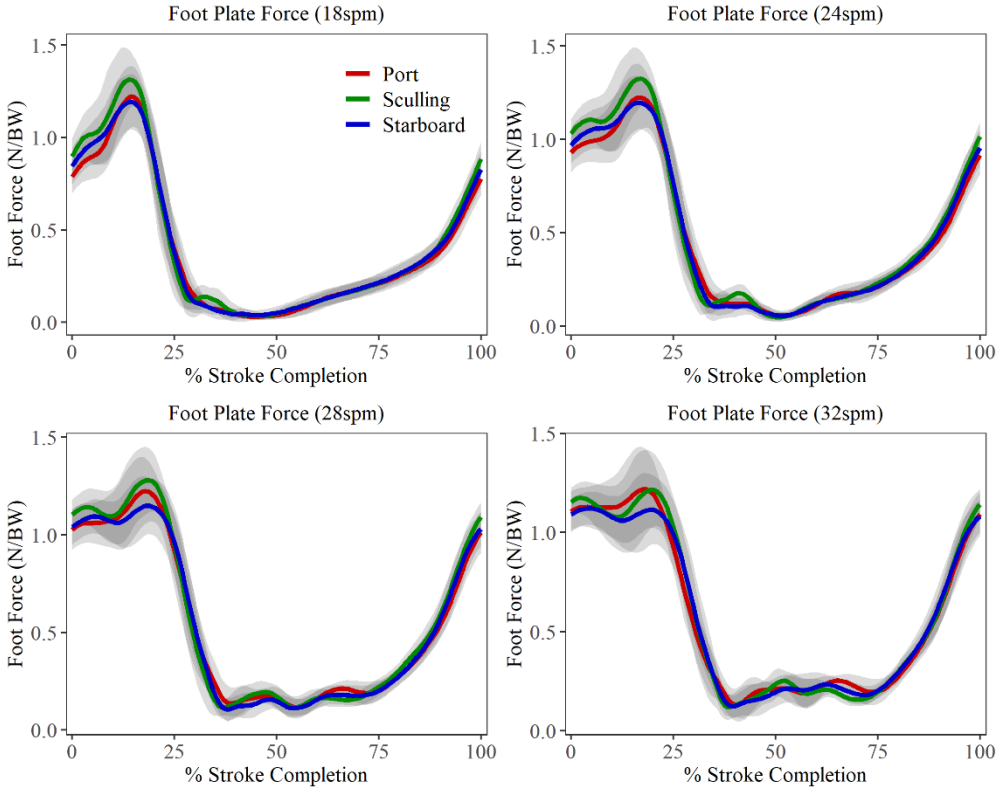

Figure 0.15: Body weight normalized footplate force (mean ± std) by preferred rowing modality at all stroke rates.

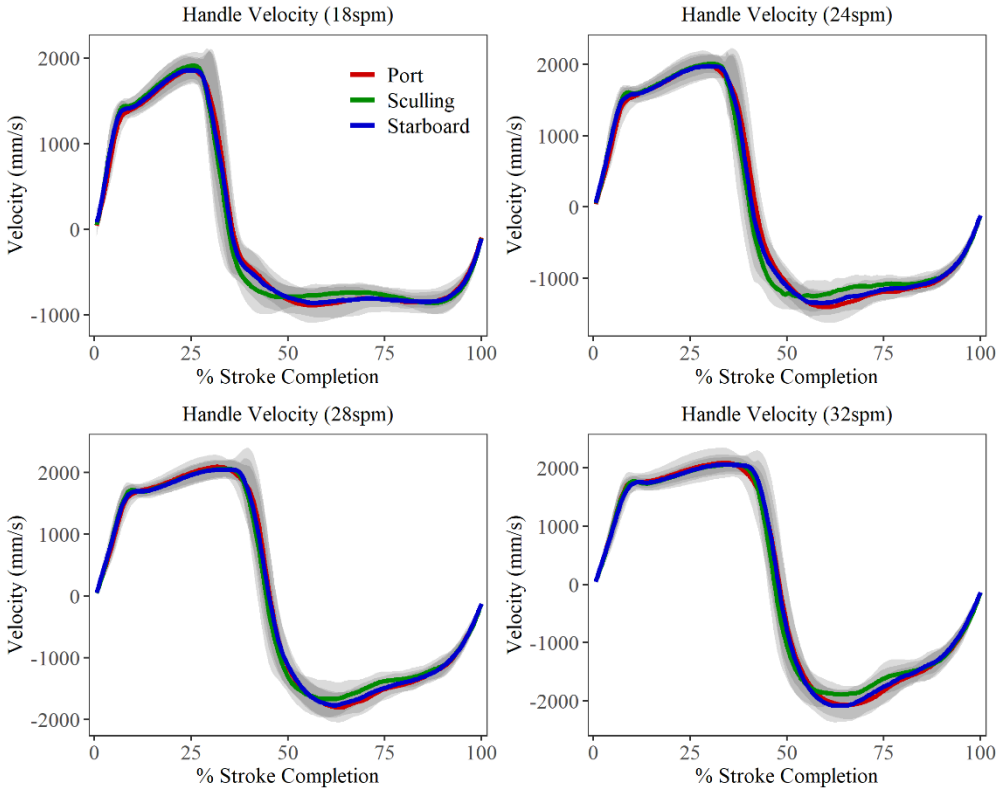

Figure 0.16: Handle velocity (mean ± std) for preferred rowing modality cohorts at all stroke rates.

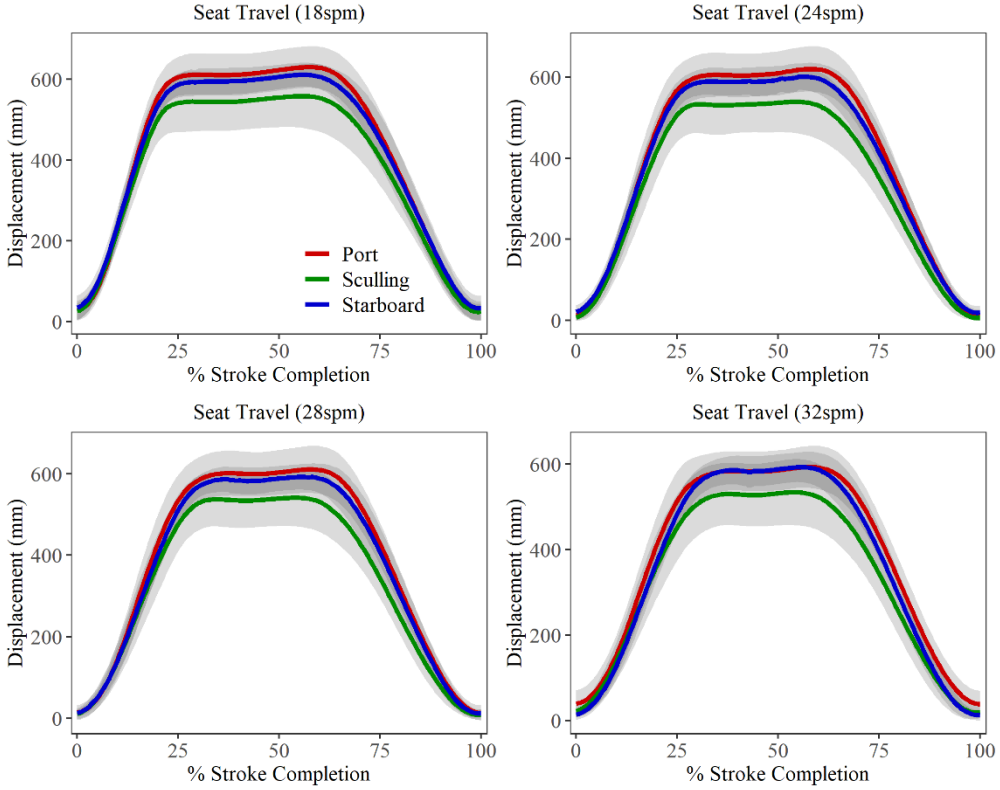

Figure 0.17: Seat displacement (mean ± std) for preferred rowing modality cohorts at all stroke rates.

APPENDIX D: SUPPLEMENTAL BIOMECHANICS RESULTS

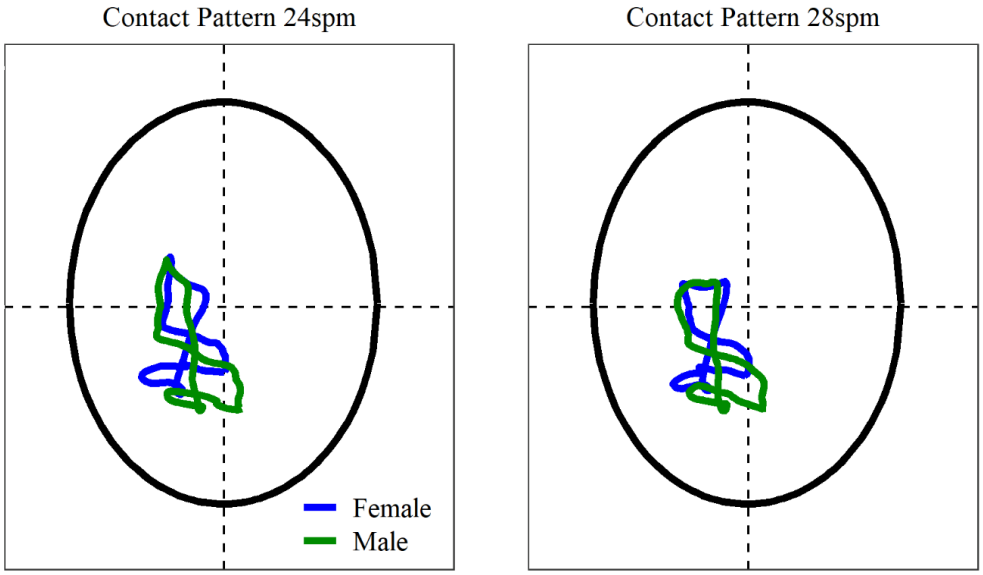

Figure 0.1: Glenoid contact patterns (mean paths) for male versus female rowers.

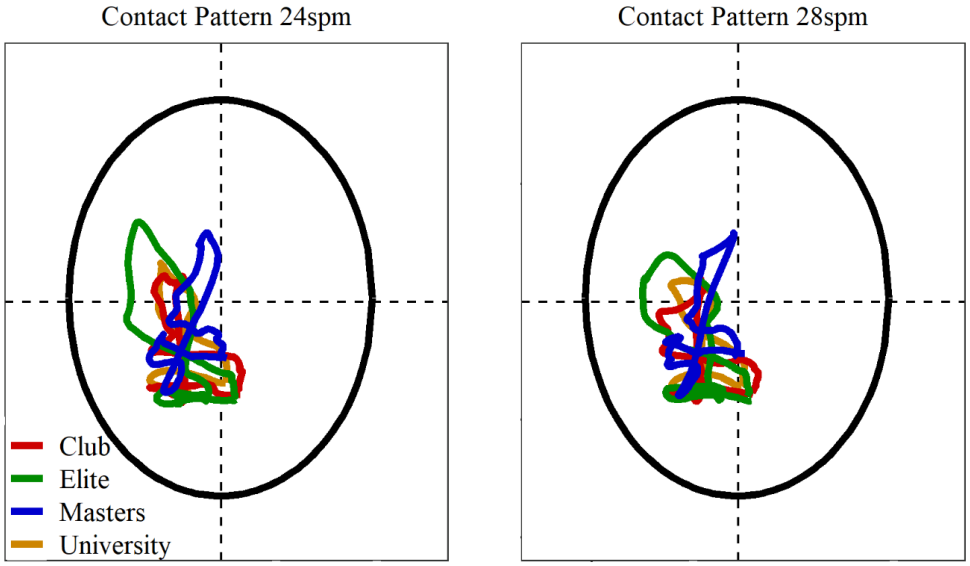

Figure 0.2: Glenoid contact patterns (mean paths) for age/competition level cohorts.

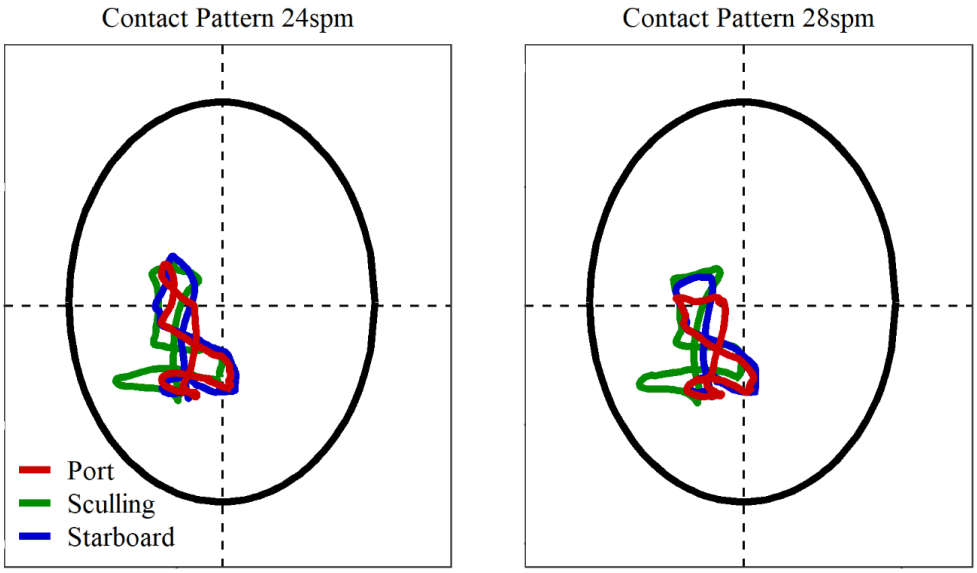

Figure 0.3: Glenoid contact patterns (mean paths) by preferred rowing modality.

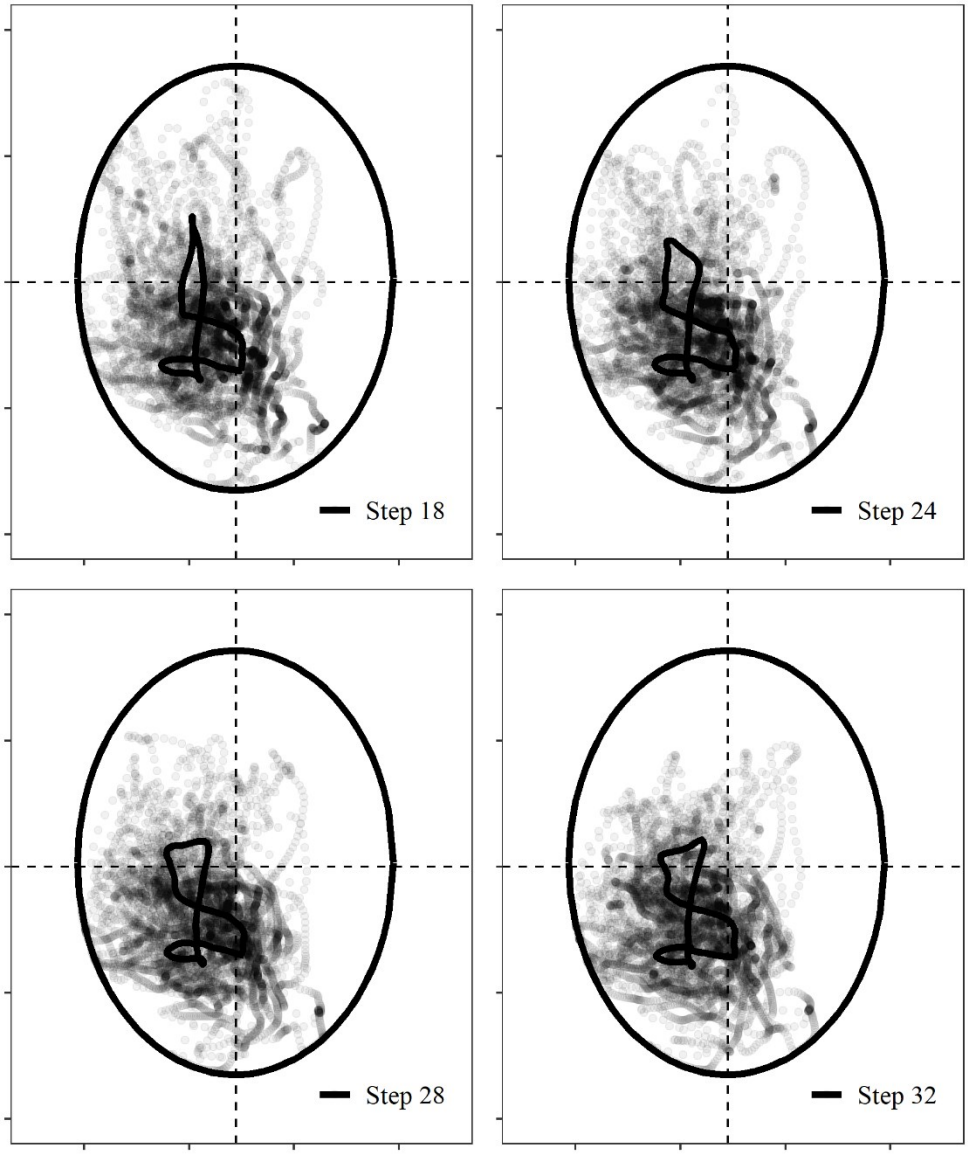

Figure 0.4: Population-wide glenoid contact patterns (mean paths and point clouds) at all stroke rates.

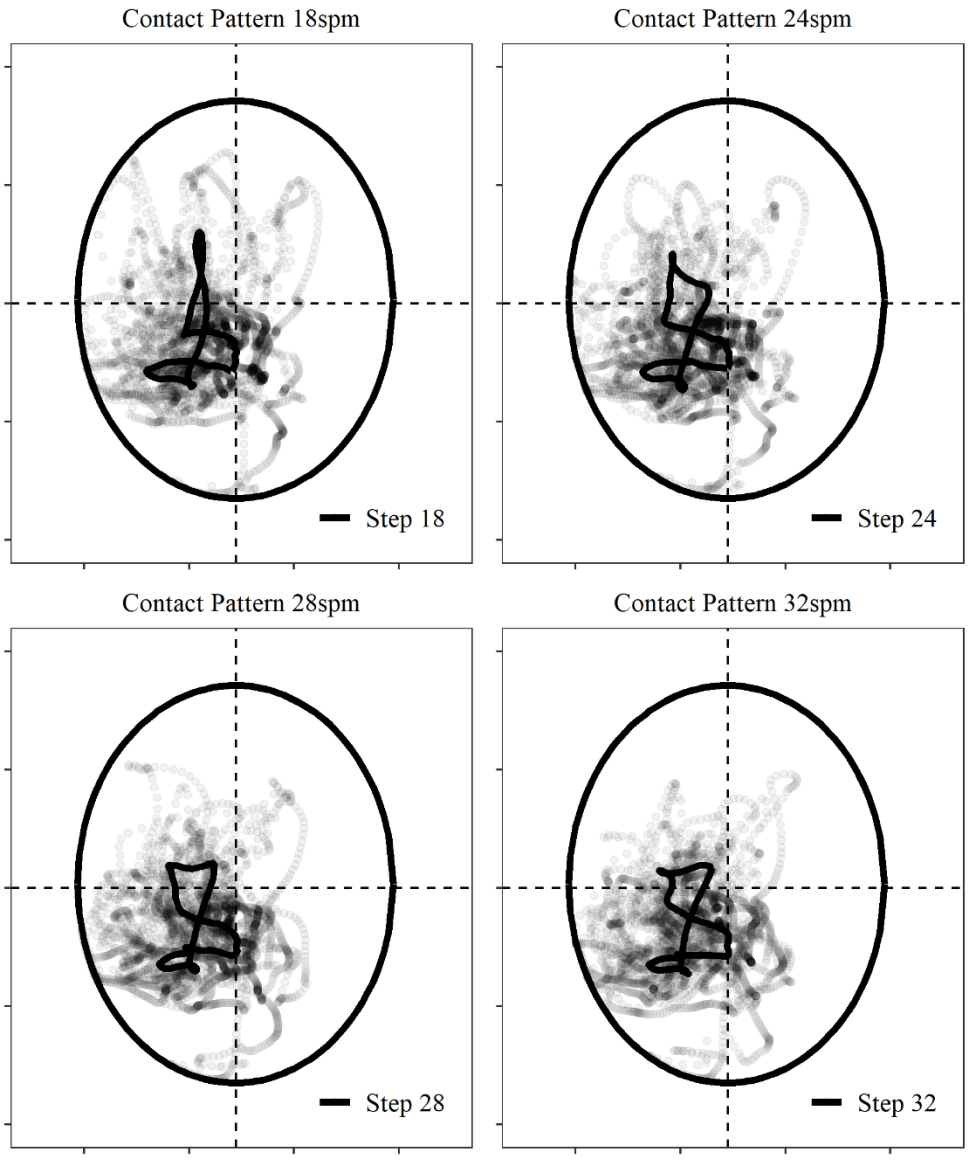

Figure 0.5: Glenoid contact patterns (mean paths and point clouds) for female rowers at all stroke rates.

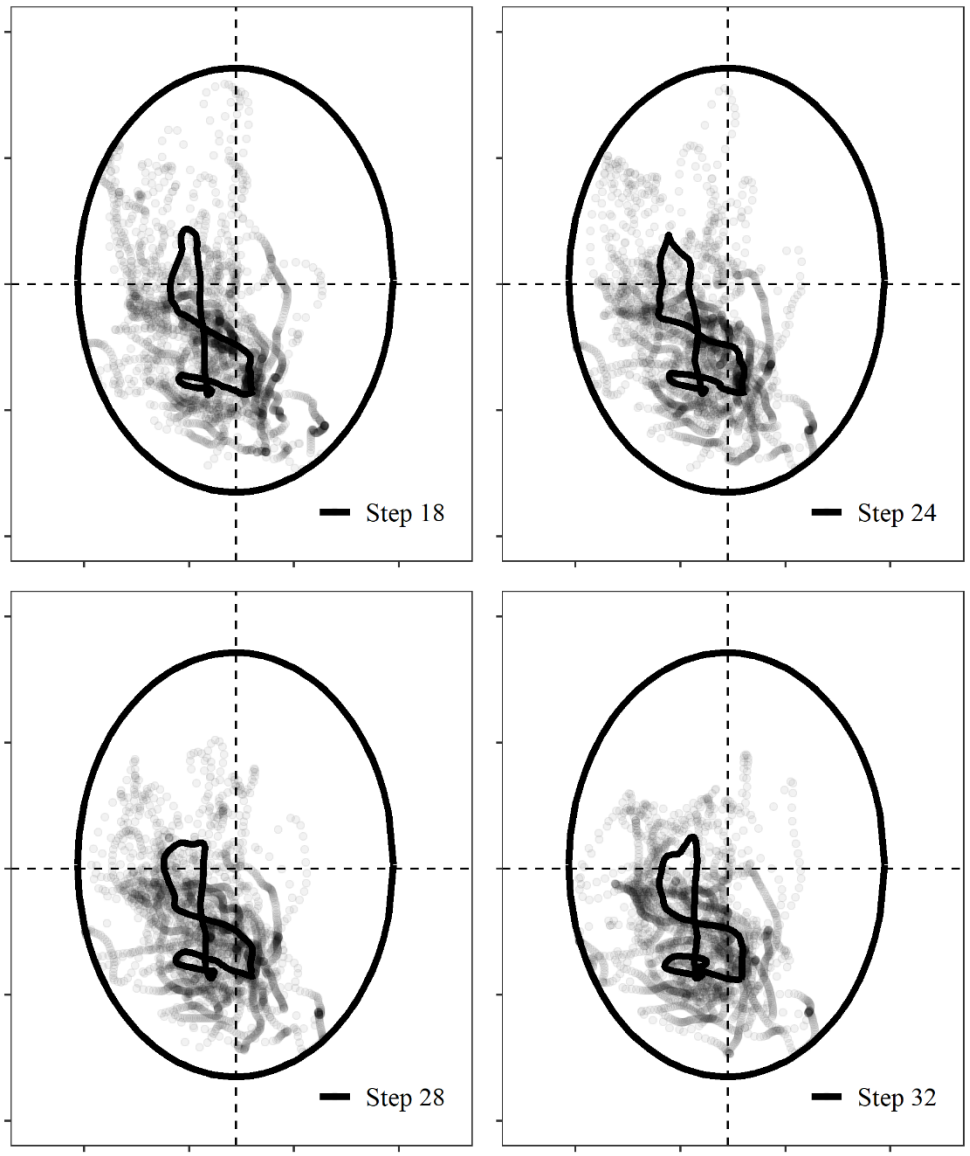

Figure 0.6: Glenoid contact patterns (mean paths and point clouds) for male rowers at all stroke rates.

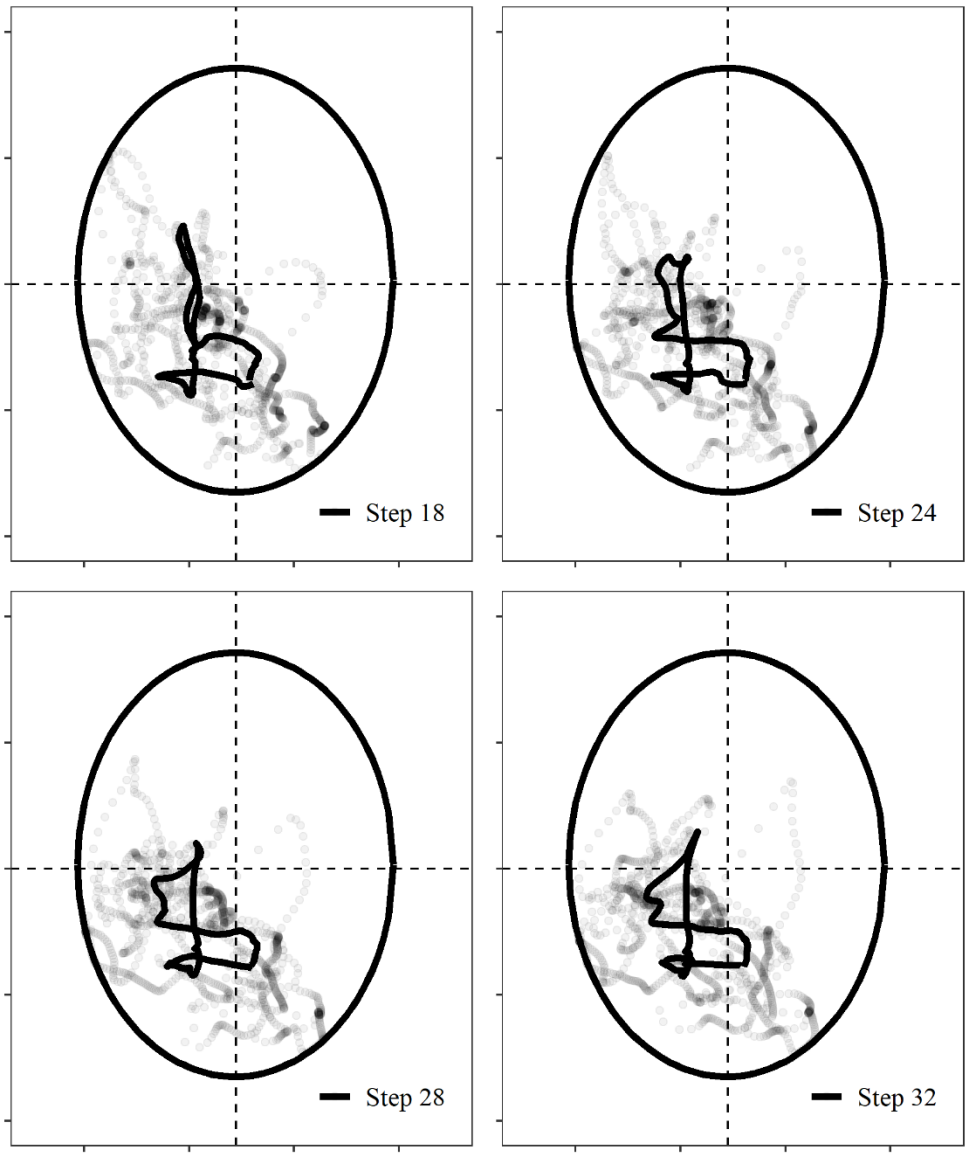

Figure 0.7: Glenoid contact patterns (mean paths and point clouds) for club rowers at all stroke rates.

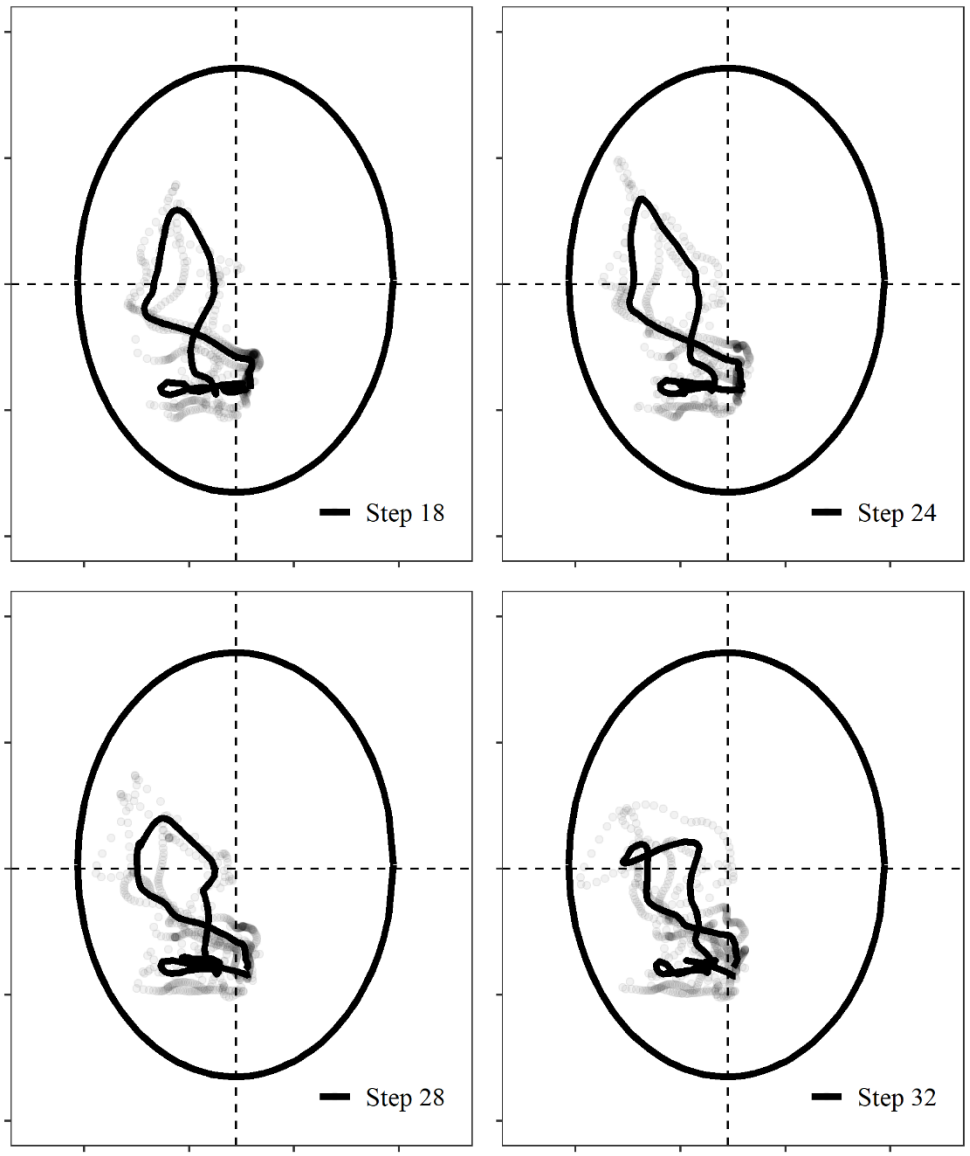

Figure 0.8: Glenoid contact patterns (mean paths and point clouds) for elite rowers at all stroke rates.

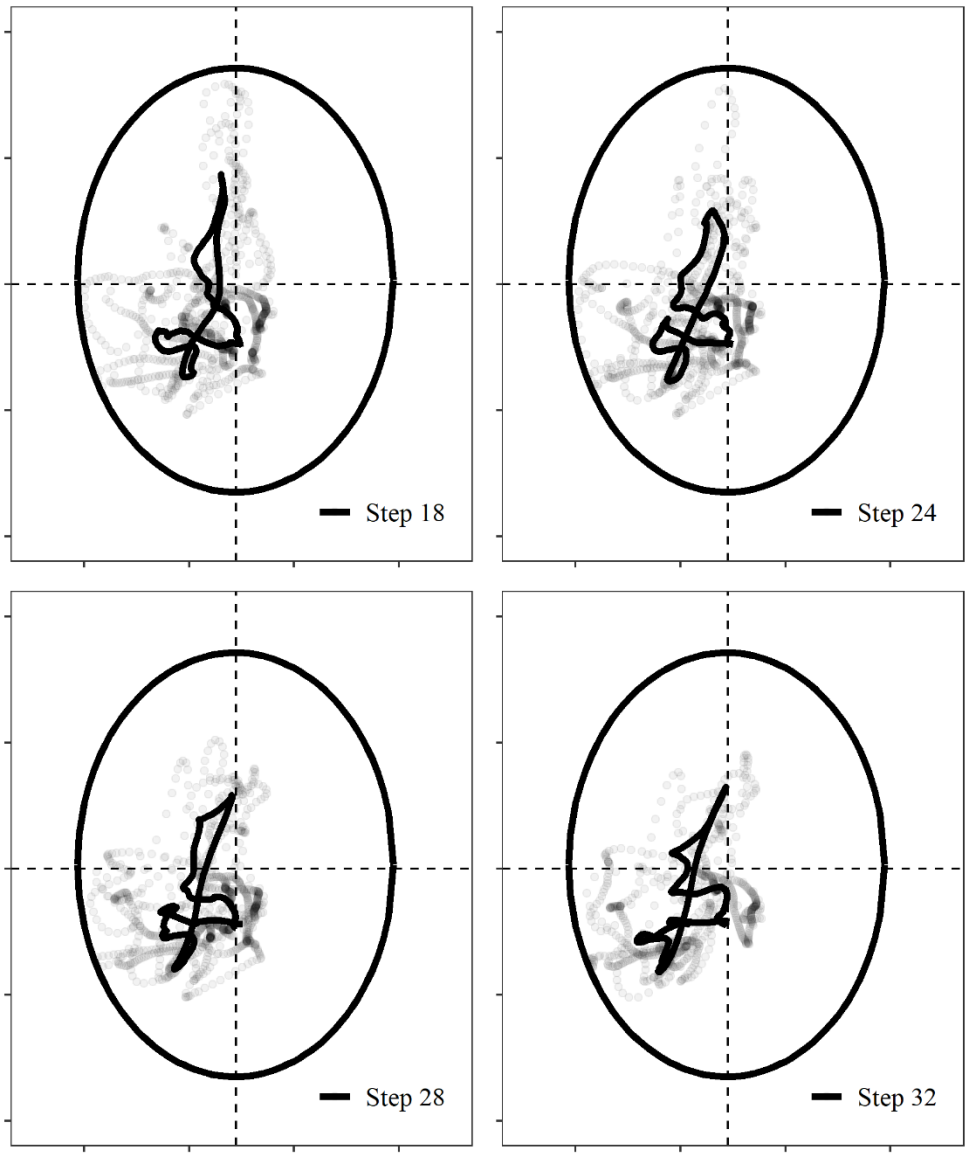

Figure 0.9: Glenoid contact patterns (mean paths and point clouds) for masters rowers at all stroke rates.

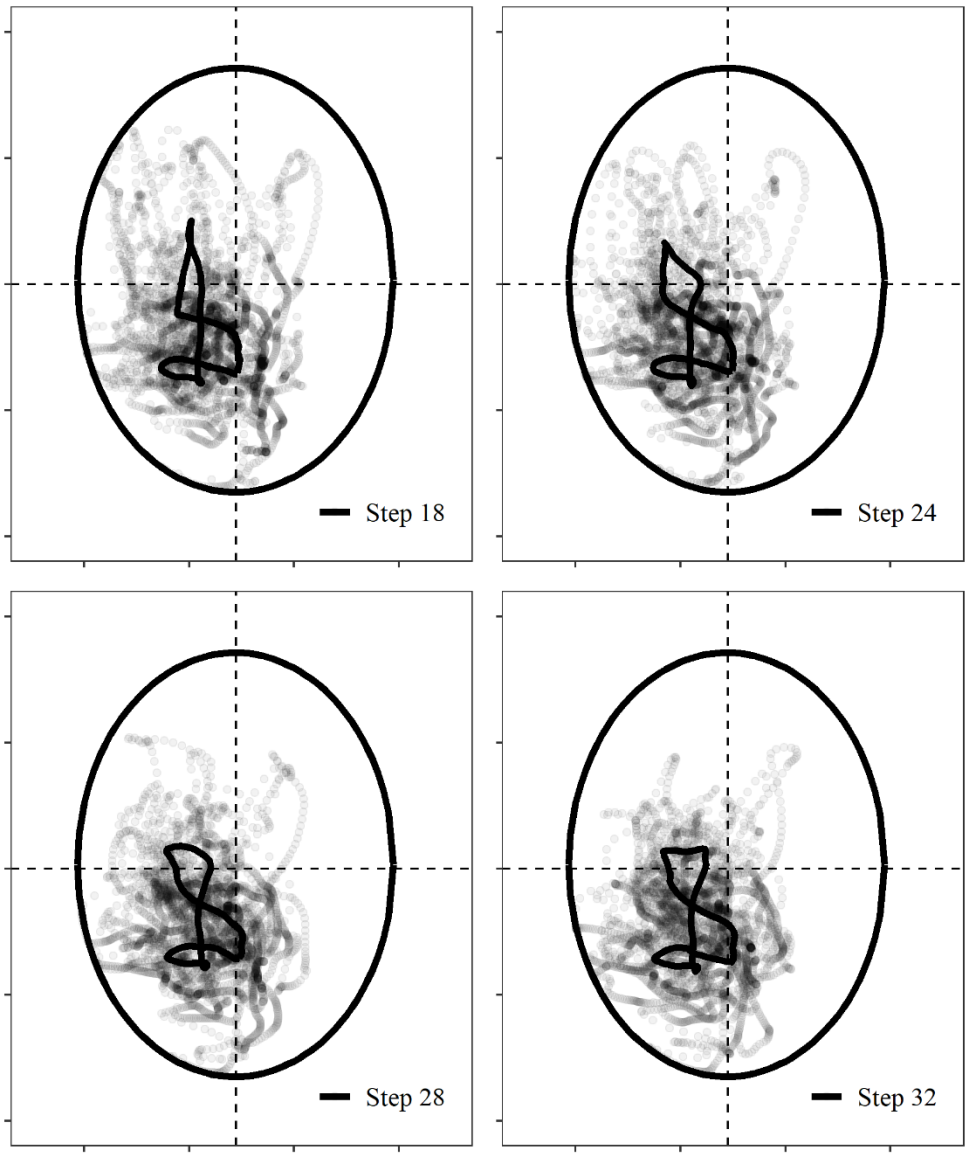

Figure 0.10: Glenoid contact patterns (mean paths and point clouds) for university rowers at all stroke rates

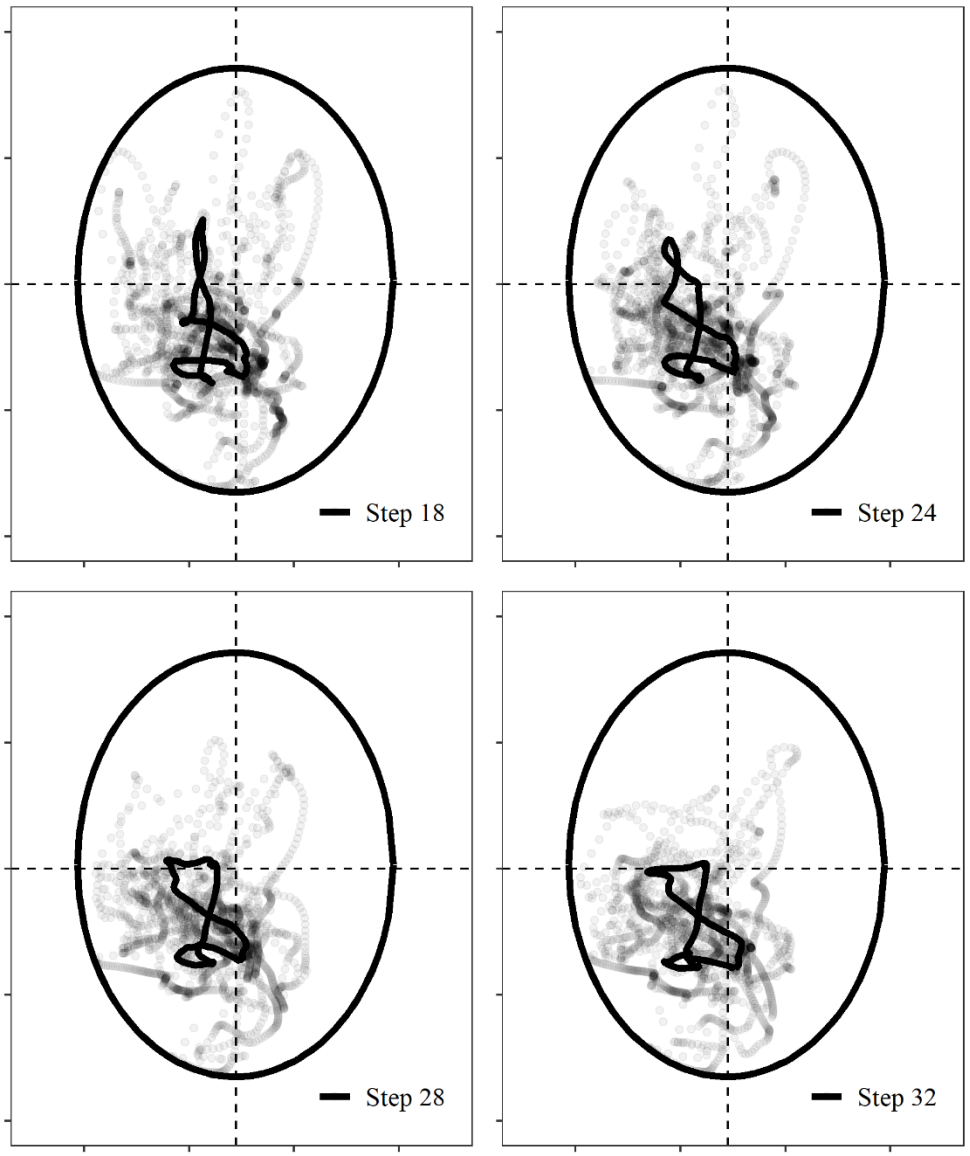

Figure 0.11: Glenoid contact patterns (mean paths and point clouds) for port rowers at all stroke rates.

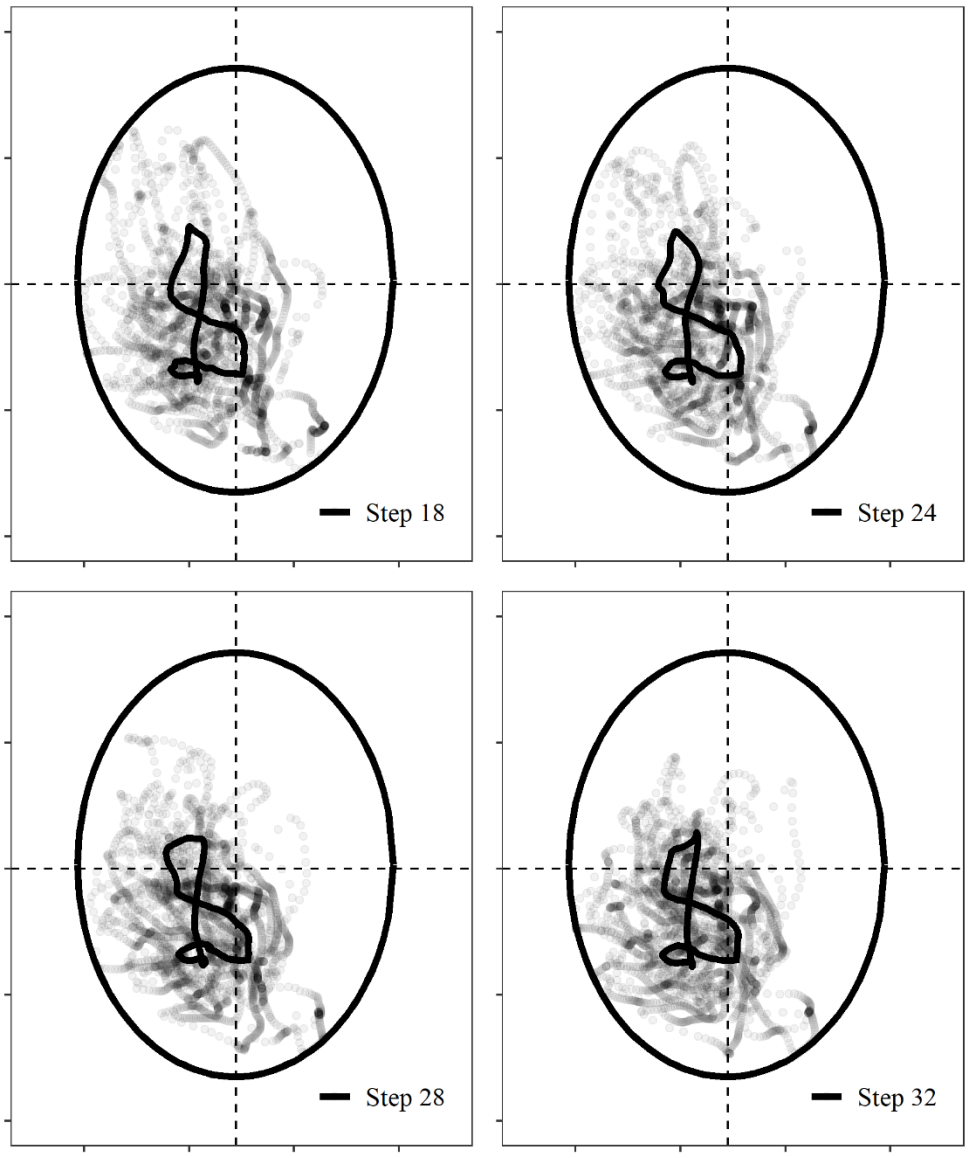

Figure 0.12: Glenoid contact patterns (mean paths and point clouds) for starboard rowers at all stroke rates.

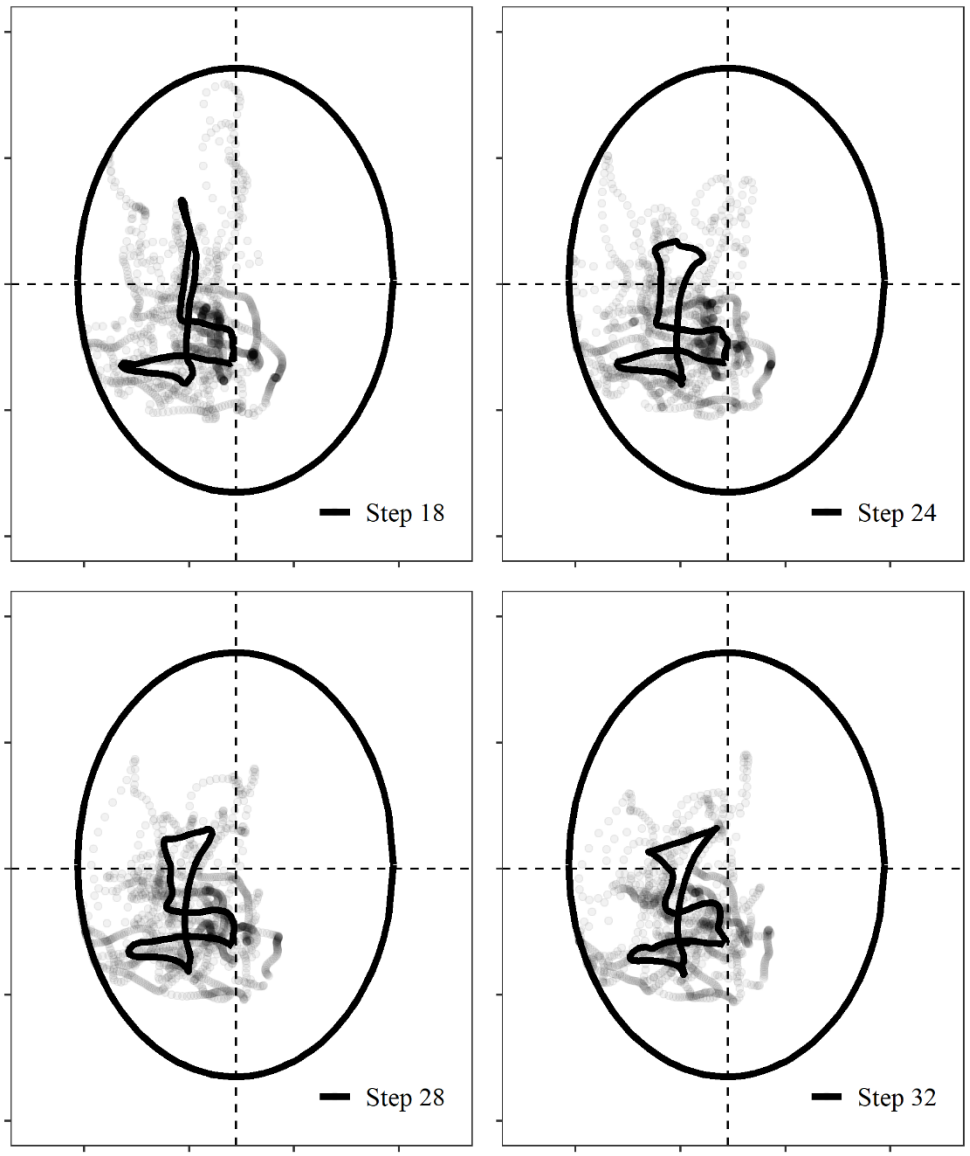

Figure 0.13: Glenoid contact patterns (mean paths and point clouds) for scullers at all stroke rates.

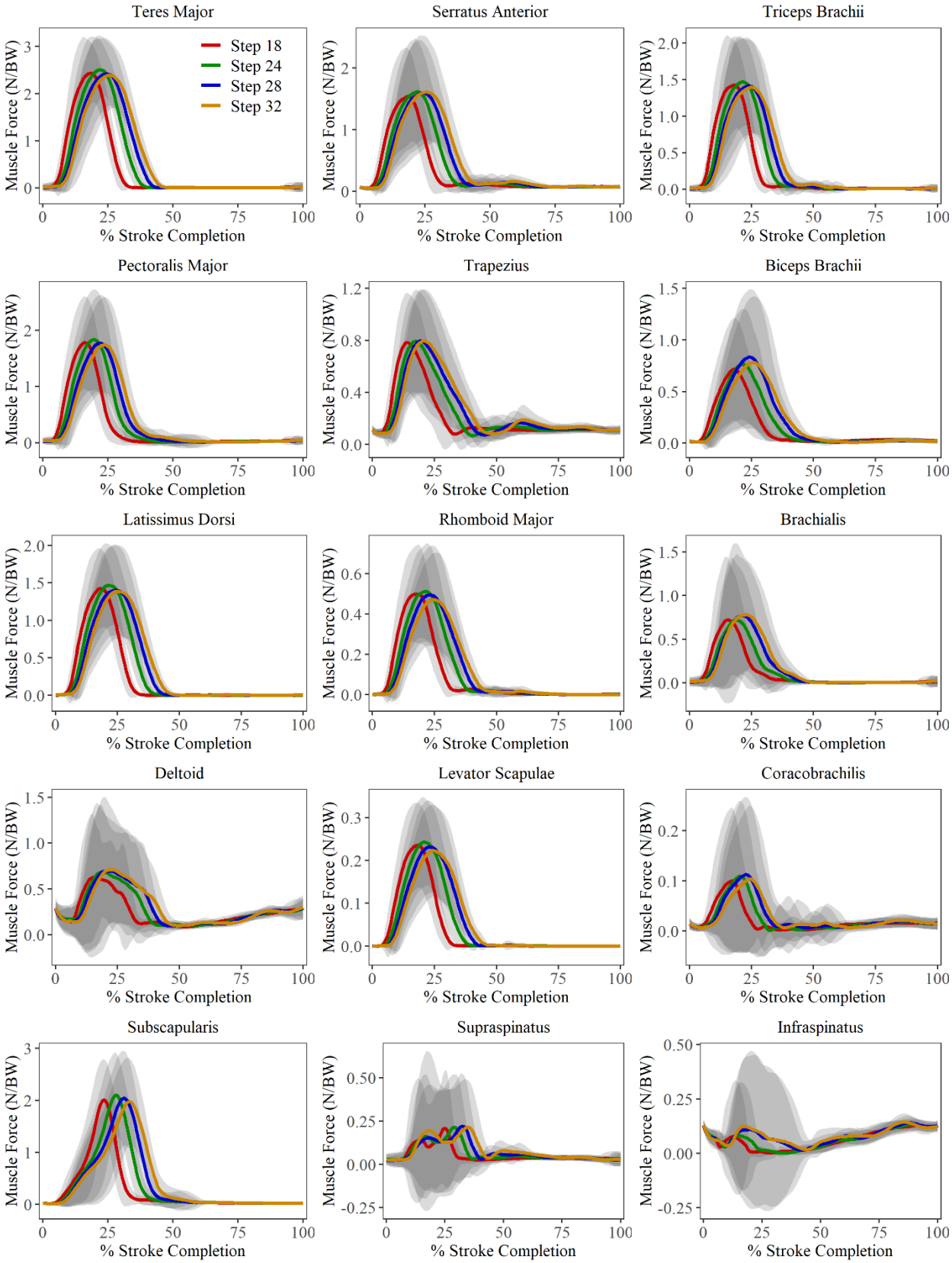

Figure 0.14: Population-wide body weight normalized muscle forces (mean ± std) at all stroke rates.

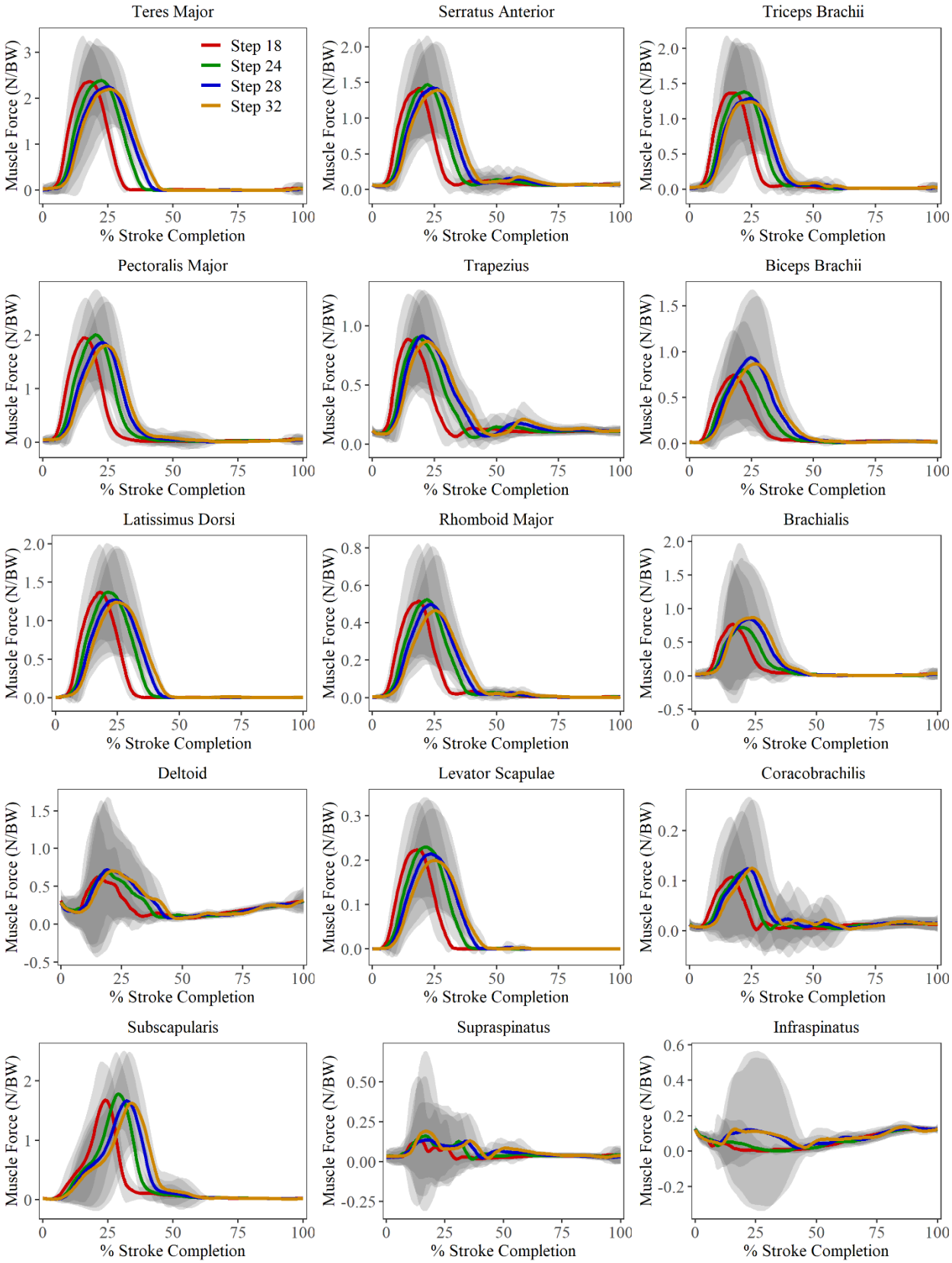

Figure 0.15: Female rower body weight normalized muscle forces (mean ± std) at all stroke rates.

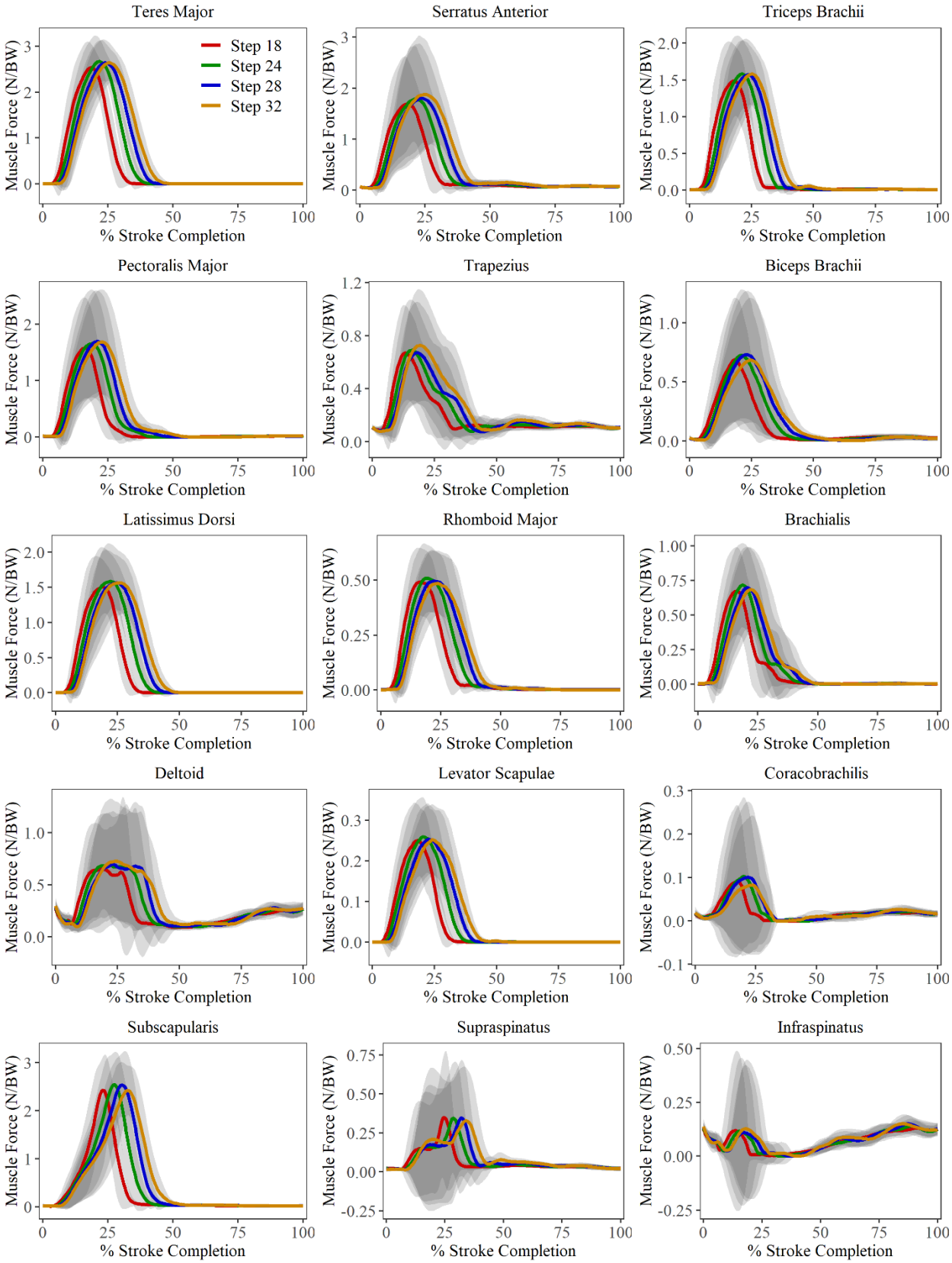

Figure 0.16: Male rower body weight normalized muscle forces (mean ± std) at all stroke rates.

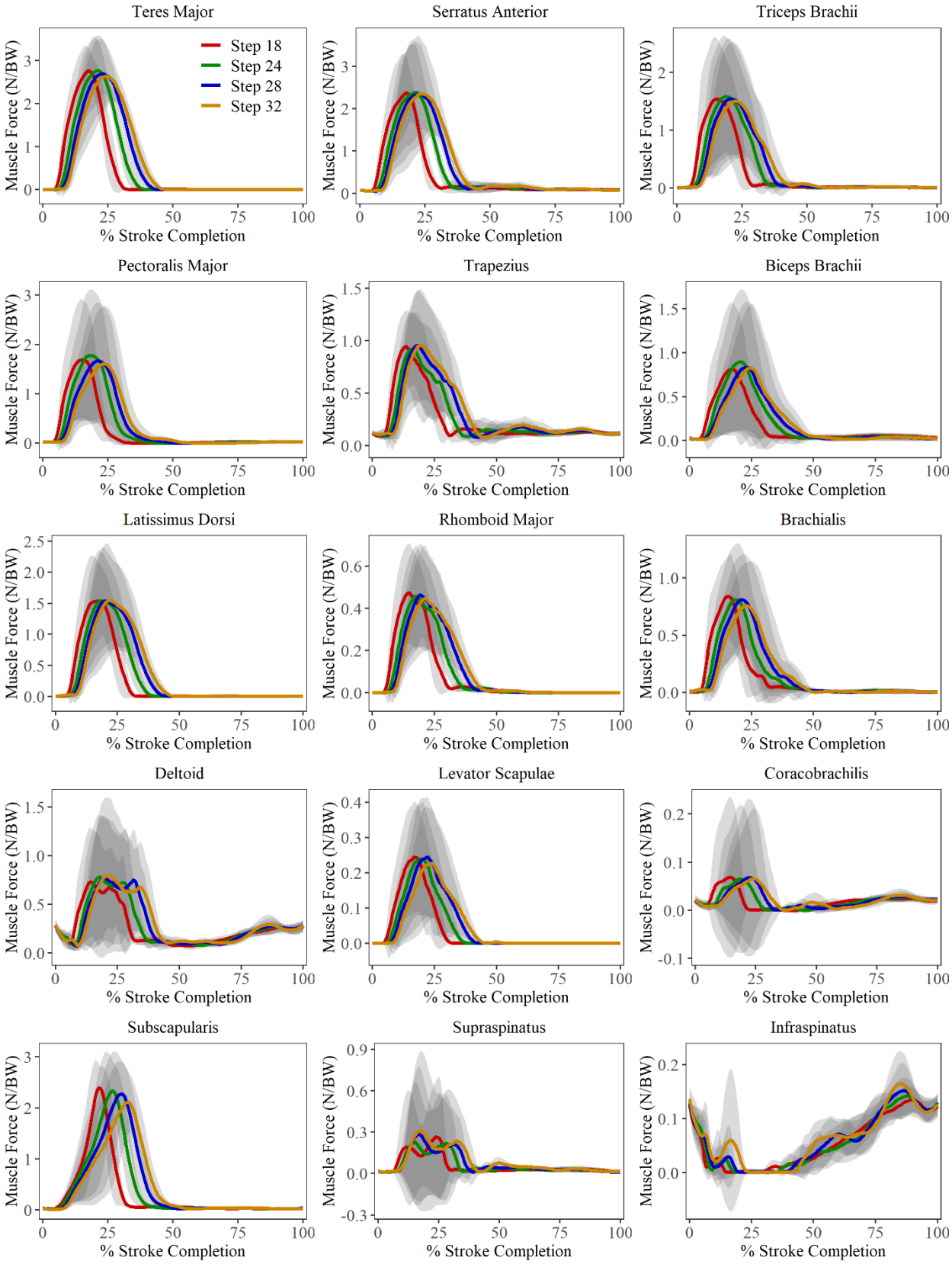

Figure 0.17: Club rower body weight normalized muscle forces (mean ± std) at all stroke rates.

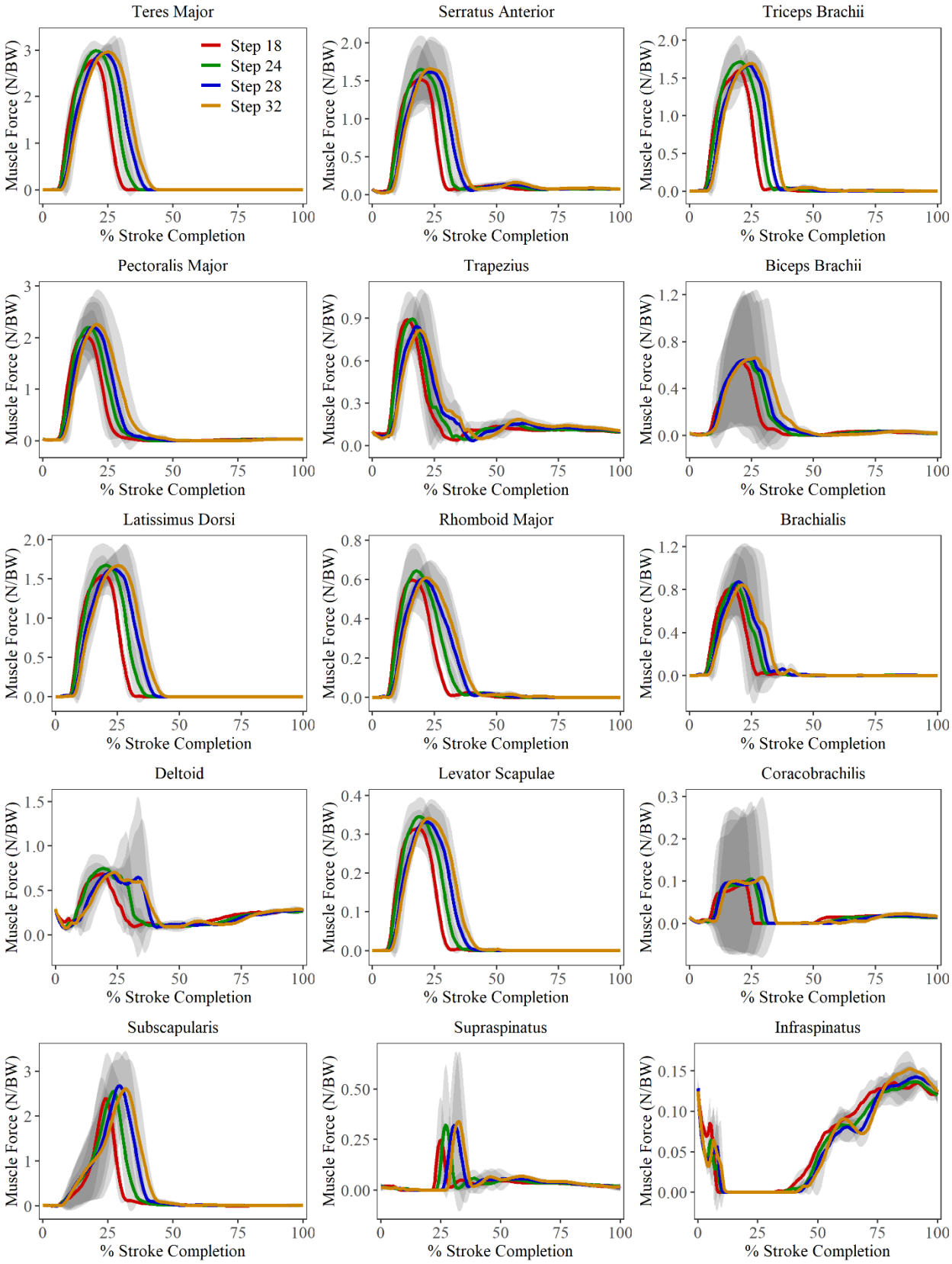

Figure 0.18: Elite rower body weight normalized muscle forces (mean ± std) at all stroke rates.

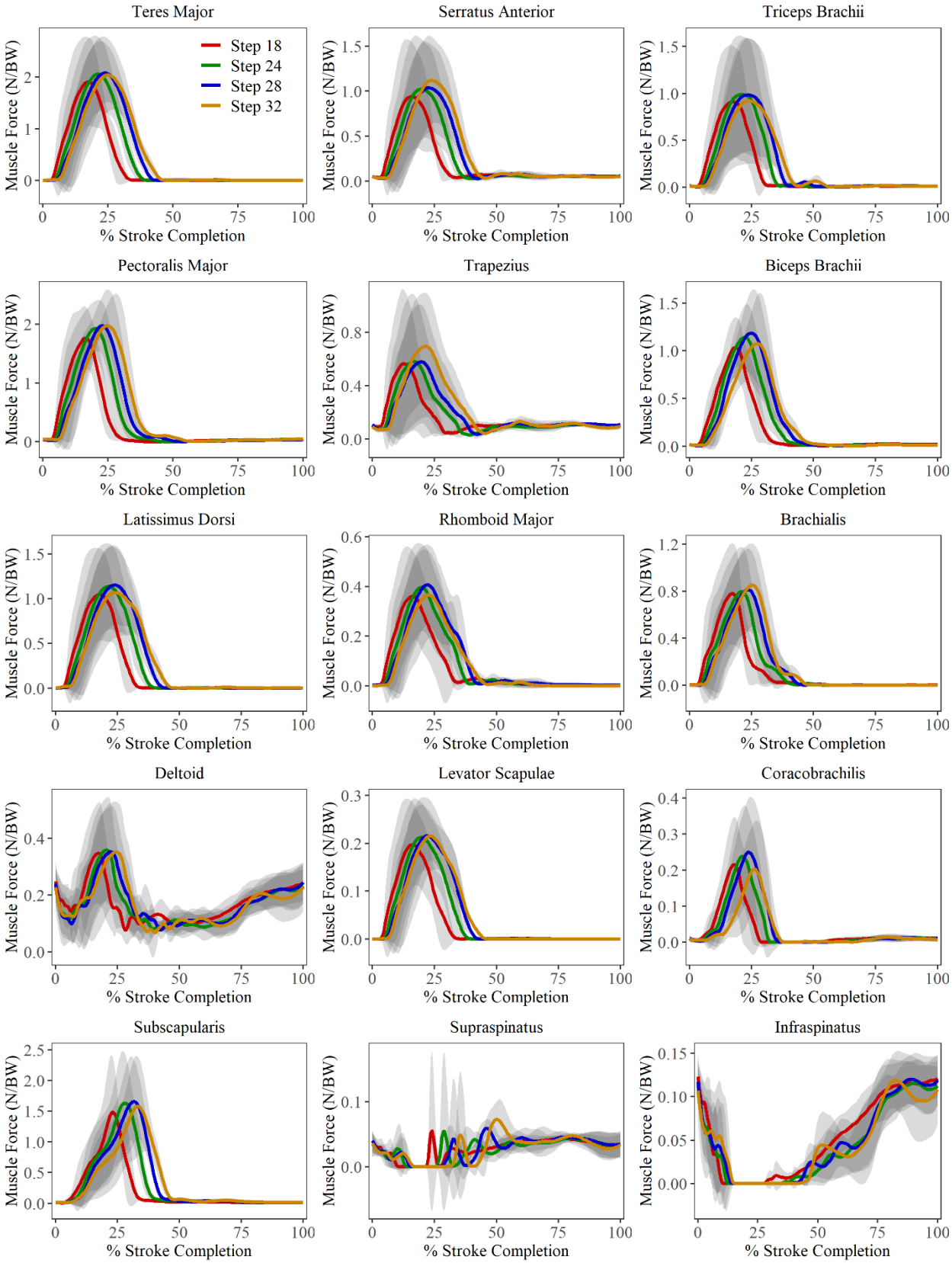

Figure 0.19: Masters rower body weight normalized muscle forces (mean ± std) at all stroke rates.

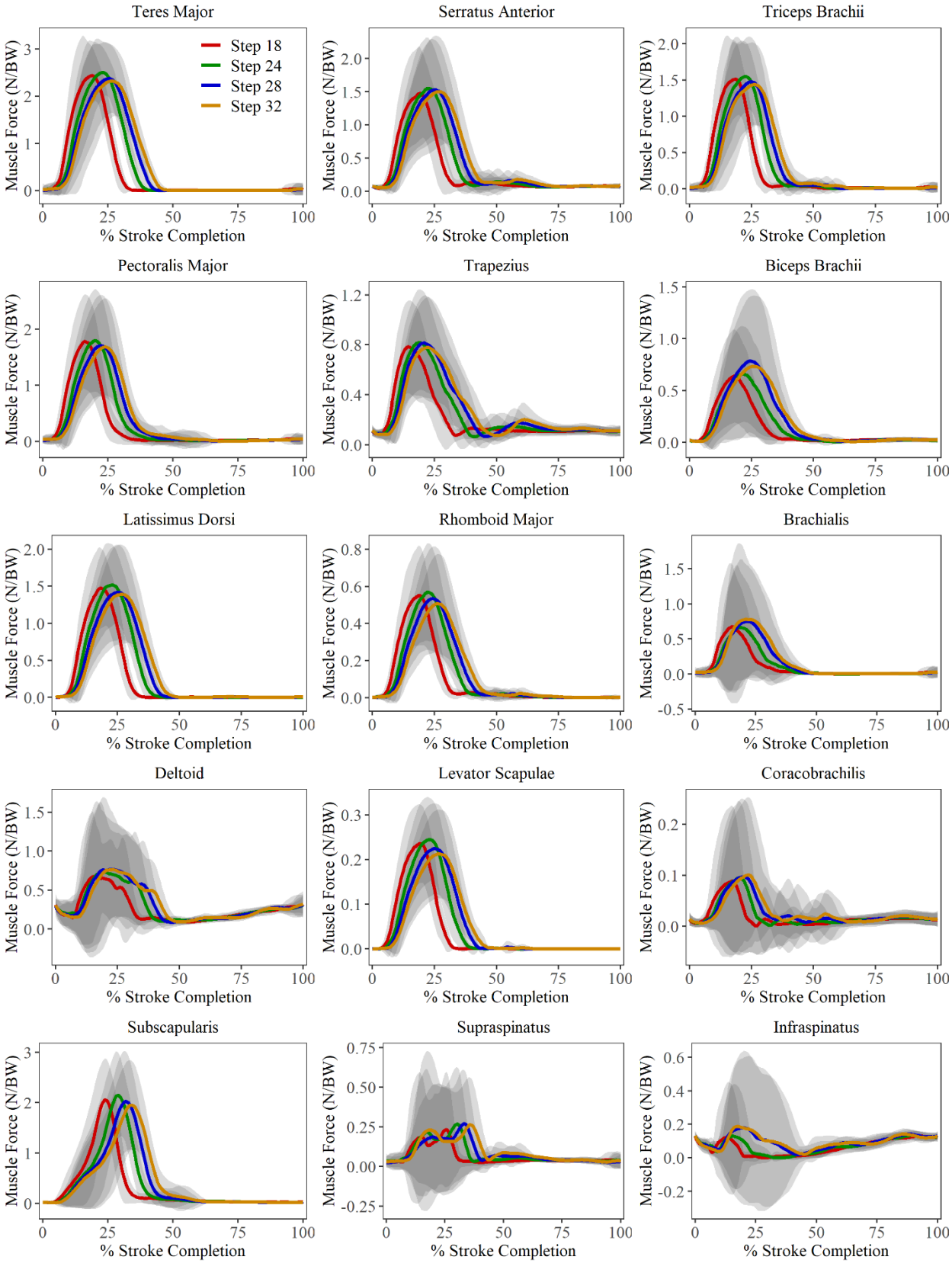

Figure 0.20: University rower body weight normalized muscle forces (mean ± std) at all stroke rates.

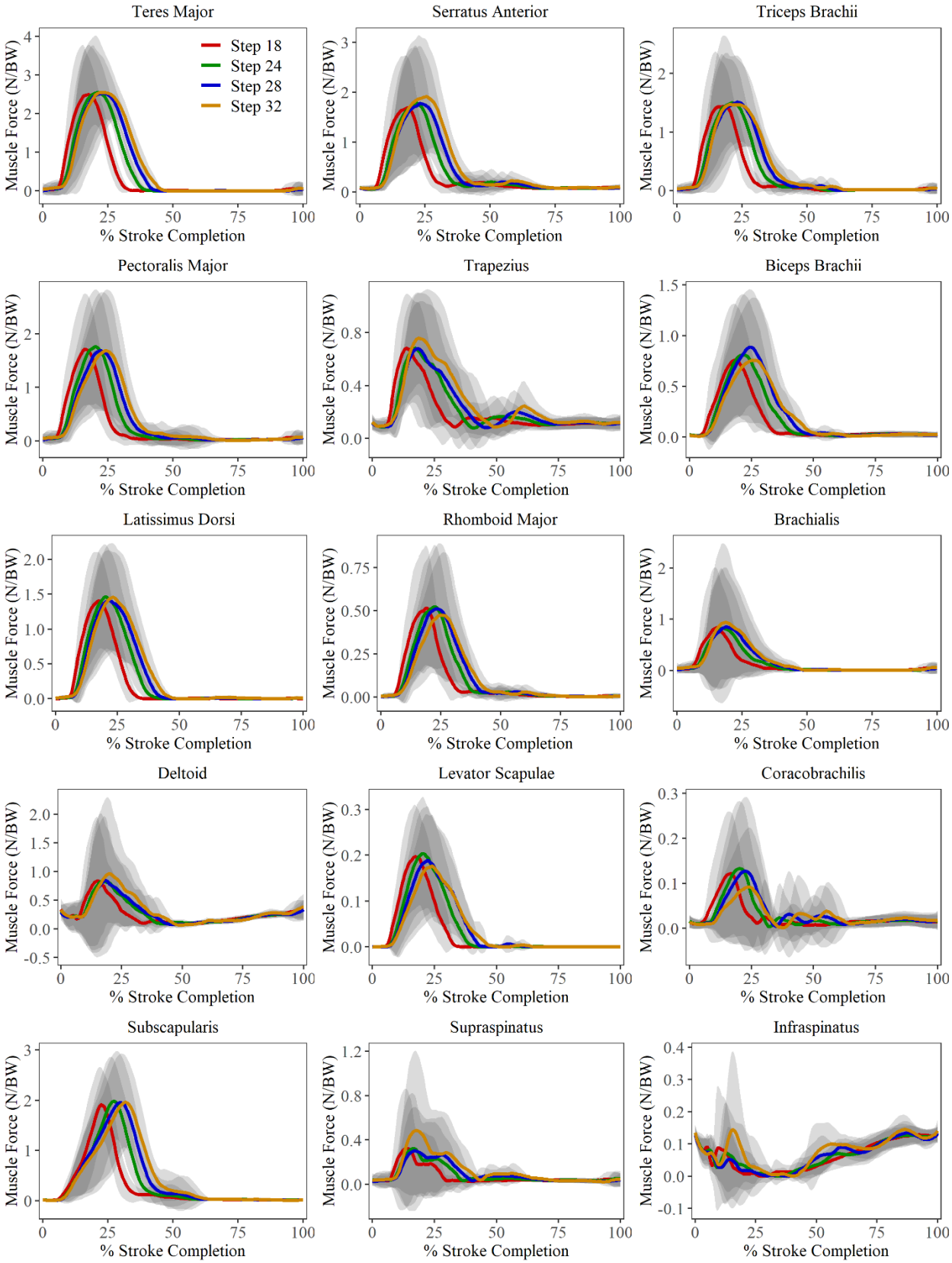

Figure 0.21: Port preferred modality body weight normalized muscle forces (mean ± std) at all stroke rates.

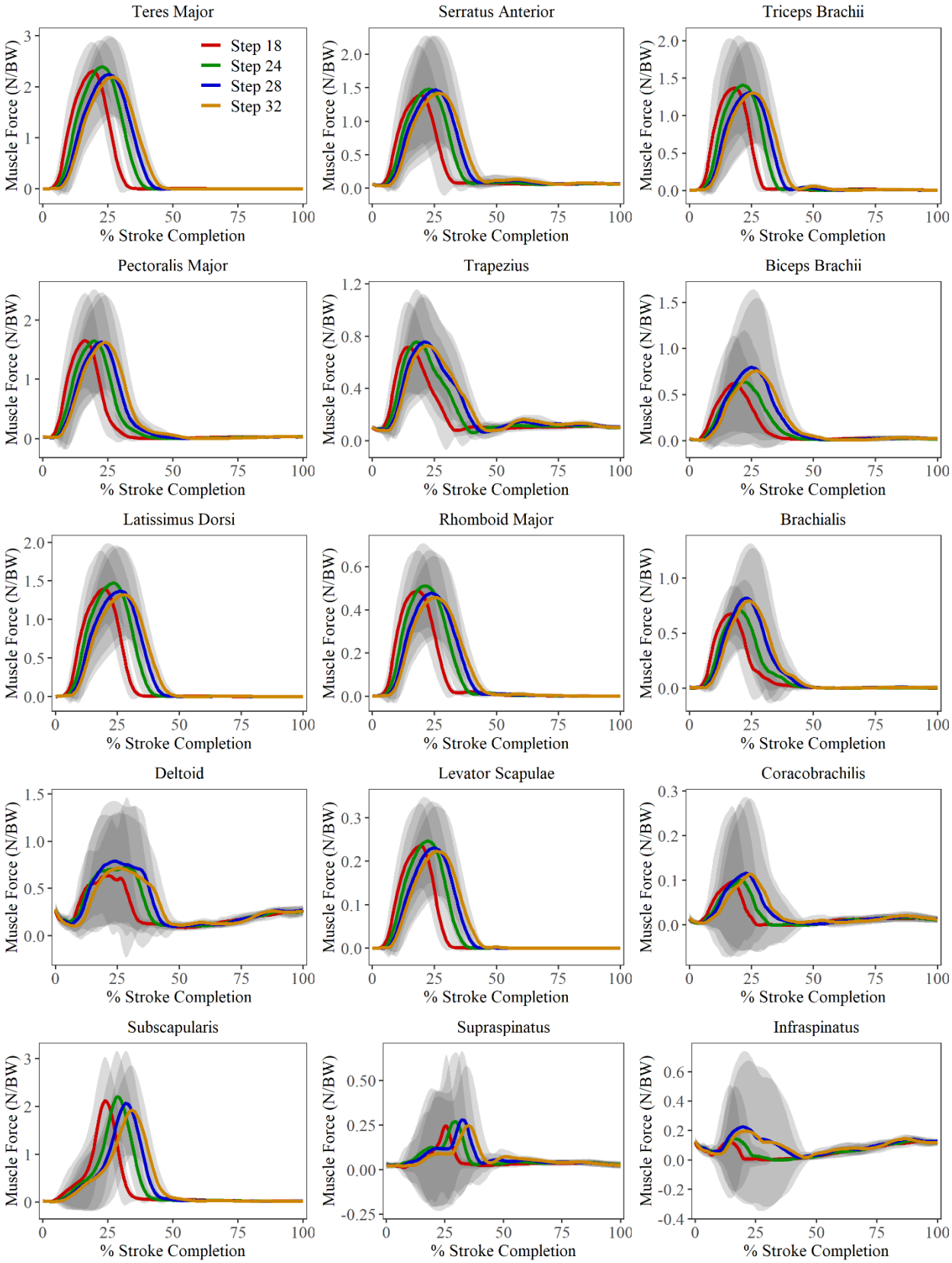

Figure 0.22: Starboard preferred modality body weight normalized muscle forces (mean ± std) at all stroke rates.

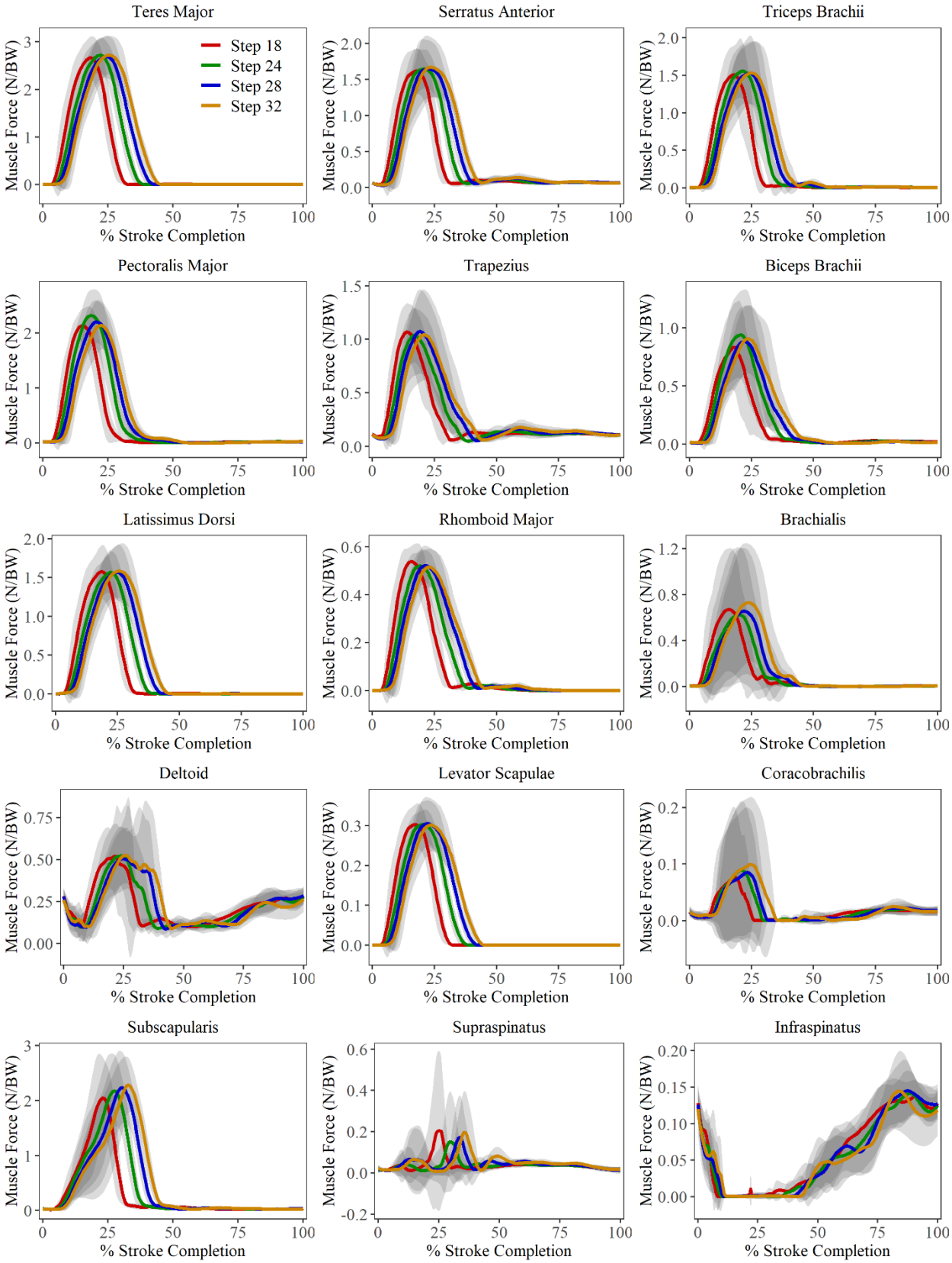

Figure 0.23: Sculling preferred modality body weight normalized muscle forces (mean ± std) at all stroke rates.